
# GEOLOGICAL SURVEY OF CANADA
# COMMISSION GÉOLOGIQUE DU CANADA



# CURRENT RESEARCH 1999-E

# RECHERCHES EN COURS 1999-E

Natural Resources Canada
Ressources naturelles Canada

Canada

## NOTICE TO LIBRARIANS AND INDEXERS

The Geological Survey's Current Research series contains many reports comparable in scope and subject matter to those appearing in scientific journals and other serials. Most contributions to Current Research include an abstract and bibliographic citation. It is hoped that these will assist you in cataloguing and indexing these reports and that this will result in a still wider dissemination of the results of the Geological Survey's research activities.

## AVIS AUX BIBLIOTHÉCAIRES ET PRÉPARATEURS D'INDEX

La série Recherches en cours de la Commission géologique contient plusieurs rapports dont la portée et la nature sont comparables à celles des rapports qui paraissent dans les revues scientifiques et autres périodiques. La plupart des articles publiés dans Recherches en cours sont accompagnés d'un résumé et d'une bibliographie, ce qui vous permettra, on l'espère, de cataloguer et d'indexer ces rapports, d'où une meilleure diffusion des résultats de recherche de la Commission géologique.

GEOLOGICAL SURVEY OF CANADA
COMMISSION GÉOLOGIQUE DU CANADA

# CURRENT RESEARCH 1999-E
# RECHERCHES EN COURS 1999-E

**1999**

**Includes/comprend:**

**Cordillera and Pacific Margin**
**Cordillère et marge du Pacifique**

**Interior Plains and Arctic Canada**
**Plaines intérieures et région arctique du Canada**

**Canadian Shield**
**Bouclier canadien**

**Eastern Canada and National and General Programs**
**Est du Canada et programmes nationaux et généraux**

Catalogue No. M44-1999/5E
ISBN 0-660-17824-9

Available in Canada from
Geological Survey of Canada offices:

601 Booth Street
Ottawa, Ontario K1A 0E8

3303-33rd Street N.W.
Calgary, Alberta T2L 2A7

101-605 Robson Street
Vancouver, B.C. V6B 5J3

A deposit copy of this publication is also available for reference
in selected public libraries across Canada

Price subject to change without notice

**Cover illustration**

Thinly layered, middle-amphibolite-facies, quartzofeldspathic gneiss of the ca 1.45 Ga Montauban group, south-central Grenville Province, Quebec. This gneiss is interpreted as thinly bedded felsic tuff from a submarine tephra fallout deposit. *See* paper by L. Nadeau et al., this volume. Photograph by L. Nadeau. GSC 1999-017

**Photo en page couverture**

Gneiss quartzofeldspathique finement rubané du faciès des amphibolites, centre sud de la Province de Grenville, Québec. Ce gneiss, attribué au groupe de Montauban (env. 1,45 Ga), serait un tuf finement lité issu de la sédimentation de cendre volcanique en milieu sous-marin. Cette photo se rapporte à l'article de L. Nadeau et al. dans le présent volume. Photo : L. Nadeau, GSC 1999-017

## Separates

A limited number of separates of the papers that appear in this volume are available by direct request to the individual authors. The addresses of the Geological Survey of Canada offices follow:

Geological Survey of Canada
601 Booth Street
Ottawa, Ontario
K1A 0E8
(FAX: 613-996-9990)

Geological Survey of Canada (Calgary)
3303-33rd Street N.W.
Calgary, Alberta
T2L 2A7
(FAX: 403-292-5377)

Geological Survey of Canada (Pacific)
101-605 Robson Street
Vancouver, British Columbia
V6B 5J3
(FAX: 604-666-1124)

Geological Survey of Canada (Pacific)
P.O. Box 6000
9860 Saanich Road
Sidney, British Columbia
V8L 4B2
(FAX: 604-363-6565)

Geological Survey of Canada (Atlantic)
Bedford Institute of Oceanography
P.O. Box 1006
Dartmouth, Nova Scotia
B2Y 4A2
(FAX: 902-426-2256)

Geological Survey of Canada (Quebec)
2535, boulevard Laurier
C.P. 7500
Sainte-Foy (Québec)
G1V 4C7
(FAX: 418-654-2615)

## Tirés à part

On peut obtenir un nombre limité de «tirés à part» des articles qui paraissent dans cette publication en s'adressant directement à chaque auteur. Les adresses des différents bureaux de la Commission géologique du Canada sont les suivantes :

Commission géologique du Canada
601, rue Booth
Ottawa (Ontario)
K1A 0E8
(Télécopieur : 613-996-9990)

Commission géologique du Canada (Calgary)
3303-33rd Street N.W.,
Calgary, Alberta
T2L 2A7
(Télécopieur : 403-292-5377)

Commission géologique du Canada (Pacifique)
101-605 Robson Street
Vancouver, British Columbia
V6B 5J3
(Télécopieur : 604-666-1124)

Commission géologique du Canada (Pacifique)
P.O. Box 6000
9860 Saanich Road
Sidney, British Columbia
V8L 4B2
(Télécopieur : 604-363-6565)

Commission géologique du Canada (Atlantique)
Institut océanographique Bedford
P.O. Box 1006
Dartmouth, Nova Scotia
B2Y 4A2
(Télécopieur : 902-426-2256)

Commission géologique du Canada (Québec)
2535, boulevard Laurier
C.P. 7500
Sainte-Foy (Québec)
G1V 4C7
(Télécopieur : 418-654-2615)

# CONTENTS

## CORDILLERA AND PACIFIC MARGIN
## CORDILLÈRE ET MARGE DU PACIFIQUE



## INTERIOR PLAINS AND ARCTIC CANADA
## PLAINES INTÉRIEURES ET RÉGION ARCTIQUE DU CANADA

## CANADIAN SHIELD
## BOUCLIER CANADIEN



## EASTERN CANADA AND NATIONAL AND GENERAL PROGRAMS
## EST DU CANADA ET PROGRAMMES NATIONAUX ET GÉNÉRAUX

# Cordillera and Pacific Margin

# Cordillère et marge du Pacifique

# Summary of 1998 fieldwork in Trutch and Toad River map areas, Central Forelands NATMAP Project, northeastern British Columbia[1]

Larry S. Lane, Michael P. Cecile, Lisel D. Currie, and Glen S. Stockmal
GSC Calgary, Calgary

*Lane, L.S., Cecile, M.P., Currie, L.D., and Stockmal, G.S., 1999: Summary of 1998 fieldwork in Trutch and Toad River map areas, Central Forelands NATMAP Project, northeastern British Columbia;* in *Current Research 1999-E; Geological Survey of Canada, p. 1–8.*

**Abstract:** Significant parts of seven 1:50 000 scale map areas were mapped in detail, and part of the Trutch map area was mapped at 1:250 000 scale during seven weeks of fieldwork. In the Trutch area, facies changes within the Triassic succession presented difficulties in the definition of mappable units across the area. Individual folds are mappable for long distances in the foothills of the Trutch map area. In the foothills, numerous folds truncate against a subtle, but distinct, domain 70–80 km long, containing long, continuous, north-trending folds. Within and adjacent to this zone, some structures exhibit abrupt changes in plunge, others show pronounced local swings in axial surface traces, and on other structures, shortening is transferred en échelon to adjacent structures. Also, disparities exist between the trends of local structures and the trends of regional structures. Altogether these indicate that surface structures are influenced by features that are present in the subsurface.

**Résumé :** Pendant sept semaines de travail de terrain, des parties importantes de sept régions cartographiques ont été cartographiées en détail à l'échelle de 1/50 000 et une partie de la région cartographique de Trutch a été cartographiée à l'échelle de 1/250 000. Dans la région de Trutch, des changements de faciès à l'intérieur de la succession du Trias ont présenté des difficultés pour la définition d'unités cartographiables à travers la région. On peut cartographier les plis individuels sur de longues distances dans les avant-monts de la région cartographique de Trutch. Dans les avant-monts, plusieurs des plis sont tronqués sur un domaine subtil mais distinct de 70 à 80 km de longueur qui contient des plis longs et continus d'orientation nord. À l'intérieur de cette zone et à proximité, certaines structures accusent un changement abrupt de plongement, d'autres montrent des changements locaux brusques de la trace des surfaces axiales, alors que sur d'autres structures le raccourcissement est transféré en échelon à des structures adjacentes. De plus, il existe des différences entre les directions des structures locales et celles des structures régionales. Pris ensemble, ces phénomènes indiquent que des éléments dans la subsurface influent sur les structures de surface.

[1] Contribution to the Central Forelands NATMAP Project

## INTRODUCTION

The Central Foreland NATMAP Project is a multidisciplinary project including bedrock and surficial mapping, surface and subsurface correlation studies, detailed biostratigraphic and stratigraphic studies in support of mapping and regional paleogeographic problems, and thematic studies including lead-zinc mineralization in breccia zones in Paleozoic carbonates. The mapping project will study two areas of the Cordilleran foothills in detail to investigate the nature of regional variations in stratigraphy and structural style between a southern domain in the Fort St. John–Fort Nelson area of northeastern British Columbia (Fig.1), and a northern domain in the Liard–La Biche area of adjacent Yukon and Northwest Territories. Previous regional syntheses have suggested that these variations were inherited from the geometry of continental rifting during the initial formation of the proto-Pacific continental margin in latest Proterozoic time (e.g. Cecile et al., 1997).

The first field season of the Central Foreland project focused on 1:50 000 and 1:250 000 scale mapping and stratigraphic studies in the Trutch map area (94 G), and on 1:50 000 scale mapping in the Trout River area (94 N4) (Fig.1). Previous regional reconnaissance mapping (Taylor, 1979; Thompson, 1989; Taylor and Stott, 1998) provided a regional context, but subsequent stratigraphic studies of late Paleozoic strata (Richards et al., 1993; Henderson et al., 1993) and Triassic strata (Gibson, 1993) have permitted more detailed mapping and further delineation of stratigraphic variations. Also, the co-operation and participation of the petroleum industry in the Central Foreland NATMAP project will enable us to fully integrate new surface data with existing seismic and well data as mapping progresses.

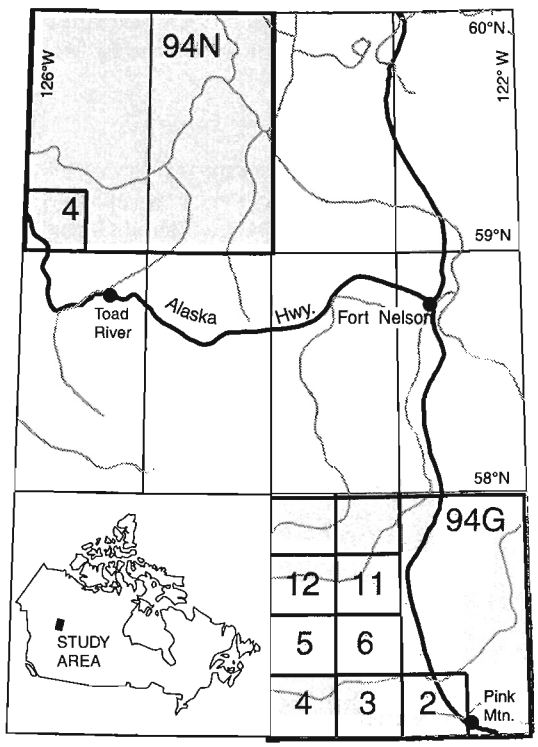


***Figure 1.*** *Location map of northeastern British Columbia showing 1:50 000 scale NTS map areas with new mapping in 1998.*

Significant exploration activities are ongoing in this environmentally sensitive area. One of the many benefits of this project's emphasis on integration of bedrock geological mapping with subsurface data will be to improve the focus of exploration activities, thereby reducing the cumulative environmental impact of future exploration. In addition, concurrent mapping of the surficial geology includes the identification of areas prone to landslides, which will facilitate land-use planning in the region (Bednarski, 1999).

The Trutch map area in northeastern British Columbia includes Plains, Foothills, and Rocky Mountains physiographic provinces. Extensive petroleum development in the region includes significant gas fields tapping Triassic reservoirs (e.g. Bubbles field, Jedney field, Fig. 2), and Carboniferous Debolt Formation reservoirs (e.g. Sikanni field, Pocketknife field, Fig. 2). Known fields occur within, or adjacent to, the eastern margin of the Foothills. Devonian targets are being actively explored in the western Foothills.

During fieldwork in 1998, parts of seven 1:50 000 scale maps in the western part of the Trutch map area were mapped in detail (Fig.1), and six are available as colour Open File maps (Cecile, 1999; Currie and Cecile, 1999; Khudoley, 1999; Lane, 1999; Legun 1999a; Stockmal, 1999). Also, part of the east half of the Trutch map area was mapped at 1:250 000 scale. In Toad River map area, approximately half of 94 N/4 was mapped at 1:50 000 scale, together with a small part of 94 N/3.

## STRATIGRAPHY

Exposed strata in the study area include Ordovician to Devonian carbonate rocks in the Rocky Mountains in the west, Devonian to Cretaceous clastic and carbonate successions in the Foothills, and Cretaceous sandstone and shale in the Plains to the east (Fig. 3). Detailed mapping in the western and southern parts of 94 G focused largely on areas underlain by Carboniferous–Permian, Triassic and Jurassic–Cretaceous strata. In each instance, significant changes in facies or preserved thickness occur over distances on the order of 40 km along and across strike.

In 1998, the lower Paleozoic succession in Mount McCusker (94 G/4) was mapped in detail by project partners from the British Columbia Geological Survey (Legun, 1999a, b). Also, the stratigraphic context and the nature of hydrothermal brecciation at the Robb Lake Mississippi Valley–type (MVT) Pb-Zn deposit was examined (Paradis et al., 1999; Nelson et al., 1999a, b).

Carboniferous strata of the Prophet Formation (Fig. 3) are exposed in the western parts of the project area. Prophet A and Prophet B are the lowest members, forming a regionally consistent succession comprising interbedded chert and shale (Richards et al., 1993). The highest member, Prophet C, is approximately equivalent to the Debolt Formation in the

subsurface, and is a 25–30 m thick carbonate unit over most of the project area. However, northward and westward over distances as small as 10 km, the carbonate becomes progressively replaced by secondary chert such that it becomes difficult to distinguish from the chert-dominant Prophet B member. Above the Prophet Formation, the preserved thickness of the Carboniferous Stoddart Group (Fig. 3) is highly variable over short distances. A thick succession is intersected by petroleum wells in the subsurface beneath the eastern Foothills (B. Richards, pers. comm., 1998). In exposures in the western Foothills, the unit is present on some ridges, but locally it is absent and the Permian Fantasque Formation lies directly on carbonates of the Prophet C member.

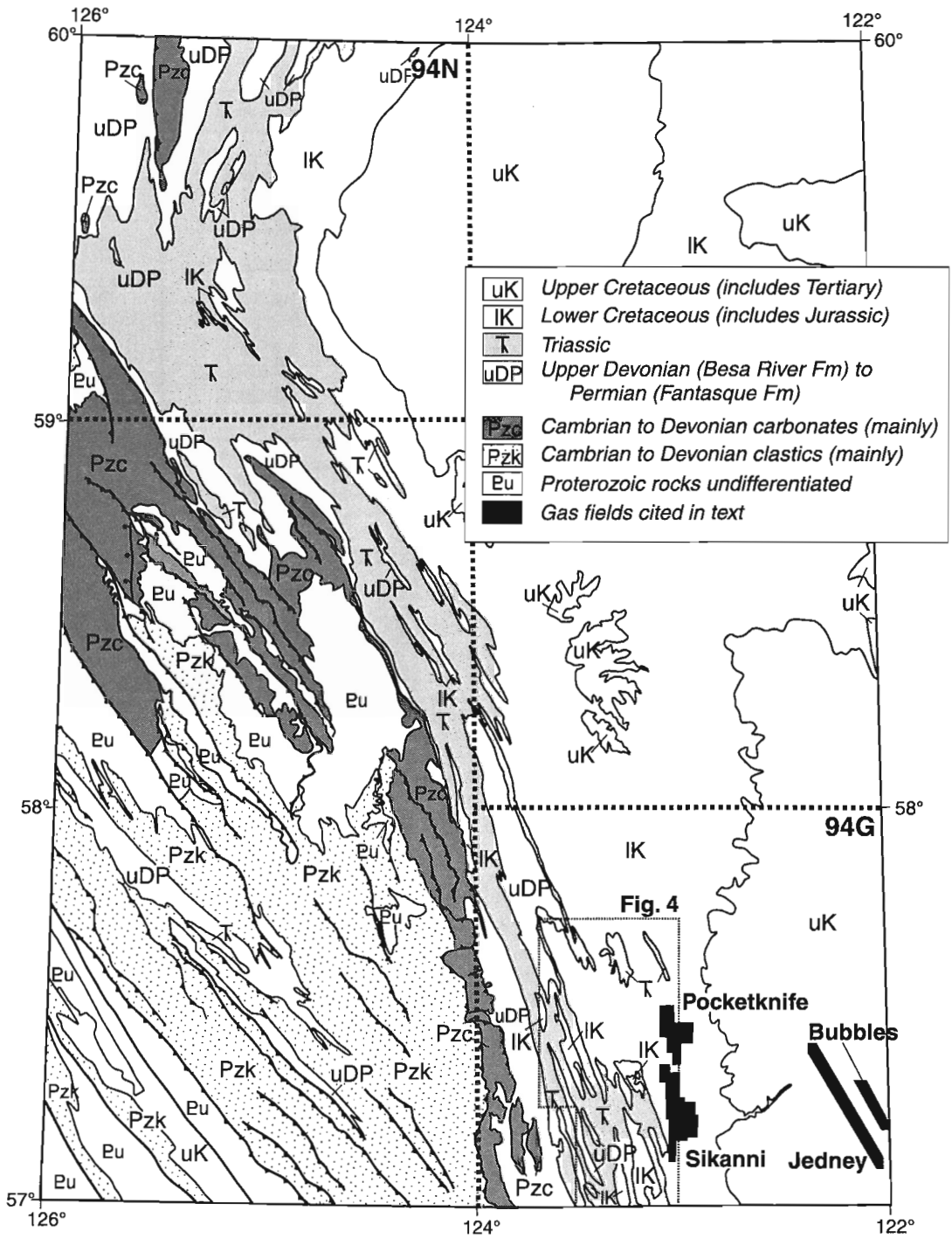


***Figure 2.*** *Generalized regional geology map simplified from the Fort Nelson geological compilation of MacIntyre et al. (1998), showing regional northwest-southeast structural trends with superimposed northerly trends coincident with the early Paleozoic shale-out. Map areas 94 N and 94 G are outlined. The area shown in Figure 4 is also identified.*

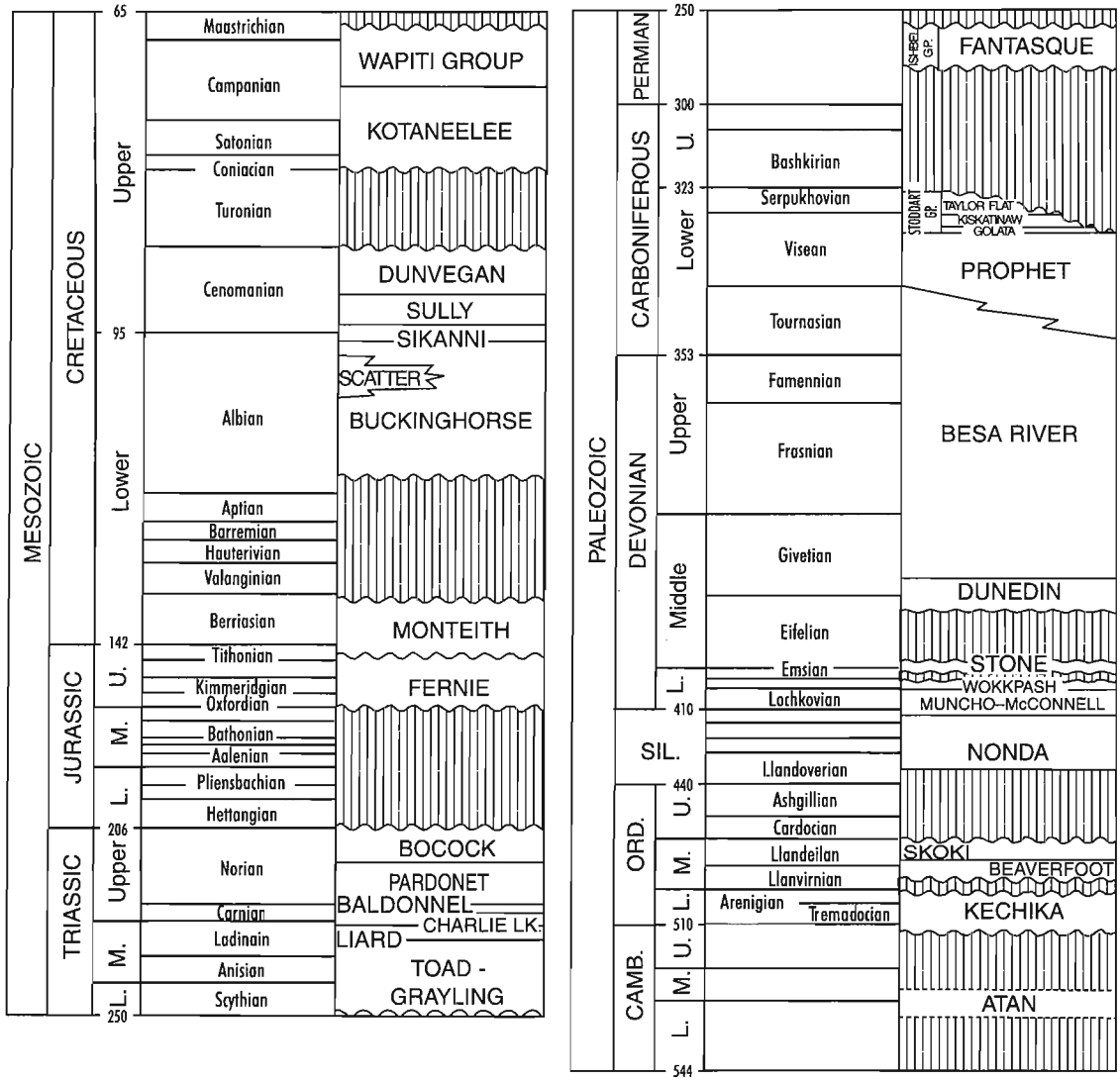


***Figure 3.*** *Stratigraphic nomenclature used in this report.*

The Triassic succession is particularly variable across the project area. Our mapping has highlighted the need for a more detailed understanding of the age and facies variations in this part of the succession. This is complicated by the fact that in many places the degree of exposure is insufficient to adequately document these variations. Stratigraphic and biostratigraphic studies of the Triassic succession (Orchard, 1999; Johns et al., 1999) are important components of the project in relation to surface-subsurface correlations, paleogeographic studies, mapping support, and in providing context to ongoing vertebrate paleontology research in the area (Nicholls et al., 1998).

Although the Triassic Toad–Grayling succession is variable in thickness, its character on the scale of the project area is consistent. In the eastern part of the Redfern Lake area (94 G/5), it consists of a poorly exposed, lower, black shale sequence varying in thickness from as little as 20 m to as much as 200 m within 3 km across strike. The upper part of the succession is dominated by brown-weathering, dark grey calcareous siltstone and argillaceous limestone, interbedded with bluish-black shale. Near the top, a few thick units of quartz sandstone are locally exposed, and in the south a resistant 10 m thick sandstone unit occurs some 50 m below the top of the formation.

The Liard and Charlie Lake formations constitute a succession of quartz sandstone, calcareous sandstone and siltstone, sandy carbonate, and carbonate as much as 300 m thick in total. Thickness and lithology both vary considerably in detail across the project area. Over much of the area, the contact between the (calcareous) quartz sandstone of the Liard Formation and the carbonate-dominant Charlie Lake has been difficult to define consistently and is considered a significant mapping problem that has not yet been resolved (*see* Gibson, 1993). In the south, where the Charlie Lake Formation is almost entirely calcareous, the definition is not problematic. However, farther north, at least three significant

(>5 m) quartz sandstone units occur within the succession, raising the question of where to place the Liard–Charlie Lake contact. The Charlie Lake Formation also contains a prominent light grey bluff-forming limestone unit 10–15 m thick close to the top of the formation. This unit is readily mistaken for the overlying Baldonnel Formation in areas of poor exposure.

In the outer Foothills, quartzite (interbedded with 10–20% black shale) of the Upper Jurassic to Lower Cretaceous Monteith Formation overlies a thin Jurassic Fernie shale. Westward, the preserved thickness of the Fernie increases to more than 200 m. Consistently in the west, and in places in the east, the top of the Fernie is transitional over more than 10 m into the Monteith Formation. Locally in the east, this contact is abrupt, or the Fernie is missing and the Monteith lies directly on the Triassic Pardonet Formation. This interval is the focus of ongoing detailed stratigraphic and biostratigraphic studies.

## STRUCTURE

Along the western edge of the Trutch map area, the north-south strike of thrust faults and folds in the early Paleozoic carbonate succession diverges from the northwest-southeast structural grain typical of the region (Fig. 2). This belt of Rocky Mountain structures is just east of the north-south-trending early Paleozoic carbonate shale-out and the structural trends reflect the influence of this Paleozoic depositional ramp, which in turn is likely controlled by basement structure. The Besa River shales are complexly deformed and constitute the major regional detachment to structures in the overlying Prophet/Debolt and Triassic strata in the eastern Foothills.

Although the lower Paleozoic carbonate succession of the Rocky Mountains in the southwest corner of the project area is dominated by spectacular shallowly dipping thrust faults and tight, overturned folds (Legun, 1999a, b), the upper Paleozoic and Mesozoic successions are dominated by folds displaying a variety of geometries. These include simple box and chevron folds, commonly with nearly flat crests and troughs in the outer Foothills. Farther west, geometries are dominated by tight chevrons, commonly overturned eastward, and are locally disrupted by thrust faults. Previously published structural interpretations from the region indicate that the structures are detached on flat décollement structures in the subsurface (Thompson, 1989).

## EASTERN FOOTHILLS

Gentle mountain topography characterizes the western three quarters of the Foothills comprising 94 G/3, G/6, and G/11 (Fig. 4), where rocks of the Carboniferous Prophet Formation to Cretaceous Buckinghorse Formation are exposed. The Prophet Formation is exposed in the cores of anticlines in the southwestern corner of the three map areas. The ridges are primarily underlain by anticlines that bring Jurassic Monteith and Fernie formations, along with Triassic Pardonet, Baldonnel, Charlie Lake, Liard, Toad, and Grayling formations to the surface. The Buckinghorse Formation and locally Gething Formation are preserved in valleys, along the traces of major synclines. To the east of the physiographic Foothills, the Plains are underlain by folded Monteith, Gething, and Buckinghorse formations, and the uppermost Triassic Pardonet is exposed in an anticline crossing the Sikanni Chief River (Fig. 4).

Major folds have wavelengths of a few kilometres and generally trend north-northwest. Box folds, sometimes with minor parasitic folds, dominate the folding style. In general, the fold axes have remarkably shallow plunges. Few major faults reach the surface in this area (Fig. 4). Thrust faults are also known at the level of the Debolt Formation in the Sikanni gas field, east of the foothills (Fig. 2).

The southern part of the eastern Foothills is transected by a distinct north-trending structural domain up to 8 km wide and 70–80 km long (Fig. 4). Its western margin is defined by the conspicuous termination of south-southeast-trending fold trains against a continuous multiple-hinge anticlinal culmination. Some 5–10 km east of this culmination is a second anticline-syncline-anticline culmination that forms the eastern margin of this domain. Within and adjacent to this domain, a series of anomalous local features includes folds with axial surfaces curved into a z-shaped map pattern, northwest-trending en échelon folds, and abrupt northward steepening of plunges from near zero to as much as 17°N, localized where the domain crosses Sikanni Chief Valley and Besa River–Pocketknife Creek valley (Fig. 4). Some of these features imply a component of right-lateral oblique convergence associated with this domain. We speculate that this domain likely is controlled by reactivated structures within the Proterozoic–Paleozoic miogeoclinal succession in the subsurface.

## WESTERN FOOTHILLS

Structures in Richards Creek map area (94 G/12) have an overall gentle southerly plunge resulting in the exposure of a number of structural levels and associated detachments. At the highest structural level, Triassic through Cretaceous strata are folded into open and upright to tight and overturned structures with wavelengths and amplitudes varying from a few hundred metres to 2 km. Faulting is negligible at map scale. The sense of vergence is typically toward the foreland, although local reversals occur. Within individual structures, the style varies along strike from rounded hinges to chevron-style hinges, and box folds transform into approximately concentric styles.

Where the Toad–Grayling Formation becomes thicker north of Richards Creek (Fig. 4), it becomes a secondary detachment horizon permitting structures within the overlying Triassic succession to evolve independently from structures in the underlying Carboniferous–Permian succession. Beneath the thick basal Triassic Toad–Grayling succession, a lower structural level comprising the Carboniferous Prophet Formation and Permian Fantasque Formation are deformed into a series of spectacular, tight, steeply inclined to overturned folds. These folds broadly correspond with structures in the overlying Triassic section, but are distinctly foreland-vergent. They are cut by shallow, east-northeast directed thrust faults that apparently root in the underlying Devonian Besa River shale.

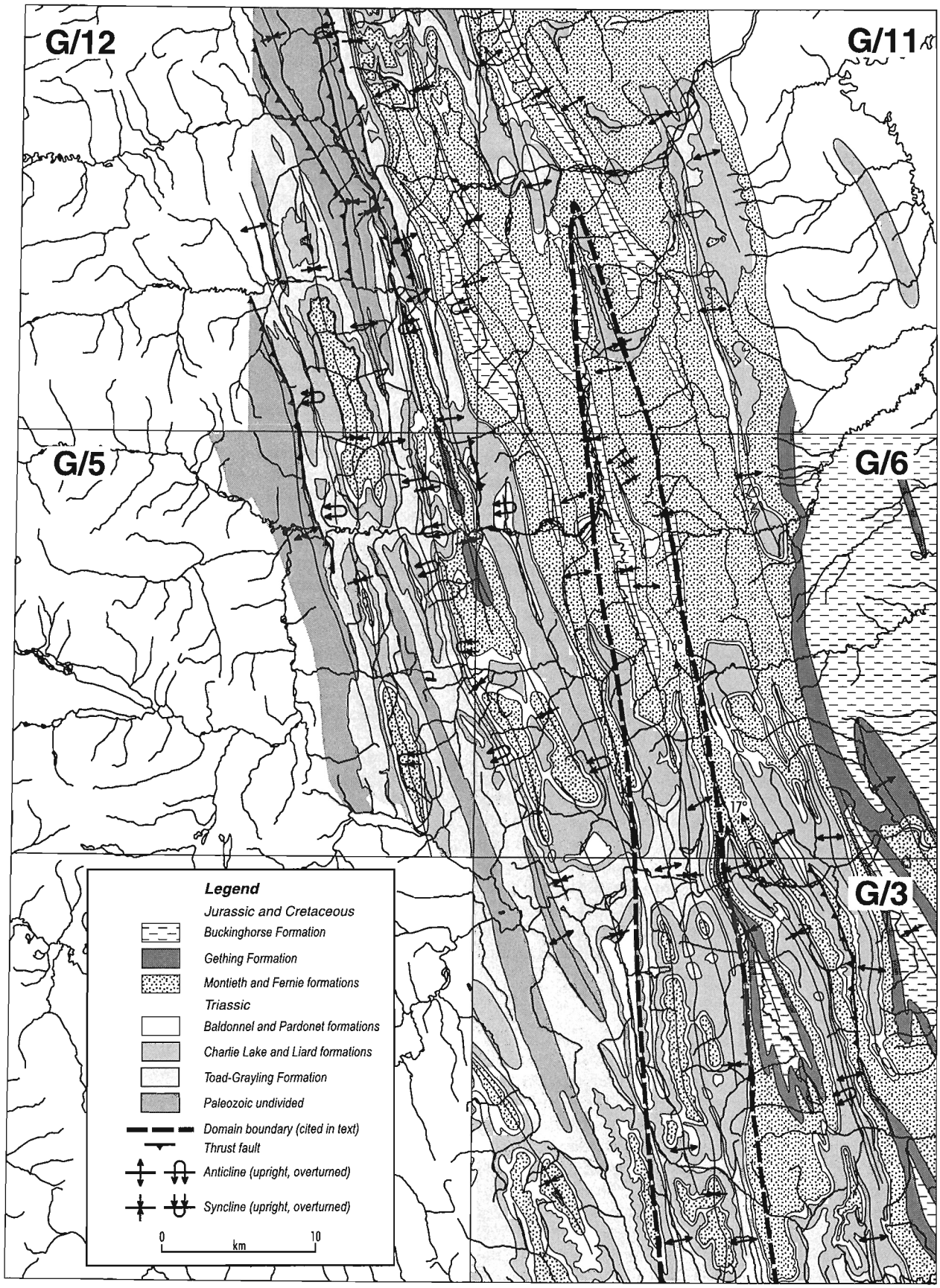


***Figure 4.*** *Geological compilation simplified from new colour Open File maps produced from mapping in 1998 (Cecile, 1999; Currie and Cecile, 1999; Khudoley, 1999; Lane, 1999; Stockmal, 1999).*

## TROUT RIVER (94 N/4)

Two weeks of fieldwork focused on the southern part of the map area, where Silurian to Devonian carbonate strata are exposed. In this most rugged part of the area, structures are dominated by shallowly west-dipping thrust faults and associated detached folds. The folds vary from upright to eastward overturned and are commonly open to tight. The faults are eastward-directed, except for two local backthrusts. The exposed strata include the Silurian Nonda Formation, and the overlying Devonian succession (Muncho–McConnell, Wokkpash, Stone, and Dunedin formations). The carbonate succession was thrust over shales of the Besa River Formation.

Carboniferous to Triassic strata, equivalent to those units exposed farther south in the Trutch map area, are poorly exposed in timbered hills in the eastern part of the Trout River area. Here, preliminary results suggest that structures are dominated by tight, upright folds with dominant wavelength on the order of 4 km, but containing abundant minor folds on the order of 300–500 m wavelength.

## SUMMARY AND CONCLUSIONS

After one year of detailed mapping in Trutch and Toad River areas, the Central Foreland NATMAP project has produced five new colour open file maps at 1:50 000 scale. Compilation of these detailed maps has clearly elucidated structural domains. Regional structural trends are northwestward, but significant trend deviations exist over substantial parts of the Trutch map area. These deviations are inferred to relate to stratigraphic facies belts and reactivation of pre-existing structures affecting the lower Paleozoic succession in the subsurface. Reprocessing and reinterpretation of donated seismic-reflection data is ongoing and, in conjunction with the mapping, will be used to test the hypothesis of subsurface structural control.

Stratigraphic facies vary substantially across the Trutch map area at most stratigraphic levels. Of particular significance are variations in Triassic facies. The positions and character of these facies variations are targets of ongoing detailed stratigraphic study.

## REFERENCES


**Bednarski, J.**
1999: Preliminary report on mapping surficial geology of Trutch map area, northeastern British Columbia; *in* Current Research 1999-A; Geological Survey of Canada, p. 35–43.

**Cecile, M.P. (comp.)**
1997: Geology, Sikanni Chief River area, parts of NTS sheets 94 G/3 (Marion Lake), 94 G/6 (Mount Withrow); Geological Survey of Canada, Open File 3471, scale 1:50 000.

**Cecile, M.P.**
1999: Preliminary geology of Marion Lake map area (94 G/3), British Columbia; Geological Survey of Canada, Open File 3736, scale 1:50 000.

**Currie, L.D. and Cecile, M.P.**
1999: Preliminary geology of Mount Withrow map area (94 G/6), British Columbia; Geological Survey of Canada, Open File 3737, scale 1:50 000.

**Cecile, M.P., Morrow, D.W., and Williams, G.K.**
1997: Early Paleozoic (Cambrian to Early Devonian) tectonic framework, Canadian Cordillera; Bulletin of Canadian Petroleum Geology, v. 45, p. 54–74.

**Gibson, D.W.**
1993: Triassic; *in* Chapter 4 of Sedimentary Cover of the Craton in Canada; (ed.) D.F. Stott and J.D. Aitken; Geological Survey of Canada, Geology of Canada No. 5, p.294–320 (*also* Geological Society of America, The Geology of North America, v. D-1, p. 294–320).

**Henderson, C.M., Bamber, E.W., Richards, B.C., Higgins, A.C., and McGugan, A.**
1993: Permian; *in* Chapter 4 of Sedimentary Cover of the Craton in Canada; (ed.) D.F. Stott and J.D. Aitken; Geological Survey of Canada, Geology of Canada No. 5, p. 272–293. (*also* Geological Society of America, The Geology of North America, v. D-1, p. 272–293).

**Johns, M.J., Barnes, C.R., and Orchard, M.J.**
1999: Progress on Triassic ichthyolith biostratigraphy and regional thermal-maturation studies, Trutch and Halfway map areas, northeastern British Columbia; *in* Current Research 1999-A; Geological Survey of Canada, p. 51–59.

**Khudoley, A.K.**
1999: Preliminary geology of Minaker Creek map area (94 G/11), British Columbia; Geological Survey of Canada, Open File 3735, scale 1:50 000.

**Lane, L. S.**
1999: Preliminary Geology of Redfern Lake east half map area (94 G/5E), British Columbia; Geological Survey of Canada, Open File 3734, scale 1:50 000.

**Legun, A.S.**
1999a: Geology of the Mount McCusker area west half, northeastern British Columbia (NTS 94 G/4W); British Columbia Ministry of Energy and Mines, Geological Survey Branch, Open File 99-13, scale 1:50 000.
1999b: Geology of the Mount McCusker area, northeastern British Columbia (94G/4W); *in* Geological Fieldwork 1998; British Columbia Ministry of Energy and Mines, Paper 1999-1, p. 115–125.

**MacIntyre, D.G., Okulitch, A.V., Taylor, G.C., Cullen, B., Massey, N., and Bellefontaine, K. (comp.)**
1998: Geology, Fort Nelson, British Columbia; Central Foreland Map NO-10-G, Geological Survey of Canada, Open File 3604, scale 1:500 000.

**Nelson, J.L., Gabites, J.E., and Paradis, S.**
1999a: New galena lead isotopic data from carbonate rocks in northeastern B.C. – implications for regional MVT fluid migration; *in* Geological Fieldwork 1998; British Columbia Ministry of Energy and Mines Paper 1999-1, p. 81–87.

**Nelson, J.L., Paradis, S., and Zantvoort, W.**
1999b: The Robb Lake carbonate-hosted lead-zinc deposit, northeastern British Columbia: a Cordilleran MVT deposit; *in* Geological Fieldwork 1998; British Columbia Ministry of Energy and Mines Paper 1999-1, p. 89–101.

**Nicholls, E.L., Brinkman, D.B., Wu, X-C.**
1998: A new Archosaur from the Upper Triassic Pardonet Formation of British Columbia; Canadian Journal of Earth Sciences, v. 35, p. 1134–1142.

**Orchard, M. J.**
1999: Conodont faunas and Upper Triassic stratigraphy, Trutch map area, northeastern British Columbia; *in* Current Research 1999-A; Geological Survey of Canada, p. 45–50.

**Paradis, S., Nelson, J.L., and Zantvoort, W.**
1999: A new look at the Robb Lake carbonate-hosted lead-zinc deposit, northeastern British Columbia; *in* Current Research 1999-A; Geological Survey of Canada, p. 61–70.

**Richards, B.C., Bamber, E.W., Higgins, A.C., and Utting, J.**
1993: Carboniferous; *in* Chapter 4 of Sedimentary Cover of the Craton in Canada; (ed.) D.F. Stott and J.D. Aitken; Geological Survey of Canada, Geology of Canada No. 5, p. 202–271. (*also* Geological Society of America, The Geology of North America, v. D-1, p. 202–271).

**Stockmal, G.S.**
1999: Preliminary geology of Richards Creek east half map area (94 G/12E), British California; Geological Survey of Canada, Open File 3733, scale 1:50 000.

**Taylor, G.C.**
1979: Trutch and Ware (east half) map areas; Geological Survey of Canada, Open File 606, scale 1:125 000.

**Taylor, G.C., and Stott, D.F.**
1998: Geology, Toad River, Peace River District, British Columbia; Geological Survey of Canada Open File 3598, scale 1:250 000.

**Thompson, R.I.**
1989: Stratigraphy, tectonic evolution and structural analysis of the Halfway River map area (94 B), northern Rocky Mountains, British Columbia; Geological Survey of Canada Memoir 425, 119 p.

---

Geological Survey of Canada Project 850032

# Mineralogy of amygdaloidal, mafic flow rocks of the Endako Group in the Kenney Dam area, northeastern Nechako River map area, central British Columbia[1]

E.M. Barnes[2] and R.G. Anderson
GSC Pacific, Vancouver

*Barnes, E.M. and Anderson, R.G., 1999: Mineralogy of amygdaloidal, mafic flow rocks of the Endako Group in the Kenney Dam area, northeastern Nechako River map area, central British Columbia;* in *Current Research 1999-E; Geological Survey of Canada, p. 9–20.*

**Abstract:** Eleven samples of Endako Group amygdaloidal, olivine basalt and basaltic-andesite flows represent fresh and altered basal, medial, and upper parts of an approximately 150 m thick sequence at Kenney Dam (NTS 93 F/10 SW). Petrographic, X-ray diffraction, and scanning electron-microscopic studies determined primary, secondary, and amygdaloidal minerals. Olivine, clinopyroxene (augite), orthopyroxene, andesine, magnetite, and ilmenite phenocrysts in an opaque or feldspar-microlite-rich groundmass characterize the flow rocks.

Limonite, goethite, hematite, siderite, chalcedony, opal, and calcite, in approximate order of crystallization, occur as vesicle fillings and/or are common alteration products of the groundmass and clinopyroxene. Calcite, siderite, and iron hydroxides have several crystal habits, textures, and layering, suggesting multistage crystal growth. The abundance of later carbonate mineralization likely derived from alteration of local limestone units.

Modelling of the secondary-mineral parageneses suggests they likely precipitated within a wide range of intermediate pH and low temperatures.

**Résumé :** Onze échantillons de coulées de basalte à olivine et d'andésite basaltique amygdoïdes du Groupe d'Endako représentent les parties basale, médiane et supérieure fraîches et altérées d'une séquence d'environ 150 m d'épaisseur au barrage Kenney (SNRC 93 F/10 SW). Des études pétrographiques, diffractométriques et de microscopie électronique à balayage ont permis de déterminer les minéraux primaires, secondaires et des amygdales. Les roches des coulées sont caractérisées par des phénocristaux d'olivine, de clinopyroxène (augite), d'orthopyroxène, d'andésine, de magnétite et d'ilménite dans une matrice opaque ou riche en microlite et feldspath.

La limonite, la gœthite, l'hématite, la sidérite, la calcédoine, l'opale et la calcite, en ordre approximatif de cristallisation, remplissent les vésicules ou sont des produits communs d'altération de la matrice et du clinopyroxène. La calcite, la sidérite et les hydroxydes de fer ont plusieurs formes cristallines et textures et se présentent en couches, ce qui laisse supposer qu'il y a eu une croissance en plusieurs étapes. L'abondance de minéraux carbonatés tardifs serait attribuable à l'altération d'unités de calcaire locales.

Une simulation de la paragénèse des minéraux secondaires permet de penser que ces minéraux ont probablement précipité à l'intérieur d'une vaste gamme de pH intermédiaires et de basses températures.

[1] Contribution to the Nechako NATMAP Project.
[2] Division of Earth Sciences, University of Glasgow, Lilybank Terrace, Glasgow, Scotland G12 8QQ

## INTRODUCTION

Sequences of Tertiary basaltic rocks in the Fort Fraser (NTS 93 K) and Nechako River (NTS 93 F) areas are widespread (e.g. Armstrong, 1941, 1949; Tipper, 1963; Kimura et al., 1980; Bellefontaine et al., 1995; Struik et al., 1997; Williams, 1997) (Fig. 1). One of these sequences, the Eocene Endako Group mafic rocks, is widely exposed in the south-central part of the Fort Fraser and the north-central part of the Nechako River map areas. The rocks display a variety of volcanological features and textures. The distinction of the mafic volcanic rocks of the Endako Group from those in the underlying Eocene Ootsa Lake Group (e.g. Anderson et al., 1999; Grainger and Anderson, 1999) and overlying Neogene mafic flows (formerly called the Chilcotin Group; e.g. Resnick et al., 1999; Fig. 1) is difficult, partly due to incomplete mineralogical descriptions of the rocks in the reference areas for the Endako Group.

Haskin et al. (1998) and Anderson et al. (1998a, b) described four well exposed stratigraphic sections of Endako Group rocks, established their regional setting, and summarized their geochemical characteristics. The sections near the Nautley River (*see* Struik et al., 1997), northeast of Bungalow Lake, and at Mount Greer span the contact between the Endako Group and the underlying Ootsa Lake Group. The study area, near Kenney Dam northwest of Knewstubb Lake, includes the thickest and most continuous sequence of Endako Group volcanic rocks preserved in the Nechako River area. The unit includes basaltic andesite and lesser basalt flows, with minor associated hyaloclastite and tuffaceous sedimentary rocks; the flow rocks are aphyric to plagioclase- and pyroxene-phyric, and rarely olivine-phyric, and are commonly amygdaloidal.

The regional setting (Anderson et al., 1998a), lithology, stratigraphy, and physical volcanology of the Endako Group rocks at the Kenney Dam locality described by Haskin et al. (1998) are supplemented in this study by petrographic, X-ray diffraction, and scanning electron-microscope (energy-dispersive) methods used to characterize samples, collected in early July 1998, from the base, middle, and upper parts of the well exposed sequence. The work is part of a baccalaureate study (Barnes, 1999) and represents the first detailed petrographic description of the Endako Group.

## GEOLOGY

The study area is readily accessible via maintained and disused gravel roads, including the Holy Cross, 500, and Kenney Dam forestry roads in the southwestern part of the Big Bend map area (NTS 93 F/10; Fig. 1). A disused gravel road leads west and south from the Kenney Dam Road to the basal part of the sequence northeast of, and at the foot of, Kenney Dam.

At the Kenney Dam site (Haskin et al., 1998), the comparatively thick sequence of mafic flows is believed to mark the Nechako graben, part of a series of synvolcanic extensional Eocene structures (Anderson et al., 1998a, b). At this locality, the sequence comprises approximately 150 m of mafic-intermediate volcanic flows and minor hyaloclastite and clastic sedimentary rocks (base of section at UTM E370875, N5938430, zone 10; site A, Fig. 1). The base of the Endako Group at Kenney Dam is not exposed.

The section (Fig. 2a, b) consists of consecutively stacked 3–5 m thick flows in which a finely crystalline texture imparts a sparkly appearance. The rocks have an orange oxidized rind on weathered surfaces. Microphenocrysts consist of subhedral, elongate plagioclase, up to 3 mm long, and minor pyroxene. The flows are subhorizontal, dipping gently (<20°) to the northwest. The flow tops are commonly brecciated.

Clinopyroxene- and plagioclase-phyric basaltic andesite and lesser basalt are variably vesicular ranging from at least 5% vesicles in the massive blocky interior of a flow, to 50% vesicles in the upper and lower portions (Haskin et al., 1998; and this study, Table 1a). The flow bases are thin (10–30 cm) and only sparsely vesicular. Vesicles are generally round, 0.5–6 cm in diameter, and evenly distributed throughout. The transition from flow interior to top is marked by a gradual increase in vesicle abundance and size range. The larger vesicles are flattened parallel to the flow contacts (Fig. 3a). Flow tops are 0.5–1 m thick and their porosity provided excellent sites for deposition of secondary minerals.

## ANALYTICAL METHODS

Representative samples of units were collected for petrographic and mineralogical studies. Magnetic susceptibility (m.s.) measurements were routinely obtained at most outcrops over a 5 min period using a hand-held Exploranium KT-9 Kappameter. These data are an average of at least 5 measurements, reported in $10^{-3}$ SI units (Table 1a), and are typical of the magnetic susceptibility range for Endako Group rocks regionally.

Samples for analysis were selected to represent the regionally occurring secondary minerals typical of this unit. Five sites (sites 0101, 0102, 0103, 0104, and 0105) included horizons similar to, but not identical to, those established by Haskin et al. (1998) for their subsequent geochemical studies (e.g. Anderson et al., 1998b). At each site, at least two samples were taken from the same flow. They included one fresh sample, usually from the more massive central flow area, and one or more altered samples from the vesicular and/or amygdaloidal, upper or lower parts of the flow; the number and sampling location was dependent on the nature and abundance of the secondary minerals. The sites span an almost continuous cliff representing relief of at least 150 m.

Sites 0101 (in the lowest accessible flow) and 0102 were taken from the lower 80 m of the cliff which lies north of Kenney Dam at the base of the dam wall (Fig. 2a). Sites 0103, 0104, and 0105 (in the highest flow) were taken from the upper 70 m of the sequence, exposed in a disused forestry road, aggregate quarry, and log-loading site, 200 m south of the dam (Fig. 2b). No distinctive amygdaloidal or secondary minerals were observed at site 0105, and it will not be considered further. Four fresh rock samples and seven secondary-mineral samples were studied in detail. Iron and carbonate

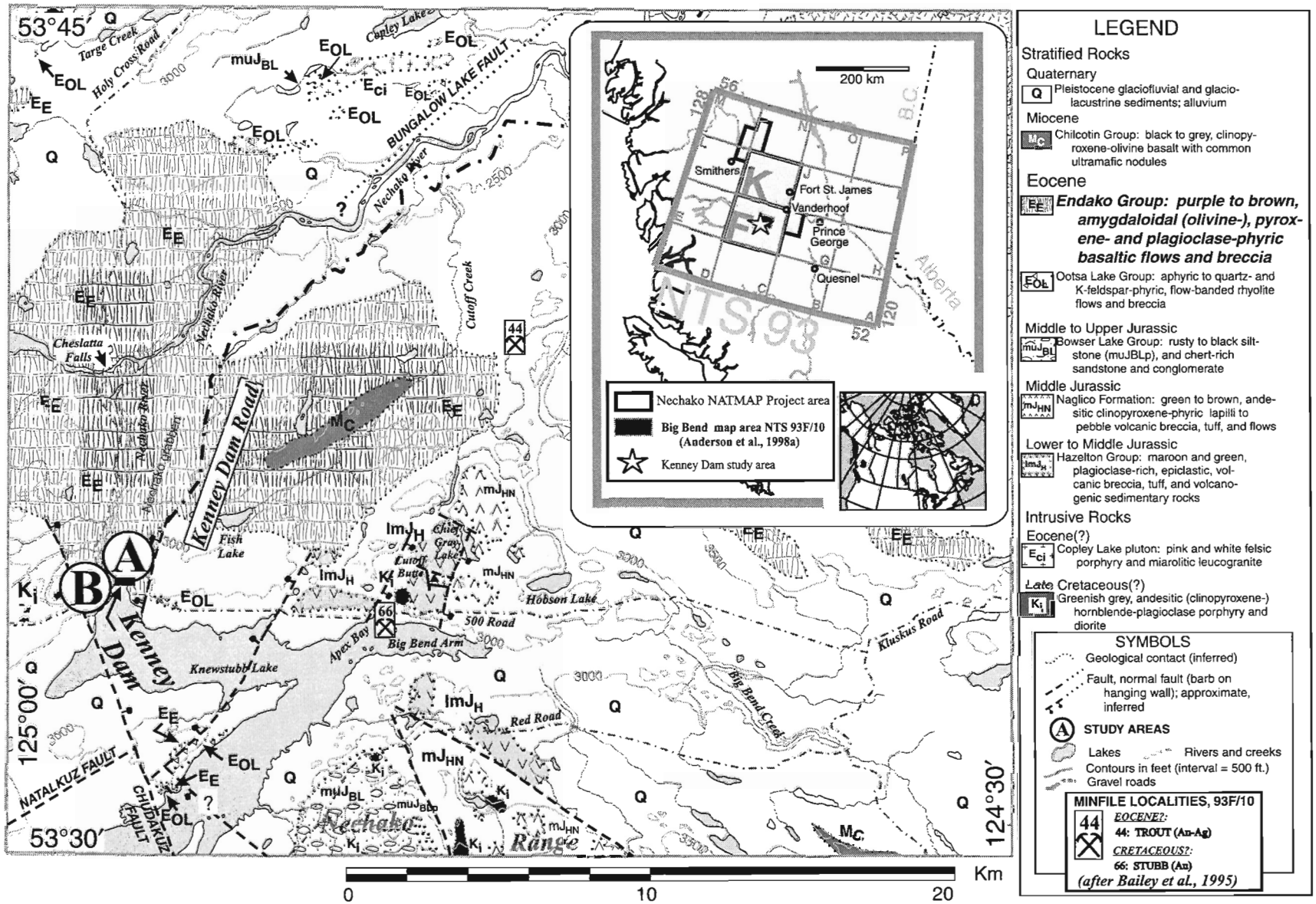


***Figure 1.*** *Geological map of Big Bend area (after Anderson et al., 1998a) and location of sampling areas A (UTM E370875, N5938430, zone 10) and B (UTM E370746, N5937806, zone 10); inset map shows study area location within Nechako NATMAP Project area.*

**Table 1a.** Mineralogy of basaltic-andesite flow rocks.

| Sample | UTM; zone 10 | Fresh colour | Weathered colour | Magnetic susceptibility | Vesicle content | Amydule character and colour (Munsell Rock Colour) | Lustre | Pyroxene | Plagioclase | Fe-Ti Oxides | Groundmass |
|---|---|---|---|---|---|---|---|---|---|---|---|
| 0101E | E370875, N5938430; base of section, site A, Figure 1 | dark grey | dark red brown | 28.2 | 5% (centre)–50% (flow top); spherical to flattened; 0.5–5 cm diameter | resinous; black to olive grey (5 Y 3/2) to light olive grey (5 Y 5/2); common coarse-grained calcite | fine-grained matte material | clinopyroxene: 30%; euhed.–subhed.; ophitic; 2 mm; nearly completely replaced by limonite | andesine; unaligned; <50%; 1 mm; euhed.–subhed. | 5–10%; euhed.–subhed.; approx. 0.5 mm | opaque; rare plagioclase microlites and dendritic ilmenite |
| 0102G | E370875, N5938430; 20 m above site 0101, site A, Figure 1 | dark grey | dark red brown | 11.1 | 20–30%; spherical to slightly elongate; 2–6 cm diameter | dusky yellow (5 Y 6/4) | fine-grained minerals overlying thin, paler, concentric layers | clinopyroxene: 15%; 0.5–1.5 mm; completely replaced by calcite, opal and chalcedony and iron hydroxides | andesine; unaligned; 30–50%; 1 mm; euhed.–subhed. | rare accumulations of opaque spherules; 0.1 mm; entrained at base of iron hydroxide vesicle lining | opaque |
| 0103 | E370746, N5937806; base of east cliff in quarry, site B, Figure 1 | dark grey | dark grey brown | 12.2 | <10%; spherical; 0.5–6 cm diameter | moderate brown (5 YR 3/4) 0.5 cm thick, earthy rim on vesicle overlain by 0.2 cm thick very pale orange (10 YR 8/2) and dark reddish brown (10 R 3/4) fine crystalline material with iridescent sheen | | clinopyroxene: <10%; subhed.; ophitic; commonly replaced by limonite | andesine; 60–75%; slightly altered | subhedral; 5% | common plagioclase microlites |
| 0103E | E370746, N5937806; base of east cliff in quarry, site B, Figure 1 | dark grey | dark grey brown | 12.2 | <10%; spherical; 0.5–6 cm diameter | dark reddish brown (10 R 3/4) lath-shaped crystals with iridescent sheen | | clinopyroxene: <10%; subhed.; ophitic; commonly replaced by limonite | andesine; 60–75%; slightly altered | subhedral; 5% | common plagioclase microlites |
| 0103F | E370746, N5937806; base of east cliff in quarry, site B, Figure 1 | dark grey | dark grey brown | 12.2 | <10%; spherical; 0.5–6 cm diameter | moderate brown (5 YR 3/4 to 5 YR 4/4) fine crystalline lining; common, spaced, greyish orange (10 YR 7/4) spheres, 5 mm diameter, attached to vesicle lining | | clinopyroxene: 10–15%; subhed.–euhed.; ophitic; fresh | andesine; unaligned; 60%; 1 mm in size | commonly euhedral distal to vesicle margin; increase in abundance and decrease in crystallinity towards it; proximal to vesicle, oxides altered to prismatic, aligned rutile | intersertal plagioclase microlites and dendritic ilmenite |
| 0104D | E370746, N5937806; 25 m above site 0103 | dark grey | dark reddish brown | — | 20–30%; spherical; 0.5–5 cm diameter | 0.5 mm thick layer of very fine-grained, light bluish-grey, matte material; similar in texture and thickness to sample 0102G; mineralized biogenic(?) tubules <1 mm diameter and 0.5 cm long | | augite(?) and rare orthopyroxene; ophitic variety, approx. 5%; euhed. grains 10-15%; very altered; locally completely replaced by microcrystalline iron hydroxide | andesine; unaligned; 50–60%; 1 mm in size; euhed. to subhed.; slightly altered | common acicular and dendritic ilmenite | plagioclase microlites |
| 0104G | E370746, N5937806; 25 m above site 0103 | dark grey | middle brown | — | 25–30%; spherical; 0.5–3 cm diameter | moderate brown (5 YR 3/4 to 5 YR 4/4) fine crystalline lining; common, spaced, greyish orange (10 YR 7/4) discs, 2 cm in diameter and 0.5 cm deep, attached to vesicle lining | | augite and rare orthopyroxene; ophitic, 20–25%; 0.5–2 mm; euhed. to anhed. locally replaced by microcrystalline limonite | andesine; unaligned; 50–60%; approx. 1–2 mm in size; euhed. to subhed.; unaltered | approx. 5%; approx. 0.3 mm; euhed. to suhed. | intersertal devitrified glass, approx. 10–15%; plagioclase microlites, <1 mm in size |

**Table 1b.** Mineralogy of secondary minerals.

| Sample | Limonite | Goethite | Calcite | Chalcedony | Hematite | Siderite | Opal |
|---|---|---|---|---|---|---|---|
| 0101E | replaced clinopyroxene; microcrystalline, contains singular to bifurcating 'shatter cracks'; formed geopetal structure within vesicle; rare reversed zoning | vesicle and geopetal structure lining; as microfibrous fringe and as ptygmatic bands in limonite layer | overgrowth on iron hydroxide layer; as aligned to sub-aligned irregular fibres and as fibres grown through iron hydroxide radial spherules | | | | |
| 0102G | replaced clinopyroxene; as rare geopetal structures within vesicle | vesicle and geopetal structure lining; as microfibrous fringe and as radial microfibrous spherules in calcitic overgrowth of iron hydroxide layer | rare spherules (1 mm across); or rare amydule (0.5–1 cm across) | as a) two distinct, consecutively-precipitated uniform layers over calcite and iron hydroxides; and, b) spherules lining the vesicle | | | |
| 0103 | | | coarse-grained; enclosed common siderite rhombs | | as thin, red-brown, microcrystalline layer | 0.5 cm thick layer of unaligned, zoned rhombs overlies and alternates with iron hydroxide layer | subspherical growth patterns and faint growth banding; partly recrystallized(?) to quartz |
| 0103E | as geopetal structure with shatter cracks | | | | | layer of zoned rhombs overlies iron hydroxide layer; rhombs aligned approximately perpendicular to limonite geopetal structure | |
| 0103F | | | as a) anhedral variety which filled microfractures and replaced clino-pyroxene; b) granular variety which overlies hematite layer; and c) common late spherical growths 1 cm in diameter and characterized by growth zoning | rare, finely crystalline spherules attached to rhombic siderite; ragged base or altered outer rim | lined vesicles as irregular layer with minor entrained, anhedral Fe-Ti oxides | rhombic siderite grades away from calcite layer; growth zones outlined by iron-rich zones | |
| 0104D | microcrystalline limonite replaced pyroxene; also as clustered spheres which form an irregular layer overlying the hematite | | granular variety overlies iron hydroxide layer | | as reddish brown, microcrystalline vesicle lining | rhombic siderite (rare) overlies iron hydroxide layer | very thin final layer of vesicle lining |
| 0104G | | | as a) as fringe lining vesicles, characterized by at least 2 growth zones outlined by iron-rich zones; b) common late disc-like growths characterized by growth zoning distal from rock surface and outlined by entrained minor Fe-Ti oxides | | | rhombic siderite (rare) overlies calcite layer | |

secondary-mineral phases were mainly studied in this project (Fig. 3). Common opal and chalcedony were not sampled due to their straightforward identification.

Standard petrographical techniques were used to identify minerals, alteration, and textures in covered thin sections of the rock-vesicle contact prepared from each of the seven altered samples. The compositions of plagioclase phenocrysts were estimated by the Michel Levy method (Kerr, 1959). The Munsell Rock-Color Chart was used to designate the colours of the secondary minerals as seen in hand sample (Table 1b).

X-ray powder-diffraction (XRD) methods were used to study samples of fresh rock from each site, as well as specific secondary-mineral material (as highlighted in petrographic observations) or entire vesicle linings or amygdules of each mineralized sample. Each sample, comprising hand-picked grains, was ground to a paste with acetone to provide 'smear mounts' for analysis.

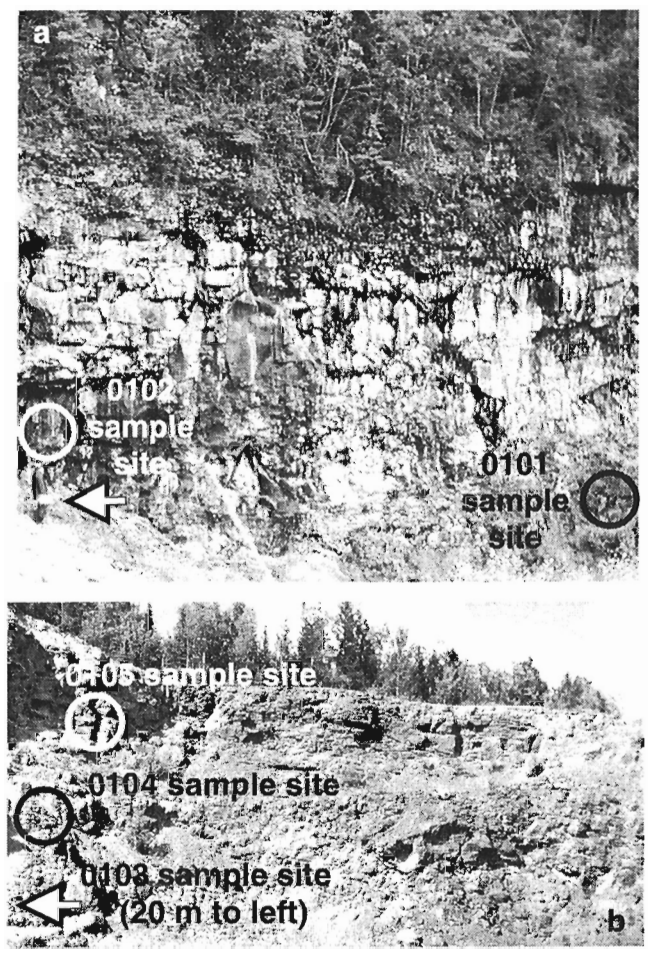


***Figure 2.*** *Location of samples:* ***a****) Lower part of Endako Group sequence north of, and at the base of, Kenney Dam; figure (see arrow) is 1.8 m tall. Samples 0101 and 0102 locations shown;* ***b****) Upper part of Endako Group sequence, south of Kenney Dam; cliff is ca. 70 m tall. Locations of samples 0103, 0104, and 0105 shown. No distinctive amygdaloidal minerals were observed in sample 0105.*

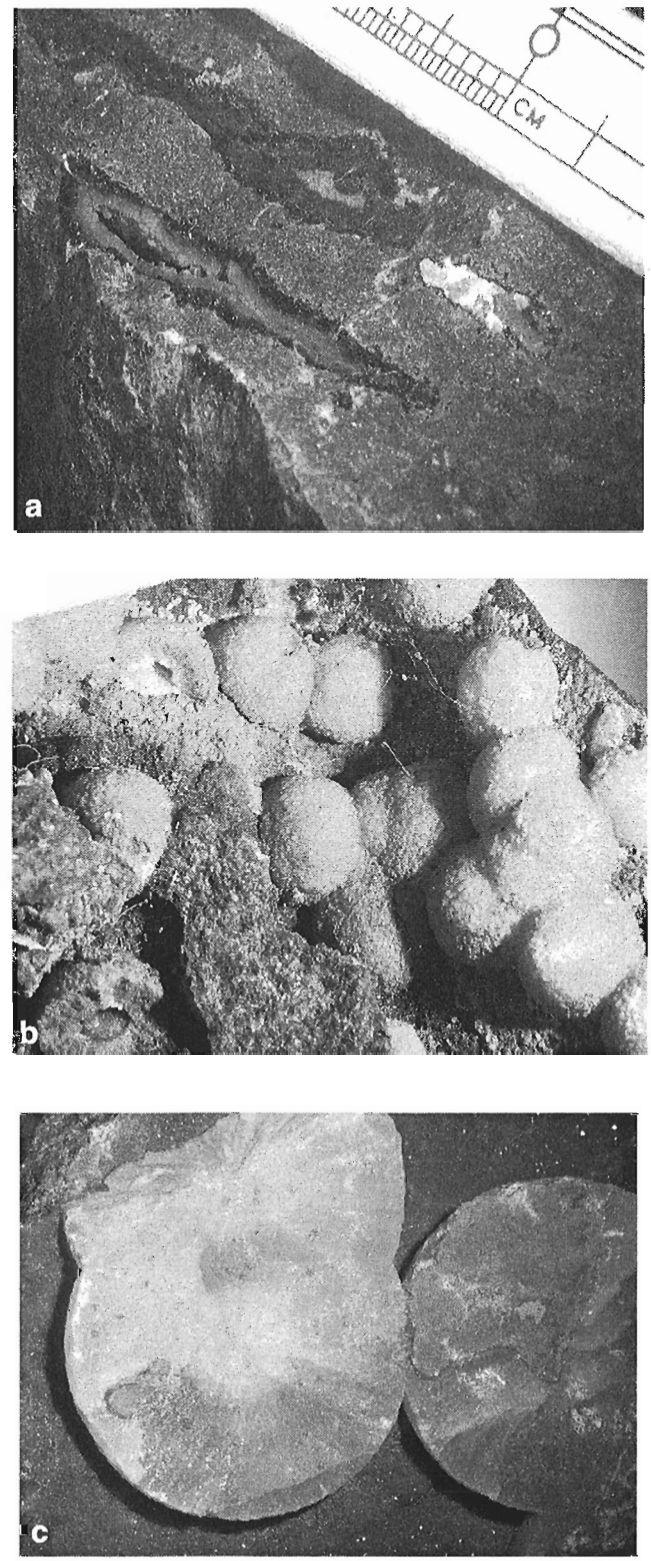


***Figure 3.*** *Typical mineral habits for amygdules in hand sample for samples:* ***a****) 0101E: flattened vesicle contains black iron hydroxides with shatter cracks and inner zone of chlorite(?);* ***b****) 0103F: calcite spherules (greyish orange, 5YR 4/4; field of view 5.5 cm wide); and,* ***c****) 0104G: zoned calcite disk-like amygdules (greyish orange, 10YR 7/4; disks 2 cm in diameter).*

A Philips X-ray diffractometer with vertical goniometer and computer-controlled step scanner fitted with a standard Co tube was used, and °2θ was measured between 4 and 60 in 1 °2θ steps, at a scanning speed of 2°2θ/min. The data were compared with the Traces V4.0 database and the Division of Earth Sciences, University of Glasgow reference collection.

A Leica Electron Optical S360 Stereoscan scanning electron microscope (SEM), utilizing an electron beam accelerated at 20 kV, was used to image and provide a semiquantitative analyses of primary minerals from a polished thin section of sample 0102G to characterize the mineral compositions.

Geochemical modelling was undertaken via The Geochemist's Workbench™ v3.0 (Bethke, 1996), a computer package that enables the modelling of aqueous geochemical reactions through the use of computational equilibrium thermodynamics using the'thermo.dat 1994' data set. The REACT program was used to test the reaction of fluid with minerals in an attempt to determine under what conditions the secondary minerals may have been produced. The graphing program GTPLOT was used to illustrate the reaction.

## PRIMARY MINERALS OF THE HOST VOLCANIC FLOW ROCKS

The four fresh samples representative of the host volcanic-flow rocks contain variable amounts of augite and andesine, lesser magnetite and ilmenite, and rare olivine and orthopyroxene phenocrysts set in an opaque or feldspar-microlite-rich groundmass (cf. Table 1a; Fig. 4–7).

Pyroxene is subhedral to euhedral, <10 to 30% in abundance, 0.5–2 mm in size, and commonly shows an ophitic texture. Andesine is euhedral to subhedral, makes up 30–75% of the rock, is commonly 1 mm, but up to 2 mm in length, and not aligned. Common albite and less common Carlsbad twinning are typical, and oscillatory twinning is restricted to larger plagioclase phenocrysts. Magnetite and ilmenite constitute 5–10% of the rock, are euhedral to subhedral, or rarely occur as spherules entrained within an iron hydroxide vesicle lining, as in sample 0104D. Ilmenite occurs rarely in a dendritic form.

Confirmation of the presence of olivine was only available from SEM imaging and semiquantitative analysis of polished slabs of sample 0102G.

A variable degree of alteration of the pyroxene is characteristic. Complete replacement of pyroxene by microcrystalline iron hydroxide or by calcite with minor silica-rich layers is common, with iron hydroxide commonly appearing as the first secondary mineral to be precipitated. Fresh pyroxene, however, is common, even at the rock/vesicle interface.

Intersertal glass (with dendritic ilmenite and plagioclase microlites constituting the rarely identifiable portion of the groundmass) is commonly altered, turning the plagioclase microlites green. With more extensive alteration, the groundmass is opaque (e.g. Fig. 4a, 5a). Rare alignment of elongate acicular to prismatic rutile, spatially associated with andesine(?) and the alteration product of the Fe-Ti oxides, occurs proximal to the vesicle margin (Fig. 6c).

Plagioclase commonly appears fresh throughout, with only minor alteration.

## SECONDARY MINERALS

Analysis of the secondary minerals with X-ray powder diffraction, identifies chlorite, iron hydroxide, calcite, and siderite, which corroborated petrographic observations (Table 1b; Fig. 4–7). The identities of clay minerals, found in the XRD analyses of the samples with the most extensive pyroxene alteration, were not further investigated. The abundance of clay increased with the intensity of pyroxene alteration in the samples (e.g. samples 0101E and 0102G).

Petrographic analyses helped identify the nature, textures, and parageneses of secondary minerals, in approximate order of crystallization in vesicles: limonite, goethite, hematite, siderite, chalcedony, opal, and calcite (cf. Table 1b; Fig. 4–7).

Goethite and hematite do occur together, but goethite is more common in the two basal sites and hematite in the upper two sample sites. Limonite is ubiquitous throughout, microcrystalline, straw brown to dark brown in plane-polarized light, and exhibits strong absorption and isotropic character under cross polars. It exhibits a 'scaly' texture and 'shatter cracks'. Goethite resembles limonite in crystallinity and colour, but commonly crystallizes as radially acicular grains with extinction parallel to the elongate crystal axis. A subradial crystal habit occurs in microfibrous fringes on, and ptygmatic bands found within, limonite. Hematite is vibrant red brown and microcrystalline.

A geopetal structure is believed to be indicated by the asymmetrical, but consistent, distribution of the iron hydroxides and other secondary minerals within the vesicles. The structure is commonly characterized by a localized crystallization of goethite or limonite as the earliest mineral species in contact with the host rock along the vesicle wall. This texture is accompanied by a proximal increase in the abundance of other secondary minerals in comparison to the remainder of the vesicle (Fig. 4, 6).

Siderite is absent from the two basal samples, but is abundant in all 0103 site samples and both 0104 site samples. It commonly occurs with iron-rich zones distinguishing growth bands, forms layers which overlie iron hydroxide and calcite, and also appears as distinct rhombs entrained within coarse, calcite-rich areas (*see* Fig. 6, 7). Where precipitated as a layer, siderite crystals commonly display chevron growth patterns (Fig. 7a).

Chalcedony appears in samples 0102G and 0103F, and as a replacement for opal in sample 0103. Opal is also found in sample 0104D. However, as samples showing obviously silica-rich precipitates were not studied in detail, no correlation with stratigraphic height is implied. Chalcedony occurs in finely crystalline radial spherules (e.g. Fig. 5) and layers,

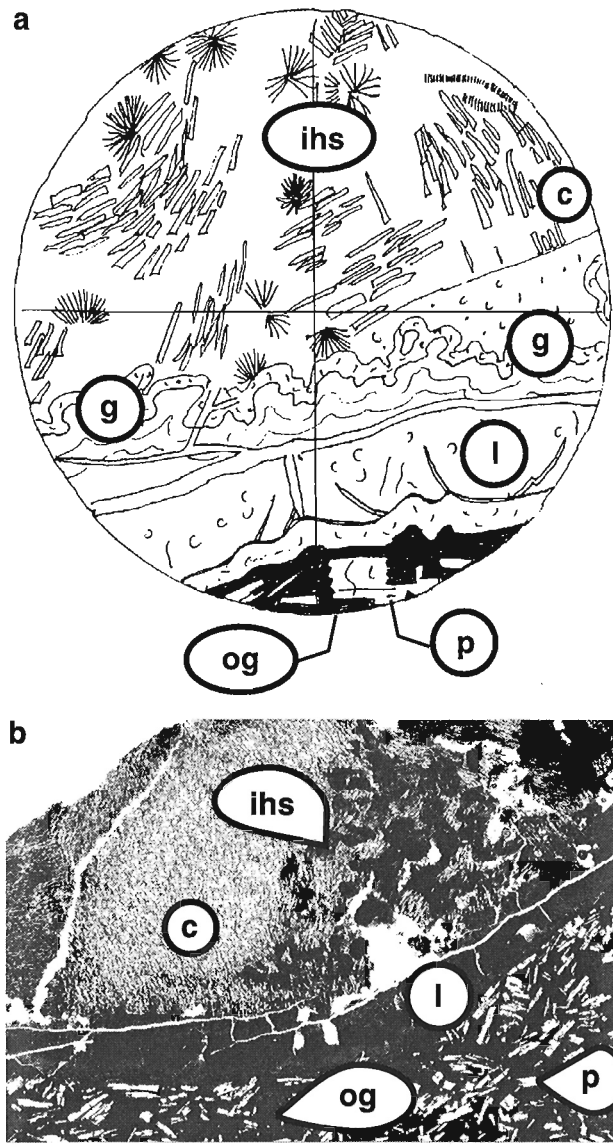


***Figure 4.*** *a) Camera lucida sketch, and* ***b****) photomicrograph (plane-polarized light) of distinctive petrographic textures for sample 0101E. Note limonite geopetal structure characterized by shatter cracks as initial vesicle filling and later iron hydroxide spherules overgrown by calcite crystal. Magnification in sketch is 10x; width of photomicrograph image is 5.6 mm.*

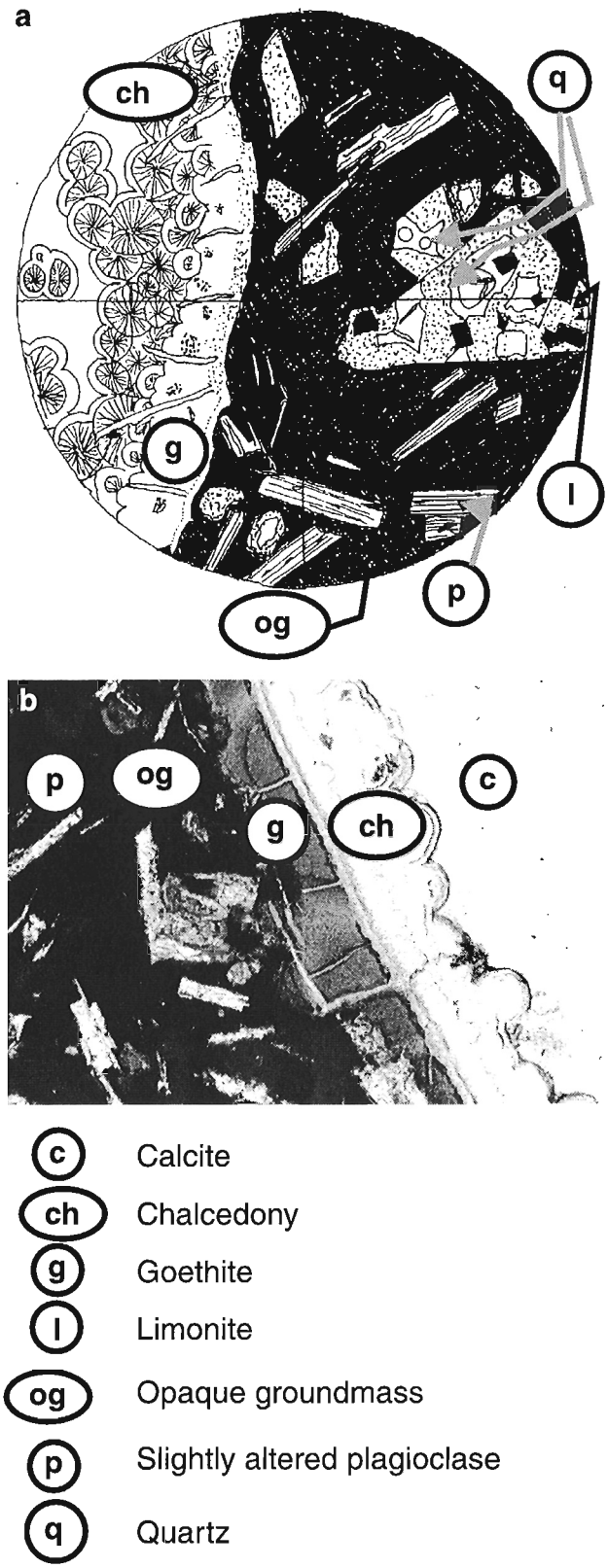


***Figure 5.*** *a) Camera lucida sketch, and* ***b****) photomicrographs (plane-polarized light) of distinctive petrographic textures for sample 0102G. Note goethite and geopetal structures characterized by shatter cracks as initial vesicle fillings. Iron hydroxides are overgrown by chalcedony and calcite. Magnification in sketch is 10x; width of photomicrograph images is 1.4 mm.*

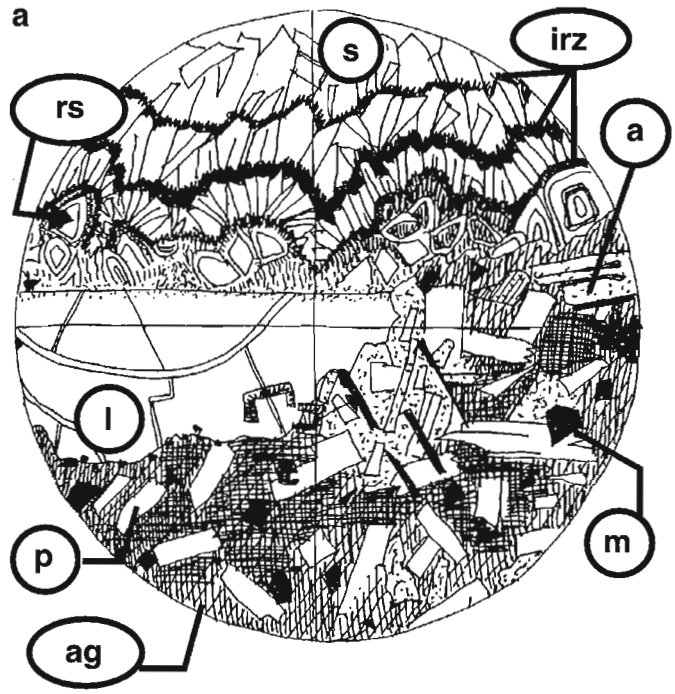


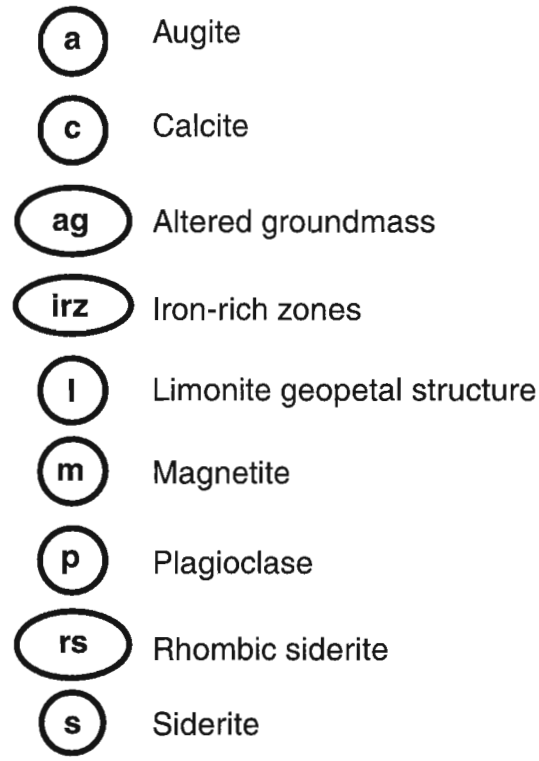


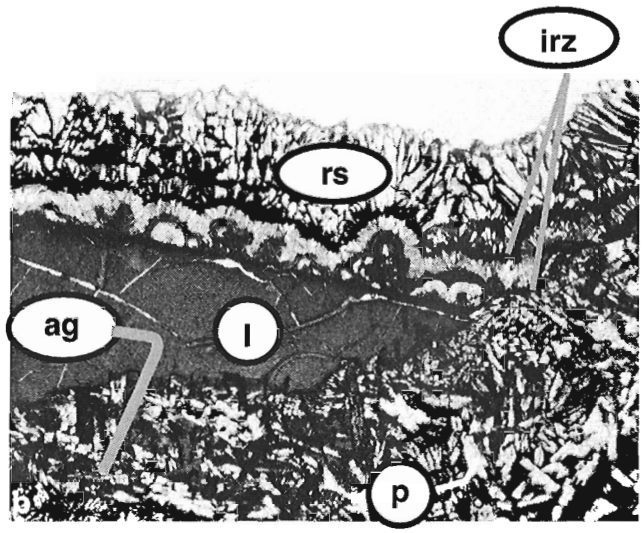


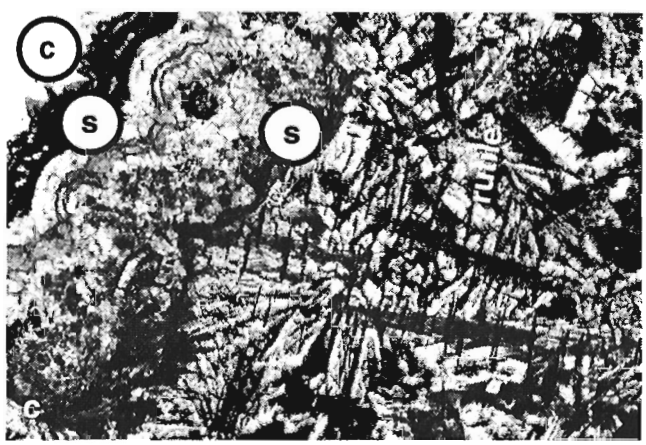


***Figure 6.***

***a)*** *Camera lucida sketch, and* ***b)****,* ***c)*** *photomicrographs (plane-polarized light) of distinctive petrographic textures for sample 0103E (a, b) and 0103F (c). Note sequential vesicle filling by limonite geopetal structure, rhombic siderite, several periods of alternation of siderite and iron-rich zones, and late siderite growth in a) and b). Magnification in sketch is 10x; width of photomicrograph image b) is 5.6 mm. Photomicrograph of sample 0103F (c) shows alignment of rutile in volcanic flow host subparallel to vesicle margin coated sequentially by calcite and siderite (width of photomicrograph image c) is 1.4 mm).*

and in mosaic textures as a replacement for opal. Colourless opal appears as a colloform layer with a rare, fine banding indicating periodic growth.

Extensive calcite precipitation occurs in a wide variety of crystal habits and is commonly the last secondary mineral precipitated. Crystal textures include coarse, granular calcite occurring as a vesicle lining; as the replacement mineral for pyroxene; as microfracture filling; or as vesicle filling exhibiting the fibrous textures in sample 0101E (Fig. 3a), the spherical growths of sample 0103F (Fig. 3b), and the discs of 0104G (Fig. 3c).

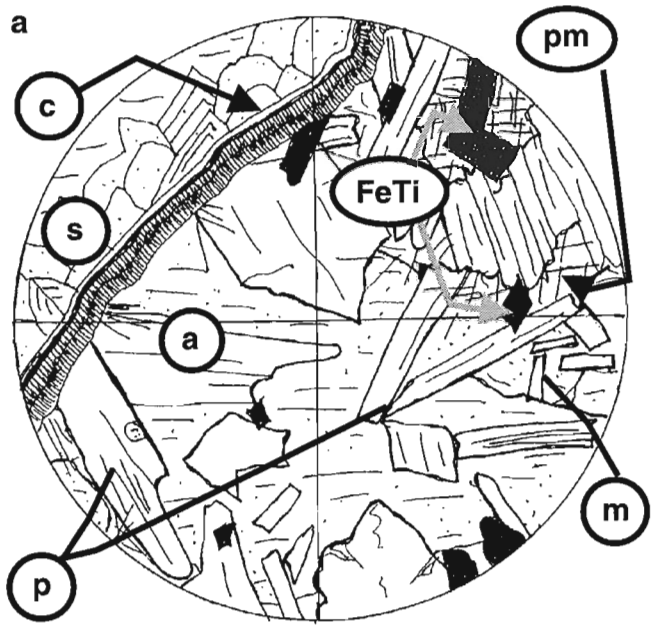


a Unaltered augite
c Calcite
FeTi Fe-Ti oxide
l Limonite
m Magnetite
o Opal
og Opaque groundmass
p Plagioclase
pm (Locally altered) plagioclase microlites
s Siderite

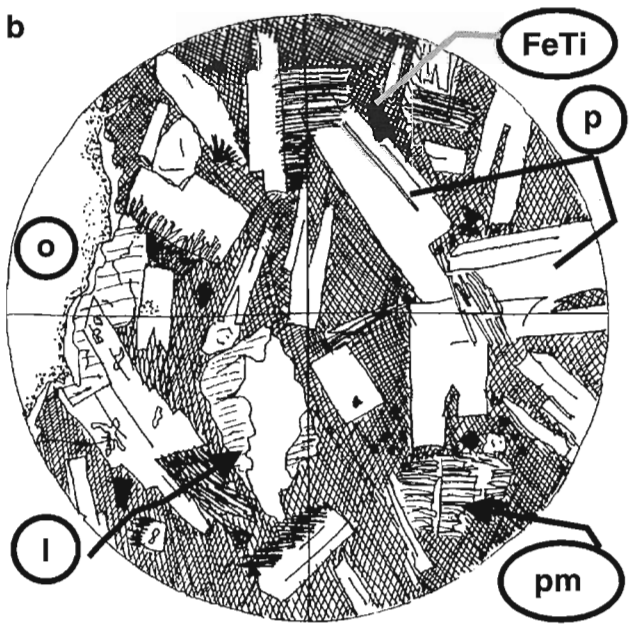


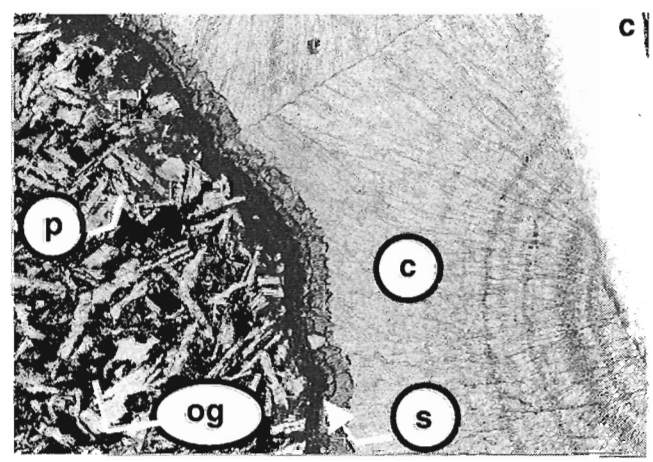


***Figure 7. a), b)*** *Camera lucida sketches, and* ***c)*** *photomicrograph (plane-polarized light) of distinctive petrographic textures for sample 0104D (a) and 0104G (b, c). Opal is the sole vesicle filling for sample 0104D. Magnification in sketches is 10x; width of photomicrograph image is 1.4 mm.*

The calcite discs are unusual. In hand sample, the top surface is smooth, slightly concave and commonly pocked; in thin section they are characterized by entrainment of Fe-Ti oxides (?) and slight variations in crystal habit, which indicate a growth pattern originating distal from the rock surface (*see* Fig. 7c).

The late-stage carbonate mineral precipitation may reflect interaction of meteoric water with scattered limestone units to the southeast of the Kenney Dam site (Tipper, 1963) now submerged beneath the Nechako reservoir (Knewstubb Lake).

## TOWARDS A MODEL FOR PRECIPITATION OF SECONDARY MINERALS IN THE ENDAKO GROUP FLOWS

From thin-section observation, augite $(Ca, Mg, Fe2+, Ti, Al)_2 [Si_2O_6]$, is commonly replaced by limonite, $FeO(OH)\cdot nH_2O$, and goethite, FeO(OH), in the presence of opal, $SiO_2\cdot nH_2O$, and/or chalcedony, $SiO_2$.

This reaction provided the basis for a conceptual model to be tested on Geochemist's Workbench™ v3.0 (GWB; Bethke, 1996):

$$(Ca, Mg, Fe^{2+}, Ti, Al)_2 [Si_2O_6] + H_2O = FeO(OH) + SiO_2 + \text{Ca-nontronite}.$$

The initial system is then defined in terms of mass and chemical composition of the fluid, amounts of minerals present, gas fugacities, temperature, and Eh and pH.

Fresh water is the most probable fluid to have been in contact with the rock, given that the area was inland during the Tertiary. Therefore, salinity was assumed to be low, and the initial solute concentration was kept to a minimum in the modelling. A model 100 mg of iron-rich pyroxene end-member ferrosilite (representing augite which is not part of the GWB database) was reacted with 1 kg water at pH 7 at 25°C. The experiment was run to a temperature of 50°C. The gases, $O_2$ and $CO_2$, were given a normal atmospheric pressure at the start of the experiment. Hematite was suppressed from the products to allow goethite to be shown as a reaction product.

A very stable reaction producing goethite (also representative of the observed limonite and hematite), quartz (also representative of the observed opal and chalcedony), and Ca-nontronite (smectite), was modelled. In the simulations, the reaction was shown to be stable between the starting temperature and at least 50°C, and between pH 5 and 8. The reaction produced a nominal increase in acidity of 0.1 pH unit.

Secondary minerals found by petrography and X-ray powder diffraction were successfully modelled in this simplified system. Smectite has not been positively identified in this project, but fine-grained silicates were found to be present in the X-ray powder-diffraction data. The relative stability of the model reaction suggests that the secondary mineral assemblages and textures found in the Endako Group in the Kenney Dam area might have regional significance.

## CONCLUSION

Eleven samples of amygdaloidal olivine basalt and basaltic-andesite flow rocks represent basal, medial, and upper parts of an approximately 150 m thick sequence of thin mafic flows of the Eocene Endako Group at Kenney Dam. A variety of techniques confirm the essential mafic and feldspar mineralogy of the flow rocks and provide a case study of the variety and range of parageneses of limonite, goethite, hematite, siderite, chalcedony, opal, and calcite mineral species that make up the amygdules which characterize the flow rocks of the Endako Group.

## ACKNOWLEDGMENTS

The senior author would like to express her sincere thanks to the GSC and especially NATMAP project leader Bert Struik; her participation was under the auspices of the GSC's Volunteer Program, with the approval of Brian Bell of the University of Glasgow, and supported by the financial assistance of the estate of the late Jo Wylie; their backing is deeply appreciated. A sincere thank you to Jonah Resnick for his excellent field assistance, and to Lori Snyder for sharing her field experience and unpublished petrographic descriptions.

Support of the Division of Earth Sciences (University of Glasgow) through the expertise of Robert McDonald (SEM technician), Bill Higgison (XRD technician), and John Gilleece (thin-section preparation), critical to the data acquisition, is gratefully acknowledged. The assistance, guidance and support of Dr. Allan Hall is greatly appreciated.

We appreciate the time spent by Glenn Woodsworth, whose constructive review of an earlier version of the manuscript hopefully led to a better final version. Bev Vanlier is thanked for her digital preparation of the pre-press version of the manuscript.

## REFERENCES

**Anderson, R.G., Snyder, L.D., Resnick, J., and Barnes, E.**
1998a: Geology of the Big Bend Creek map area, central British Columbia; *in* Current Research 1998-A; Geological Survey of Canada, p. 145–154.

**Anderson, R.G., Snyder, L.D., Resnick, J., Grainger, N., and Barnes, E.M.**
1999: Bedrock geology of the Knapp Lake map area, central British Columbia; *in* Current Research 1999-A; Geological Survey of Canada, p. 109–118.

**Anderson, R.G., Snyder, L.D., Wetherup, S., Struik, L.C., Villeneuve, M.E., and Haskin, M.**
1998b: Mesozoic to Tertiary volcanism and plutonism in southern Nechako NATMAP area: part 1: influence of Eocene tectonics and magmatism on the Mesozoic arc and orogenic collapse: new developments in the Nechako River map area; *in* New Geological Constraints on Mesozoic to Tertiary Metallogenesis and on Mineral Exploration in central British Columbia: Nechako NATMAP Project, (ed.) L.C. Struik and D.G. MacIntyre; Geological Association of Canada, Cordilleran Section, March 27, 1998, Short Course Notes, 26 p.

**Armstrong, J.E.**
1941: Fort Fraser, west half, Coast District, British Columbia; Geological Survey of Canada, Map 631A, scale 1:253 440.

**Armstrong, J.E.** (cont.)
1949: Fort St. James map-area, Cassiar and Coast Districts, British Columbia; Geological Survey of Canada, Memoir 252, 210 p.

**Bailey, D.G., Jakobsen, D.E., and Lane, R.**
1995: MINFILE 093F Nechako River mineral occurrence map; British Columbia Ministry of Energy, Mines and Petroleum Resources, MINFILE, scale 1:250 000 (revised March 1995).

**Barnes, E.M.**
1999: The Eocene Endako Group basalts, central British Columbia, alteration and secondary minerals; B.Sc. thesis, University of Glasgow, Glasgow, Scotland, 64 p.

**Bellefontaine, K.A., Legun, A., Massey, N., and Desjardins, P.**
1995: Digital Geological Compilation of Northeast B.C. — Southern Half (NTS 83 D, E, 93 F, G, H, I, J, K, N, O, P); British Columbia Ministry of Energy, Mines and Petroleum Resources, Open File 1995-24, scale 1:250 000.

**Bethke, C.M.**
1996: Geochemical reaction modeling, concepts and applications; Oxford University Press, New York, New York, 397 p.

**Grainger, N.C. and Anderson, R.G.**
1999: Geology of the Eocene Ootsa Lake Group in northern Nechako River and southern Fort Fraser map areas, central British Columbia; *in* Current Research 1999-A; Geological Survey of Canada, p. 139–148.

**Haskin, M.L., Snyder, L.D., and Anderson, R.G.**
1998: Tertiary Endako Group volcanic and sedimentary rocks at four sites in the Nechako River and Fort Fraser map areas, central British Columbia; *in* Current Research 1998-A; Geological Survey of Canada, p. 155–164.

**Kerr, P.F.**
1959: Optical mineralogy; McGraw–Hill, New York, New York, 442 p.

**Kimura, E.T., Bysouth, G.D., Cyr, J., Buckley, P., Peters, J., Boyce, R., and Nilsson, J.**
1980: Geology of parts of southeast Fort Fraser and northern Nechako River map areas, central British Columbia; Placer Dome Incorporated, Internal Report and Maps, Vancouver, British Columbia, scale 1:50 000.

**Resnick, J., Anderson, R.G., Russell, J.K., Edwards, B.R., and Grainger, N.C.**
1999: Neogene basaltic flow rocks, xenoliths, and related diabase, northern Nechako River map area, central British Columbia; *in* Current Research 1999-A; Geological Survey of Canada, p. 157–167.

**Struik, L.C., Whalen, J.B., Letwin, J., and L'Heureux, R.**
1997: General geology of southeast Fort Fraser map area, British Columbia; *in* Current Research 1997-A; Geological Survey of Canada, p. 65–76.

**Tipper, H.W.**
1963: Nechako River map area, British Columbia; Geological Survey of Canada, Memoir 324, 59 p.

**Williams, S.P.**
1997: Geological compilation of the Nechako River (93 F) map area, British Columbia; Geological Survey of Canada, Open File 3429, scale 1:250 000.

---

Geological Survey of Canada Project 950036-04

# Stratigraphy of the Hazelton Group in southwestern Nechako River map area, central British Columbia[1]

M.B. Quat and L.C. Struik
GSC Pacific, Vancouver

*Quat, M.B. and Struik, L.C., 1999: Stratigraphy of the Hazelton Group in southwestern Nechako River map area, central British Columbia;* in *Current Research 1999-E; Geological Survey of Canada, p. 21–29.*

**Abstract:** Hazelton Group rocks in southwestern Nechako River map area formed in an Early to Middle Jurassic volcanic arc. The succession consists of subaerial and submarine volcanic rocks interbedded with marine sediments assigned to the Entiako and Naglico formations. The Entiako Formation correlates to the Telkwa Formation in the Whitesail Reach map area and the Unuk River and Betty Creek formations in the Iskut River map area. The Naglico Formation roughly correlates to the Smithers Formation in the Whitesail Reach map area and the Salmon River Formation of the Iskut River–Telegraph Creek map areas. These units represent a silica-bimodal volcanic and sedimentary succession deposited in an arc-backarc complex of the Stikine Terrane (Stikinia). The Hazelton Group is the oldest rock succession in southwest Nechako River map area. It is overlain by Eocene Ootsa Lake Group rhyolite, Endako Group basalt, and Miocene basalt and intruded by (?)Jurassic diorite and granodiorite.

**Résumé :** Les roches du Groupe de Hazelton dans le sud-ouest de la région cartographique de la rivière Nechako ont été formées dans un arc volcanique du Jurassique précoce à moyen. La succession comprend des roches volcaniques subaériennes et sous-marines interlitées avec des roches sédimentaires marines des formations d'Entiako et de Naglico. La Formation d'Entiako est mise en corrélation avec la Formation de Telkwa de la région cartographique de Whitesail Reach et avec les formations d'Unuk River et de Betty Creek de la région cartographique de la rivière Iskut. La Formation de Naglico est plus ou moins mise en corrélation avec la Formation de Smithers de la région cartographique de Whitesail Reach et avec la Formation de Salmon River des régions cartographiques de la rivière Iskut et du ruisseau Telegraph. Ces unités représentent une séquence silicatée bimodale volcanique et sédimentaire mise en place dans un complexe d'arc et d'arrière-arc du terrane de Stikine (Stikinia). Le Groupe de Hazelton est la plus vieille succession de roches dans le sud-ouest de la région cartographique de la rivière Nechako. Il est recouvert par de la rhyolite du Groupe d'Ootsa Lake (Éocène), par du basalte du Groupe d'Endako et par du basalte miocène et est recoupé par de la diorite et du granodiorite (?)jurassiques.

[1] Contribution to the Nechako NATMAP Project.

## INTRODUCTION

The Hazelton Group in the Tetachuck Lake area (Fig. 1, 2) forms the upper part of the Stikine Terrane (Stikinia) that began amalgamation and convergence with the other terranes of the Intermontane Belt during the Triassic. The Hazelton Group comprises arc volcanic rocks and related sedimentary rocks formed in response to subduction of the Wrangellia and/or Cache Creek terranes (Gabrielse, 1991; Marsden and Thorkelson, 1992) under Stikinia in the Early and Middle Jurassic.

This study describes and interprets depositional characteristics of the Hazelton Group of Tetachuck Lake map area (NTS 93 F/5), central British Columbia (Fig. 2). It compares the stratigraphy with that of the Fawnie and Nechako ranges (NTS 93 F/2, 3, 6, 7) (Diakow et al., 1997), the Whitesail Reach (NTS 93 E/10)–Troitsa Lake (NTS 93 E/6) map areas (Diakow and Mihalynuk, 1987), and the Iskut River map area (NTS 104 B) (Anderson, 1993) (Fig. 1, 2). Tetachuck Lake (NTS 93 F/5) map area was mapped in conjunction with Qualcho Lake (NTS 93 F/4) as part of the Nechako NATMAP Project (Fig. 1, 2) during the 1998 field season (Struik and MacIntyre, 1999). This area was originally mapped by Tipper (1963), who included some of the older mafic volcanic and sedimentary rocks in the Triassic Takla Group. Subsequently these rocks were interpreted as Jurassic Hazelton Group by Schiarizza et al. (1994).

Tetachuck Lake map area is accessible by forest service roads from Burns Lake, Fraser Lake, or Vanderhoof; those roads lead to a barge that crosses Ootsa Lake to join the Chelaslie–Main forest service road. Chelaslie–Main forest service road is the main artery of the road network in the Tetachuck Lake area.

Extensive glacial deposits limit outcrop in the area. Three study sites (A–C, Fig. 3) were chosen for their accessibility and exposure. The study area west of Chelaslie–Main forest service road (A) and the area north of Tetachuck Lake (C) are close to good logging roads and well exposed by logging clear cuts. The section exposed along the north bank of Chelaslie River (B) is accessible by boat from Chelaslie Arm (Fig. 3).

Jurassic Hazelton Group rocks of British Columbia attract considerable attention because they host many economic and potentially economic mineral occurrences, such as gold at Eskay Creek in the Iskut map area and silver, lead, zinc, copper, and molybdenum at the Huckleberry mine in the Whitesail Reach map area. Other important mines hosted by Hazelton Group include Core Mountain and Chikamin Mountain in the Chikamin Mountain (NTS 93 E/06) map area and Premier, Kerr, and Inel deposits in the Iskut River map area.

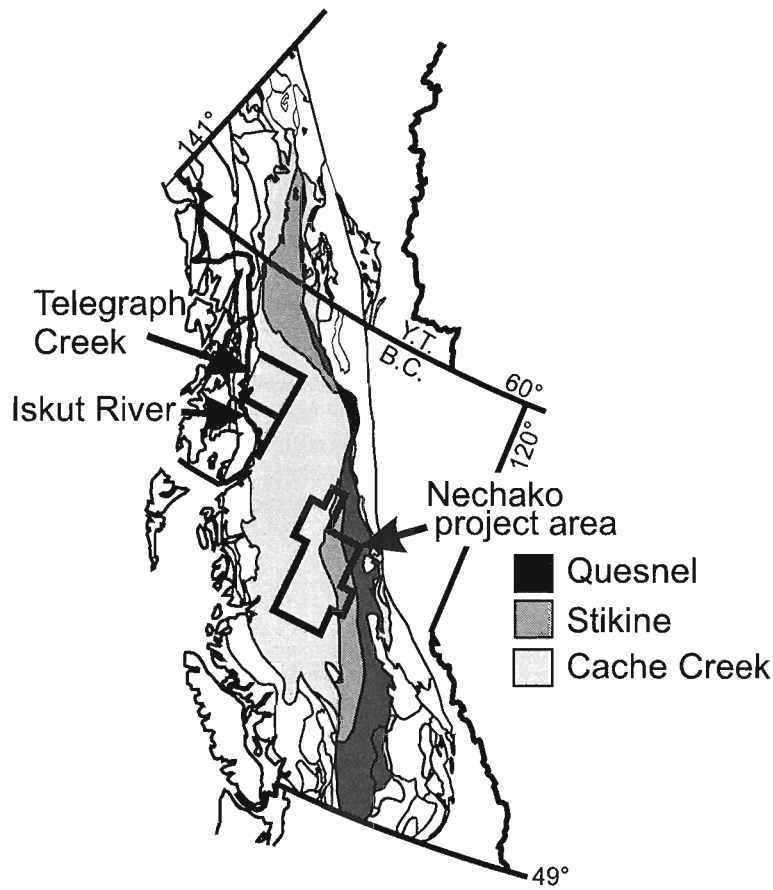


***Figure 1.***

*Location of the Nechako NATMAP Project and the Iskut River and Telegraph Creek map areas with respect to terranes of the Intermontane Belt of the Canadian Cordillera (modified from Wheeler and McFeely (1991)).*

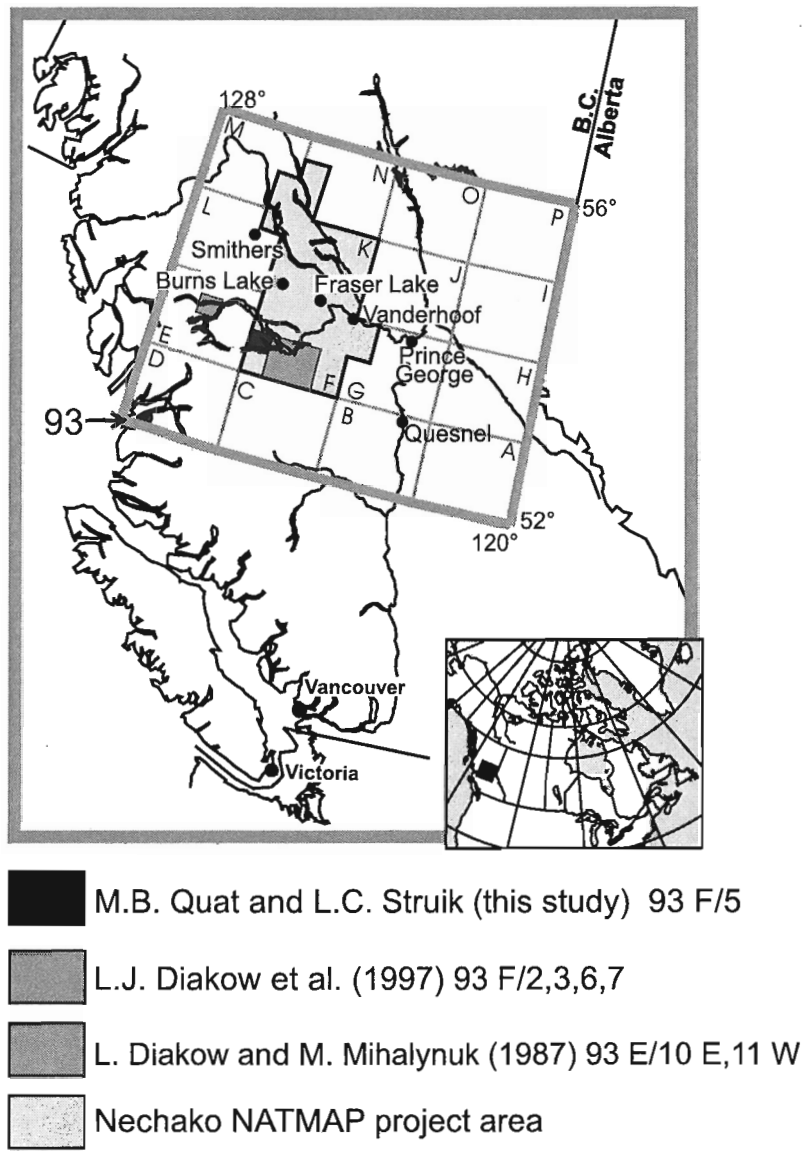


***Figure 2.*** *Location of the study area and comparison areas in central British Columbia.*

## GEOLOGY

Rocks in the Tetachuck Lake map area form four stratified units ranging in age from Early Jurassic to Miocene, and four suites of plutons of Jurassic to Eocene age. The four stratified units are the Early to Middle Jurassic Hazelton Group, the Eocene Ootsa Lake and Endako groups, and Miocene basalt (Fig. 3).

Hazelton Group ranges in age from Toarcian (late Early Jurassic) to Bajocian (early Middle Jurassic) and is divided into two formations, Entiako and the younger Naglico (Diakow et al., 1997). These divisions will be used here as well as provisional subdivisions used by Struik et al. (1999). The contact between the Entiako and Naglico formations is paraconformable, except west of the Chelaslie–Main forest service road where it is conformable.

The Entiako Formation records subaerial felsic to mafic volcanism ending with a period of marine deposition marking the top of the formation. The Naglico Formation marks a time of plagioclase-phyric andesite flows and tuffs containing interbeds of marine volcaniclastic sediments. The Hazelton Group in the Tetachuck Lake area is unconformably overlain by Ootsa Lake Group rhyolite, Endako Group basalt, and Miocene basalt.

The Ootsa Lake Group rhyolite is characterized by white to cream, light yellow-weathering flows, which are sometimes banded but usually massive in the Tetachuck Lake area. It contains phenocrysts of quartz, plagioclase, and minor biotite. At the downstream end of the rapids on the Chelaslie River, the Ootsa Lake Group disconformably overlies Hazelton Group strata.

Endako Group basalt is found in small patches in the area. The basalt is generally massive, dark aphanitic flows with few phenocrysts of pyroxene and trace olivine. Outcrops of this unit can be found north of Chelaslie River and Chelaslie Arm (Fig. 3).

Miocene basalt is dark grey to black, flat lying, and locally contains mantle xenoliths up to 10 cm in diameter. The xenoliths are made up of crystals of olivine, pyroxene, diopside, and augite within a massive aphanitic groundmass. This unit overlies the Hazelton Group west of Chelaslie–Main forest service road and in the area of Blanchet–Main forest service road. This basalt correlates with the Chilcotin Group of south-central British Columbia.

Diorite, granodiorite, and monzonite of Jurassic or possibly younger age are scattered throughout the area in four plutonic suites and intrude Hazelton Group rocks. The intrusions are fine- to medium-grained, equigranular, contain biotite and hornblende, are slightly foliated, and contain local andesite and rhyolite dykes. Some of these intrusions are described by Billesberger et al. (1999).

## HAZELTON GROUP (lmJH)

### *Entiako Formation* (lmJHE)

The Entiako Formation is divided into two facies following Diakow et al. (1997), 1) a subaerial felsic to mafic volcanic facies containing rhyolite to andesite tuff and breccia with minor rhyolite flows, and 2) a near-shore to deeper marine sedimentary facies, characterized by volcanically derived sandstone, conglomerate, tuffaceous siltstone, and mudstone. Entiako Formation correlates lithologically to the Telkwa Formation in the Whitesail Reach map area and to the Unuk

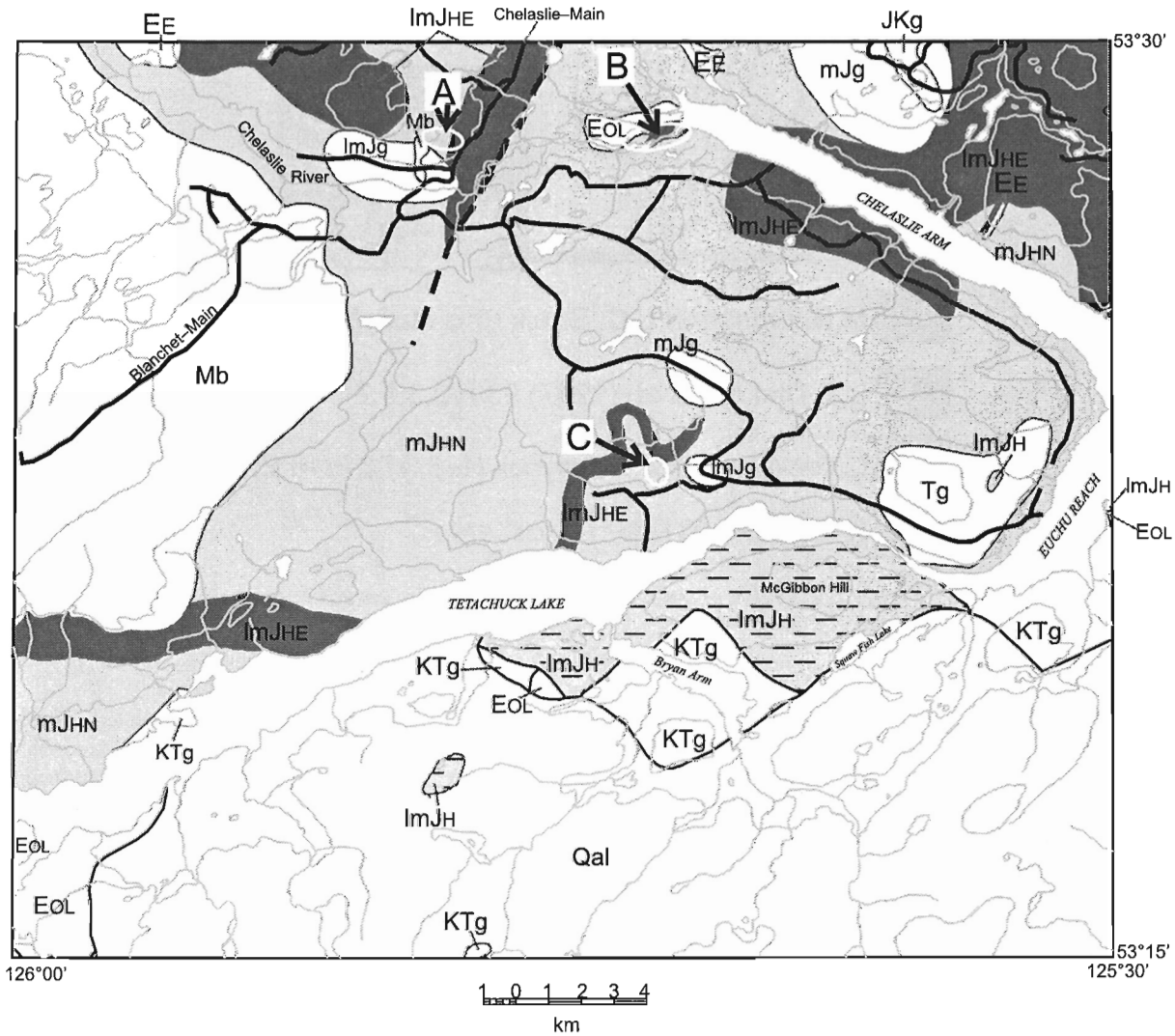


***Figure 3.*** *Location of the three measured sections and bedrock geology of the Tetachuck Lake map area (NTS 93 F/5). Locality A is the location for the Chelaslie Main section, locality B is the Chelaslie River section, and locality C is the Tetachuck Lake section. Legend differentiates formations of the Hazelton Group.*

River, Betty Creek, and (?) Mount Dilworth formations in the Iskut River area (Fig. 4). These formations all contain silica-bimodal ash and lapilli tuff and breccia and volcaniclastic fossiliferous sediments. Their age as determined by the fossil record in the Fawnie and Nechako ranges is Toarcian (Diakow et al., 1997); U-Pb ages in the Iskut River area are 197 ± 14 Ma (Brown, 1987).

The subaerial felsic to mafic facies is found at the Chelaslie–Main forest service road and Chelaslie River sections, A and B, respectively. In the measured section near Tetachuck Lake (C) no Entiako formation rocks were encountered. Characteristic of the Chelaslie–Main (A) and Chelaslie River (B) sections are the abundance of rhyolite and/or andesite tuff. The Chelaslie River section has a good exposure of the rhyolite tuff interbedded with andesite tuff (Fig. 5A). The felsic tuff is not exposed in the Chelaslie–Main section; rather it contains andesite breccia which grades upsection to andesite tuff. The rhyolite tuff is buff to green and contains quartz phenocrysts, pyroclasts of flow-laminated rhyolite, and fragments of plagioclase and hornblende. This tuff is well bedded, locally graded, and alternates between beds of lapilli and ash tuff. The andesite tuff and breccia is maroon to dark green, contains phenocrysts of quartz, slender plagioclase, and hornblende fragments and is slightly graded and locally bedded.

The near-shore and deeper marine sedimentary facies is best displayed in the Chelaslie–Main section and is mostly absent in the Chelaslie River section except for a feldspathic sandstone interbedded with rhyolite and andesite tuff. The sandstone is grey to pink, medium to coarse grained, and contains large feldspar fragments and rhyolitic and andesitic detritus. In the section west of the Chelaslie–Main forest service road the Entiako Formation contain marine fossiliferous volcanic sediment, mudstone, conglomerate, and siltstone.

The volcanic sediment of the Chelaslie–Main section has a well bedded, fine-grained, grey to green matrix that weathers in bands of white, pink, and green (Fig. 5B) and contains bivalve and gastropod fossils (Fig. 5C). Mudstone is dark grey to black, finely laminated, tuffaceous, and contains andesite and rhyolite fragments and thin (less than 5 mm thick) interlayers of light brown ash tuff. Within the thick beds of mudstone are interbeds of conglomerate and siltstone. The conglomerate is grey to brown and is dominated by clasts of andesite, rhyolite, and bivalve shells (Fig. 5D). The clasts are rounded, range in size from 2 cm to 30 cm and make up 40–60% of the rock. This conglomerate contains fewer clasts further upsection but is still fossiliferous as it grades into siltstone. The siltstone is light to dark grey, fossiliferous at the base, and is overlain by finely laminated tuffaceous mudstone similar to that below the conglomerate.

The Entiako Formation in the Tetachuck Lake map area records subaerial to subaqueous deposition of an eruptive volcanic episode, followed by near-shore to deeper marine clastic sedimentation. The bimodal and fragmental nature of the formation indicates concurrent mafic and felsic explosive volcanic events from a nearby volcanic island. The facies change between the Chelaslie River and Chelaslie–Main sections from coarse-grained sandstone to fine-grained siltstone and mudstone indicates that this was formed in a west-facing slope of a volcanic island, with the source of the detritus and volcanic debris to the east.

### LEGEND TO FIGURE 3

**QUATERNARY**

Qal — Undivided; unconsolidated glacial till, fluvial deposits, and poorly sorted alluvium

**TERTIARY**

Tg — Granite

Miocene

Mb — Olivine-phyric basalt

Eocene

EE — Endako Group: andesite, basalt, dacite, rhyodacite; flows, breccia; vesicular, amygdaloidal

EOL — Ootsa Lake Group: rhyolite, dacite, basalt; vesicular, amygdaloidal; breccia, tuff

**MESOZOIC AND TERTIARY**

Late Cretaceous–Early Tertiary

KTg — Hornblende diorite, granodiorite

**MESOZOIC**

Jurassic to Cretaceous

JKg — Fine-grained biotite hornblende monzonite, minor feldspar porphyry

Lower to Middle Jurassic

mJg — Biotite hornblende diorite

lmJg — Hornblende biotite diorite

Hazelton Group

lmJH — Undifferentiated Hazelton Group: basaltic, andesitic and rhyolitic pyroclastics and flow; feldspar-phyric andesite; flows, breccia, tuff

mJHN — Naglico Formation: feldspar augite andesite flows, tuff, breccia, and agglomerate; limestone, sandstone

mJHE — Entiako Formation: andesitic greywacke, conglomerate, rhyolite tuff, and minor flows; mudstone, feldspathic sedimentary rocks

### *Naglico Formation* (mJHN)

In the Tetachuck Lake map area the Naglico Formation is subdivided into three lithological units following Struik et al. (1999) in the Euchiniko map area. One unit is a feldspar-phyric andesite flow and lapilli tuff. Andesite agglomerate and breccia form a second unit. The third unit is sedimentary and contains sandstone interbedded with limy ash tuff and limestone with zones of densely packed gastropod and clam shell debris. The Naglico Formation lithologically correlates to the Smithers Formation in the Whitesail Reach map area and to the Salmon River Formation of the Iskut River–Telegraph Creek map areas (Fig. 4). These formations all contain andesitic (usually feldspar- or pyroxene-phyric) flow,

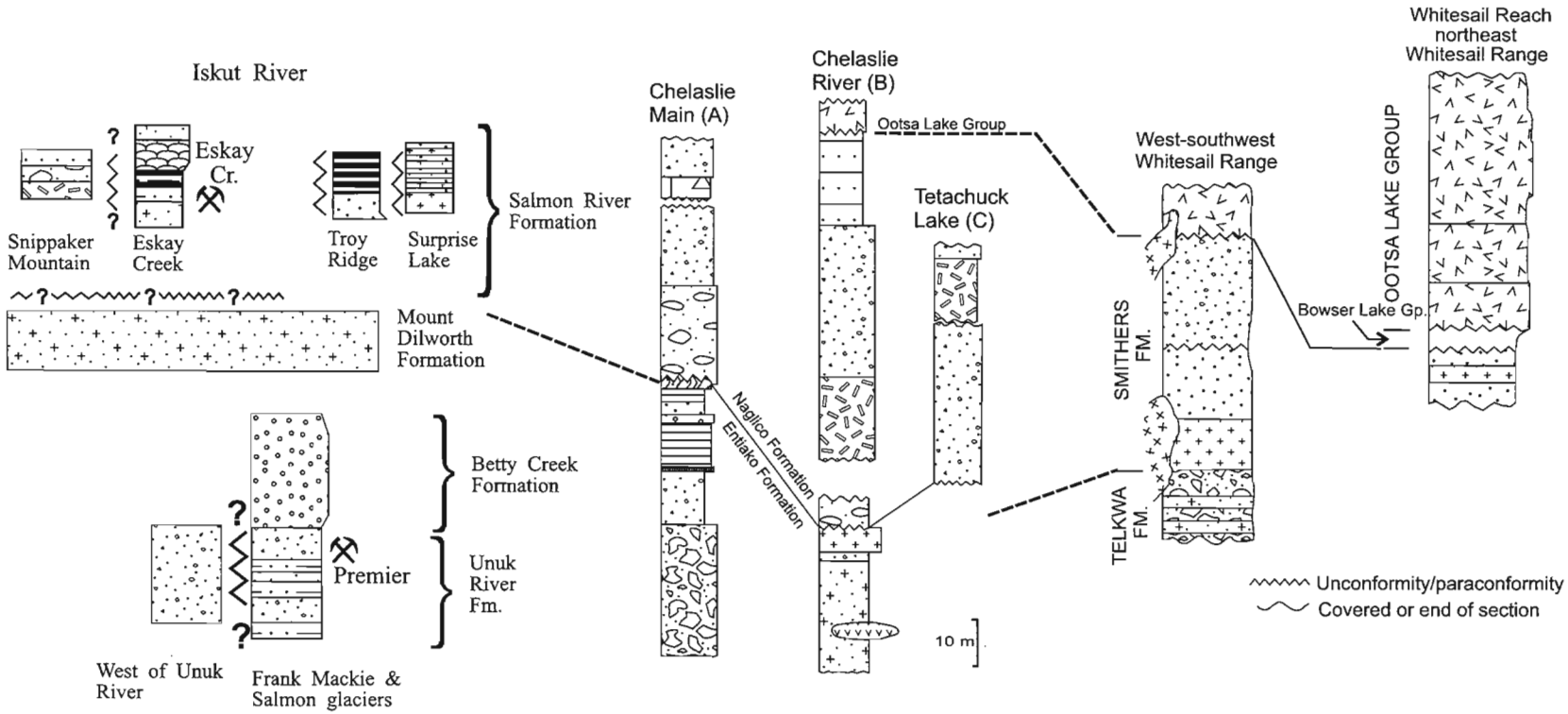


## Lithology

- Miocene basalt dyke
- Cretaceous to Eocene Ootsa Lake Group: rhyolite, andesite
- Cretaceous intrusives diorite, granite, gabbro
- Middle Jurassic Bowser Lake Group: siltstone, shale arkosic wacke; fossiliferous
- Lower to Middle Jurassic Hazelton Group
- Sandstone interbedded with limy ash
- Andesitic tuff
- "Pajama beds": laminated siliceous siltstone
- Pillowed lava
- Limestone and mudstone; densely packed fossils
- Plagioclase-phyric andesite agglomerate
- Plagioclase-phyric andesite flow
- Tuff bedded with some conglomerate and breccia
- Mudstone; finely laminated
- Silty shale, shale, and siliceous shale
- Siltstone; fossiliferous at base
- Conglomerate; fossiliferous
- Volcanic sediment; fossiliferous
- Andesite breccia and tuff
- Feldspathic sandstone; coarse grained
- Rhyolite tuff with minor flows

***Figure 4.*** *Stratigraphic sections of the Hazelton Group in three areas of the Tetachuck Lake map area (centre) with comparisons to the Whitesail Reach (right, modified from Diakow and Mihalynuk (1987)) and Iskut River (left, modified from Anderson (1993)) map areas.*




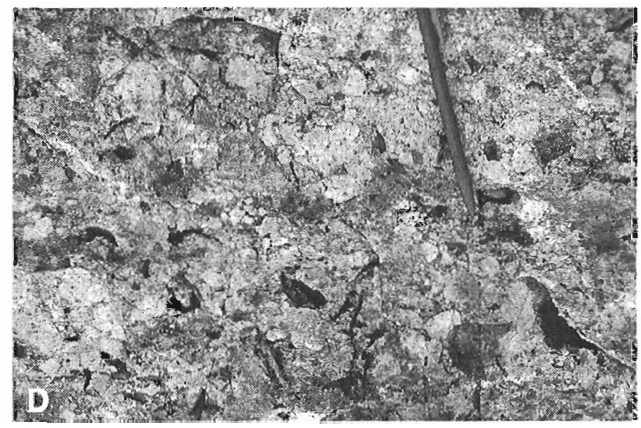


***Figure 5.*** *Rocks typical of the Entiako Formation.* ***A)*** *Beds of lapilli and ash tuff from the mouth of the Chelaslie River. Person is standing on green ash tuff.* ***B)*** *Bedded and slightly graded tuff found in section A.* ***C)*** *Fossiliferous ash tuff.* ***D)*** *Conglomerate with clasts of andesite tuff and gastropod and bivalve shells.*

breccia, or tuff, sandstone, and fossiliferous limestone. Their age as determined by the fossil record in the Fawnie and Nechako ranges is Bajocian (Diakow et al., 1997) and upper Aalenian to Bajocian in the Iskut River area (Anderson, 1993).

The first unit containing feldspar-phyric andesite flow and tuff is found in the Chelaslie River (B) and Tetachuck Lake (C) sections. It is thickest and least variable at the Chelaslie River section. Characteristic to both sites is the massive feldspar-phyric andesite flow and tuff. The flow rocks of this unit are generally maroon to dark grey and contain plagioclase phenocrysts (up to 10 cm long and 20% of volume), acicular hornblende, and minor pyroxene phenocrysts (Fig. 6A). The lapilli tuff contains fragments of the flow unit in a groundmass of the same composition. Unique to the Tetachuck Lake section is epidotization of the flow and tuff rocks and quartz veining. Local sulphide mineralization is found in quartz veins and disseminated throughout andesite tuff and consists of pyrite and minor chalcopyrite and bornite. The quartz veins are up to 3 mm wide, 2–3% of volume, and occur in two episodes. The first episode contains minor sulphides and is near horizontal and the second episode is sulphide rich and crosscuts the first set of veins. The quartz veins and sulphide mineralization may be related to the epidotization found in the Tetachuck Lake section and suggests hydrothermal alteration.

The second unit of andesite agglomerate and breccia is found at the Chelaslie–Main and Chelaslie River sections and occurs stratigraphically under the flow and tuff unit in this area. To the east in the Euchiniko map area this unit occurs within the flow and tuff unit (Struik et al., 1999). This unit is maroon to brown and contains large (up to 15 cm in diameter), rounded to subangular clasts of fine-grained porphyritic andesite in a medium-grained matrix of the same material (Fig. 6B).

The third unit of the Naglico Formation is found in the Chelaslie–Main and Chelaslie River sections. Both of these sections contain different sedimentary rocks of this unit and may represent a facies change. Collectively, the third unit is comprised of limestone and mudstone with zones of densely packed gastropod and bivalve shells, and sandstone interbedded with limy ash tuff. The limestone and mudstone is found in the Chelaslie–Main section. This limestone and mudstone package is well bedded with zones of densely packed fossil debris. The limestone is black, massive, and contains mostly

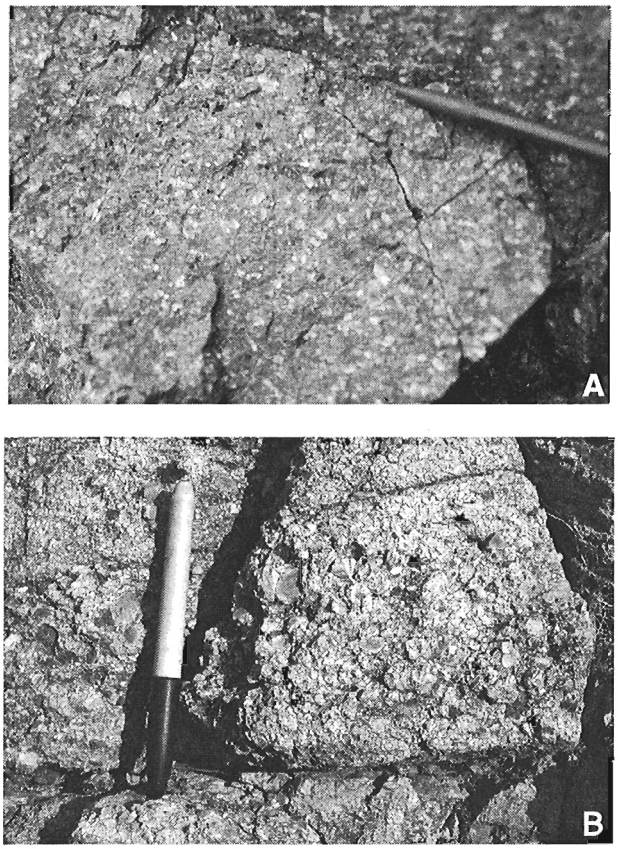



***Figure 6.*** *Typical rocks of the Naglico Formation.* ***A)*** *Feldspar-phyric andesite of the Chelaslie River.* ***B)*** *Andesite agglomerate found in the Chelaslie–Main and Chelaslie River sections.* ***C)*** *Limestone and mudstone containing bivalve and gastropod shells, photograph by M.G. Hrudey.*

gastropods. The mudstone is dark grey, weathers brown, and bedding is interrupted by local bioturbation (Fig. 6C). The sandstone package is found in the Chelaslie River (B) section. This sandstone is cream to yellow, is limy, and has beds up to 45 cm thick with interbeds of limy ash. It is overlain with angular unconformity by Ootsa Lake Group rhyolite.

The Naglico Formation in the Tetachuck Lake map area records another eruptive event and associated marine sedimentation. The maroon colour and the texture of the volcanic rocks of this formation suggest a period of subaerial effusive and explosive deposition. The feldspar-phyric andesite flow represents proximal effusive deposition near the Chelaslie River and Tetachuck Lake sections. Further from the source the eruption is recorded as andesitic agglomerate and tuff at the Chelaslie–Main section. The sedimentary facies change also suggests that the Chelaslie–Main section is more distal from the source of detritus than the near-shore sandstone of the Chelaslie River section.

## CONCLUSIONS

Through lithological comparisons to Hazelton Group rocks of the Fawnie and Nechako ranges to the east, volcanic and sedimentary successions of the Tetachuck Lake map area can be differentiated into Entiako and Naglico formations of the Jurassic Hazelton Group. This correlation indicates the likely age of these rocks in the Tetachuck Lake map area to be late Early to early Middle Jurassic. Correlation to Hazelton Group in the Whitesail Reach map area to the west and to the Iskut River map area to the northeast is also suggested. From lithological comparisons the Entiako Formation can be correlated to the Telkwa Formation in the former and to the Unuk River, Betty Creek, and possibly the Mount Dilworth formations of the latter. The Naglico Formation is correlated to the Smithers Formation of the Whitesail Reach map area and to the Salmon River Formation of the Iskut River map area.

## ACKNOWLEDGMENTS

The authors gratefully acknowledges the field assistance of Selena Billesberger, Kelly Franz, and Ruth Paterson for the Hazelton portion of this project and the mapping expertise of Mike Hrudey, Karen Fallas, and Crystal Huscroft for the rest of the bedrock geology for the map area. The authors would also like to thank S.P. Gordey for critical revision and Bev Vanlier for editing help.

## REFERENCES

**Anderson, R.G.**
1993: A Mesozoic stratigraphic and plutonic framework for northwestern Stikinia (Iskut River area), northwestern British Columbia, Canada; *in* Mesozoic Paleogeography of the Western United States—II, (ed.) G. Dunne and K. McDougall; Pacific Section Society of Economic Paleontologists and Mineralogists, v. 71, p. 477–494.

**Billesberger, S.M., Anderson, R.G., and Quat, M.B.**
1999: Geology of four plutons in central and northern Tetachuck Lake map area, central British Columbia; *in* Current Research 1999-E; Geological Survey of Canada.

**Brown, D.A.**
1987: Geological setting of the volcanic-hosted Silbak Premier Mine, northwestern British Columbia (104 A/4); MSc thesis, University of British Columbia, Vancouver, British Columbia, 216 p.

**Diakow, L. and Milhalynuk, M.**
1987: Geology of Whitesail Reach and Troitsa Lake map areas (93E/10W, 11E); *in* Geological Fieldwork 1986; British Columbia Ministry of Energy, Mines and Petroleum Resources, Paper 1987-1, p. 171–179.

**Diakow, L.J., Webster, I.C.L., Richards, T.A., and Tipper, H.W.**
1997: Geology of the Fawnie and Nechako Ranges, southern Nechako Plateau, central British Columbia (93F/2,3,6,7); *in* Interior Plateau Geoscience Project: Summary of Geological, Geochemical and Geophysical Studies, (ed.) L.J. Diakow and J.M. Newell; British Columbia Geological Survey Branch, Open File 1996-2 and Geological Survey of Canada, Open File 3448, p. 7–30.

**Gabrielse, H.**
1991: Late Paleozoic and Mesozoic terrane interactions in north-central British Columbia; Canadian Journal of Earth Sciences, v. 28, p. 947–957.

**Marsden, H. and Thorkelson, D.J.**
1992: Geology of the Hazelton volcanic belt in British Columbia: Middle Jurassic evolution of Stikinia; Tectonics, v. 11, no. 6, p. 1266–1287.

**Schiarizza, P., Panteleyev, A., Gaba, R.G., and Glover, J.K.**
1994: Mineral Potential Project, Cariboo-Chilcotin Area (92 J, K , N , O , P; 93 A, B, C, F, G, H); British Columbia Ministry of Energy, Mines and Petroleum Resources, Open File 1994-7.

**Struik, L.C. and MacIntyre, D.G.**
1999: Nechako NATMAP Project overview, central British Columbia, year four: part 1; *in* Current Research 1999-A; Geological Survey of Canada, p. 71–78.

**Struik, L.C., Anderson, R.G., and Plouffe, A.**
1999: Geology of the Euchiniko map area, central British Columbia; *in* Current Research 1999-A; Geological Survey of Canada, p. 119–128.

**Tipper, H.W.**
1963: Nechako River map area, British Columbia; Geological Survey of Canada, Memoir 324, 59 p.

**Wheeler, J.O. and McFeely, P. (comp.)**
1991: Tectonic assemblage map of the Canadian Cordillera and adjacent parts of the United States of America; Geological Survey of Canada, Map 1712, scale 1:2 000 000.

---

Geological Survey of Canada Project 950036

# Geology of four plutons in central and northern Tetachuck Lake map area, central British Columbia[1]

S.M. Billesberger[2], R.G. Anderson, and M.B. Quat
GSC Pacific, Vancouver

*Billesberger, S.M., Anderson, R.G., and Quat, M.B., 1999: Geology of four plutons in central and northern Tetachuck Lake map area, central British Columbia;* in *Current Research 1999-E; Geological Survey of Canada, p. 31–43.*

**Abstract:** At least four homogeneous and composite plutons intruded the Middle Jurassic Hazelton Group and were overlain by Tertiary volcanic rocks in the Tetachuck Lake map area (NTS 93 F/5). Field relationships, composition, and petrographic and geochemical features help characterize the plutons. The Chelaslie River and Tetachuck-south plutons comprise biotite-hornblende (clinopyroxene) diorite and resemble the Middle Jurassic Stag Lake plutonic suite in geochemical composition. Hornblende-biotite quartz monzodiorite of the Tetachuck-north pluton is the most felsic except for parts of the Chelaslie Arm pluton. Biotite-hornblende (clinopyroxene) monzodiorite of the Chelaslie Arm-1 phase within the composite Chelaslie Arm pluton is mineralogically unique due to the presence of rare orthopyroxene. The Chelaslie Arm-2 phase within the composite Chelaslie Arm pluton is characterized by biotite-hornblende quartz monzonite, its peraluminous affinity, and the most geochemically evolved composition of the plutons studied. It resembles felsic members of the Stag Lake Suite or the (?)Eocene Copley Lake plutonic suite.

**Résumé :** Au moins quatre plutons homogènes et composites ont fait intrusion dans le Groupe de Hazelton du Jurassique moyen et ont été recouverts par des roches volcaniques du Tertiaire dans la région cartographique du lac Tetachuck (SNRC 93 F/5). Les relations de terrain, la composition et les caractéristiques pétrographiques et géochimiques permettent de caractériser les plutons. Les plutons de Chelaslie River et de Tetachuck-sud sont constitués de diorite à biotite et hornblende (clinopyroxène) et ont une composition géochimique similaire à celle de la suite plutonique de Stag Lake du Jurassique moyen. La monzodiorite quartzifère à biotite et hornblende du pluton de Tetachuck-nord est la plus felsique sauf pour des parties du pluton de Chelaslie Arm. La monzodiorite à biotite et hornblende (clinopyroxène) de la phase Chelaslie Arm-1 du pluton composite de Chelaslie Arm a une minéralogie unique à cause de la présence d'orthopyroxène rare. La phase Chelaslie Arm-2 du pluton composite de Chelaslie Arm est caractérisée par la présence d'une monzonite quartzique à biotite et hornblende, une affinité hyperalumineuse et la composition géochimique la plus évoluée des plutons étudiés. Elle est similaire aux membres felsiques de la suite de Stag Lake ou encore à la suite plutonique (?)éocène de Copley Lake.

[1] Contribution to the Nechako NATMAP Project.
[2] Department of Earth and Ocean Sciences, University of British Columbia, 6339 Stores Road, Vancouver, British Columbia V6T 1Z4

## INTRODUCTION

This paper summarizes a detailed study of four mafic to felsic plutons, examined during regional-scale bedrock mapping of the Tetachuck Lake map area (NTS 93 F/5) in 1998, as a part of the Nechako NATMAP Project (Fig. 1; Struik and MacIntyre (1999) and references therein). The project contributes to the ongoing revision of the Nechako River 1:250 000 scale geological map (Tipper, 1963).

All four plutons are located north of Tetachuck Lake and intrude volcanic rocks of the Hazelton Group (Fig. 2). One underlies a portion of the Chelaslie River in the northwestern portion of the map area and is informally named the 'Chelaslie River pluton'. The second and third are located farther to the southeast, north of Tetachuck Lake, and are best exposed along Tetachuck Road. The more northern pluton is referred to as 'Tetachuck-north' and the more southern pluton as 'Tetachuck-south'. The fourth occurs in the northeastern part of the map, north of Chelaslie Arm, along the border of the Marilla map area (NTS 93 F/12). The pluton is divided into two parts: an elongate phase referred to as 'Chelaslie Arm-2' which intrudes the main phase known as 'Chelaslie Arm-1'.

Field relationships and geochemical and petrographical studies help distinguish the four plutons and phases. One sample from each of the Chelaslie River and Tetachuck-north plutons is currently being dated by U-Pb methods and the results will be reported elsewhere. Modal analyses (Table 1), chemical analyses, and the magnetic-susceptibility measurements (Table 2) of the samples are part of the database.

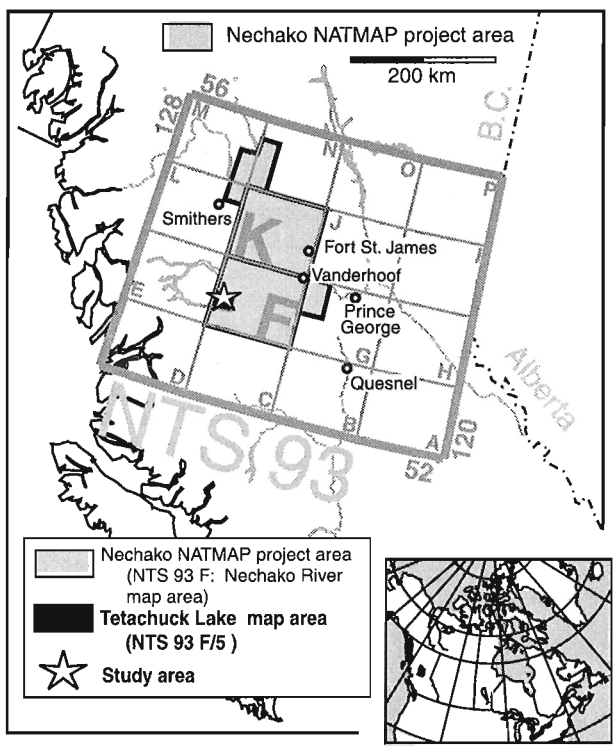


*Figure 1. Location of Tetachuck Lake map area within the Nechako NATMAP bedrock mapping area.*

## PHYSIOGRAPHY, ACCESS, AND FIELD METHODS

The Tetachuck Lake map area is characterized by rolling hills and low relief typical of the Interior Plateau. Outcrops are entirely below the tree line and extensive logging and road building enhance the access and exposure. Quaternary sediments cover a large portion of the map area, extending over most of the low-lying and/or swampy terrain, and are especially prominent in the west and south.

New data reported in this paper were based upon 11 traverses done during 5 weeks in July and August 1998. Standard geological-mapping techniques were supplemented by global-positioning-system measurements taken at each station, providing a lateral location precision of 50–100 m (depending on the number and orientation of available satellites). Magnetic-susceptibility readings were recorded for most outcrops using a hand-held Exploranium KT-9 Kappameter, with the values quoted (10-3 S.I. units) being averages of at least 5 measurements per outcrop. Representative samples were collected at each outcrop location for use in petrographic, geochemical, and geochronological analyses, as well as for reference and use in making specific-gravity measurements.

Geological contacts are inferred and extrapolated beyond the outcrop distributions across the extensive Quaternary cover, which mainly consist of unconsolidated glacial till, fluvial deposits, and poorly sorted alluvium (Fig. 2). The geology of the area south of Tetachuck Lake is derived from previous mapping (Tipper, 1963).

## REGIONAL GEOLOGY

Two bedrock units predominate in the Tetachuck Lake map area: the Lower to Middle Jurassic Hazelton Group volcanic rocks, and various Jurassic to Tertiary plutons which intrude the Hazelton Group rocks. Eocene Endako and Ootsa Lake groups and Neogene Chilcotin Group volcanic rocks (Resnick et al., 1999) are locally important.

### *Stratified units*

#### Lower to Middle Jurassic Hazelton Group (units lmJH, lmJHE and lmJHN)

Basaltic, andesitic and rhyolitic pyroclastic rocks and flows, as well as breccia, tuff, and flows of feldspar-phyric andesite of the Hazelton Group (country rocks to the plutons) are mainly exposed along the western edge of Chelaslie Arm and inland along the south edge of Tetachuck Lake (Fig. 2). Locally, the unit is divisible into the Entiako and Naglico formations described by Diakow et al. (1997) and Quat and Struik (1999).

Greywacke derived from andesitic flows, conglomerate, rhyolite tuff and minor flows, mudstone and feldspathic sedimentary rocks make up the Entiako formation (unit lmJHE, Fig. 2) which is localized along the north edge of Tetachuck

Lake, and to the northeast, along the southwestern and northeastern Chelaslie Arm. It occurs along the northwestern and eastern margins of the Chelaslie River pluton and along the southern and eastern flanks of the Chelaslie Arm pluton.

Extensive Naglico formation rocks (unit lmJHN, Fig. 2) include tuff, breccia, agglomerate and flows of feldspar-augite andesite composition, as well as sandstone and fossiliferous limestone, and host the four plutons studied.

### Tertiary volcanic rocks

Vesicular, amygdaloidal, and brecciated rhyolite flows and tuff, and dacite of the Eocene Ootsa Lake Group (unit EOL, Fig. 2) are exposed primarily along the shoreline of Tetachuck Lake, Euchu Reach and Chelaslie Arm.

Eocene Endako Group volcanic rocks (unit EE, Fig. 2) include vesicular and amygdaloidal andesite, basalt, dacite and rhyodacite flows and breccia. The Ootsa Lake and Endako groups rocks unconformably overlie rocks of the Hazelton Group.

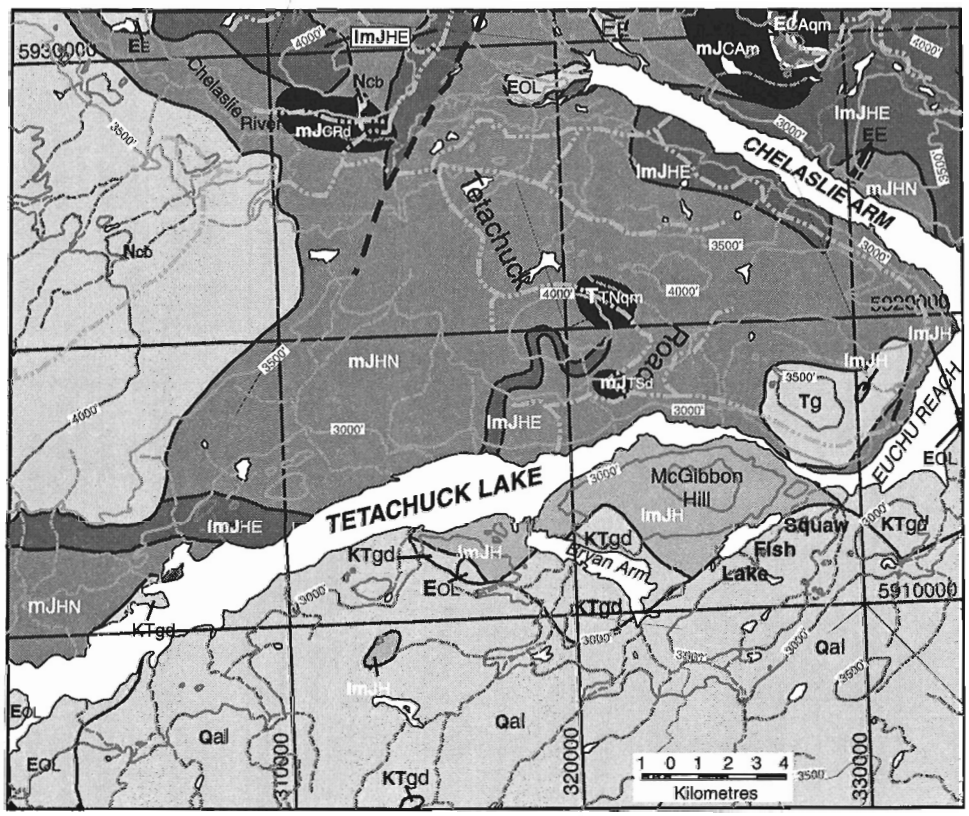


QUATERNARY

Qal

Neogene

Ncb Chilcotin Group

TERTIARY

Tg Granite

TTNqm Tetachuck-north pluton: quartz monzodiorite

Eocene

EE Endako Group

EOL Ootsa Lake Group

ECAqm Chelaslie Arm-2 phase: quartz monzonite

Late Cretaceous-Early Tertiary

KTgd diorite, granodiorite

MESOZOIC

(?)Middle Jurassic

mJCAm Chelaslie Arm-1 phase: monzonite to monzodiorite

mJCRd Chelaslie River pluton: diorite

mJTSd Tetachuck-south pluton: diorite

Lower to Middle Jurassic

lmJH Hazelton Group (undivided)

mJHN Naglico formation

lmJHE Entiako formation

SYMBOLS

lakes

gravel roads

contours (interval 500 feet)

streams

approximate or inferred geological contacts

fault

5910000N / 320000E UTM coordinates (zone 10)

***Figure 2.*** *Geological map of the Tetachuck Lake map area showing locations of plutons studied. Country-rock geology is from L.C. Struik and M.B. Quat (unpub. data, 1998).*

**Table 1.** Summary of the modes estimated from hand samples and determined by image analysis as well as the thin-section mineralogies of the four plutons.

**Hand-sample estimation**

| | Chelaslie River | | | Tetachuck-north | | | Tetachuck-south | | Chelaslie Arm-1 | | | Chelaslie Arm-2 | | |
|---|---|---|---|---|---|---|---|---|---|---|---|---|---|---|
| **Sample #** | **3002** | **806** | **0701c** | **2804** | **4707** | **0804a** | **605** | **3208** | **5804** | **5806** | **5807** | **3406** | **5802** | **5808** |
| Alkali-feldspar | 5 | 10 | 2 | 20 | 20 | 18 | 0 | 0 | 5 | 10 | 12 | 35 | 25 | 35 |
| Plagioclase | 60 | 65 | 63 | 55 | 50 | 58 | 65 | 65 | 65 | 58 | 65 | 40 | 50 | 33 |
| Quartz | 0 | 0 | 0 | 8 | 12 | 12 | 0 | 0 | 0 | 2 | 1 | 15 | 5 | 12 |
| Mafics | 35 | 25 | 35 | 17 | 18 | 12 | 35 | 35 | 30 | 30 | 22 | 10 | 20 | 20 |
| Total | 100 | 100 | 100 | 100 | 100 | 100 | 100 | 100 | 100 | 100 | 100 | 100 | 100 | 100 |
| QAP rock name | Diorite | Monzodiorite | Diorite | Quartz monzodiorite | Quartz monzonite | Quartz monzodiorite | Diorite | Diorite | Diorite | Monzodiorite | Monzodiorite | Quartz monzonite | Quartz monzodiorite | Quartz monzonite |

**Image Analysis**

| | Chelaslie River | | | Tetachuck-north | | | Tetachuck-south | | Chelaslie Arm-1 | | | Chelaslie Arm-2 | | |
|---|---|---|---|---|---|---|---|---|---|---|---|---|---|---|
| **Sample #** | **3002** | **806** | **0701c** | **2804** | **4707** | **0804a** | **605** | **3208** | **5804** | **5806** | **5807** | **3406** | **5802** | **5808** |
| Alkali feldspar | 3.0 | 13.2 | 4.3 | 19.9 | 19.4 | 16.9 | 0.0 | 0.0 | 6.1 | 10.8 | 16.5 | 34.0 | 22.1 | 29.9 |
| Plagioclase | 62.3 | 61.0 | 59.1 | 48.5 | 46.6 | 57.1 | 65.0 | 70.1 | 57.0 | 52.0 | 58.6 | 44.3 | 56.9 | 40.6 |
| Quartz | 0.0 | 0.0 | 0.0 | 11.0 | 15.1 | 11.9 | 0.0 | 0.0 | 0.0 | 0.0 | 2.8 | 8.4 | 4.4 | 8.3 |
| Mafics | 34.7 | 25.8 | 36.6 | 20.6 | 18.9 | 14.0 | 35.0 | 29.9 | 36.9 | 37.2 | 22.1 | 13.3 | 16.6 | 21.3 |
| Total | 100.0 | 100.0 | 100.0 | 100.0 | 100.0 | 100.0 | 100.0 | 100.0 | 100.0 | 100.0 | 100.0 | 100.0 | 100.0 | 100.0 |
| QAP rock name | Diorite | Monzodiorite | Diorite | Quartz monzonite | Quartz monzonite | Quartz monzodiorite | Diorite | Diorite | Diorite | Monzodiorite | Monzodiorite | Quartz monzonite | Quartz monzodiorite | Quartz monzonite |

| Chelaslie River | Tetachuck-north | Tetachuck-south | Chelaslie Arm-1 | Chelaslie Arm-2 |
|---|---|---|---|---|
| >5% | >5% | >5% | >5% | >5% |
| Plagioclase | Plagioclase | Plagioclase | Plagioclase | Plagioclase |
| Amphiboles (clinopyroxene) | Alkali feldspar | Actinolite (clinopyroxene) | Clinopyroxene | Alkali feldspar |
| Biotite | Biotite | Biotite | Amphiboles (clinopyroxene) | Quartz |
| <5% | Hornblende | <5% | Biotite | Biotite |
| Alkali feldspar | Quartz | Opaques | Alkali feldspar | Amphiboles (clinopyroxene) |
| Orthopyroxene | <5% | Apatite | <5% | <5% |
| Quartz | Titanite | Titanite | Orthopyroxene | Orthopyroxene |
| Opaques | Opaques | | Quartz | Opaques |
| Apatite | Apatite | | Opaques | Apatite |
| Titanite | Zircon | | Apatite | |

**Table 2.** Sample locations, elevations, magnetic susceptibility measurements (in $10^{-3}$ S.I. Units), geochemical analyses, normative mineralogies, and geochemical affinities for the four plutons.

| | Chelaslie River | | | Tetachuck-north | Tetachuck-south | Chelaslie Arm-1 | | Chelaslie Arm-2 |
|---|---|---|---|---|---|---|---|---|
| | **3002** | **0603AVG** | **0606AVG** | **4707** | **605** | **5804** | **5806** | **5808** |
| Easting | 312800 | 312941 | 313690 | 321173 | 321527 | 327532 | 326723 | 328226 |
| Northing | 5927460 | 5926734 | 5927440 | 5921312 | 5917934 | 5928896 | 5929242 | 5930740 |
| Elevation | 1030 | | | 1145 | 1070 | 1035 | 1080 | 1155 |
| Magnetic susceptibility | 55.6 | | | 43.8 | | 20.4 | 6.3 | 13.9 |
| $SiO_2$ | 53.95 | 48.39 | 51.13 | 65.52 | 58.36 | 54.85 | 56.63 | 66.86 |
| $TiO_2$ | 1.18 | 1.26 | 1.22 | 0.54 | 0.77 | 1.02 | 1.08 | 0.49 |
| $Al_2O_3$ | 17.45 | 17.75 | 17.64 | 16.21 | 16.51 | 16.79 | 16.37 | 14.70 |
| $Fe_2O_3$ | 3.62 | 5.12 | 4.35 | 1.99 | 1.82 | 3.24 | 2.07 | 1.13 |
| FeO | 4.71 | 5.94 | 5.16 | 2.08 | 6.35 | 5.34 | 5.98 | 2.47 |
| MnO | 0.13 | 0.17 | 0.15 | 0.07 | 0.15 | 0.12 | 0.12 | 0.06 |
| MgO | 4.12 | 6.17 | 4.98 | 1.54 | 3.84 | 4.39 | 3.94 | 1.45 |
| CaO | 7.43 | 10.17 | 8.53 | 3.90 | 6.48 | 7.14 | 5.91 | 2.14 |
| $Na_2O$ | 4.52 | 3.08 | 4.19 | 4.30 | 4.03 | 4.04 | 3.88 | 3.46 |
| $K_2O$ | 2.40 | 0.92 | 1.25 | 3.14 | 1.39 | 1.72 | 2.79 | 4.58 |
| $P_2O_5$ | 0.44 | 0.70 | 0.53 | 0.25 | 0.15 | 0.48 | 0.42 | 0.16 |
| LOI | 0.32 | 0.70 | 1.14 | 0.41 | 0.64 | 0.97 | 0.93 | 2.44 |
| TOTAL | 100.27 | 100.34 | 100.25 | 99.95 | 100.50 | 100.10 | 100.13 | 99.94 |
| Ba | 813 | 424 | 857 | 1087 | 458 | 965 | 1195 | 1108 |
| Cr | 556 | 290 | 586 | 744 | 313 | 660 | 817 | 758 |
| V | 196 | 268 | 211 | 83 | 178 | 194 | 165 | 59 |
| Ce | 51 | 46 | 54 | 61 | 41 | 53 | 68 | 65 |
| Ga | 21 | 24 | 22 | 19 | 15 | 20 | 19 | 15 |
| Nb | 10.7 | 1.2 | 6.2 | 8.1 | 4.5 | 6.1 | 9.9 | 10.2 |
| Pb | 10 | 6 | 7 | 9 | 9 | 11 | 23 | 15 |
| Rb | 69 | 36 | 28 | 83 | 34 | 49 | 85 | 179 |
| Sr | 949 | 1326 | 1049 | 664 | 313 | 732 | 577 | 367 |
| Th | 5.9 | 3.8 | 1.9 | 5.6 | bd | 3.9 | 6.0 | 21.9 |
| U | 1.8 | bd | bd | 3.5 | bd | bd | 0.8 | 8.2 |
| Y | 17 | 13 | 16 | 9 | 27 | 17 | 19 | 14 |
| Zr | 146 | 18 | 51 | 98 | 124 | 72 | 156 | 219 |
| **Normative minerals (wt. %)** | | | | | | | | |
| Quartz | 0.00 | 0.00 | 0.00 | 18.43 | 8.05 | 3.83 | 4.19 | 22.14 |
| Corundum | | | | | | | | 0.56 |
| Orthoclase | 14.19 | 5.45 | 7.45 | 18.64 | 8.23 | 10.25 | 16.62 | 27.76 |
| Albite | 38.26 | 26.15 | 35.76 | 36.55 | 34.15 | 34.48 | 33.10 | 30.03 |
| Anorthite | 20.24 | 31.98 | 25.85 | 15.72 | 22.88 | 22.79 | 19.16 | 9.81 |
| Cpx | 11.06 | 11.24 | 10.69 | 1.66 | 6.88 | 7.92 | 6.26 | 0.00 |
| Opx | 4.70 | 10.44 | 7.06 | 4.48 | 15.35 | 12.91 | 14.59 | 6.68 |
| Magnetite | 5.25 | 7.45 | 6.36 | 2.90 | 2.64 | 4.74 | 3.03 | 1.68 |
| Ilmenite | 2.24 | 2.40 | 2.34 | 1.03 | 1.46 | 1.95 | 2.07 | 0.95 |
| Apatite | 1.03 | 1.64 | 1.25 | 0.59 | 0.35 | 1.13 | 0.99 | 0.38 |
| Forsterite | 2.12 | 2.40 | 2.37 | | | | | |
| Fayalite | 0.90 | 0.85 | 0.87 | | | | | |
| **Shand index** | 0.7412 | 0.7229 | 0.7426 | 0.923 | 0.829 | 0.7813 | 0.8125 | 1.011 |
| **QAP rock name** | monzodiorite | diorite | monzodiorite/ diorite | monzogranite/ quartz-monzonite | quartz-monzodiorite | quartz-monzodiorite | quartz-monzodiorite | monzogranite |
| | | **Chelaslie River** | | **Tetachuck-north** | **Tetachuck-south** | **Chelaslie Arm-1** | | **Chelaslie Arm-2** |
| **Tectonic affinity** | | Volcanic arc | | Volcanic arc | Volcanic arc | Volcanic arc | | Volcanic arc |
| **Shand Index** | | Metaluminous | | Metaluminous | Metaluminous | Metaluminous | | Peraluminous |
| **Calc-alkaline / tholeiitic** | | Calc-alkaline | | Calc-alkaline | Calc-alkaline | Calc-alkaline | | Calc-alkaline |
| **Alkaline / subalkaline** | | Alkaline | | Subalkaline | Subalkaline | Borderline | | Subalkaline |
| **K vs Na vs Ca** | | Ca>Na>K | | Na>Ca>K | Ca>Na>K | Ca>Na>K | | K>Na>Ca |
| **Rb vs Ba vs Sr** | | Sr>Ba>Rb | | Ba>Sr>Rb | Ba>Sr>Rb | Ba>Sr>Rb | | Ba>Sr>Rb |
| **High/medium/low K** | | Medium to high | | High | Medium | Medium to high | | High |

Neogene Chilcotin Group includes locally columnar-jointed basalt flows which contain lherzolite nodules (e.g. Chelaslie River locality of Resnick et al., 1999) and are sparsely exposed but widespread in the northwest (Fig. 2; Tipper, 1963; L.C. Struik, pers. comm., 1998). The unit nonconformably overlies the Chelaslie River pluton (Fig. 3).

## *Plutonic rocks*

### Undivided Late Cretaceous to Early Tertiary plutons (units KTgd and Tg)

Plutons, other than those in this study, encompass a Late Cretaceous to (?)Early Tertiary granodiorite to hornblende diorite pluton south of Tetachuck Lake (unit KTgd, Fig. 2) and a (?)Tertiary granite pluton northwest of Euchu reach (unit Tg, Fig. 2).

### Chelaslie River pluton (unit mJCRd)

The Chelaslie River pluton underlies an area of about 6.5 km$^2$ in the northwestern Tetachuck Lake map area (Fig. 2). It is mainly medium grey, fine- to medium-grained, hypidiomorphic-granular biotite-hornblende of actinolite (clinopyroxene) diorite (Fig. 4). The pluton intruded rocks of Naglico and Entiako formations of the Hazelton Group.

The pluton intruded beds of andesitic tuff, plagioclase-phyric andesitic agglomerate, and fossiliferous limestone (Naglico formation) along its northern and western contacts. Along its northwestern and its eastern contacts (Fig. 5), it intruded andesite breccia and tuff, and a volcaniclastic sedimentary rock package of the Entiako formation. The pluton's intrusive contact with the Naglico formation is covered and inferred along its southern margin.

Along Chelaslie River, the pluton is crosscut by rhyolite, basalt, and andesite dyke equivalents to the Eocene Ootsa Lake and Endako groups. Neogene Chilcotin Group basalt locally nonconformably overlies the pluton (Fig. 2, 3).

A zone of highly altered, fractured, and pyrite-bearing rocks, is located along the northeastern contact of the pluton with the Naglico formation. The diorite in the zone weathers rusty, appears leached, and contains pyrite disseminations and fracture coatings. The northernmost part of the diorite pluton is distinguished by heterogeneous texture and composition of the mafic minerals, a diminished biotite-to-hornblende ratio, and northerly increase in the size of the hornblende crystals (Fig. 6). Also in the north is a southeast-trending distribution of uncommon, fine-grained, mafic-rich enclaves (Fig. 7), and a localized exposure of diorite that contains open fractures coated with calcite and chlorite.

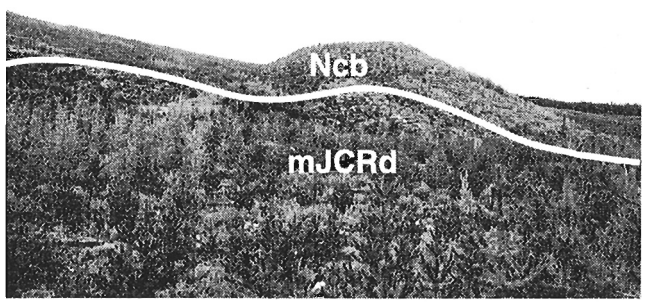


***Figure 3.*** *View east to the contact between the Chelaslie River pluton and the Neogene Chilcotin Group basalt; width of picture is approximately 150 m.*

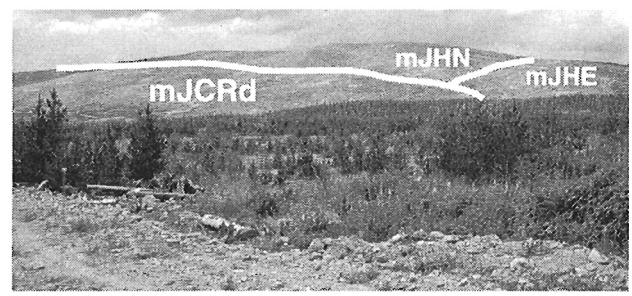


***Figure 5.*** *View northwest to the contact between the Chelaslie River pluton and the Middle Jurassic Hazelton Group Naglico formation volcanic rocks; relief of the hill above tree tops is approximately 800 m.*

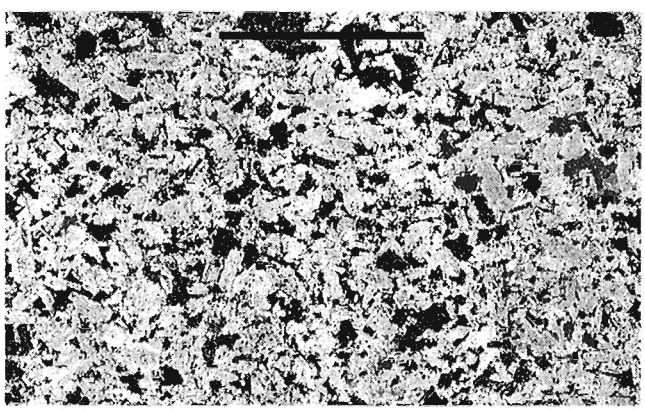

***Figure 4.*** *Texture of sample SCBB98-3003 from the Chelaslie River pluton; scale bar is 1 cm long. Pale grey is plagioclase and black is hornblende (clinopyroxene) and biotite.*

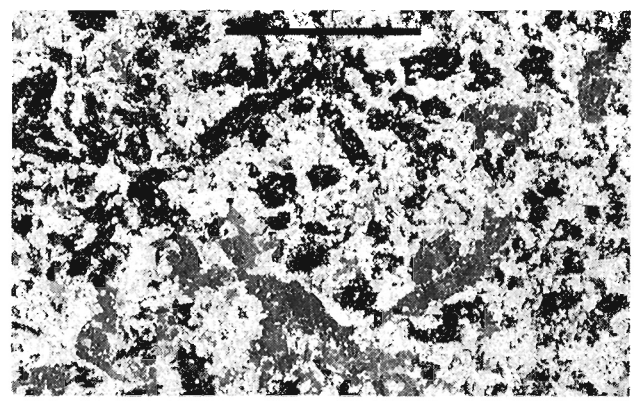

***Figure 6.*** *Texture in the Chelaslie River pluton (sample SCBB98-0701c); scale bar is 1 cm long. Plagioclase is pale grey and hornblende (clinopyroxene) and biotite are black. Note large euhedral hornblende crystals.*

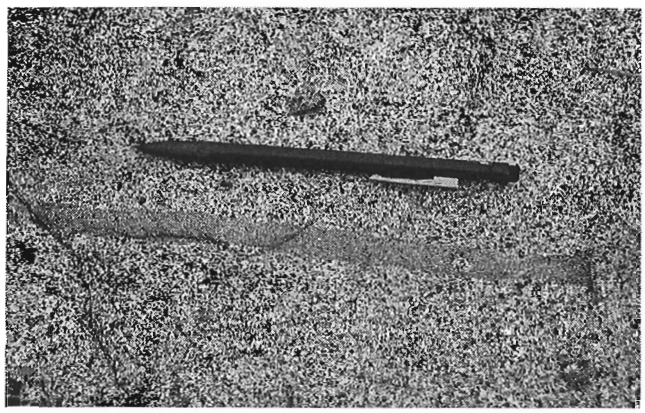

*Figure 7. Outcrop view of an aligned, mafic enclave in the Chelaslie River pluton which trends southeast; pencil is 15 cm long.*

### Tetachuck-north pluton (unit TTNqm)

The Tetachuck-north pluton underlies about 3.5 km$^2$ in the east-central portion of the Tetachuck Lake map area and is best exposed along discontinuous outcrops which extend a distance 1.5 km along and 300 m to the east and west of Tetachuck Road (Fig. 2). The pluton mainly comprises white, medium-grained, hypidiomorphic-granular hornblende-biotite quartz monzodiorite (Fig. 8). The pluton is surrounded by, and is inferred to intrude, rocks of the Hazelton Group Naglico formation. The pluton's contacts with country rock are covered; the location of its western and southern contacts is inferred from the nearest exposures of Hazelton Group volcanic rocks. Locally, within the pluton, there are areas of finer-grained, mafic-rich enclaves (Fig. 9), as well as areas containing unusually coarse-grained plagioclase.

### Tetachuck-south pluton (unit mJTSd)

The Tetachuck-south pluton is located south of the Tetachuck-north pluton in the east-central portion of the map area, but is otherwise unrelated to it (Fig. 2). The pluton probably underlies an area of about 2 km$^2$ and is best exposed along a 0.5 km roadside exposure. It is a medium grey, fine- to medium-grained, hypidiomorphic-granular biotite-hornblende or actinolite (clinopyroxene) diorite (Fig. 10). The pervasive alteration of the pluton observed in thin section analyses is not seen in hand sample. Locally, an epidote vein in the diorite trends 068° and dips 48° to the northwest.

The pluton is in intrusive contact with rocks of the Hazelton Group Naglico formation along most of its margin and with rocks of the Entiako formation along its western flank. The intrusive nature of its southwestern contact with the Naglico formation was inferred from inclusions of hornfelsed tuff in the diorite; the tuff country rock changes to plagioclase-phyric andesitic tuff farther west. The northeastern contact between the pluton and the Naglico formation is covered.

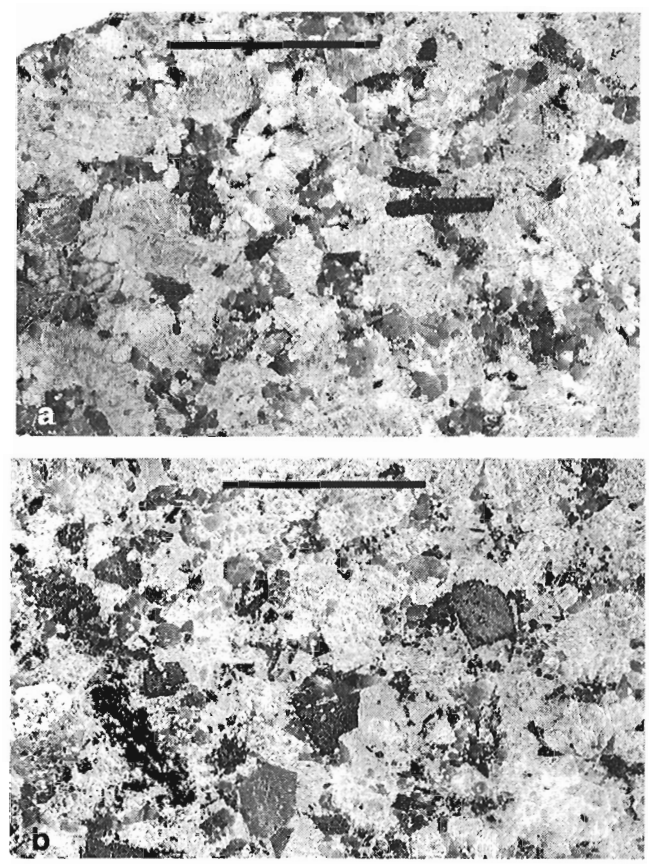


*Figure 8. Textures in Tetachuck-north pluton: **a**) sample SCBF98-4708; scale bar is 1 cm long. Plagioclase is pale grey, quartz is darker grey, and mafic minerals are black. Note the euhedral hornblende crystal. **b**) Sample SCBB98-0803; scale bar is 1 cm long. Plagioclase is pale grey, quartz is darker grey and mafic minerals are black. Note the euhedral biotite crystals.*

*Figure 9. Outcrop view of a mafic enclave in the Tetachuck-north pluton; pencil is 15 cm long.*

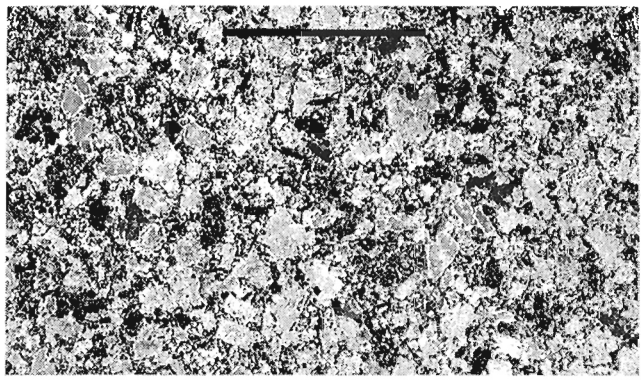

*Figure 10. Texture in the Tetachuck-south pluton (sample SCBQ98-3208); scale bar is 1 cm long. Plagioclase is pale grey and hornblende (clinopyroxene) and biotite are black.*

### Composite Jurassic and (?)Eocene Chelaslie Arm pluton (units mJCAm and ECAqm)

The composite Chelaslie Arm pluton is exposed over a 5 $km^2$ area, with a total inferred extent of approximately 9 $km^2$ in northeastern Tetachuck Lake map area (Fig. 2). The pluton extends into the Marilla map area (NTS 93 F/12), north of the study area. The composite pluton is divided into two units referred to as Chelaslie Arm-1 and Chelaslie Arm-2 (units mJCAm and ECAqm respectively, Fig. 2). The Chelaslie Arm-2 unit is a younger, more felsic-rich phase within the Chelaslie Arm-1 phase.

Chelaslie Arm-1 phase consists of grey to olive-grey, medium- to coarse-grained, hypidiomorphic-granular to plagioclase-megacrystic biotite-hornblende or actinolite-clinopyroxene monzodiorite (Fig. 11a, 11b). The primary rock type of the Chelaslie Arm-2 phase is a white-pink, fine- to medium-grained, hypidiomorphic-granular, hornblende or actinolite (clinopyroxene)-biotite quartz monzonite (Fig. 12).

Country rocks of the Chelaslie Arm-1 phase include Hazelton Group Naglico formation on the west and the south, and Entiako formation on the east. In the southeast, the contact between the monzodiorite and plagioclase-phyric basalt and gabbro is covered. Monzodiorite in the southeast is heavily weathered to saprolite, leaving only plagioclase and fresh biotite grains. Farther northwest, the monzodiorite is intruded by a dacite dyke a few metres thick that contains scattered small phenocrysts of hornblende, plagioclase, and biotite in an aplitic groundmass.

### *Petrography*

Modal analysis of the rock samples was completed with an image-analysis technique using computer software to analyze a photograph of the rock sample and calculate the area underlain by the minerals in the sample (Duncan, 1999). The results of the image analysis conducted for this study and the comparison with estimates from the stained hand sample are summarized in Table 1.

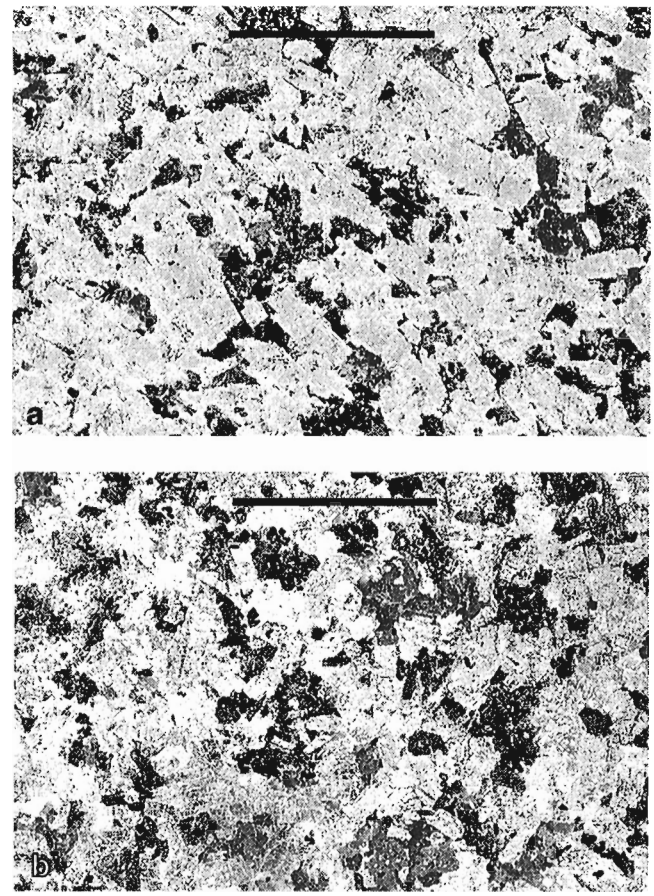


***Figure 11.*** *Textures in the Chelaslie Arm-1 pluton; scale bar is 1 cm long:* ***a)*** *sample SCBH98-5807: plagioclase megacrysts are pale grey and hornblende, clinopyroxene, and biotite are black.* ***b)*** *Sample SCBH98-5809: plagioclase megacrysts are pale grey and clinopyroxene, hornblende, and biotite are black.*

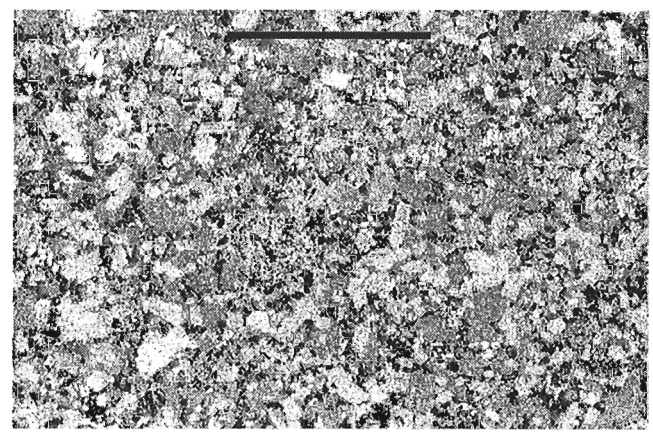

***Figure 12.*** *Texture in the Chelaslie Arm-2 pluton (sample SCBBQ98-3406); scale bar is 1 cm long. Plagioclase is pale grey, alkali-feldspar is dark grey, and hornblende (clinopyroxene) and biotite are black.*

The discrepancy between rock names established from the image-analysis technique and hand-sample estimation are accountable to two types of error: error in the estimation of mineral abundances in the hand sample or problems in isolating the distinctive area covered by a mineral in the image-analysis technique. Errors in hand-sample analysis occur as a result of the tendency to overestimate the percentage of the most abundant mineral in the hand sample (plagioclase). Small variations in colour affect the image-analysis technique that uses homogeneous colour patches to select minerals. A difficulty arises in selecting the entire area covered by a mineral when the resolution of photographs allows the detailing of small-scale variations in colour and shade. The variations may be due to natural, alteration, or stain-quality phenomena. Plagioclase determinations were derived using the Michel-Levy and Carlsbad-albite methods, and the results for each pluton are summarized in the petrographic descriptions below.

### Chelaslie River pluton

The primary mineralogy for the Chelaslie River samples is clinopyroxene and plagioclase, with minor quartz, orthopyroxene, titanite, opaque minerals, and apatite. Amphibole (actinolite and hornblende) crystallization was late and produced overprint textures and/or growth around clinopyroxene crystals as well as interstitial to subhedral biotite. Grain size varies from 0.5–4 mm for biotite, 0.25–2 mm for amphibole (clinopyroxene), and 0.25–4 mm for plagioclase. Plagioclase crystals are euhedral and elongate to stubby in nature, and have been subject to sausseritization along the edges, in cracks, and within cores. They are characterized by albite and Carlsbad twinning, as well as oscillatory zoning, both normal and reverse in character, with the average plagioclase composition ranging from andesine to labradorite, ($An_{32}$ to $An_{52}$). The majority of the elongate plagioclase crystals have been bent and fractured to produce a deviation in the trend of albite twins of an average angle of 5°, and in some thin sections, the crystals are weakly aligned.

Clinopyroxene (and rare orthopyroxene) cores within amphiboles (mainly actinolite), were identified by relict clinopyroxene birefringence, twinning, and in some cases, crystal form, even where they may have anomalous green–pale yellow pleochroism typical of amphibole. Many amphibole crystals cored by clinopyroxene are either partially altered to sericite or replaced by biotite, which is in turn altered to chlorite.

Biotite crystals are subhedral to interstitial and occur along the rims of, or in clusters with, amphibole. Biotite occurs in lesser amounts than amphibole, and some biotite is altered to hematite. Quartz occurs in minor amounts as poikilitic plates.

The order of crystallization (early to late) was apatite, opaque minerals (titanite), clinopyroxene (orthopyroxene), plagioclase, amphibole, biotite, and quartz.

### Tetachuck-north pluton

Subhedral biotite (2–4 mm in size), hornblende (1–4 mm), plagioclase (3–6 mm), and alkali feldspar (1–2.5 mm), subhedral to interstitial quartz, and subhedral, minor apatite, titanite, opaque minerals, and zircon characterize the primary mineralogy for the pluton.

Plagioclase crystals exhibit textures indicating two distinct phases of crystallization with the dominant later phase crystals containing crystals of the earlier phase. The earlier phase of plagioclase crystallization is distinguished by crystals with heavily corroded cores, subhedral crystal forms, and oscillatory zonation which is either normal or reverse in nature. Euhedral crystal forms, albite and Carlsbad twinning, and normal oscillatory zonation characterize the later phase plagioclase crystals. The average plagioclase composition is ($An_{30}$ to $An_{33}$). Alkali feldspar crystals are scattered and subhedral to poikilitic.

Hornblende is euhedral to bladed, glomeroporphyritic, altered along fractures, and commonly exhibits good cleavage and twinning. Biotite crystals are euhedral and partially altered to chlorite. Titanite is subhedral to euhedral and occurs mainly with opaque minerals and biotite.

The order of crystallization (early to late) was apatite, zircon, opaque minerals, titanite, corroded plagioclase cores, hornblende, biotite, later phase plagioclase, alkali feldspar, and quartz.

### Tetachuck-south pluton

The main mineralogy includes clinopyroxene (amphibole; 0.5–1.5 mm) and plagioclase (1–4 mm) with minor opaque minerals, apatite, and titanite.

Plagioclase crystals are euhedral and elongate, and their alteration to sausserite is so pervasive and intense that plagioclase compositions could not be determined. Amphibole (primarily actinolite) crystals are determined to be reaction products as they so completely replace clinopyroxene (and rare orthopyroxene) that relict birefringence and, rarely, crystal shape are all that remain as relics of the original pyroxene crystal. Biotite is uncommon, exhibits interstitial to subhedral crystal forms, and exhibits rare alteration to hematite.

The order of crystallization (early to late) was apatite, opaque minerals (titanite), clinopyroxene (orthopyroxene), plagioclase, amphibole, and biotite.

### Composite Chelaslie Arm pluton

*Chelaslie Arm-1 phase*

The primary mineralogy of the Chelaslie Arm-1 phase is clinopyroxene(2–3 mm in size) and plagioclase (0.75–9 mm) with minor orthopyroxene (0.5–2 mm), apatite, and opaque minerals. Reaction and later stage mineral phases include alkali feldspar (1–3 mm in size), amphibole, biotite (1 mm), and quartz (1 mm).

Plagioclase crystals are either small and stubby, or large and elongate, show minor sausseritization, and are characterized by albite and Carlsbad twinning. The average plagioclase composition in this pluton ranges from andesine to labradorite ($An_{45}$ to $An_{57}$). Alkali feldspar is subhedral to poikilitic.

Clinopyroxene occurs either as crystals rimmed with biotite, or is preserved as cores within amphibole (primarily actinolite). In both cases, the euhedral crystal shape and twinning of the clinopyroxene is almost always evident, and most crystals exhibit good cleavage. Orthopyroxene is much more rare and smaller than clinopyroxene, with the smallest pyroxene crystals more completely replaced by amphibole.

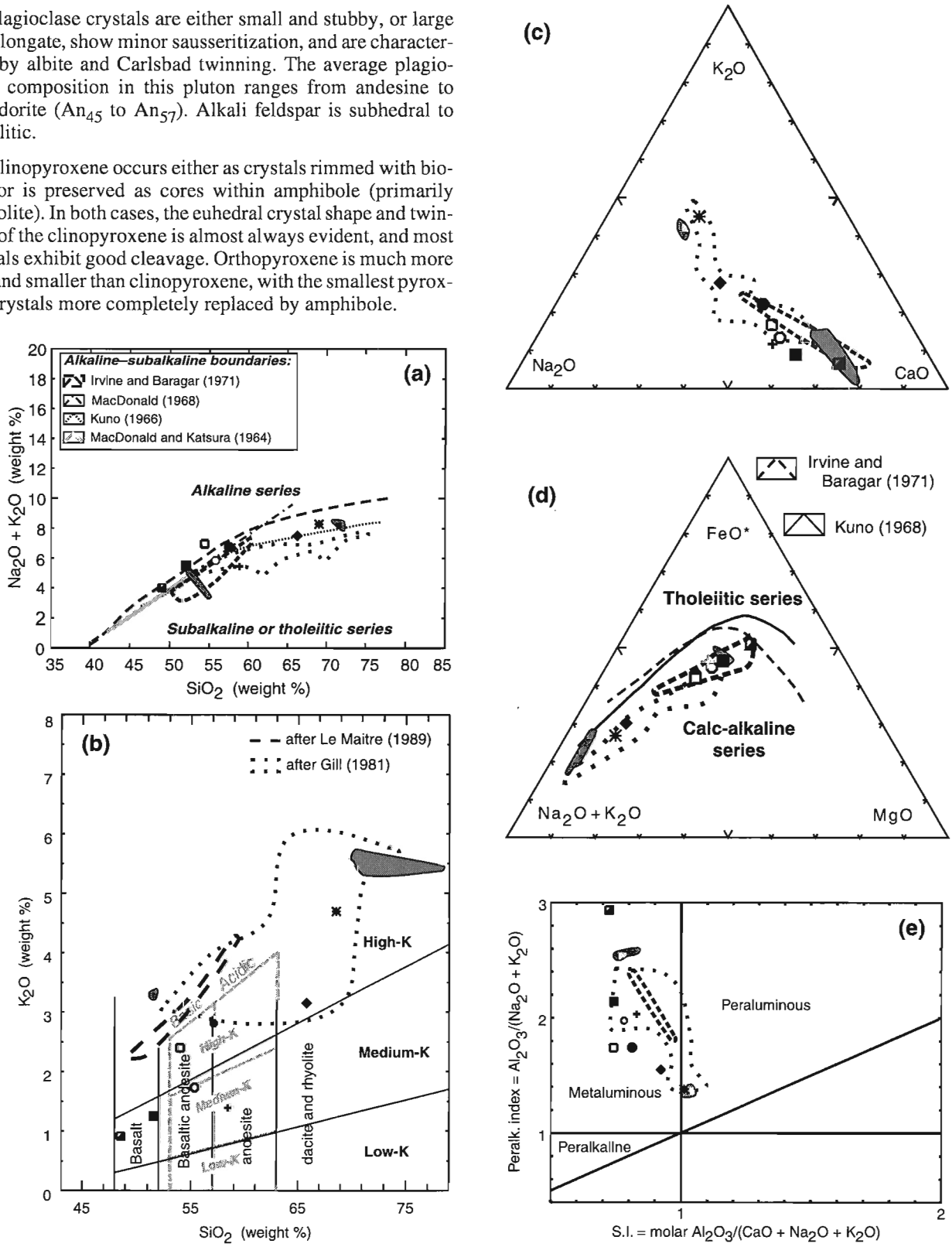


***Figure 13.*** *Summary of geochemical variation within the studied plutons and comparisons to other plutonic suites within the northwestern Nechako River map area (Anderson et al., 1998c):* ***a****) total alkali-silica plot and variety of alkaline-subalkaline divisions;* ***b****) potash-silica plot;* ***c****) $Na_2O$-$K_2O$-CaO ternary plot;* ***d****) alkali-total iron as FeO-magnesia ternary plot and calc-alkaline-tholeiitic divisions;* ***e****) peraluminous-metaluminous (Shand) indices;* ***f****) log Rb - log (Y + Nb) plot of Pearce et al. (1984);* ***g****) Ba-Rb-Sr ternary plot.*

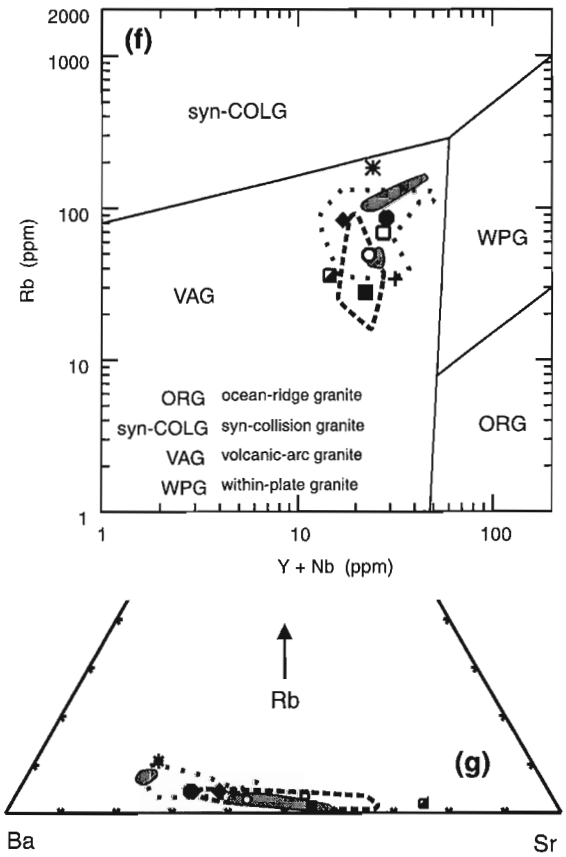


**Legend for Figure 13**

(?)Eocene

Copley Lake pluton (n = 8; NTS 93 F/15)

Chelaslie Arm-2 pluton

✳

Chelaslie Arm-1 pluton

○

●

Tetachuck-south pluton

+

Tetachuck-north pluton

◆

Chelaslie River pluton

□ 601

◪ 603_AVG

■ 606_AVG

Middle Jurassic Stag Lake plutonic suite (NTS 93 F/15)

intermediate phase (n = 17)

mafic phase (n = 4)

Amphibole occurs primarily as a replacement mineral (of orthopyroxene and clinopyroxene) and rarely, as small clusters of acicular actinolite crystals. Epidote alteration is evident along fractures in amphibole crystals and many crystals exhibit incomplete alteration to sericite. Biotite occurs interstitially in clusters around opaque minerals, or as rims around clinopyroxene. Quartz is minor and poikilitic.

The order of crystallization was apatite, opaque minerals, orthopyroxene, clinopyroxene, plagioclase, amphibole, biotite, alkali feldspar, and quartz.

*Chelaslie Arm-2 phase*

Clinopyroxene (surrounded by amphibole; 1 mm), biotite, plagioclase (1–3 mm in size), alkali feldspar (2 mm), quartz (1 mm), and minor orthopyroxene, opaque minerals, and apatite make up this younger phase of the Chelaslie Arm pluton.

Plagioclase (andesine, $An_{36}$ to $An_{43}$) crystals are stubby to elongate and euhedral, are characterized by Carlsbad and albite twinning, and are partially altered to sausserite. Alkali feldspar crystals are subhedral and exhibit minor perthite. Quartz crystals are subhedral to poikilitic in character.

Clinopyroxene occurs as subhedral to euhedral crystals which were incompletely changed to amphibole. Clinopyroxene within the amphibole is recognized by its relict birefringence. Orthopyroxene crystals are very small, subhedral to euhedral, and rare. Amphibole (mainly actinolite) occurs as a replacement of clinopyroxene as in other plutons described above, and in turn was partly replaced by biotite. Biotite is subhedral to poikilitic, mainly occurs as alteration products of amphibole, and is altered to chlorite.

The order of crystallization was apatite, opaque minerals, clinopyroxene (orthopyroxene), plagioclase, alkali feldspar, biotite, and quartz.

## GEOCHEMISTRY

Representative samples from each pluton and constituent phases were collected for geochemical analyses. Powdered samples were prepared at the University of British Columbia using a jaw crusher and a tungsten-carbide mill, and analyzed at the Geochemical Laboratories, Department of Earth and Planetary Sciences, McGill University. Two duplicate samples for each of SCBB98-0603 and SCBB98-0606, and two previously analyzed samples unrelated to the plutons studied were included to test precision and accuracy. The geochemical analyses, the normative mineralogy, and a variety of geochemical affinities for the samples and plutons are listed in Table 2 and plotted in Figure 13a–g. The results for samples SCBB98-0603 and SCBB98-0606 are the averaged compositions from the duplicate analyses.

Samples from all four plutons are mostly subalkaline (Fig. 13a), calc-alkaline (orthopyroxene-normative; Fig. 13d), contain medium to high potassium (Fig. 13b), exhibit volcanic-arc affinities (Fig. 13f), and are calc-alkaline in nature. All samples are metaluminous (clinopyroxene-normative)

except the sample from the Chelaslie Arm-2 phase, which is peraluminous (corundum-normative) (Fig. 13e). The more evolved character of the samples from the Tetachuck-north pluton and Chelaslie Arm-2 phase help distinguish them from the other samples on most variation diagrams; e.g. on the basis of the relative abundances of alkali-alkaline earth elements (Fig. 13c), alkaline-femic major elements (Fig. 13d), and lithophile trace elements (Fig. 13g) and resemble that for the felsic Middle Jurassic Stag Lake and (?)Eocene Copley Lake plutonic suites (Anderson et al., 1998c).

The Tetachuck area pluton samples are generally more alkaline (Fig. 13a) but less potash rich (Fig. 13b, c) than other Middle Jurassic and (?)Eocene plutonic suites studied within the Nechako Plateau (Anderson et al., 1998c; Fig. 13), but otherwise overlap compositions of those suites as represented on conventional variation diagrams.

## CONCLUSIONS

Mineralogical and textural comparisons can be drawn between the biotite-hornblende (clinopyroxene) diorite of Chelaslie River and the Tetachuck-south plutons including composition, fine to medium grain size, hypidiomorphic-granular texture, and calc-alkaline, medium- to high-potassium, metaluminous, and volcanic-arc characteristics. In addition, their mineralogical, textural, petrographic, and geochemical resemblance suggest a possible correlation to the regionally extensive Middle Jurassic Stag Lake plutonic suite to the east (Anderson et al., 1998c). The Chelaslie Arm-2 phase of the composite Chelaslie Arm pluton has some similarities in composition, textures, grain size, and geochemical characteristics with the (?)Eocene Copley Lake plutonic suite to the east (Anderson and Snyder, 1998; Anderson et al., 1997, 1998a, b, c). The Tetachuck-north and Chelaslie-Arm-1 plutons show no unique or comparable geochemical or compositional characteristics which might link them to another plutonic suite recognized within the Nechako NATMAP area. Uranium-lead dating of samples from the Chelaslie River and Tetachuck-north plutons will test some of these correlations.

## ACKNOWLEDGMENTS

We would like to thank Bert Struik for logistical support, leadership, and assistance with the fieldwork. Karen Fallas and Mike Hrudey are thanked for their assistance with the fieldwork, Steve Piercey and Richard Friedman for their help with the preparation of the geochemistry samples, and Liz Hilton is thanked for her assistance with the petrography.

We appreciate the time spent by Bert Struik, whose constructive review of an earlier version of the manuscript hopefully led to a better final version. Stephen Williams' usual skill in the preparation of the digital maps is also gratefully acknowledged. Bev Vanlier is thanked for her digital preparation of the pre-press version of the manuscript.

## REFERENCES

**Anderson, R.G., L'Heureux, R., Wetherup, S., and Letwin, L.**
1997: Geology of the Hallett Lake map area, central British Columbia: Triassic, Jurassic, Cretaceous, and Eocene? plutonic rocks; *in* Current Research 1997-A; Geological Survey of Canada, p. 107–116.

**Anderson, R.G., and Snyder, L.D.**
1998: Jurassic to Tertiary volcanic, sedimentary, and intrusive rocks in the Hallett Lake area, central British Columbia; *in* Current Research 1998-A; Geological Survey of Canada, p. 135–144.

**Anderson, R.G., Snyder, L.D., Resnick, J., and Barnes, E.**
1998a: Geology of the Big Bend Creek map area, central British Columbia; *in* Current Research 1998-A; Geological Survey of Canada, p. 145–154.

**Anderson, R.G., Snyder, L.D., Wetherup, S., Struik, L.C., Villeneuve, M.E., and Haskin, M.**
1998b: Mesozoic to Tertiary volcanism and plutonism in southern Nechako NATMAP area part 1: influence of Eocene tectonics and magmatism on the Mesozoic arc and orogenic collapse: new developments in the Nechako River map area; *in* New Geological Constraints on Mesozoic to Tertiary Metallogenesis and on Mineral Exploration in central British Columbia: Nechako NATMAP Project, (ed.) L.C. Struik and D.G. MacIntyre; Geological Association of Canada, Cordilleran Section, March 27, 1998, Short Course Notes, 26 p.

**Anderson, R.G., Whalen, J.B., Struik, L.C., and Villeneuve, M.E.**
1998c: Mesozoic to Tertiary volcanism and plutonism in southern Nechako NATMAP area part 2: Triassic to Eocene composite intrusions and molybdenum metallogeny: the Endako Batholith redefined; *in* New Geological Constraints on Mesozoic to Tertiary Metallogenesis and on Mineral Exploration in central British Columbia: Nechako NATMAP Project, (ed.) L.C. Struik and D.G. MacIntyre; Geological Association of Canada, Cordilleran Section, March 27, 1998, Short Course Notes, 19 p.

**Diakow, L.J., Webster, I.C.L., Richards, T.A., and Tipper, H.W.**
1997: Geology of the Fawnie and Nechako Ranges, southern Nechako Plateau, central British Columbia (93 F/2, 3, 6, 7); *in* Interior Plateau Geoscience Project: Summary of Geological, Geochemical, and Geophysical Studies, (ed.) L.J. Diakow, J.M. Newell, and P. Metcalfe; Geological Survey of Canada, Open File 3448, p. 7–30 (*also* British Columbia Geological Survey Branch, Open File 1996-2).

**Duncan, R.A.**
1999: Physical and chemical zonation in the Emerald Lake pluton, Yukon Territory; M.Sc. thesis, University of British Columbia, Vancouver, British Columbia, 178 p.

**Gill, J.B.**
1981: Orogenic andesites and plate tectonics; Springer-Verlag, Berlin, 389 p.

**Irvine, T.N. and Baragar, W.R.A.**
1971: A guide to the chemical classification of the common volcanic rocks; Canadian Journal of Earth Sciences, v. 8, p. 523–548.

**Kuno, H.**
1966: Lateral variation of basaltic magma types across continental margins and island arcs; Bulletin Volcanologique, v. 29, p. 195–222.
1968: Differentiation of basalt magmas; *in* Basalts: The Poldervaart Treatise on Rocks of Basaltic Composition, vol. 2., (ed.) H.H. Hess and A. Poldervaart; Interscience, New York, New York, p. 623–688.

**Le Maitre, R.W. (ed.)**
1989: A classification of igneous rocks and glossary of terms, Blackwell, Oxford, England, 193 p.

**MacDonald, G.A.**
1968: Composition and origin of Hawaiian lavas; *in* Studies in Volcanology: A Memoir in Honour of Howel Williams, (ed.) R.R. Coats, R.L. Hay, and C.A. Anderson; Geological Society of America, Memoir 116, p. 477–522.

**MacDonald, G.A. and Katsura, T.**
1964: Chemical composition of Hawaiian lavas; Journal of Petrology, v. 5, p. 83–133.

**Pearce, J.A., Harris, N.B.W., and Tindle, A.G.**
1984: Trace element discrimination diagrams for the tectonic interpretation of granitic rocks; Journal of Petrology, v. 25, p. 956–983.

**Quat, M.B. and Struik, L.C.**
1999: Stratigraphy of the Hazelton Group in southwestern Nechako River map area, central British Columbia; *in* Current Research 1999-E; Geological Survey of Canada.

**Resnick, J., Anderson, R.G., Russell, J.K., Edwards, B.R., and Grainger, N.**
1999: Neogene basaltic flow rocks, xenoliths, and related diabase, northern Nechako River map area, central British Columbia; *in* Current Research 1999-A; Geological Survey of Canada, p. 157–167.

**Struik, L.C. and MacIntyre, D.J.**
1999: Nechako NATMAP Project overview, central British Columbia, year four; *in* Current Research 1999-A; Geological Survey of Canada, p. 79–87.

**Tipper, H.W.**
1963: Nechako River map-area, British Columbia; Geological Survey of Canada, Memoir 324, 59 p.

---

Geological Survey of Canada Project 950036

# Interior Plains and Arctic Canada

# Plaines intérieures et région arctique du Canada

# Rift-related structures in Jurassic and Lower Cretaceous strata near the Canadian polar margin, Yukon Territory, Northwest Territories, and Nunavut

J.C. Harrison, J.H. Wall, T.A. Brent, T.P. Poulton, and E.H. Davies[1]
GSC Calgary, Calgary

*Harrison, J.C., Wall, J.H., Brent, T.A., Poulton, T.P., and Davies, E.H., 1999: Rift-related structures in Jurassic and Lower Cretaceous strata near the Canadian polar margin, Yukon Territory, Northwest Territories, and Nunavut;* in *Current Research 1999-E; Geological Survey of Canada, p. 47–58.*

**Abstract:** Geological and geophysical data from Prince Patrick Island and adjacent areas reveal rift-related sedimentation and deformation in Jurassic and Lower Cretaceous strata of the western Arctic Islands. The syntectonic succession includes offshore marine shale; mixed siliciclastic rocks of shoreface and inner shelf-deltaic associations; fluvial, overbank, and braidplain quartz sandstone; minor coal; and some coarse alluvial deposits. Evidence for as many as eight late Toarcian through Aptian deformational stages is contained in pre-rift and syn-rift strata preserved in a series of grabens and half grabens, and over intervening horst blocks. Transfer faults, including one believed to define the limits of Banks and Eglinton basins in M'Clure Strait, strike west and northwest. Parallelism of normal faults to the local shelf edge is consistent with an extensional origin for the Canadian portion of the polar margin adjacent to the Amerasian Basin.

**Résumé :** Des données géologiques et géophysiques obtenues à l'île Prince Patrick et dans les régions environnantes montrent qu'il y a eu sédimentation et déformation reliées aux rifts dans les strates du Jurassique et du Crétacé inférieur de l'archipel Arctique occidental. La succession syntectonique comporte des shales marins extracôtiers, des roches silicoclastiques mixtes d'associations d'avant-plage et de plate-forme intérieure/delta, des grès quartzeux fluviatiles, de débordement et de plaine anastomosée, un peu de charbon et quelques dépôts alluvionnaires à grain grossier. Les strates antérieures au rifting et contemporaines du rifting qui ont été préservées dans une série de grabens et de demi-grabens et sur les horsts qui les séparent témoignent de jusqu'à huit épisodes de déformation s'échelonnant du Toarcien tardif à l'Aptien. Les failles de décrochement, y compris une faille que l'on croit définir les limites des bassins de Banks et d'Eglinton dans le détroit de M'Clure, ont une direction ouest et nord-ouest. Le parallélisme des failles normales avec le bord local de la plate-forme continentale vient appuyer l'origine par extention de la portion canadienne de la marge polaire adjacente au bassin amérasien.

[1] Mobil Oil Canada, 330-5th Avenue SW, Calgary, Alberta T2P 0L4

## INTRODUCTION

Previous work on the geology and geophysics of the North American polar margin on the Arctic Ocean indicates that (?)Hauterivian and later Cretaceous seafloor spreading within the Amerasian Basin was preceded by an interval of Middle Jurassic through Early Cretaceous rifting (Hubbard et al., 1987; Moore, et al., 1994; Dixon, 1996). This paper describes the local depocentres and high blocks associated with a portion of the mapped rift system between 75°45′N and 77°45′N, and defines the nature and duration of the rift phase and provides new constraints on viable tectonic models for the origin of the adjacent ocean basin.

## PRINCIPAL GEOLOGICAL FEATURES

Upper Triassic through Lower Cretaceous (Albian) strata, lying within the Sverdrup Basin, are present throughout the northeastern Prince Patrick Island region both onshore and beneath the adjacent interisland channels (Fig. 1; Harrison, 1993). Correlative strata have been mapped westwards on seismic profiles beneath unconformable Pliocene cover to the limits of available data (inset, Fig. 1). Four small, Jurassic–Cretaceous intracratonic basins lie southwest of the Sverdrup Basin (Fig. 1, 2). These include Eglinton Basin, the northern part of Banks Basin, M'Clure Strait Basin in the western end of M'Clure Strait, and Tullett Basin (most of which underlies Neogene cover of west-central Prince Patrick Island; inset, Fig. 1). The basins are roughly elliptical in plan and crescent-shaped in cross-section with gently inward-dipping basin fill, the highest beds commonly occurring in the basin centres. Lower Paleozoic basement rocks occur in high blocks between the basins and comprise thermally overmature sandstones of an extensive Middle and Upper Devonian foreland clastic wedge succession (Embry, 1991a) which were deformed into open folds and eroded to a peneplain before basin formation. The region is transected by northerly striking normal faults, horst blocks, and grabens which contain Jurassic and Cretaceous sedimentary rocks.

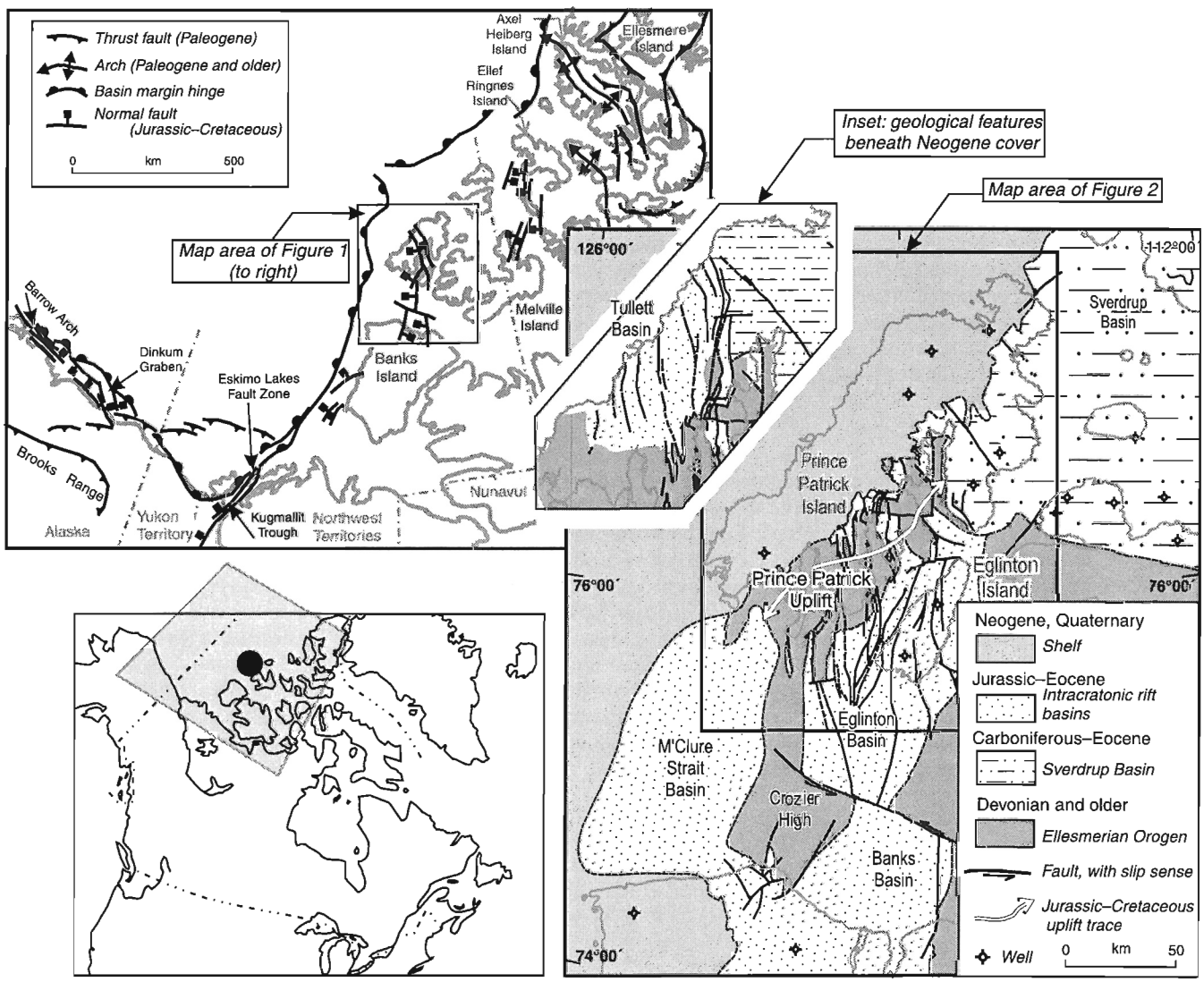


***Figure 1.*** *Regional context for major geological features of the western Canadian Arctic Islands. The inset illustrates some significant features present beneath Neogene cover.*

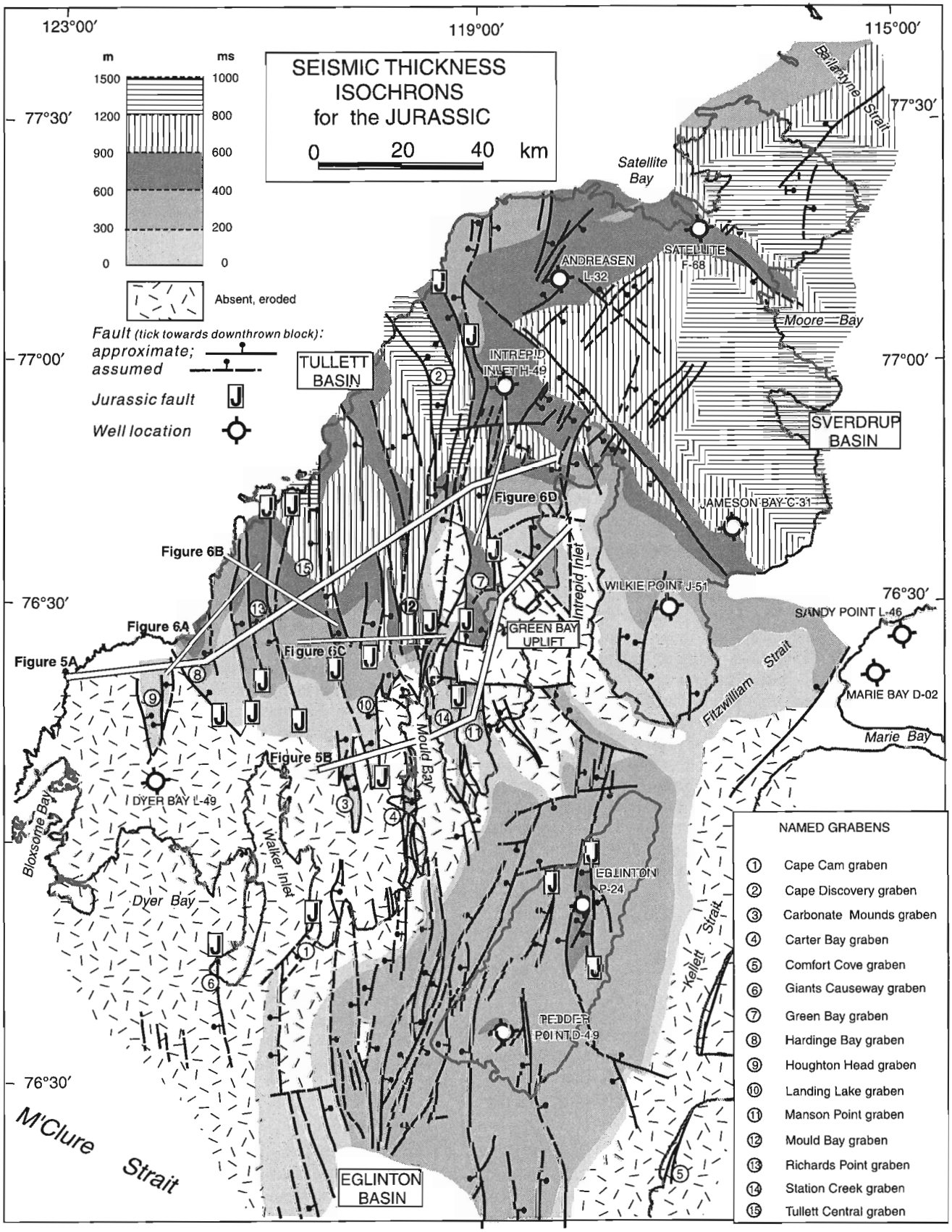


***Figure 2.*** *Seismic thickness isochrons for the Jurassic of Prince Patrick and Eglinton islands area. Contour interval is 200 ms or approximately 300 m at 3 km/s two-way travel time.*

Unconsolidated Pliocene sand and gravel form an unconformable blanket above deformed Cretaceous and older rocks throughout the western half of Prince Patrick Island (Fig. 1).

In this account we abandon the term "Eglinton Graben", first proposed by Thorsteinsson and Tozer (1960), in order to distinguish this feature from the array of small, locally developed half grabens and to underscore the geological similarities shared by Eglinton Basin and the three other intracratonic basins within the region. Eglinton Basin is aligned with the long axis of Eglinton Island (Fig. 1); however, the full extent of the basin is defined by seismic profiles acquired in adjacent interisland channels. Basin fill is up to 900 m thick and features sediments of Lower Jurassic (Toarcian) through Upper Cretaceous (upper Campanian) age. Eglinton Basin terminates southward in M'Clure Strait. Regional gravity and some seismic data are interpreted to indicate that the southern and northern limits, of Eglinton and Banks basins, respectively, may coincide with a northwesterly striking sinistral transcurrent fault located in midchannel. To the west, on the opposite side of a Devonian high block, is M'Clure Strait Basin, a structure mostly outlined by gravity data. Seismic profiles acquired over the northern edge of the basin, south of Prince Patrick Island, are interpreted to feature at least 600 m of faulted (?)Cretaceous strata.

Tullett Basin is separated from M'Clure Strait Basin by a Devonian high block located beneath southern Prince Patrick Island and from Eglinton Basin by the northeast-trending Prince Patrick Uplift (Fig. 1, 2). Exposed within the uplift are Devonian basement rocks, erosional remnants of at least seven Jurassic–Cretaceous grabens and numerous other faulted Jurassic outliers. The grabens and horst blocks of Prince Patrick Uplift continue to the south into the western margin of Eglinton Basin and, to the north, extend across the centre of Tullett Basin. Strata of Prince Patrick Uplift and Tullett Basin range from Carnian through Albian and account for up to 1500 ms (ca. 2300 m) of section on seismic profiles acquired over the eastern part of the basin. However, stratigraphic evidence indicates that the fault system responsible for the horst and graben system running through these intracratonic basins was inactive prior to the Late Toarcian.

## JURASSIC STRATA OF THE WESTERN ARCTIC ISLANDS

### *Correlation and biostratigraphy*

Measured outcrop sections have been correlated to wells and seismic profiles (Fig. 2) using standard lithostratigraphic, well-log, and synthetic seismogram methods. These correlations are supported by local and regional studies of ammonites, bivalves, foraminifera, and dinoflagellates.

Ammonite collections were first made on Prince Patrick Island during exploration voyages (Haughton *in* M'Clintock, 1857). Subsequent work throughout Sverdrup Basin allowed recognition of at least 22 discrete ammonite and four bivalve (*Buchia*) assemblages representing every stage of the Jurassic in marine facies, possibly including the Hettangian (Frebold, 1957, 1958, 1960, 1961, 1975; Tozer and Thorsteinsson, 1964; Jeletzky, 1966, 1973, 1984; Poulton, 1994, T.P. Poulton, unpub. data, 1993, 1998). These assemblages, which include some undescribed taxa and previously unreported occurrences (Fig. 3), are plotted against standard Boreal and Subboreal zones, adapted from Cope et al. (1980a, b), Sei and Kalacheva (1993), Callomon (1994), and Rostovtsev and Prozorowsky (1997). The Arctic Canada *Buchia* zones have been adjusted to partially reflect ages provided by ammonites in Greenland and Siberia (i.e. Surlyk and Zakharov, 1982).

The foraminiferal subdivisions are primarily based on collections obtained from outcrop sections of western Axel Heiberg Island and more distal surface and subsurface sections of eastern Axel Heiberg and west-central Ellesmere islands (Fig. 3; Wall, 1983; J.H. Wall, unpub. data, 1993, 1998; Basov et al., 1992). The same assemblages are recognizable in sequences representing the basin margin on Prince Patrick (Fig. 4) and western Melville islands but are generally less diverse there than those from the basin centre. The Late Hettangian–Sinemurian foraminiferal assemblage (with *Glomospira perplexa* Franke as nominate component) has not been encountered in the predominantly deltaic rocks of this age in the eastern Arctic Islands. The assemblage is defined by collections from two outcrop sections of the Grosvenor Island Formation near Cape Canning on Prince Patrick Island (locality 16 on Fig. 4) and from two well intersections (Jameson Bay C-31 and Satellite F-68). Associated ammonites in the outcrop sections include *Coroniceras* sp. (Early Sinemurian) and *Echioceras* sp. (Late Sinemurian). *Glomospira perplexa* (and several associated fauna) has been obtained from beds tentatively identified as Hettangian from the South Barrow Test Well No. 3 in northern Alaska by Tappan (1955, chart 1 facing p. 26 and p. 27).

The dinoflagellate zonation derives from the original "Oppel-zonation" of Davies (1983) and subsequent revisions in a series of palynological studies by E.H. Davies on outcrop sections and exploration wells, most notably from the thicker Jurassic intervals of the central Sverdrup Basin (Fig. 3). Correlation to the Jurassic time scale is based on similarities of the Canadian Arctic microflora to dinoflagellate assemblages of the North Sea region and western Europe. Two new zones are now recognized in the Sinemurian and lower strata of Prince Patrick Island. The (?) Upper Hettangian and Lower Sinemurian is represented by *Dapcodinium priscum* in association with other newly discovered species of *Dapcodinium, Hebecysta?,* and *Valvaedinium.* The Upper Sinemurian is represented by newly discovered species of *Dapcodinium, Hebecysta?, Leuhendia,* and *Nannoceratopsis.*

### *Seismic units*

Correlated seismic horizons include 1) the top of the Intrepid Inlet Member (about top Pliensbachian) which is 175 ms above the base of the Jurassic of northeasternmost Prince Patrick Island, 2) the top of the Sandy Point Formation (top Aalenian), 3) the top of the upper Hiccles Cove Formation

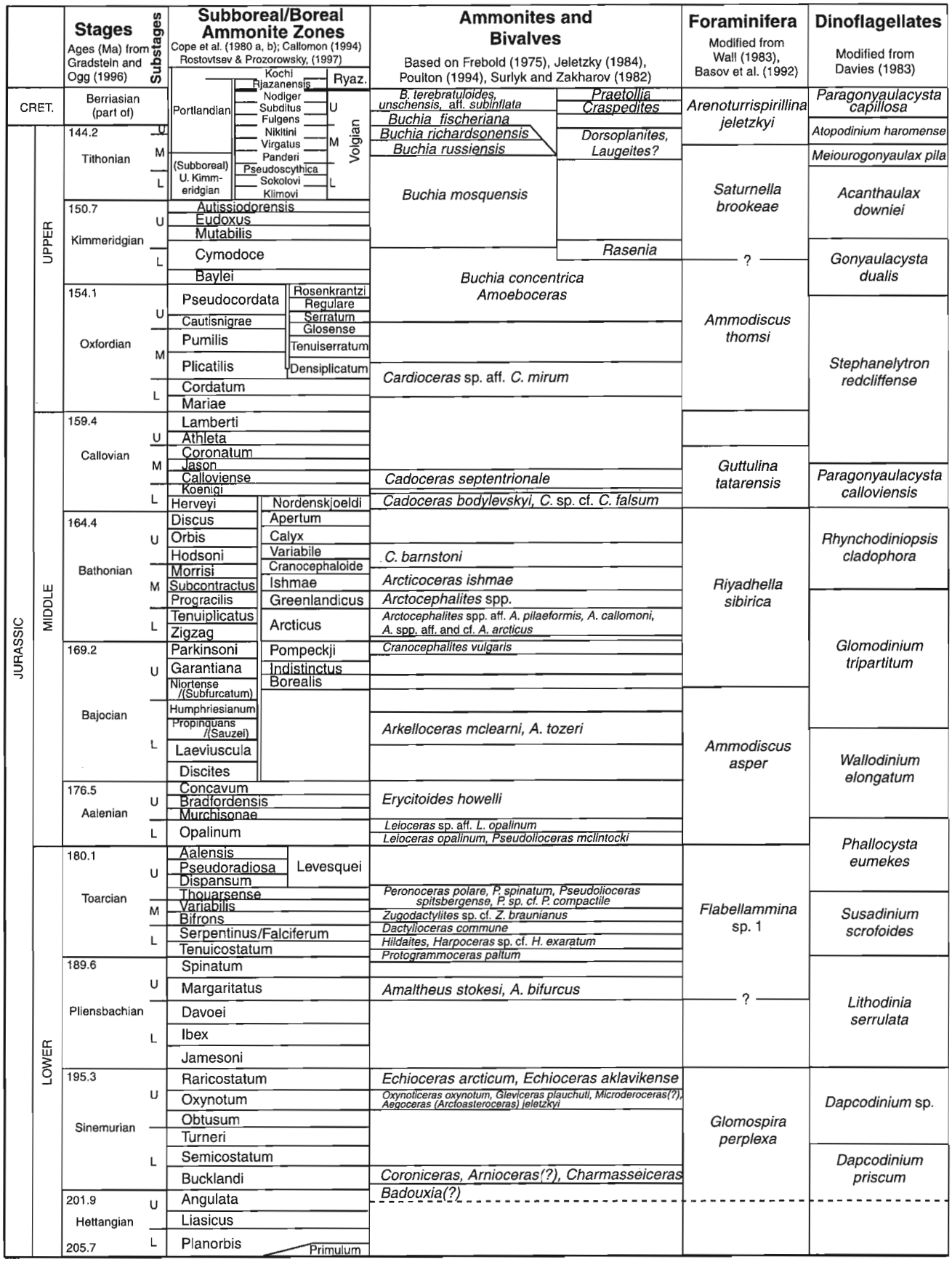


***Figure 3.*** *Correlation of boreal Jurassic biozones. Ryaz.=Ryazianian*

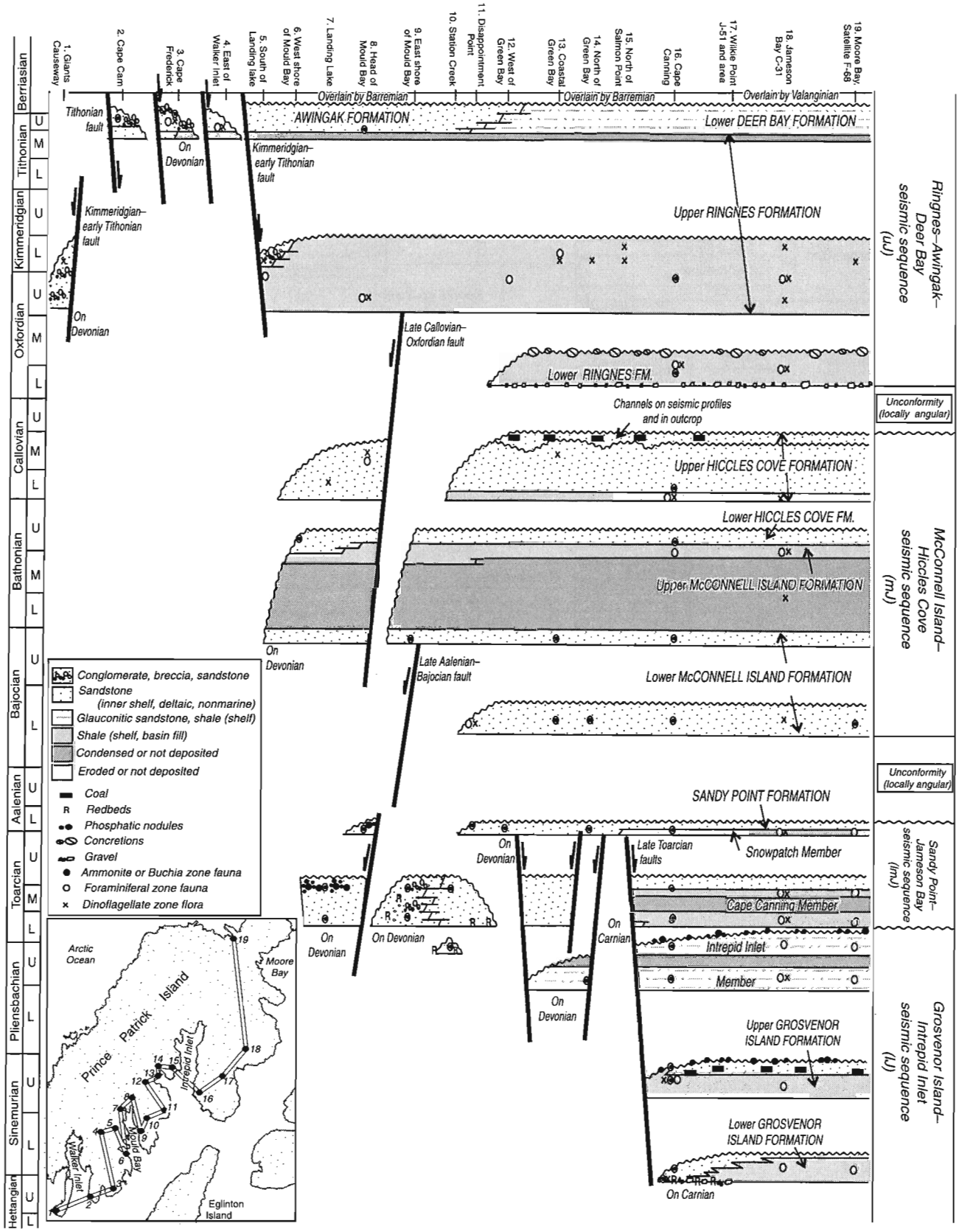


***Figure 4.*** *Correlation of Jurassic strata and associated deformation features of Prince Patrick Uplift and the western Sverdrup Basin on Prince Patrick Island. Age range of displayed rock units are provided by the known range of the locally collected ammonite and/or bivalve zone fauna. Intervals of nondeposition (condensed and eroded intervals) are indicated wherever zone fauna are missing. Duration of nonmarine sediment accumulation is debatable, and it is likely that a more complete record of the Jurassic is present north of Cape Canning (locality 16) on the line of profile.*

(top Callovian), 4) the top of the Deer Bay Formation (Valanginian) in the northeast which seismically correlates with the top of the Awingak Formation (Tithonian) in the southwest, and 5) the base of the Neogene.

The intervals between the correlated reflectors are regionally mappable seismic sequences (Fig. 4) distinguished by internal seismic features (seismic depositional facies). For example, weak, more or less continuous parallel reflections for the Lower Jurassic shale units below the Intrepid Inlet Member are clearly separable from parallel discontinuous reflections that increase in frequency and amplitude upsection in the overlying progradational Sandy Point–Jameson Bay sequence. The quartz sandstone-dominated McConnell Island–Hiccles Cove sequence has locally developed seismic channels and several high-amplitude continuous reflectors in the upper part. This interval is also capped by a high-amplitude continuous reflector where it is overlain by organic-rich shale of the lower Ringnes Formation. The Ringnes–Awingak sequence (deltaic sandstone, minor shale) is mostly devoid of internal reflections but is characterized by short discontinuous reflection segments where the correlative Deer Bay Formation (marine shelf sandstone and shale) is present in the northeast. The overlying Lower Cretaceous interval (braidplain sandstone and coal overlain by marine shale) is distinguished by numerous discontinuous reflection segments of variable amplitude.

### *Distribution and thickness variations*

General features of the Jurassic strata within the report area are summarized on a seismic isochron thickness map and two simplified structural cross-sections (Fig. 2, 5). The thickness of the Jurassic succession reflects three distinct tectonic phases. Regional thinning of the entire Jurassic succession from northeastern to southwestern Prince Patrick Island is attributed to erosion of pre-Aalenian depositional sequences beneath younger strata imposed on a pattern of declining subsidence rate with distance from the centre of the Sverdrup Basin. Likewise, the Lower Jurassic thins progressively to the southwest by basin margin onlap and younging of units lying on Devonian basement.

Seismic isochron contours also show regional thinning towards the northwest across northeastern Prince Patrick Island (Fig. 2). Cospatial with the location of this change are two southeastward-plunging, narrow faulted anticlines and two broad regional synclines. Fold axial traces are not shown on the isochron map, however, the anticlines were tested, unsuccessfully, by the Intrepid Inlet H-49 and Satellite F-68 wells. The intervening and adjacent synclines lie to the northeast. Regional considerations indicate that these and other smaller folds are likely the product of southwesterly directed compressive deformation during the Cenozoic. Closures within regional anticlines, and in similar contraction features of smaller size, were a common target for exploratory drilling

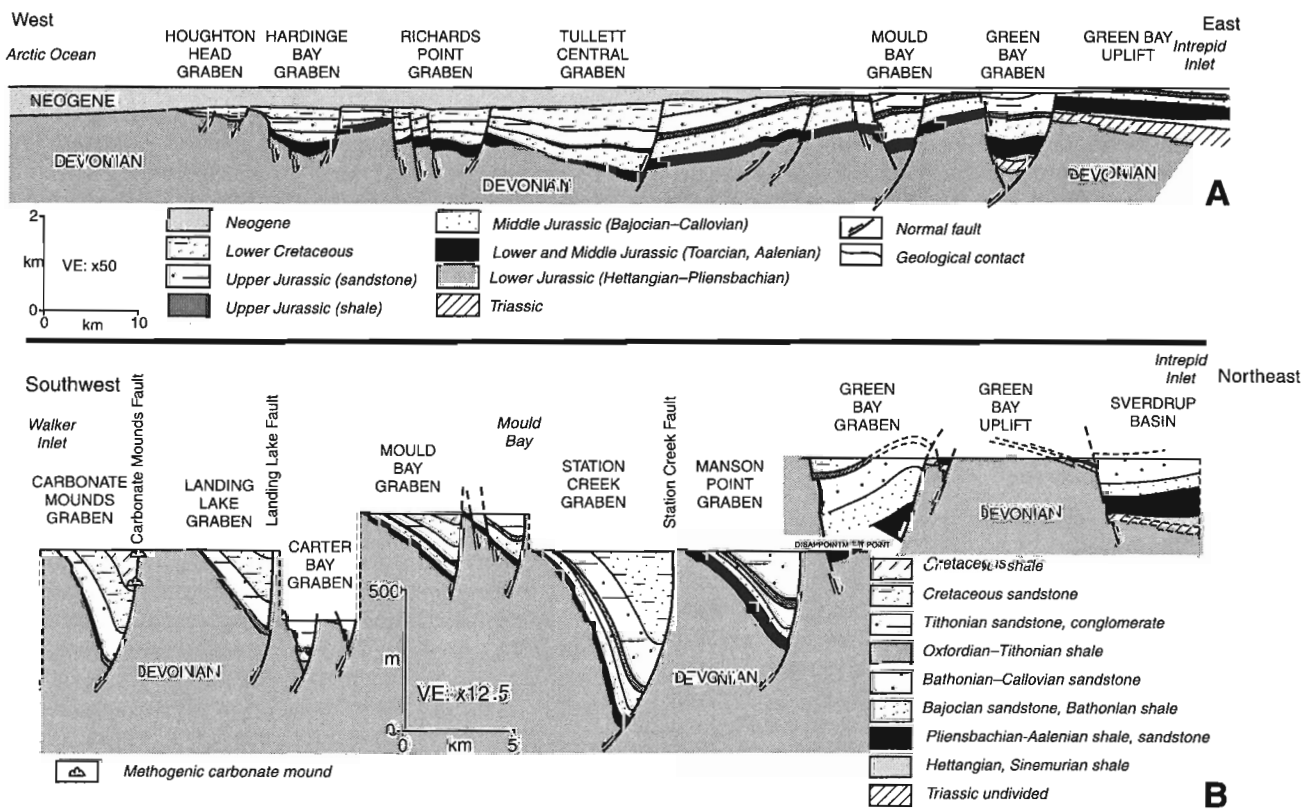


***Figure 5.*** *Simplified structural cross-sections of Tullett Basin and Prince Patrick Uplift.*

in the Mesozoic rocks of the western Arctic Islands (i.e. Jameson Bay C-31); however, results within the study area were not encouraging.

Other local variations in the thickness of the Jurassic succession within the study area, especially those observed within the mapped fault array, are the product of differential sediment accumulation and/or footwall uplift during various stages of fault movement in the Middle and Late Jurassic. There is also evidence, provided by seismic profiles and bedrock mapping, for Early Cretaceous and pre-Neogene stages of slip. The nature of each stage of extensional deformation is summarized below.

## *Deformation history*

### Pre-Jurassic rift strata

The oldest strata predating the Jurassic rift phase on Prince Patrick Island comprise thin, transgressive oolitic sandstone beds that lie unconformably above Carnian limestones east of Intrepid Inlet (Fig. 4). These contain (?) Late Hettangian and Early Sinemurian *Badouxia*(?), *Coroniceras* sp., and *Arnioceras*(?) sp. and are, tentatively, correlated with the lower part of the Grosvenor Island Formation which contains various Late Hettangian and Sinemurian foraminifera, including *Ammodiscus siliceus* (Terquem) and *Glomospira perplexa* Franke. Above the basal oolite are greenish-grey shale beds of the upper Grosvenor Island Formation which contain Sinemurian dinoflagellates and foraminifera, and an ammonite assemblage that includes *Echioceras arcticum* Frebold, *Echioceras* sp., *Cenoceras* sp., and *Gleviceras*(?) sp. of Late Sinemurian age. Also assigned to the pre-rift succession are glauconitic sandstone and phosphatic shale of the Intrepid Inlet Member (of the Jameson Bay Formation) with a Pliensbachian macrofauna including *Amaltheus* sp. and an indeterminate form resembling *A. stokesi*. The highest pre-rift beds are shale, with minor cemented sandstone and pebble conglomerate of the Cape Canning Member. These beds carry Early Toarcian ammonites especially *Pseudolioceras* sp. aff. *compactile* (Simpson) and *Dactylioceras* sp. aff. *commune* (Simpson).

### Rift phase

*Stage 1: Late Toarcian*

The oldest structural disturbance, potentially associated with the onset of the Jurassic rift phase, features uplift and erosion of the Jameson Bay Formation (Intrepid and Cape Canning members) prior to deposition of overlapping nearshore marine quartz sandstone of the Sandy Point Formation on Green Bay Uplift (Fig. 2) but differential preservation of Jameson Bay rocks in grabens to the southwest. Seismically defined normal faults may also have been active during this interval, for example, within Hardinge Bay graben (Fig. 5; in unit lmJ on Fig. 6A). The termination of this first stage of local uplift is provided by macrofauna in the overlapping Sandy Point Formation including Early Aalenian *Pseudolioceras m'clintocki* (Haughton).

*Stage 2: Late Aalenian and Early Bajocian*

Geophysical profiles indicate widespread development of normal faults throughout Tullett Basin during the Late Aalenian to the mid-Early Bajocian. This resulted in differential preservation of the Sandy Point–Jameson Bay seismic sequence in the downthrown hanging wall of normal faults associated with Hardinge Bay, Richards Point, Tullett Central, and Landing Lake grabens, and local angular unconformities over and adjacent to various high blocks (Fig. 5, 6A–C). Some of these faults terminate below the McConnell Island–Hiccles Cove sequence (unit mJ) which, on Prince Patrick Uplift, contains a mid-Early Bajocian macrofaunal assemblage at the base including *Arkelloceras tozeri* Frebold, *Arkelloceras* sp., *Retroceramus* sp., and *Camptonectes* sp.

*Stage 3: Mid-Bajocian through Callovian*

Indirect evidence for deformation during this interval includes preservational limits for strata that shift from northwesterly trending in the Aalenian (i.e. parallel to the Sverdrup Basin margin) to northerly trending and parallel to many of the mapped faults (Fig. 2) during the Bajocian and Bathonian. Strata of these ages are found throughout Eglinton Basin and may be preserved as far south as central Banks Basin (Miall, 1979). Locally divergent seismic reflectors and growth faults occur within the McConnell Island–Hiccles Cove seismic sequence of Green Bay and Landing Lake grabens (Fig. 5, 6C, D). Additional evidence for erosional unroofing is provided by braidplain sandstone channels identified in outcrops of the upper Hiccles Cove Formation and seismically defined channels that occur within the upper part of the same sequence (unit mJ on Fig. 6B).

Timing of events during this interval is provided by the occurrence, for example, of *Cranocephalites vulgaris* Spath (latest Bajocian) and *Arctocephalites* sp. indet. (Early Bathonian) in the lower McConnell Island Formation of Carter Bay graben west of Mould Bay; Late Bathonian *Arcticoceras ishmae* (Keyserling) in the lower Hiccles Cove Formation, and *Cadoceras* sp. cf. *C. bodylevskyi* Frebold (Early Callovian) in the upper Hiccles Cove Formation east of Intrepid Inlet.

*Stage 4: Callovian through Early Oxfordian*

Constraints on the duration of deformation during this interval are provided by the erosion of Callovian and older sandstone and subsequent onlap by upper Lower Oxfordian and younger marine shale (Ringnes Formation). Evidence for tectonism prior to deposition of the Ringnes Formation is widespread throughout both Tullett Basin and Prince Patrick Uplift. Examples include evidence for erosion of the entire Callovian part of the Hiccles Cove Formation in Station Creek graben (locality 9, Fig. 4), differential preservation of the same Callovian portion of the Hiccles Cove Formation below Ringnes Formation in grabens west and north of Mould Bay localities 6 to 8), sub-Ringnes channelling, and local angular unconformity above the McConnell Island–Hiccles Cove sequence (unit mJ) on seismic profiles of Hardinge Bay, Richards Point, Tullett Central, and Landing Lake grabens (Fig. 5, 6A–D).

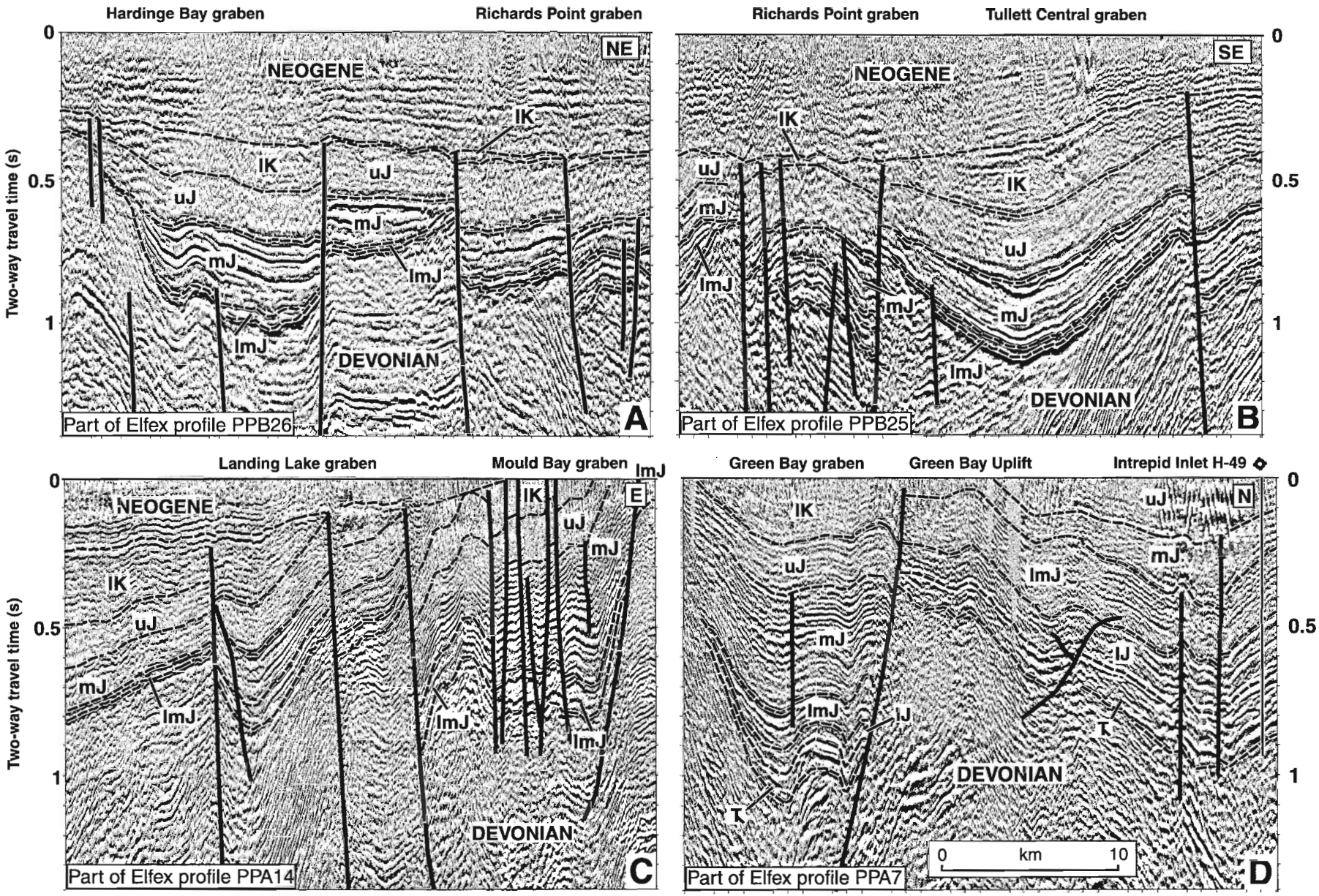


***Figure 6.*** *Representative seismic profiles of Tullett Basin, subsurface western Prince Patrick Island. Lines of profile are located on Figure 2. Abbreviations: Tr: Upper Triassic; lJ: Lower Jurassic ((?)Hettangian to Pliensbachian); lmJ: Lower and Middle Jurassic (Toarcian, Aalenian); mJ: Middle Jurassic (Bajocian–Callovian); uJ (Oxfordian–Tithonian); lK: Lower Cretaceous.*

Timing constraints are provided by macrofauna and foraminiferal assemblages collected locally from the overlapping Ringnes Formation. These include *Cardioceras* sp. (Early Oxfordian) and *Amoeboceras* sp. (Late Oxfordian to Early Kimmeridgian) east of Intrepid Inlet, and *Ammodiscus thomsi* Chamney with associated microfauna (Oxfordian–Kimmeridgian) around Mould Bay and elsewhere on southern Prince Patrick Island.

*Stage 5: Early to mid-Kimmeridgian*

Evidence for deformation during this interval is circumstantial and limited. Clast-supported gravel and pebble conglomerate units in Landing Lake graben, and boulder beds in Giants Causeway graben, are interbedded with marine shale of the Ringnes Formation. The coarser sediments are interpreted as deltaic channel-fill deposits of potential syntectonic origin. However, distance of transport may be significant as clasts (Devonian sandstone and chert) are mostly subrounded. The shale units contain Early to Middle Kimmeridgian dinoflagellates and *Ammodiscus thomsi* assemblage foraminifera (Oxfordian–Kimmeridgian).

*Stage 6: Tithonian*

Cobble conglomerate and breccia occur with variously well rounded to angular clasts of locally derived Devonian sandstone in the Awingak Formation in Cape Cam graben. Similar cobble conglomerate units are interbedded with marginal marine sandstone and minor shale of the Awingak Formation in Comfort Cove graben on southwestern Melville Island (Harrison, 1995). Diagnostic assemblages include *Buchia russiensis* and related Early to Middle Tithonian fauna at Comfort Cove, and probable Late Tithonian bivalves, including *Buchia fischeriana?* (d'Orbigny) at Cape Cam and nearby at Cape Frederick.

*Stage 7: Berriasian to Hauterivian*

Differential preservation of the mostly Upper Jurassic Ringnes–Awingak–Deer Bay sequence below unconformable cover of Lower Cretaceous Isachsen Formation (Barremian–Aptian), including the correlative seismic units, supports an inference of rift-related fault motion during the Berriasian through Hauterivian depositional hiatus. This evidence has been acquired from seismic profiles of northern Eglinton Island within central Eglinton Basin, from surface sections on Prince Patrick Uplift, and from seismic profiles over Houghton Head, Hardinge Bay, and Richards Point grabens in Tullett Basin. Both locally and regionally the Lower Cretaceous oversteps the Jurassic and rests directly on the Devonian.

*Stage 8: Barremian to Aptian*

The highest widespread occurrence of rift-related faulting and record of associated deposition occurs in the Lower Cretaceous Isachsen Formation. Features include differential preservation of Isachsen Formation sandstone and the equivalent seismic interval (unit lK) in the hanging wall of normal faults in Eglinton and M'Clure Strait basins, and various grabens of Prince Patrick Uplift and Tullett Basin (Fig. 5, 6). Age of these strata is provided by Barremian dinoflagellates and other microflora collected from the lower and medial part of the Isachsen Formation in Station Creek graben. Braidplain gravels of potential syntectonic origin also occur in the uppermost preserved part of the Isachsen Formation in Station Creek graben where microflora are Barremian to Aptian. Syntectonic conglomerate and differentially preserved Lower Cretaceous strata have been documented from northern Banks Basin (Miall, 1979) and on southeastern Melville Island (Goodarzi et al., 1994; Harrison, 1995).

## REGIONAL TECTONIC IMPLICATIONS

The basins and uplifts, horsts, and grabens documented in the present account are part of a Jurassic and Lower Cretaceous rift system that extends from the Prince Patrick Island area southwestwards across Banks Island to the eastern Mackenzie Delta region. Rift-related structures of similar age are documented by wells and are interpreted on seismic profiles in the offshore north of Alaska.

Features tectonically active in the Jurassic included Storkerson Uplift of western Banks Island (Miall, 1979). This structure was probably continuous with Crozier High (west of Eglinton Basin; Fig. 1) prior to the Albian. Banks Basin, presently understood from surface geology, exploratory wells, and potential-field data, may have offered a continuous marine connection to the south during the Upper Jurassic (Miall, 1979). Seismic profiles are numerous in the area but an interpretation has not been published.

Deltaic, nearshore and outer shelf sandstone units containing a continuous ammonite and bivalve biochronology for the Jurassic, are preserved in various formations exposed throughout northern Yukon Territory (up to 1300 m thick; Poulton (1997) and references therein), and by well penetrations in the Mackenzie Delta area of the Northwest Territories (Dixon, 1996). Provenance areas are indicated southeast of the Eskimo Lakes fault zone which was likely active at this time (Dixon, 1996; Poulton, 1997). Seismically defined, syn-rift, Lower Jurassic through Lower Cretaceous rocks are also interpreted to represent the fill in the northeasterly trending Kugmallit Trough in the eastern Mackenzie Delta (Lane and Dietrich, 1995).

A northerly provenance for the Jurassic section (about 300–1200 m thick) in northern Alaska is indicated by various shelf sand units encountered in wells along the southern flank of Barrow Arch. Likewise, evidence for an ancestral rift phase commencing in the Jurassic along the north Alaskan margin is provided by seismic profiles over Dinku graben (Hubbard et al., 1987). Although the Jurassic–Neocomian succession (up to 3500 m thick) in the graben has not been penetrated by exploration wells, a Lower and lower Middle Jurassic pre-rift interval is interpreted to be overlain by a syn-rift Bathonian to sub-Hauterivian succession (Hubbard et al., 1987).

The extent of the rift system north of Prince Patrick Island is unknown. The mapped faults (Fig. 2) continue northward off the existing seismic profiles and it would appear likely

that similar structures should be encountered on the Arctic continental shelf and on the submerged portions of the Sverdrup Rim northwest of the Sverdrup Basin. Likewise, an array of northeasterly striking extension faults were active, and gabbro dykes and other mafic and halokinetic intrusive bodies were emplaced in the (?)Jurassic and Lower Cretaceous throughout the central and western Sverdrup Basin (Harrison, 1995). Indirect evidence for tectonic elevation of the Sverdrup Rim during the Jurassic is provided by Bajocian–Bathonian sandstone of distant northwestern provenance in exploratory wells of western Ellef Ringnes Island (Embry, 1991b).

## CONCLUSIONS

1. Jurassic and Lower Cretaceous rift-related structures in the western Arctic Islands are part of a rift system of comparable age that is parallel and close to the present Arctic continental margin and is traceable southwards to the Mackenzie Delta region. Similar structures exist along the same plate margin north of Alaska.
2. Rifting began not earlier than the Late Toarcian. As many as eight pre-Albian rift stages are indicated by field and subsurface data, with local age constraints provided by diagnostic shelly macrofauna, foraminifera, and dinoflagellate assemblages.
3. Normal faults in the rift zone are parallel to the adjacent continental margin, and transcurrent faults are more or less perpendicular to this margin. These observations are consistent with plate tectonic models that require extension perpendicular to the Canadian portion of the continental margin during ocean-floor spreading in the Amerasian Basin.

## ACKNOWLEDGMENTS

The authors would like to thank Finn Surlyk (University of Copenhagen), and Bob Anderson and Ashton Embry (Geological Survey of Canada) for their thorough and valuable review comments. Drafting was completed with the help of Peter Neelands and David Sargent.

## REFERENCES

**Basov, V.A., Wall, J.H., Sokolov, A.R., Yakovlev, S.P., Poulton, T.P., and Embry, A.F.**
1992: The *Riyadhella sibirica* foraminiferal zone in the Middle Jurassic of northern Russia and Canada; Abstracts International Conference on Arctic Margins, Anchorage, Alaska, p. 63.

**Callomon, J.H.**
1994: Jurassic ammonite biochronology of Greenland and the Arctic; Geological Society of Denmark, Bulletin 41, p. 128–137.

**Cope, J.C.W., Duff, K.L., Parsons, C.F., Torrens, H.S., Wimbledon, W.A., and Wright, J.K.**
1980a: A correlation of Jurassic rocks in the British Isles, Part 2, Middle and Upper Jurassic; Geological Society of London, Special Report 15, 109 p.

**Cope, J.C.W., Getty, T.A., Howarth, M.K., Morton, N., and Torrens, H.S.**
1980b: A correlation of Jurassic rocks in the British Isles, Part 1, Introduction and Lower Jurassic; Geological Society of London, Special Report 14, 73 p.

**Davies, E.H.**
1983: The dinoflagellate Oppel-zonation of the Jurassic-Lower Cretaceous sequence in the Sverdrup Basin, Arctic Canada; Geological Survey of Canada, Bulletin 359, 59 p.

**Dixon, J.**
1996: Geological atlas of the Beaufort-Mackenzie area; Geological Survey of Canada; Miscellaneous Report 59, 173 p.

**Embry, A.F.**
1991a: Middle-Upper Devonian clastic wedge of the Arctic Islands; *in* Chapter 10, Geology of the Innuitian Orogen and Arctic Platform of Canada and Greenland, (ed.) H.P. Trettin; Geological Survey of Canada, Geology of Canada, no. 3, p. 263–279 (*also* Geological Society of America, The Geology of North America, v. E).
1991b: Mesozoic history of the Arctic Islands; *in* Chapter 14, Geology of the Innuitian Orogen and Arctic Platform of Canada and Greenland, (ed.) H.P. Trettin; Geological Survey of Canada, Geology of Canada, no. 3, p. 369–433 (*also* Geological Society of America, The Geology of North America, v. E).

**Frebold, H.**
1957: The Jurassic Fernie Group in the Canadian Rocky Mountains and Foothills; Geological Survey of Canada, Memoir 287, 197 p.
1958: Stratigraphy and correlation of the Jurassic in the Canadian Rocky Mountains and Foothills; *in* Jurassic and Carboniferous of Western Canada, (ed.) A.J. Goodman; John Andrew Allan Memorial Volume, American Association of Petroleum Geologists, p. 10–26
1960: The Jurassic faunas of the Canadian Arctic, Lower Jurassic and lowermost Middle Jurassic ammonites; Geological Survey of Canada, Bulletin 59, 33 p.
1961: The Jurassic faunas of the Canadian Arctic, Middle and Upper Jurassic ammonites; Geological Survey of Canada, Bulletin 74, 43 p.
1975: The Jurassic faunas of the Canadian Arctic, Lower Jurassic ammonites, biostratigraphy and correlations; Geological Survey of Canada, Bulletin 243, 35 p.

**Goodarzi, F., Harrison, J.C., and Wall, J.H.**
1994: Stratigraphy and petrology of Lower Cretaceous coal, southeastern Melville Island, District of Franklin, Arctic Canada; *in* The Geology of Melville Island, Arctic Canada, (ed.) R.L. Christie and N.J. McMillan; Geological Survey of Canada, Bulletin 450, p. 229–245.

**Gradstein, F.M. and Ogg, J.**
1996: A Phanerozoic time scale; Episodes, v.19, p. 3–5, 26 (chart).

**Harrison, J.C.**
1993: Geology of Prince Patrick and Eglinton islands, Canadian Arctic Archipelago; Geological Survey of Canada, Open File 2654, scale 1:125 000 (five sheets).
1995: Melville Island's salt-based fold belt, Arctic Canada; Geological Survey of Canada, Bulletin 472, 331 p.

**Hubbard, R.J., Edrich, S.P., and Rattey, R.P.**
1987: Geologic evolution and hydrocarbon habitat of the "Arctic Alaska microplate"; *in* Alaskan north slope geology, (ed.) I. Tailleur and P. Weimer; The Pacific Section of Society of Economic Paleontologists and Mineralogists and The Alaskan Geological Society, v. 2, p. 797–830.

**Jeletzky, J.A.**
1966: Upper Volgian (latest Jurassic) ammonites and buchias of Arctic Canada; Geological Survey of Canada, Bulletin 128, 51 p.
1973: Biochronology of the marine boreal latest Jurassic Berriasian and Valanginian in Canada; *in* The Boreal Lower Cretaceous, (ed.) R. Casey and P.F. Rawson; Geological Journal, Special Issue 5, p. 41–80.
1984: Jurassic-Cretaceous boundary beds of western and Arctic Canada and the problem of the Tithonian-Berriasian stages in the Boreal Realm; *in* Jurassic-Cretaceous biochronology and paleogeography of North America, (ed.) G.E.G. Westermann; Geological Association of Canada, Special Paper 27, p. 175–255.

**Lane, L.S. and Dietrich, J.R.**
1995: Tertiary structural evolution of the Beaufort Sea-Mackenzie Delta region, Arctic Canada; Bulletin of Canadian Petroleum Geology, v. 43, p. 293–314.

**M'Clintock, F.L.**
1857: Reminiscences of Arctic ice travel in search of Sir John Franklin and his companions; Journal of the Royal Society, Dublin, v. 1, p. 183–280.

**Miall, A.D.**
1979: Mesozoic and Tertiary geology of Banks Island, Arctic Canada; Geological Survey of Canada, Memoir 387, 235 p.

**Moore, T.E., Wallace, W.K., Bird, K.J., Karl, S.M., Mull, C.G., and Dillon, J.T.**
1994: Geology of northern Alaska; *in* Chapter 3, The Geology of Alaska, (ed.) G. Plafker and H.C. Berg; Geological Society of America, Boulder, Colorado, The Geology of North America, v. G-1, p. 49–140.

**Poulton, T.P.**
1994: Jurassic stratigraphy and fossil occurrences - Melville, Prince Patrick, and Borden islands; *in* The Geology of Melville Island, Arctic Canada, (ed.) R.L. Christie and N.J. McMillan; Geological Survey of Canada, Bulletin 450, p. 161–193.
1997: Jurassic, Chapter 10; *in* The Geology, Mineral and Hydrocarbon Potential of Northern Yukon Territory and Northwestern District of Mackenzie, (ed.) D.K. Norris; Geological Survey of Canada, Bulletin 422, p. 267–299.

**Rostovstev, K.O. and Prozorowsky, V.A.**
1997: Information on resolutions of standing commissions of the Interdepartmental Stratigraphic Committee (ISC) on the Jurassic and Cretaceous systems; International Subcommission on Jurassic Stratigraphy, Newsletter v. 24, p. 48–49.

**Sei, I.I. and Kalacheva, E.D.**
1993: Biostratigraphic criteria of Jurassic-Cretaceous boundary in Russia; VSEGEI, p. 1–60.

**Surlyk, F. and Zakharov, V.A.**
1982: Buchiid bivalves from the Upper Jurassic and Lower Cretaceous of East Greenland; Paleontology, v. 25, p. 727–753.

**Tappan, H.**
1955: Foraminifera from the Arctic Slope of Alaska: Part 2, Jurassic Foraminifera; United States Geological Survey, Professional Paper 236B, p. 21–90.

**Thorsteinsson, R. and Tozer, E.T.**
1960: Summary account of structural history of the Canadian Arctic Archipelago since Precambrian time; Geological Survey of Canada, Paper 60-7, 25 p.

**Tozer, E.T. and Thorsteinsson, R.**
1964: Western Queen Elizabeth Islands, Arctic Archipelago; Geological Survey of Canada, Memoir 332, 242 p.

**Wall, J.H.**
1983: Jurassic and Cretaceous foraminiferal biostratigraphy in the eastern Sverdrup Basin, Canadian Arctic Archipelago; Bulletin of Canadian Petroleum Geology, v. 31, p. 246–281.

---

Geological Survey of Canada Project 860006

# Adsorbed-water characteristics of sediments from depths of 850–950 m in the JAPEX/JNOC/GSC Mallik 2L-38 gas hydrate research well, Northwest Territories

N. Scromeda, S. Connell, and T.J. Katsube
Mineral Resources Division, Ottawa

*Scromeda, N., Connell, S., and Katsube, T.J., 1999: Adsorbed-water characteristics of sediments from depths of 850–950 m in the JAPEX/JNOC/GSC Mallik 2L-38 gas hydrate research well, Northwest Territories*; in *Current Research 1999-E; Geological Survey of Canada, p. 59–63.*

**Abstract:** The adsorbed-water content has been determined for 17 sediment samples from depths of 850–950 m in the JAPEX/JANOC/GSC Mallik 2L-38 gas hydrate research well (Mackenzie Delta, Northwest Territories). The purpose was to obtain information on the adsorbed-water characteristics of unconsolidated to moderately consolidated sediments, to obtain data required to determine the thickness of the adsorbed molecular water layers, and to determine if the adsorbed-water content shows an increase with decreased temperature.

The results indicate that the adsorbed-water values ($S_I$) for the naturally dried samples at 4°C are generally larger than those for the samples naturally dried at 25°C, implying an increase in bound-water layers for decreased temperature. They also indicate, however, that under certain conditions the grain-size distribution (clay, silt, and sand content) has a significant effect on the $S_I$ values at the lower temperatures, with opposite trends seen in some cases.

**Résumé :** On a déterminé le contenu en eau adsorbée de 17 échantillons de sédiments prélevés à des profondeurs de 850 à 950 m dans le puits de recherche JAPEX/JNOC/GSC Mallik 2L-38 destiné à l'étude des hydrates de gaz, foré dans le delta du Mackenzie (Territoires du Nord-Ouest). Le but était d'obtenir de l'information sur les caractéristiques relatives à l'eau adsorbée des sédiments non consolidés ou moyennement consolidés, d'acquérir les données requises pour déterminer l'épaisseur des couches d'eau moléculaire adsorbée et de déterminer si le contenu en eau adsorbée augmente avec une baisse de la température.

Les résultats indiquent que le contenu en eau adsorbée ($S_I$) des échantillons séchés à l'air à 4 °C est généralement plus grand que celui des échantillons séchés à l'air à 25 °C, ce qui laisse supposer qu'il y a un accroissement des couches d'eau liée avec une baisse de la température. Toutefois, ils indiquent également que dans certaines conditions, la répartition granulométrique (contenu en argile, silt et sable) a un effet important sur les valeurs de $S_I$ aux basses températures, des tendances opposées étant observées dans certains cas.

## INTRODUCTION

The adsorbed-water content has been determined for 17 sedimentary rock samples from 850–950 m in the Mallik 2L-38 well (Mackenzie Delta, Northwest Territories; Dallimore et al., in press), in order to obtain information on the adsorbed-water characteristics of unconsolidated to moderately consolidated sediments, and to obtain data required to determine the thickness of the adsorbed molecular-water layers (double layers) on such sedimentary material. Information similar to 'adsorbed-water characteristics', in the form of 'static irreducible water saturation', has been reported on a routine basis for various types of rocks as part of the immersion porosity-determination procedure (e.g. Scromeda and Katsube, 1994). The moisture in moist rocks consists of free-water molecules and water molecules adsorbed to the grain surfaces. When the rock is dried under vacuum conditions, or naturally dried at temperatures below 100°C, only the free-water content is evacuated, and the adsorbed water remains on the grain surfaces (e.g. Hinch, 1980). However, the amount of adsorbed water decreases with increased temperature, with all adsorbed water evacuated at 116°C (e.g., Hinch, 1980). Another purpose of this study is to determine if the adsorbed-water content shows a significant increase with decreased temperature below 25°C. This paper reports the results of tests that have been performed at temperatures of 4°C, 25°C, and 50°C. Further studies will be carried out in the future to quantitatively determine the thickness of adsorbed-water layers (double layers) and how they can vary with temperature.

## INVESTIGATIVE METHOD

### *Samples and sample preparation*

Seventeen sediment samples were selected from the core material collected in the Mallik 2L-38 well (located in the Mackenzie Delta, Northwest Territories). The specimens used for testing were taken from subsamples which had been stored first at low temperatures (4°C), and then at room temperature. Information on sample depth and lithology are listed in Table 1.

### *Experimental approach*

Two specimens (A and B) were initially taken from each of the unconsolidated to moderately consolidated subsamples. They were then placed in a weighed beaker at room temperature (25°C). The specimens were saturated with 5–10 mL of deionized water, just enough to fully cover the specimens. The A specimens were left at room atmosphere and temperature (25°C), while the B specimens were placed in a refrigerator at 4°C. The specimens remained at these temperatures until all of the excess water evaporated out of the beakers, leaving only the moist specimens. The specimens were placed in a vacuum chamber for the initial natural-drying procedure (Katsube and Scromeda, 1995). The vacuum was then applied at 760 mm Hg for 420 min at room temperature (25°C), until a constant weight ,$W_{d1}$, was reached. Following the natural drying under vacuum, the specimens were placed in the vacuum oven under a vacuum of 760 mm Hg and dried for 24 hours at two different temperatures: 50°C and 100°C. Weights, $W_{d2}$ and $W_{d3}$, were measured after constant weights were reached at 50°C and subsequently at 100°C, respectively. These drying procedures are described in further detail elsewhere (Scromeda and Katsube, 1993).

The $W_d$ values ($W_{d1}$, $W_{d2}$, and $W_{d3}$) were used to determine the adsorbed water, $S_I$, values at each temperature, using the following equation:

$$S_I = (V / V_D) \times 100\%, \quad (1)$$

where V is the general expression for the volume of a moist specimen and $V_D$ is the volume of the specimen after the final drying at 100°C. The $S_{I(W)}$, $S_{I(d1)}$, and $S_{I(d2)}$ represent $S_I$ at room temperature without vacuum drying, at vacuum-dried room temperature (25°C), and at 50°C vacuum-oven-dried temperature, respectively. First, $S_{I(W)}$ is determined for the specimens before they are placed in the vacuum chamber at room temperature (25°C):

$$S_{I(W)} = (V_W / V_D) \times 100\%, \quad (2)$$

where $V_W$ is the volume of the moist specimen at room temperature determined by

$$V_W = (W_W - W_D)/ \delta W, \quad (3)$$

where $W_W$ is the weight of the moist specimen at room temperature (25°C), $W_D$ is the vacuum-oven-dried weight of the specimen at 100°C, and $\delta W$ is the specific density of water which is considered to be 1.0 g/mL in this study. The dry

**Table 1.** Information on sample depth and lithology (Jenner et al., in press).

| Sample number | Depth (m) | Lithology |
|---|---|---|
| EJA-1 | 896.8 | Silt |
| EJA-2 | 896.4 | Clayey silt |
| EJA-3 | 887.3 | Silt |
| EJA-4 | 897.1 | Sandy silt |
| EJA-5 | 906.2 | Sand |
| EJA-6 | 919.1 | Sand |
| EJA-8 | 927.6 | Clayey silt |
| EJA-9 | 949.4 | Clayey silt |
| EJA-11 | 897.1 | Quartzite (sand) |
| EJA-12 | 893.9 | Sand |
| EJA-13 | 903.9 | Silt, clayey silt |
| EJA-14 | 936.7 | Clayey silt |
| EJA-15 | 944.5 | Clayey silt |
| EJA-19 | 949.4 | Clayey silt |
| EJA-20 | 896.7 | Clayey silt |
| EJA-21 | 928.3 | Clayey silt |
| EJA-22 | 928.6 | Clayey silt |

**Table 2a.** Adsorbed-water ($S_I$) values recorded at each temperature level for samples saturated and initially dried at room temperature (25°C).

| Sample | $\delta_G$ (g/mL) | $W_W$ (g) | $W_{d1}$ (g) | $W_{d2}$ (g) | $W_D$ (g) | $V_W$ (mL) | $V_{d1}$ (mL) | $V_{d2}$ (mL) | $S_{I(W)}$ (%) | $S_{I(d1)}$ (%) | $S_{I(d2)}$ (%) |
|---|---|---|---|---|---|---|---|---|---|---|---|
| EJA-1a | 2.73 | 0.8702 | 0.8695 | 0.8620 | 0.8611 | 0.0091 | 0.0084 | 0.0009 | 2.89 | 2.66 | 0.29 |
| EJA-2a | 2.66 | 0.5398 | 0.5391 | 0.5356 | 0.5355 | 0.0043 | 0.0036 | 0.0001 | 2.14 | 1.79 | 0.05 |
| EJA-3a | 2.65 | 1.3733 | 1.3726 | 1.3662 | 1.3658 | 0.0075 | 0.0068 | 0.0004 | 1.46 | 1.32 | 0.08 |
| EJA-4a | 2.65 | 1.4195 | 1.4190 | 1.4094 | 1.4092 | 0.0103 | 0.0098 | 0.0002 | 1.94 | 1.84 | 0.04 |
| EJA-5a | 2.66 | 0.8010 | 0.8007 | 0.7993 | 0.7991 | 0.0019 | 0.0016 | 0.0002 | 0.63 | 0.53 | 0.07 |
| EJA-6a | 2.65 | 0.7032 | 0.7029 | 0.7022 | 0.7021 | 0.0011 | 0.0008 | 0.0001 | 0.42 | 0.30 | 0.04 |
| EJA-8a | 2.63 | 1.4942 | 1.4936 | 1.4838 | 1.4835 | 0.0107 | 0.0101 | 0.0003 | 1.90 | 1.79 | 0.05 |
| EJA-9a | 2.65 | 1.1605 | 1.1598 | 1.1546 | 1.1542 | 0.0063 | 0.0056 | 0.0004 | 1.45 | 1.29 | 0.09 |
| EJA-11a | 2.60 | 2.5048 | 1.8634 | 1.4935 | 1.4921 | 1.0127 | 0.3713 | 0.0014 | 176 | 64.7 | 0.24 |
| EJA-12a | 2.66 | 0.5596 | 0.5630 | 0.5586 | 0.5585 | 0.0011 | 0.0045 | 0.0001 | 0.52 | 2.14 | 0.05 |
| EJA-13a | 2.60 | 2.3518 | 1.7919 | 1.3907 | 1.3890 | 0.9628 | 0.4029 | 0.0017 | 180 | 75.4 | 0.32 |
| EJA-14a | 2.52 | 2.9682 | 2.1568 | 1.6140 | 1.6127 | 1.3555 | 0.5441 | 0.0013 | 212 | 85.0 | 0.20 |
| EJA-15a | 2.57 | 3.9536 | 3.4149 | 3.0408 | 3.0356 | 0.9180 | 0.3793 | 0.0052 | 77.7 | 32.1 | 0.44 |
| EJA-19a | 2.60 | 5.9090 | 5.0552 | 3.7749 | 3.7699 | 2.1391 | 1.2853 | 0.0050 | 148 | 88.6 | 0.34 |
| EJA-20a | 2.63 | 2.3496 | 1.7242 | 1.5701 | 1.5686 | 0.7810 | 0.1556 | 0.0015 | 131 | 26.1 | 0.25 |
| EJA-21a | 2.61 | 4.0309 | 3.1554 | 2.3899 | 2.3899 | 1.6410 | 0.7655 | 0.0000 | 179 | 83.6 | 0.00 |
| EJA-22a | 2.62 | 5.4129 | 4.5831 | 3.0272 | 3.0225 | 2.3904 | 1.5606 | 0.0047 | 207 | 135 | 0.41 |

The samples in this table are represented by the 'a' specimens (e.g., EJA-1a, EJA-2a .....EJA-22a).

$\delta_W$ = density of water
$W_W$ = weight of sample at room temperature (25°C)
$W_{d1}$ = vacuum-dried weight of sample at 25°C
$W_{d2}$ = vacuum-oven-dried weight of sample at 50°C
$W_D$ = vacuum-oven-dried weight of sample at 100°C
$V_W = W_W - W_D / \delta_W$
$V_{d1} = W_{d1} - W_D / \delta_W$
$V_{d2} = W_{d2} - W_D / \delta_W$

$\delta_W = 1.0$ g/mL
$S_{I(W)} = (V_W / V_D) \times 100\%$
$S_{I(d1)} = (V_{d1} / V_D) \times 100\%$
$S_{I(d2)} = (V_{d2} / V_D) \times 100\%$
$V_D = W_D / \delta_G$

**Table 2b.** Adsorbed-water ($S_I$) values recorded at each temperature level for samples saturated and initially dried at 4°C.

| Sample | $\delta_G$ (g/mL) | $W_W$ (g) | $W_{d1}$ (g) | $W_{d2}$ (g) | $W_D$ (g) | $V_W$ (mL) | $V_{d1}$ (mL) | $V_{d2}$ (mL) | $S_{I(W)}$ (%) | $S_{I(d1)}$ (%) | $S_{I(d2)}$ (%) |
|---|---|---|---|---|---|---|---|---|---|---|---|
| EJA-1b | 2.73 | 2.1057 | 1.4722 | 1.1540 | 1.1510 | 0.9547 | 0.3212 | 0.0030 | 226 | 76.2 | 0.71 |
| EJA-2b | 2.66 | 0.5694 | 0.5655 | 0.5450 | 0.5438 | 0.0256 | 0.0217 | 0.0012 | 12.5 | 10.6 | 0.59 |
| EJA-3b | 2.65 | 1.7893 | 1.5528 | 1.5104 | 1.5080 | 0.2813 | 0.0448 | 0.0024 | 49.4 | 7.87 | 0.42 |
| EJA-4b | 2.65 | 1.5879 | 1.2039 | 1.1746 | 1.1736 | 0.4143 | 0.0303 | 0.0010 | 93.6 | 6.84 | 0.23 |
| EJA-5b | 2.66 | 0.9300 | 0.7862 | 0.7846 | 0.7845 | 0.1455 | 0.0017 | 0.0001 | 49.3 | 0.58 | 0.03 |
| EJA-6b | 2.65 | 0.6508 | 0.6420 | 0.6396 | 0.6396 | 0.0112 | 0.0024 | 0.0000 | 4.64 | 0.99 | 0.00 |
| EJA-8b | 2.63 | 1.6356 | 1.5127 | 1.4565 | 1.4516 | 0.1840 | 0.0611 | 0.0049 | 33.3 | 11.1 | 0.89 |
| EJA-9b | 2.65 | 1.1251 | 1.1195 | 1.0846 | 1.0822 | 0.0429 | 0.0373 | 0.0024 | 10.5 | 9.13 | 0.59 |
| EJA-11b | 2.60 | 2.7573 | 2.2376 | 1.7897 | 1.7837 | 0.9736 | 0.4539 | 0.0060 | 142 | 66.2 | 0.87 |
| EJA-12b | 2.66 | 0.7066 | 0.5940 | 0.5893 | 0.5888 | 0.1178 | 0.0052 | 0.0005 | 53.2 | 2.35 | 0.23 |
| EJA-13b | 2.60 | 1.7915 | 1.3311 | 0.9782 | 0.9753 | 0.8162 | 0.3558 | 0.0029 | 218 | 94.9 | 0.77 |
| EJA-14b | 2.52 | 2.8959 | 2.5052 | 2.4355 | 2.4319 | 0.4640 | 0.0733 | 0.0036 | 48.1 | 7.60 | 0.37 |
| EJA-15b | 2.57 | 3.2469 | 2.8752 | 2.6895 | 2.6783 | 0.5686 | 0.1969 | 0.0112 | 54.6 | 18.9 | 1.07 |
| EJA-19b | 2.60 | 4.7653 | 4.1873 | 3.6148 | 3.6056 | 1.1597 | 0.5817 | 0.0092 | 83.6 | 42.0 | 0.66 |
| EJA-20b | 2.63 | 2.2906 | 1.8452 | 1.7764 | 1.7716 | 0.5190 | 0.0736 | 0.0048 | 77.1 | 10.9 | 0.71 |
| EJA-21b | 2.61 | 3.5501 | 3.0666 | 2.8340 | 2.8255 | 0.7246 | 0.2411 | 0.0085 | 66.9 | 22.3 | 0.79 |
| EJA-22b | 2.62 | 3.9611 | 3.4131 | 2.7107 | 2.7014 | 1.2597 | 0.7117 | 0.0093 | 122 | 69.0 | 0.90 |

The samples in this table are represented by the "b" specimens (e.g., EJA-1b, EJA-2b .....EJA-22b).

$\delta_G$ = grain density
$W_W$ = weight of sample at room temperature (25°C)
$W_{d1}$ = vacuum-dried weight of sample at 25°C
$W_{d2}$ = vacuum-oven-dried weight of sample (50°C)
$W_D$ = vacuum-oven-dried weight of sample (100°C)
$V_W = W_W - W_D / \delta_W$
$V_{d1} = W_{d1} - W_D / \delta_W$
$V_{d2} = W_{d2} - W_D / \delta_W$

$\delta_W = 1.0$ g/mL
$S_{I(W)} = (V_W / V_D) \times 100\%$
$S_{I(d1)} = (V_{d1} / V_D) \times 100\%$
$S_{I(d2)} = (V_{d2} / V_D) \times 100\%$
$V_D = W_D / \delta_G$

weight ($W_D$) is the constant weight at 100°C, and is considered to represent the sample when it is devoid of any free and adsorbed (or bound) water (American Petroleum Institute, 1960). Following these steps, $S_{I(d1)}$ and $S_{I(d2)}$ were determined by replacing $V_W$ and $W_W$ with $V_{d1}$, $V_{d2}$, $W_{d1}$, and $W_{d2}$ in equations (2) and (3) for the $S_I$ determinations under 50°C and 100°C vacuum-oven-dried temperature conditions.

## EXPERIMENTAL RESULTS

Results of the adsorbed-water ($S_I$) determinations for the specimens, using equations (1) to (3), are listed in Tables 2a and 2b for the initial natural drying at 25°C and 4°C, respectively. Three $S_I$ values, $S_{I(W)}$, $S_{I(d1)}$, and $S_{I(d2)}$ in Table 2a, were determined a) for specimens naturally dried for 3 days at room temperature (25°C); b) for specimens vacuum-dried for 7 hours at room temperature (25°C); and c) for specimens vacuum-oven-dried at 50°C for 24 hours, respectively. The $S_{I(W)}$ values represent the initial adsorbed-water condition before any vacuum drying was started. The three $S_I$ values in Table 2b represent the same values as those in Table 2a, but this time the natural drying (3 days) procedure occurred at 4°C for 6 days. The $W_D$ values needed for the $S_I$ calculations (equations 1–3) are determined by vacuum-oven-drying the specimens at 100°C for 24 hours, and are considered to represent the weight of the fully dried specimens.

The $S_{I(W)}$, $S_{I(d1)}$ and $S_{I(d2)}$ values for the specimens representing these 17 samples are in the ranges of 0.42–207%, 0.3–135%, and 0.00–0.41%, respectively for the naturally dried specimens at room temperature (25°C). The same three values for the naturally dried specimens at the temperature of 4°C are 4.6-226%, 0.6-95% and 0.00-1.07%, respectively. There are few known data available for comparison with these. However, there are some irreducible water saturation ($S_r$) data on a shale sample (Scromeda and Katsube, 1994) that can be used to calculate the $S_{I(d1)}$ and $S_{I(d2)}$ values for a shale sample with the natural drying procedure carried out at room temperature (25°C). The two values ($S_{I(d1)}$ and $S_{I(d2)}$) for that sample are 0.68% and 0.16%, respectively. These are similar to the values in the lower end of those listed in Table 2a and 2b.

The two $S_{I(d1)}$ and $S_{I(d2)}$ values were derived by the following procedure. The $S_r$ previously reported is defined by the following equation (Scromeda and Katsube, 1994):

$$S_r = (W_r - W_D)/(W_W - W_D), \quad (4)$$

where $W_r$ is the weight of the sample at any given drying time and temperature. The other parameters are the same as those in equations (1)–(3). This implies that all $W_r$, $W_D$, and $W_W$ values are known for the shale sample reported (Scromeda and Katsube, 1994). Since from equations (1) and (2), $S_I$ can be expressed as

$$S_{I(W)} = V_W / V_D, \quad (5)$$

and since specimen volume (V) can be expressed as weight over density (e.g. $V = W/\delta_D$), we then obtain

$$(W_W/\delta_D)/(W_D/\delta_D) = V_W / V_D, \quad (6)$$

where $\delta_D$ = bulk density (g/mL) of the sample. From these we obtain

$$S_{I(W)} = W_W/W_D. \quad (7)$$

This implies that by selecting stable $W_r$ values for temperatures of 25°C and 50°C for the shale sample in the previous study, the $S_{I(d1)}$ and $S_{I(d2)}$ values can be calculated for that sample by replacing $W_W$ in equation (7) with those selected $W_r$ values.

## DISCUSSIONS AND CONCLUSIONS

It has been demonstrated that the adsorbed-water values ($S_I$) for the naturally dried silt and sand specimens at 4°C (Table 2b) are generally larger than those for the samples naturally dried at 25°C (Table 2a). This is especially true for the $S_{I(d2)}$ values, which represent the $S_I$ values for the vacuum-oven-drying at 50°C, where they are 0.00–1.07% for all the specimens naturally dried at 4°C (Table 2b) and 0.00–0.44% at 25°C (Table 2a). This does not occur, however, for six of the clayey-silt samples (EJA-14, 15, 19, 20, 21, 22). Excluding these six clayey-silt samples (EJA-14, 15, 19, 20, 21, 22), the $S_{I(W)}$ and $S_{I(d1)}$ values are 4.6–226% versus 0.99–95% and 0.42-180% versus 0.3-75% for the two naturally dried temperatures (4°C versus 25°C), respectively. This suggests that there are more layers of bound water on the specimens when naturally dried at 4°C compared to the natural drying at room temperature (25°C). The reasons for the very large $S_I$ values (e.g. >100%) are unexplained at present. These values are 48–122% versus 78–212%, and 7.6–69% versus 26–135% for the two natural drying temperatures (4°C versus 25°C), respectively, for the six clayey-silt samples. That is, $S_{I(W)}$ and $S_{I(d1)}$ for the natural-drying temperature of 25°C display the larger values. It is currently not known why the $S_{I(W)}$ and $S_{I(d1)}$ values for the six clayey-silt samples display the opposite trend from the rest, and further studies are required.

## ACKNOWLEDGMENTS

The authors acknowledge the support provide by S.R. Dallimore (Geological Survey of Canada) for this study, and for his supplying the samples used in this study. The authors also thank Barbara Medioli (Geological Survey of Canada) for critically reviewing this paper.

## REFERENCES

**American Petroleum Institute**
1960: Recommended practices for core-analysis procedure; API Recommended Practice 40 (RP 40), American Petroleum Institute, Washington, D.C., p. 55. (first edition).

**Dallimore, S.R., Collett, T.S., and Uchida, T.**
in press: Overview of science program, JAPEX/JNOC/GSC Mallik 2L-38 gas hydrate research well; *in* Scientific Results from JAPEX/JNOC/GSC Mallik 2L-38 Gas Hydrate Research Well, Northwest Territories, Canada, (ed.) S.R. Dallimore, T. Uchida, T.S. Collett; Geological Survey of Canada, Bulletin 544.

**Hinch, H. H.**
1980: The nature of shales and the dynamics of hydrocarbon expulsion in the Gulf Coast Tertiary section; *in* Problems of petroleum migration, (ed.) W.H. Roberts III and R.J. Cordell; American Association of Petroleum Geologists, p. 1–18.

**Jenner, K.A., Dallimore, S.R., Clark, I.D., Paré, D., and Medioli, B.E.**
in press: Sedimentology of gas hydrate host strata from JAPEX/JNOC/GSC Mallik 2L-38 gas hydrate research well; *in* Scientific Results from JAPEX/JNOC/GSC Mallik 2L-38 Gas Hydrate Research Well, Mackenzie Delta, Northwest Territories, Canada, (ed.) S. R. Dallimore, T. Uchida, and T. S. Collett; Geological Survey of Canada, Bulletin 544.

**Katsube, T.J. and Scromeda, N.**
1995: Accuracy of low porosity measurements in granite; *in* Current Research, 1995-C; Geological Survey of Canada, p. 265–270.

**Scromeda, N., and Katsube, T.J.**
1993: Effect of vacuum-drying and temperature on effective porosity determination for tight rocks; *in* Current Research, Part E; Geological Survey of Canada, Paper 93-1E, p. 313–319.
1994: Effect of temperature on drying procedures used in porosity measurements of tight rocks; *in* Current Research, 1994-E; Geological Survey of Canada, p. 283–289.

---

Geological Survey of Canada Project 870057

# Laboratory physical characteristics of kimberlites from Smeaton, Saskatchewan[1]

T.J. Katsube, N. Scromeda, and B.A. Kjarsgaard
Mineral Resources Division, Ottawa

*Katsube, T.J., Scromeda, N., and Kjarsgaard, B.A., 1999: Laboratory physical characteristics of kimberlites from Smeaton, Saskatchewan;* in *Current Research 1999-E; Geological Survey of Canada, p. 65–71.*

**Abstract:** Bulk density ($\delta$), porosity ($\phi_E$), and electrical resistivity ($\rho_r$) have been determined for ten kimberlite samples from Smeaton (Fort à la Corne field), Saskatchewan, as part of a basic physical rock property study underway to provide information required for exploration activity in progress for kimberlite-hosted diamond deposits in Canada.

Results indicate that the range of values, 2.1–2.6 g/mL, 13–20%, and 20–280 $\Omega \cdot$ m for $\delta$, $\phi_E$, and $\rho_r$ of these samples, respectively, are typical of those previously reported for crater-facies kimberlites, and generally resemble the values for sedimentary rocks. Electrical resistivity ($\rho_r$) variations appear to be independent of $\phi_E$, also a trend consistent with previous findings for crater-facies kimberlite.

**Résumé :** Les propriétés physiques des roches, soit masse volumique apparente ($\delta$), porosité ($\phi_E$) et résistivité électrique ($\rho_r$), ont été déterminées pour dix échantillons de kimberlite de Smeaton (champ de Fort à la Corne), Saskatchewan, dans le cadre d'une étude de base sur les propriétés physiques des roches réalisée pour fournir l'information requise par les activités d'exploration en cours sur les gisements de diamant dans des kimberlites au Canada.

Les résultats indiquent que les valeurs (2,1–2,6 g/mL pour $\delta$, 13–20 % pour $\phi_E$ et 20–280 $\Omega \cdot$ m pour $\rho_r$) pour ces échantillons sont typiques de celles déjà rapportées pour des kimberlites de faciès de cratère et ressemblent en général aux valeurs obtenues pour des roches sédimentaires. Les variations de résistivité électrique ($\rho_r$) semblent être indépendantes de la valeur de la porosité ($\phi_E$), ce qui concorde également avec les résultats obtenus précédemment pour la kimberlite de faciès de cratère.

[1] Contribution to Canada-Saskatchewan Partnership Agreement on Mineral Development (1990-1995), a subsidiary agreement under the Canada-Saskatchewan Economic and Regional Development Agreement

## INTRODUCTION

Physical rock properties (electrical resistivity, bulk density, and porosity) have been determined for ten kimberlite samples from Smeaton, Saskatchewan. This is part of a basic physical rock property study (Katsube et al., 1992a; Katsube and Scromeda, 1994) being carried out to provide information required for exploration (planning of geophysical surveys and interpretation of the data). This is a response to the vigorous Canadian mineral exploration activity now in progress for kimberlite-hosted diamond deposits (LeCheminant et al., 1996). Use of airborne magnetics and electromagnetics as exploration tools for kimberlites has been demonstrated in various parts of the world (e.g. Atkinson, 1989). Basic physical rock property information is required to aid in the further development of geophysical methods with improved detection capabilities for kimberlites below overburden. For this reason, a physical rock property study on kimberlites consisting of electrical resistivity, formation factor, magnetic susceptibility, density, and porosity measurements is underway.

Results of parts of this study have previously been reported (Katsube et al., 1992a; Katsube and Scromeda, 1994; Scromeda et al., 1994). They include physical property data on kimberlite samples from Somerset Island (Northwest Territories), Sturgeon Lake and Fort à la Corne (Saskatchewan), and Kirkland Lake (Ontario). This paper is primarily a documentation of physical properties of samples from the Smeaton kimberlite drill hole #169, drilled by the Geological Survey of Canada (GSC core #2125). Interpretive and modelling studies are currently continuing on quantitative relationships between mineralogy (primary and secondary), petrographic textural type (crater, diatreme, or hypabyssal facies), and physical properties. While rock property data on electrical resistivity, magnetic susceptibility, and density can be used directly for interpretation of surface and airborne geophysical methods, porosity is used to analyze the physical structure of the rocks, and help link the geophysical parameters (electrical resistivity, magnetic susceptibility, and density) to the geological characteristics of the kimberlites. Examples of such analyses using these parameters can be found in the literature (Katsube and Hume, 1987; Katsube et al., 1991; Katsube and Mareschal, 1993).

## METHOD OF INVESTIGATION

### *Samples and sample preparation*

Ten split core samples of kimberlite were collected from various depths (119–210 m) in Smeaton, Saskatchewan for this study (Table 1). The samples are representative of different types of the Smeaton kimberlite drill core (Fig. 1), which include marine reworked material (olivine-rich shoreface sands), olivine-rich crystal tuffs, and juvenile lapilli tuffs. These samples were partial discs with diameters and thicknesses of 4.6 cm and 1.1–1.6 cm, respectively. An irregular-shaped chip specimen was cut off from each of nine of these sample and used for porosity measurements. Each of the remaining specimens (partial discs) had their surfaces polished and prepared for electrical resistivity and other measurements. Two rectangular specimens were cut from sample SM-4 for both porosity and the other measurements.

### *Preparatory and bulk density measurements*

The caliper method (American Petroleum Institute, 1960) was used to determine the bulk density, $\delta$, of the samples. This method requires measurement of dimensions and weight of the specimens and is derived from

$$\delta = W/V, \tag{1}$$

where V and W are the volume and weight of the room dry (humidity 40%) specimen, respectively. The volume of the partial-disc specimens are determined using the following equations:

$$V = A\ell \tag{2}$$

$$A = r_D^2[\alpha\pi/180 - \sin(2\alpha)/2] \tag{3}$$

$$r_D = (d^2 + t^2)/(2t) \tag{4}$$

$$\alpha = \cos^{-1}[(d^2 - t^2)/(d^2 + t^2)] \tag{5}$$

where A, $\ell$, $r_D$, and $\alpha$ are the area, thickness, radius, and separation angle, respectively, of the partial disc specimens, respectively (Fig. 2). The parameters t and d are two of the specimen dimensions that are actually measured, and are defined in Figure 2. The geometric factor, $K_G$

$$K_G = A/\ell \tag{6}$$

is determined for specimens used for the electrical measurements.

The volume (V) and geometric factor ($K_G$) values of the rectangular specimen (sample SM-4) were determined using the conventional methods (Katsube et al., 1992b). The geometric characteristics of the specimens for all ten samples are listed in Table 2.

**Table 1.** Kimberlite core samples from Smeaton drill core 169/8 (GSC #21250) identifying laboratory sample numbers with depth interval and facies.

| Sample number | Depth interval (m) | Facies |
|---|---|---|
| SM-4 | 119.00–119.12 | Marine reworked material |
| SM-8 | 145.11–145.28 | Crystal tuff |
| SM-9 | 153.05–153.21 | Crystal tuff |
| SM-10 | 160.02–160.26 | Crystal tuff |
| SM-11 | 169.68–170.00 | Crystal tuff |
| SM-12 | 175.00–175.20 | Crystal tuff |
| SM-13 | 182.00–182.20 | Juvenile lapilli |
| SM-15 | 195.15–195.35 | Juvenile lapilli |
| SM-16 | 205.00–205.25 | Juvenile lapilli |
| SM-17 | 209.80–210.00 | Juvenile lapilli |

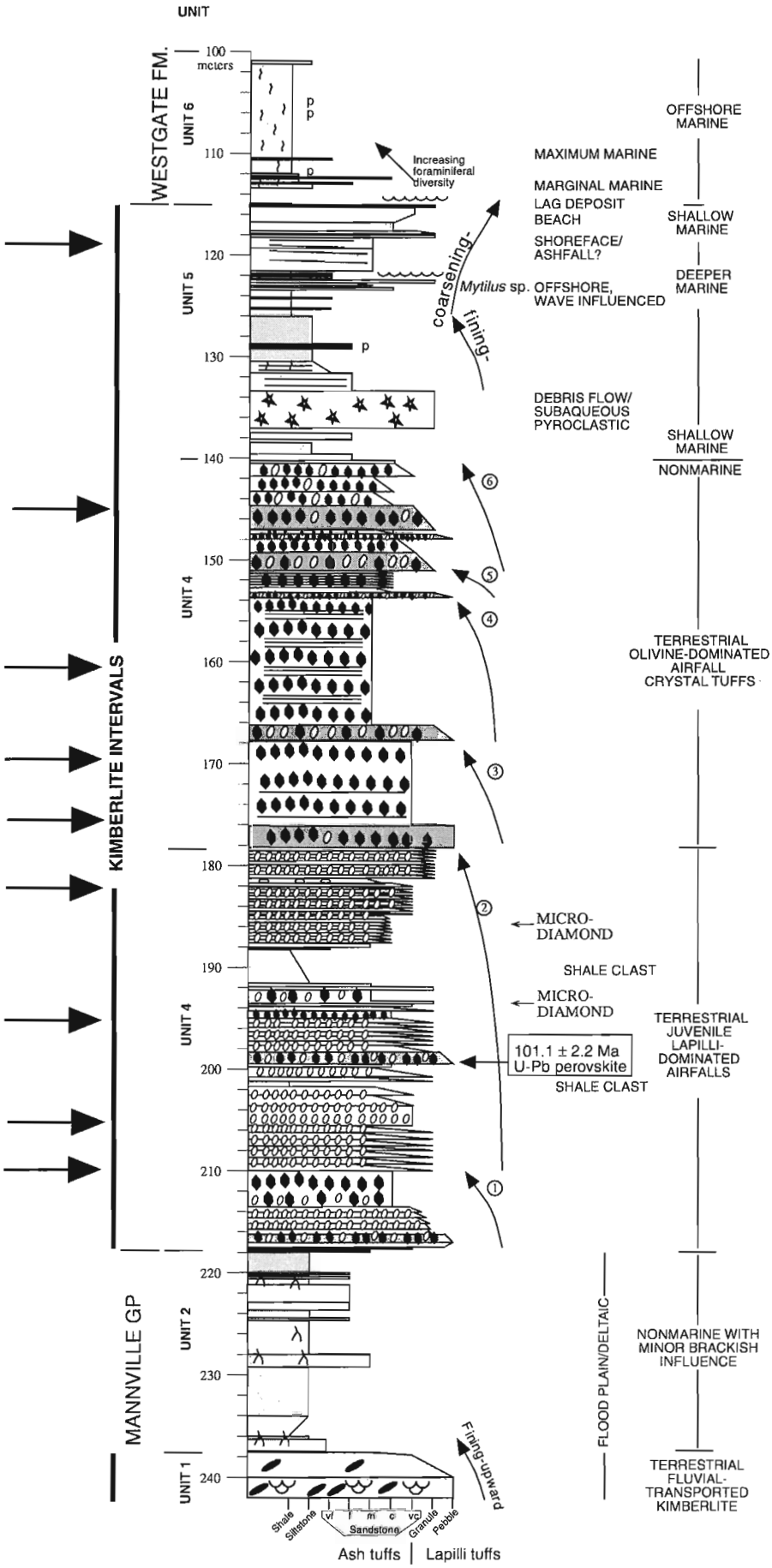


***Figure 1.***

*Measured section of Smeaton drill core 169/8 (Kjarsgaard et al., 1995) indicating depth of samples used in this study. Arrows at the left-hand side of the column indicate the positions of the samples.*

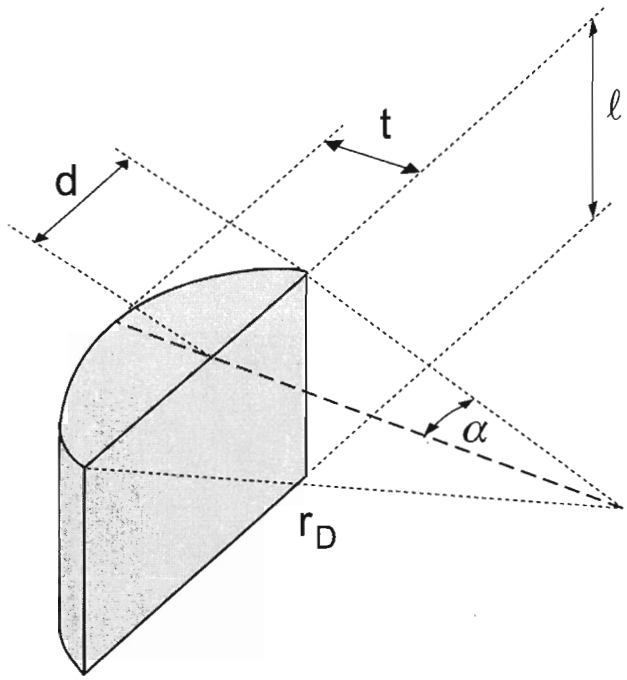


***Figure 2.*** *Description of a partial disc specimen, and its dimensions. ℓ, $r_D$, and α are the thickness, radius, and half the separation angle of the partial disc specimen. The parameters t and d are illustrated here.*

### *Effective porosity measurements*

Effective porosity, $\phi_E$, in principle includes the pore volume of all interconnected pores, and is determined from the difference in weight between the oven-dried and water-saturated rock specimen:

$$\phi_E = \delta(W_w - W_D) / (\delta_W W_D) \quad (7)$$

where $W_w$ and $W_D$ are the wet and dry weight of the specimen, respectively, and $\delta_w$ is the density of the pore water (usually considered as unity). Details of the technique, including its advantages and limitations are described in the literature (e.g. Katsube and Scromeda, 1991; Katsube et al., 1992b; Scromeda and Katsube, 1993). The *Recommended Practices for Core-analysis Procedures* (American Petroleum Institute, 1960) has generally been followed in these papers.

The static irreducible water saturation, $S_{rD}$, which is expressed as follows:

$$S_{rD} = (W_{rD} - W_D)/ (W_W - W_D), \quad (8)$$

where $W_{rD}$ is the weight of the specimen when it reaches a constant value under vacuum drying at 23°C, represents the degree of moisture bound to the pore surfaces. A constant weight ($W_{rD}$) is defined by the sample weight variation being less than 0.1 mg/h. Further details of the technique are described in the literature (Katsube et al., 1992b; Scromeda and Katsube, 1993).

**Table 2a.** Dimensions of partial disc specimens cut out from the split core samples.

| Samples | $r_D$ (cm) | α (°) | A ($cm^2$) | ℓ (cm) | V ($cm^3$) | W (g) | $K_G$ ($10^{-2}$ m) | δ ($g/cm^3$) |
|---|---|---|---|---|---|---|---|---|
| SM-8 | **4.65** | 137 | 4.6 | 1.356 | 6.2 | 13.2677 | 3.39 | 2.13 |
| SM-9 | **4.74** | 138 | 4.9 | 1.570 | 7.7 | 18.2804 | 3.12 | 2.38 |
| SM-10 | **4.63** | 134 | 4.3 | 1.441 | 6.2 | 13.6252 | 2.99 | 2.19 |
| SM-11 | **4.39** | 133 | 3.8 | 1.218 | 4.7 | 11.8420 | 3.14 | 2.54 |
| SM-12 | **4.69** | 139 | 4.9 | 1.320 | 6.5 | 15.8398 | 3.71 | 2.45 |
| SM-13 | **4.69** | 122 | 3.5 | 1.163 | 4.1 | 9.9497 | 3.03 | 2.43 |
| SM-15 | **4.69** | 135 | 4.5 | 1.137 | 5.2 | 12.4820 | 3.99 | 2.41 |
| SM-16 | **4.60** | 135 | 4.4 | 1.323 | 5.8 | 14.2780 | 3.31 | 2.47 |
| SM-17 | **4.63** | 134 | 4.3 | 1.293 | 4.9 | 12.6612 | 3.32 | 2.57 |

$r_D$ = Diameter; V = Volume of specimen
α = Half of separation angle (Fig. 2); W = Weight
A = Area; $K_G$ = Geometric factor
ℓ = Thickness; δ = Bulk density

**Table 2b.** Dimensions of the specimen cut out from sample SM-4.

| Sample | $a_1$ (cm) | $a_2$ (cm) | ℓ (cm) | V ($cm^3$) | W (g) | $K_G$ ($10^{-2}$m) | δ (g/mL) |
|---|---|---|---|---|---|---|---|
| SM-4 | 2.199 | 1.391 | 1.004 | 3.07 | 7.4200 | 3.047 | 2.42 |

$a_1$,$a_2$ = Length of the two sides of the rectangular specimen
ℓ = Thickness of specimen
W = Weight of specimen under room dry conditions
$K_G$ = Geometric factor
δ = Bulk density

### *Bulk electrical resistivity measurements*

The bulk electrical resistivity, $\rho_r$, is determined from the complex electrical resistivity, $\rho^*$, measurements made by methods described in recent publications (e.g. Katsube et al., 1991; Katsube and Salisbury, 1991). The complex electrical resistivity ($\rho^*$) measurements were made on specimens saturated in distilled water for 24–48 h (Katsube and Salisbury, 1991). The $\rho^*$ is measured over a frequency range of 1–$10^6$ Hz, with $\rho_r$ usually representing an electrical resistivity at a frequency of about $10^2$–$10^3$ Hz. It is a function of the pore structure and pore-fluid resistivity, and is assumed to exclude any other effects, such as dielectric or any other pore-surface polarizations (Katsube, 1975; Katsube and Walsh, 1987).

First, the complex resistivity, $\rho^*$, is measured:

$$\rho^* = \rho_R + i\rho_I, \tag{9}$$

where $\rho_R$ is the real resistivity and $\rho_I$ is the imaginary resistivity, from impedance $Z(\Theta)$ measurements:

$$\rho^* = K_G Z(\Theta), \tag{10}$$

where $\Theta$ is the phase angle. Then the bulk electrical resistivity ($\rho_r$) is determined from the Cole-Cole plots of the complex resistivity ($\rho^*$) measurements by the method described in Katsube (1975) and Katsube and Walsh (1987), or in more recent publications (e.g. Katsube et al., 1991; Katsube and Salisbury, 1991).

### *Measurement errors*

Effective porosity ($\phi_E$) and complex resistivity measurements for bulk electrical resistivity ($\rho_r$) determinations were made at room temperature. The errors for these measurements are estimated to be generally in the ranges of ±9–10% and ±10–20%, respectively (Katsube and Salisbury, 1991).

## EXPERIMENTAL RESULTS

The results of the bulk density ($\delta$) determinations are listed in Table 2. They are in the range of 2.1–2.6 g/mL, results similar to those previously reported for crater-facies kimberlites (Katsube et al., 1992a; Katsube and Scromeda, 1994), and resemble those for sedimentary rocks (Daly et al., 1966).

The results of the effective porosity ($\phi_E$) measurements are listed in Table 3, displaying values in the range of 13–20%. These values are very similar to those previously reported for crater- and diatreme-facies kimberlites, and also resemble those for sedimentary rocks (Daly et al., 1966).

The results of the bulk electrical resistivity ($\rho_r$) measurements are listed in Table 4. Determinations have been made at 24 h and 48 h after saturation, to ensure that they represent $\rho_r$ values stable with time. Under this state, it is expected that the distilled water has chemically equilibrated with the rock, and represents the in situ condition. Normally, differences up to ±20% of their mean are considered to be within measurement error and represent stability. In this case there are some that slightly exceed that value (e.g. sample SM-9), for reasons not

**Table 3.** Results of the effective porosity measurements.

| Sample | $\delta$ (g/mL) | $W_w$ (g) | $W_D$ (g) | $S_{rD}$ (%) | $\phi_E$ (%) |
|---|---|---|---|---|---|
| SM-4 | 2.42 | 5.0232 | 4.7509 | 9.9 | 13.9 |
| SM-8 | 2.13 | 9.0867 | 8.3131 | 10.1 | 19.8 |
| SM-9 | 2.38 | 10.2009 | 9.5620 | 7.4 | 15.9 |
| SM-10 | 2.19 | 8.7109 | 8.0591 | 6.5 | 17.7 |
| SM-11 | 2.54 | 9.7964 | 9.3061 | 9.4 | 13.4 |
| SM-12 | 2.45 | 9.2625 | 8.7582 | 10.9 | 14.1 |
| SM-13 | 2.43 | 8.4173 | 7.9461 | 11.8 | 14.4 |
| SM-15 | 2.41 | 5.5002 | 5.2038 | 13.2 | 13.7 |
| SM-16 | 2.47 | 6.4571 | 6.0744 | 13.8 | 15.6 |
| SM-17 | 2.57 | 4.4355 | 4.1982 | 15.8 | 14.5 |

$W_w$ = Wet weight
$W_D$ = Dry weight
$S_{rD}$ = Static irreducible water saturation
$\delta$ = Bulk density
$\phi_E$ = Effective porosity

**Table 4.** Results of electrical resistivity measurements.

| Sample | $\rho_r$ (Ωm) Mes. #1 | Mes. #2 | Mean* |
|---|---|---|---|
| SM-4 | 170 | 130 | 150 ± 20 |
| SM-8 | 140 | 140 | 140 ± 0 |
| SM-9 | 190 | 120 | 155 ± 35 |
| SM-10 | 45 | 66 | 56 ± 11 |
| SM-11 | 26 | 27 | 27 ± 1 |
| SM-12 | 14 | 19 | 17 ± 3 |
| SM-13 | 180 | 210 | 195 ± 15 |
| SM-15 | 300 | 250 | 275 ± 25 |
| SM-16 | 200 | 180 | 190 ± 10 |
| SM-17 | 190 | 270 | 230 ± 40 |

$\rho_r$ = Bulk electrical resistivity
Mes. (#1) = Measurement after 24 h of saturation
Mes. (#2) = Measurement after 48 h of saturation
*The values following the ± sign represent the larger of the two differences between the mean and the two measurement (#1 and #2) values. Since the $\rho_r$ values decrease immediately after saturation, it is necessary to make at least two measurements, reasonably timed apart, to ensure a stable value has been reached. equal, a difference within ±20%, or a larger value for the second $\rho_r$ measurement is interpreted to imply that stability has been reached.

yet known. The $\rho_r$ values are in the range of 20–280 Ω · m, typical of those previously reported (Katsube and Scromeda, 1994) for crater-facies kimberlites, and also resemble those of Palaeozoic and Precambrian sedimentary and volcanic rocks (Keller, 1982).

## DISCUSSION AND CONCLUSIONS

Results for the four parameters, bulk density (δ), effective porosity ($\phi_E$), static irreducible water saturation ($S_{rD}$), and bulk electrical resistivity ($\rho_r$) are compiled in Table 5 for all 10 Smeaton kimberlite samples. Previously published results from the Fort à la Corne kimberlite field (Scromeda et al., 1994) are also included in this table. The range of values, 2.1–2.6 g/mL, 13–20%, and 20–280 Ω · m for bulk density (δ), effective porosity ($\phi_E$), and bulk electrical resistivity ($\rho_r$), respectively, for these samples, are typical of those previously reported (Katsube and Scromeda, 1994) for crater-facies kimberlites, and generally resemble the values for sedimentary rocks (Daly et al., 1966; Keller, 1982).

A relatively good correlation exists between bulk density (δ) and effective porosity ($\phi_E$), as shown in Figure 3a. No correlation seems to exist between $\rho_r$ and $\phi_E$ (Fig. 3b). That is, the variation of $\rho_r$ appears to be independent of $\phi_E$. These trends are consistent with those previously observed for crater-facies kimberlites (T.J. Katsube and B.A. Kjarsgaard, unpub. report, 1995). Further studies are underway to determine the quantitative relationship between the mineralogy and these physical properties.

**Table 5.** Summary of physical and petrophysical properties of the Smeaton kimberlite samples.

| Samples | δ (g/mL) | $\phi_E$ (%) | $S_{rD}$ (%) | $\rho_r$ (Ω•m) | Facies |
|---|---|---|---|---|---|
| SM-4 | 2.42 | 13.9 | 9.9 | 150 ± 20 | mrt |
| SM-8 | 2.13 | 19.8 | 10.1 | 140 ± 5 | ct |
| SM-9 | 2.38 | 15.9 | 7.4 | 160 ± 40 | ct |
| SM-10 | 2.19 | 17.7 | 6.5 | 56 ± 11 | ct |
| SM-11 | 2.54 | 13.4 | 9.4 | 27 ± 1 | ct |
| SM-12 | 2.45 | 14.1 | 10.9 | 17 ± 3 | ct |
| SM-13 | 2.43 | 14.4 | 11.8 | 200 ± 20 | lt |
| SM-15 | 2.41 | 13.7 | 13.2 | 280 ± 30 | lt |
| SM-16 | 2.47 | 15.6 | 13.8 | 190 ± 10 | lt |
| SM-17 | 2.57 | 14.5 | 15.8 | 230 ± 40 | lt |
| CS-1 | 2.62 | 8.89 | 19.1 | 11 ± 0.5 | lt |
| CS-2 | 2.17 | 18.23 | 4.9 | 22 ± 3 | lt |
| CS-3 | 2.40 | 14.70 | 8.0 | 25 ±14 | lt |
| CS-4 | 2.35 | 16.06 | 7.5 | 10 ± 1 | lt |
| CS-5 | 2.43 | 12.68 | 11.7 | 310 ± 40 | lt |

CS- = Fort à la Corne samples from previously published results (Scromeda et al., 1994)
δ = Bulk density
$\phi_E$ = Effective porosity
$S_{rD}$ = Static irreducible water saturation
$\rho_r$ = Bulk electrical resistivity
mr = Marine reworked
c = Crystal
l = Lapilli
t = Tuff

## ACKNOWLEDGMENTS

The authors acknowledge support from the Canada-Saskatchewan Mineral Development Agreement (1990-1995) for this study. The authors are grateful to the Uranerz/ Cameco/Monopros Fort a la Corne Joint Venture for

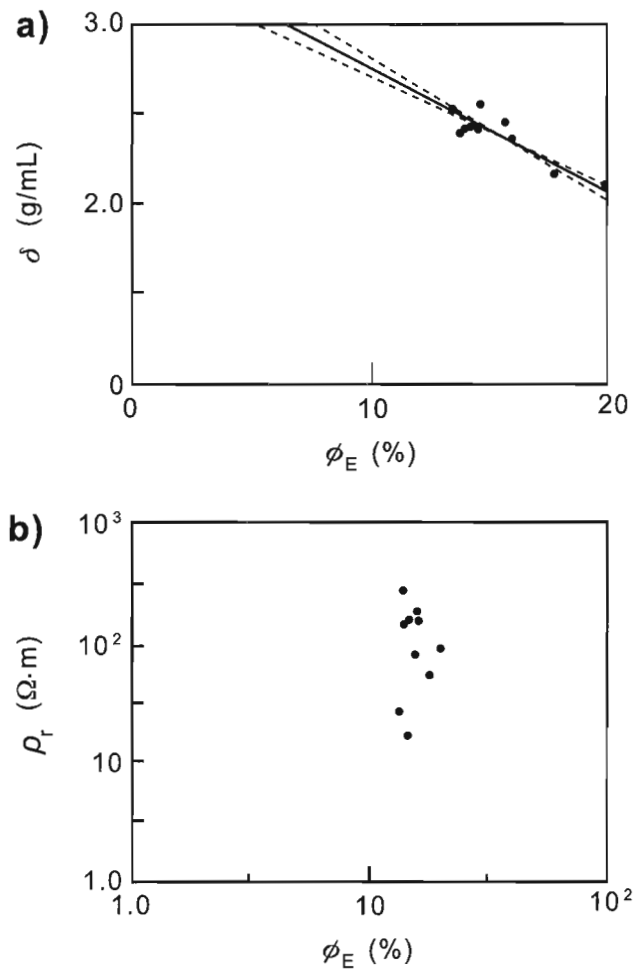


***Figure 3. a)*** *Bulk density ( ) as a function of effective porosity ($\phi_E$) (RMA: = -0.068$\phi_E$ + 3.44, r = -0.88); RMA is represented by a solid line and the normal regression lines are represented by dashed lines;* ***b)*** *bulk electrical resistivity ($\rho_r$) as a function of effective porosity ($\phi_E$); RMA is the reduced major axis and r is the correlation coefficient. The principles of the RMA are described in Davis (1986), and examples of related applications are found in Katsube and Agterberg (1990).*

permitting us to publish the results of this study. The authors are also grateful for the critical review of this paper and useful suggestions by K.A. Richardson and Q. Bristow (Geological Survey of Canada), and by D. Gendzwill (University of Saskatchewan).

## REFERENCES

**American Petroleum Institute**
1960: Recommended practices for core-analysis procedure; *in* API Recommended Practice 40 (RP 40) First Edition, American Petroleum Institute, Washington, D.C., p. 55.

**Atkinson, W.J.**
1989: Diamond exploration philosophy, practice and promises; a review; *in* Proceedings of the Fourth International Kimberlite Conference, Kimberlites and Related Rocks, Volume 2, (ed.) J. Ross; Geological Society of Australia, Special Publication No.14, p. 1075–1107.

**Daly, R.A., Manger, E.G., and Clark, S.P., Jr.**
1966: Density of rocks; *in* Handbook of Physical Constants; The Geological Society of America, Inc., Memoir 97, p. 23.

**Davis, J.C.**
1986: Statistics and Data Analysis in Geology; John Wiley & Sons, New York, New York, p. 200–204.

**Katsube, T.J.**
1975: The electrical polarization mechanism model for moist rocks; *in* Current Research, Part C; Geological Survey of Canada, Paper 75-1C, p. 353–360.

**Katsube, T.J. and Agterberg, F.P.**
1990: Use of statistical methods to extract significant information from scattered data in petrophysics; *in* Statistical Applications in the Earth Sciences, (ed.) F.P. Agterberg and G.F. Bonham-Carter; Geological Survey of Canada, Paper 89-9, p. 263–270.

**Katsube, T.J. and Hume, J.P.**
1987: Permeability determination in crystalline rocks by standard geophysical logs; Geophysics, v. 52, p. 343–352.

**Katsube, T.J. and Mareschal, M.**
1993: Petrophysical model of deep electrical conductors; Graphite lining as a source and its disconnection due to uplift; Journal of Geophysical Research, v. 98, no. B5, p. 8019–8030.

**Katsube, T.J. and Salisbury, M.**
1991: Petrophysical characteristics of surface core samples from the Sudbury structure; *in* Current Research, Part E; Geological Survey of Canada, Paper 91-E, p. 265–271.

**Katsube, T.J. and Scromeda, N.**
1991: Effective porosity measuring procedure for low porosity rocks; *in* Current Research, Part E; Geological Survey of Canada, Paper 91-E, p. 291–297.
1994: Physical properties of Canadian kimberlites; Somerset Island and Saskatchewan; *in* Current Research, Part B; Geological Survey of Canada, Paper 94-1B, p. 35–42.

**Katsube, T.J. and Walsh, J.B.**
1987: Effective aperture for fluid flow in microcracks; International Journal of Rock Mechanics and Mining Sciences and Geomechanics Abstracts, v. 24, p. 175–183.

**Katsube, T.J., Best, M.E., and Mudford, B.S.**
1991: Petrophysical characteristics of shales from the Scotian shelf; Geophysics, v. 56, p. 1681–1689.

**Katsube, T.J., Scromeda, N., Bernius, G., and Kjarsgaard, B.A.**
1992a: Laboratory physical property measurements of kimberlites; *in* Current Research, Part E; Geological Survey of Canada, Paper 92-1E, p. 357–364.

**Katsube, T.J., Scromeda, N., and Williamson, M.**
1992b: Effective porosity of tight shales from the Venture Gas Field, offshore Nova Scotia; *in* Current research, Part D; Geological Survey of Canada, Paper 92-1D, p. 111–119.

**Keller, G.V.**
1982: Electrical properties of rocks and minerals; *in* Handbook of Physical Properties of Rocks, Volume I (ed.) R.S. Carmichael; CRC Press, Inc., Boca Raton, Florida, p. 217–293.

**Kjarsgaard, B.A., Leckie, D.A., McIntire, D.J., McNeil, D.H., Haggart, J.M., Stasiuk, L., and Bloch, J. (ed.)**
1995: Smeaton kimberlite drill core, Fort a la Corne Field, Saskatchewan; Geological Survey of Canada, Open File 3170, 58 p.

**LeCheminant, A.N., Richardson, D.G., Dilabio, R.N., and Richardson, K.A. (ed.)**
1996: Searching for Diamonds in Canada; Geological Survey of Canada, Open File 3228, p. 1–3.

**Scromeda, N. and Katsube, T.J.**
1993: Effect of vacuum-drying and temperature on effective porosity determination for tight rocks; *in* Current Research, Part E; Geological Survey of Canada, Paper 93-1E, p. 313–319.

**Scromeda, N., Katsube, T.J., Bernius, G., and Kjarsgaard, B.A.**
1994: Physical properties of Canadian kimberlites from Fort a la Corne, Saskatchewan; *in* Current Research 1994-E; Geological Survey of Canada, p. 171–175.

Geological Survey of Canada Project 870057

# CANADIAN SHIELD

# BOUCLIER CANADIEN

# Geochemistry of gabbroic rocks from the 1.9 Ga Kramanituar Complex and surrounding country rocks of the Archean western Churchill Province, Nunavut

M. Sanborn-Barrie
Continental Geoscience Division, Ottawa

*Sanborn-Barrie, M., 1999: Geochemistry of gabbroic rocks from the 1.9 Ga Kramanituar Complex and surrounding country rocks of the Archean western Churchill Province, Nunavut;* in *Current Research 1999-E; Geological Survey of Canada, p. 75–89.*

**Abstract:** The Paleoproterozoic Kramanituar Complex is a window of deep-crustal rocks exposed in the interior of the Archean western Churchill Province. It is dominated by high-pressure, granulite-facies, mafic metaplutonic rocks, including gabbro, gabbroic anorthosite, norite, and anorthosite. Major- and trace-element geochemistry indicate that these rocks likely represent a cogenetic suite derived from an undepleted mantle source at 1902 ± 1 Ma, the U-Pb zircon age for a gabbroic anorthosite sample. Gabbroic rocks hosted within Archean country rocks north and east of the Kramanituar Complex are petrochemically distinct from the Kramanituar suite and appear to have been derived through partial-melt processes.

**Résumé :** Le complexe paléoprotérozoïque de Kramanituar est une fenêtre de roches crustales profondes exposées à l'intérieur de la province archéenne de Churchill occidentale. Il est dominé par des roches mafiques métaplutoniques de haute pression du faciès des granulites, notamment du gabbro, de l'anorthosite gabbroïque, de la norite et de l'anorthosite. La géochimie des éléments majeurs et des éléments traces indique que ces roches représentent probablement une suite cogénétique dérivée d'une source mantellique non appauvrie à 1902 ± 1 Ma, l'âge U-Pb des zircons dans un échantillon d'anorthosite gabbroïque. Les roches gabbroïques encaissées dans les roches archéennes au nord et à l'est du complexe de Kramanituar diffèrent du point de vue pétrochimique de la suite de Kramanituar et seraient dérivées de processus de fusion partielle.

## INTRODUCTION AND REGIONAL SETTING

The Kramanituar Complex is one of several high-grade, mafic-dominated, tectonometamorphic complexes that coincide with the surface trace of the Snowbird tectonic zone, a geophysically defined feature that extends more than 2000 km from the foothills of the Rocky Mountains to Hudson Bay (Fig. 1). In order to better understand the role of the Snowbird tectonic zone in the tectonometamorphic evolution of the western Churchill Province, several recent studies have investigated lithotectonic, geothermobarometric, and geochronological aspects of its associated high-grade complexes (Gordon, 1988; Tella et al., 1994; Snoeyenbos et al., 1995; Hanmer, 1997; Aspler et al., 1999; M. Sanborn-Barrie, unpub. data, 1999; M. Sanborn-Barrie, S.D. Carr, and R.J. Thériault, unpub. data, 1999; M. Sanborn-Barrie and R.G. Berman, unpub. data, 1999). Collectively, these studies have shown that high-grade complexes along the Snowbird tectonic zone share similarities in terms of lithological association, structural style, and metamorphic grade, but that they differ with respect to the timing of latest penetrative tectonomorphism and magmatism. Available constraints indicate that the regional northeast-striking segment of the Snowbird tectonic zone (Fig. 1) experienced latest penetrative tectonomorphism during Neoarchean time (Hanmer et al., 1994; Hanmer, 1997; Aspler et al., 1999), whereas the regional east-striking Chesterfield segment (Fig. 1) experienced high-grade tectonic and magmatic activity during the Paleoproterozoic (Gordon, 1988; Tella et al. 1994; M. Sanborn-Barrie, S.D. Carr, and R.J. Thériault, unpub. data, 1999), subsequent to Neoarchean events.

The presence of ca. 1.9 Ga mafic intrusive rocks within the Chesterfield segment of the Snowbird tectonic zone allowed the opportunity to investigate processes of Paleoproterozoic crustal evolution in this part of the Archean western Churchill Province. The geochemistry of gabbroic rocks of the Kramanituar Complex, and of gabbroic country rocks to the complex, are presented and analyzed here to address magmatic relationships that could not be resolved by field mapping, petrographic, and/or isotopic methods alone. Trace-element geochemistry is used to assess whether gabbroic and anorthositic rocks of the Kramanituar Complex are cogenetic with gabbroic anorthosite, dated at 1902 ± 1.6 Ma (M. Sanborn-Barrie, S.D. Carr, and R.J. Thériault, unpub. data, 1999), in order to better constrain the extent of Paleoproterozoic magmatic activity in this area. Similarly, trace-element data are used to compare the Kramanituar gabbroic suite with gabbroic country rocks to determine the extent of

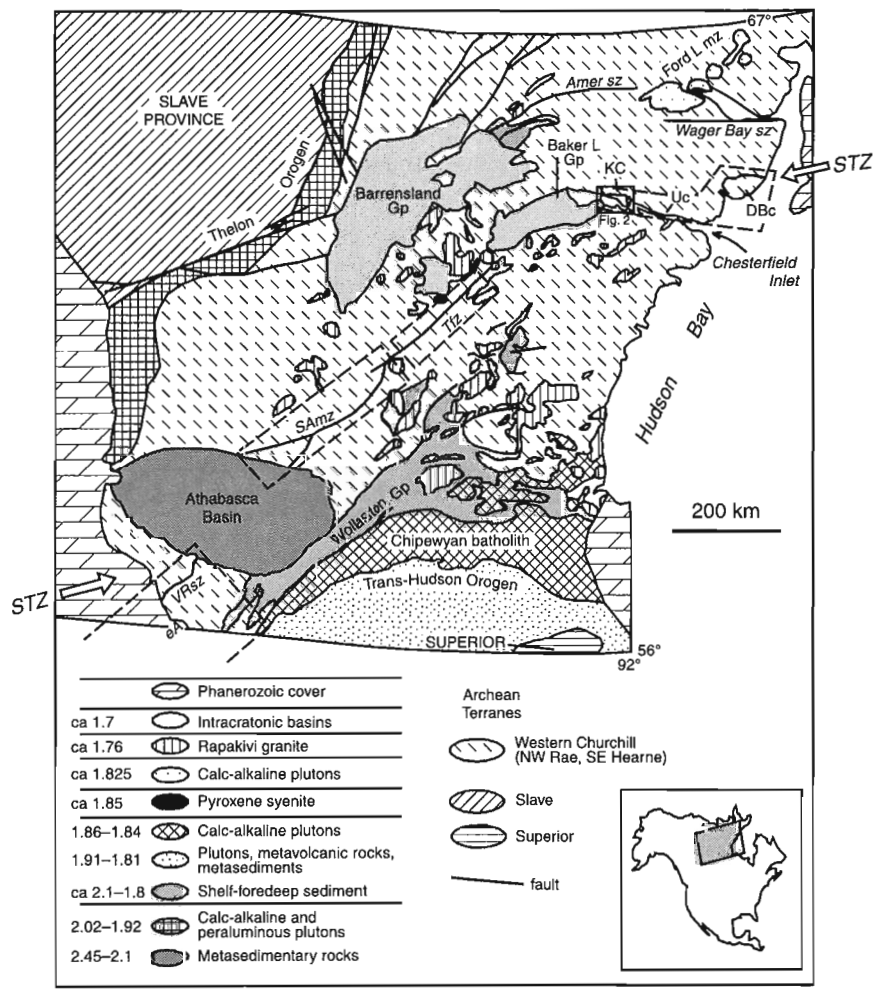


***Figure 1.***

*Geology of the western Canadian Shield after Hoffman (1989). Segments of the Snowbird tectonic zone (STZ), from northeast to southwest, are the Chesterfield segment which includes the Daly Bay complex (DBc), Uvauk complex (Uc) and Kramanituar Complex (KC); the Tulemalu fault zone (Tfz); the Striding–Athabasca mylonite zone (SAmz); and the Virgin River shear zone (VRsz) and subsurface east Alberta (eA) segment.*

magmatism of similar chemistry, and perhaps similar age. Lastly, geochemical characterization of the Kramanituar Complex gabbroic suite is considered in the context of mantle-source composition, and the tectonic setting within which these rocks evolved.

## THE KRAMANITUAR COMPLEX

The Kramanituar Complex is a coherent, 850 km$^2$ elliptical exposure of high-grade rocks (Fig. 2) that is dominated by granulite-facies, metagabbro-gabbroic, anorthosite-norite-anorthosite, dated at 1902 ± 1.6 Ma (M. Sanborn-Barrie, S.D. Carr, and R.J. Thériault, unpub. data, 1999) from one locality (*K*-676b, this study). It includes charnockite layers of Archean age (ca. 2573 +28/-5 Ma; Schau, 1980) and panels of sillimanite- and kyanite-bearing paragneiss and diatexite of probable primary Archean age. Penetrative Paleoproterozoic (ca. 1.91–1.90 Ga) tectonometamorphism of the complex has obscured essentially all primary magmatic features of these rocks (M. Sanborn-Barrie, unpub. data, 1999) and has resulted in the penetrative development of steeply dipping, northwest- to west-striking L/S fabrics defined mainly by granulite-facies assemblages (12–15 kbar, 800–850°C; M. Sanborn-Barrie and R.G. Berman, unpub. data, 1999). These fabrics include a steep belt, 3–6 km wide, of granulite-facies ribbon mylonites (Northern shear zone; inset Fig. 2), which is cut by a leucogranite dyke dated at 1902.6 ± 1 Ma, providing a minimum age of penetrative ductile deformation for the complex (M. Sanborn-Barrie, S.D. Carr, and R.J. Thériault, unpub. data, 1999).

Prograde metamorphism of the complex at 1910–1908 Ma, and possibly as early as 1917 Ma, is recorded by monazite ages from sillimanite- and kyanite-bearing paragneiss. High-grade conditions continued until at least 1902 ± 1.6 Ma, the primary magmatic U-Pb zircon age of gabbroic anorthosite. Exhumation of the complex is recorded by rocks with disequilibrium textures, in that these record a

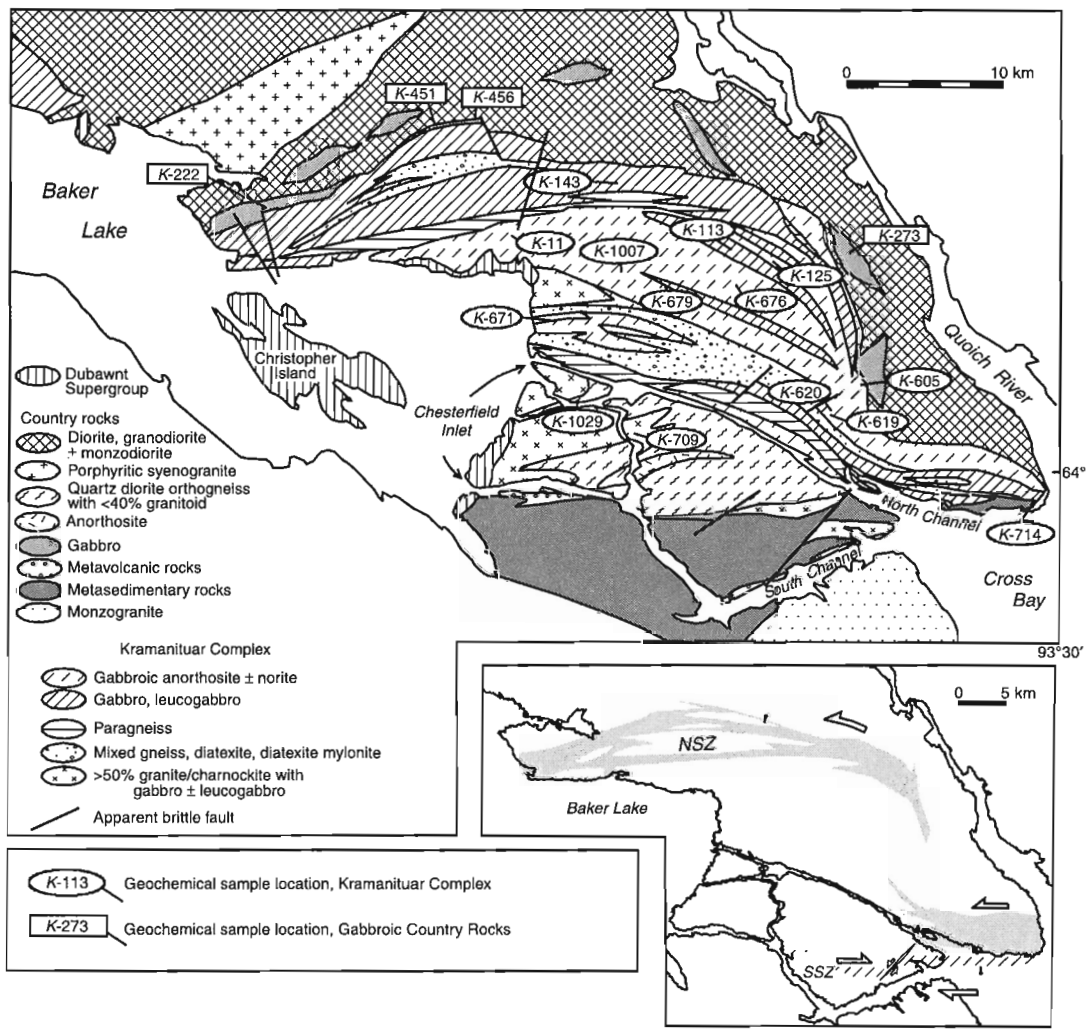


***Figure 2.*** *General geology of the Kramanituar Complex and its country rocks, modified from Schau and Ashton (1980) and Sanborn-Barrie (unpub. data, 1999). NSZ = Northern shear zone, SSZ = Southern shear zone.*

near-isothermal (850–750°C) decompression history from peak conditions of ca. 13 kbar to 8–9 kbar (M. Sanborn-Barrie and R.G. Berman, unpub. data, 1999). Exhumation to mid-crustal levels led to very rapid cooling (>450°C/Ma) of the complex between 1902 Ma and 1901 Ma. This is recorded by widespread titanite and rutile data (M. Sanborn-Barrie, S.D. Carr, and R.J. Thériault, unpub. data, 1999) and is reflected by the general absence of textures indicative of re-equilibration or thermal relaxation in these rocks.

## COUNTRY ROCKS TO THE KRAMANITUAR COMPLEX

The Kramanituar Complex is in contact with mainly amphibolite-facies Archean rocks. Geothermobarometric and geochronological constraints on their tectonometamorphic evolution point to a similar Paleoproterozoic history to the north, but indicate an older, mainly Neoarchean, history to the south.

North and east of the complex, foliated to gneissic quartzofeldspathic plutonic rocks, with a U-Pb zircon age of 2675 +33/-11 Ma from one locality (Schau, 1980) host hornblende-bearing gabbroic rocks. Two of these gabbroic units yield estimated *P-T* conditions of 8–13 kbar and 760 ± 60°C (garnet-clinopyroxene-plagioclase-amphibole), indicating the presence of high-pressure rocks beyond the north and east boundaries of the Kramanituar Complex.

South of the complex, metasedimentary rocks and minor, ca. 2.68 Ga metavolcanic rocks (Davis and Sanborn-Barrie, unpub. data, 1998) contain a regional, northeast-striking, moderately northwest-dipping foliation which is intensified and deflected into the dextral, right-stepping Southern shear zone (Fig. 2 inset). An age of ca. 2550 Ma for syntectonic syenogranite pegmatite within the Southern shear zone dates movement on the shear zone and provides a minimum Neoarchean age for structures south of the complex.

## GEOCHEMISTRY

### *Analytical Techniques*

Representative samples of gabbroic units were analyzed at the Geological Survey of Canada for major, minor, and trace elements (GSC, unpublished internal schedule, 1996). Major- and minor-element oxides were analyzed by fused-disk wavelength-dispersive X-ray fluorescence with limits of determination better than 0.5%. Trace elements, including Ba, Be, Co, Cr, Cu, Ni, Sc, Sr, V, and Zn, were analyzed by inductively coupled plasma (ICP) emission spectrometry with limits of determination better than ±20 ppm for Ba, Rb, and Sr, and better than ±10 ppm for the other elements listed. All other trace elements, including the rare-earth elements, were analyzed by ICP mass spectrometry, for which determination limits better than 0.1 ppm are obtained for all trace elements except for Mo and Ta (0.2 ppm), Zr (0.5 ppm), and Pb (2 ppm). Major- and trace-element geochemical data for gabbroic rocks are presented in Table 1 and described below.

### *Geochemistry of gabbroic rocks within the Kramanituar Complex*

Major-element data for gabbroic to anorthositic rocks of the Kramanituar Complex are plotted on AFM and Jensen ternary diagrams in Figure 3. These diagrams are intended for samples representative of liquid compositions, such as the gabbro samples which are mainly from dikes/sills less than 15 m wide, two of which are interpreted to cut country rocks presently exposed south of the complex (samples *K*-1029 and *K*-709; Fig. 2). Regardless, the diagrams serve to portray the range of rock compositions and highlight the geochemical continuity shown by the samples. The gabbros plot in the high-Fe tholeiite basalt field, with two samples between the tholeiitic andesite and calc-alkalic basalt fields. With decreasing colour index, samples plot progressively closer to

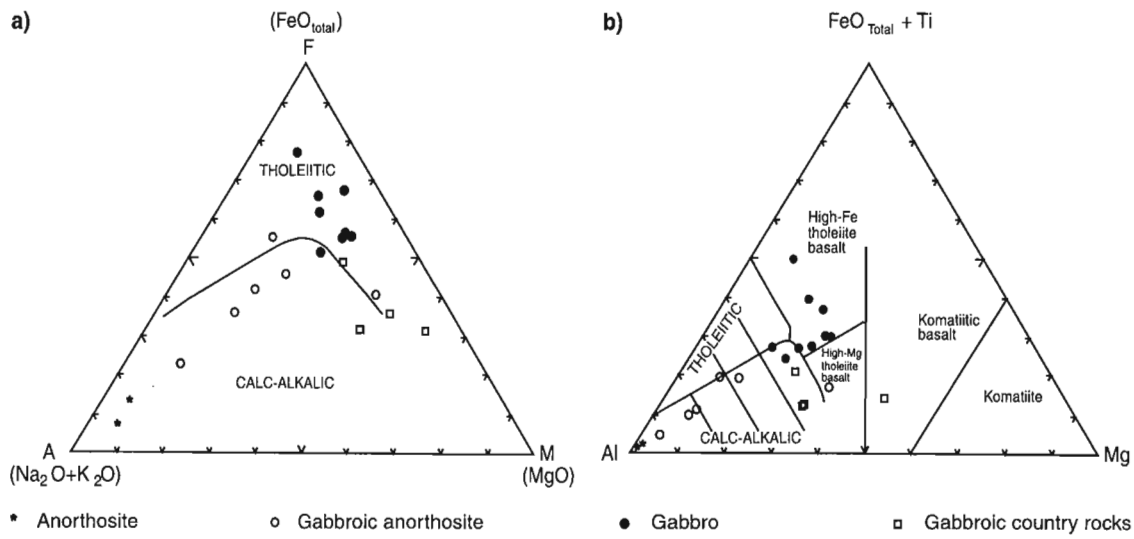


***Figure 3.*** *Ternary variation diagrams.* ***a)*** *AFM diagram after Irvine and Baragar (1971).* ***b)*** *Jensen cation plot (Jensen and Pyke, 1982).*

the alkali apex on the AFM diagram and toward the $Al_2O_3$ apex on the Jensen diagram. Magnesium numbers for the suite range from 37 to 70, except for the most ferroan sample (*K*-113a) which has a Mg number of 19.4 (Table 1). Chromium and Ni contents for gabbro and gabbroic anorthosite are moderate to low, ranging between 13 and 260 ppm, and 14 and 220 ppm, respectively; both elements are generally below detection limits in anorthosite. Rare-earth element (REE) data for rocks of gabbroic composition (Fig. 4a) show two main patterns: 1) flat REE patterns at 10 times (*K*-679b) to 30 times (*K*-113a) chondrite values without substantial enrichment or depletion in Eu (Eu/Eu* = 0.86–1.08); or 2) gently sloped patterns ($La_N/Yb_N$ = 2.2–5.2) with small negative europium anomalies (Eu/Eu* = 0.78–0.87) (Eu/Eu* = $Eu_N\sqrt{/[(Sm_N)(Gd_N)]}$). Gabbroic anorthosite samples typically have moderately sloped patterns ($La_N/Yb_N$ = 5.1–13),

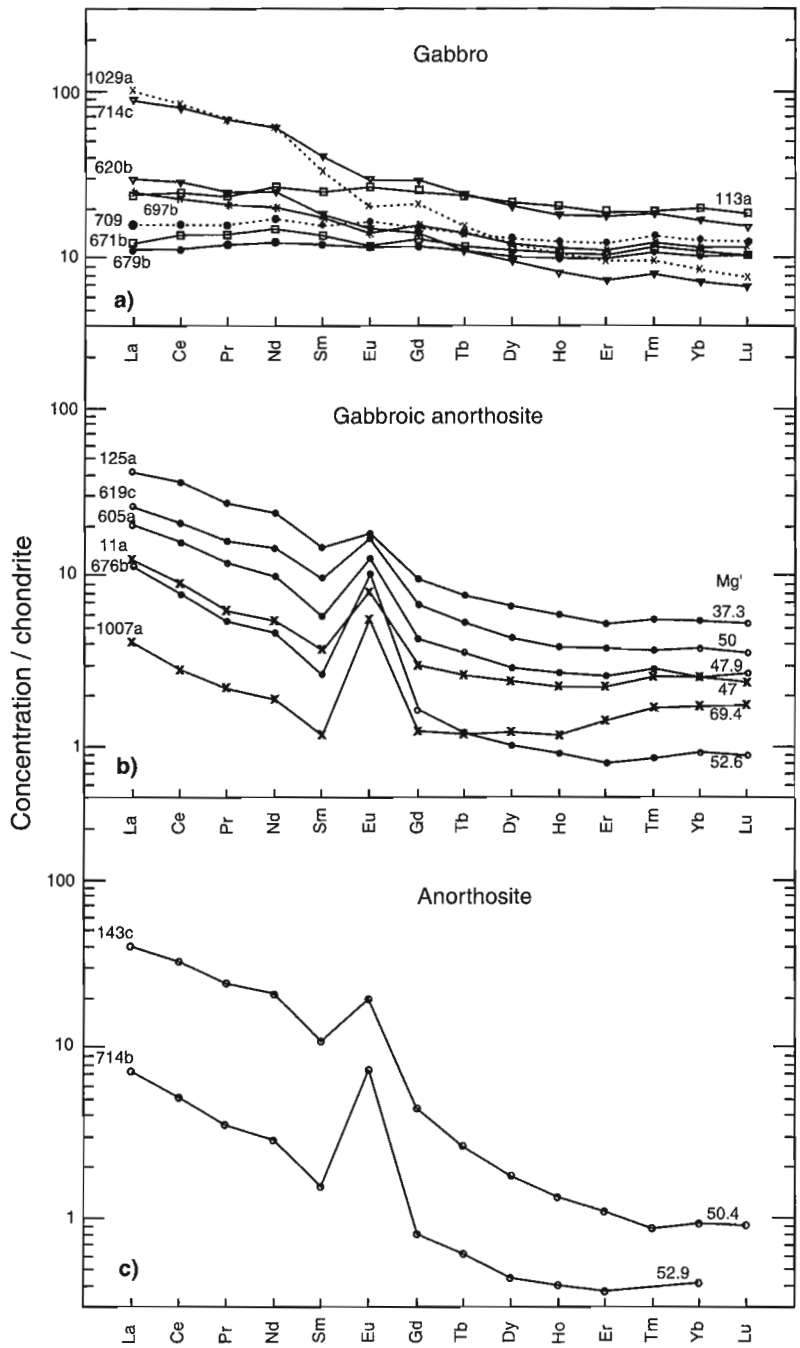


***Figure 4.*** *REE abundances for mafic rocks from the Kramanituar Complex normalized to chondrite values of Sun (1980).* ***a****) Gabbro.* ***b****) Gabbroic anorthosite with Mg number (see Table 1) for each representative sample shown.* ***c****) Anorthosite with Mg number.*

**Table 1.** Geochemical data for representative gabbroic samples from the Kramanituar Complex and surrounding country rocks.

| | Kramanituar gabbroic suite | | | | | | | | | | | | | | | | Gabbroic country rocks | | | |
|---|---|---|---|---|---|---|---|---|---|---|---|---|---|---|---|---|---|---|---|---|
| | Anorthosite | | Gabbroic anorthosite | | | | | | Gabbro | | | | | | | | | | | |
| | K-143c | K-714b | K-11a | K-125a | K-605a | K-619c | K-676b | K-1007a | K-113a | K-620b | K-671b | K-679b | K-697b | K-709 | K-714c | K-1029a | K-222 | K-273a | K-451b | K-456a |
| $SiO_2$ | 51.60 | 53.80 | 51.90 | 50.60 | 53.30 | 51.60 | 54.60 | 53.00 | 48.50 | 50.70 | 47.60 | 50.40 | 49.50 | 51.90 | 50.20 | 50.50 | 50.20 | 50.90 | 46.90 | 50.30 |
| $TiO_2$ | 0.21 | 0.08 | 0.30 | 1.27 | 0.31 | 2.18 | 0.14 | 0.18 | 3.14 | 1.38 | 1.05 | 1.04 | 1.43 | 1.25 | 2.50 | 1.29 | 0.28 | 0.27 | 0.17 | 0.40 |
| $Al_2O_3$ | 28.60 | 28.30 | 24.60 | 22.50 | 24.80 | 21.60 | 26.50 | 17.30 | 13.10 | 14.10 | 15.60 | 18.40 | 14.60 | 12.10 | 13.10 | 17.60 | 18.70 | 12.40 | 22.20 | 18.00 |
| $Fe_2O_3$ | 0.00 | bdl | 1.60 | 2.90 | 1.20 | 1.70 | 0.40 | 1.60 | 7.30 | 3.40 | 5.90 | 2.60 | 3.10 | 4.60 | 5.40 | 3.20 | 1.50 | 1.90 | 2.00 | 3.60 |
| FeO | 0.80 | 0.60 | 3.10 | 4.90 | 2.80 | 5.20 | 1.30 | 6.80 | 13.20 | 9.60 | 6.40 | 9.20 | 10.10 | 10.20 | 10.10 | 6.80 | 4.00 | 4.50 | 4.90 | 6.00 |
| MnO | 0.01 | 0.01 | 0.06 | 0.09 | 0.05 | 0.09 | 0.02 | 0.14 | 0.24 | 0.20 | 0.20 | 0.18 | 0.23 | 0.33 | 0.24 | 0.13 | 0.08 | 0.14 | 0.09 | 0.14 |
| MgO | 0.41 | 0.34 | 2.03 | 2.25 | 1.80 | 3.38 | 0.93 | 9.41 | 2.40 | 7.24 | 6.41 | 4.26 | 6.93 | 5.26 | 4.42 | 5.27 | 7.89 | 12.00 | 9.43 | 6.48 |
| CaO | 11.00 | 11.50 | 10.70 | 10.60 | 10.10 | 9.21 | 10.50 | 8.40 | 8.52 | 10.70 | 11.50 | 11.00 | 10.80 | 10.70 | 9.00 | 9.60 | 9.48 | 14.40 | 10.60 | 9.90 |
| $Na_2O$ | 3.60 | 4.10 | 4.00 | 3.70 | 4.40 | 3.60 | 4.40 | 2.50 | 3.10 | 2.30 | 1.60 | 2.80 | 2.20 | 1.20 | 1.90 | 3.50 | 2.80 | 1.10 | 1.80 | 2.90 |
| $K_2O$ | 1.32 | 0.39 | 0.30 | 0.37 | 0.42 | 0.83 | 0.51 | 0.27 | 0.19 | 0.23 | 1.19 | 0.13 | 0.55 | 0.36 | 1.09 | 0.32 | 0.83 | 0.47 | 0.56 | 0.35 |
| $H_2O$ | 1.00 | 0.50 | 0.50 | 0.50 | 0.90 | 0.50 | 0.60 | 0.50 | 0.70 | 0.60 | 1.80 | 0.40 | 0.80 | 1.30 | 1.80 | 1.10 | 2.10 | 0.80 | 1.60 | 1.50 |
| $CO_2$ | 0.70 | 0.60 | 0.20 | 0.40 | 0.20 | 0.20 | 0.30 | 0.20 | bdl | bdl | 1.20 | 0.20 | 0.40 | bdl | 0.20 | 0.50 | 1.30 | 0.30 | 0.40 | 0.30 |
| $P_2O_5$ | 0.01 | bdl | bdl | 0.07 | 0.04 | 0.11 | 0.02 | bdl | 0.15 | 0.11 | 0.08 | 0.08 | 0.10 | 0.10 | 0.31 | 0.39 | 0.03 | bdl | 0.02 | 0.12 |
| TOTAL | 99.40 | 100.40 | 99.30 | 100.30 | 100.40 | 100.40 | 100.30 | 100.50 | 100.80 | 100.90 | 100.80 | 100.80 | 101.00 | 100.70 | 100.40 | 100.60 | 99.80 | 99.30 | 100.80 | 100.20 |
| Mg[1] | 50.40 | 52.90 | 46.99 | 37.26 | 47.91 | 49.89 | 52.62 | 69.36 | 19.40 | 53.13 | 52.04 | 42.26 | 51.59 | 42.10 | 36.94 | 51.91 | 74.51 | 79.30 | 73.62 | 58.16 |
| Rb | 14.00 | 7.00 | 0.65 | 0.93 | 2.90 | 6.10 | 3.30 | 2.10 | 1.10 | 1.10 | 24.00 | 0.78 | 10.00 | 8.90 | 40.00 | 1.30 | 6.40 | 21.00 | 9.40 | 5.60 |
| Sr | 340.00 | 430.00 | 410.00 | 360.00 | 390.00 | 390.00 | 440.00 | 260.00 | 150.00 | 270.00 | 160.00 | 130.00 | 130.00 | 64.00 | 150.00 | 430.00 | 1300.0 0 | 350.00 | 280.00 | 490.00 |
| Cs | 0.92 | 0.46 | 0.07 | 0.09 | 0.11 | 0.13 | 0.07 | 0.05 | 0.06 | 0.08 | 0.73 | 0.03 | 0.20 | 0.67 | 2.40 | 1.60 | 0.73 | 0.53 | 0.21 | 0.21 |
| Ba | 420.00 | 150.00 | 130.00 | 140.00 | 150.00 | 400.00 | 200.00 | 110.00 | 80.00 | 130.00 | 190.00 | 50.00 | 90.00 | 90.00 | 210.00 | 260.00 | 410.00 | 140.00 | 200.00 | 150.00 |
| Y | 3.00 | 1.00 | 5.70 | 14.00 | 6.70 | 9.60 | 2.20 | 2.90 | 48.00 | 20.00 | 26.00 | 24.00 | 28.00 | 29.00 | 42.00 | 23.00 | 4.30 | 8.00 | 3.70 | 6.30 |
| Zr | 17.00 | 14.00 | 32.00 | 86.00 | 34.00 | 80.00 | 20.00 | 17.00 | bdl | 97.00 | 81.00 | 67.00 | 91.00 | bdl | bdl | bdl | 100.00 | 61.00 | 24.00 | 25.00 |
| Hf | 0.41 | 0.30 | 0.71 | 2.10 | 0.81 | 1.70 | 0.45 | 0.40 | 4.30 | 2.40 | 2.00 | 1.70 | 2.30 | 2.70 | 5.00 | 3.80 | 2.10 | 1.50 | 0.55 | 0.71 |
| Nb | 2.30 | 1.20 | 0.59 | 5.10 | 2.20 | 7.60 | 0.54 | 0.21 | 8.60 | 7.00 | 3.10 | 3.60 | 5.80 | 5.50 | 33.00 | 8.40 | 0.93 | 0.42 | 0.58 | 0.48 |
| Ta | 0.50 | 0.50 | bdl | 0.50 | 0.20 | 0.50 | bdl | 0.20 | 0.80 | 0.40 | 0.20 | 0.30 | 0.50 | 0.70 | 2.20 | 0.50 | 0.20 | bdl | 0.20 | 0.20 |
| Th | 1.40 | 0.13 | 0.43 | 2.60 | 1.30 | 0.59 | 0.23 | 0.18 | 0.42 | 0.10 | 0.28 | 0.33 | 1.20 | 0.64 | 0.87 | 0.28 | 0.16 | 0.33 | 0.37 | 0.38 |
| U | 0.49 | 0.07 | 0.08 | 0.52 | 0.41 | 0.13 | 0.06 | 0.07 | 0.11 | 0.04 | 0.08 | 0.09 | 0.24 | 0.43 | 0.71 | 0.08 | 0.10 | 0.08 | 0.08 | 0.08 |
| La | 13.00 | 2.40 | 4.20 | 14.00 | 6.80 | 8.80 | 3.90 | 1.40 | 8.00 | 10.00 | 4.10 | 3.80 | 8.50 | 5.30 | 29.00 | 33.00 | 22.00 | 4.50 | 2.70 | 7.90 |
| Ce | 28.00 | 4.40 | 7.90 | 32.00 | 14.00 | 18.00 | 7.00 | 2.50 | 22.00 | 25.00 | 12.00 | 10.00 | 20.00 | 14.00 | 68.00 | 72.00 | 41.00 | 12.00 | 5.80 | 17.00 |
| Pr | 3.10 | 0.46 | 0.83 | 3.60 | 1.60 | 2.10 | 0.74 | 0.29 | 3.10 | 3.30 | 1.80 | 1.60 | 2.80 | 2.10 | 8.60 | 8.90 | 4.40 | 1.60 | 0.68 | 2.10 |
| Nd | 13.00 | 1.80 | 3.50 | 15.00 | 6.40 | 9.40 | 3.00 | 1.20 | 17.00 | 16.00 | 9.40 | 8.00 | 13.00 | 11.00 | 38.00 | 37.00 | 19.00 | 8.40 | 2.90 | 9.70 |
| Sm | 2.20 | 0.31 | 0.75 | 3.00 | 1.20 | 2.00 | 0.54 | 0.24 | 5.10 | 3.80 | 2.80 | 2.50 | 3.70 | 3.20 | 8.30 | 6.70 | 3.00 | 2.00 | 0.59 | 1.90 |
| Eu | 1.50 | 0.58 | 0.64 | 1.40 | 0.99 | 1.30 | 0.81 | 0.44 | 2.10 | 1.20 | 0.89 | 0.92 | 1.10 | 1.30 | 2.30 | 1.60 | 0.99 | 0.60 | bdl | 0.74 |
| Gd | 1.20 | 0.22 | 0.83 | 2.70 | 1.20 | 1.90 | 0.46 | 0.34 | 7.00 | 4.00 | 3.60 | 3.30 | 4.40 | 4.30 | 8.00 | 5.90 | 1.90 | 1.70 | 0.65 | 1.60 |
| Tb | 0.13 | 0.03 | 0.13 | 0.39 | 0.18 | 0.27 | 0.06 | 0.06 | 1.20 | 0.56 | 0.59 | 0.57 | 0.72 | 0.72 | 1.20 | 0.77 | 0.18 | 0.25 | 0.10 | 0.20 |
| Dy | 0.59 | 0.15 | 0.83 | 2.30 | 1.00 | 1.50 | 0.35 | 0.42 | 7.50 | 3.40 | 3.90 | 3.50 | 4.40 | 4.50 | 7.00 | 4.20 | 0.86 | 1.40 | 0.59 | 1.10 |
| Ho | 0.10 | 0.03 | 0.17 | 0.46 | 0.21 | 0.30 | 0.07 | 0.09 | 1.60 | 0.65 | 0.82 | 0.79 | 0.92 | 0.98 | 1.40 | 0.82 | 0.14 | 0.28 | 0.12 | 0.22 |
| Er | 0.24 | 0.08 | 0.50 | 1.20 | 0.58 | 0.85 | 0.18 | 0.32 | 4.40 | 1.70 | 2.30 | 2.30 | 2.60 | 2.80 | 4.00 | 2.20 | 0.35 | 0.70 | 0.36 | 0.53 |
| Tm | 0.03 | bdl | 0.09 | 0.20 | 0.10 | 0.13 | 0.03 | 0.06 | 0.75 | 0.29 | 0.41 | 0.39 | 0.44 | 0.48 | 0.65 | 0.34 | 0.06 | 0.11 | 0.06 | 0.09 |
| Yb | 0.20 | 0.09 | 0.55 | 1.20 | 0.56 | 0.84 | 0.20 | 0.38 | 4.50 | 1.60 | 2.40 | 2.30 | 2.60 | 2.80 | 3.70 | 1.90 | 0.35 | 0.66 | 0.33 | 0.48 |
| Lu | 0.03 | bdl | 0.08 | 0.18 | 0.09 | 0.12 | 0.03 | 0.06 | 0.64 | 0.23 | 0.35 | 0.36 | 0.40 | 0.43 | 0.53 | 0.26 | 0.06 | 0.09 | 0.05 | 0.08 |
| Co | 15.00 | 11.00 | 34.00 | 39.00 | 21.00 | 29.00 | 11.00 | 52.00 | 66.00 | 49.00 | 51.00 | 39.00 | 46.00 | 45.00 | 39.00 | 34.00 | 49.00 | 42.00 | 51.00 | 39.00 |
| Ni | bdl | bdl | 31.00 | 34.00 | 35.00 | 88.00 | 19.00 | 220.00 | 14.00 | 57.00 | 130.00 | 49.00 | 100.00 | 49.00 | 15.00 | 60.00 | 260.00 | 180.00 | 340.00 | 75.00 |
| Cr | bdl | 10.00 | 19.00 | 16.00 | 23.00 | 150.00 | 13.00 | 210.00 | bdl | 74.00 | 260.00 | 27.00 | 160.00 | 150.00 | 39.00 | 99.00 | 170.00 | 520.00 | 50.00 | 60.00 |
| Cu | bdl | bdl | 17.00 | 49.00 | 31.00 | 17.00 | bdl | 91.00 | 97.00 | 79.00 | 49.00 | 110.00 | 68.00 | 120.00 | 79.00 | 63.00 | 15.00 | bdl | 22.00 | 73.00 |
| Zn | bdl | bdl | 16.00 | 37.00 | 20.00 | 46.00 | bdl | 45.00 | 140.00 | 72.00 | 99.00 | 71.00 | 93.00 | 210.00 | 120.00 | 74.00 | 50.00 | 14.00 | 24.00 | 53.00 |
| Pb | 8.00 | 3.00 | 3.00 | 2.00 | 6.00 | 5.00 | 3.00 | bdl | 2.00 | 2.00 | 2.00 | 6.00 | 2.00 | bdl | 3.00 | 3.00 | 13.00 | bdl | 6.00 | 4.00 |
| Mo | 0.30 | 1.10 | 0.30 | 0.70 | 2.60 | 2.00 | 0.20 | bdl | 2.20 | 0.30 | 0.50 | 1.10 | 1.10 | 1.80 | 1.30 | 0.40 | 22.00 | 0.30 | 0.30 | 0.60 |
| V | bdl | bdl | 53.00 | 120.00 | 25.00 | 110.00 | bdl | 99.00 | 450.00 | 310.00 | 310.00 | 270.00 | 290.00 | 310.00 | 370.00 | 220.00 | 24.00 | 130.00 | bdl | 200.00 |
| Sc | 1.80 | 0.80 | 11.00 | 16.00 | 8.30 | 14.00 | 2.90 | 20.00 | 42.00 | 36.00 | 43.00 | 31.00 | 36.00 | 39.00 | 40.00 | 25.00 | 11.00 | 53.00 | 7.70 | 23.00 |
| Be | 1.80 | bdl | 2.20 | 12.00 | 2.10 | 16.00 | 0.80 | 1.00 | 31.00 | 10.00 | 7.50 | 7.30 | 10.00 | 8.60 | 17.00 | 8.50 | 2.60 | 2.50 | 1.50 | 3.60 |
| Ga | 31.00 | 22.00 | 24.00 | 24.00 | 23.00 | 19.00 | 24.00 | 14.00 | 26.00 | 20.00 | 18.00 | 19.00 | 19.00 | 18.00 | 24.00 | 22.00 | 16.00 | 12.00 | 14.00 | 19.00 |
| In | bdl | 0.07 | 0.08 | bdl | bdl | bdl | bdl | bdl | 0.12 | 0.17 | 0.07 | 0.06 | 0.08 | 0.17 | 0.20 | 0.11 | bdl | 0.14 | 0.10 | 0.11 |
| Tl | 0.20 | 0.03 | bdl | bdl | 0.03 | 0.02 | bdl | bdl | bdl | bdl | 0.22 | bdl | 0.08 | 0.09 | 0.19 | bdl | 0.04 | 0.19 | 0.08 | 0.03 |

[1] Mg number = mol % MgO/mol % FeO, where mol % FeO = $0.9 \cdot FeO_{total}$ or $0.9 \cdot (FeO/71.9 + Fe_2O_3 \cdot 0.9/71.9)$

bdl = below detection limit

with LREE (light rare-earth elements) from 10 to 45 times chondrite values and HREE from 0.9 to 6 times chondrite values (Fig. 4b). Strong positive Eu anomalies (Eu/Eu*=1.5–5.0) characterize the REE pattern of gabbroic anorthosite and are consistent with variable cumulate plagioclase in these rocks. One gabbroic anorthosite sample (*K*-1007a) shows less LREE enrichment ($La_N/Yb_N$ = 2.5) with LREE at 4.5 times and HREE at 1.8 times chondrite values. Anorthosite is characterized by LREE enrichment ($La_N/Yb_N$ >17.8) and strong positive Eu anomalies (Eu/Eu*=2.8–6.8; Fig. 4c).

Incompatible trace-element data for the Kramanituar gabbros, those samples most closely approximating liquid compositions, are shown on a multielement diagram (Fig. 5), in order of decreasing incompatibility from left to right. A gentle concave-down pattern, interrupted only by Th, Sr ± Rb troughs, characterizes these gabbroic rocks.

### *Geochemistry of gabbroic country rocks, north and east of the Kramanituar Complex*

Country rocks of gabbroic composition, though not demonstrated to represent a suite of petrogenetically coherent rocks, are described here as a group for comparison with those of the Kramanituar Complex. Their major-element compositions plot near the tholeiitic/calc-alkalic boundary (open squares in Fig. 3a) and lie within the calc-alkalic basalt and komatiitic basalt (*K*-273a) fields (Fig. 3b). This suite has higher Mg numbers, from 58 to 80, Cr contents of 50 to 520 ppm, and Ni

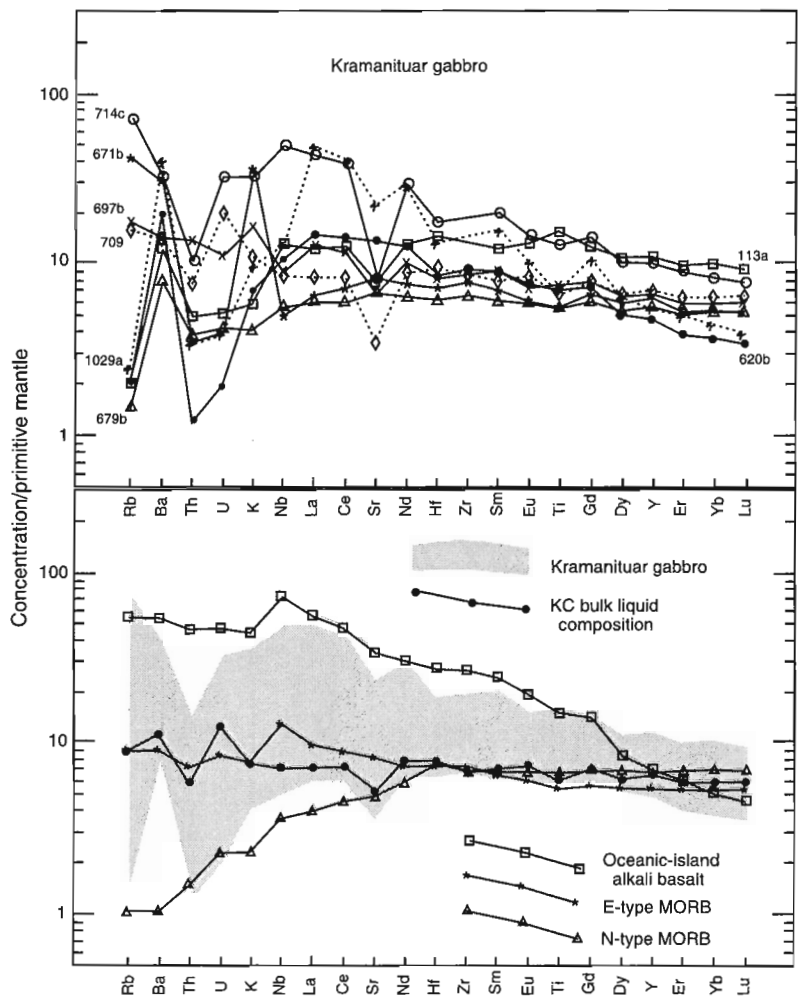


***Figure 5.*** *Incompatible trace-element plot for gabbros from the Kramanituar Complex normalized to primitive mantle values of Hofmann (1988). Also shown is the pattern for N-type MORB, E-type MORB, and P-type MORB for comparison (values of Sun and McDonough, 1989).*

contents of 75 to 340 ppm, relative to the Kramanituar gabbro samples. Rare-earth element data show moderately sloped patterns ($La_N/Yb_N$ = 4.5–46), with LREE from 8 to 70 times chondrite values and HREE from 1.5 to 3 times chondrite values (Fig. 6a). They show either minor enrichment or depletion in Eu (Eu/Eu* = 0.97–1.27). Normalized incompatible-element abundance patterns for gabbroic country rocks show a decreasing abundance of less-incompatible elements, resulting in a negatively sloped pattern which is punctuated by strong spikes. Negative spikes occur at Th, Nb, and Ti, with positive spikes at Rb, K, and a lesser positive peak at La-Sr (Fig. 6b).

### *Geochemical modelling of crustal magmatic processes*

The trace-element geochemistry data of gabbroic rocks from the study area show several features of petrogenetic interest. Flat REE patterns for gabbroic rocks from the Kramanituar Complex suggest that several of the analyzed samples may represent bulk liquid compositions from which cumulate rocks of gabbroic anorthosite composition have been derived. Petrochemical modelling, presented below, investigates the potential for a cogenetic relationship between these suites.

### *Parameters for geochemical modelling*

Gabbro compositions characterized by flat REE patterns from 10 to 25 times chondrite values (Fig. 4a, Table 1) are permissive of bulk liquid compositions for the Kramanituar gabbroic suite. Of these, samples *K*-679b and *K*-709 are most appropriate, with 50 to 52 weight per cent $SiO_2$, 4.26 to 5.26 weight per cent MgO, Mg numbers of 42, 27–150 ppm Cr, and 49 ppm Ni, values that are typical of tholeiitic basalts that have fractionated some olivine (Basaltic Volcanism Study Project, 1981). An estimate of the bulk liquid composition for the Kramanituar Complex gabbroic suite (Table 2) is therefore taken as an average of samples *K*-679b and *K*-709 and is high-Fe tholeiitic basalt with a flat REE pattern ($La_N/Yb_N$ = 1.19, Eu/Eu* = 1.04) at 14 times chondrite values.

Mineral/melt partition coefficients used for AFC modelling are listed in Table 3. The partition coefficients for plagioclase are from the Proterozoic Kiglapait Intrusion of Labrador (Morse, 1988), a layered complex of similar size, modal lithology and anorthite content to the Kramanituar Complex. Kiglapait partition coefficients for plagioclase are similar to those for other granulite-facies anorthosite complexes (Phinney and Morrison, 1990), and are an order of magnitude higher than those of McKay (1982) which are appropriate for lower pressure conditions. The modal mineralogy used to determine bulk partition coefficients representative of a gabbroic anorthosite fractionate is 74% plagioclase, 8% orthopyroxene, 12% clinopyroxene, 3% amphibole, 2% ilmenite, and 1% magnetite. This is based on petrographic observation of gabbroic anorthosite samples, excluding garnet as a fractionating phase. In a separate series of AFC models, 1% garnet, which strongly sequesters the middle and heavy rare-earth elements (HREE), was included. It was

**Table 2.** Geochemical data for derived Kramanituar bulk liquid and crustal contaminant compositions.

| | Kramanituar bulk liquid | Paragneissic leucosome | | |
|---|---|---|---|---|
| | | *K*-86b | *K*-289a | Contaminant |
| $SiO_2$ | 51.15 | 64.20 | 70.70 | 67.45 |
| $TiO_2$ | 1.14 | 0.89 | 0.35 | 0.62 |
| $Al_2O_3$ | 15.25 | 18.40 | 16.30 | 17.35 |
| $Fe_2O_3$ | 3.60 | 4.90 | 1.60 | 3.25 |
| FeO | 9.70 | 3.60 | 2.00 | 2.80 |
| MnO | 0.25 | 0.16 | 0.04 | 0.10 |
| MgO | 4.76 | 2.85 | 1.85 | 2.35 |
| CaO | 10.85 | 0.91 | 1.02 | 0.96 |
| $Na_2O$ | 2.00 | 2.10 | 1.80 | 1.95 |
| $K_2O$ | 0.24 | 1.44 | 3.51 | 2.47 |
| $H_2O$ | 0.85 | 1.20 | 0.40 | 0.80 |
| $CO_2$ | bdl | bdl | 0.40 | bdl |
| $P_2O_5$ | 0.09 | 0.03 | 0.03 | 0.03 |
| TOTAL | 100.75 | 100.90 | 100.10 | 100.50 |
| Mg[1] | 42 | | | |
| Rb | 4.84 | 30.00 | 76.00 | 53.00 |
| Sr | 97.00 | 170.00 | 140.00 | 155.00 |
| Cs | 0.35 | 0.40 | 0.10 | 0.25 |
| Ba | 70.00 | 370.00 | 590.00 | 480.00 |
| Y | 26.50 | 27.00 | 29.00 | 28.00 |
| Zr | 67.00 | bdl | bdl | bdl |
| Hf | 2.20 | 4.10 | 3.20 | 3.65 |
| Nb | 4.55 | 11.00 | 7.70 | 9.35 |
| Ta | 0.50 | 0.50 | 0.70 | 0.60 |
| Th | 0.48 | 5.60 | 0.58 | 3.09 |
| U | 0.26 | 0.69 | 0.19 | 0.44 |
| La | 4.55 | 38.00 | 29.00 | 33.50 |
| Ce | 12.00 | 79.00 | 53.00 | 68.00 |
| Pr | 1.85 | 7.90 | 4.80 | 6.35 |
| Nd | 9.50 | 31.00 | 17.00 | 24.00 |
| Sm | 2.85 | 5.40 | 3.20 | 4.30 |
| Eu | 1.11 | 1.30 | 1.20 | 1.25 |
| Gd | 3.80 | 4.90 | 3.70 | 4.30 |
| Tb | 0.64 | 0.74 | 0.65 | 0.69 |
| Dy | 4.00 | 4.40 | 4.30 | 4.35 |
| Ho | 0.88 | 0.86 | 0.90 | 0.88 |
| Er | 2.55 | 2.40 | 2.60 | 2.50 |
| Tm | 0.43 | 0.41 | 0.48 | 0.44 |
| Yb | 2.55 | 2.40 | 2.70 | 2.55 |
| Lu | 0.39 | 0.35 | 0.39 | 0.37 |
| Co | 42.00 | 43.00 | 40.00 | 41.50 |
| Ni | 49.00 | 29.00 | bdl | 9.50 |
| Cr | 88.50 | 120.00 | 92.00 | 108.00 |
| Cu | 115.00 | 34.00 | bdl | 12.00 |
| Zn | 140.50 | 82.00 | 47.00 | 64.50 |
| Pb | 2.00 | 31.00 | 28.00 | 29.50 |
| Mo | 1.45 | 1.80 | 1.80 | 1.80 |
| V | 290.00 | 140.00 | 52.00 | 96.00 |
| Sc | 35.00 | 23.00 | 13.00 | 18.00 |
| Be | 7.95 | 8.60 | 3.30 | 5.95 |
| Ga | 18.50 | 23.00 | 21.00 | 22.00 |
| In | 0.11 | 0.10 | bdl | 0.02 |
| Tl | 0.03 | 0.15 | 0.39 | 0.27 |

[1] Mg number = mol % MgO/mol % FeO, where mol % FeO = 0.9•$FeO_{total}$ or 0.9•(FeO/71.9+$Fe_2O_3$•0.9/71.9)
bdl = below detection limit

**Table 3.** Mineral/melt partition coefficients used for AFC modelling of gabbro-anorthosite suite from liquid gabbro composition.

| REE | Plagioclase[1] | Orthopyroxene[2] | Clinopyroxene[3] | Amphibole[4] | Garnet[5] | Magnetite[6] | Ilmenite[7] |
|---|---|---|---|---|---|---|---|
| La | 0.65 | 0.0067 | 0.058 | 0.17 | 0.01 | 0.2 | 0.0064 |
| Ce | 0.49 | 0.0078 | 0.1 | 0.26 | 0.07 | 0.2 | 0.0065 |
| Nd | [0.321] | 0.011 | 0.22 | 0.44 | 0.26 | 0.25 | 0.0085 |
| Sm | 0.152 | 0.019 | 0.45 | 0.76 | 1 | 0.3 | 0.014 |
| Eu | 0.813 | 0.022 | 0.48 | 0.88 | 1.58 | 0.25 | 0.00655 |
| Gd | 0.09 | 0.033 | 0.5 | 0.86 | 2.16 | 0.25 | 0.0065 |
| Tb | 0.072 | 0.05 | 0.5 | 0.83 | 2.74 | 0.25 | 0.0062 |
| Dy | [0.068] | 0.061 | 0.5 | 0.78 | 3.32 | 0.25 | 0.0067 |
| Er | [0.058] | 0.094 | 0.61 | 0.68 | 5.95 | 0.25 | 0.0062 |
| Yb | 0.048 | 0.14 | 0.58 | 0.59 | 8 | 0.25 | 0.0067 |
| Lu | 0.047 | 0.18 | 0.53 | 0.51 | 10 | 0.25 | 0.0065 |

[1] Mesoproterozoic Kiglapait intrusion (Morse, 1988)
[2,3,4] Basalt at 10–20 kb (Irving and Frey, 1984)
[5] Basalt at 30 kb and 1240°C (Nicholls and Harris, 1980)
[6] Andesitic liquids (Gill, 1981)
[7] Mare basalt composition at 1 atm and 1140°C (MacKay and Weill, 1976)

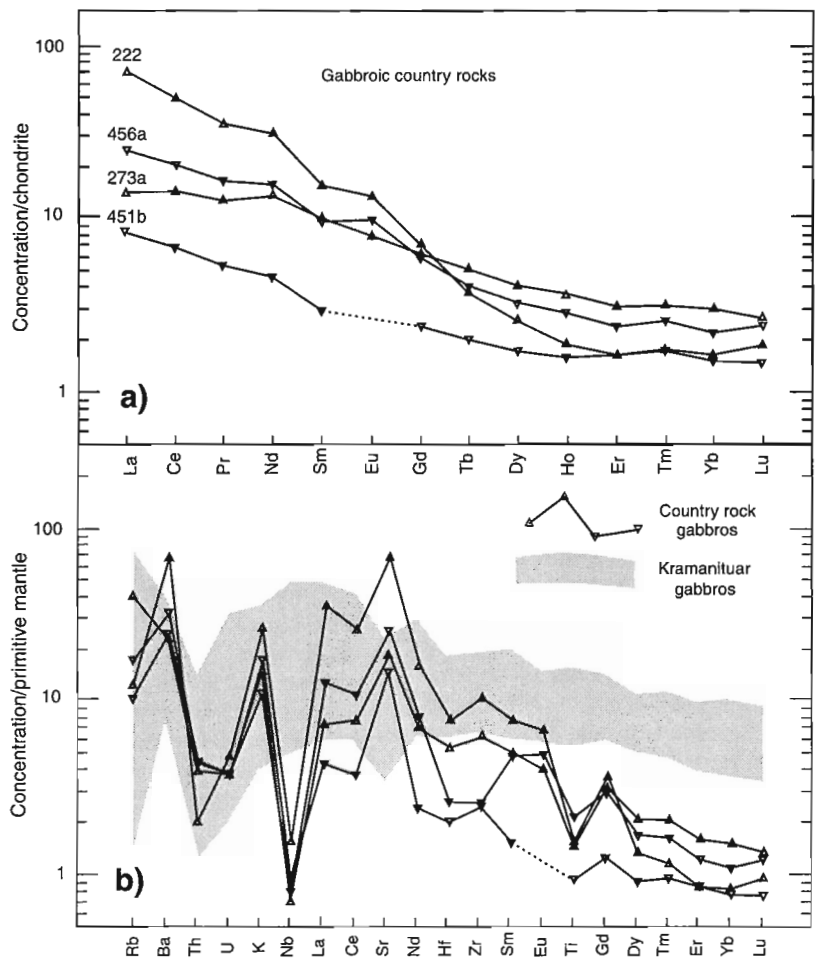


***Figure 6.*** *Trace-element geochemistry of gabbroic country rocks.* ***a)*** *REE abundances normalized to chondrite values of Sun (1980).* ***b)*** *Spider diagram showing REE and other incompatible trace-element abundances normalized to primitive mantle values of Hofmann (1988). Shaded region is the field for Kramanituar gabbro samples, for comparison (discussed in text).*

determined that even this low proportion of garnet was inappropriate for most samples with the possible exception of *K*-1007a (discussed below).

### *Fractionational crystallization model*

Fractional crystallization describes the crystallization of solid phases from a melt. It is best described by the Rayleigh Law, whereby crystals are removed from their site of formation after crystallization such that the distribution of trace elements is not an equilibrium process. Rayleigh fractionation is modeled by according to

$$C_L/C_O = F^{(D-1)}$$

where $C_L$ is the weight concentration of a trace element in the fractionating liquid, $C_O$ is the weight concentration of a trace element in the parental liquid, F is the fraction of melt remaining, and D is the bulk partition coefficient (based on mode) for the fractionating assemblage (Rollinson, 1993). A simple Rayleigh fractionation model is shown in Fig. 7a for cumulates derived from a parent composition represented by the estimated bulk composition of the Kramanituar gabbro suite. The model REE profiles for simple Rayleigh fractionation show a poor fit to the observed gabbroic anorthosite compositions due to the shallower negative slope to the model REE profiles and the restricted compositional range they represent for 10 to 50% fractionation (shaded; Fig. 7a).

A separate model investigated derivation of the gabbroic anorthosite suite via Rayleigh fractionation from a more enriched bulk liquid composition (i.e. modelled after sample *K*-714c; Fig. 4a). Since even the initial fractionate in equilibrium with such a liquid (Fig. 7b) is more enriched in the LREE than any of the observed cumulate rocks (shaded), it is unlikely that the gabbroic anorthosites were derived from a parental melt of this composition.

### *Assimilation-fractional crystallization model*

Assimilation of wall rock during fractional crystallization is a common process driven by the enthalpy of the magma and the latent heat of crystallization. The role of simultaneous assimilation and fractional crystallization (AFC) in generating cumulate rocks was investigated by using a crustal contaminant (Table 2) which is an average of sillimanite- (*K*-86b) and kyanite-bearing (*K*-289a) leucosome from the Kramanituar Complex. These are interpreted as partial-melt phases derived from paragneiss and are presently in contact with, and occur as partially digested xenoliths within, gabbroic anorthosite. Assimilation is modeled on a 1:1 ratio with fractionation; that is, removal of 10% fractionate is accompanied by assimilation of 10% metasedimentary leucosome. This degree of assimilation is geologically reasonable in an AFC process where derivative mafic magmas can contain up to 50 to 80% contaminant (Longhi et al., 1983; Sparks, 1986). Assimilation of crustal material is enhanced 1) for more primitive and hotter mafic magmas; 2) where crustal rocks have low fusion temperatures; and, 3) where crustal rocks are already at temperatures close to fusion upon intrusion of magma (Sparks, 1986). The second and third factors pertain to the Kramanituar Complex, where quartzofeldspathic metasedimentary rocks were at high-grade conditions just prior to intrusion of the mafic magma (M. Sanborn-Barrie, S.D. Carr, and R.J. Thériault, unpub. data, 1999). Furthermore, contamination of tholeiitic magma within the Kramanituar Complex by siliceous material is consistent with the presence of orthopyroxene as a significant cumulus phase in many of these rocks (Stolper, 1980; Ashwal 1993). Results of a simplified AFC process are shown in Fig. 7c. The model REE profiles for 10–50% AFC (shaded; Fig. 7c) are parallel to the observed profiles for gabbroic anorthositic rocks from the complex; however, the highly restricted range in REE abundances that can be derived by up to 50% fractionation does not match the range in REE abundances observed for the gabbroic anorthosite suite.

### *Modified assimilation-fractional crystallization model*

The model that best fits the observed REE patterns for gabbroic anorthosite cumulates is one of AFC with increasing degrees of intercumulus trapped liquid (Fig. 8). The proportion of intercumulus liquid was increased incrementally during fractionation, from 1% intercumulus liquid at 10% fractionation, to 25% liquid at 50% fractionation. This is consistent with adcumulus and intercumulus textures in anorthositic rocks worldwide (Ashwal, 1993). Furthermore, the cumulates with the lowest REE patterns are also the most primitive (Fig. 4b), consistent with the observation that adcumulate textures (<5% intercumulus liquid) are more common in hotter, more primitive cumulates (ie. Stillwater Complex, Ashwal 1993). Four gabbroic anorthosite samples correspond closely to model REE patterns for 10 to 50% AFC (Fig. 8a). The flat HREE pattern which characterizes these samples cannot be modelled if even 1% garnet is included in the fractionate mode. That garnet was not fractionating from the magma implies magmatic crystallization at depths corresponding to $P \leq 15$ kbar (Thompson, 1972). One gabbroic anorthosite sample (*K*-676b) has LREE which are modeled for 10% AFC, but has much lower HREE than predicted by this model. This sample has a low colour index (no normative diopside and 4.18 weight per cent normative hypersthene) and a mode of 85% plagioclase, 8% orthopyroxene, 3% clinopyroxene, 2% pargasitic amphibole, 1% magnetite, 1% ilmenite, and trace zircon. Modified AFC modelling using a bulk partition coefficient based on this mode results in close agreement between sample *K*-676b and a model REE pattern for 5% fractionate (Fig. 8b).

Only one gabbroic anorthosite REE pattern could not be modelled. Sample *K*-1007a, with a distinctive REE pattern showing much less LREE enrichment than other gabbroic anorthosite samples ($La_N/Yb_N = 2.5$), has a high colour index (4.31 weight per cent normative diopside and 32.52 weight per cent normative hypersthene). A bulk partition coefficient was calculated for the observed mode of 58% plagioclase, 30% orthopyroxene, 7% clinopyroxene, 2% amphibole, 1% magnetite, 1% ilmenite, and 1% garnet. Model REE patterns generated from this are *parallel* to the distinctive REE pattern of *K*-1007a (Fig. 8c); however, even the initial fractionate,

with no intercumulus liquid and no assimilated country rock, produces a pattern which is higher by 1.5 times chondrite values. This sample is the only gabbroic anorthosite with HREE that shows a marked concave-up pattern, a feature generally attributed to garnet±hornblende fractionation.

### *Comparison between the Kramanituar gabbroic suite and gabbroic country rocks*

Foliated gabbroic country rocks north and east of the Kramanituar Complex are characterized by an incompatible trace-element pattern which is distinct from that of the Kramanituar gabbroic suite (Fig. 5b). The two most distinctive features of

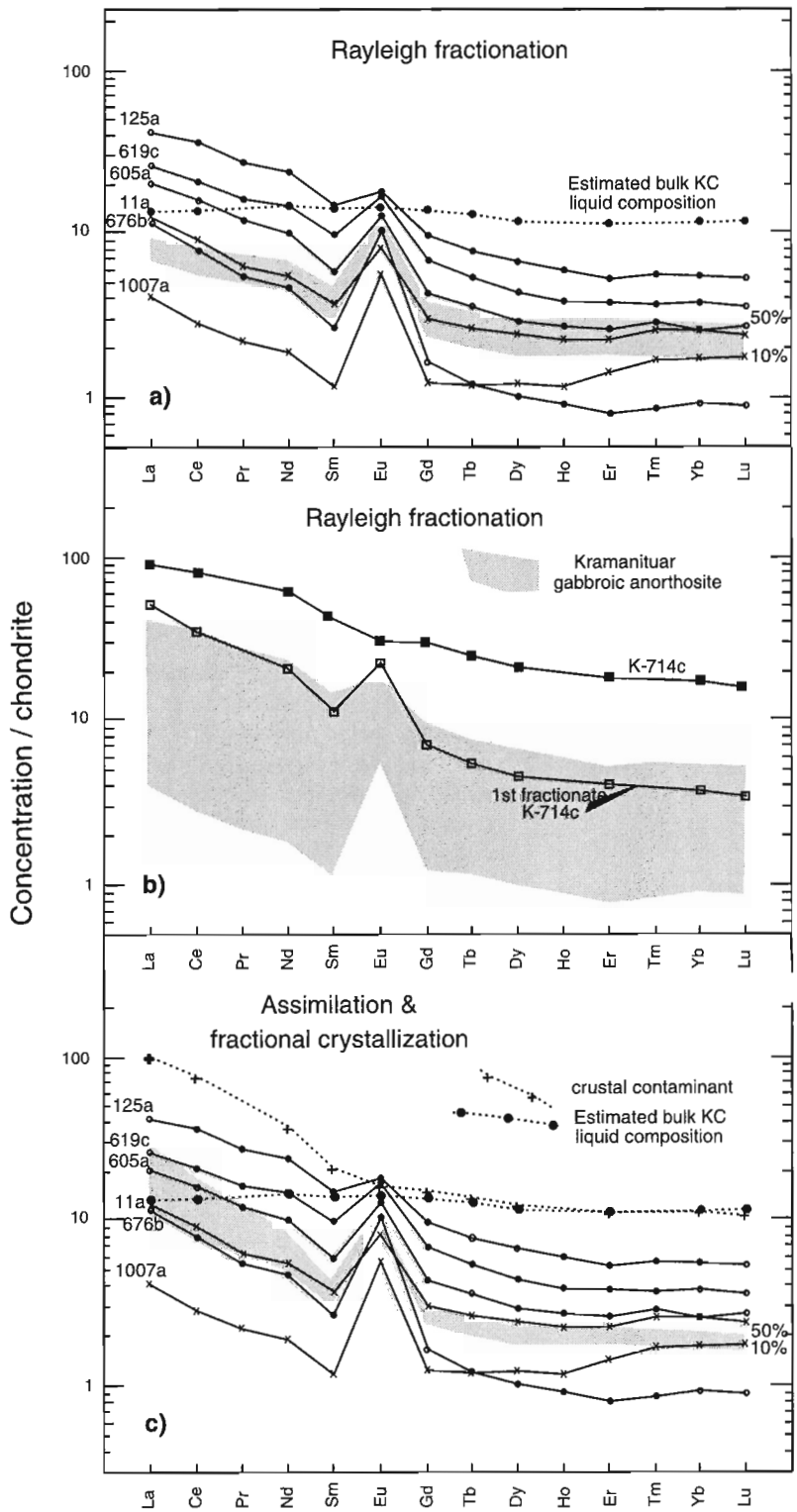


***Figure 7.***

*Results of Rayleigh fractionation and simplified AFC modelling for the Kramanituar gabbroic suite.* ***a****) Shaded region represents field for cumulates derived by 10–50% Rayleigh fractionation from an estimated bulk liquid composition (shown). Actual abundances for gabbroic anorthosite samples are indicated for comparison.* ***b****) First fractionate derived via simple Rayleigh fractionation in equilibrium with an enriched bulk liquid composition (K-714c). Shaded region represents field for actual gabbroic anorthosite cumulates, for comparison.* ***c****) Shaded region represents field for cumulates derived by 10–50% simplified AFC from an estimated bulk liquid composition (shown) with a crustal contaminant (also shown). Actual abundances for gabbroic anorthosite samples are indicated for comparison.*

the country-rock gabbro samples are the moderate, negative slope of the patterns, and depletion of high-field-strength elements (HFSE: Th, Nb, Ti), neither of which characterize the Kramanituar gabbroic suite. Negatively sloped multielement patterns are diagnostic of rocks derived through partial melting of a hydrated crust, or of rocks derived from a source which itself was a product of partial melting, since products of partial melting will be enriched in the most incompatible elements and depleted in the least incompatible elements (Wilson, 1989). Depletion of HFSE, especially Nb, indicates decoupling between the HFSE and the large-ion lithophile elements (LILE). This has been attributed to the presence of a Nb-compatible residual Ti-rich phase (e.g. rutile, sphene, ilmenite) in a source region (e.g. convergent plate margin) undergoing partial melting (Nicholls and Ringwood, 1973; Saunders et al., 1980; Smedley, 1986; Green and Pearson, 1987). Alternatively, it may reflect relative enrichment in the LILE, as observed in arc settings. The important point here is that incompatible trace-element geochemistry reveals significant differences between gabbroic country rocks and the Kramanituar gabbroic suite. The data are consistent with derivation of gabbroic country rocks by partial-melt processes or from metasomatized mantle lithosphere, where trace elements are decoupled, in contrast to the Kramanituar gabbroic suite, whose geochemistry is consistent with a more pristine mantle source.

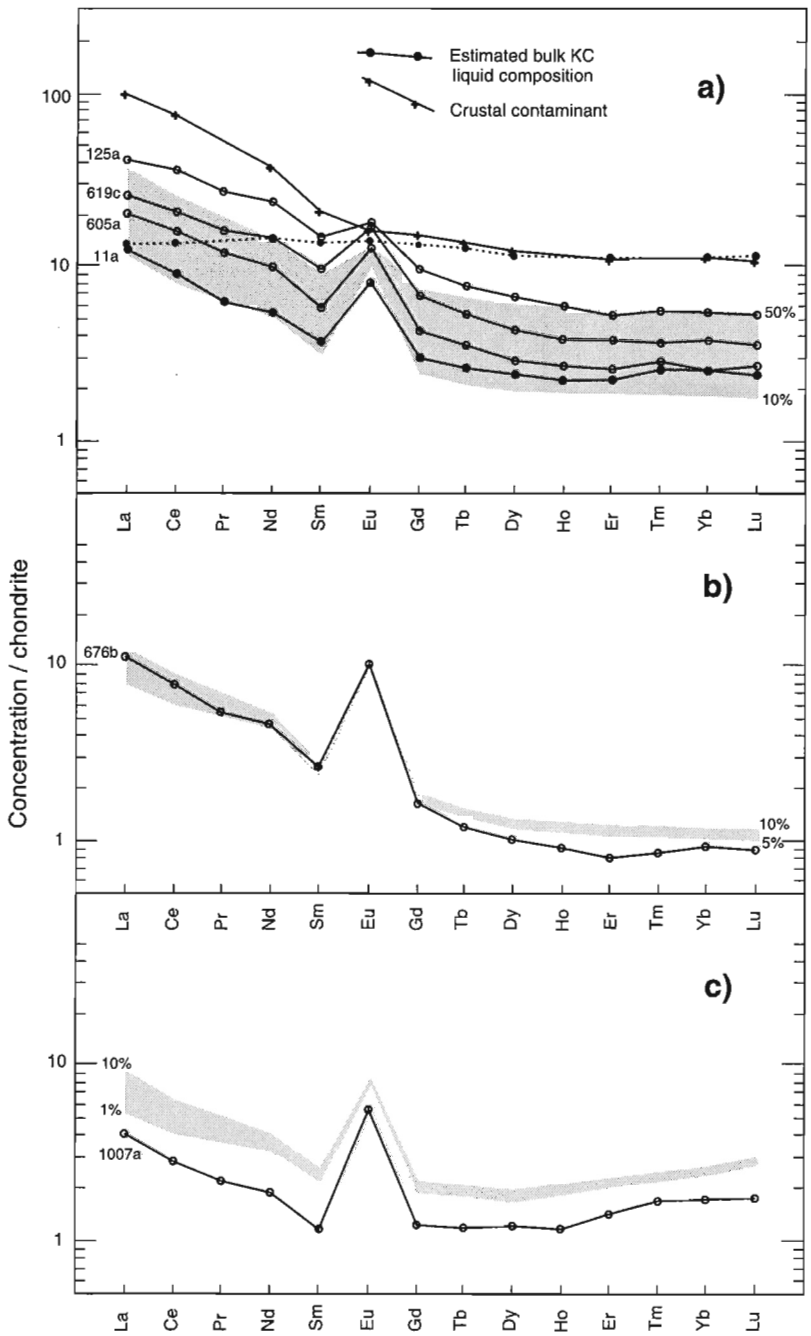


***Figure 8.***

*Results of modified AFC modelling of REE for the Kramanituar gabbroic suite. Shaded regions represent fields for cumulates derived through AFC ± trapped interstitial liquid from the estimated bulk liquid composition (shown) with a crustal contaminant (also shown). Actual abundances for Kramanituar gabbroic anorthosite samples are indicated for comparison.* ***a****) For 10–50% AFC;* ***b****) For 5–10% AFC with a mode representative of gabbroic anorthosite sample K-676b, shown for comparison.* ***c****) For <10% AFC for a mode representative of gabbroic anorthosite sample K-1007a and including 1% garnet.*

## DISCUSSION AND CONCLUSIONS

### *A cogenetic suite*

Modelling of trace-element data for mafic plutonic rocks of the Kramanituar Complex, presented here, is consistent with a cogenetic relationship between gabbroic anorthosite and gabbroic rocks within the complex. Limited isotopic data for these rocks further supports this finding. Granulite-facies gabbro (*K*-1053) from the complex yields an $\varepsilon_{Nd}$ (1902 Ma) value of +2.8, in accordance with (*see* further discussion below) extraction from the mantle at 1.9 Ga (DePaolo, 1981), the U-Pb (zircon) magmatic crystallization age of gabbroic anorthosite (*K*-676b) (M. Sanborn-Barrie, S.D. Carr, and R.J. Thériault, unpub. data, 1999).

### *Deep-crustal conditions*

Within the Kramanituar Complex, the association of a high-pressure (12 ± 1.5 kbar) metagabbroic suite (M. Sanborn-Barrie and R.G. Berman, unpub. data, 1999) intruding metasedimentary migmatites indicates that the complex was metamorphosed at deep-crustal conditions at ca. 1.9 Ga. The cogenetic relationship demonstrated for rocks of gabbroic, gabbroic anorthositic, and anorthositic composition indicate that *fractionation* of mantle melts took place at deep-crustal conditions at ca. 1902 Ma, the U-Pb (zircon) age of gabbroic anorthosite. Indications of garnet fractionation in sample *K*-1007a, as reflected by its HREE profile (Fig. 7c) support crystallization of mantle-derived melts in the deep crust at conditions of 12–15 kbar. The low $fO_2$ for the Kramanituar Complex gabbroic suite, reflected by a mineral/melt partition coefficient of close to 1 for Eu in plagioclase as required for the AFC modelling, is more typical of magmatism in the lower crust than in the upper crust (Drake and Weill, 1975). Drake and Weill (1975) have shown that high (~1) partition coefficients for plagioclase imply low $fO_2$ conditions, because a strong correlation exists between oxygen activity ($fO_2$) and the partition coefficient for Eu in plagioclase: europium forms $Eu^{2+}$ at low oxygen activities and $Eu^{3+}$ at high oxygen activities. The $Eu^{2+}$ and $Eu^{3+}$ behave very differently in their partitioning between plagioclase and basaltic melts, with $Eu^{2+}$ much more compatible than $Eu^{3+}$ in plagioclase. In the case of the Kramanituar Complex gabbroic suite, low $fO_2$ conditions are consistent with lower crust/mantle conditions, not the more-oxidized conditions characteristic of the upper crust.

### *Mantle source*

The trace-element data allow preliminary speculation on the composition of the mantle source for the Kramanituar gabbroic suite, and on aspects of the tectonic setting of this region. The bulk liquid composition of the Kramanituar gabbroic suite shows moderate enrichment in incompatible trace elements (Fig. 5), comparable to that of enriched mid-ocean ridge basalt (MORB). The degree of enrichment shown is comparable to basaltic compositions variably referred to as *plume*-type MORB (Sun, 1980), E-type MORB (Wilson, 1989; McKenzie and O'Nions, 1991); or T- (transitional) type MORB (Humphris et al., 1985). These compositions are all enriched relative to N- (normal) type MORB, but are depleted relative to an enriched MORB end-member. The enriched nature of the Kramanituar bulk liquid is displayed by the enrichment in LREE for the Kramanituar gabbros relative to N-type MORB (Fig. 4a), by the gentle concave-down pattern of the incompatible-element abundances for the gabbros (Fig. 5) which reveals no significant depletion in these elements, and by the virtually flat pattern at 1x produced when the Kramanituar Complex bulk liquid composition is normalized to E-type MORB (values of Sun and McDonough, 1989). Enrichment is *not* attributed simply to crustal contamination, since attributes of continental crust such as high silica, a pronounced negative Nb anomaly, and high La/Nb ratios of 1.5 to 7.0 (Thompson et al., 1984; Campbell and Griffiths, 1993), do not characterize the Kramanituar gabbroic suite (Table 1). As previously discussed, crustal contamination has been important in derivation of gabbroic anorthosite *from* this bulk liquid. An $\varepsilon_{Nd}$ value of +2.8 for these gabbroic rocks, slightly lower than the predicted value of +4 for depleted mantle at ca. 1900 Ma (DePaolo, 1981), is consistent with an enriched (E-type) MORB source for the Kramanituar Complex gabbroic suite (Campbell and Griffiths, 1992). The modified AFC model presented here predicts that more-fractionated gabbroic rocks from the Kramanituar Complex would yield a range of significantly lower $\varepsilon_{Nd}$ values, reflecting the assimilation of crustal rocks of probable Archean age.

Whereas normal or N-type MORB is derived by partial melting of an isotopically homogeneous, depleted mantle reservoir, E-type MORB is thought to be derived by partial melting from an undepleted, variably enriched reservoir which is isotopically heterogeneous (Allegre et al., 1984; Zindler et al., 1984; Wilson, 1989). Parts of this reservoir may reflect recycled subduction-altered oceanic crust (±pelagic and terrigenous sediments) and are generally designated the ocean-island basalt (OIB) reservoir (Zindler and Hart, 1986). Other parts are believed to be primordial (undepleted) in composition. It is partial melting of near-primordial portions of the mantle that is thought by Sun (1980), Wilson (1989), and Campbell and Griffiths (1992) to give rise to E-type MORB geochemical signatures.

The production of tholeiitic magma with an E-type MORB signature is attributed by Campbell and Griffiths (1992) to thermal plumes because they believe that thermal anomalies at the core-mantle boundary are required to cause partial melting of a lower, primordial part of the mantle. This relationship is demonstrated in Iceland, where plume-related basalts derived from deeper levels in the mantle have an E-type MORB signature in contrast to more shallowly derived normal or N-type MORB (McKenzie and O'Nions, 1991). Initiation of a thermal plume is considered by some workers to arise as a result of the insulating properties of a stable craton (Anderson 1994; Hoffman 1989). Stability of the Laurentian craton from ca. 2.5 to 2.0 Ga may have contributed to elevated mantle temperatures below the western Churchill Province.

An undepleted E-type MORB source for the Kramanituar gabbroic suite at 1.9 Ga is similar to that proposed for mafic rocks of similar age presently exposed in this part of

Laurentia. These include enriched, plume-related mafic volcanic rocks of the ca. 1.96 Ga Povungnituk Group, Cape Smith Belt (Campbell and Griffiths, 1992; Lucas et al., 1992), and ca. 1904 Ma basalts with E-type MORB geochemistry which form the oldest Paleoproterozoic units in the Trans-Hudson Orogen (Stern et al., 1995). Although it is premature to speculate on the presence of a plume in the generation of high-grade, mafic-dominated complexes of Paleoproterozoic age along the Chesterfield segment of the Snowbird tectonic zone (Fig. 1), migration of a plume-related hotspot could explain the apparent diachroneity of events along this 250 km long segment, where granulite-facies metamorphism and mafic magmatism are bracketed between ca. 2067 and 1950 Ma at the Daly Bay Complex (Gordon, 1988) in the east, ca. 1920–1940 Ma at the Uvauk complex (Tella et al., 1994), and ca. 1910–1902 Ma at the Kramanituar Complex (M. Sanborn-Barrie, S.D. Carr, and R.J. Thériault, unpub. data, 1999) in the west.

In considering the tectonic setting of the western Churchill Province, it is notable that the small degree of enrichment of the Kramanituar Complex gabbros does not approach that of continental tholeiites (high K, Sr, Ba; low Nb) or alkali basalts (i.e., Nb/Y >1.4; high $K_2O$; higher $P_2O_5$). These rocks are derived by partial melting of more-enriched mantle, and showing significant degrees of crustal contamination (Wilson, 1989; Anderson, 1996). Continental tholeiites and alkali basalts are generally associated with the initial stages of lithospheric extension or rifting. Accordingly, trace-element geochemistry for the Kramanituar gabbroic suite does not appear to reflect the onset of intracontinental rifting and alkalic magmatism of the western Churchill Province which is well expressed by rocks dated at ca. 1.83–1.75 Ga (Peterson, 1994).

Detailed investigation of the petrogenesis of gabbroic country rocks surrounding the Kramanituar Complex is not addressed in this study; however, the geochemical signature of these rocks (Fig. 6) provides preliminary evidence of a supra-subduction environment during their evolution, presumably in the late Archean. Their geochemical signature may indirectly link them to Neoarchean, subduction-related, calc-alkaline volcanic rocks and associated tonalite-granodiorite that dominate this part of the Archean western Churchill Province.

## ACKNOWLEDGMENTS

I thank Tucker Barrie for assistance in petrochemical modelling and for many helpful discussions on aspects of geochemistry. Tucker Barrie, Simon Hanmer, Tom Skulski, and Richard Stern are thanked for critical reviews of this paper which resulted in numerous improvements to it.

## REFERENCES

**Allegre, C.J., Hamelin, B., and Dupre, B.**
1984: Statistical analysis of isotopic ratios in MORB; the mantle blob cluster model and the convective regime of the mantle; Earth and Planetary Science Letters, v. 71, no. 1, p. 71–84.

**Anderson, D.L.**
1994: Superplumes or supercontinents; Geology, v. 22, p. 39–42.
1996: Enriched asthenosphere and depleted plumes; International Geology Review, v. 38, p. 1–21.

**Ashwal, L.D:**
1993: Anorthosites; Springer-Verlag, Berlin, Germany, 422 p.

**Aspler, L.B., Chiarenzelli, J.R., Cousens, B.L., and Valentino, D.**
1999: Precambrian geology, northern Angikuni Lake, and a transect across the Snowbird tectonic zone, western Angikuni Lake, Northwest Territories (Nunavut); *in* Current Research 1999-C; Geological Survey of Canada, p. 107–118.

**Basaltic Volcanism Study Project**
1981: Basaltic volcanism on the terrestrial planets; Pergamon Press, New York, New York, 1286 p.

**Campbell, I.H. and Griffiths, R.W.**
1992: The changing nature of mantle hotspots through time: implications for the chemical evolution of the mantle; Journal of Geology, v. 92, 497–523.
1993: The evolution of the mantle's chemical structure; Lithos, v. 30, p. 389–399.

**DePaolo, D.J.**
1981: Trace element and isotopic effects of combined wallrock assimilation and fractional crystallization; Earth and Planetary Science Letters, v. 53, p. 189–202.

**Drake, M.J. and Weill, D.F.**
1975: Partition of Sr, Ba, Ca, Y, Eu2+, Eu3+ and other REE between plagioclase feldspar and magmatic liquid: an experimental study; Geochimica et Cosmochimica Acta, v. 39, 689–712.

**Gill, J.B.**
1981: Orogenic andesites and plate tectonics; Springer-Verlag, Berlin, Germany, 401 p.

**Gordon, T.M.**
1988: Precambrian geology of the Daly Bay area, District of Keewatin; Geological Survey of Canada, Memoir 422, 21 p.

**Green, T.H. and Pearson, N.J.**
1987: An experimental study of Nb and Ta partitioning between Ti-rich minerals and silicate liquids at high pressure and temperature; Geochimica et Cosmochimica Acta, v. 51, p. 55–62.

**Hanmer, S.**
1997: Geology of the Striding–Athabasca mylonite zone, northern Saskatchewan and southeastern District of Mackenzie, Northwest Territories; Geological Survey of Canada, Bulletin 501, 92 p.

**Hanmer, S., Parrish, R., Williams, M., and Kopf, C.**
1994: Striding–Athabasca mylonite zone: complex Archean deep-crustal deformation in the East Athabasca mylonite triangle, northern Saskatchewan; Canadian Journal of Earth Sciences, v. 31, p. 1287–1300.

**Hoffman, P.F.**
1989: Precambrian geology and tectonic history of North America; *in* The Geology of North America — an overview, (ed.) A.W. Bally and A.R. Palmer; The Geological Society of America, The Geology of North America, v. A, p. 447–512.

**Hofmann, A.W.**
1988: Chemical differentiation of the Earth: the relationship between mantle, continental crust, and oceanic crust; Earth and Planetary Science Letters, v. 90, p. 297–314.

**Humphris, S.E., Thompson, G., Schilling, J.G., and Kingsley, R.H.**
1985: Petrological and geochemical variations along the Mid-Atlantic Ridge between 46°S and 32°S: influence of the Tristan da Cunha mantle plume; Geochimica et Cosmochimica Acta., v. 49, p. 1445–1464.

**Irvine, T.N. and Baragar, W.R.A.**
1971: A guide to the chemical classification of the common volcanic rocks; Canadian Journal of Earth Sciences, v. 8, p. 523–548.

**Irving, A.J. and Frey, F.A.**
1984: Trace element abundances in megacrysts and their host basalts; constraints on partition coefficients and megacryst genesis; Geochimica et Cosmochimica Acta, v. 48, no. 6, p. 1201–1221.

**Jensen, L.S. and Pyke, D.R.**
1982: Komatiites in the Ontario portion of the Abitibi belt; *in* Komatiites, (ed.) N.T. Ardnt and E.G. Nisbet; George Allen and Unwin, London, England, p. 147–157.

**Longhi, J., Wooden, J.L., and Coppinger, K.D.**
1983: The petrology of high-Mg dikes from the Beartooth Mountains, Montana: a search for the parent magma of the Stillwater Complex; Journal of Geophysical Research, v. 88 (Suppl.), p. B53–B69.

**Lucas, S.B., St-Onge, M.R., Parrish, R.R., and Dunphy, J.M.**
1992: Long-lived continent-ocean interaction in the Early Proterozoic Ungava orogen, northern Quebec, Canada; Geology, v. 20, p. 113–116.

**McKay, G.A.**
1982: Partitioning of REE between olivine, plagioclase, and synthetic melts: implications for the origin of lunar anorthosite; *in* Lunar and Planetary Instiute Technical Report, v. XIII; Lunar and Planetary Institute, Houston, p. 493–494.

**McKay, G.A. and Weill, D.F.**
1976: Petrogenesis of KREEP; *in* Proceedings of the seventh Lunar Science conference; Volume 2, Petrogenetic Studies of Mare and Highland Rocks, (ed.) R.B. Merrill, R.V. Morris, J.M. Rhodes, and T.M. Usselman; Pergamon Press, New York, New York, p. 2427–2447.

**McKenzie, D. and O'Nions, R.K.**
1991: Partial melt distributions from inversion of rare earth element concentratons: Journal of Petrology, v. 32, p. 1021–1091.

**Morse, S.A.**
1988: Partition coefficients for anorthosites; Chemical Geology, v. 70, p. 154 (abstract).

**Nicholls, I.A. and Harris, K.L.**
1980: Experimental rare earth element partition coefficients for garnet, clinopyroxene and amphibole coexisting with andesitic and basaltic liquids; Geochimica et Cosmochimica Acta, v. 44, no. 2, p. 287–308.

**Nicholls, I.A. and Ringwood, A.E.**
1973: Effect of water on olivine stability in tholeiites and the production of silica saturated magmas in the island arc environment; Journal of Geology, v. 81, no. 3, p. 285–300.

**Peterson, T.D.**
1994: Early Proterozoic ultrapotassic volcanism of the Keewatin hinterland, Canada; *in* Kimberlites, Related Rocks and Mantle Xenoliths, (ed.) O.A. Meyer-Henry and H. Leonardos-Othon; Companhia de Pesquisa de Recursos Minerais, Rio de Janeiro, Brazil, Special Publication, v. 1A, p. 221–235.

**Phinney, W.C. and Morrison, D.A.**
1990: Partition coefficients for calcic plagioclase: Implications for Archean anorthosites; *in* Geochimica et Cosmochimica Acta, v. 54, p. 1639–1654.

**Rollinson, H. R.**
1993: Using geochemical data: evaluation, presentation, interpretation; Geochemistry Series, Longman Group Ltd., Essex, England, 352 p.

**Saunders, A.D., Tarney, J., Marsh, N.G., and Wood, D.A.**
1980: Ophiolites as ocean crust or marginal basin crust: a geochemical approach; *in* Ophiolites; Proceedings of the International Opholite Symposium, (ed.) A. Panayiotou; Cyprus Ministry of Agriculture–Cyprus Geological Survey Department, p. 193–204.

**Schau, M.**
1980: Zircon ages from a granulite-anorthosite complex and a layered gneiss complex northeast of Baker Lake, District of Keewatin; *in* Rb-Sr and U-Pb Isotopic Age Studies, Current Research, Part C, Geological Survey of Canada, Paper 80-1C, p. 237–238.

**Schau, M. and Ashton, K.E.**
1980: Geological map of the granulite and anorthosite complex at the southeast end of Baker Lake, 56D1, 56C4, parts of 55M16 and 55N13; Geological Survey of Canada, Open File 712, scale 1:50 000.

**Smedley, P.L.**
1986: The relationship between calc-alkaline volcanism and within-plate continental rift volcanism, evidence from Scottish Palaeozoic lavas; Earth and Planetary Science Letters, v. 77, no.1, p. 113–128.

**Snoeyenbos, D.R., Williams, M.L., and Hanmer, S.**
1995: Archean high-pressure metamorphism in the western Canadian Shield; European Journal of Mineralogy, v. 7, p. 1251–1272.

**Sparks, R.S.J.**
1986: The role of crustal contamination in magma evolution through geological time; Earth and Planetary Science Letters, v. 78, p. 211–223.

**Stern, R.A., Syme, E.C., and Lucas, S.B.**
1995: Geochemistry of 1.9 Ga MORB- and OIB-like basalts from the Amisk collage, Flin Flon Belt, Evidence for an intra-oceanic origin; Geochimica et Cosmochimica Acta., v. 59, p. 3131–3154.

**Stolper, E.**
1980: A phase diagram for mid-ocean ridge basalts: preliminary results and implications for petrogenesis; Contributions to Mineralogy and Petrology, v. 74, p. 13–28.

**Sun, S.-S.**
1980: Lead isotope study of young volcanic rocks from mid-ocean ridges, ocean islands and island arcs; Royal Society of London, Philosophical Transactions, v. A297, p. 409–445.

**Sun, S-S and McDonough, W.F.**
1989: Chemical and isotopic systematics of oceanic basalts, implications for mantle composition and processes; *in* Magmatism in the ocean basins, (ed.) A.D. Saunders and M.J. Norry; Geological Society of London, Special Publications, v. 42, p. 313–345.

**Tella, S., Roddick, J.C., Schau, M., and Mader, U.**
1994: Geochronological constraints on the tectono-metamorphic history of the allochthonous Uvauk gabbro-anorthosite-granulite complex, central Churchill Province, District of Keewatin, NWT., Canada; *in* Proceedings, Geological Association of Canada–Mineralogical Association of Canada, Joint Annual Meeting, v.19, p. A111 (abstract).

**Thompson, R.N.**
1972: Melting behavior of two Snake River lavas at pressures up to 35 kb; Carnegie Institute, Washington, Geophysical Laboratory Yearbook, v. 71, p. 406–410.

**Thompson, R.N., Morrison, M.A., Hendry, G.L., and Parry, S.J.**
1984: An assessment of the relative roles of crust and mantle in magma genesis; an elemental approach; *in* The Relative Contributions of Mantle, Oceanic Crust and Continental Crust to Magma Genesis, Philosophical Transactions of the Royal Society of London, Series A: Mathematical and Physical Sciences, v. 310, p. 549–590.

**Wilson, M.**
1989: Igneous Petrogenesis, Unwin Hyman; London, England, 466 p.

**Zindler, A. and Hart, S.**
1986: Chemical geodynamics; Annual Review of Earth and Planetary Sciences, v. 14, p. 493–571.

**Zindler, A., Staudigel, H., and Batiza, R.**
1984: Isotope and trace element geochemistry of young Pacific seamounts, implications for the scale of upper mantle heterogeneity; Earth and Planetary Science Letters, v. 70, no. 2, p. 175–195.

---

Geological Survey of Canada Project 970006

# Neodymium-isotopic characteristics of the Uchi–Confederation Lakes region, northwestern Ontario[1]

K.Y. Tomlinson and N. Rogers
Continental Geoscience Division, Ottawa.

*Tomlinson, K.Y. and Rogers, N., 1999: Neodymium-isotopic characteristics of the Uchi–Confederation Lakes region, northwestern Ontario;* in *Current Research 1999-E; Geological Survey of Canada, p. 91–99.*

**Abstract:** The Uchi–Confederation greenstone belt of the Uchi Subprovince, Superior Province, records a prolonged history of mafic to felsic volcanism (~2975–2740 Ma) and tonalitic plutonism (~2840–2700 Ma). Neodymium-isotopic data from the Trout Lake batholith (εNd values of -1.1 to +2.7, compared to values of +2 to +3 for late Archean depleted mantle) suggest that a felsic component older than 3 Ga may be present. Volcanic rocks of the Balmer assemblage have εNd values of +0.3 to +1.9 at 2.96 Ga, also suggestive of an older crustal component to Balmer assemblage volcanism. Volcanic rocks from the Woman assemblage have εNd values from 0.0 to +1.9 at 2.84 Ga, again suggesting recycling of older crust. Volcanic rocks in the lower half of the Confederation assemblage are relatively juvenile with εNd values of +1.4 to +2.0 at 2.74 Ga. Confederation assemblage rocks in the upper half of the sequence have lower values of -0.4 to +1.1.

**Résumé :** La ceinture de roches vertes d'Uchi-Confederation de la sous-province d'Uchi de la Province du lac Supérieur fait état d'une longue histoire de volcanisme mafique à felsique (env. 2975–2740 Ma) et de plutonisme tonalitique (env. 2840–2700 Ma). Les données isotopiques de Nd du batholite de Trout Lake (valeurs de εNd variant de -1,1 à +2,7 comparées aux valeurs de +2 à +3 pour le manteau tardi-archéen appauvri) permettent de penser qu'une composante felsique antérieure à 3 Ga pourrait être présente. Les roches volcaniques de l'assemblage de Balmer ont des valeurs de εNd variant de +0,3 à +1,9 à 2,96 Ga, ce qui permet aussi de supposer la présence d'une composante crustale antérieure à 3 Ga dans plus ancienne de l'assemblage volcanique de Balmer. Les roches volcaniques de l'assemblage de Woman ont des valeurs de εNd qui varient de 0,0 à +1,9 à 2,84 Ga, ce qui laisse encore supposer qu'il y a eu recyclage de coûte préexistante. Les roches volcaniques dans la moitié inférieure de l'assemblage de Confederation sont relativement juvéniles et ont des valeurs de εNd allant de +1,4 à +2,0 à 2,74 Ga. Les roches de l'assemblage de Confederation dans la moitié supérieure de la séquence ont des valeurs plus basses variant de -0,4 à +1,1.

[1] Contribution to the Western Superior NATMAP

## INTRODUCTION

The Uchi–Confederation greenstone belt occurs in the Uchi Subprovince of the Superior Province, and contains dated units that span more than 250 Ma (Fig. 1). The belt has been divided into three main volcanic-dominated components which, from oldest to youngest, are the Balmer assemblage (~2975–2960 Ma), the Woman assemblage (~2840 Ma), and the Confederation assemblage (~2740 Ma) (Nunes and Thurston, 1980; Noble, 1989; Stott and Corfu, 1991; Rogers et al., 1999). The adjacent Trout Lake batholith contains at least three phases including ~2840 Ma and ~2806 Ma tonalitic phases, and a ~2700 Ma granodiorite phase (Noble, 1989; Fig. 1). It intrudes the Balmer assemblage, but also contains gneissic tonalites that may represent basement to the greenstone belt. The aim of this study is to investigate the role of crustal recycling within the greenstone belt and the Trout Lake batholith using Nd isotopes and trace-element geochemistry.

## METHODOLOGY FOR ND-ISOTOPIC ANALYSES

Sample powders, spiked with a mixed $^{148}Nd$-$^{149}Sm$ solution, were dissolved in an HF-$HNO_3$ mixture. Separation of REEs was done by cation-exchange chromatography using TruSpec® resin optimized for REE separation. Separation of Sm and Nd from other REEs followed HDEHP (Di (2-ethylexyl) orthophosphoric acid)–teflon-powder chromatography. Total procedural blanks were approximately 50 pg for Nd and 20 pg for Sm. Mass analysis was carried out on a MAT-261 solid-source mass spectrometer in static multicollection mode. Neodymium-isotopic compositions were normalized to $^{146}Nd/^{144}Nd = 0.7219$. Repeated measurements of an AMES Nd standard solution yielded $^{143}Nd/^{144}Nd = 0.512195 \pm 17$ (2 standard deviations). The $^{143}Nd/^{144}Nd$ ratios were corrected to LaJolla $^{143}Nd/^{144}Nd = 0.511860$. The $^{147}Sm/^{144}Nd$ ratios are reproducible to 0.5%. The εNd values were calculated assuming Chondritic Uniform Reservoir (CHUR) $^{147}Sm/^{144}Nd = 0.1967$ and present-day $^{143}Nd/^{144}Nd = 0.512638$.

## TROUT LAKE BATHOLITH

The Trout Lake batholith intrudes the Balmer assemblage at the western edge of the Uchi–Confederation greenstone belt. The oldest phase of tonalite that has been dated has an age of 2840 Ma (Noble, 1989), apparently coeval with Woman assemblage volcanism. However, the existence of isolated rafts of gneissic tonalite within the predominant 2840 Ma foliated tonalite indicates that older phases (>2840 Ma) may exist within the batholith. A sample of the gneissic tonalite (RAX98-407) has a depleted mantle model age ($T_{DM}$) of 3347 Ma and an εNd value at 3.0 Ga of -1.1 (Table 1, Fig. 2; or for comparison, an εNd of -2.4 at 2840 Ma). Such a low epsilon value at 3 Ga suggests that the true age of this rock may be even older, or that it contains a much older, recycled, felsic componant. The ~2840 Ma phase of the Trout Lake batholith (sample RAX98-419) has an εNd value of +0.6, again suggesting recycling of older crust (at least 3.0 Ga). Tonalite which may represent a younger phase of the Trout Lake batholith (2806 Ma) has an εNd value of +2.7 (RAX98-531). This value is similar to depleted mantle at 2.8 Ga (Fig. 2) and suggests a predominantly juvenile contribution to part of the Trout Lake batholith.

## BALMER ASSEMBLAGE

The Balmer assemblage occurs to the east of, and is intruded by, the Trout Lake batholith, and consists of predominantly pillowed and massive tholeiitic flows, gabbro sills, and layered gabbro (Rogers et al., 1999). The assemblage has been dated at 2959 Ma at its western margin (Fig. 1; Nunes and Thurston, 1980), and at Spot Lake towards the east (Fig. 1) at 2975 Ma (V. McNicoll, unpublished data, 1998). The abundance of deformed gabbro and associated plagiogranite dykes within the structural base of the Balmer assemblage led Rogers et al. (1999) to draw analogies with modern ophiolitic sequences and hence suggest a possible oceanic setting for the Balmer assemblage. A sample of pegmatitic gabbro from the Balmer assemblage has since been dated at ~2700 Ma (V. McNicoll, unpub. data, 1999). Some of these gabbros may still be related to Balmer assemblage volcanism but others are obviously later.

Three samples of volcanic rock from the Balmer assemblage have been analyzed for Nd isotopes (Table 1; Fig. 2). A sample of felsic tuff collected adjacent to the Trout Lake batholith (sample RAX98-405) has an εNd value of +0.3 at 2.96 Ga and a $T_{DM}$ of 3132 Ma. Depleted mantle at this time would have an εNd value of around +2.5 (Fig. 2). This data is therefore suggestive of older crustal involvement within the Balmer assemblage. A basalt from the Balmer assemblage (RAX98-016) has an εNd value of +1.85 at 2.96 Ga. This rock is enriched in Th and light REEs, with a small negative Nb anomaly (N. Rogers, unpub. data, 1999) and hence may have recycled, or been contaminated by, a small amount of older crust. A quartz-feldspar porphyry (RAX98-408) thought to be near the structural top of the Balmer assemblage has an εNd value of +1.6. This rock has a very pronounced negative Nb anomaly, and appears to be crustally contaminated on the basis of both geochemistry and Nd isotopes.

Rocks with MORB-like geochemical signatures have not been found in the Balmer assemblage of the Uchi–Confederation greenstone belt. All analyzed mafic and felsic rocks are enriched in Th and light REEs, and have negative Nb anomalies (K.Y. Tomlinson, unpub. data, 1998; N. Rogers, unpub. data, 1999). This suggests that the Balmer assemblage is unlikely to have formed in an oceanic setting. This is consistent with data from the Balmer assemblage of the neighbouring Red Lake greenstone belt, which also indicate crustal contamination in mafic rocks (Tomlinson et al., 1998; Hollings, 1998).

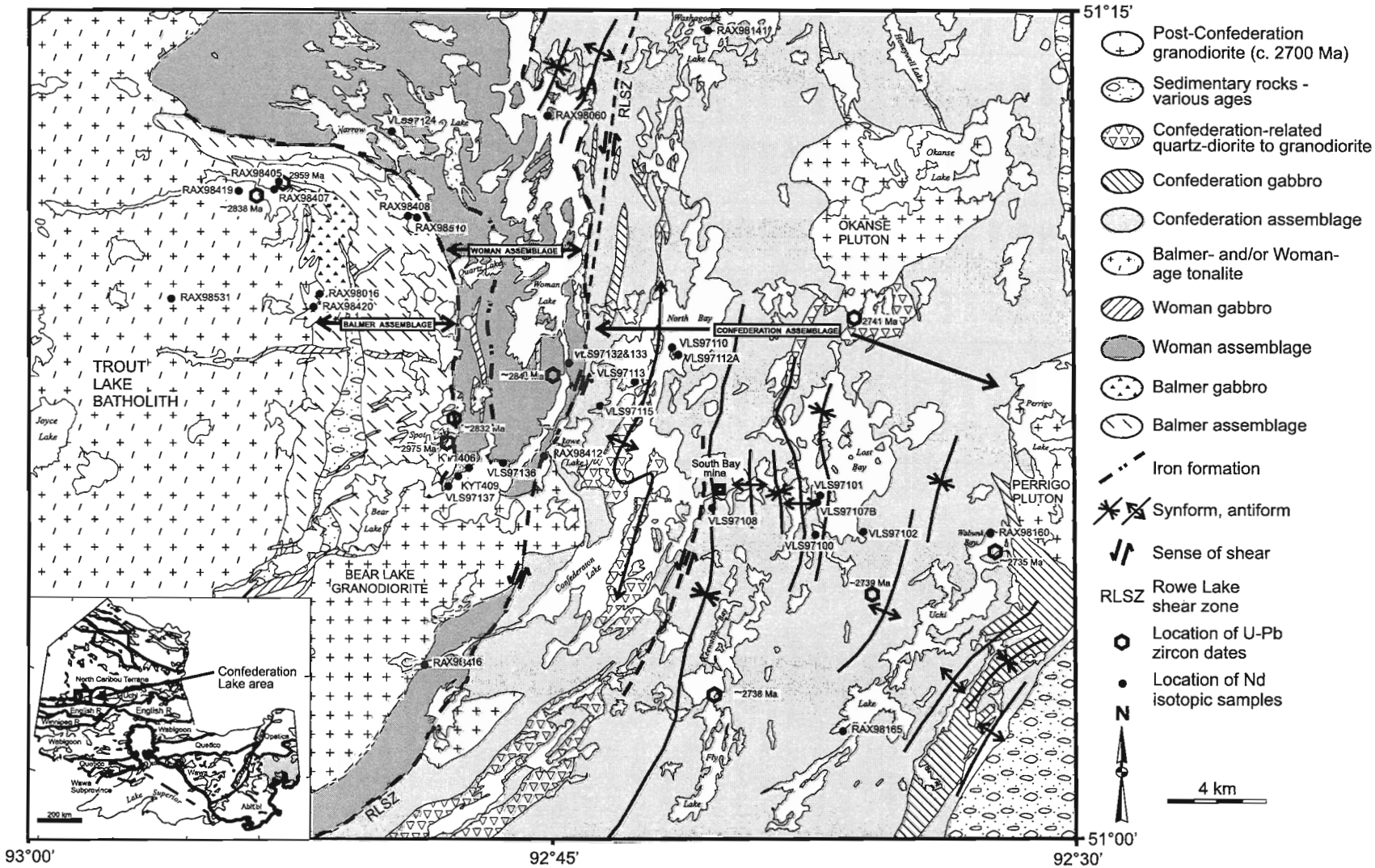


***Figure 1.*** *Geology of the Confederation Lake area (after Rogers et al., 1999). The locations of samples analyzed for Nd isotopes are shown.*

**Table 1.** Nd isotopic data for the Woman–Confederation Lake area.

| Sample | Measured $^{143}Nd/^{144}Nd$[a] | Measured $^{147}Sm/^{144}Nd$ | Age (Ga) | Epsilon Nd (T) | Sm (ppm) | Nd (ppm) | DePaolo $T_{(DM)}$ |
|---|---|---|---|---|---|---|---|
| **Balmer assemblage** | | | | | | | |
| RAX98-405 felsic tuff | 0.511324 ± 6 | 0.1287 | 2.96 | **0.28** | 4.15 | 19.5 | 3132 |
| RAX98-408 QFP | 0.510641 ± 7 | 0.0903 | 2.96 | **1.62** | 1.44 | 9.62 | 2996 |
| RAX98-016 basalt | 0.512504 ± 7 | 0.1850 | 2.96 | **1.85** | 1.99 | 6.52 | |
| **Woman assemblage** | | | | | | | |
| RAX98-416 ignimbrite | 0.511201 ± 6 | 0.1149 | 2.84 | **1.90** | 8.58 | 45.14 | 2869 |
| VLS97-133 felsic volc. | 0.510924 ± 7 | 0.1043 | 2.84 | **0.36** | 6.73 | 38.99 | 2983 |
| VLS-97-136 andesite | 0.510839 ± 6 | 0.0990 | 2.84 | **0.63** | 6.09 | 37.16 | 2957 |
| VLS-97-124 basalt | 0.513065 ± 17 | 0.2149 | 2.84 | **1.69** | 0.98 | 2.75 | |
| VLS-97-137 basalt | 0.512708 ± 6 | 0.1966 | 2.84 | **1.43** | 2.14 | 6.57 | |
| KYT406 basalt | 0.512476 ± 17 | 0.1855 | 2.84 | **0.93** | 2.12 | 6.91 | |
| KYT-409 basalt | 0.512441 ± 10 | 0.1863 | 2.84 | **-0.04** | 1.42 | 4.61 | |
| RAX98-510 basalt | 0.513203 ± 11 | 0.2234 | 2.84 | **1.28** | 1.61 | 4.37 | |
| RAX98-060 basalt | 0.513223 ± 11 | 0.2241 | 2.84 | **1.39** | 1.33 | 3.58 | |
| VLS-97-132 gabbro | 0.513083 ± 6 | 0.2204 | 2.84 | **0.01** | 1.51 | 4.14 | |
| **Confederation assemblage** | | | | | | | |
| VLS97-108 rhyolite (Keewatin) | 0.510783 ± 6 | 0.0917 | 2.736 | **0.80** | 1.57 | 10.37 | 2846 |
| RAX98-160 rhyolite (Wabunk) | 0.511187 ± 5 | 0.1141 | 2.735 | **0.78** | 2.18 | 11.56 | 2868 |
| VLS97-107B dacite (Mitchell Fm) | 0.512194 ± 9 | 0.1671 | 2.739 | **1.80** | 15.15 | 54.80 | 2823 |
| VLS97-112A dacite (Mitchell Fm) | 0.51224 ± 4 | 0.1691 | 2.739 | **1.98** | 14.80 | 52.89 | 2790 |
| VLS97-110 andesite | 0.511932 ± 7 | 0.1539 | 2.740 | **1.35** | 2.51 | 9.87 | 2872 |
| VLS-97-113 basaltic andesite | 0.512523 ± 9 | 0.1855 | 2.740 | **1.73** | 5.23 | 17.05 | |
| VLS-97-102 basalt | 0.511733 ± 13 | 0.1428 | 2.740 | **1.37** | 3.62 | 15.34 | 2850 |
| VLS-97-100 basalt | 0.512704 ± 11 | 0.1978 | 2.738 | **0.90** | 1.53 | 4.69 | |
| VLS97-115 basalt | 0.512823 ± 12 | 0.2016 | 2.738 | **1.91** | 1.33 | 3.99 | |
| VLS-97-101 basalt | 0.512291 ± 6 | 0.1785 | 2.738 | **-0.36** | 5.97 | 20.20 | |
| RAX98-165 basalt | 0.511631 ± 9 | 0.1377 | 2.734 | **1.13** | 4.15 | 18.2 | 2866 |
| RAX98-141 basalt | 0.512356 ± 19 | 0.1790 | 2.739 | **0.76** | 1.30 | 4.39 | |
| **Young intrusions** | | | | | | | |
| RAX98-420 gabbro | 0.512425 ± 12 | 0.1834 | 2.70 | **0.48** | 3.00 | 9.90 | |
| RAX98-412 granite | 0.511306 ± 7 | 0.1216 | 2.705 | **0.18** | 2.01 | 9.99 | 2904 |
| **Trout Lake batholith** | | | | | | | |
| RAX98-419 tonalite | 0.510823 ± 12 | 0.0983 | 2.84 | **0.57** | 1.47 | 9.06 | 2961 |
| RAX98-531 tonalite | 0.511221 ± 5 | 0.1128 | 2.806 | **2.68** | 1.27 | 6.81 | 2776 |
| RAX98-407 tonalite | 0.511431 ± 10 | 0.1387 | 3.0 | **-1.14** | 1.51 | 6.6 | 3347 |

[a] In-run error (2 sigma)

## WOMAN ASSEMBLAGE

The Woman assemblage extends eastwards from Spot Lake to a sedimentary unit just east of Woman Lake, and its eastern boundary in part follows the Rowe Lake shear zone (Fig. 1; Rogers et al., 1999). The assemblage has been dated at ~2840 Ma (Stott and Corfu, 1991) on a suite of rhyolitic, welded tuffs (the Woman Lake tuff of Thurston, 1985), which represents the near-stratigraphic top of the assemblage. A gabbro dyke at Spot Lake has been dated at ~2832 Ma (V. McNicoll, unpub. data, 1998). This dyke crosscuts the Balmer assemblage and is a feeder to the Woman assemblage, indicating that Woman assemblage volcanic rocks erupted through Balmer assemblage basement (Rogers et al., 1999). The Woman assemblage is dominated by eastward-facing, mafic, pillowed and massive flows, with minor sedimentary and felsic volcanic units. A clastic sedimentary unit (and laterally continuous iron formation) occurs within the assemblage (Fig. 1) and contains detrital zircons which are dated at ~2890 to 2873 Ma (V. McNicoll, unpub. data, 1998). Rocks underlying (west of) this unit may represent a slightly older phase of volcanism, while rocks overlying (east of) this unit may represent true Woman-aged (~2840 Ma) volcanism (Rogers et al., 1999). Ten samples have been analyzed for Nd isotopes from this assemblage (Table 1; Fig. 2).

Trace-element geochemistry and Nd-isotopic data for rocks to the west and east of the sedimentary marker horizon are shown separately on Figure 3. To the west, the lavas show a large range of εNd values from +1.7 to 0.0 at 2.84 Ga (Fig. 2, 3). Geochemically, the lavas are fairly primitive, with

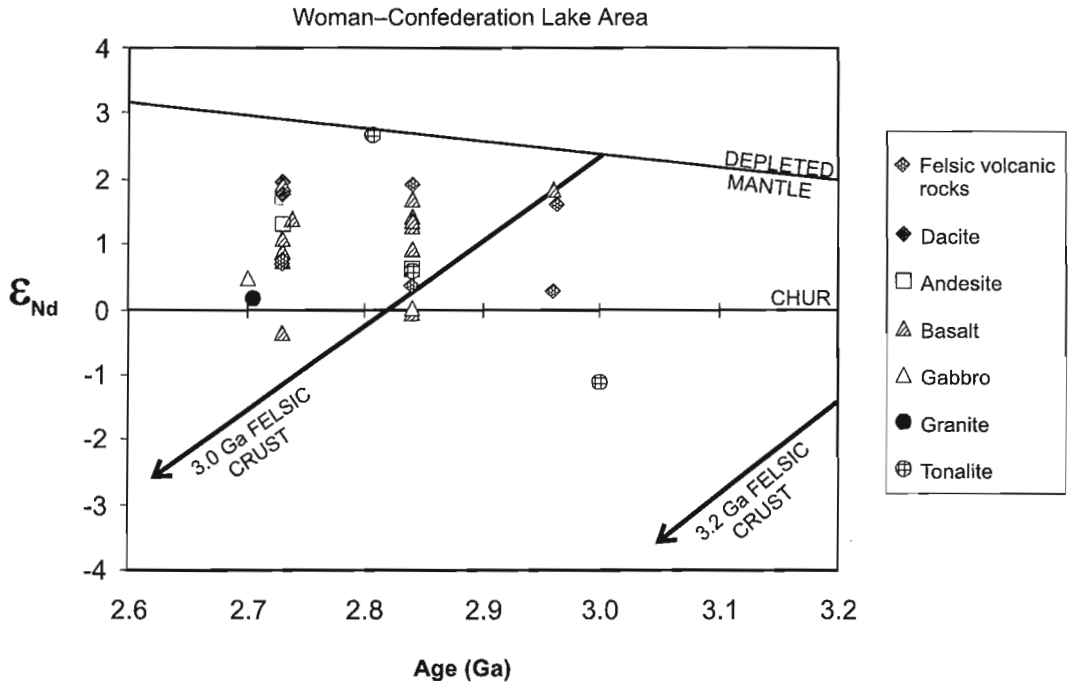


***Figure 2.*** *Epsilon Nd versus time diagram for samples analyzed from the Confederation Lake area (Depleted mantle model of DePaolo, 1981).*

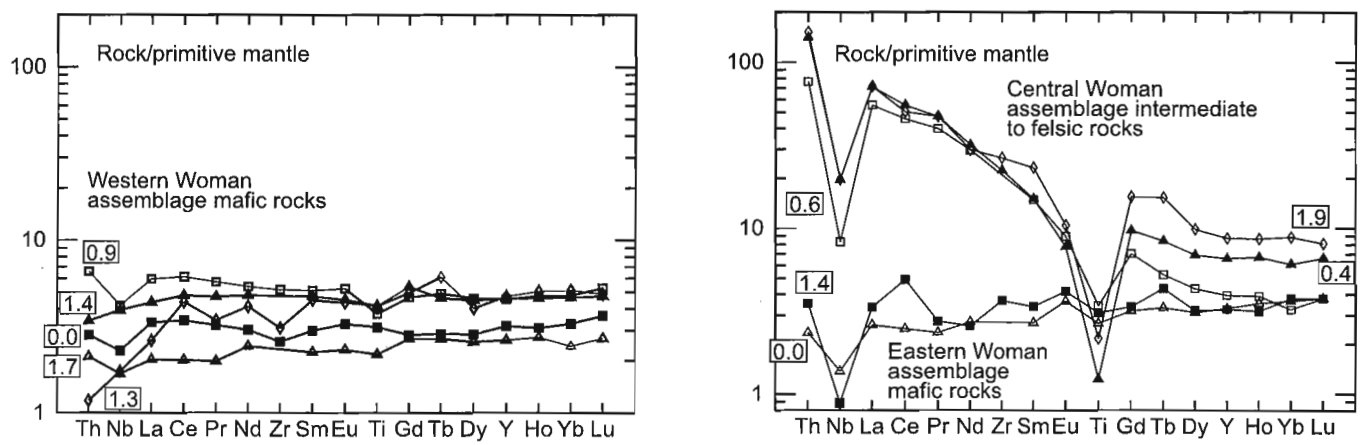


***Figure 3.*** *Mantle-normalized multi-element diagrams and epsilon Nd values for Woman assemblage rocks. Labels in boxes are the εNd values of the samples at 2.84 Ga.*

relatively flat REE profiles and although some display Th enrichment and small negative Nb anomalies, the degree of crustal involvement appears to be minor (Fig. 3). Some of the low εNd values do, however, suggest that older crust must have been involved in their petrogenesis. Due to the small amount of crust involved (as suggested by their geochemistry), this crust would need to have been significantly older than the Woman assemblage rocks (probably older than 3 Ga) to account for the Nd-isotopic data.

An intermediate lava sample from the centre of the Woman assemblage (VLS97-136) and a sample of Woman Lake tuff (VLS97-133) have similar εNd values of +0.6 and +0.4, respectively, again suggesting involvement of older crust. A petrographically similar felsic tuff (sample RAX98-416) to the south of the Bear Lake pluton, which was suggested by Rogers et al. (1999) to possibly correlate with the Woman Lake tuff, is geochemically similar to the Woman Lake tuff, but has a much more juvenile εNd value of +1.9 at 2.84 Ga (Fig. 3, Table 1).

Mafic rocks to the east of the Woman Lake tuff unit again have variable isotopic characteristics, with one sample having +1.4 εNd and another sample having 0.0 εNd. Rogers et al. (1999) suggested that this part of the sequence may represent repetition by either faulting or combined folding and faulting, of a more westerly part of the Woman assemblage. The initial geochemical and isotopic results are consistent with structural repetition of the Woman assemblage rocks. Without further geochronological controls however, it is impossible to determine if this is truly a series of structurally repeated sequences or a separate pulse of younger (?) magmatism.

## CONFEDERATION ASSEMBLAGE

The Confederation assemblage comprises the supracrustal rocks east of the Rowe Lake shear zone (Fig. 1). Dated rocks within the assemblage range from 2741 to 2735 Ma (Noble, 1989; Nunes and Thurston, 1980), but errors generally overlap, so the internal stratigraphy cannot currently be constrained by geochronological data. Rogers et al. (1999) suggested, on the basis of crosscutting gabbro dykes, that the Confederation assemblage was erupted through the Woman assemblage, although this hypothesis is under further investigation. Mafic flows are predominant in the Confederation assemblage, but exhibit no macroscopic petrographic variations and so the spatially associated felsic volcanic rocks act as important marker units within the stratigraphy. Based on field studies, Rogers et al. (1999) recognized three different suites of felsic rock (Fig. 4). The lowermost felsic suite has informally been referred to as the Mitchell formation (Rogers et al., 1999) and comprises felsic tuffs and dacitic flows that locally exhibit a pronounced perlitic texture. Partly contemporaneous with the Mitchell formation are a distinct suite of aphyric, felsic volcanic rocks that are centred on Uchi Lake. They have been referred to as the Wabunk rhyolites (Fig. 4; Rogers et al., 1999). A stratigraphically higher suite of quartz and quartz-feldspar porphyries occur in the South Bay and Fly Lake area. They are termed the Keewatin porphyries (Fig. 4) and comprise felsic tuffs, tuff breccias, and hypabyssal intrusions (Rogers et al., 1999).

Using these felsic horizons as marker units, it has been possible to subdivide the mafic flows as occurring beneath, between, or above the felsic units, and hence examine the isotopic and geochemical characteristics of the entire Confederation package in terms of stratigraphic evolution (Fig. 5). Twelve samples have been analyzed for Nd isotopes from the Confederation assemblage (Table 1; Fig. 1, 2).

Lavas beneath the Mitchell formation are mafic to intermediate in composition and have εNd values of +1.4 to +1.7 at 2.74 Ga. They are slightly to moderately enriched in light REEs with flat to moderately fractionated heavy rare-earth element (HREE) profiles (Fig. 5). Some samples show Th enrichment and negative Nb anomalies, but others do not. These lavas may contain a minor older crustal component as their εNd values are slightly low compared to depleted mantle values of around +3 at 2.74 Ga (Fig. 2). This may represent crustal contamination by underlying Woman assemblage or Balmer assemblage rocks, or crustal recycling within the mantle.

The Mitchell formation contains the most juvenile rocks in the Confederation assemblage, which is surprising for rocks of dacitic to rhyolitic composition. Two dacitic flows have εNd values of +2.0 and +1.8 and an F3 rhyolite of Noble (1989) has an εNd = +1.6 (Fig. 5). These rocks have generally flat REE profiles and high abundances of heavy REEs, consistent with extended fractionation from a mafic tholeiitic liquid (as suggested by Thurston and Fryer, 1983). They display small negative Nb anomalies and minor Th enrichment. Like the mafic lavas beneath them, the εNd values of this sequence can be accounted for by only a small amount of older crustal involvement which could be accommodated by either Woman and/or Balmer assemblage contamination or crustal recycling within the mantle.

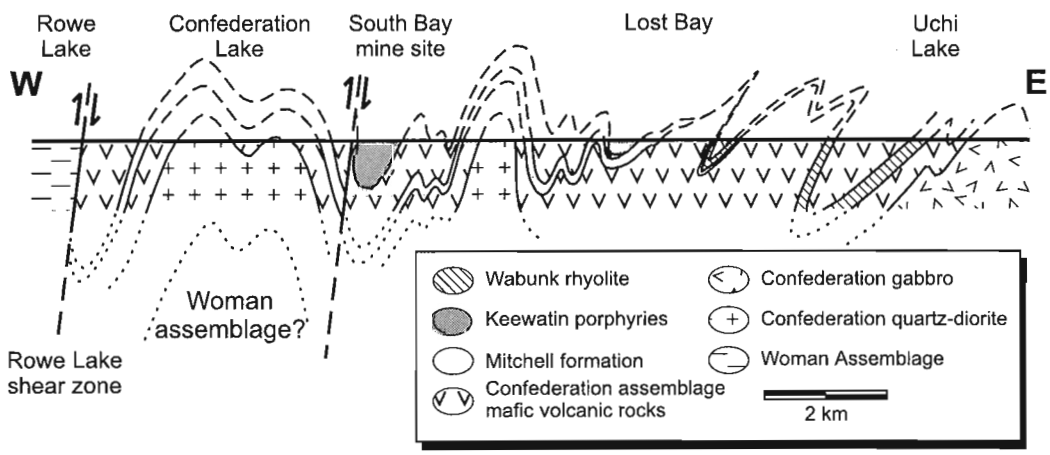


***Figure 4.*** *Schematic cross-section through the Confederation assemblage (after Rogers et al. (1999).*

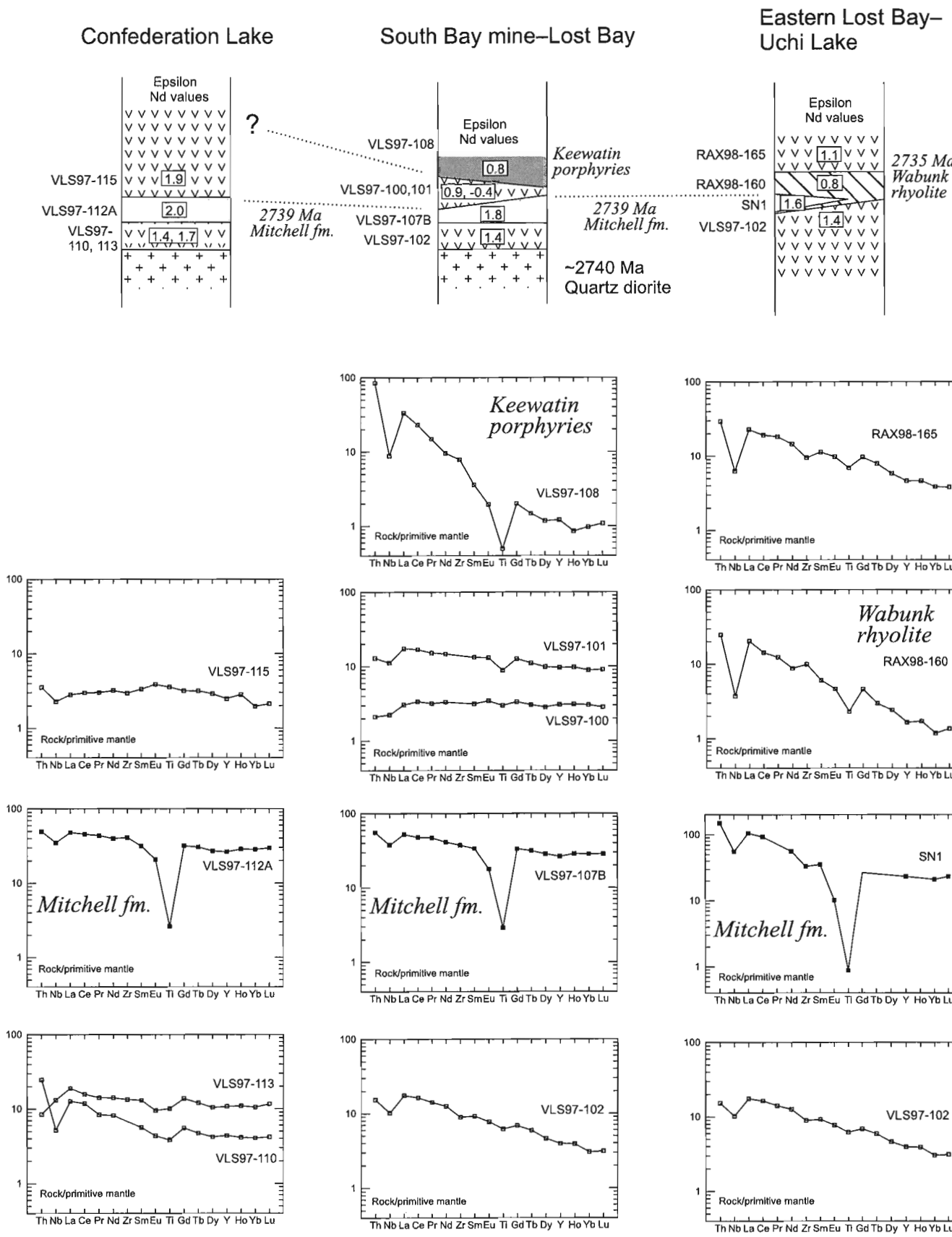


***Figure 5.*** *Top: simplified sections showing the relative position of felsic units and mafic units within the Confederation assemblage and the εNd values (at 2.74 Ga) of samples analyzed. (Legend is the same as Figure 4.) Bottom: corresponding mantle-normalized multi-element diagrams for the same samples (and their relative position stratigraphically).*

Mafic to intermediate lavas between the Mitchell formation and the overlying felsic suites display a variety of characteristics. West of Confederation Lake, the lavas have relatively flat mantle-normalized profiles with slight Th enrichment and comparatively juvenile εNd values of +1.9 (at 2.74 Ga). To the east of Confederation Lake, where the sequence thins (Fig. 5), the mafic lavas have rather lower εNd values of +0.9 and –0.4 (at 2.74 Ga). The lavas have flat to slight light-REE-enriched multielement profiles with small negative Nb anomalies. In terms of geochemistry alone, they do not appear to have recycled more than a few per cent of felsic crust. Their isotopic characteristics, however, require crustal involvement, which suggests that a small amount of very old crust (i.e. older than 3 Ga) may have been involved in their petrogenesis by either crustal contamination or recycling within the mantle

Rocks of the Keewatin and Wabunk felsic suites also have relatively low εNd values of +0.8. These rocks are extremely rich in light-REEs, with Th enrichment and Nb depletion. Their $T_{DM}$ model ages of 2846 and 2868 Ma (Table 1) suggest that they separated from the depleted mantle reservoir during, or prior to, Woman assemblage magmatism. These rocks may represent melts of crust older than the Woman assemblage, or the model ages may represent mixed ages involving Woman-aged crust and an older (>3 Ga) component.

A basaltic lava from Uchi Lake that may be stratigraphically above the Wabunk rhyolite has an εNd value of +1.1. It is moderately light-REE enriched, with a negative Nb anomaly, again suggesting that it may have recycled or been contaminated by older (>3 Ga) felsic crust.

To summarize the data from the Confederation assemblage, felsic rocks of the Mitchell formation, and stratigraphically lower mafic rocks are relatively juvenile, with εNd values of +1.4 to +2.0. They require only a small amount of recycling of crust, younger than 3 Ga, probably represented by the Woman and/or the Balmer assemblage. Most rocks overlying the Mitchell formation have rather lower εNd values (-0.4 to +1.1) and require an older (>3 Ga) crustal component to their petrogenesis.

## YOUNG INTRUSIONS

A ~2705 Ma granite (V. McNicoll, unpub. data, 1999) from the Bear Lake pluton (RAX98-412) which intrudes the Woman and Confederation assemblages (Fig. 1) and a ~2700 Ma gabbro (V. McNicoll, unpub. data, 1999) which intrudes the Balmer assemblage (RAX98-420) have both been analyzed for Nd isotopes. Both samples have low εNd values of +0.2 (granite) and +0.5 (gabbro) (Table 1; Fig. 2). These data are consistent with reworking of Balmer/Woman/Confederation-aged crust in the late-stage development of the greenstone belt.

## CONCLUSIONS

The geochronology, geochemistry, and field relationships of the Uchi–Confederation Lake greenstone belt and the Trout Lake batholith are still under investigation, but Nd-isotopic data and preliminary geochemistry on 30 samples presented here place some important constraints on the evolution of the area. The two most significant findings are 1) that the Balmer assemblage appears to contain crustally contaminated rocks and therefore may have formed on pre-existing felsic crust, and 2) that a phase of the Trout Lake batholith older than 2840 Ma most likely exists. Indeed, an early phase of the Trout Lake batholith may represent basement to the Balmer assemblage.

As shown by Rogers et al. (1999), the Woman assemblage erupted through the Balmer assemblage. The isotopic data is consistent with this but also suggests that a component older than 3 Ga is necessary, via crustal contamination or crustal recycling within the mantle, to explain some of the low εNd values within the Woman assemblage. The same can be said for the upper half of the Confederation assemblage; however, the lower half of the Confederation assemblage (the Mitchell formation and lower units) is notably more juvenile.

## ACKNOWLEDGEMENTS

K.Y. Tomlinson is extremely grateful to R. Thériault and T. Skulski for training in Nd-isotopic analysis. T. Skulski and C. van Staal are acknowledged for initiating this study and for subsequent discussions on the area. V. McNicoll provided access to her unpublished geochronological data. V. McNicoll, J. Percival, and R. Thériault are thanked for reviewing the manuscript. This work is a contribution to the Western Superior NATMAP Project.

## REFERENCES

**DePaolo, D.J.**
1981: Neodymium isotopes in the Colorado Front Range and crust-mantle evolution in the Proterozoic; Nature, v. 291, p. 193–196.

**Hollings, P.N.**
1998: Geochemistry of the Uchi Subprovince, northern Superior Province: an evaluation of the geodynamic evolution of the northern margin of the Superior Province ocean basin; Ph.D. thesis, University of Saskatchewan, Saskatoon, Saskatchewan, 229 p.

**Noble, S.R.**
1989: Geology, geochemistry and isotope geology of the Trout Lake batholith and the Uchi–Confederation lakes greenstone belt, northwestern Ontario, Canada; Ph.D. thesis, University of Toronto, Toronto, Ontario, 288 p.

**Nunes, P.D and Thurston, P.C.**
1980: Two hundred and twenty million years of Archean evolution: a zircon U-Pb age stratigraphic study of the Uchi–Confederation lakes greenstone belt, northwestern Ontario; Canadian Journal of Earth Sciences, v. 17, p. 710–721.

**Rogers, N., van Staal, C.R., and McNicoll, V.**
1999: Recent advances in the geology and structure of the Confederation Lake region, northwestern Ontario; *in* Current Research 1999-C; Geological Survey of Canada, p. 187–195.

**Stott, G.M. and Corfu, F.**
1991: Uchi Subprovince; *in* Geology of Ontario, Ontario Geological Survey, Special Volume 4, part 1, p. 145–236.

**Thurston, P.C.**
1985: Physical volcanology and stratigraphy of the Confederation Lake area, District of Kenora (Patricia Portion); Ontario Geological Survey, Report 236, 117 p.

**Thurston P.C. and Fryer, B.J.**
1983: The geochemistry of repetitive cyclical volcanism from basalt through rhyolite in the Uchi–Confederation greenstone belt, Canada; Contributions to Mineralogy and Petrology, v. 83, p. 204–226.

**Tomlinson, K.Y., Stevenson, R.K., Hughes, D.J., Hall, R.P, Thurston, P.C, and Henry, P.**
1998: The Red Lake greenstone belt, Superior Province: evidence of plume-related magmatism at 3 Ga and evidence of an older enriched source; Precambrian Research, v. 89, p. 59–76.

---

Geological Survey of Canada Project 970014

# Seismic-reflection data from the Sturgeon Lake mining camp, northern Ontario

Brian Roberts and Erick Adam
Continental Geoscience Division, Ottawa

*Roberts, B. and Adam, E., 1999: Seismic-reflection data from the Sturgeon Lake mining camp, northern Ontario;* in *Current Research 1999-E; Geological Survey of Canada, p. 101–110.*

**Abstract:** In November 1997, Noranda Mining and Exploration Inc. acquired a 7.8 km seismic line in the vicinity of the Sturgeon Lake mining camp in Northwestern Ontario. The data processing was done by the Geological Survey of Canada and the results are presented in this report. Recent studies have shown that the seismic-reflection technique can be an important tool in mineral exploration if certain geological criteria are met, and the data are carefully processed. The main focuses in the processing were noise elimination, static corrections, and determination of the correct velocity field. We also tested prestack migration by utilizing an equivalent-offset technique. This method provided an alternative final section which aided in the data interpretation. The dynamite data displayed high signal levels and we observed strong reflectivity at depth. However, the near-surface reflectivity is weak, likely due to the complexity and steepness of the geological structures.

**Résumé :** En novembre 1997, un profil sismique d'une longueur de 7,8 km a été collecté dans la région du camp minier de Sturgeon Lake, situé dans le nord-ouest de l'Ontario, par Mines et Exploration Noranda Inc. La Commission géologique du Canada a été choisie pour le traitement des données, et les résultats sont présentés dans ce rapport. Des études récentes démontrent que la méthode de sismique-réflexion peut être utile à l'exploration minérale lorsque certains critères géologiques sont rencontrés et que les données sont traitées adéquatement. Lors du traitement des données, une attention particulière a été accordée à l'élimination du bruit, aux corrections statiques et à la détermination des vitesses sismiques. La migration avant-sommation a aussi été testée en utilisant la méthode des séparations équivalentes. Cette méthode procure une section somme finale pouvant aider l'interprétation des données. La source de dynamite a généré des arrivées d'amplitudes élevées et on observe de fortes réflexions en profondeur. Toutefois, il y a peu de réflexions proches de la surface, ce qui est probablement dû à la complexité et à la pente abrupte des structures géologiques.

## INTRODUCTION

There are an increasing number of studies which demonstrate the benefits of using the seismic technique in existing mining camps. In particular, they show that it is a cost-effective way to map favourable mine horizons (e.g. Milkereit et al., 1996; Perron et al., 1997), and is potentially capable of directly detecting massive sulphide deposits (e.g. Adam et al., 1997). It has been shown that the success of seismic studies in a crystalline environment is dependent on prior knowledge of the structures (i.e. dip, strike, thickness) and the physical properties (i.e. density and velocity) of the host rocks and mineralization. This information is obtained by geophysical logging in existing boreholes, performing lab measurements on rock samples, and examining the geological database.

In November 1997, Noranda Mining and Exploration Inc. took the opportunity to utilize a seismic crew that had been mobilized from Calgary for the acquisition of the LITHOPROBE Western Superior seismic transect to acquire a 7.8 km seismic line near several existing mining camps in the Sturgeon Lake greenstone belt, Northern Ontario (Fig. 1). The area is well mapped, and Noranda has a number of boreholes in the vicinity of the seismic line to aid in the interpretation of the data.

Processing of the seismic data was undertaken at the Seismology and Electromagnetism Section of the Geological Survey of Canada using the ProMAX seismic data-processing software. Detailed geological information on the study area was not available, and, as a result, this report outlines the processing performed and displays the final sections along with a description of the main features in the data, rather than providing a complete interpretation of the data.

## GEOLOGICAL SETTING

The Sturgeon Lake greenstone belt lies in the Superior Province at the boundary between the central and western Wabigoon Subprovince where Mesoarchean crust (central Wabigoon) appears to lie adjacent to younger supracrustal belts (western Wabigoon) (Thurston et al., 1991). Greenstone belts (ca. 2.73 Ga) are widespread in the Wabigoon Subprovince and host numerous base-metal occurrences. The

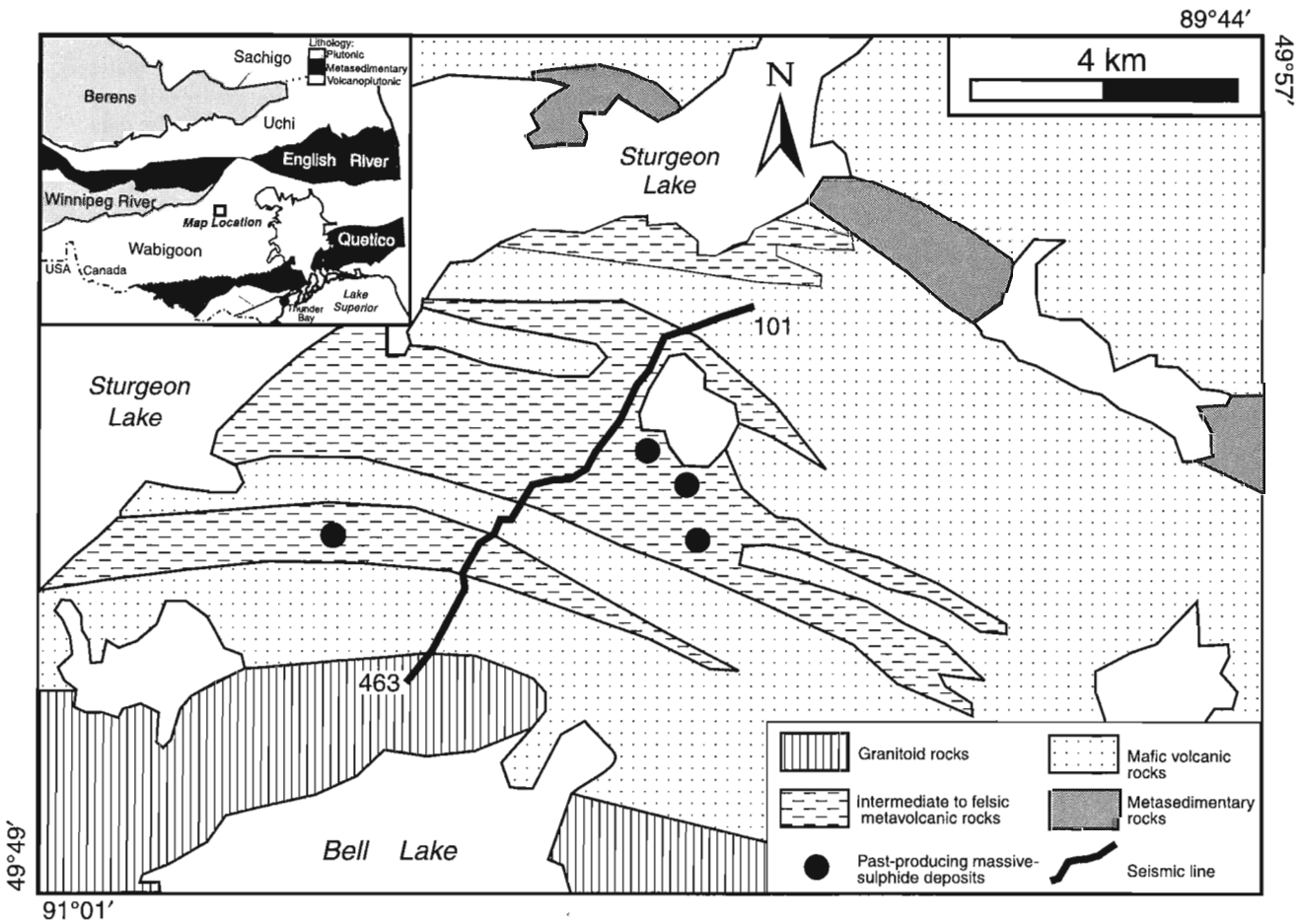


***Figure 1.*** *Map showing the location of Sturgeon Lake seismic line 1 and the regional setting of the Sturgeon Lake mine camp area within the Archean Superior Province (inset). Geology is modified from Sanborn-Barrie et al. (1998).*

area of interest for this study has been mapped in detail, and the zone which contains the known mineral occurrences has been interpreted as an Archean submarine caldera complex (Morton et al., 1991). The caldera volcanic rocks overlie a pre-caldera volcanic cycle to the south, and are overlain by younger mafic volcanic rocks to the north (Fig. 1). All the metavolcanic units in the Sturgeon Lake mine-camp area are dated in the 2.70–2.735 Ga range.

## SEISMIC-DATA ACQUISITION PARAMETERS

Receivers along the entire seismic line were active for all the shots, and 3 s of 393-channel data were recorded with a sampling rate of 1 ms for each of the 223 dynamite shots. The 393 trace spread used a receiver spacing of 20 m and the shot spacing was 40 m. A visual inspection of the shot gathers indicated that the dynamite shots provided ample source energy with strong first-break energy along the entire spread of receivers and obvious reflection energy is seen at 1.5 and 2.5 s.

## DATA PROCESSING

The processing of seismic data can be divided into those steps which are performed prior to stacking the seismic traces (referred to as prestack) and those done after stack (or poststack).

### *Prestack*

The prestack processing of the shot gathers focuses mainly on the elimination of noise (both source generated and ambient background), the application of static corrections, and the determination of the correct velocity function for stacking the data (including the application of dip-moveout correction). Noise elimination is critical, because in the crystalline environment we are dealing with low-reflection coefficients and thus, a low signal-to-noise ratio. Below we have listed the highlights of the prestack processing with applicable comments.

#### Geometry definition

The seismic line was not straight (Fig. 1); however, a smooth binning line could be fitted through the source-receiver midpoints such that most of the common-depth-point (CDP) bins contain a full range of offsets. The CDP fold is as high as 224 in the middle of the line, smoothly tapering to a low fold at the ends of the line. Elevations vary by only 10 m along the length of the line.

#### True amplitude recovery

To correct for amplitude loss due to spherical divergence, the data were scaled using a time-variant factor [1/(time•velocity$^2$)] with a constant velocity of 6000 m/s. As well, a full-trace (3 s) automatic-gain function was applied to all traces in order to correct for variations in source and receiver coupling.

#### Deconvolution

Deconvolution improves the temporal resolution of seismic data by compressing the seismic wavelet. After testing, a minimum-phase spiking deconvolution was performed using an operator length of 120 ms.

#### Bandpass filter

The low-frequency end of the spectrum primarily contains the dispersive ground-roll energy and air blast (*see* Fig. 2a) along with ambient noise related to workings at the mine site, small streams, etc. To remove this energy, the low cut of the bandpass filter was set at 32 Hz. The shot gathers also contain abundant high-frequency energy, beyond 200 Hz, but it was observed that the reflective energy in the shot gathers was below 150 Hz. The bandpass filter was thus set to be quite wide, between 32 and 150 Hz, at this early stage of the processing.

#### Elevation statics

The data are corrected to a flat datum of 430 m using a replacement velocity of 5900 m/s.

#### 2-D spatial filtering

After deconvolution and bandpass filtering, there still remains a relatively strong, but discrete, refracted shear-wave arrival (head wave) (Fig. 2a). In order to remove as much of this as possible, we applied a median filter which is focused along a specific velocity (± 3450 m/s in this case). Strong energy travelling at that velocity should be much reduced. This process was about 80% effective, but it was anticipated that the dip moveout (DMO) correction would attenuate the remaining coherent shear-wave energy.

#### Mute first-break energy

Trace muting is based on the first-break picks. The data is muted from 30 ms below the first-break pick to the top (time 0).

Figure 2b displays the top 1 s of a processed shot gather at this point of the processing sequence. The coherent noise has been effectively removed and the reflectivity, although weak, can now be identified.

#### Refraction-statics application

The Canadian shield typically has ground conditions that vary from bedrock at surface to variably thick overburden and an unpredictable height for the water table. Seismic waves travel slowly through overburden, especially if it is dry, and are consistently fast in bedrock. Therefore, along the length of a receiver spread, a variation in the traveltimes to the receivers is normally observed that is related to the thickness of the weathering layer at each location. This static correction is vital in obtaining a good seismic image in any mining-camp-scale seismic survey. In this case, a one-layer

refraction-statics model was defined using the uphole times from the shots and the ProMAX refraction-statics package. Three methods were used for the computations (diminishing residual matrices (DRM), generalized residual method (GRM), and delay times) and all came up with comparable results. The depth-of-overburden model and the source and receiver statics used to correct for the weathering layer are shown in Figure 3.

### Residual statics

The lateral continuity of reflection energy can be improved prior to the stacking process by calculating source and receiver statics which yield a maximum CDP-stack power over a given window on each CDP gather. This process can be effective in low signal-to-noise data. Surface consistent residual statics were calculated using a 600 ms window centred on the strong package of reflectivity at approximately 1 s.

### Dip moveout correction (DMO)

In complex geological environments, reflections with various dips are commonly observed and this is true at Sturgeon Lake. The dipping events are typically related to steeply dipping contacts, faults, or diffractions from structural discontinuities and high-impedance scatterers. In applying the normal moveout correction there is no velocity function that will simultaneously optimize stacking of both dipping and

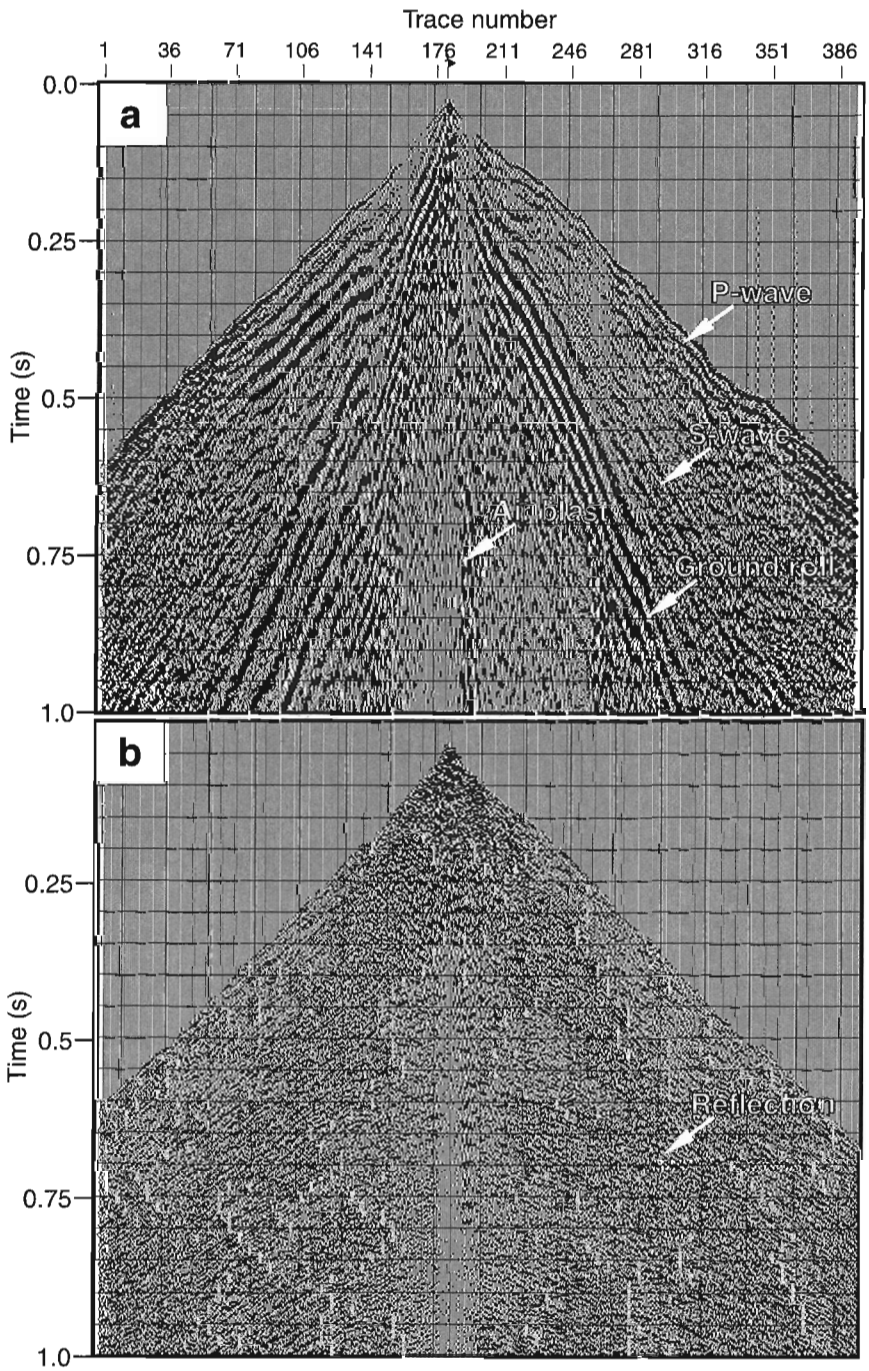


*Figure 2.*

*A display of the top 1 s of a raw (**a**) and processed (**b**) shot gather from station 255 on line 1 The weak reflectivity is apparent on b after the removal of all the coherent noise.*

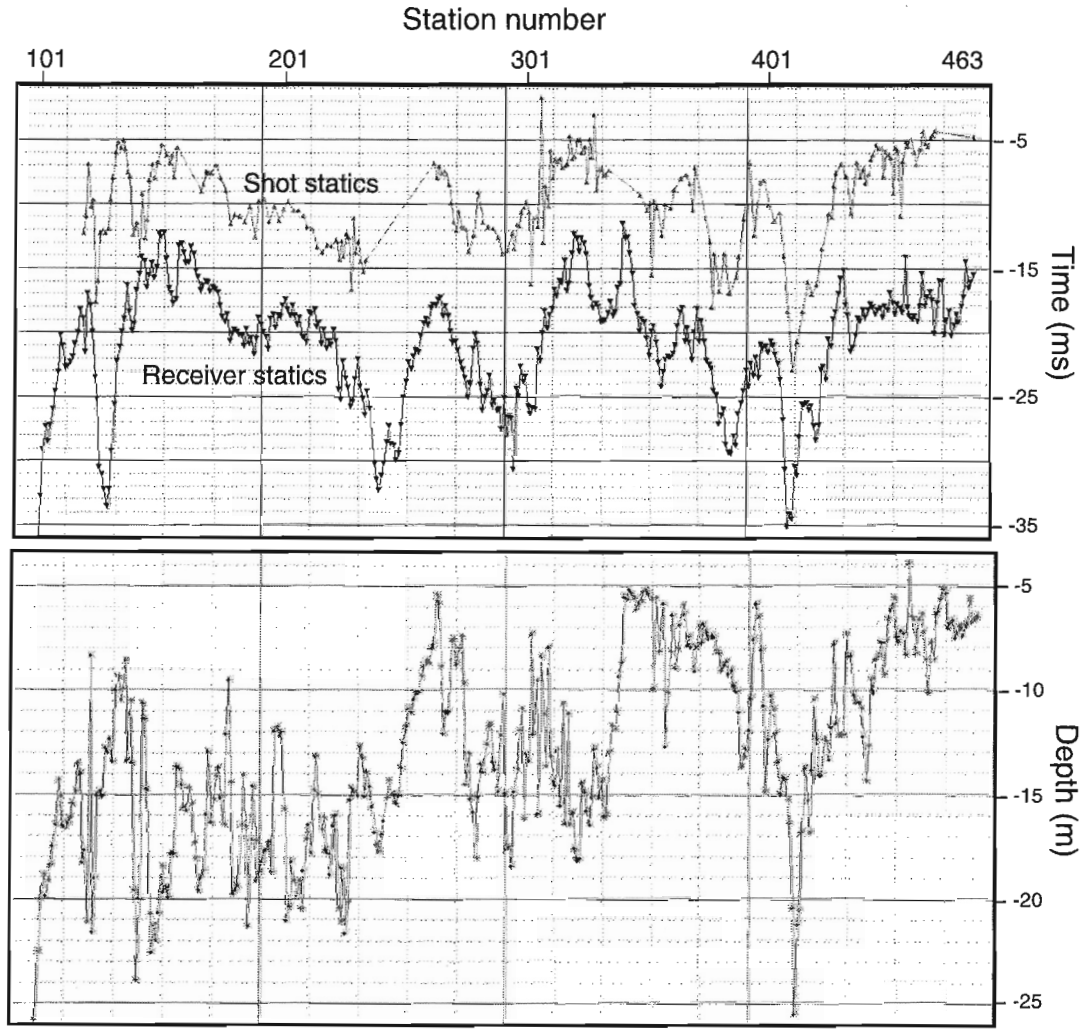


***Figure 3.*** *Shot and receiver refraction statics (top) and depth of overburden (bottom).*

subhorizontal events. The dipping events stack at anomalously high velocities. To circumvent this problem, DMO is used to effectively create a zero-offset section, in which dipping events will stack at realistic velocities. Prior to DMO, an average background velocity (6000 m/s) is used to correct the data, then a full velocity analysis is performed following DMO.

### Velocity analysis

The velocity analysis was performed using a combined semblance/constant-velocity stack display every 50 CDPs (500 m). The velocities varied somewhat along the line, but on average the velocity function varies from 5600 m/s at the surface to 6350 m/s at depth (*see* Table 1).

**Table 1.** Typical velocity function used for NMO correction of Sturgeon Lake line 1.

| Time (ms) | RMS Velocity (m/s) |
|---|---|
| 50.0 | 5600 |
| 300.0 | 5900 |
| 500.0 | 6000 |
| 1000.0 | 6100 |
| 2400.0 | 6350 |

### Normal moveout (NMO) correction and CDP stack

Following the NMO correction, the data are stacked using a straight mean stack with a maximum fold of 224.

### *Poststack*

### Bandpass filter

Up to this point we have maintained a wide frequency spectrum in the data. This is to ensure that every chance is given to enhance the high-frequency data, especially in the top 0.5 s. In analyzing the data poststack, it is observed that most of the coherent energy lies in the 30–80 Hz range, with some higher frequency signals (up to 120 Hz) in the upper part of the section. Because of this, a time-variant bandpass filter was applied at this point (0–0.3 s, 30–120 Hz; 0.3–0.45 s, 30–100 Hz; 0.45–3.0 s, 30–80 Hz).

### F-K migration

Stolt F-K migration with a constant velocity of 6000 m/s (average background velocity) was applied.

### Automatic gain control (AGC)

A scale factor is calculated using a 1 s window and applied to the sample at the centre of the window.

## OBSERVATIONS FROM THE STACKED AND MIGRATED SECTIONS

The data acquired at Sturgeon Lake are of high quality and the data processing was fairly routine with no major problems encountered. The geological information required to do a

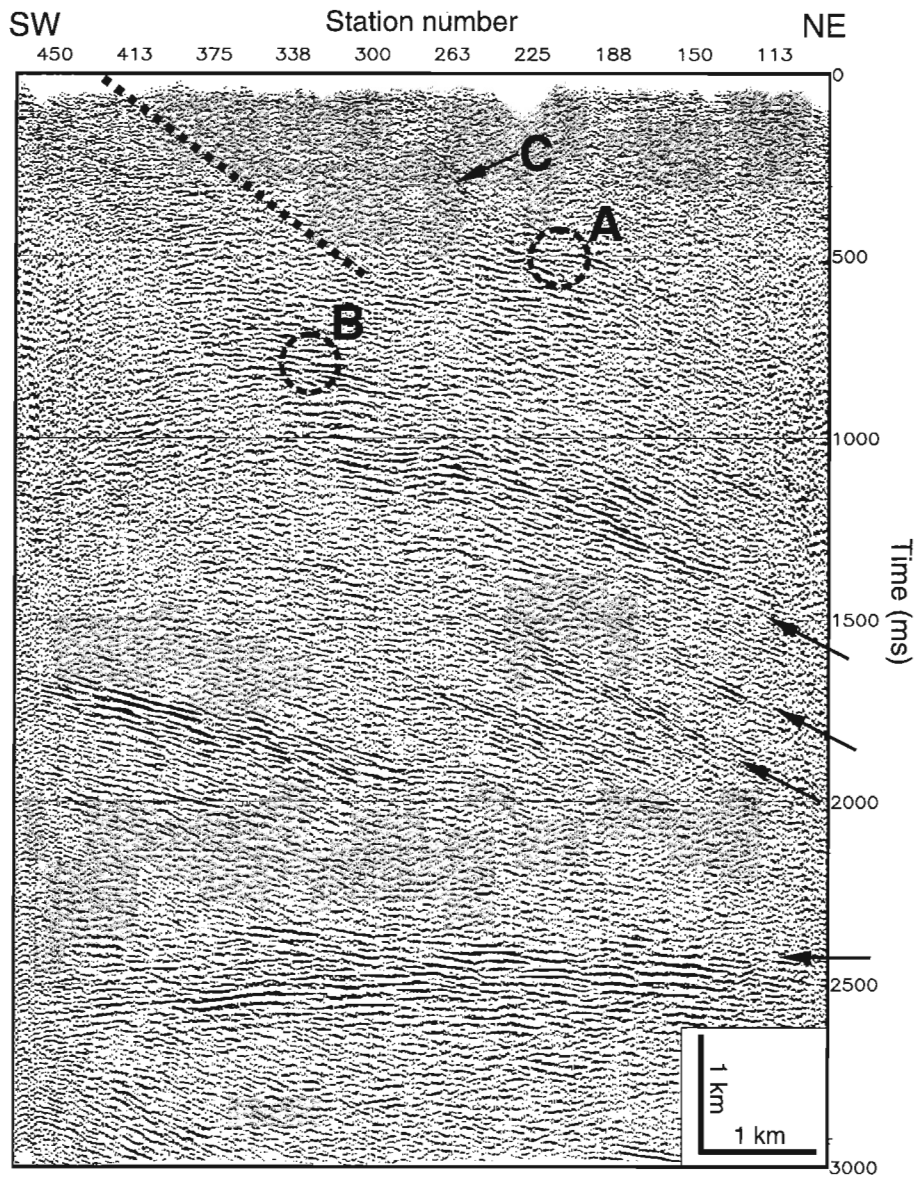


***Figure 4.***

*Sturgeon Lake line 1 dip moveout (DMO) stack (1:1 scale). **A** and **B** indicate diffractions, **C** points to steeply dipping, near-surface reflectivity, and the dotted line joins the apparent truncations of the horizontal reflectivity seen in the southwest part of the section. The arrows indicate reflections referred to in the text.*

meaningful interpretation was not available; however, useful observations can be made about the major features displayed on the seismic section.

Below 1 s on the DMO section (Fig. 4) we see a series of dipping interfaces (apparent dip of 20 to 30° NE) and a strong subhorizontal reflection package at 2.5 s. The dipping events are of varying strength, but continuous from station 463 to the northeast end of the section. The exception to this is the lowest layer of dipping reflections, which is strong at the southwest end of the line, but becomes incoherent at approximately the halfway point (around station 250). Above 1 s, the picture is more complex with strong, but patchy reflectivity in the southwest end of the line and a more transparent section to the northeast (at least above 0.4 s). At least two diffractions that can be identified; one with an apex at station 220 and 0.5 s (A on Fig. 4), and one at station 345 and 0.8 s (B on Fig. 4). The first diffraction (A) also appears to have a series of weaker diffractions below it, but they are not so continuous. Also of note in the top part of the section are some weak, steep, northeasterly dipping reflections (approximatley 40° dip) between stations 240 and 290 and 150–400 ms (C on Fig. 4). The subhorizontal reflections which make up the strong reflectivity in the west part of the line appear to truncate rather abruptly as they extend east. A hypothetical line (*see* dotted line on Fig. 4) joining these truncations (a fault?) would extend to surface at about station 420, near the contact between the older mafic volcanic group and the intrusive volcanic rocks to the south (Fig. 1).

The migrated section (Fig. 5) is noisier and contains more artifacts than the DMO section; however, it does clarify the picture somewhat in the upper section. Below 3 km the events are as described above except that the dipping events have moved updip to the southwest and appear to flatten towards the northeast end of the line. Above 3 km we see that

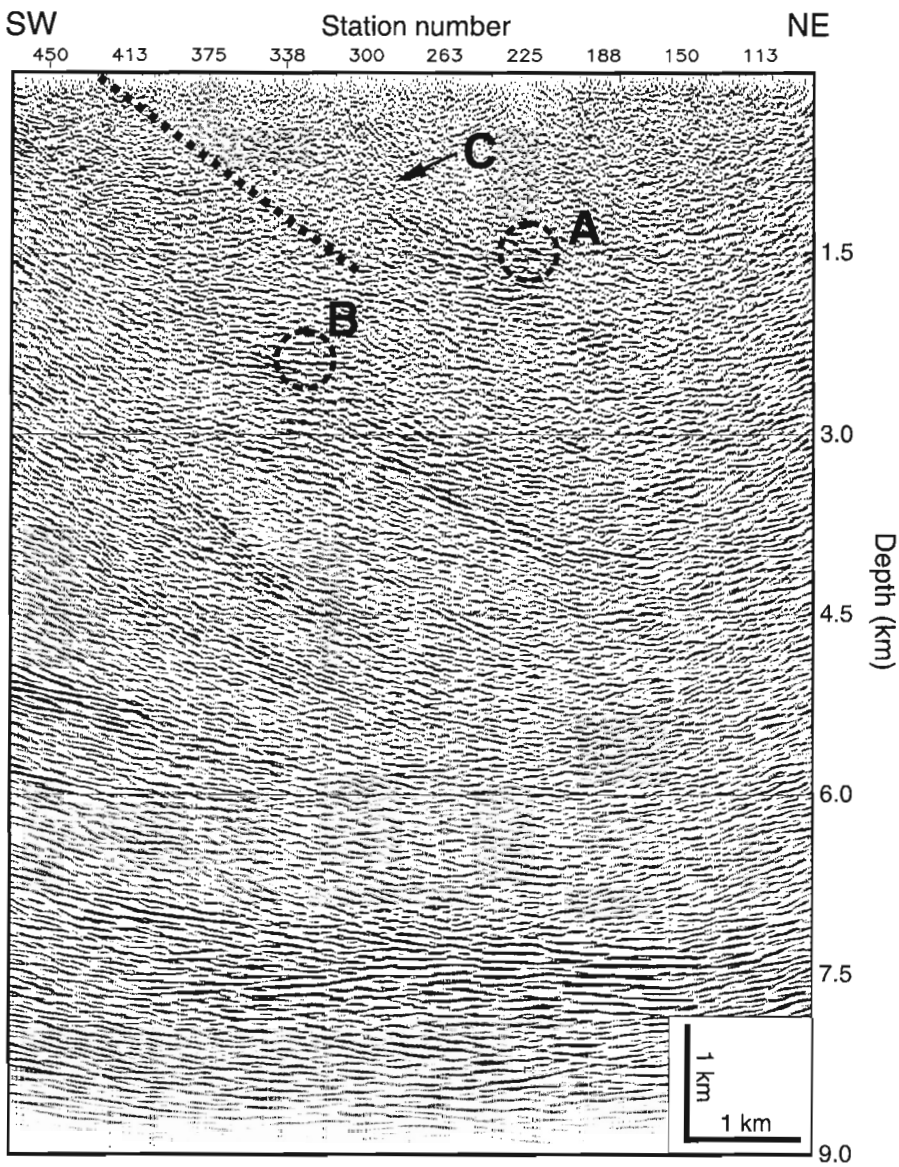


***Figure 5.***

*Sturgeon Lake line 1 migrated stack (F-K migration at 6.0 km/s). See Figure 4 for description of features.*

the two diffractions mentioned above have collapsed to fairly discrete zones of moderate- to high-amplitude reflections. The dipping reflections between stations 240 and 290 (referred to as C above) have steepened up, and now we can project them from the surface at approximately station 315 down to a package of subhorizontal reflections at 1.5–1.8 km (stations 210–220). Again, the subhorizontal events to the west end of the line appear to truncate against some east-dipping plane.

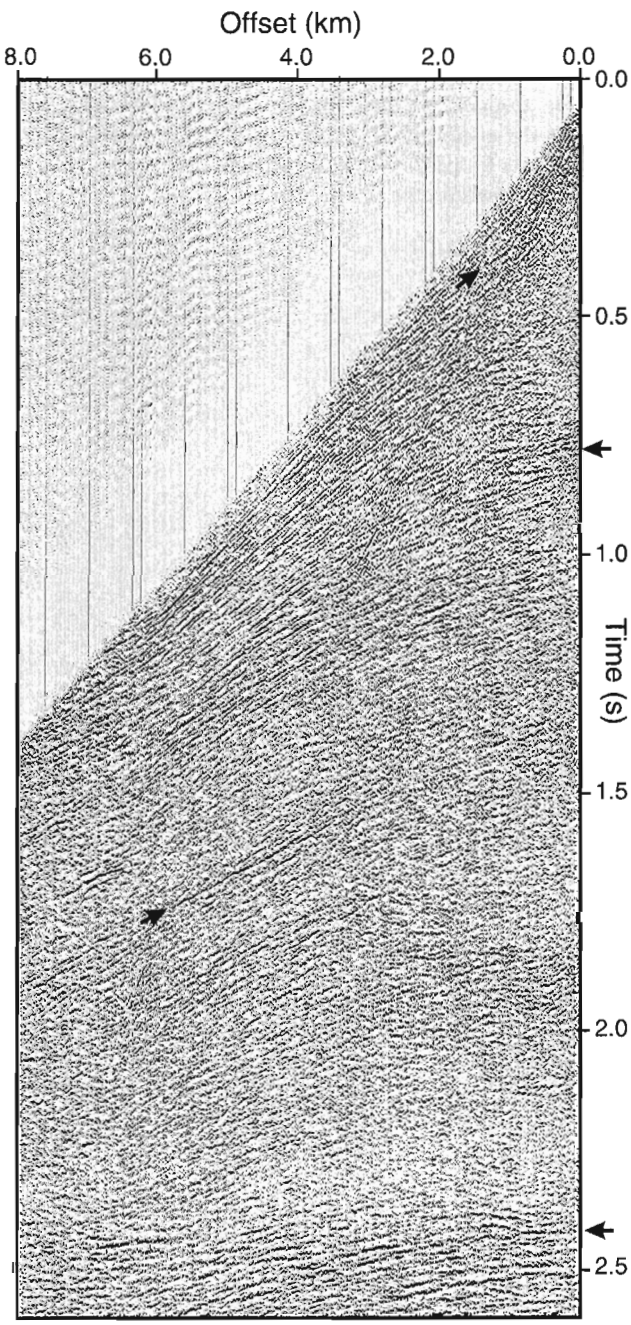


***Figure 6.*** *Common-scatter-point (CSP) gather at station 330. Offsets between 0 and 8 km are displayed. A 30–130 Hz spectral equalization with a 1.5 s window has been applied Arrows indicate reflections observed at various depths.*

## EQUIVALENT-OFFSET MIGRATION

Equivalent-offset prestack migration (EOM) has been applied to Sturgeon Lake line 1 using an ITA/Insight module developed at the GSC. Theory and various application of equivalent-offset migration are described by Bancroft et al. (1998). For a constant velocity, the typical NMO, DMO, CMP stack process is kinematically equivalent to prestack migration (Hale, 1984). However, EOM provides an efficient method for acquiring detailed velocity information, and comparisons with poststack migrations have shown that equivalent-offset migrations have better coherency and hence, are more interpretable (Bancroft, 1998). In the application of this method, common-scatter-point (CSP) gathers are assembled at the CDP locations along the processing line.

A CSP bin width of 20 m (twice the CDP spacing) was selected based on receiver spacing and trial-and-error testing with other data, generating 694 CSP gathers. Each CSP gather consisted of 500 traces with equivalent offsets between 0 and 10 000 m (Fig. 6). Note that different bin sizes were not tested. The migration velocity used to assemble the CSP gathers was 6.0 km/s and the maximum migration time was 3 s. The 3 s maximum migration time and the large offsets (10 km) were selected to avoid excessive smearing at depth.

The input traces for the CSP migration were preprocessed using the prestack processing flow described above, up to and including the DMO correction step. After the CSP gathers were assembled, NMO corrections and stacking were performed using ITA/Insight software. A single stacking-velocity function was used: 0.0 s, 5500 m/s; 0.2 s, 5900 m/s; 0.5 s, 6000 m/s. A NMO stretch mute factor of 50% was selected as a compromise between frequency content at shallow depth and imaging of shallow reflections. Stack sections using 0 and 30% stretch mutes were produced and showed strong subhorizontal events near the surface, which were probably caused by remnants of unmuted first-break energy.

The EOM prestack migrated section of the Sturgeon Lake line (Fig. 7) overall shows better continuity of events between 200 and 3000 ms than the F-K migrated section (Fig. 5). However, the migrated DMO section shows better images in the top 600 m and we attribute this difference to the wide aperture of the equivalent offset migration. Data points having an aperture close to 90° often include remnants of first-break energy, creating high amplitudes on the CSP gathers. These were attenuated by applying spectral equalization with a 500 ms sliding window. While this approach has greatly reduced the noise, some is still visible in the top 600 m and the data can no longer be considered 'true amplitude'.

## DISCUSSION AND CONCLUSION

We have observed strong reflectivity at Sturgeon Lake and some potentially interesting structures, both at depth and in the top 0.5 s. It is possible to compare this data to the LITHOPROBE regional seismic data that also crosses part of the Sturgeon Lake greenstone belt. The southern end of regional line 1A extends into the north end of the belt for

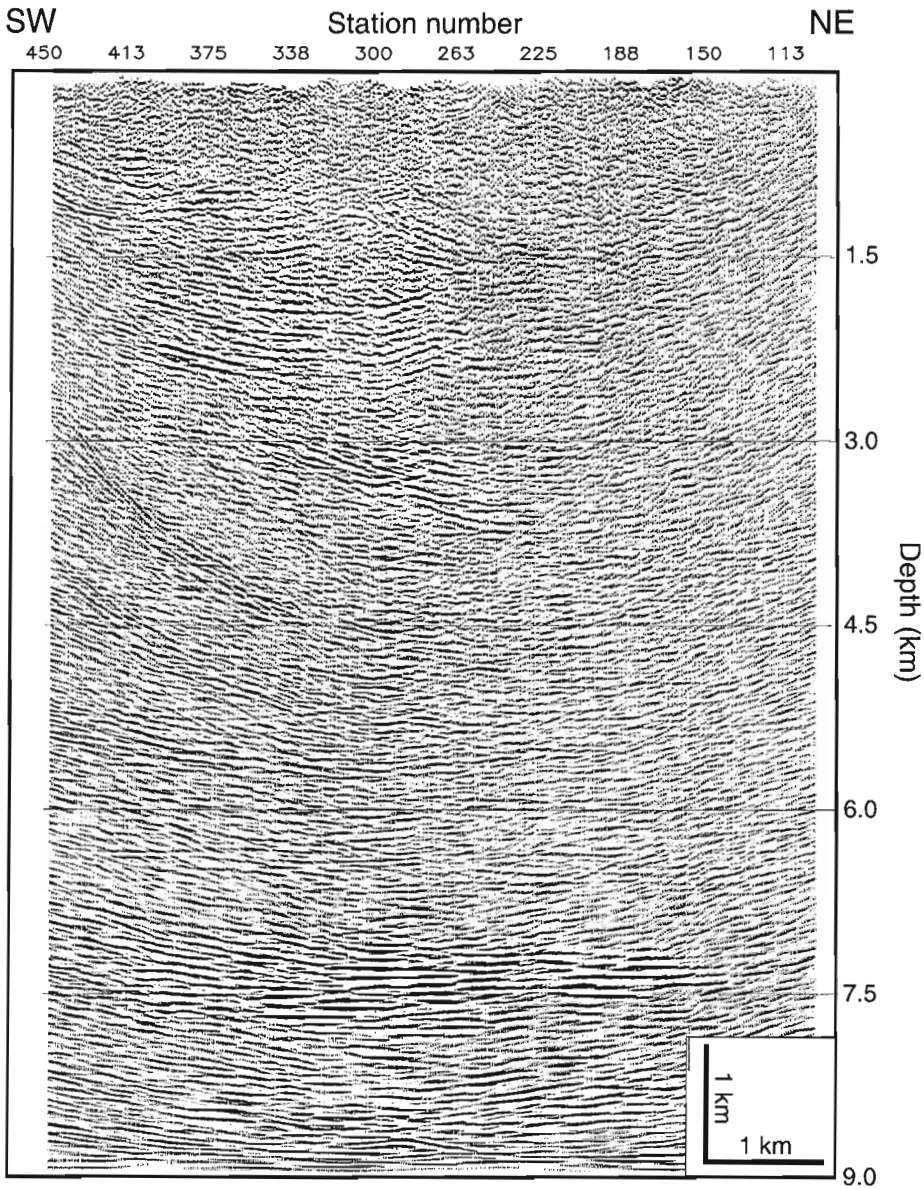


***Figure 7.***

*Equivalent-offset migration stack of Sturgeon Lake line 1.*

roughly 30 km ending approximately 40 km northeast of Sturgeon Lake line 1. The most prominent reflector in the upper crustal part of line 1A is a strong south dipping package that lies at 2.5–4.0 s (D. White et al., written communication, 1999). This event may correlate with the strong subhorizontal reflection we see at 2.5 s on the high-resolution line and indicate that this is a regional reflection underlying the greenstone belt.

The final stacks (DMO structure stack and migrated stack) could possibly be improved by more effort in at least two areas.

1. The refraction-statics solution appears to be at least adequate, but it may be that a better solution could be arrived at through the use of a more robust refraction-statics program. It is possible that this would lead to an improved image in the upper section.
2. The velocity analysis could be redone using the common-scatter-point gathers. The large equivalent offsets of the CSP gathers and better signal-to-noise ratio than standard common-midpoint (CMP) gathers translate into a more accurate velocity analysis. This would result in minor tuning of the velocities leading to a more accurate picture of the true velocities, and perhaps a slightly better image.

The key processing steps for these data were bandpass and 2-D spatial filtering (for coherent noise removal), refraction and residual statics (for improved signal continuity), and DMO (to enable the definition and application of the correct velocity function). In this case, the application of a prestack migration was worth the computational overhead and we would recommend the use of equivalent-offset prestack migration for all short- and moderate-length, high-resolution seismic lines in mining camps.

## ACKNOWLEDGMENTS

The seismic data was collected by J.R.S. Exploration Co. Ltd. of Calgary. We are grateful to Noranda Mining and Exploration Ltd. for allowing the publication of these data. Azad Rafeek provided invaluable drafting assistance and Ian Kay supplied the inset for Figure 1.

## REFERENCES

**Adam, E., Arnold, G., Beaudry, C., Matthews, L., Milkerriet, B., Perron, G., and Pineault, R.**
1997: Seismic exploration for VMS deposits, Matagami, Quebec; *in* Proceedings of Exploration 97, (ed.) A.G. Gubins: Fourth Decennial Conference on Mineral Exploration, p. 433–438.

**Bancroft, J.**
1998: The equivalent offset method of prestack time migration; Geophysics, v. 63, no. 6, p. 2042–2053.

**Hale, D.**
1994: Dip-moveout by Fourier transform; Geophysics, v. 49, no. 6, p. 741–757.

**Milkereit, B., Eaton, D., Wu, J., Perron, G., Salisbury, M., Berrer, E., and Morrison, G.**
1996: Seismic imaging of massive sulphide deposits, part 2: reflection seismic profiling; Economic Geology, v. 91, p. 829–834.

**Morton, R.L., Walker, J.S., Hudak, G.J., and Franklin, J.M.**
1991: The early development of an Archean submarine caldera complex with emphasis on the Mattabi ash-flow tuff and its relationship to the Mattabi massive sulphide deposit; Economic Geology, v. 86, p. 1002–1011.

**Perron, G., Milkereit, B., Reed, L., Salisbury, M., Adam, E., and Wu, J.**
1997: Integrated seismic reflection and borehole geophysical studies at Les Mines Selbaie, Quebec; CIM Bulletin, v.90, p. 75–82.

**Sanborn-Barrie, M., Skulski, T., and Whalen, J.B.**
1998: Tectonostratigraphy of central Sturgeon Lake, Ontario: deposition and deformation of submarine tholeiites and emergent calc-alkaline volcano-sedimentary sequences; *in* Current Research 1998-C; Geological Survey of Canada, p. 115–136.

**Thurston, P.C., Osmani, I.A., and Stone, D.**
1991: Northwestern Superior Province: review and terrane analysis; *in* Geology of Ontario, (ed.) P.C. Thurston, H.R. Williams, R.H. Sutcliffe, and G.M. Stott; Ontario Geological Survey, Special Volume 4, Part 1, p. 81–144.

Geological Survey of Canada Project 970012

# Regional groundwater and stream chemistry survey, Oak Ridges Moraine, Ontario

Larry Dyke
Terrain Sciences Division, Ottawa

*Dyke, L., 1999: Regional groundwater and stream chemistry survey, Oak Ridges Moraine, Ontario;* in *Current Research 1999-E; Geological Survey of Canada, p. 111–121.*

**Abstract:** Water from 310 private wells and 158 stream sites in the Oak Ridges Moraine area of southern Ontario, an important aquifer complex, was sampled over three months during the summer of 1994. Chloride or nitrate in well- and stream-water samples, as components frequently associated with land use, are distributed in such a way as to suggest that shallow groundwater flow is responsible for most of the subsurface transport of these components. Very low sulphate concentrations occur in wells with intakes generally below the lowest elevation of Oak Ridges Moraine exposure. This result suggests groundwater flow also occurs on a larger scale approximately defined by the distance between the regional recharge area along the moraine crest and the low sulphate well area outside the Oak Ridges Moraine exposure.

**Résumé :** On a échantillonné un complexe aquifère important pendant trois mois durant l'été de 1994. L'eau prélevée provenait de 310 puits privés et de 158 sites sur des cours d'eau dans la région de la Moraine d'Oak Ridges, dans le sud de l'Ontario. La répartition du chlorure ou du nitrate, substances souvent associées à l'utilisation des terres, dans les échantillons d'eau de puits ou de cours d'eau permet de supposer que les eaux souterraines à faible profondeur sont à l'origine de la plus grande partie du transport souterrain de ces substances. Les concentrations de sulfate sont très faibles dans les puits dont l'eau provient généralement d'un point sous l'affleurement le plus bas de la Moraine d'Oak Ridges. Ce résultat permet de supposer que l'écoulement des eaux souterraines se produit aussi à une échelle plus grande, approximativement définie par la distance entre l'aire d'alimentation régionale le long de la crête de la moraine et la zone de puits à faible teneur en sulfate située au-delà du dernier affleurement de la Moraine d'Oak Ridges.

## INTRODUCTION

The Oak Ridges Moraine is a broad, east-trending ridge of glaciofluvial and glaciolacustrine sediments lying between Lake Simcoe and Lake Ontario (Fig. 1; Sharpe et al., 1996). It was deposited as a late Quaternary ice-marginal feature during the last deglaciation of southern Ontario. The Oak Ridges Moraine is underlain by the less permeable Newmarket Till which in turn separates the moraine from less well known ice-marginal sediments below. The Geological Survey of Canada has carried out a hydrogeology study of the Oak Ridges Moraine area which includes the moraine and adjacent glacial deposits. Approximately 250 000 people rely on groundwater pumped by municipal and private wells from the moraine or deeper aquifers. As part of the study, a regional groundwater chemistry survey was carried out over the moraine crest and immediate flanks. This sampling was done to acquire a modern assessment of water quality over the entire Oak Ridges Moraine area in a short time interval. The results from this chemical analysis are also used to provide insight into the scale of groundwater flow systems. These results are then compared with well-water analyses carried out by GSC in the 1940s to determine if changes associated with urbanization can be detected.

A considerable body of groundwater quality data exists for the Oak Ridges Moraine area, including analyses of well waters done in association with groundwater assessments by the Geological Survey of Canada in the late 1940s, selected watershed surveys (e.g. Funk, 1977; Sibul et al., 1977; Howard and Beck, 1986; Howard et al., 1993), and a recent regional compilation of data by Hunter and Associates and Raven/Beck (unpub. report, 1996). The watershed studies vary in detail and objective but include evidence that groundwater chemistry evolves between recharge and discharge areas based on ion exchange and mineral dissolution. The present study was carried out in part to determine if such processes are typical of the Oak Ridges Moraine area in general. It was also undertaken to gain a general indication of the level of water quality alteration due to the introduction of substances associated with land use. Although water quality data is available for this entire area, observations cluster at sites of topical interest and are spread over several decades. In an attempt to reduce inconsistencies in the spacing and timing of these data, a regional sampling of water wells and streams was carried out over a three-month period in 1994.

## SIGNIFICANCE OF CHEMICAL COMPONENTS

The chemical evolution that proceeds as rain and snowmelt infiltrate and move through the subsurface can assist in defining the lateral extent and depth of groundwater flow systems in a geological feature. Products of chemical solution at or near the ground surface which are detected in deeper groundwater offer a means of establishing flowpaths. Ion exchange and reduction-oxidation reactions will alter the chemical composition if residence time is long enough and the appropriate chemical environment is encountered. Thus detection of groundwater with evolved chemical compositions can also assist in establishing flowpaths. In this study, the chemical characterization of waters was limited to normally abundant inorganic components or components likely originating from known sources.

Water hardness is a measure of all divalent cations, usually dominated by calcium and magnesium. These cations are contributed mainly from dissolution of the carbonate mineral component of Oak Ridges Moraine area sediments. Tills in the area typically contain 20–40% $CaCO_3$ in the matrix (Karrow, 1967) and similar contents are probably present in the finer

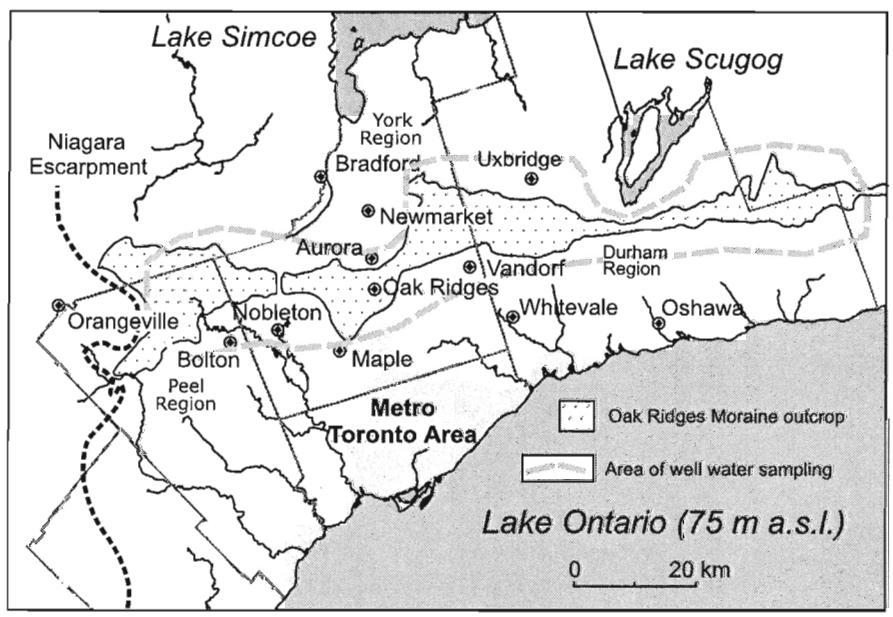


***Figure 1.*** *Location map showing outcrop of Oak Ridges Moraine and general area of well water sampling in the context of the Greater Toronto Area.*

grained facies of the Oak Ridges Moraine. Although maximum concentrations are probably reached quickly as groundwater infiltrates, subsequent cation exchange, as groundwater passes through clay-rich strata, may provide an indication of chemical evolution and groundwater travel. Alkalinity, the capacity of a water to neutralize an acid, is derived principally from the bicarbonate anion by dissolution of carbonate rocks. Although hardness and alkalinity are both customarily expressed as the amount of calcium carbonate dissolved that would give the measured value, the two may differ for a given water sample due to processes other that calcium carbonate dissolution. For example, cation exchange may result in divalent cations removed from solution, dissolution of gypsum produces calcium ion, and bicarbonate is a product of reduction-oxidation reactions. Sulphate is also most likely derived from the dissolution of gypsum or the weathering of pyrite. The tendency of sulphate to be chemically reduced in an evolving reduction-oxidation environment and hence consumed during movement in the subsurface may provide a means of distinguishing flow on different scales. Chloride and nitrate in the glacial sediments likely originate from non-natural sources and are indicators of urbanization and agriculture, respectively. They are transported from on or near the ground surface but the distribution of these components in groundwater may be complicated by the uneven distribution of releases and partitioning between surface runoff and infiltration.

The chemical components included in this analysis also have aesthetic and health implications. Most have no strictly defined maximum desirable concentrations. Chloride has no significant health implications and limits are specified to prevent undesirable taste. However, because of its common association with septic field or landfill leachate, the presence of chloride may imply other contamination. Nitrate is derived from fertilizer or can be associated with livestock and can cause oxygen deprivation to the blood in infants. Sulphate may have a mild laxative effect and hardness is an aesthetic parameter, preventing the lathering of soap and producing calcium deposits in water-heating appliances and fixtures. Alkalinity is a measure of the acid-neutralizing capability of a water and usually correlates with hardness. Table 1 gives maximum desirable concentrations as defined by Health Canada (1996).

## PROCEDURE

The primary sample source was 310 domestic water wells, ranging in depth up to 150 m. Most well samples were screened at depths of less than 100 m. The area of coverage includes both the flanks and the moraine crest (Fig. 1), therefore providing an opportunity to detect water quality evolution both with distance from the crest and with the depth of sampling in the recharge area. Well sampling was complemented with stream sampling at 158 locations within the general area of well coverage (*see* Fig. 5). The initial stream sampling was carried out during an interval of little or no rainfall in mid- to late June and so captured water supplied predominantly by stream baseflow. Therefore, the stream survey provided additional samples derived directly from groundwater discharge.

Well sampling locations were chosen using a random selection technique. The area to be sampled was superimposed with a 5 x 5 km grid based on the National Topographic System 1 km grid system. This grid was overlain on maps showing the locations of all wells for each of the three following depth categories: 0–30 m, 30–60 m, and greater than 60 m. Within each 5 x 5 km grid cell, wells for sampling were chosen on the basis of a 1 km grid square location chosen by random selection. The well closest to the centre of this grid element was selected for sampling. Unfiltered samples of 0.5 L were collected from tap outlets left running long enough to ensure that the sampled water was drawn form the well bore at the time of sampling. The sampling bottle was rinsed with sample water at least three times. Care was taken to ensure that the sample had not been routed through a water softener. However, some results appear to indicate a softener was present. Field duplicates were taken for about 10% of the sampling locations and an equal number of duplicate analyses run in the laboratory. Stream samples were treated the same way, with the restriction that stagnant reaches were avoided. However, sampling locations were determined mainly by the location of road stream crossings. All samples were immediately stored in coolers with ice, transported to a refrigerator, and analyzed within 3–4 days of collection.

Samples were analyzed for a selection of the inorganic components normally most abundant in groundwater and surface water. Components for analysis were chosen either to 1) serve as indicators of natural chemical evolution during travel from recharge to discharge areas (hardness, alkalinity, sulphate) or 2) serve as tracers to broadly define groundwater flowpaths and the extent to which contaminants introduced at the ground surface are dispersed (chloride, nitrate). Hardness and alkalinity were analyzed by titration techniques and are expressed as milligrams per litre of calcium carbonate. The other ions were analyzed by spectrophotometry (Table 2).

**Table 1.** Water quality guidelines.

| Chemical component | Maximum concentration guideline (mg/L) |
|---|---|
| Chloride | 250, onset of taste[1] |
| Nitrate | 45[2] |
| Sulphate | 500[1] |
| Hardness | More than 200 considered hard[3] |
| Alkalinity | 500, associated with excessive hardness at this concentration[3] |

[1] Aesthetic objective
[2] Maximum acceptable concentration
[3] Not a Health Canada guideline

**Table 2.** Analytical techniques used for water analyses.

| Chemical component | Analytical technique |
|---|---|
| Hardness | Titration with EDTA |
| Alkalinity | Titration with sulphuric acid |
| Sulphate | Spectrophotometry, barium sulphate precipitate |
| Chloride | Titration with mercuric nitrate |
| Nitrate | Spectrophotometry, cadmium complexion |

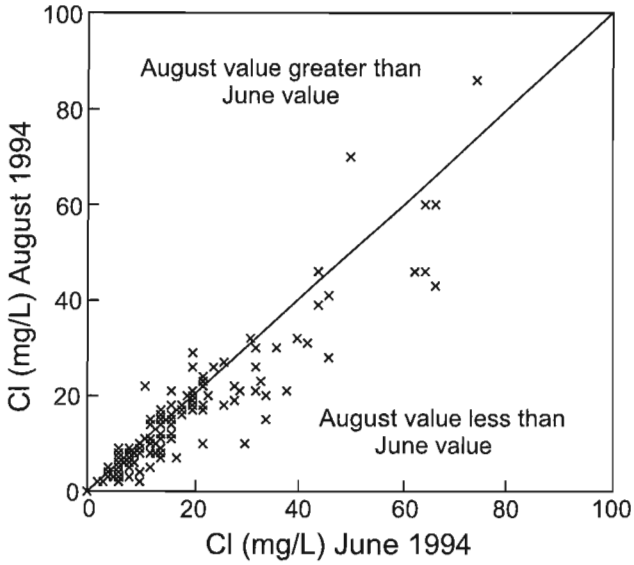


***Figure 2.*** *Comparison of chloride in stream waters sampled in June and in August 1994. The diagonal line shows the locations of equal concentration.*

Errors on duplicate analyses were generally within a range of 10–15% and detection limits in most cases are approximately 2 mg/L (hardness: 4 mg/L).

All streams and 40 wells were resampled about two months after the initial sampling. Streams showed variabilities between the first and second samplings of up to 50% in all components. For chloride concentrations above about 20 mg/L, chloride concentration was consistently 20–30% lower on the second stream sampling (Fig. 2). All other components in streams averaged the same but showed the wide variation for specific sites. Chemical analyses of the first stream sampling are discussed. The well subsample showed much less variability, generally less than 20%, except for hardness which had several second samples differing by up to 50% from the initial sampling. The behaviour of hardness, together with a small number of very low hardness values, suggests that, despite the care taken, some water samples may be affected by passage through water softeners. It is not possible to positively identify samples treated by water softeners because sodium, which a softener exchanges for divalent cations, was not included for analysis. Interpretation of hardness values is thus subject to this limitation.

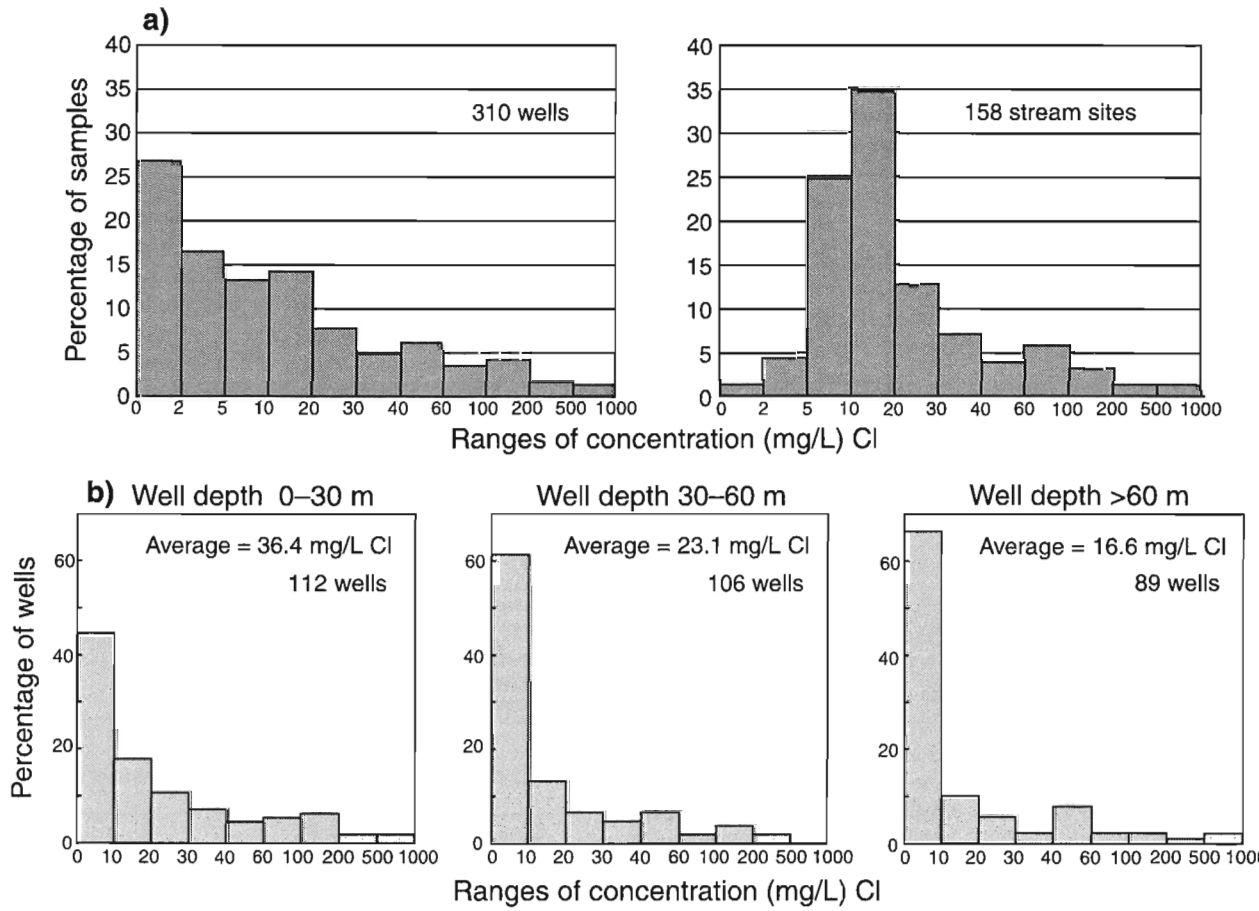


***Figure 3. a)*** *Distribution of chloride concentrations in well and stream samples.* ***b)*** *Distribution of chloride in wells based on well intake depths of 0–30 m, 30–60 m, and greater than 60 m.*

## CHLORIDE

Chloride in well-water samples shows a wide range in concentration (Fig. 3a). A few samples have chloride concentrations between 500 and 1000 mg/L but most are under 60 mg/L and one quarter contain less than 2 mg/L. The lowest chloride values may represent a background level where wells are drawing water originating at recharge areas uncontaminated with chloride or where time has not been sufficient for water containing chloride to reach the well. The overall wide range of chloride values can be attributed to well intakes which intersect some of the many chloride plumes which must originate from surface sources such as road de-icing salt and septic field leachate. Although chloride is present in shale bedrock groundwaters in the southern half of Peel Region (Hickinbotham, 1979) and chloride from bedrock waters is suspected from wells penetrating bedrock and screened close to the bedrock surface (Howard and Beck, 1986), it is unlikely that this source contributes to stream waters or well waters in the sampling area. None of the wells sampled in this study penetrate bedrock. Also, chloride concentrations show a general trend to lower concentrations for increasing well intake depth (Fig. 3b). This trend is more consistent with the dilution of chloride in groundwater as it moves to deeper levels rather than with upward movement from a bedrock chloride source. The sampled wells are plotted in plan view in Figure 4 and categorized by chloride concentration. No systematic distribution of chloride concentration is apparent, suggesting that chloride occurrence is not related to a regional source such as bedrock pore waters. More likely, high chloride concentrations are determined by proximity of well intakes to surface chloride sources.

Introduction of chloride probably began with urbanization and so its dispersal offers a means of assessing the rate of groundwater flow. However, at the broad scale of this survey and despite knowledge of the depth and location of water wells, the required geological detail for delineating probable flowpaths is not known. Dispersal plumes from individual point sources, such as septic tank leach fields, may be responsible for some of the chloride occurrences in Figure 4. Otherwise, as indicated above, there is no obvious pattern to the distribution of well values at the scale of this general survey. Deeper wells typically have low chloride values compared with the Health Canada water quality objective of 250 mg/L for chloride and few shallow wells exceed this value. However, chloride above background levels may be an indication that other contaminants are present because of the typical association of chloride with septic field or landfill leachate. This cautionary note aside, the likelihood of intercepting water with low chloride values, especially for wells away from already developed areas, is high.

In contrast to well waters, chloride in stream waters is highest in the western, more urbanized part of the sampled area (Fig. 5). This occurrence coincides with the area of most extensive use of road de-icing salt. Although the highest concentrations for both streams and wells are no higher than 1000 mg/L, probable dilution as seepage enters a stream suggests that some stream seepage sources of chloride probably exceed 1000 mg/L. To produce the distribution shown in Figure 5 and the probable high chloride values in seepage to streams, most groundwater flow to streams must largely follow short, near-surface flowpaths, minimizing the dilution of incorporated salts. The frequency distribution of chloride concentrations in stream waters differs from that for wells in the lack of stream

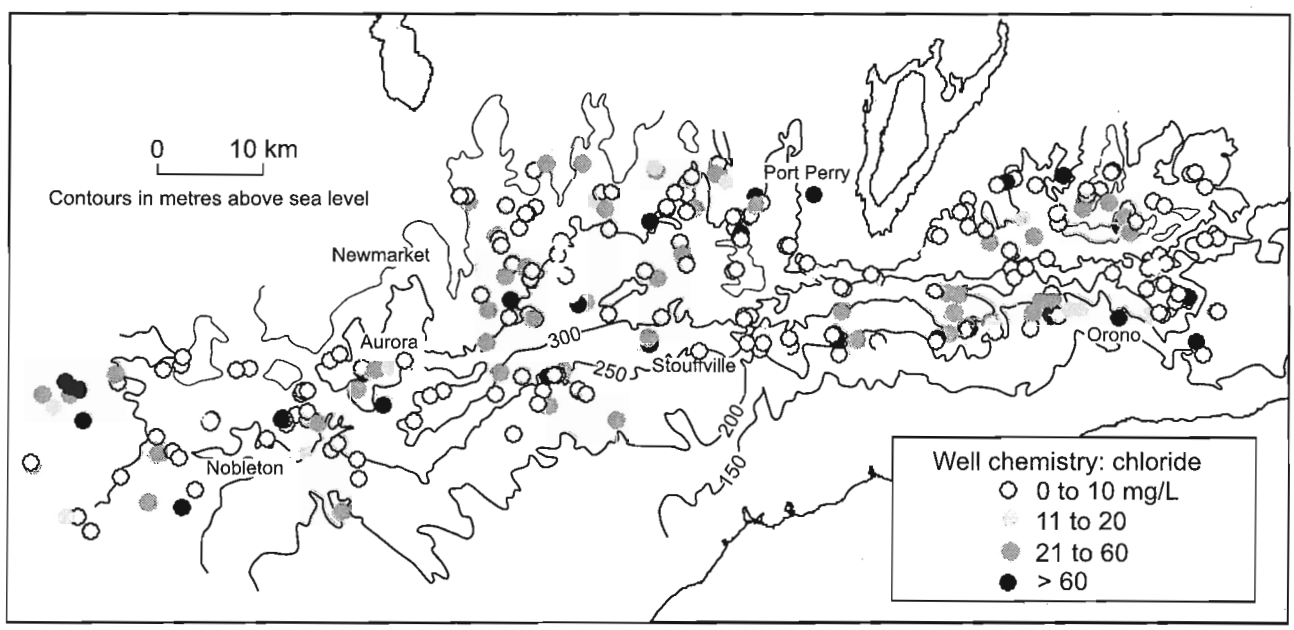


***Figure 4.*** *Locations of wells sampled for the groundwater chemistry survey, shaded to indicate the range of chloride concentration in which the chloride content falls. Contours show the general topographic expression of the Oak Ridges Moraine.*

samples with chloride concentrations of less than 2 mg/L (Fig. 3a). Low chloride values for streams are rare because of the likelihood that some chloride is contributed by surface runoff or shallow groundwater flow at points in the watershed above the sampling location. The association of highest chloride concentrations with shallow groundwater in Figure 3b supports the contention that stream baseflow is provided mainly by shallow groundwater flow. Deeper well waters include a large number of low chloride concentrations probably because they are derived partly from groundwater circulation paths separate from local circulation toward streams or, alternatively, chloride has not reached them yet.

## NITRATE

The general character of nitrate occurrence is similar to that of chloride. Like chloride, the source is unevenly distributed over the sampling area, consisting mainly of fertilized fields, livestock feeding areas, and septic tank seepage. This characteristic is suggested by the distribution of well-water nitrate levels in Figure 6. Stream-sample nitrate concentrations are shown in Figure 7. The eastern, more rural part of the sampling area shows the highest nitrate values, suggesting an influence of rural nitrate sources on stream water quality. A small number of well samples exceed the water quality objective of 45 mg/L nitrate. Although stream samples do not exceed this level, dilution of contributing groundwater sources is probably taking place, indicating that higher nitrate concentrations in stream seepage sources may exist. As with chloride, groundwater with the higher concentrations probably have very short transport routes, either by surface water flow or very shallow groundwater flow.

## SULPHATE

Unlike chloride or nitrate, sulphate concentrations in wells have a bimodal distribution (Fig. 8a). Concentrations below 10 mg/L are rare, except for concentrations below 2 mg/L, which make up 15% of the wells sampled. Like hardness, sulphate is most likely acquired by groundwater during travel rather than from a surface source. The most likely source for sulphate is pyrite distributed throughout the glacial sediment body. Gypsum as an accessory mineral in road de-icing salt is unlikely as a major source of sulphate because of the lack of correlation between sulphate and chloride and also because of the frequency distribution of sulphate concentrations is distinctly different from that of chloride. Sulphate values are distributed around a mean value distinctly above zero, with the notable addition of the near-zero values.

The nature of the bimodal distribution in sulphate values is also shown in Figure 8b where sulphate concentrations are plotted according to well intake level. The lowest values are essentially below the detection limit of about 2 mg/L. There is a distinct gap before readings again become common above 10 mg/L. The large proportion of very low sulphate concentrations suggests that sulphate is being removed from groundwater rather than simply not encountered. With downward movement in recharge areas, sulphate that is produced by the oxidation of pyrite or other source is subsequently reduced to sulphide and precipitated or transformed to $HS^-$ or $H_2S$. The distance over which this transformation takes place is probably highly variable but, within the Oak Ridges Moraine, the location of wells with the very low values provides an indication of this distance. Almost all the wells with very low readings are below a surface elevation of 300 m (Fig. 8c), at the base of or below the lowest elevation of Oak Ridges Moraine exposure. This observation suggests that sulphate is not yet

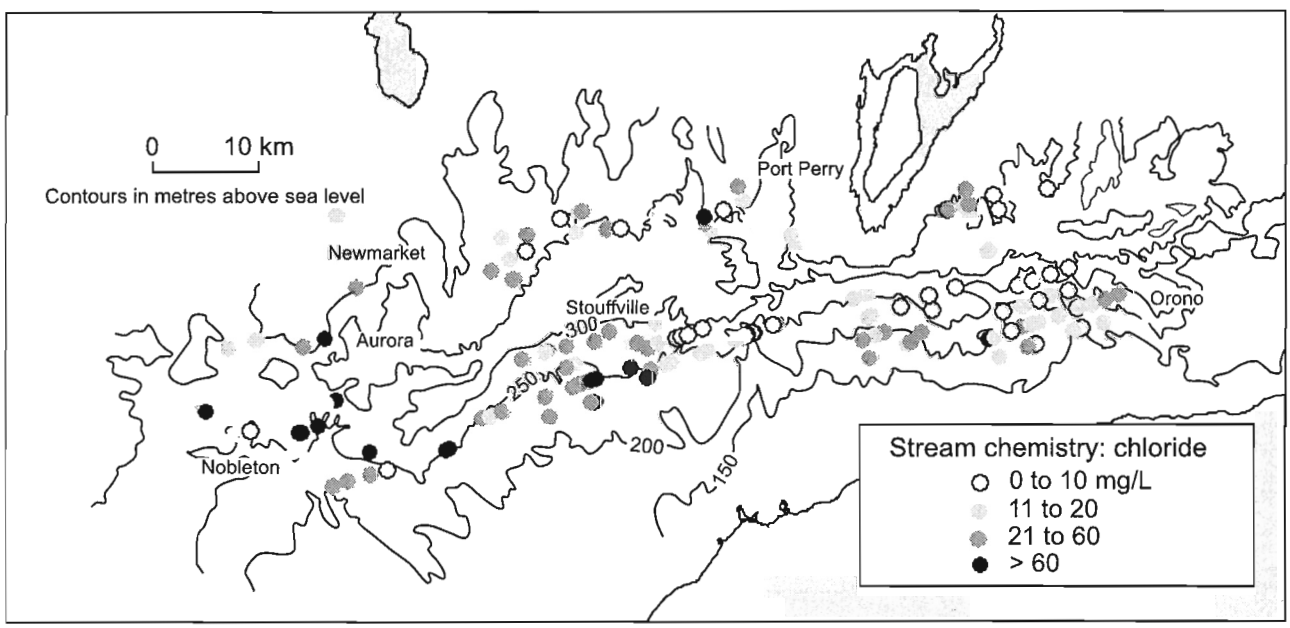


***Figure 5.*** *Locations of stream samples. Shading indicates range of chloride concentration in which each sample falls for chloride.*

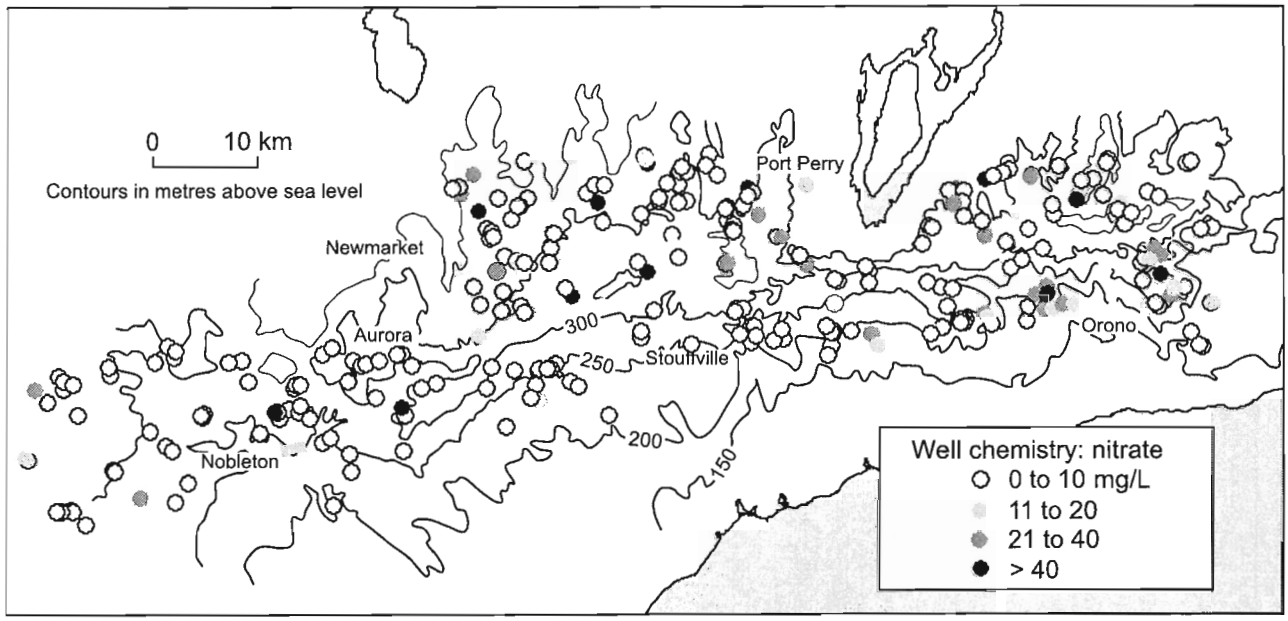


***Figure 6.*** *Well-water analysis for nitrate. Shading indicates range of nitrate concentrations into which each sample falls.*

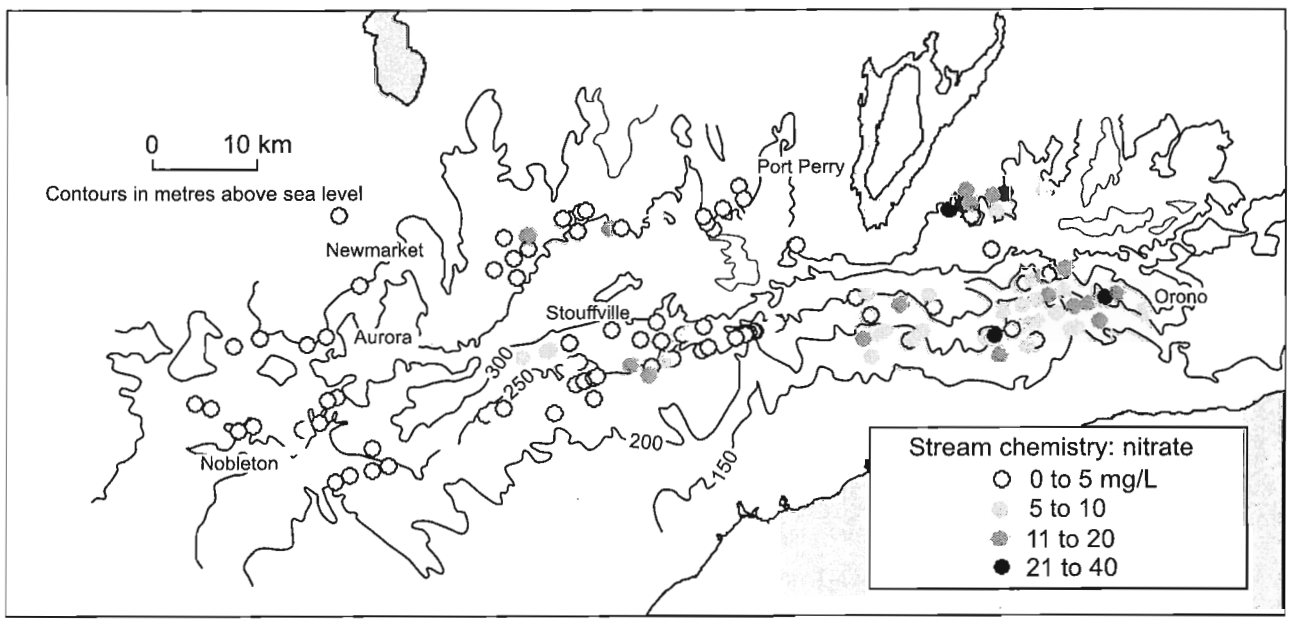


***Figure 7.*** *Stream-water analysis for nitrate. Shading indicates range of nitrate concentrations into which each sample falls.*

reduced along the moraine crest at shallow to intermediate depths but becomes reduced along longer flowpaths on the order of 5–10 km. Therefore, low groundwater sulphate in the Oak Ridges Moraine area may indicate waters flowing along intermediate to regional groundwater pathways. Also chloride concentrations associated with the low sulphate wells are low, averaging about 11 mg/L, further suggesting that longer flowpaths and slower velocities have prevented the arrival of chloride in concentrations more typical of shallow aquifers.

## HARDNESS AND ALKALINITY

Moderately hard water is present in most of the wells sampled. Hardness generally ranges between 100 and 300 mg/L as $CaCO_3$, with about 4% of the well samples below 50 mg/L. Hardness affects the aesthetic appeal of water, restricting its ability to produce soap lather and causing calcareous precipitates on kettles and water fixtures. Hardness is most likely contributed by the dissolution of the carbonate fraction of the glacial sediments. Dissolution probably occurs rapidly on initial infiltration because soil-generated $CO_2$, which

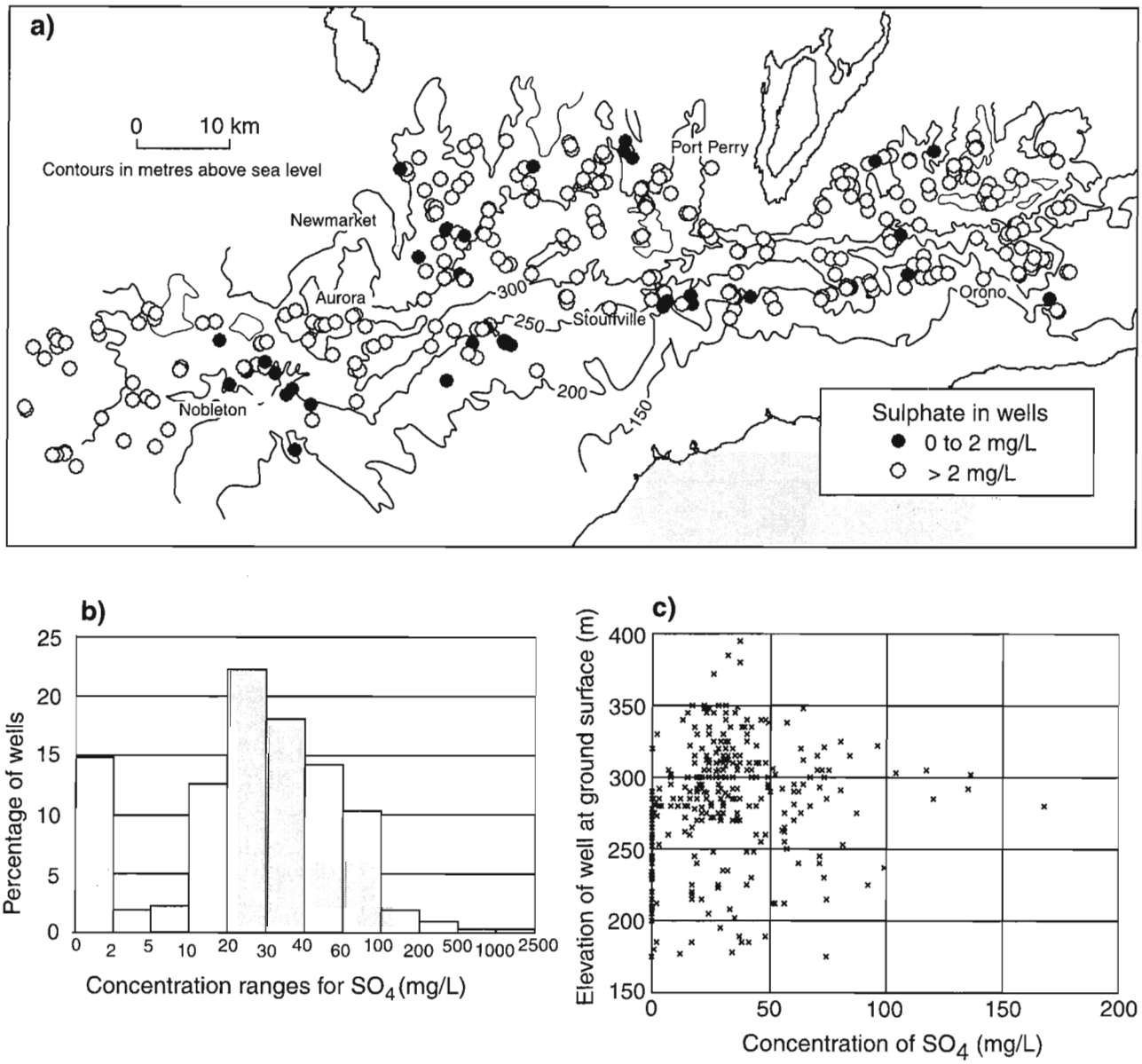


***Figure 8. a)*** *Well-water analysis for sulphate showing samples with very low sulphate concentrations. Note that most well locations with very low sulphate fall below 300 m elevation.* ***b)*** *Histogram showing bimodal distribution of sulphate concentrations. Note the expanded concentration scale below 10 mg/L and that the range 0 to 2 mg/L $SO_4$ comprises about 15% of the wells. These samples come from wells with collar elevations of less than 300 m, as shown in* ***c)****.*

dissociates to carbonic acid, influences the ability of infiltrating groundwater to dissolve calcium carbonate. Sandy sediments with little or no organic soil cover are present along parts of the Oak Ridges Moraine crest, hence little or no elevation of $CO_2$ partial pressure will exist within the soil in these areas. Where soils are well developed, $CO_2$ partial pressures will be higher, favouring dissolution of calcium carbonate. Thus variations in the organic component of soils may account for some of the variation in hardness in well-water samples.

Attempting to reconcile hardness variations with soil properties is unlikely to yield a correlation at the scale of this survey. Groundwater sampled in wells has probably moved primarily laterally from its infiltration point and precipitation of calcium carbonate or mixing may have occurred. Removal of hardness cations, primarily $Ca^{2+}$ and $Mg^{2+}$, by cation exchange may be a process operating on a more regional scale and has been related to groundwater flow on a watershed scale in the Oak Ridges Moraine area (Howard and Beck, 1986). Alkalinity of well waters, also in terms of $CaCO_3$, was measured and can be related to hardness as a means of detecting possible depletion or enrichment in hardness cations. Ideally, hardness and alkalinity, both attributed only to the dissolution of $CaCO_3$, should be equal if $CaCO_3$ is the only source. This hypothesis is tested by plotting hardness against alkalinity in Figure 9. Although there is a general tendency for the two to be linearly related, major departures from equivalence are present.

In Figure 9, well samples with very low sulphate values have been distinguished as black squares. This subsample falls in the zone of the graph where the ratio of hardness to alkalinity is below 1. Ratios below 1 can be interpreted as a depletion in divalent cations or as an enrichment in $HCO_3^-$,

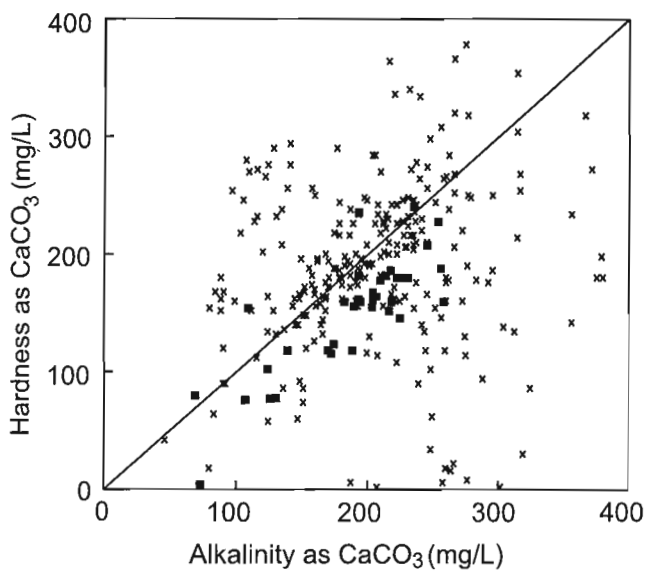


***Figure 9.*** *Hardness plotted against alkalinity for all well water samples (xs). The diagonal line shows the locations of equal concentration. The black squares represent the analyses for all wells with very low sulphate concentrations (0 to 2 mg/L $SO_4$).*

the ion responsible for most of the alkalinity. This result could be produced either by oxidation of organic matter by the reduction of sulphate, i.e.

$$2CH_2O + SO_4^{2-} \text{ —> } HCO_3^- + HS^- + CO_2 + H_2O$$

or by cation exchange. Examination of Figure 9 indicates that the low sulphate samples have lower than average hardness (145 versus 200 mg/L for the rest of the samples) and lower than average alkalinity (181 versus 213 mg/L for the rest of the samples). Acid produced by pyrite weathering may be reducing the alkalinity but cation exchange is also suggested by the lower hardness values associated with the low sulphate samples.

## COMPARISON WITH OLDER REGIONAL WATER CHEMISTRY SURVEYS

Studies under the Water Supply Paper series of GSC were carried out in the late 1940s (Caley et al., 1947; Hainstock et al., 1948a, b, 1952) in the Toronto area and provide chemical analyses of well waters for several townships. For the purpose of comparison with the 1994 survey, early surveys that coincide with the 1994 area of coverage (King and Whitchurch townships) and surveys immediately south, in townships that are presently less dependent on groundwater (Vaughan and Markham townships), were analyzed (Fig. 10). Contaminants associated with urbanization are most likely to show changes between the two surveys. Of those included in the 1994 survey, only chloride is available from the Water Supply Paper surveys and is compared with the 1994 survey in Figure 11. For the area where the two surveys overlap, the histogram of chloride concentration groupings (Fig. 11a) shows significant differences between them. At concentrations below 10 mg/L, the 1994 survey shows a marked number of analyses at the very lowest chloride values (0–2 mg/L) whereas the 1940s survey has almost no values in this range. This result is also apparent in the Vaughan and Markham township survey (Fig. 11b). The very few values at what might be considered a background level for the 1940s survey is counter-intuitive. Because no estimate of chloride detection limit is available for these earlier surveys, interpretation of this difference is problematic.

There is also a difference at higher concentrations, with less than 2% of the wells from the 1940s having more than 100 mg/L but about 10% of the 1994 surveyed wells having chloride values above this level. Although the percentage of wells with the higher values in the 1994 survey may appear small, the maximum value in 1994 is about 10 times greater than the maximum from the 1940s survey. Records of stream-water chloride content reported by Hunter and Associates and Raven/Beck (unpub. report, 1996) and Bowen and Hinton (1998) supply independent evidence that chloride availability has increased markedly since these records were begun in the mid-1960s. The groundwater response may be subdued partly because chloride plumes may not have reached more wells. There is no modern comparison with the Vaughan and Markham township survey but close to 10% of the sampled wells contain chloride above 100 mg/L and concentrations are generally higher than in the King and

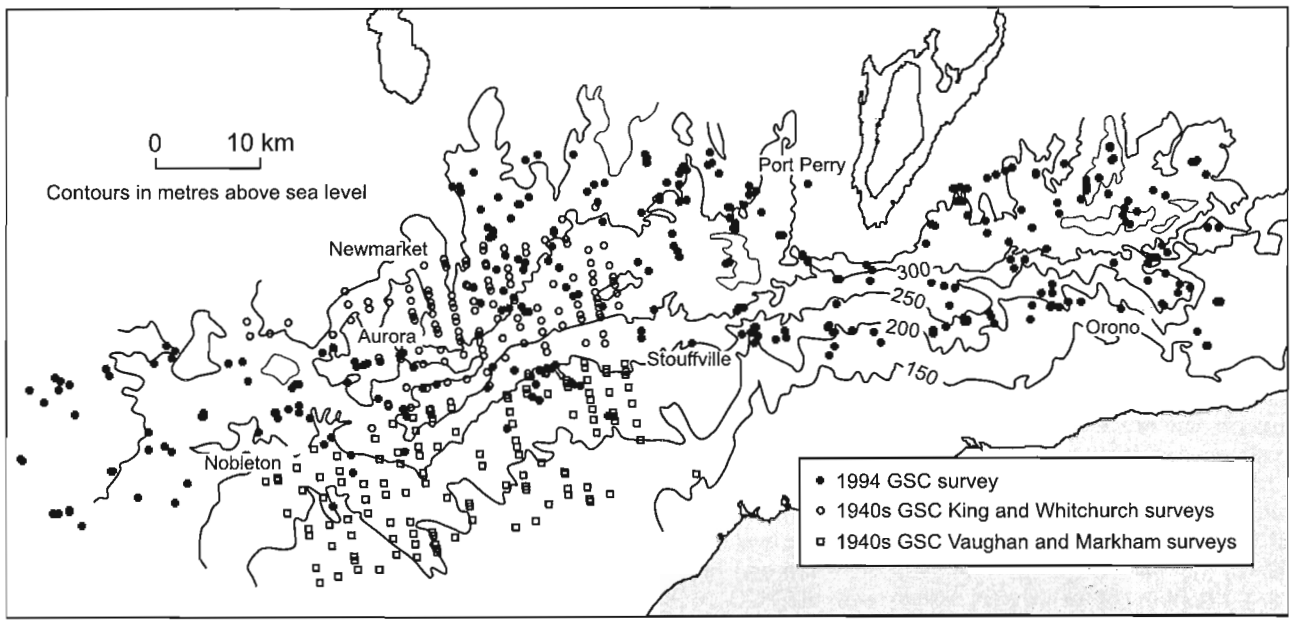


***Figure 10.*** *Locations of wells sampled in 1940s and 1994 Geological Survey of Canada wellwater chemistry surveys.*

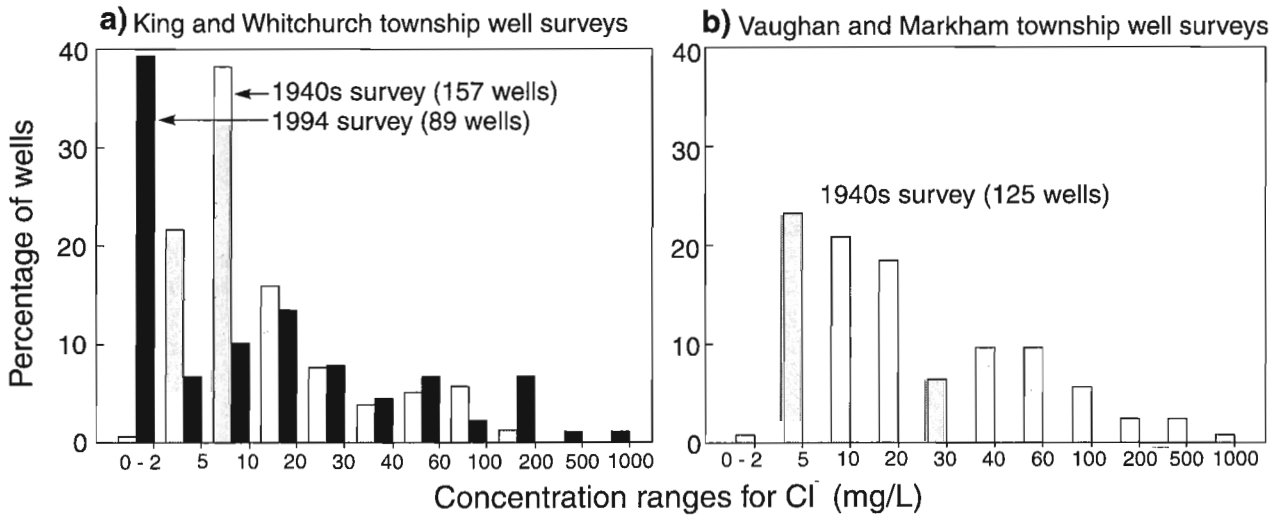


***Figure 11.*** *Histograms a) comparing all the 1940s results for chloride with the corresponding area of the 1994 survey and b) showing chloride results for the 1940s Vaughan and Markham township surveys.*

Whitchurch township area. These characteristics may be explained by 1) longer and denser urbanization in the Vaughan and Markham township area or 2) because of decreased glacial sediment thicknesses in this area, the possible encounter of saline groundwater by wells drawing water from bedrock.

## CONCLUSIONS

In this ground and surface water chemistry survey, only stream waters show a broad spatial pattern of higher concentrations of substances (chloride and nitrate) associated with land use practices. Well waters show no similar grouping on a regional scale. This result, along with the occurrence of the highest chloride concentrations in shallow wells, suggests that stream baseflow is supplied in part by local, shallow

groundwater flow. The distribution of wells with very low sulphate values on the flanks of the Oak Ridges Moraine suggests that chemical reduction of sulphate is occurring somewhere along a flowpath between the moraine crest and the location of these wells. The lack of low sulphate values on the moraine, the low elevation of well intakes showing very low sulphate, the association of generally low chloride concentrations with low sulphate concentrations, and the limitation of stream sampling sites with very low sulphates to catchments off the moraine all suggest that groundwater with these very low values is part of a more extensive flow regime that is passing through the Newmarket Till underlying the Oak Ridges Moraine. Shallow aquifers within the Oak Ridges Moraine would appear to be most vulnerable to contamination from substances introduced at the ground surface. Deeper aquifers, i.e. below the Newmarket Till, appear to be much less susceptible to surface contamination, probably because of the longer flowpaths and slower flow rates for groundwater reaching these levels.

## ACKNOWLEDGMENTS

Paul Chin, Hany Hassan, and Michele Wright are thanked for their capable assistance with sample collection and chemical analysis. Reviews of the manuscript by Marc Hinton and David Sharpe resulted in significant improvements.

## REFERENCES

**Bowen, G.S. and Hinton, M.J.**
1998: The temporal and spatial impacts of road salt on streams draining the Greater Toronto Area; Proceeding of the Groundwater in a Watershed Context Symposium, Canadian Water Resources Association, Cambridge, Ontario, p. 303–309.

**Caley, J.F., Clark, T.H., and Owen, E.B.**
1947: Ground-water resources of Markham Township, York County, Ontario; Geological Survey of Canada, Water Supply Paper No. 284, 19 p.

**Funk, G.F.**
1977: Geology and water resources of the Bowmanville, Soper and Wilmot Creek IHD representative drainage basin; Ontario Ministry of Environment, Water Resources Branch, Water Resources report 9a, 96 p.

**Hainstock, H.N., Owen, E.B., and Caley, J.F.**
1948a: Ground-water resources of Vaughan Township, York County, Ontario; Geological Survey of Canada, Water Supply Paper No. 287, 18 p.
1948b: Ground-water resources of King Township, York County, Ontario; Geological Survey of Canada, Water Supply Paper No. 293, 20 p.
1952: Ground-water resources of Whitchurch Township, York County, Ontario; Geological Survey of Canada, Water Supply Paper No. 320, 20 p.

**Health Canada**
1996: Guidelines for Canadian Drinking Water Quality; Canada Communications Group - Publishing, Ottawa, Ontario, (6th edition), 90 p.

**Hickinbotham, A.**
1979: Ground Water Probability, Regional of Peel; Ontario Ministry of Environment, Water Resources Map 3128, scale 1:100 000.

**Howard, K.W.F. and Beck, P.**
1986: Hydrochemical interpretation of groundwater flow systems in Quaternary sediments in southern Ontario; Canadian Journal of Earth Sciences, v. 23, p. 938–947.

**Howard, K.W.F., Boyce, J.I., Livingstone, S.J., and Salvatori, S.L.**
1993: Road salt impacts on groundwater quality - the worst is still to come; Geological Society of America, GSA Today, v. 3, p. 1.

**Karrow, P.F.**
1967: Pleistocene geology of the Scarborough area; Ontario Department of Mines, Geological Report 46, 104 p.

**Sharpe, D.R., Dyke, L.D., Hinton, M.J., Pullan, S.E., Russell, H.A.J., Brennand, T.A., Barnett, P.J., and Pugin, A.**
1996: Groundwater prospects in the Oak Ridges Moraine area, southern Ontario: application of regional geological models; *in* Current Research 1996-E, Geological Survey of Canada, p. 181–190.

**Sibul, U., Wang, K.T., and Vallery, D.**
1977: Groundwater resources of the Duffins Creek - Rouge River drainage basins; Ontario Ministry of Environment, Water Resources Branch, Water resources Report 8, 109 p.

Geological Survey of Canada Project 920046

# Regional geological mapping of the Oak Ridges Moraine, Greater Toronto Area, southern Ontario[1]

D.R. Sharpe, P.J. Barnett[2], H.A.J. Russell, T.A. Brennand[3], and G. Gorrell[4]

Terrain Sciences Division, Ottawa

*Sharpe, D.R., Barnett, P.J., Russell, H.A.J., Brennand, T.A., and Gorrell, G., 1999: Regional geological mapping of the Oak Ridges Moraine, Greater Toronto Area, southern Ontario;* in *Current Research 1999-E; Geological Survey of Canada, p. 123–136.*

**Abstract:** Geological maps are keys to communicating earth science information and their use is fundamental to land-use planning. A new 1:200 000 scale surficial geology map synthesizes recent 1:50 000 and 1:20 000 mapping in the Oak Ridges Moraine–Greater Toronto Area. These regional geological data provide consistent mapping across the area in aid of terrain analysis, resource evaluation, and environmental assessment. The mapping provides, for the first time, the basis for developing regional geological models within the area.

The geological mapping synthesizes approximately 20 000 new and archival ground observations that are grouped into 11 deposits or map units. Map units have been organized into major sediment packages depicted in a three-dimensional regional geological model that highlights six principal stratigraphic elements. These regional strata, from oldest to youngest, are: 1) bedrock, 2) lower deposits, 3) Newmarket Till, 4) Channel fill, 5) Oak Ridges Moraine, and 6) Halton Till.

**Résumé :** Les cartes géologiques constituent un moyen efficace de communiquer l'information géoscientifique et leur emploi est essentiel à la planification et à l'utilisation des terres. Une nouvelle carte de la géologie de surface de la région de la Moraine d'Oak Ridges et du grand Toronto à l'échelle de 1/200 000 fait la synthèse de récents travaux de cartographie dont les résultats ont été publiés aux échelles de 1/50 000 et de 1/20 000. Ces données géologiques à l'échelle régionale permettent de dégager une image cartographique uniforme du territoire, ce qui s'avère utile aux fins d'analyse de terrain, d'évaluation des ressources et d'évaluation environnementale. La cartographie fournit, pour la première fois, une base solide permettant d'élaborer des modèles géologiques à l'échelle régionale.

La carte géologique fait la synthèse d'environ 20 000 observations de terrain, nouvelles ou déjà disponibles, que l'on a attribuées à 11 unités sédimentaires ou cartographiques. Ces unités ont été regroupées en grands assemblages sédimentaires qui sont illustrés dans un modèle géologique tri-dimensionnel de la région mettant en évidence 6 entités stratigraphiques principales. De la plus ancienne à la plus récente, ces entités sont les suivantes : 1) substratum rocheux; 2) dépôts inférieurs; 3) Till de Newmarket; 4) matériaux de remplissage de chenal; 5) Moraine d'Oak Ridges; et 6) Till de Halton.

[1] Contribution to the Oak Ridges Moraine NATMAP project
[2] Ontario Geological Survey, 933 Ramsey Lake Road, Sudbury, Ontario P3E 6B5
[3] Department of Geography, Simon Fraser University, Burnaby, British Columbia V5A 1S6
[4] Gorrell Resource Investigations, RR # 1, Oxford Mills, Ontario K0G 1S0

## INTRODUCTION

Awareness of earth science is fundamental to rational land-use planning and is a prerequisite for informed debate on resource management, environmental health, and public safety (e.g. Clague et al., 1997). Geological maps are a key means of communicating earth-science information and are important tools for organizing, summarizing, and analyzing data about the spatial pattern of the Earth's landscape and sediments.

A regional, 1:200 000 scale, surficial geology map of the Oak Ridges Moraine (ORM) and Greater Toronto Area (GTA; Sharpe et al., 1997a) summarizes a recent series of twelve 1:50 000 maps for the area (Fig. 1). The regional map also incorporates data from a series of 9 recent 1:20 000 geology maps published by the Ontario Geological Survey (OGS), covering the central area of the ORM (e.g. Barnett, 1996a). Mapping was initiated in response to a number of earth- and water-resource planning and management issues identified by the Ontario Ministry of Natural Resources, ORM Technical Working Committee (1994). Regional mapping was sponsored by the National Geoscience Mapping Program (NATMAP) of the Geological Survey of Canada in collaboration with the OGS and a number of other provincial and municipal agencies and local groups.

### *Objectives and scope of the report*

The objective of the regional map, and of this paper, is to present the geology of the ORM-GTA area as baseline data for terrain evaluation, regional planning, resource management, and environmental analysis. This paper is aimed at informed

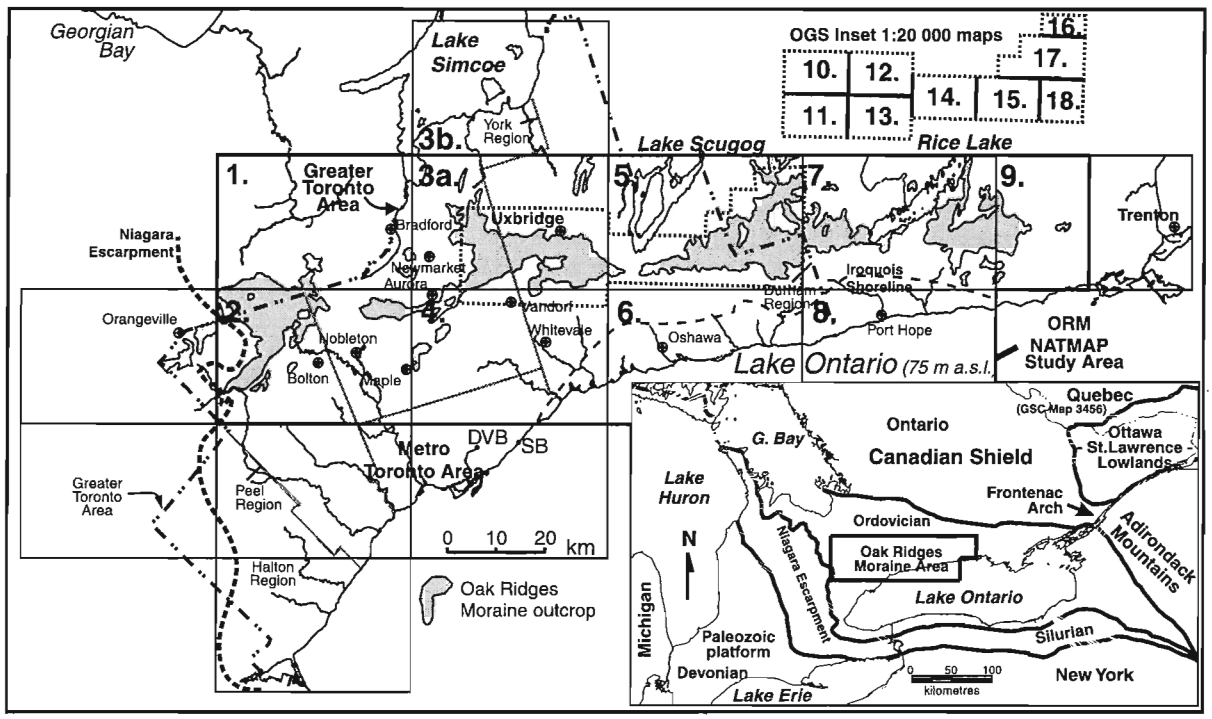


***Figure 1.*** *Location of GTA map area (GSC Open File 3062; Sharpe et al., 1997a) with regional geology inset. The NATMAP study area is covered by GSC Open File 3456 (Sharpe et al., 1997b). Map names and publication numbers for Geological Survey of Canada (GSC) and Ontario Geological Survey (OGS) maps are listed and linked to the index map with numbers:*

***1:50 000 scale maps:*** *1. Alliston: GSC, Open File 3334 (Russell and Dumas, 1997). 2. Bolton: GSC, Open File 3299 (Russell and White, 1997). 3a. Newmarket: GSC, Open File 3329 (Barnett and Gwyn, 1977); 3b. Beaverton: OGS Map 2560 (Barnett and Mate, 1998). 4. Markham: GSC, Open File 3300 (Sharpe and Barnett, 1997). 5. Scugog: GSC, Open File 3330 (Barnett, 1997b); OGS, Map 2644 (Barnett et al., 1996). 6. Oshawa: GSC, Open File 3331(Brennand, 1997a). 7. Rice Lake: GSC, Open File 3332 (Gorrell and Brennand, 1997). 8. Port Hope: GSC, Open File 3298 (Brennand, 1997b). 9. Trenton: GSC, Open File 3333 (Gorrell, 1997).*

***1:20 000 scale maps:*** *10. Mt. Albert: OGS, Map 2631 (Barnett and McCrae, 1996a). 11. Stouffville: OGS, Map 2632 (Barnett and McCrae, 1996b). 12. Uxbridge: OGS, Map 2633 (Barnett and Dodge, 1996). 13. Claremont: OGS, Map 2634 (Barnett, 1996a). 14. Port Perry: OGS, Map 2635 (Barnett and Henderson, 1996). 15. Enniskillen: OGS, Map 2636 (Barnett, 1996b). 16. Kendal area: OGS, Map 2637 (Barnett, 1996c). 17. Bethany: OGS, Map 2638 (Barnett, 1996d). 18. Brunswick: OGS, Map 2639 (Barnett, 1996e).*

users (e.g. terrain consultants) who can help communicate this geological knowledge to a wider group of users. The report describes 11 map units discussed within the framework of a regional geological model. The mapping provides a consistent geological synthesis across the region as required for standardized land-use and resource evaluation. The map also provides a basis for understanding the surficial geology of the area in three dimensions when used with the geological model (Sharpe et al., 1996). This report describes the geological context for the sedimentary units and their distribution. It also provides a regional geological synthesis for the origin and depositional setting of strata in the ORM-GTA. More detailed accounts of the geology of the ORM area are being published separately (e.g. Barnett et al., 1998; Pugin et al., in press).

### *Previous and present geological mapping*

Sediment mapping in the ORM-GTA has been ongoing throughout the twentieth century. Taylor (1913) identified the moraines in the GTA while Coleman (1913, 1932) added three-dimensional geological perspective by examining the lake bluffs along Lake Ontario. Chapman and Putnam (1984) defined the physiography of the ORM/GTA.

Gadd (1950), Watt (1957, 1968) and other GSC workers introduced the early work on geological mapping related to water resources. Singer (1974), Funk (1979), Sibul et al. (1977), and Ostry (1979) provided modern hydrogeological mapping to the GTA. This included the introduction of three-dimensional methods such as drilling and borehole geophysics (Sibul et al., 1977; Fligg and Rodrigues, 1983; Eyles et al., 1985). Recent geological mapping has been summarized by Karrow (1967), Sharpe (1980), Barnett et al. (1991), and Sharpe et al. (1997a).

The nine maps within the NATMAP area (Fig. 1) are based on new fieldwork and conceptual understanding, complemented by archival field data; most maps have approximately 1000 field sites. Maps outside the NATMAP area (Fig. 1) have been remapped with a minimum of new fieldwork, but include reassessed archival data and a standardized legend. All new maps are structured in a Geographic Information System (GIS) with supporting data in a relational database (e.g. Russell et al., 1996). GSC Open File 3062 (Sharpe et al., 1997a) is available digitally, along with related 1:200 000 scale map products (Russell et al., in press).

## SURFICIAL GEOLOGICAL MAP

Geological maps generalize earth-science information, but they are technical documents that portray complex three-dimensional earth relationships in plan view. Hence, there is a need to simplify and explain map content so that it is more accessible to a range of users (e.g. Clague et al., 1997). Geological Survey of Canada Open File 3062 (Sharpe et al., 1997a) presents a 1:200 000 scale map, a simple legend, and side-bar figures showing the regional location, terrain, and geological context of the area. The legend uses 11 classes of sediment and rock to describe the geological landscape in the ORM-GTA (Table 1). Sediments are grouped under terms

**Table 1.** Glacial and Recent sediments shown on GSC Open File 3062.

| Map unit | Name (origin) | Sediment | Thickness | Landform type |
|---|---|---|---|---|
| 11 | Recent deposits | sand, gravel and diamicton | 1–3 m | dunes, lakeshores, slopes |
| 10 | River deposits | **a.** gravel, sand, silt, clay, muck<br>**b.** gravel, sand, silt, clay | 1–2 m<br>1–8 m | modern floodplains<br>river and delta terraces |
| 9 | Organic deposits | peat, muck and marl | 1–7 m | wetlands |
| 8 | Glacial lake deposits | **a.** sand and silty sand<br>**b.** gravely sand | 1–50 m<br>1–5 m | basins and nearshore flats<br>raised shorelines |
| 7 | Glacial lake deposits | **a.** silt, clay, diamicton<br>**b.** silt and clay | 1–10 m<br>1–5 m | basins<br>basins |
| 6 | Glacial river deposits | **a.** sand<br>b. gravel | 1–15 m<br>1–15 m | eskers, fills and terraces<br>eskers, fills and terraces |
| 5 | Morainal deposits | **a.** sand, silt, gravel, diamicton,<br>**b.** sand and gravel | 1–100 m<br>1–20 m | broad moraines<br>channels, hills, depressions |
| 4 | Glacial deposits (till) | clayey silt to silt, 1–2% stones (e.g. Halton and Kettleby Tills) | 1–15 m | plains |
| ---------- erosional unconformity | | | | |
| 3 | Glacial deposits (till) | sandy silt, sand, 3–10% stones (e.g. Newmarket Till) | 1–50 m | plains and uplands |
| 2 | Lower sediments | sand, silt, clay and till | 1–100 m | bluffs, buried plains |
| | **g.** Upper Thorncliffe Formation/Clarke beds; **h.** Seminary/Meadowcliffe/ Bondhead tills | | | |
| | **i.** Lower Thorncliffe Formation/Clarke beds; **j.** Sunnybrook Till; **k.** Scarborough Formation | | | |
| | **l.** Don Formation; **m.** York Till; **n.** Stratified sediment, sand **o.** Stratified sediment, silt and clay | | | |
| **Unconformity** (long interval with no deposits and/or major erosion) | | | | |
| **Paleozoic** | | | | |
| 1 | Bedrock | limestone, sandstone, or shale | ~50–500 m | Niagara Escarpment; buried valleys |
| Note: Glacial deposits (till) are grouped as coarse and fine textured. | | | | |

such as glacial-lake or glacial-river deposits. Unit descriptions and colours on the map emphasize primary sediment textures (e.g. sand, silt, clay, gravel, and diamicton), followed by the thickness, landform type, and origin of material. A digital elevation model of the area allows the land contours and terrain to be more easily recognized (Fig. 2; Kenney et al., 1999). A three-dimensional block model portrays the regional geology in a manner that allows the structural and functional link between map elements and map units to be clarified (Fig. 3, 4).

## GEOLOGICAL SETTING

Regional terrain elements include the Precambrian Shield to the north, and underlying flat-lying Paleozoic rocks of the St. Lawrence Lowlands and Great Lakes (Fig. 1). Limestones, shales, and sandstones (Table 1, unit 1) of Ordovician age (Sanford and Baer, 1981), mainly outcrop along the Niagara Escarpment, Lake Simcoe, and in streams close to Lake Ontario (Fig. 5h).

A major regional unconformity separates the Paleozoic bedrock and overlying sediments. A new map of this surface (Brennand et al., 1997) shows major valleys trending southeasterly across the area, including the ancient Laurentian Valley (Spencer, 1881), but no bedrock ridge beneath the ORM (Eyles et al., 1993). Sediment thickness is highly variable (0–200 m; Russell et al., 1998a), being influenced by bedrock topography and ice-controlled sedimentation. It is thinnest atop the Niagara Escarpment and thickest along Laurentian Valley.

From analysis of surface texture and digital elevation data (Skinner and Moore, 1997; Kenny, 1997), the region can be divided into seven physiographic areas that are significant to

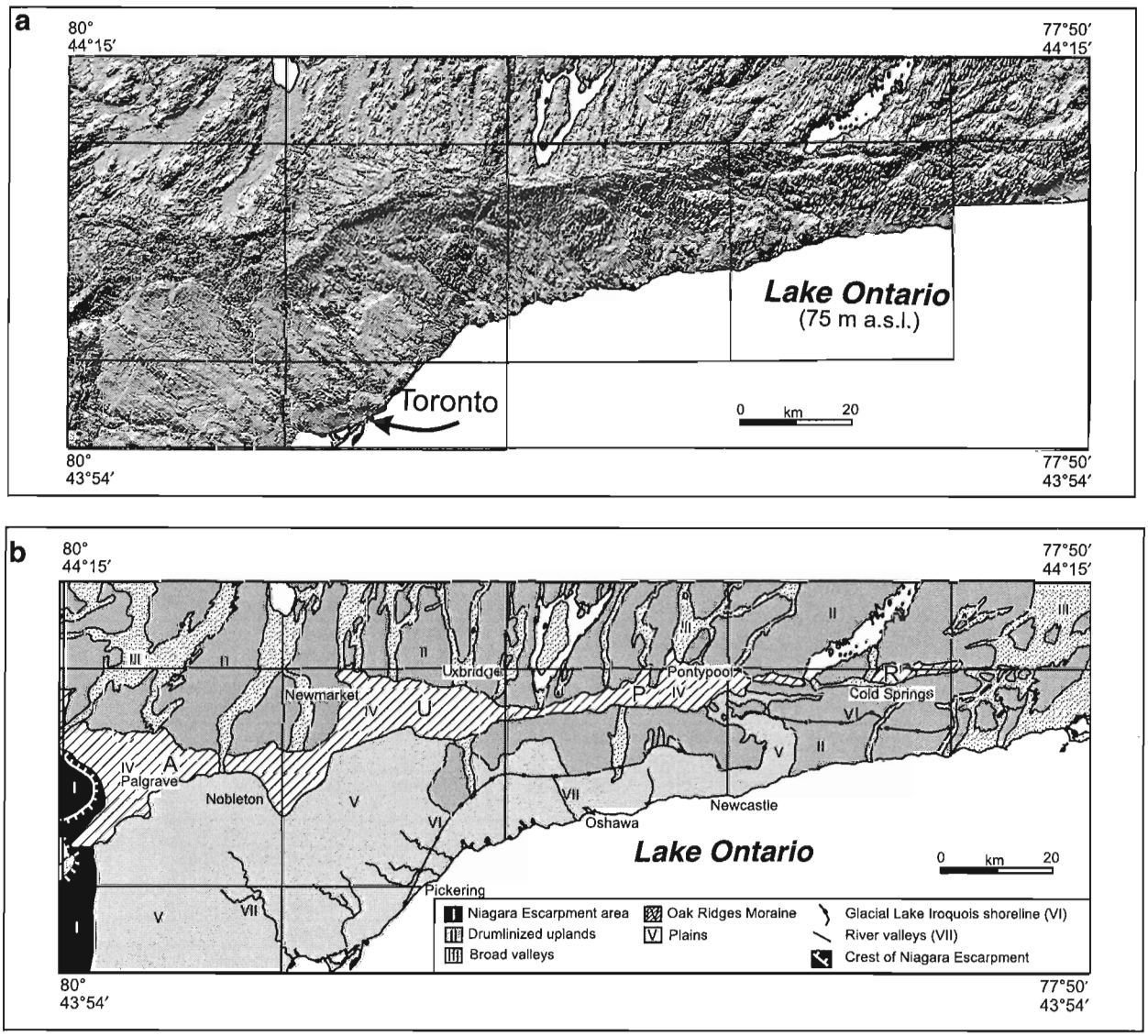


***Figure 2. a)*** *Relief of the central ORM area (Skinner and Moore, 1997).* ***b)*** *Physiographic units of the GTA/ORM area based on the digital elevation model (DEM) (see Barnett et al., 1998 for additional discussion).*

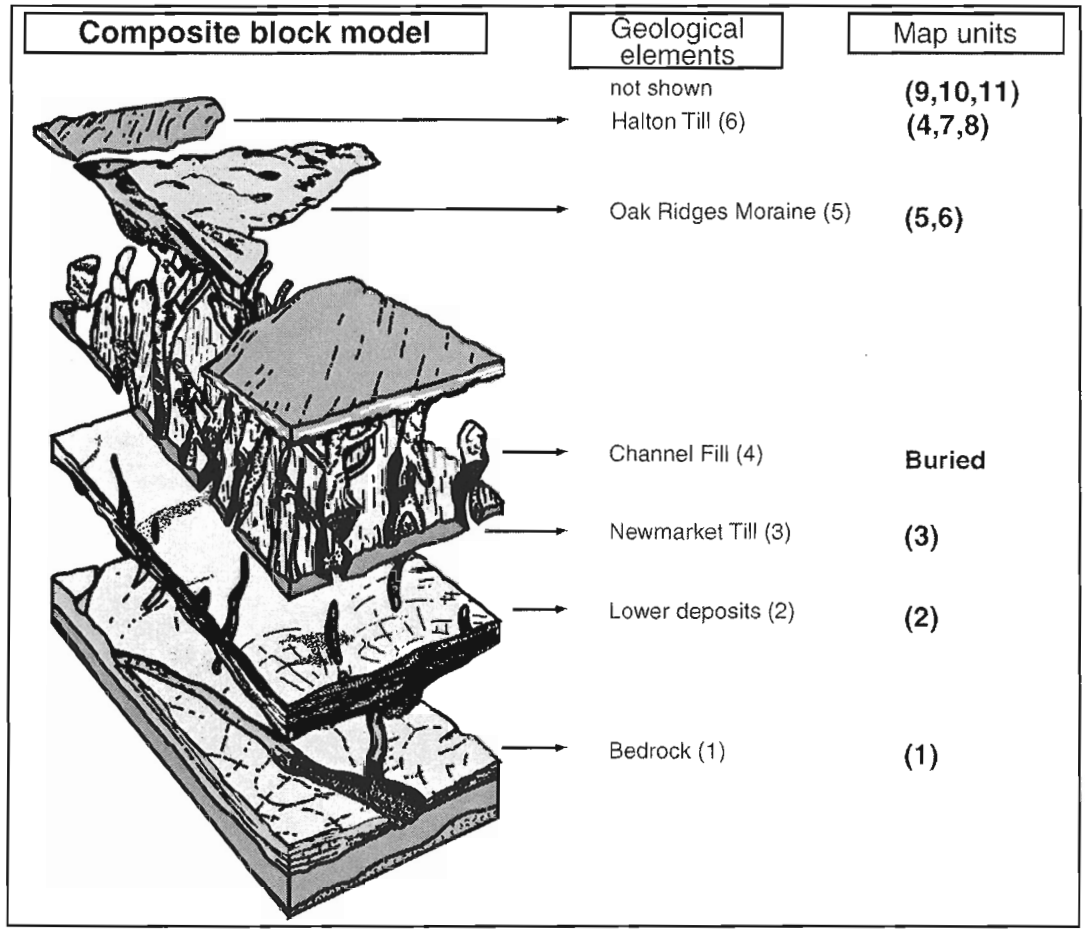


***Figure 3.*** *Geological model of major stratigraphic elements of the GTA, showing relationship of 6 stratigraphic elements to the 11 map units.*

understanding the regional geology (Fig. 2). 1) The Niagara Escarpment is an approximately 100 m topographic rise that affected ice and meltwater flow across the area , particularly during formation of the ORM (Barnett et al., 1998). 2) Drumlinized uplands of the Peterborough drumlin field occur north and south of the ORM (Fig. 2); they also underlie it (Fig. 4a; Barnett et al., 1998). 3) Large flat-floored valleys are eroded into the drumlin upland north of the ORM (Fig. 2); some continue south of the moraine, e.g. Duffins Creek (Sharpe and Barnett, 1997; Kenny, 1997). 4) The Oak Ridges Moraine is an east-west drainage divide extending from the Niagara Escarpment to east of Rice Lake (Fig. 2). 5) Broad, gently sloping plains border the southwestern margin of the ORM (Fig. 2; Barnett et al., 1991). 6) The Lake Iroquois shoreline truncates this plain (Fig. 2b) at elevations ranging from about 110 m a.s.l. near Hamilton (Karrow, 1987) to ~140 m a.s.l. at the eastern margin of the area. And, 7) river valleys dissect the area (Fig. 2b), rising in drumlinized uplands or in the ORM.

## SURFICIAL GEOLOGY AND A THREE-DIMENSIONAL GEOLOGICAL MODEL OF THE ORM-GTA

Sediments in the ORM-GTA are described and subdivided using grain size, thickness, landform type, and sediment origin (Table 1; GSC Open File 3062; Sharpe et al., 1997a). More detailed sediment descriptions, which can improve understanding of the processes of formation and their environments of deposition, are published separately (e.g. Russell et al., 1998a). The major sediment packages of the area are displayed as a regional geological model (Fig. 3; Sharpe et al., 1996). Six principal stratigraphic elements are discussed below in chronological order to place the surface map units (Sharpe et al., 1997a) in their appropriate geological and stratigraphic context (Fig. 3).

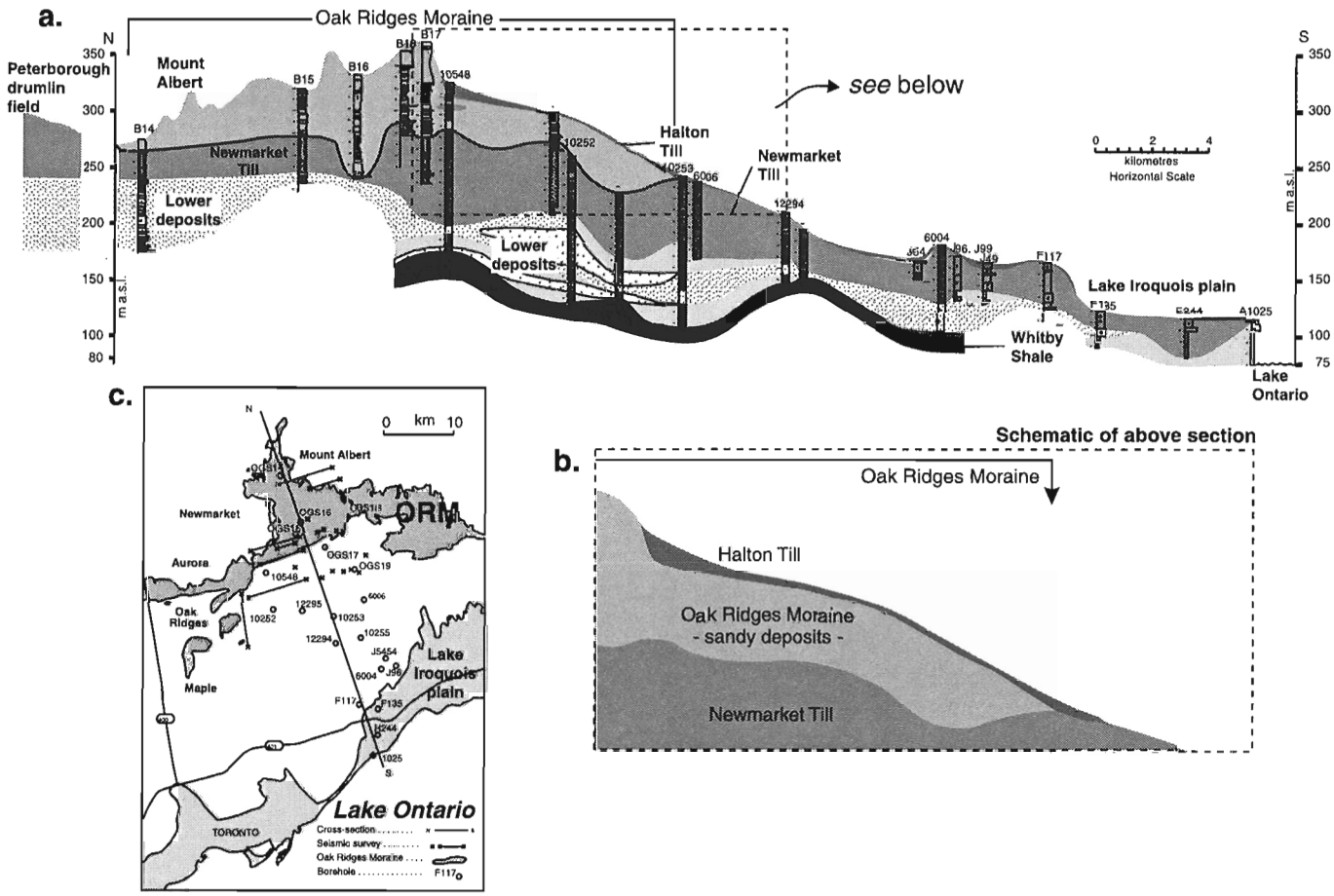


***Figure 4.*** *Cross-section and geological model showing central GTA stratigraphic elements.* ***a)*** *N-S section from Scarborough Bluffs to Mount Albert;* ***b)*** *inset cross-section of Newmarket, Halton and ORM showing the thin and restricted distribution of Halton strata.* ***c)*** *map of borehole control. The regional extent of the Newmarket Till and the broad expanse of ORM sediments below a very thin Halton sediment package (inset) are easily seen in cross-section (from Sharpe et al., 1994).*

### *Lower deposits*

Lower deposits comprise thick, complex, sediment packages that rest on bedrock and that occur below the Newmarket Till (Fig. 3, 4). These deposits are poorly exposed at surface and individual sediment sequences can only be mapped at scattered locations. The oldest exposed sediments (unit 2, Table 1) are found along the Lake Ontario bluffs and river valleys (Fig. 5f, g; e.g. Karrow, 1967), in sequences up to 100 m thick. Some units may extend as far north as Lake Simcoe as defined by borehole geophysics (e.g. Fligg, 1983; Eyles et al., 1985) and reflection seismic profiling (Pugin et al., in press). These sediments are mainly sand, silt, and clay, but they also include older tills, and distinctive fossil-bearing beds that form important markers in regional investigations and correlations (Karrow, 1990). Recent mapping has revealed sandy beds near Lake Scugog (unit 2n and 2o; Barnett and Dodge, 1996). Lower sediments were mainly deposited in proglacial lakes. From the base up, the lower sediments include York Till, Don Interglacial beds, Scarborough Formation, Sunnybrook Till, and the Thorncliffe Formation.

The York Till is dense, clay-sand diamicton with 5–10% gravel. It occurs at Don Valley Brickyards (Karrow, 1967), Woodbridge (White, 1975) and in boreholes to the north near Nobleton (Russell and Arnott, 1998). In places (e.g. Etobicoke Creek; Watt, 1968), this till is difficult to distinguish from younger tills (e.g. Newmarket). The Don Formation is found at the Don Valley Brickyards (Fig. 1; Karrow, 1967), near Woodbridge, and in boreholes. It consists of fine sand, silt, and clay with warm-climate fossils interpreted as a fluvial environment (Karrow, 1990). The Scarborough Formation

***Figure 5.*** *Major types of sediment and rock in the ORM/GTA.* ***a)*** *Halton interbedded sediments;* ***b)*** *ORM fine sand and silt;* ***c)*** *ORM gravel;* ***d)*** *channel gravel;* ***e)*** *Newmarket Till;* ***f)*** *lower sediment, Scarborough sand and organics;* ***g)*** *lower sediment, rhythmites;* ***h)*** *Shale-carbonate bedrock (below shovel) overlain by Newmarket and Halton tills, Etobicoke Creek.*

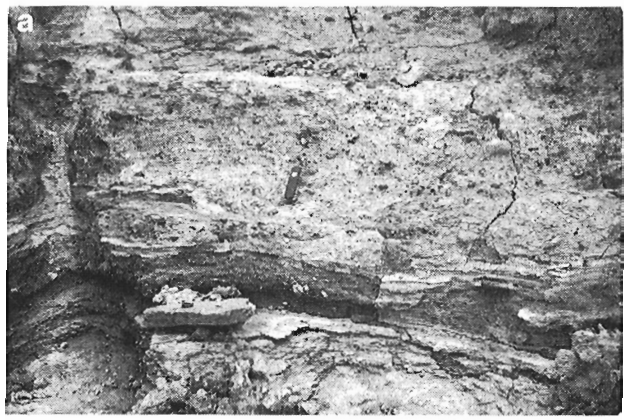
a

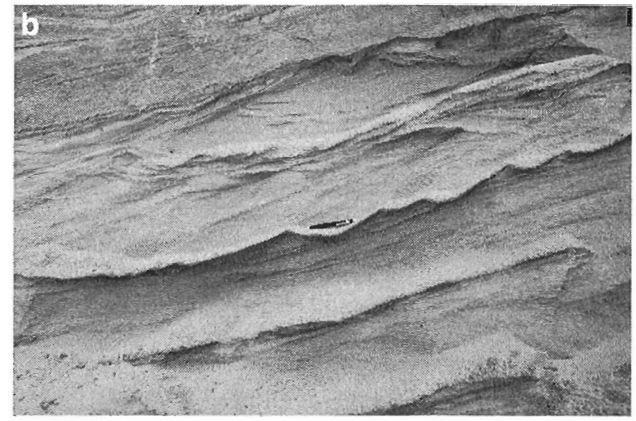
b

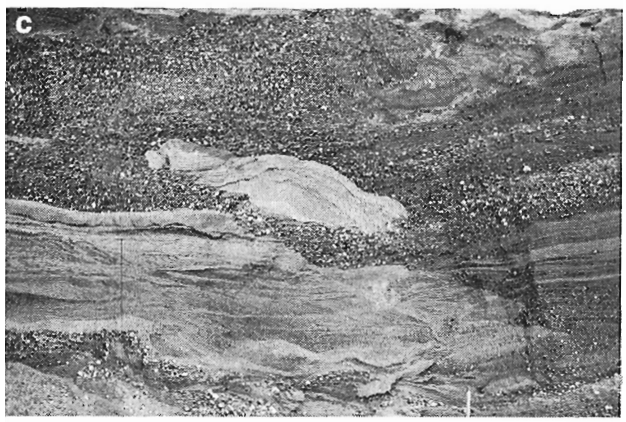
c

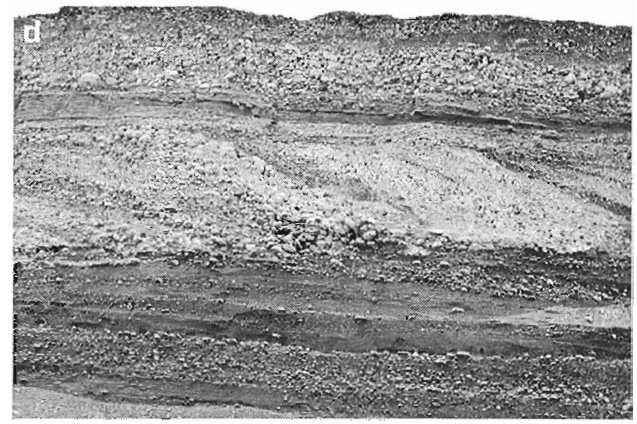
d

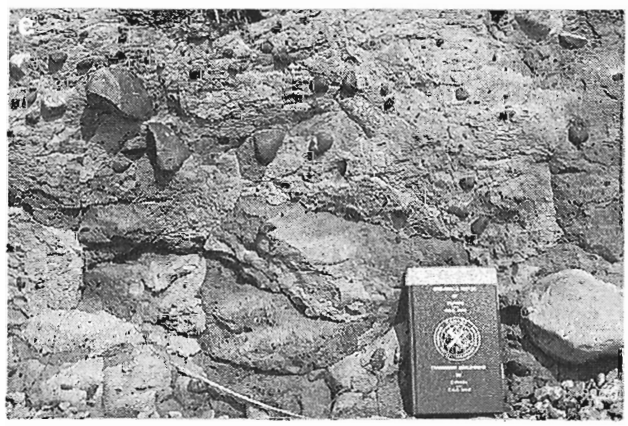
e


f


g

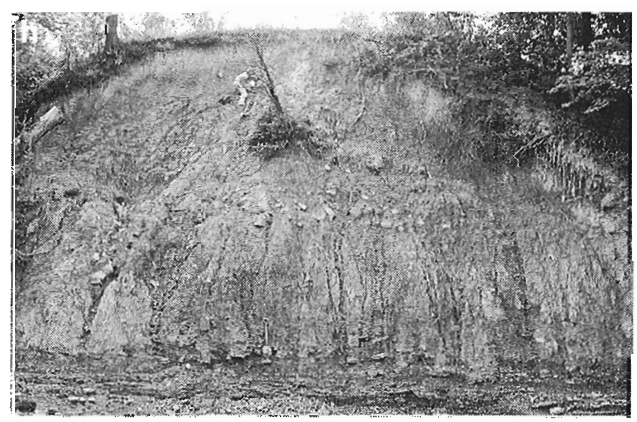
h

forms approximately 50–100 m high bluffs along the Lake Ontario shore and adjacent creeks (Fig. 1). It is recognized in drill core north of Lake Ontario between 120–150 m a.s.l. It consists of a lower 30 m of silt-clay rhythmites and massive silt, overlain by 20 m of sand (Kelly and Martini, 1986). Disseminated organic material and wood fragments are common, making it a subsurface marker bed across the area (Fig. 5f). The Sunnybrook Till , a clayey-silt diamicton with low stone content (~1%), is prominent at Scarborough Bluffs and river valleys south of Woodbridge (Karrow, 1967; White, 1975). It can include rhythmites (Karrow, 1967) and massive clay that indicate glacial-lake affinities (Eyles and Eyles, 1983), but striated stones at its base suggest that it may be a till. The Thorncliffe Formation is also exposed along lake and rivers bluffs and extends in the subsurface well to the north, as recorded by thick sequences interpreted on seismic profiles (Pugin et al., 1996) and in drill core. Thorncliffe beds extend east along the Port Hope lake bluffs (Brookfield et al., 1982). Thorncliffe sediments consist of lower silt-clay rhythmites (Fig. 5g) and crosslaminated and crossbedded sands. The package is up to 50 m thick at Scarborough, thinning to 20 m thick at Duffins Creek (Karrow, 1967). The extent and thickness of this formation makes it a significant aquifer in the area (Sibul et al., 1977; Gerber and Howard, 1996).

### *Newmarket Till*

The Newmarket Till (Table 1, unit 3; Gwyn and DiLabio 1973) can be traced across the GTA as a distinct and consistent lithology (Fig. 5e), making it an excellent regional marker unit (Fig. 3a, 4a). It was mapped as the Leaside till near Toronto (Karrow, 1967) and its correlatives have been identified across the area (Sharpe et al., 1994; Gerber and Howard, 1996; Boyce et al., 1995) after it was recognized to underlie the ORM (Gwyn and Cowan, 1978) and extend into Lake Ontario (Lewis et al., 1998). This widespread till sheet forms the main sediment in the regional (Peterborough) drumlin field (Fig. 4) and is extensive in the Markham area. It is a dense, stony (~5–15% gravel), silty sand to sandy silt diamicton that occurs as beds 3–5 m thick, separated in places by stone lines and sandy interbeds, 1–5 m thick; total thickness is 5–50 m.

The Newmarket Till commonly has a planar lower contact on undisturbed rippled sand (Thorncliffe Formation); in places sand is interbedded. This planar contact is present on seismic profiles (Pullan et al., 1994; Boyce et al., 1995; Pugin et al., in press) at elevations ranging from approximately 210–190 m a.s.l. where it shows as a continuous, high-velocity reflector (2500–3000 m/sec on downhole velocity logs (Hunter et al., 1998)). The advance of the Late Wisconsinan ice sheet from the north and along the Lake Ontario basin lead to initial deposition of Newmarket Till into standing water.

### Regional unconformity

Cutting across the Newmarket Till, and into Lower Deposits in places, is an unconformity (Table 1); a regional erosion surface marked by channels and drumlins (Fig. 3, 4; Barnett et al., 1998). The channels form a south-southwest-oriented network (Fig. 2) cut into Newmarket Till north of the Oak Ridges Moraine (e.g. Barnett 1990; Brennand and Shaw 1994). The link between channels and adjacent drumlin fields on this regional erosion surface is interpreted from landforms (Shaw and Sharpe, 1987) and displayed on reflection seismic profiles (Pugin et al., in press). The unconformity and channel fill sediments are part of a closely-linked event sequence that scoured Newmarket Till and deposited coarse-grained sediment on parts of the erosional surface (Barnett et al., 1998).

### *Channel fill sediments*

The tunnel channels of the regional unconformity form an extensive network with valleys 1–5 km across, tens of kilometres long and 50–100 m deep (Barnett, 1990). They contain thick buried deposits (Fig. 3), several with 10–25 m thick gravel sequences (Fig. 5d; Shaw and Gorrell 1991; Pugin et al., 1996). However, channels fills are mainly 10–75 m thick sandy sediments that fine upwards to silt and clay (Barnett et al., 1998). Surface sediments within the buried channels contain fine sand, silt, and organic material. Both channels, and eskers within them, appear to be related to the ORM complex (Barnett et al., 1998); channel fills form the lower portions of the ORM sediment package and eskers are linked to upper ORM sediments. The coarse channel sediments were deposited during waning flow from inferred regional meltwater floods (e.g. Shaw and Gorrell, 1991). Sediments deposited during subsequent seasonal meltwater flow (Brennand and Shaw, 1994) form eskers, exposed at small surface outcrops areas in the area (unit 6a). Other near-surface glaciofluvial channels sediments (unit 6; Table 1) are found atop the ORM (Sharpe and Barnett, 1997a).

### *Oak Ridges Moraine and morainal deposits*

On Open File 3062 (Sharpe et al., 1997a), stratified sediment ridges are shown as morainal deposits (unit 5), including the ORM and several similar, but smaller, deposits found to the north of the ORM. The ORM is an extensive deposit, 160 km long, 5–15 km wide and more than 100 m thick (Fig. 3), but it is not identified with a precise line on Open File 3062. This is because it may be more extensive (5–10 km) in the subsurface, where it underlies Halton Till (Russell and Arnott, 1997) and the ORM comprises several map units (Fig. 3). The ORM consists of four major wedges of stratified sediment (Fig. 1, 2b) forming plains, hummocks, kettles, narrow beads, and gaps. The lower contact of the ORM is an irregular, scoured surface (channel and drumlin unconformity), which, in part, controls the thickness and distribution of ORM sediments. Rhythmically interbedded fine sands and silts are the dominant near-surface sediments (Fig. 5b), but coarse sands and gravels (Fig. 5c) are prominent locally, at depth, and in fans (Barnett, 1995; Paterson and Cheel, 1997). Some areas of the ORM consist of a few fining-upward packages of tens of metres (e.g. Sharpe et al., 1996; Gilbert, 1997; Russell et al., 1998b), which grade from medium sand to silt-clay laminae. Composite landform relations (Barnett, 1995), textural trends, and structural data indicate formative meltwater flow from the northeast, changing to westward during later fan- and delta-building stages (e.g. Barnett, et al., 1998; Duckworth, 1979). ORM sediments were deposited in a deep glacial lake (Gilbert, 1997)

ponded between the ice and the Niagara Escarpment, where spillover channels formed at elevations around 425–250 m a.s.l. (Chapman, 1985; Barnett et al., 1998). On Open File 3062 (Sharpe et al., 1997a), several similar, but small, stratified sediment ridges are found to the north of the ORM.

### *Halton Till*

The Halton (and Kettleby) Till and related sediments (unit 4, Table 1) occur as thin (~10–20 m) surface tills and interbedded lake sediments that onlap the south (Halton) and north (Kettleby) flanks of the ORM. The Halton sediment complex covers 150–200 km$^2$ as predominantly clayey silt to silt till with interbedded sand, silt and clay (Fig. 5a). The Kettleby Till covers a smaller area and occurs as a thin (1–2m) clayey diamicton, interbedded with fine sand, silt, and clay. The Halton sediments are approximately 20–40 m thick along the Humber Valley (Russell and Arnott, 1997), and they thin towards the north and east (Fig. 4). Where these sediments onlap the south flank of the ORM (Bolton to Port Perry) they are characterized by a zone of hummocks and kettles (Fig. 2). Toward the end of final glacial cover, Halton ice melted back into Lake Ontario (Fig. 4, 6b) and deposition apparently ceased when ice floated off a local grounding position or it became stagnant, signaling, in broad terms, the end of ORM-building events.

### Extent of Halton Till redefined

The extent of Halton sediments has been overestimated in recent correlations (e.g. M.M. Dillon, unpub. rept.,1994; Gerber and Howard, 1996) and is now redefined east of the Humber watershed (Fig. 6), on the basis of continuity, texture, and a well defined stratigraphy (Fig. 4). Halton forms a thin, narrow sequence that onlaps the Oak Ridges Moraine between Bolton and Oshawa (Fig. 1 and 4, inset). Halton sediments occur as patchy outliers as far south as Highway 401, but these small areas are not all shown on 1:50 000 scale maps (e.g. Sharpe and Barnett, 1997). Its distinct fine texture, low stone content, and interbedded relationship with lacustrine beds (Fig. 5a) contrasts markedly with the coarse-textured, stony, generally massive, amalgamated beds of Newmarket Till (Fig. 5c). This new regional mapping results in a more extensive surface exposure of Newmarket Till (e.g. Sharpe and Barnett 1997a). The restricted, thin, distribution of Halton sediment constrains the southern extent of the underlying ORM sediments (Fig. 4).

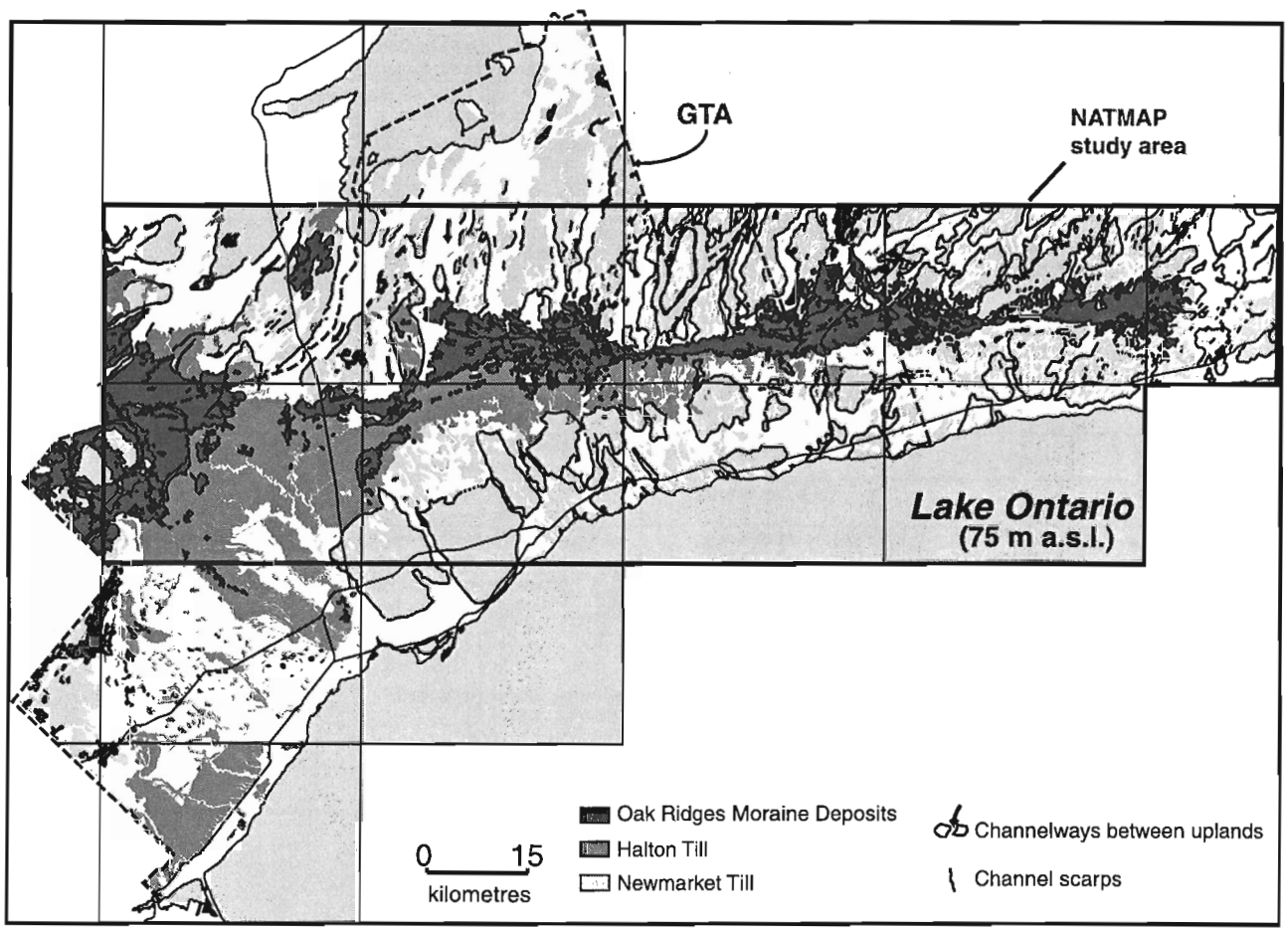


***Figure 6.*** *Generalized terrain and geology map of the ORM-GTA emphasing three regionally extensive units and a channel network of the stratigraphic model, Figure 3. (See Figure 1 for context)*

**Table 2.** Stratigraphic elements of the ORM-GTA

| | | Stratigraphic unit[1] (youngest on top) | Map units | Explanation/description[2] (reference to stratigraphic name) |
|---|---|---|---|---|
| Quaternary | | | | Period covering last 2 million years of glacial climates |
| | Recent | | | Last 10 000 years B.P. following glacial climates |
| | | Lake Ontario deposits | 11 | Deposits along shore of modern lake (75 m a.s.l.) |
| | | Alluvium (river deposits) | 10a | Sediment deposits by modern rivers in Recent time |
| | | Organic deposits | 9 | Plant and animal matter accumulating in wetlands |
| | | Older alluvium | 10b | Sediment deposited by rivers in modern valleys during glacier melt |
| | Pleistocene | | | Time of advance and retreat of the great ice sheets (~2 million - 10 000 years BP) |
| | | Peel/Schomberg pond deposits | 7,8 | Two of a series of lake beds deposited as melting ice blocked drainage (~180 m a.s.l.) |
| | | Lake Iroquois/ Algonquin deposits | 7,8 | Largest of postglacial lakes in Lake Ontario/Lake Huron basins |
| | | Glaciofluvial deposits | 6 | Deposits of high-energy streams or currents issuing from a glacier (may form core of ORM) |
| | | a. Wilfield/Kettleby Till[3,4] | 4a | |
| | | b Halton /Boucette Till[5] | 4b | Clay, silt till; few stones; thick in Humber Valley, thins rapidly to the east; Karrow, 1959 |
| | | c. Oak Ridges Moraine | 5 | Thick fine sand, silt and gravel resting on eroded Newmarket Till; Chapman and Putnam, 1943 |
| | | d. Wentworth/Leaside[6] | 3d | Sandy, stony till: may grade upward into Halton Till; Karrow, 1959; Leaside, Karrow, 1967 |
| | | e. Port Stanley/Tavistock Till | 3e/4c | Port Stanley: Lake Ontario sandy stony till; Tavistock: Lake Huron silt till |
| | Unconformity[7] | | | Major erosional episode marked by channel cutting and scouring; produced by subglacial floods (cf Barnett et al., 1998) |
| | | f. Newmarket /northern Till | 3f | Sandy, stony till extending beneath the ORM; Gwyn and Dilabio, 1973; Sharpe et al, 1994 |
| | | g.Thorncliffe Formation / Clarke Beds | 2g[8] | Sandy beds found at Scarborough Bluffs, Karrow, 1967; and at Bowmanville, Singer, 1974 |
| | | h. Seminary/Meadowcliffe/Bond head Tills | 2h | Thin mixed sediment separating thick Thorncliffe sands at lake bluffs; Karrow, 1967 |
| | | i. Thorncliffe Formation/ Clarke Beds | 2i | Beds are considered to be 30–50,000 years old (see above) |
| | | j. Sunnybrook Till /Port Hope | 2j | Clay till with very few stones; Karrow, 1967; Brookfield, 1982 |
| | | k. Scarborough Formation | 2k | Cool-climate (-5°C) raised lake beds (122 m a.s.l.) may be ~90 000 years old; Karrow, 1967 |
| | | l. Don Formation | 2l | Warm-climate (+3°C), raised lake beds with interglacial fossils; Karrow, 1967 |
| | | m. York Till | 2m | Dense, sandy till from glacial interval prior to last major warm period; Karrow, 1967 |
| | | n. Lower sediment[9] | 2n | Undifferentiated stratified sediment, mainly sand |
| | | o. Lower sediment[9] | 2o | Undifferentiated stratified sediment, mainly silt and clay |
| | Unconformity | | | Major interval of time and erosion |
| Paleozoic | | Bedrock | | Ancient marine sand, silt,and limey mud rocks formed ~450 million years ago |
| | | a. Bedrock-drift complex | | Map unit with thin 9 (<1 m) cover of glacial deposits on lime bedrock. |
| | | b. Clastic (sandstone or shale) | | Rocks made from grains of sediment cemented together; Georgian Bay/Queenston shale |
| | | c. Carbonate | | Limestone and dolostone rocks found respectively east and west of the Niagara Escarpment |

[1] See Barnett et al., 1991 for stratigraphic scheme of southern Ontario
[2] Lithology of older sediment is described
[3] Wilfield occurs south of ORM; Kettleby occurs north of ORM
[4] Till is mixed sediment (sand, silt, clay, stone) deposited by glaciers; till, lower case, indicates local name
[5] Units in italics refer to names for strata found east of Oshawa; see Brookfield et al., 1982.
[6] May correlate with Newmarket Till; Wentworth may have been deposited from retreat phase of "Newmarket ice"
[7] Erosional episodes may be present between and within other units e.g. boulder pavements
[8] Unit 2 comprises lower sediment in block model (Fig. 3)
[9] Uncertain age designation

**Glacial deposits (till)**

Open File 3062 groups heterogeneous glacial sediment into two broad till classes, clayey and sandy, to simplify sediment types for applied users (Table 1). This simplification means that some tills are not in chronological order on the legend (Table 1) but their precise stratigraphic position is shown in Figures 3, 4, and Table 2. Not all tills are discussed here, but coarse Newmarket Till and fine-textured Halton Till (above) have been described in stratigraphic order.

## MAP UNITS NOT HIGHLIGHTED ON THE REGIONAL GEOLOGICAL MODEL

Remaining map units on Open File 3062 are briefly discussed below, but for simplicity, they are not highlighted on the regional geological model (Fig. 2).

### *Glacial Lake Deposits*

Glacial lake deposits are widespread in the GTA (Fig. 3). They form broad plains within channels and below raised lake shorelines (e.g. Glacial Lakes Algonquin and Iroquois, units 7 and 8, Table 1). These glacial lake sediments comprise sand and interbedded silt and minor clay in successions that are 3–20 m thick (Barnett, 1996a). In places, they contain interbedded diamictons, deposited during slump events. At surface, younger glaciolacustrine sediments can be difficult to distinguish from older, bedded sand and silt deposits (e.g. Thorncliffe and Scarborough sediments) where Newmarket and Halton till units are missing. Organic material within the lower deposits (e.g. Aravena and Wassenaar, 1993) is one characteristic that allows these sediments to be distinguished.

As the ice retreated eastward in the Lake Ontario basin, Glacial Lake Iroquois was impounded within the basin to a level of approximately 110–150 m a.s.l. across the area. At its margin, the lake eroded till uplands and longshore currents reworked these sediments into gravely beaches, baymouth bars, and spits (Table 1). Nearshore deposits are dominantly sand and gravel (unit 8). Offshore deposits occur in topographic lows and include massive to laminated silt and clay (unit 7). Lower, Post-Iroquois, lake levels (75–120 m a.s.l.) are locally recorded by sand spits and gravel beaches.

### *Postglacial deposits: slope, organic, eolian and river sediments*

Recent deposits formed following deglaciation and lowering of post-glacial lakes. Slope and wind erosion was active, as was the accumulation of organic sediment and the work of modern rivers. However, the extent of organic and fluvial sediments in the area warranted their identification as separate map units (Table 1). Slope erosion produced deep gullying and landsliding from run-off, and from groundwater seepage (e.g. south of Claremont; Barnett, 1997a). Holocene organic deposits (unit 9) accumulated in poorly drained basins, kettles, wetlands and groundwater discharge hollows, particularly in the large valleys north of the ORM (e.g. Pefferlaw creek). Rivers discharged water to lowering lake levels, dissected the glacial landscape, and deposited sediment on their floodplains. As the lake level fell further, these rivers incised deeper, leaving raised terraces (unit 10b) and creating new floodplains (unit 10a). While much of the area is covered with a thin veneer of wind-blown silt and sand, nearshore sands were locally reworked into sand dunes when the area was deforested for a short time, for example, northeast of Vandorf (Barnett and Dodge, 1996). Other recent deposits (unit 11) include the Lake Ontario beach, baymouth bars and spits, in addition to fill.

## HYDROGEOLOGICAL CONSIDERATIONS

The new geological mapping and the related three-dimensional reconstructions (Fig. 3) have important applications to hydrogeology (e.g. Sharpe et al., 1996). Three aspects are briefly highlighted: 1) regional stratigraphic models; 2) sediment variation within major hydrostratigraphic elements, and 3) the application of sediment mapping to regional water-budget estimates.

Prior to this work there were no comprehensive geological models in the ORM-GTA area applicable to define the regional hydrostratigraphic setting (e.g. M.M. Dillon, unpub. rept., 1994). The new systematic mapping allows hydrogeological units to be put in a regional geological context (Fig. 3, 4). For example, at least four sedimentary strata form potential aquifer targets and at least two regionally significant aquitards (Sharpe et al., 1996; Howard and Gerber, 1996) are mapped.

Major hydrostratigraphic units in the area are treated as homogeneous elements (e.g. Howard et al., 1997). The ORM is a major aquifer and recharge complex (Turner, 1977) that was traditionally considered to be a uniform hydrogeological unit. Now that its architectural (e.g. Pugin et al., in press) and sedimentological variation (e.g. Paterson and Cheel, 1997; Russell et al., 1998b; Barnett et al., 1998) has been mapped in detail, it will permit improved hydrolgeological understanding and modelling. The Newmarket Till forms a thick regional aquitard apparently possessing low, predictable, regional permeability. However, enhanced secondary permeability (Gerber and Howard, 1996) or major permeability contrasts from channel erosion (e.g. Desbarats et al., 1998) indicate significant inhomogeneities in this hydrostratigraphic map unit.

Systematic sediment mapping across the GTA may allow for infiltration estimates to be made in a more consistent manner in support of regional water-budget calculations. For example, variations in mapped sediment (soil type) and topography have a dramatic impact on estimated rates of percolation (recharge) to groundwater needed for water budget assessment (e.g. Hunter and Associates, unpub. rept., 1996). Further, the combination of digital sediment maps (Russell et al., in press), topography (Kenny, 1997) and land cover (Kenny et al., 1999) could greatly improve regional water budget calculations across the GTA.

## ACKNOWLEDGMENTS

The following organizations supported mapping efforts: Ontario Geological Survey (OGS), Ministry of Northern Development and Mines, Ontario Ministry of Environment (MOE), Ontario Ministry of Natural Resources (MNR), the Regional Municipalities of Peel and York, Credit Valley Conservation Authority, Metro Toronto Conservation Authority, University of Ottawa, and Queen's University. Paul Stacey prepared the figures. Reviews by H. Thorleifson and Marc Hinton improved the paper.

## REFERENCES

**Aravena, R., and Wassenaar, L.I.**
1993: Dissolved organic carbon and methane in a regional confined aquifer, southern Ontario, Canada: carbon isotope evidence for associated subsurface sources; Applied Geochemistry, v. 8, p. 483–493.

**Barnett, P.J.**
1990: Tunnel valleys: evidence of catastrophic release of meltwater, central-southern Ontario, Canada; *in* Abstracts with Programs, Northeast Section, 25th Annual Meeting, Geological Society of America, Syracuse, New York, 3 p.
1995: Geology of the Oak Ridges Moraine area, parts of Peterborough and Victoria counties and Durham and York regional municipalities, Ontario; *in* Summary of Fieldwork and Other Activities 1995; Ontario Geological Survey, Miscellaneous Paper 164, p. 177–182.
1996a: Quaternary Geology, Claremont area; Ontario Geological Survey, Map 2634, scale 1:20 000.
1996b: Quaternary Geology, Enniskillen area; Ontario Geological Survey, Map 2636, scale 1:20 000.
1996c: Quaternary Geology, Kendal area; Ontario Geological Survey, Map 2637, scale 1:20 000.
1996d: Quaternary Geology, Bethany area; Ontario Geological Survey, Map 2638, scale 1:20 000.
1996e: Quaternary Geology, Brunswick area; Ontario Geological Survey, Map 2639, scale 1:20 000.
1997a: Piping: an important process in the postglacial landscape development of southern Ontario; *in* Program with Abstracts, Geological Association of Canada–Mineralogical Association of Canada Annual Meeting, Ottawa, Ontario, p. A8.
1997b: Surficial geology of the Scugog area, southern Ontario; Geological Survey of Canada, Open File 3330, scale 1:50 000.

**Barnett, P.J. and Dodge, J.E.P.**
1996: Quaternary Geology, Uxbridge area; Ontario Geological Survey, Map 2633, scale 1:20 000.

**Barnett, P.J. and Gwyn, Q.H.**
1997: Surficial geology of the Newmarket area, NTS 31 D/3, southern Ontario; Geological Survey of Canada, Open File 3329, scale 1:50 000.

**Barnett, P.J. and Henderson, L.A.**
1996: Quaternary geology, Port Perry area; Ontario Geological Survey, Map 2635, scale 1:20 000.

**Barnett, P.J. and McCrae, M.K.**
1996a: Quaternary Geology, Mount Albert area; Ontario Geological Survey, Map 2631, scale 1:20 000.
1996b: Quaternary Geology, Stouffville area; Ontario Geological Survey, Map 2632, scale 1:20 000.

**Barnett, P.J. and Mate, D.J.**
1998: Quaternary geology of the Beaverton area; Ontario Geological Survey, Map 2560, scale 1:50 000.

**Barnett, P.J., Dodge, J.E.P., and Henderson, L.A.**
1996: Quaternary Geology, Scugog area; Ontario Geological Survey, Map 2644, scale 1:50 000.

**Barnett, P.J., Henry, A.P., and Cowan, W.R**
1991: Quaternary geology of Ontario, southern sheet; Ontario Geological Survey, Map 2556, scale 1:1 000 000.

**Barnett, P.J., Sharpe, D.R., Russell, H.A.J., Gorrell, G., Pullan, S.E., Brennand, T.A., and Kenny, F.M.**
1998: On the origin of the Oak Ridges Moraine, Canadian Journal of Earth Sciences, v. 35, p. 1152–1167.

**Boyce, J.J., Eyles, N., and Pugin, A.**
1995: Seismic reflection, borehole and outcrop geometry of Late Wisconsin tills at a proposed landfill near Toronto; Canadian Journal of Earth Sciences, v. 32, p.1331–1349.

**Brennand, T.A.**
1997a: Surficial geology of the Oshawa area, southern Ontario; Geological Survey of Canada, Open File 3331, scale 1:50 000.
1997b: Surficial geology of the Port Hope area, southern Ontario; Geological Survey of Canada, Open File 3298, scale 1:50 000.

**Brennand, T., and Shaw, J.**
1994: Tunnel channels and associated landforms: their implication for ice sheet hydrology; Canadian Journal of Earth Sciences, v. 31, p. 502–522.

**Brennand, T.A., Moore, A., Logan, C., Kenny, F., Russell, H.A.J., Sharpe, D.R., and Barnett, P.J.**
1997: Bedrock topography of the Greater Toronto and Oak Ridges Moraine NATMAP areas, southern Ontario; Geological Survey of Canada, Open File 3419, scale 1:200 000.

**Brookfield, M.E., Gwyn, Q.H.J., and Martini, I.P.**
1982: Quaternary sequences along the north shore of Lake Ontario: Oshawa–Port Hope; Canadian Journal of Earth Sciences, v. 19, p. 1836–1850.

**Chapman L.J.**
1985: On the origin of the Oak Ridges Moraine, southern Ontario; Canadian Journal of Earth Sciences, v. 22, p. 300–303.

**Chapman, L.J., and Putnam, D.F.**
1943: The moraines of southern Ontario; Transactions of the Royal Society of Canada, v. 37, p. 33–41.
1984: The physiography of southern Ontario; Ontario Geological Survey, Special Volume 2, 270 p. (third edition).

**Clague, J.J., Turner, R.J.W., and Groulx, B.J.**
1997: Reinventing the geological map — making geoscience more accessible to Canadians; Geoscience Canada, v. 24, no. 4, p. 161-172.

**Coleman, A.P.**
1913: Geology of the Toronto region; *in* The Natural History of the Toronto Region, Ontario, Canada; Canadian Institute, Toronto, p. 51–81.
1932: The Pleistocene of the Toronto region; Ontario Department of Mines, Annual Report XLI, pt. 7, map 42g, scale 1:63 360.

**Desbarats, A.J., Hinton, M.J., Logan, C., Russell, H., and Sharpe, D.**
1998: Geostatistical modeling of leakance in the Newmarket till aquitard; *in* Abstracts with Program, Geological Society of America, Annual Meeting 1998, Toronto, Ontario, p. A402.

**Duckworth, P.B.**
1979: The late depositional history of the western end of the Oak Ridges Moraine, southern Ontario. Canadian Journal of Earth Sciences, v. 16, p.1094–1107.

**Eyles C.H. and Eyles, N.**
1983: Sedimentation in a large lake: a reinterpretation of the late Pleistocene stratigraphy at Scarborough Bluffs, Ontario, Canada; Geology, v. 11, p. 146–152.

**Eyles, N., Boyce, J.I., and Mohajer, A.A.**
1993: The bedrock surface of the western Lake Ontario region: evidence of reactivated basement structures?; Géographie physique et Quaternaire, v. 47, p. 269 283.

**Eyles, N., Clark, B.M., Kaye, B.G. Howard, K.W.F., and Eyles, C.H.**
1985: The application of basin analysis techniques to glaciated terrains: an example from the Lake Ontario basin, Canada; Geoscience Canada, v. 12, p. 22–32.

**Fligg, K., and Rodrigues, B.**
1983: Geophysical well log correlations between Barrie and the Oak Ridges Moraine; Water Resources Branch, Ontario Ministry of the Environment, Map 2273.

**Funk, G.**
1979: Geology and water resources of the East and Middle Oakville Creeks IHD representative drainage basin; Ontario Ministry of Environment, Water Resources Report 12, 68 p.

**Gadd, N.R.**
1950: Groundwater resources of Uxbridge Township, Ontario County; Geological Survey of Canada, Water Supply Paper 307, 25 p.

**Gerber, R.E. and Howard, K.W.F.**
1996: Evidence for recent groundwater flow through Late Wisconsinan till near Toronto, Ontario; Canadian Geotechnical Journal, v. 33, p. 538–555.

**Gilbert, R.**
1997: Glaciaolacustrine environment of part of the Oak Ridges Moraine, southern Ontario; Géographie physique et Quaternaire, v. 51, p. 55–66.

**Gorrell, G.**
1997: Surficial geology of the Trenton area (west half), southern Ontario; Geological Survey of Canada, Open File 3333, scale 1:50 000.

**Gorrell, G. and Brennand, T.A.**
1997: Surficial geology of the Rice Lake area, southern Ontario; Geological Survey of Canada, Open File 3332, scale 1:50 000.

**Gwyn, Q.H.J. and Cowan, W.R.**
1978: The origin of the Oak Ridges and Orangeville Moraines of sourthern Ontario; Canadian Geographer, v. XXII, no. 4, p. 345–351.

**Gwyn, Q.H.J. and DiLabio, R.N.W.**
1973: Quaternary geology of the Newmarket area; southern Ontario; Ontario Division of Mines, Preliminary Map P836, scale 1:50 000.

**Howard, K.W.F., Eyles, N., Smart, P., Boyce, J., Gerber, R., Salvatori, S.L., and Doughty, M.**
1997: The Oak Ridges Moraine of southern Ontario: a ground-water resource at risk; *in* Environmental Geology of Urban Areas, (ed.) N. Eyles; Geological Association of Canada, p.153–172.

**Hunter, J.A., Pullan, S.E., Burns, R.A., Good, R.L., Harris, J.B., Pugin, A., Skvortsov, A., Goriainov, N.N.**
1998: Downhole seismic logging for high resolution reflection surveying in unconsolidated overburden. Geophysics, v. 63, p. 1371–1384.

**Karrow, P.F.**
1959: Pleistocene geology of the Hamilton area; Ontario Department of Mines, Geological Circular no. 8.
1967: Pleistocene geology of the Scarborough area; Ontario Department of Mines, Maps 2076, 2077, scale 1:50 000.
1987: Quaternary geology of the Hamilton–Cambridge area, southern Ontario, Ontario Geological Survey, Report 25, 94 p.
1990: Interglacial beds at Toronto, Ontario; Géographie physique et Quaternaire, v. 44, p. 289–297.

**Kelly R.I. and Martini, I.P.**
1986: Pleistocene glacio-lacustrine deltaic deposits of the Scarborough Formation, Ontario, Canada; Sedimentary Geology, v. 47, p. 27–52.

**Kenny, F.M.**
1997: A chromostereo enhanced digital elevation model of the Oak Ridges Moraine area; southern Ontario; Geological Survey of Canada and Ontario Ministry of Natural Resources, Geologoical Survey of Canada, Open File 3423, scale 1:200 000.

**Kenny, F.M., Paquette, J., Russell, H.A.J., Moore, A.M., and Hinton, M.J.**
1999: A digital elevation model for the Greater Toronto Area, southern Ontario and Lake Ontario bathymetry; Geological Survey of Canada, Open File D3678, 1 CD-ROM.

**Lewis, C.F.M., Mayer, L.A., Cameron, G.D.M., and Todd, B.J.**
1998: Drumlins in Lake Ontario; *in* Glaciated Continental Margins: an Atlas of Acoustic Images, (ed.) T.A. Davies, T. Bell, A.K. Cooper, H. Josenhans, L. Ployak, A. Sonheim, M.S. Stoker, and J.A. Stravers; Geological Survey of Canada, Contribution Series, 1996170.

**ORM Technical Working Committee**
1994: Oak Ridges Moraine: a strategy for the Greater Toronto Area: An ecological approach to the protection and management of the Oak Ridges Moraine, Ontario Ministry of Natural Resources, 106 p.

**Ostry, R.C.**
1979: The hydrogeology of the IFYGL Forty Mile and Oakville Creeks study area; Ontario Ministry of the Environment, Water Resources Report 5b, 44 p.

**Paterson, J.T. and Cheel, R.J.**
1997: The depositional history of the Bloomington Complex, an ice-contact deposit in the Oak Ridges Moraine, southern Ontario, Canada; Quaternary Science Reviews, v. 16, p. 705 719.

**Pugin, A., Pullan, S.E., and Sharpe, D.R.**
1996: Observations of tunnel channels in glacial sediments with shallow land-based seismic reflection; Annals of Glaciology, v. 22: p. 176–180.

**Pugin, A., Pullan, S.E., and Sharpe, D.R.**
in press: Seismic facies of the Oak Ridges Moraine area, southern Ontario, Canadian Journal of Earth Sciences.

**Pullan, S.E., Pugin, A., Dyke, L.D., Hunter, J.A., Pilon, J.A., Todd, B.J., Allen, V.S., and Barnett, P.J.**
1994: Shallow geophysics in a hydrogeological investigation of the Oak Ridges Moraine, Ontario; *in* Proceedings, Symposium on the Application of Geophysics to Engineering and Environmental Problems; (ed.) R.S. Bell and C.M Lepper,Boston, Massachusetts, v. 1, p. 143–161.

**Russell, H.A.J. and Arnott, W.R.C.**
1997: Halton Complex, Humber watershed; *in* Where is the Water? Regional Geological/ Hydrogeological Framework, Oak Ridges Moraine Area, southern Ontario, (ed.) D.R. Sharpe and P.J. Barnett; Geological Association of Canada-Mineralogical Association of Canada, Joint Annual Meeting, Field Trip A1 Guidebook, p 18–22.
1998: Jokulhlaup deposits in subaqueous fans: examples from the western Oak Ridges Moraine; Geological Society of America Annual Meeting, Toronto, Ontario, October 26–29.

**Russell, H A J and Dumas, S.**
1997: Surficial geology of the Alliston area, NTS 31 D/4, southern Ontario; Geological Survey of Canada, Open File 3334, scale 1:50 000.

**Russell, H. A. J. and White, O. L.**
1997: Surficial geology of the Bolton area, NTS 30 M/13, southern Ontario; Geological Survey of Canada, Open File 3299, scale 1:50 000.

**Russell, H.A.J., Logan, C., Brennand, T.A., Hinton, M., and Sharpe, D.R.**
1996: A regional geoscience database: an example from the Oak Ridges Moraine NATMAP / Hydrogeology Project; *in* Current Research 1996-E; Geological Survey of Canada, p. 191–200.

**Russell, H.A.J., Moore, A., Logan, C., Kenny, F., Brennand, T.A., Sharpe, D.R., and Barnett, P.J.**
1998a: Sediment thickness of the Greater Toronto and Oak Ridges Moraine NATMAP areas; southern Ontario; Geological Survey of Canada, Open File 2892, scale 1:200 000.

**Russell, H.A.J., Sharpe, D.R., and Arnott, W.**
1998b: Sedimentology of the Oak Ridges Moraine, Humber River watershed, southern Ontario: a preliminary report; *in* Current Research 1998-C; Geological Survey of Canada, p. 155–166.

**Russell, H.A.J., Stacey, P., Sharpe, D.R., and Moore, A.**
in press: Digital data compilation I: Oak Ridges Moraine Project; Geological Survey of Canada, OpenFile D3699, 1 CD-ROM.

**Sanford, B.V. and Baer, A.J.**
1981: Geological map of southern Ontario; Geological Survey of Canada, southern Ontario sheet 30 S, 1335A, scale 1:1 000 000.

**Sharpe, D.R.**
1980: Quaternary geology of Toronto and surrounding area; Ontario Geological Survey, Map P. 2204, scale 1:100 000.
1988: The internal structure of glacial landforms: an example from the Halton till plain, Scarborough Bluffs, Ontario; Boreas, v. 17, p. 15–26.

**Sharpe, D. and Barnett, P.J.**
1997: Surficial geology of the Markham area, NTS 30 M/14, southern Ontario; Geological Survey of Canada, Open File 3300, scale 1:50 000.

**Sharpe, D.R., Barnett, P.J., Brennand, T.A., Finley, D., Gorrell, G., and Russell, H.A.**
1997a: Surficial geology of the Greater Toronto and Oak Ridges Moraine areas, compilation map sheet; Geological Survey of Canada, Open File 3062, scale 1:200 000.
1997b: Surficial geology of the Oak Ridges Moraine NATMAP area; Geological Survey of Canada, Open File 3456, scale 1:200 000.

**Sharpe, D.R., Barnett, P.J., Dyke, L.D., Howard, K.W.F., Hunter, G.T., Gerber, R.E., Paterson, J., and Pullan, S.E.**
1994: Quaternary geology and hydrogeology of the Oak Ridges Moraine area. Geological Association of Canada-Mineralogical Association of Canada, Joint Annual Meeting, Field Trip A7: Guidebook

**Sharpe, D.R., Dyke, L.D., Hinton, M.J., Pullan, S.E., Russell, H.A.J., Brennand, T.A., Barnett, P.J., and Pugin, A.**
1996: Groundwater prospects in the Oak Ridges Moraine area, southern Ontario: application of regional geological models; *in* Current Research 1996-E; Geological Survey of Canada, p. 181–190.

**Shaw, J. and Gorrell, G. A.**
1991: Subglacially formed dunes with bimodal and graded gravel in the Trenton drumlin field, Ontario, Canada; Géographie physique et Quaternaire, v. 45, p. 21–34.

**Shaw, J. and Sharpe, D.R.**
1987: Drumlin formation by subglacial meltwater erosion; Canadian Journal of Earth Sciences, v. 24, p. 2316–2322.
**Skinner, H. and Moore, A.**
1997: A digital elevation model of the Oak Ridges Moraine, southern Ontario, Geological Survey of Canada, Open File 3297.
**Sibul, U., Wang, K.T., and Vallery, D.**
1977: Ground-water resources of the Duffins Creek–Rouge River drainage basins; Water Resources Report 8, Ministry of the Environment, Water Resources Branch, Toronto, Ontario.
**Singer, S.**
1974: A hydrological study along the north shore of Lake Ontario in the Bowmanville–Newcastle area; Ontario Ministry of Environment, Water Resources Report 5d, 72 p.
**Spencer, J.W.**
1881: Discovery of the preglacial outlet of the basin of Lake Erie into that of Lake Ontario, Canadian Naturalist (New series), v. 10, p. 65–79.
**Taylor, F.B.**
1913: The moraine systems of southwestern Ontario; Canadian Institute, Transactions, v. 10, p. 1–23; Toronto.
**Turner, M.E.**
1977: The Oak Ridges aquifer complex; Ontario Ministry of the Environment, Water Resources Branch, Hydrogeological Map 78-2, scale 1:100 000.
**Watt, A.K.**
1957: Pleistocene geology and groundwater resources of the Township of North York, York County; Ontario Department of Mines, Annual Report 1955, v. 64, pt. 7, 64 p.
1968: Pleistocene geology and groundwater resources of the Township of Etobicoke; Ontario Department of Mines, Geological Report 59, 50 p.
**White, O.L.**
1975: Quaternary Geology of the Bolton area; Ontario Geological Survey, Report 117, 119 p.

Geological Survey of Canada Project 930042

# Eastern Canada and National and General Programs

# Est du Canada et programmes nationaux et généraux

# Environmental isotope geochemistry of Laurentian piedmont groundwater, Quebec

F. Vitali, M.M. Savard, É. Bourque, and Y. Michaud
GSC Québec, Sainte-Foy

*Vitali, F., Savard, M.M., Bourque, É., and Michaud, Y., 1999: Environmental isotope geochemistry of Laurentian piedmont groundwater, Quebec;* in *Current Research 1999-E; Geological Survey of Canada, p. 139–148.*

**Abstract:** A study of stable isotope (H, C, O) analysis of groundwater from the Laurentian piedmont aquifers is underway in the Portneuf region county municipality in order to characterize both granular and fractured aquifers in the region. Isotopic results indicate a short residence time for most groundwater samples. The influence of the limestone on the composition of groundwater from a sandy unit was identified, based on $\delta^{13}C_{DIC}$ and chemistry results. The obtained $\delta^{18}O_{SMOW}$ and $\delta^{2}H$ values suggest that groundwater recharge is provided mostly by the infiltration of snowmelt. The $\delta^{18}O_{SMOW}$ and $\delta^{2}H$ ratios show a linear correlation ($r = 0.940$, $n = 36$). The Portneuf groundwater line was calculated as $\delta^{2}H = 8.7\delta^{18}O + 22.7$. The main particularity of the Portneuf region groundwater is the excess in deuterium ($d = \delta^{2}H - 8\delta^{18}O$) which averages 14.8‰. Such excess seems to be related to the specific climatic conditions of Eastern Canada which determine the oxygen and hydrogen isotopic composition of precipitation and groundwater of the Laurentian piedmont aquifers.

**Résumé :** Une étude d'analyses d'isotopes stables (H, C, O) de l'eau souterraine du piémont laurentian est en cours dans la MRC de Portneuf. Son principal objectif est de caractériser les aquifères granulaires et fracturés de la région. Les résultats des analyses isotopiques indiquent un temps de résidence court pour la plupart des échantillons d'eau souterraine. L'influence du calcaire sur la composition de l'eau souterraine provenant d'une unité sableuse a été mise en évidence à partir des valeurs de $\delta^{13}C_{DIC}$ et de la chimie de l'eau. Les valeurs de $\delta^{18}O_{SMOW}$ et $\delta^{2}H$ obtenues montrent que la recharge en eau souterraine provient principalement de l'infiltration des eaux de fonte. Les rapports $\delta^{18}O_{SMOW}$ et $\delta^{2}H$ des échantillons d'eau souterraine montrent une corrélation linéaire ($r = 0{,}940$, $n = 36$). L'équation de la ligne d'eau souterraine de Portneuf est $\delta^{2}H = 8{,}7\delta^{18}O + 22{,}7$. La principale particularité de la région de Portneuf est son excès en deutérium ($d = \delta^{2}H - 8\delta^{18}O$) dont la moyenne est de 14,8 ‰. Un tel excès serait relié aux conditions climatiques particulières de l'Est du Canada qui déterminent la composition en isotopes de l'oxygène et de l'hydrogène des précipitations et de l'eau souterraine des aquifères du piémont laurentien.

## INTRODUCTION

A regional hydrogeology project on groundwater delineation and characterization is underway in the Portneuf region county municipality (Fig. 1) (Michaud et al., 1997), involving a hydrochemistry survey to assess the groundwater quality (Bourque et al., 1996, 1998; Vitali et al., 1997). The Portneuf region harbours aquifers representative of the Laurentian piedmont. Groundwater samples are collected from three types of geological formations, 1) nonconsolidated sediments deposited in the Champlain Sea, 2) Paleozoic rocks (limestone and shale) of the St. Lawrence Lowlands, and 3) Precambrian rocks (gneiss) from the Grenville Province. The investigated area covers approximately 1900 $km^2$ in the southern part of the Portneuf region county municipality (Fig. 1).

This paper presents preliminary isotopic results ($\delta^{13}C_{DIC}$, $\delta^{18}O$, and $\delta^{2}H$) obtained from groundwater samples. The isotopic study constitutes, to date, one of the rare stable isotope studies of groundwater in Quebec (Fritz et al., 1987; Moore, 1989); it is the first isotopic study of the Laurentian piedmont aquifers and is the most extended study in Quebec in terms of density of sampling sites.

The $\delta^{13}C$ results for dissolved inorganic carbon (DIC) record chemical reactions and isotope exchange processes within the aquifer. These data are useful for identifying key factors and processes influencing groundwater and to evaluate residence time (e.g. Balderer, 1987). The $\delta^{2}H$ and $\delta^{18}O_{SMOW}$ values of groundwater are strongly influenced by climatic conditions during precipitation and infiltration (Fontes, 1980). Afterwords, $\delta^{2}H$ is generally unaffected by chemical reactions with geological materials at low temperatures (Drever, 1997), whereas exchange with limestone ($CaCO_3$) may cause a significant shift towards heavy $\delta^{18}O$ values (Lohmann, 1988; Drever, 1997). The $\delta^{18}O$ is generally unaffected by reaction with silicates at low temperatures for shorter time ($<1x10^6$ a, Drever, 1997). Thus, covariation study of $\delta^{18}O$ and $\delta^{2}H$ values provides useful information on the origin of groundwater (Fontes, 1980; *see also* Gat (1996) and Clark and Fritz (1997) for a review).

In this paper, $\delta^{13}C_{DIC}$, $\delta^{18}O_{SMOW}$, and $\delta^{2}H$ values for samples collected in the autumn of 1995 are presented in order 1) to establish a first overview of the isotopic ratios of groundwater from the Laurentian piedmont aquifers, 2) to determine the sources of dissolved inorganic carbon, and 3) to compare the isotopic attributes of these aquifers relative to those of Eastern Canada and to global meteoric waters.

## HYDROGEOLOGICAL SETTING

The study area is located on the north shore of the St. Lawrence River between Québec City and Trois-Rivières. It superposes two physiographic regions, the Laurentian Mountains to the north and the St. Lawrence Lowlands to the south (Fig. 1). The Laurentians which are part of the Precambrian shield were formed during the Grenvillian orogeny. They are characterized by rounded small mountains composed of metamorphic rocks (Globensky, 1987) and are partly covered by a veneer of glacial till or by glaciofluvial deposits on valley floors (Cloutier et al., 1997). In the Laurentian Mountains, the groundwater resource occurs mainly in fractured Precambrian gneiss and in scarce and restricted porous glaciofluvial deposits (Fagnan, 1998). On the other hand, the St. Lawrence Lowlands, in the southern portion of the study area, are composed of Ordovician sedimentary rocks which are in turn covered by a thick sequence (40–50 m) of Quaternary deposits (Parent et al., 1998). The Ordovician flat-lying rocks consist of thick sequences of limestone and shale with a thin sandstone layer at the base (Clark and Globensky, 1975). The lateral extension of these formations is often marked by normal faults. The general stratigraphic sequence of the Quaternary cover includes till and glaciomarine sediments at the base, followed by Champlain Sea marine silt and clay, deltaic and coastal sands, and organic deposits (Cloutier et al., 1997). Most groundwater resources of the Portneuf region county municipality are found in the southern portion, in numerous unconfined granular aquifers within the regressive and deltaic sands, or in both surface and deep aquifers within the sedimentary rocks (Fagnan et al., 1998).

## SAMPLING AND ANALYTICAL METHODS

Groundwater samples were collected from 36 sites in the Portneuf region (Fig. 1), between September 13 and November 8, 1995. Water samples were collected from different geological materials representative of the region, at various depths (1–122 m) and from natural groundwater outflows (Table 1). Few samples are composite samples. In order to minimize cross-sample contamination, sampling tools (bailers, bottles, syringes, and filters) were washed with acidified pure water and rinsed with pure water. Samples were taken only after purging the wells as indicated by water temperature stabilizing around 6–8°C and making sure sampled water did not reside in pipes or tanks and was fresh. Samples were taken directly from the well when possible. Fifty milligrams of $HgCl_2$ was used as a preservative to prevent dissolved inorganic carbon modification due to bacteriological reactions.

The isotopic dissolved inorganic carbon extractions were made within 4 d of sampling by vacuum line acid stripping using 100% $H_3PO_4$, converting all dissolved inorganic carbon to $CO_2$. The liberated gas was trapped cryogenically. Each sample was analyzed for $\delta^{2}H$ using the zinc-reduction method (Coleman et al., 1982). The $\delta^{18}O_{SMOW}$ was determined on $CO_2$, equilibrated with 5 mL of water at a controlled temperature of 25°C (Epstein and Mayeda, 1953). A VG-SIRA 12 mass spectrometer was used to analyze the $CO_2$ extracted for carbon and oxygen isotope analyses. Hydrogen isotopic analyses were performed with a VG 602-E spectrometer at the University of Ottawa. Carbon, oxygen, and hydrogen stable isotope results are reported in the usual $\delta$ notation as per mil (‰) deviations from either NBS-19 for carbon (V-PDB) or V-SMOW for oxygen and hydrogen. Analytical precision was ±0.2‰ for $\delta^{18}O$ and $\delta^{13}C_{DIC}$, and ±1‰ for $\delta^{2}H$.

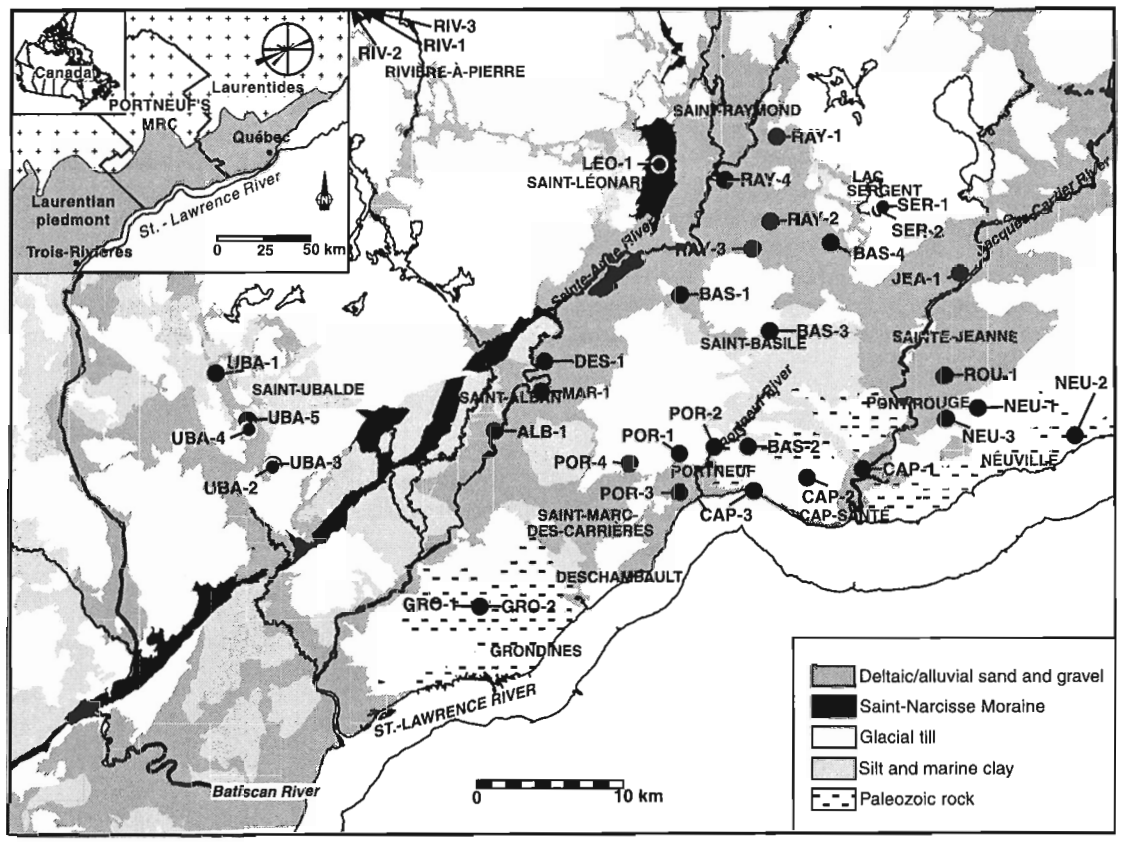


***Figure 1.*** *Hydrogeological settings of the groundwater samples from the region county municipality (MRC) of Portneuf, Quebec. A wind rose diagram gives the frequency by direction of wind speed greater than 19 miles/h as a percentage of all observation for the year (maximum 9.9 %) (modified from Wilson, 1971).*

## RESULTS

Stable carbon, oxygen, and hydrogen isotope results are reported in Table 1. Isotopic data show a broad scale of $\delta^{13}C_{DIC}$ values, ranging from -25.0‰ to -7.6‰, with 70% of the $\delta^{13}C_{DIC}$ values between -22.0 ‰ and -15.0‰ (Fig. 2a). Values of $\delta^{18}O$ range from -12.63‰ to -9.7‰, with 74% of the values between -12.5‰ and -11.5‰, whereas only three samples (8.3%) show values lower than -12.5‰ or higher than -10.5‰ (Fig. 2b). The $\delta^{2}H$ values range from -88‰ to -63‰ with 78% of the values between -88‰ and -76‰ (Fig. 2c).

Figure 3 shows the relationship between $\delta^{2}H$ and $\delta^{18}O_{SMOW}$ values found in groundwater from different aquifer types. All groundwater samples taken from gneissic aquifers show relatively homogenous isotopic values, between -11.8‰ and -11.3‰ for $\delta^{18}O$ and between -80‰ and -72‰ for $\delta^{2}H$. The $\delta^{18}O$ and $\delta^{2}H$ values are as high as -9.8‰ and - 63‰, in the carbonate aquifer of Grondines (GRO-2), and as low as -12.6‰ and -88‰, in the sandy aquifer of Sainte-Jeanne (Table 1, Fig. 3).

All groundwater results fall above the global meteoric water line (GMWL, $\delta^{2}H = 8\ \delta^{18}O + 10$; Craig, 1961). The $\delta^{2}H$ and $\delta^{18}O$ values of the Portneuf groundwater reveal a high correlation coefficient (r = 0.940). The Portneuf groundwater line was calculated as $\delta^{2}H = 8.7\delta^{18}O + 22.7$. In addition, Portneuf groundwater samples show deuterium excess (d) averaging 14.8 ±2‰ (n =36). This quantifies the position of the Portneuf groundwater line above the global meteoric water line in the $\delta^{2}H$ - $\delta^{18}O$ space, considering that deuterium excess which was defined as $d = \delta^{2}H - 8\delta^{18}O$ (Dansgaard, 1964), typically amounts to 10‰ if precipitation follows the global meteoric water line (e.g. Clark and Fritz, 1997).

## DISCUSSION

### *Carbon isotope ratios*

The main control on the carbon budget which influence the $\delta^{13}C_{DIC}$ content in groundwater is atmospheric $CO_2$ (Mook, 1980), plant respiration (O'Leary, 1988; Ebhardt and Fritsch, 1992), soil $CO_2$ derived from the decomposition of organic matter (Kendall et al., 1995), dissolution of carbonate (Klopmann et al., 1994), and silicate weathering (Probst et al., 1994).

In the Portneuf region, groundwater samples collected in the northern part of the study area present the lowest $\delta^{13}C_{DIC}$ values (Table 1, Fig. 4 for locations). Groundwater samples from that area are from shallow granular surface aquifers, excluding six samples from deeper wells (BAS-3, BAS-4, RAY-3, RIV-1, UBA-2, and SER-1) drilled in gneissic rocks. In contrast, the highest $\delta^{13}C_{DIC}$ values are mainly concentrated near the St. Lawrence River, in the southernmost portion of the region county municipality (Grondines, Portneuf, Cap-Santé, and Neuville) characterized with variable host rock formations. In that sector, groundwater samples were collected from granular, limestone, shaly, and gneissic aquifer formations (Table 1).

The $\delta^{13}C_{DIC}$ values are illustrated in a $\delta^{13}C_{DIC}$-pH diagram according to the nature of aquifer formations in Figure 5. This diagram indicates that $\delta^{13}C_{DIC}$ values vary with pH (Wigley et al., 1978; Coplen, 1993). For the Portneuf region, the lowest pH (5.8–7.0) and $\delta^{13}C_{DIC}$ values (-25.0‰ to -19.0‰ were found in shallow sandy aquifers. The organic matter-derived carbon (i.e. soil influence) seems to be preponderant for groundwater in shallow sandy aquifers. Indeed, the pH of 6–7 is commonly found in temperate soil from deciduous forest region (Heller, 1981; Gerritse and Van Driel, 1984). In addition, soil $CO_2$ derived from decomposed organic matter with initial values usually between -34‰ to -24‰ (e.g. O'Leary, 1988) can be a major carbon

**Table 1.** Autumn 1995 $\delta^{13}C_{DIC}$ (PDB), $\delta^{18}O$ and $\delta^{2}H$ (SMOW) data of groundwater from the Portneuf region. PDB=Peedee belemnite; SMOW=Standard Mean Ocean Water.

| Site | Well depth (m) | Sample depth (m) | Stratigraphy from top | $\delta^{13}C_{DIC}$ (‰) | $\delta^{18}O$ (‰) | $\delta^{2}H$ (‰) |
|---|---|---|---|---|---|---|
| BAS-2 | Spring | | Sand (>3 m) | -15.7 | -10.8 | -74 |
| BAS-1 | Spring | | Sand (>5 m) above silty clay | -20.2 | -12.2 | -84 |
| NEU-1 | Spring | | Sand (2 m) above limestone | -11.8 | -12.2 | -83 |
| CAP-3 | Spring | | Till (2 m) above shale | -17.3 | -11.9 | -80 |
| RAY-4 | Spring | | Sand (5 m) above sandy silt | -17.0 | -12.5 | -84 |
| JEA-1 | Spring | | Sand (10 m) above silt | -16.8 | -12.6 | -88 |
| MAR-1 | Spring | | Sand (15 m) above silty clay | -19.2 | -12.4 | -87 |
| ALB-1 | Spring | | Sand (15 m) above silty clay | -20.8 | -12.2 | -86 |
| POR-2 | Spring | | Sand (10 m) above clay (3 m) | -17.1 | -11.7 | -78 |
| SER-2 | 1 | 1 | Till (2 m) | -21.0 | -12.1 | -85 |
| UBA-3 | 3 | 3 | Sand (5 m) above silty clay | -20.5 | -12.1 | -82 |
| UBA-5 | 3 | 3 | Sand (>5 m) | -21.7 | -11.0 | -72 |
| RIV-3 | 4 | 4 | Sand (>4 m) | -23.9 | -12 | -78 |
| UBA-4 | 5 | 5 | Sand (>5 m) | -18.7 | -10.2 | -65 |
| ROU-1 | 6 | 6 | Sand (6 m) silt (0. 6 m) | -21.4 | -12.3 | -84 |
| RIV-2 | 7 | 6–7 | Sand (>7 m) | -25.0 | -12.3 | -84 |
| UBA-1 | 16 | 8–16 | Clay (5 m) sand (3 m) and gravel (8 m) above gneiss | -19.5 | -11.8 | -78 |
| RAY-2 | 20 | 16–20 | Sand and gravel (7.5 m) sand (13.5 m) | -20.7 | -12.2 | -85 |
| LEO-1 | 21 | 16–21 | Sand (21m) | -21.5 | -12.0 | -80 |
| DES-1 | 45 | 40–45 | Sand (47 m) above silty clay | -22.6 | -12.2 | -83 |
| RAY-1 | 16 | 14–16 | Sand (14 m) gravel (2 m) | -21.8 | -11.7 | -81 |
| POR-1 | 26 | unknown | Till (26 m) | -15.8 | -11.8 | -78 |
| POR-3 | 35 | 32–35 | Sand (4 m) silt (26 m) sand (7 m) till (2 m) | -7.6 | -11.6 | -74 |
| NEU-2 | 68 | 66–68 | Soil (2 m) sand (8 m) till (57 m) gravel (2 m) | -13.9 | -11.8 | -81 |
| CAP-1 | 11 | 9–11 | Sand and gravel (6 m) shale (6 m) | -14.1 | -12.1 | -86 |
| CAP-2 | 20 | unknown | Shale (20 m) | -10.1 | -11.5 | -78 |
| NEU-3 | 15 | 12–15 | Soil (1m) sandy silt (8 m) limestone (7 m) | -9.2 | -12.1 | -81 |
| GRO-2 | 28 | 2–28 | Limestone (28 m) | -16.1 | -9.8 | -63 |
| GRO-1 | 38 | 2–38 | Limestone (38 m) | -12.8 | -10.6 | -71 |
| RIV-1 | 30 | 11–30 | Soil (10 m) gneiss (20 m) | -20.0 | -11.8 | -77 |
| BAS-4 | 30 | 24–30 | Sandy silt (23 m) gneiss (7 m) | -16.5 | -11.7 | -80 |
| RAY-3 | 44 | 43–44 | Sand (12 m) silty clay (30 m) gneiss (2 m) | -18.2 | -11.5 | -77 |
| SER-1 | 68 | 6–68 | Till (5 m) gneiss (63 m) | -15.8 | -11.7 | -79 |
| POR-4 | 76 | 6–76 | Silty clay (4 m) gravel (0.6 m) gneiss (71 m) | -14.9 | -11.3 | -72 |
| UBA-2 | 77 | 22–77 | Sand (5 m) silty clay (17 m) gneiss (55 m) | -16.9 | -11.7 | -77 |
| BAS-3 | 122 | 3–122 | Soil (2 m) gneiss (121 m) | -17.8 | -11.5 | -74 |

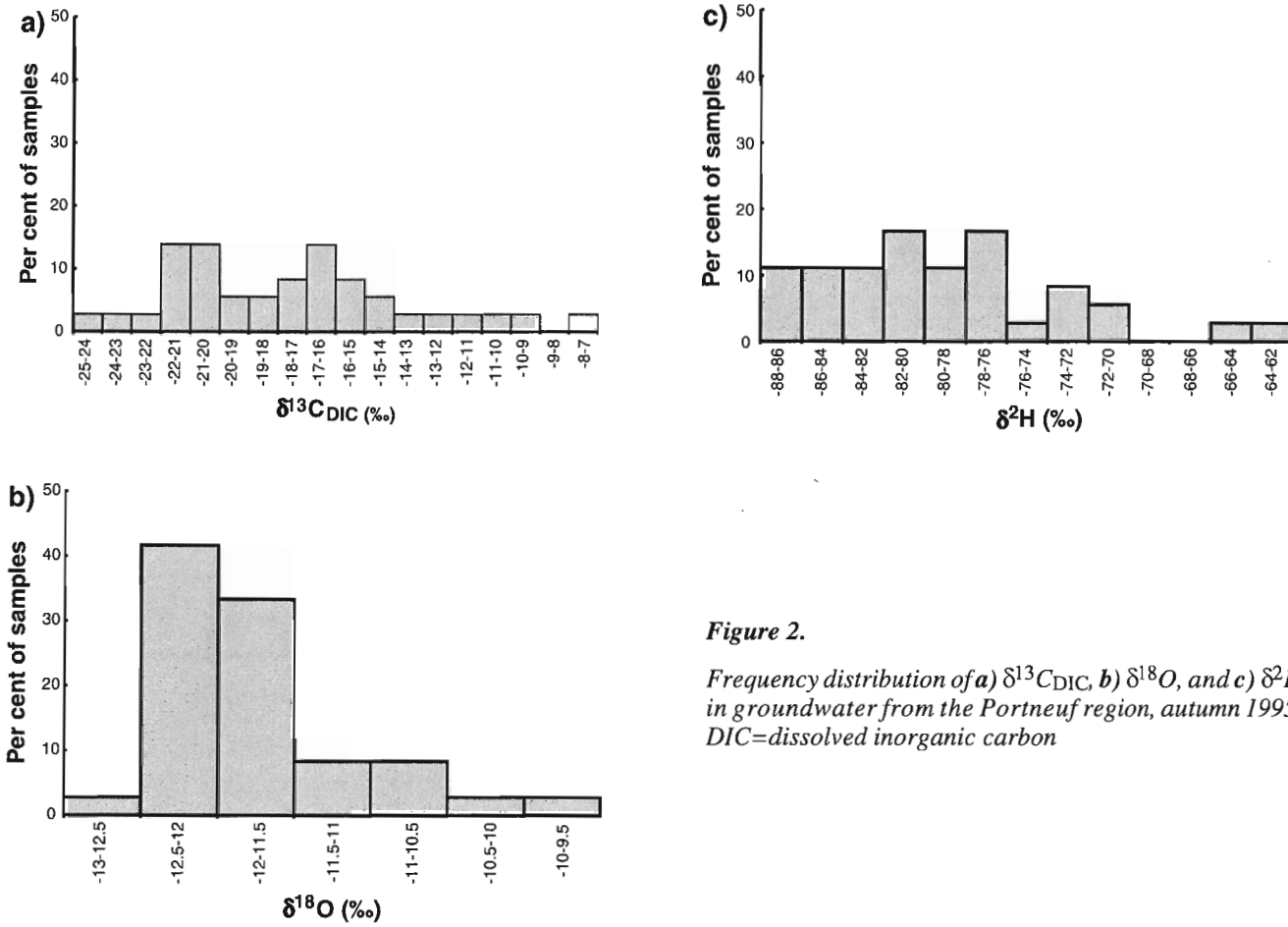


*Figure 2.*

*Frequency distribution of* ***a)*** $\delta^{13}C_{DIC}$, ***b)*** $\delta^{18}O$, *and* ***c)*** $\delta^{2}H$ *in groundwater from the Portneuf region, autumn 1995. DIC=dissolved inorganic carbon*

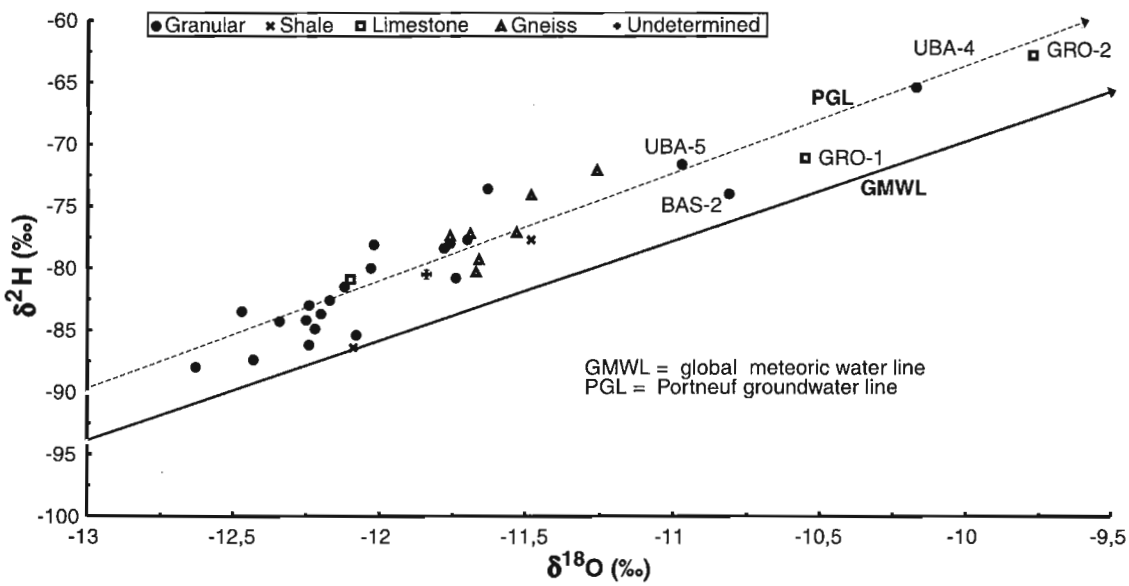


***Figure 3.*** *Plot of* $\delta^{2}H$ *versus* $\delta^{18}O$ *values from the autumn 1995 campaign classified by origin of aquifer.*

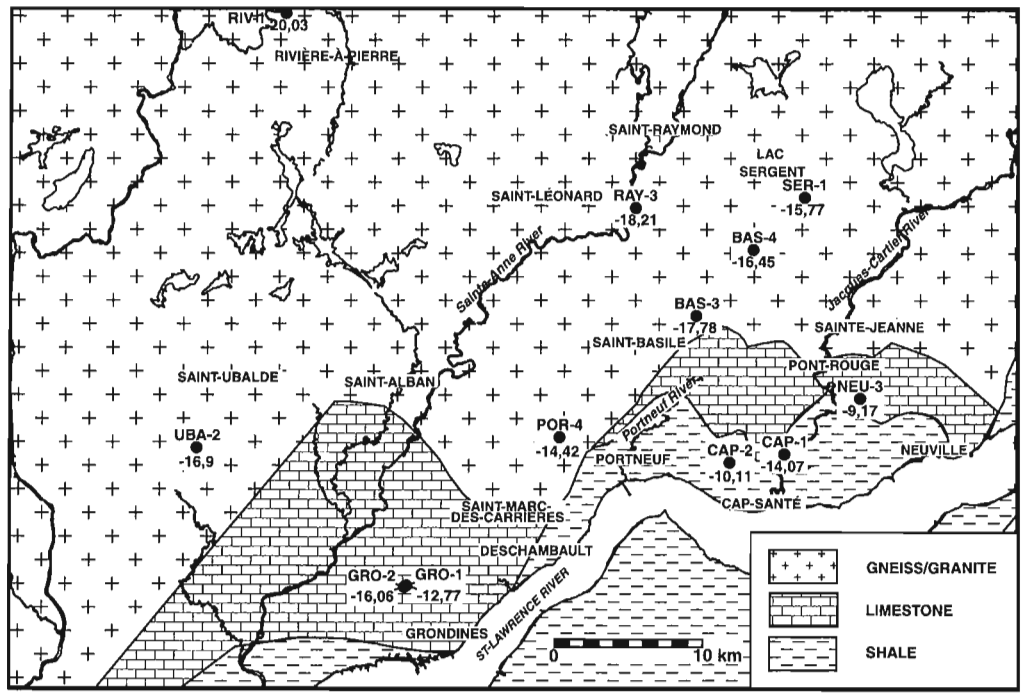


***Figure 4.*** *A $\delta^{13}C_{DIC}$ map of groundwater in rocks aquifers from the Portneuf region, autumn 1995.*

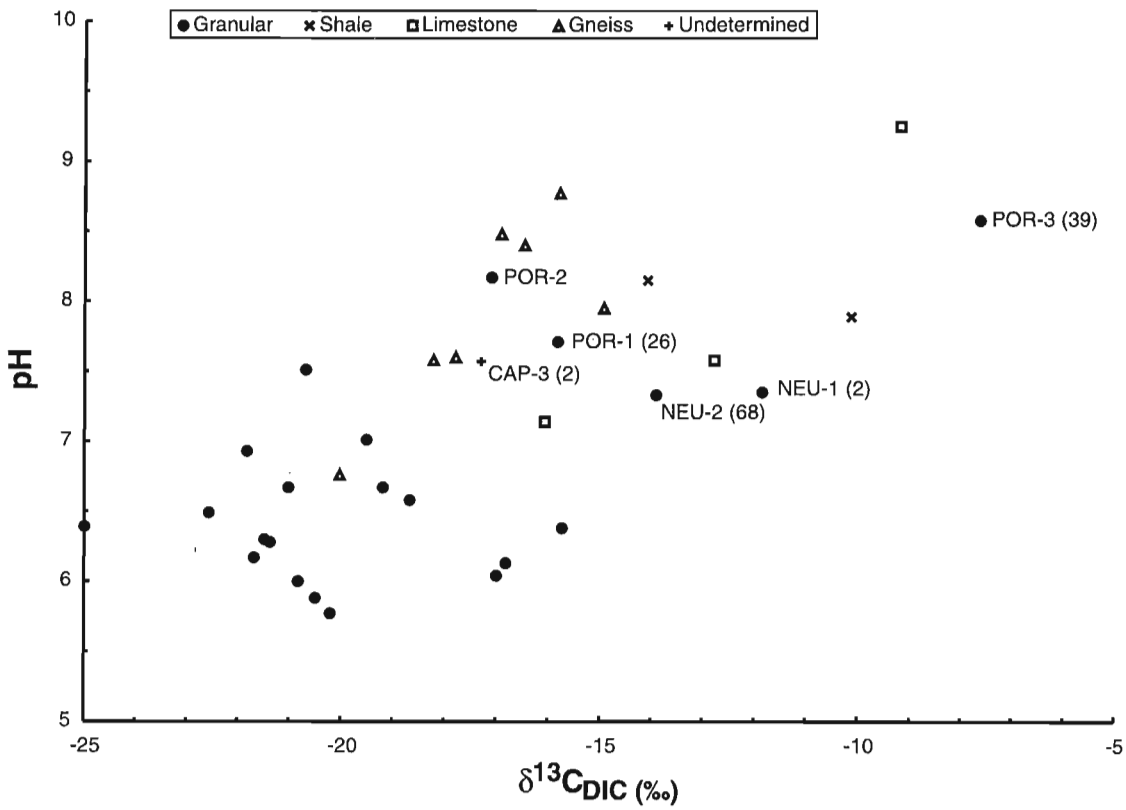


***Figure 5.*** *Relationships between $\delta^{13}C_{DIC}$ and pH of groundwater from the Portneuf region, autumn 1995.*

source contributor to groundwater $\delta^{13}C_{DIC}$ values. The fractionation during biologically mediated mineralization is non-existant and soil $CO_2$ has comparable isotopic composition as organic matter (Fry and Sherr, 1988; Ebhardt and Fritsch, 1992; Dudziak, 1994). The following dissolution of gaseous $CO_2$ into water causes a fractionation of about 7‰ (Wigley et al., 1978) and leads to values comparable to those of the shallow sandy aquifers. Groundwater samples from deeper granular aquifer of NEU-2, POR-1, and POR-3 present pH values of 7.3, 7.7, 8.6 and $\delta^{13}C_{DIC}$ of -13.9‰, -15.8‰, and -7.6‰, respectively (Fig. 5). These values seem to be due to a water-rock interaction during a relatively long period and the occurrence of carbonate.

Samples from gneissic rocks present $\delta^{13}C_{DIC}$ values ranging from -20.0‰ to -14.9‰ with associated pH between 6.8 and 9 (Fig. 5). The dissolution of biotite, K-feldspar, and plagioclase from the Grenvillian gneiss increase the pH values of the groundwater. Moreover, the range of isotopic ratios obtained from these aquifer formations could be due mostly to the variation of soil $CO_2$ in groundwater. Soil $CO_2$ seems to play a major role in weathering of silicates from gneissic rocks (Probst et al., 1994). During this process, carbonate released into groundwater has an isotopic composition of dissolved soil $CO_2$, because no fractionation is involved (e.g. Pawellek and Veizer, 1994).

Groundwater samples from limestone aquifers in the Grondines area (GRO-1, GRO-2) and Neuville (NEU-3) present higher $\delta^{13}C_{DIC}$ and pH values (Fig. 4). The high $\delta^{13}C_{DIC}$ values likely result from water interaction with marine carbonate rocks of the Trenton Group characterized with $\delta^{13}C_{VPDB}$ of -1.5‰ (Lohmann and Walker, 1989; Lavoie, 1993). This can be explained by the action of soil $CO_2$ as a catalyst for the dissolution of carbonates according to the following equations:

$$CO_2 + H_2O \longrightarrow H^+ + HCO_3^- \quad (1)$$

$$CaCO_3 + H^+ + HCO_3^- \longrightarrow Ca^{2+} + 2HCO_3^- \quad (2)$$

(Bathurst, 1975).

The $\delta^{13}C_{DIC}$ ratio of -11.8‰ and the pH of 7.4 of the spring sample (NEU-1) indicate that this water has reacted with limestone before it flowed into the sand deposit (Table 1). Finally, the high pH (8.7 and 7.9, respectively) and relatively elevated $\delta^{13}C_{DIC}$ values (-14.1‰ and -10.1‰, respectively) of samples CAP-1 and CAP-2 collected in the shaly aquifer from Cap-Santé, could be attributed to the occurrence of calcite vein into this shale and thus to water-$CaCO_3$ interactions.

### *Limestone influence*

At Neuville, groundwater sample NEU-1 outflows from a thin sandy unit (Table 1). However, an elevated $\delta^{13}C_{DIC}$ value (-11.8‰) could indicate that this water probably comes from the limestone formation underlying the sediments as it is the case for NEU-3 sampled nearby ($\delta^{13}C_{DIC}$ = -9.2‰). This is supported by other parameters such as the high specific electric conductivity of the samples NEU-1 and NEU-3 (290 and 256 µS/cm, respectively), and their high $HCO_3^-$ content (117 and 115 mg/L, respectively). In comparison, the nearby sample ROU-1 (Fig. 1), collected in a sandy aquifer at 6 m depth, presents a specific electric conductivity of 182 µS/cm and no dissolved $HCO_3^-$. Considering all these parameters, we suggest that the spring water (NEU-1) has circulated in the underlying limestone before flowing out of the sandy unit (Fig. 6).

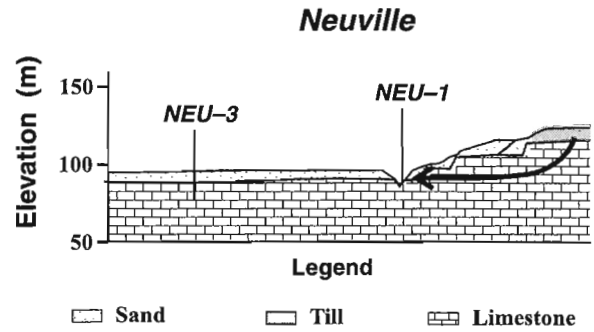


*Figure 6. Schematic hydrogeological setting of groundwater samples from Neuville, Quebec.*

### *Climatic parameters*

#### Portneuf region

Average annual directional frequency of wind speeds greater than 13 miles/h (5.8 m/s) for Québec City, close to the Portneuf region county municipality (data from Wilson, 1971) indicates that major wind directions follow the southwest-northeast axis (Fig. 1). In addition, a summary of average climatic conditions recorded at 11 meteorological stations during 30 a (1961–1990) in the Portneuf region is presented in Table 2. It includes monthly average temperatures, precipitation, snow cover thickness, and potential evapotranspiration. Meteorological data are characterized by the following seasonal attributes: 1) from June to August, evapotranspiration is equivalent to precipitation (>100 mm/mo.); 2) from December to March the snow cover thickness is between 40 cm and 70 cm, which rapidly vanishes by the end of April; 3) limited evapotranspiration (21 mm/m) during snow melting period (spring) favors major infiltration of water during this period (Paradis et al., 1997). This is confirmed by well hydrograms recorded in Saint-Léonard, Saint-Raymond, and Pont-Rouge, and hydrogeological work in the Portneuf region which indicate that the main recharge occurs during spring time, with a small secondary peak in autumn (Fagnan et al., in press).

Based on isotope effect principles such as fractionation due to temperature between water vapor and precipitation, the heaviest $\delta^{18}O$ and $\delta^{2}H$ values would be expected from autumn recharge, whereas the lightest values would be expected from snowmelt recharge, as snow has been accumulated during winter at much lower temperatures than autumnal rain. The most likely explanation for the spread of $\delta^{2}H$-$d^{18}O_{SMOW}$ results for the Portneuf aquifers (2.9‰ for $\delta^{18}O$ and 25.0‰ for $\delta^{2}H$) is that it represents waters precipitated at different temperatures and recharged at different

**Table 2.** Summary of the climatic conditions in the Portneuf region. Averages were made using data from 11 meteorological stations. Standard deviations are given in parentheses.

| Month | Average temperature (°C) | Minimum temperature (°C) | Maximum temperature (°C) | Rainfall (mm) | Snowfall (cm) | Total precipitation (mm) | Snowcover (cm) | Potential of evapotranspiration (mm) |
|---|---|---|---|---|---|---|---|---|
| January | -13.2 (0.8) | -18.7 (1.4) | -7.8 (0.4) | 16.6 (4.3) | 62.9 (9.5) | 79.2 (12.2) | 57.5 (12.4) | 0 (0) |
| February | -11.5 (0.6) | -17.3 (1.3) | -5.6 (0.3) | 14.6 (3.9) | 52.2 (10.2) | 66.9 (12.8) | 69.9 (15.9) | 0 (0) |
| March | -4.9 (0.6) | -10.4 (1.2) | 0.7 (0.4) | 35.2 (5.2) | 38.7 (6.9) | 74.3 (10.5) | 43.9 (16.6) | 0 (0) |
| April | 3.4 (0.5) | -1.9 (0.8) | 8.7 (0.4) | 60.8 (8) | 14 (3.3) | 74.9 (8.2) | 1.5 (1.8) | 21.1 (1.9) |
| May | 10.8 (0.5) | 4.5 (0.8) | 17 (0.4) | 105 (8.3) | 0.6 (0.3) | 105.6 (8.3) | 0 (0) | 72.6 (1.4) |
| June | 15.9 (0.6) | 9.7 (0.8) | 22 (0.6) | 112.4 (11.2) | 0 (0) | 112.4 (11.2) | 0 (0) | 107.4 (2.4) |
| July | 18.6 (0.6) | 12.5 (0.8) | 24.7 (0.5) | 120.1 (11.9) | 0 (0) | 120.1 (11.9) | 0 (0) | 126.6 (2.5) |
| August | 17.3 (0.6) | 11.5 (0.8) | 23.1 (0.6) | 118.7 (9.4) | 0 (0) | 118.7 (9.4) | 0 (0) | 108.4 (2.4) |
| September | 12.2 (0.6) | 6.7 (0.8) | 17.6 (0.6) | 120.7 (10.8) | 0 (0) | 120.7 (10.8) | 0 (0) | 66.3 (2) |
| October | 6.1 (0.6) | 1.5 (0.8) | 10.7 (0.6) | 100.2 (10.2) | 2 (0.8) | 102.1 (10.7) | 0.1 (0.2) | 30.6 (1.8) |
| November | -0.9 (0.6) | -4.5 (0.8) | 2.8 (0.5) | 67.9 (9) | 30.5 (6.8) | 98.8 (12.3) | 10.7 (2.9) | 0 (0) |
| December | -18.7 (1.4) | -12 (8.3) | -5 (0.5) | 28.7 (4.7) | 69.5 (10.8) | 98.4 (14.2) | 37.8 (8.8) | 0 (0) |

periods. Overall, the regional isotopic pattern shows that most samples reflect snowmelt recharge (lightest isotope ratios). The shallow sandy aquifers at Saint-Ubalde (UBA-4, UBA-5) and Saint-Basile (BAS-2), and the carbonate aquifer from Grondines (GRO-1, GRO-2) possibly reflect autumn recharge (heaviest isotope ratios) because they are all in settings that favor rapid infiltration and, as they were sampled during the autumn, their water carries an autumn signal. All the other groundwater samples reflect mixing water from snowmelt with autumnal rain water (intermediate isotopic sets).

In the following section, we will try to determine the location of the Portneuf groundwater line with regard to the global meteoric water line, and more generally to explain the available Eastern Canada groundwater and precipitation isotopic data, with regard to the global meteoric water line. As Portneuf granular aquifers are mainly formed of silicate minerals with relatively young groundwater, we consider that $\delta^{18}O$ and $\delta^{2}H$ ratios are not affected by water-rock interactions. This allows comparisons with isotopic data of meteoric waters.

## Deuterium excess

The Portneuf groundwater line is characterized by an average deuterium excess (d) of 14.8. On a global basis, deuterium excess of meteoric waters averages about 10‰, but regionally it could change due to variations in humidity, wind speed, and sea surface temperature during primary evaporation (e.g. Clark and Fritz, 1997). Deuterium excess in precipitation due to locally effective moisture source have been previously abundantly described in the Eastern Mediterranean region (e.g. Gat and Carmi, 1970; Gat and Dansgaard, 1972; Fontes, 1994; Gat, 1996) with a water line established as $\delta^{2}H = 8\delta^{18}O + 22$ (Gat and Carmi, 1970). Due to the lack of available isotopic studies, little attention has yet been paid to Eastern Canada, another part of the world where a significant deuterium excess exists. To underline this particularity of Eastern Canada, H and O isotopic data from the Portneuf region were compiled along with other available data such as groundwater from thick (50 m) Northern Till (late Wisconsinan), Toronto area, Ontario (Gerber and Howard, 1996); shallow groundwater from glacial till of the Hermine Basin, St. Hyppolyte area, southern Laurentian Mountains, Quebec (Moore, 1989), and daily precipitation collected over 7 a in Ottawa (Fritz et al., 1987). All the reported isotopic values present a high deuterium enrichment with a maximum of 22.4 reached by the Hermine Basin groundwater sampled in February–March 1987 (Fig. 7). The significance of a given deuterium value is relative and is largely dependant on the sampling period and comparison between the different studies must be handled with caution.

The compilation of numerous isotopic data obtained on groundwater during the last ten years in Eastern Canada (Moore, 1989; Gerber and Howard, 1996; this study, Fig. 7) indicates an evident deuterium excess higher than 10. This reinforces the hypothesis (Fritz et al., 1987), based on isotope ratios obtained for three meteorological stations in Ontario, one in Quebec, and one in Newfoundland, that specific climatic conditions influence the isotopic ratios of precipitation and groundwater of Eastern Canada. These climatic conditions involve mixing of three different air masses, with domination of air from the Gulf of Mexico and tropical Atlantic Ocean during summers, and Arctic airstream during winters (Brown, 1970; Bryson and Hare, 1974). However, the response of oxygen and hydrogen isotopic composition in precipitation due to this mixing of air masses is not yet well understood. Isotopic data obtained during the last ten years from Eastern Canada aquifers will probably generate more information and a better understanding of the climatic parameters controlling the deuterium excess in this part of the world.

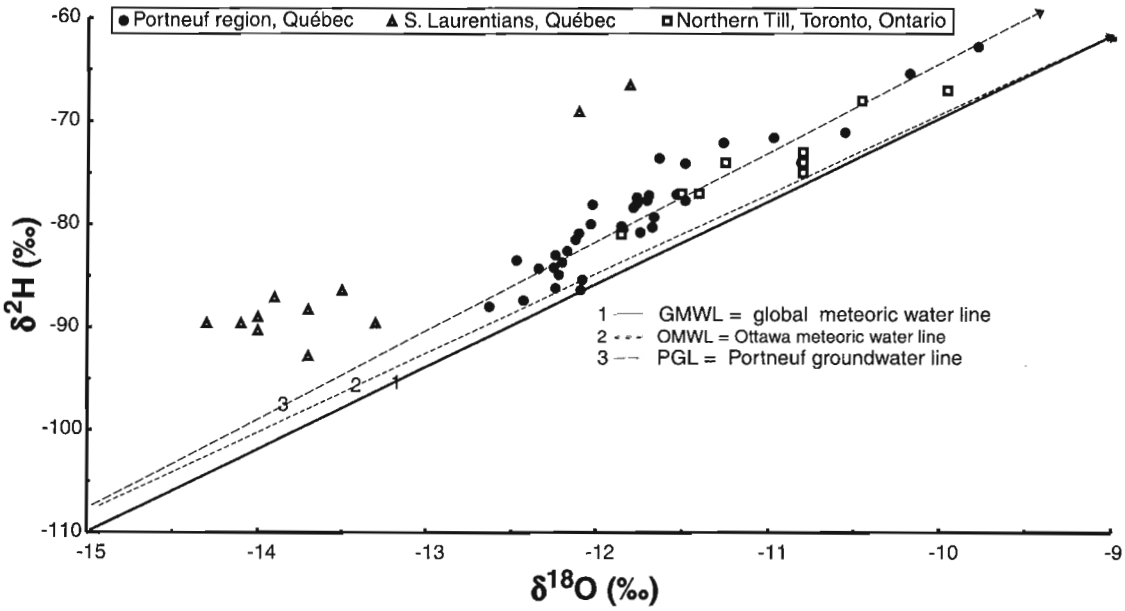


***Figure 7.*** *Comparison of $\delta^2H$ versus $\delta^{18}O$ groundwater values from Portneuf region and isotopic values from other studies from Eastern Canada: Groundwater from Northern Till, Toronto area, Ontario (Gerber and Howard, 1996); Hermine Basin, St. Hyppolyte area, southern Laurentian Mountains, Quebec (Moore, 1989), and Ottawa meteoric water line, Ontario (Fritz et al., 1987).*

## CONCLUSION

This preliminary groundwater isotopic study of the Laurentian piedmont aquifer provides useful information on the isotopic attributes of groundwater in Quebec, which are still poorly known considering the abundance and the use of this resource. Isotopic results support a relatively short residence time for most groundwater samples of the Portneuf aquifers. The $\delta^{13}C_{DIC}$ shows limestone effects on groundwater composition in a sample from a sandy aquifer formation in the Neuville municipality. Stable isotope results also suggest that recharge occurred mainly by snow melting during spring, with a minor autumnal input. At this stage of the investigation, the main particularity of the Laurentian piedmont groundwater is the uncommon deuterium excess of 14.8‰ which results from the specific climatic conditions of Eastern Canada.

## ACKNOWLEDGMENTS

The authors would like to thank G. Saint-Jean (University of Ottawa) and M. Luzincourt (Delta-lab, GSC-Québec) for their technical assistance and R. Lefebvre and M. Nastev for the thoughtful review of the manuscript. This is a contribution of the Laurentian Piedmont Hydrogeology Project funded by the GSC hydrogeology program and carried out in collaboration with the Québec Ministère de l'Environnement, Université Laval and Portneuf region county municipality. The first author was funded by a NSERC PDF research grant. Preliminary versions of the manuscript benefited from useful comments provided by internal and external readers.

## REFERENCES

**Balderer, W., Rauert, W., and Stichler, W.**
1987: Environmental isotope study of the deep groundwater in Northern Switzerland; International Atomic Energy Agency, IAEA-SM 299/114, p. 455–474.

**Bathurst, R.G.C.**
1975: Carbonate and Their Diagenesis: Development in Sedimentology No. 12; Elsevier, Amsterdam, Oxford, New York, 658 p. (second enlarged edition).

**Bourque, É., Laflèche, M.R., Lefebvre, R. et Michaud, Y.**
1996: Résultats initiaux de la caractérisation géochimique des aquifères du piémont Laurentien dans la municipalité régionale de Comtés de Portneuf (Québec); dans Recherches en cours 1996-E; Commission géologique du Canada, p. 225–232.

**Bourque, É., Michaud, Y., Lefebvre, R. et Boisvert, É.**
1998: Cartographie hydrogéologique régionale du Piémont Laurentien dans la MRC de Portneuf: hydrogéochimie des eaux souterraines; Commission Géologique du Canada, Dossier public 3664-c, 1 feuille.

**Brown, R.M.**
1970: Distribution of hydrogen in Canadians waters; *in* Isotope hydrology 1970. Proceedings of a Symposium in Hydrology; International Atomic Energy Agency, 9–13 March 1970, Proceedings Series IAEA-SM 129/1, p. 3–21.

**Bryson, R.A. and Hare, F.K. (ed.)**
1974: Climates of North America. World Survey of Climatology; (ed.) H.E. Landsberg; Elsevier, Amsterdam. v. 11, 420 p.

**Clark, I. and Fritz, P.**
1997: Environmental Isotopes in Hydrogeology; Lewis Publishers, New York, 328 p.

**Clark, T. and Globensky, Y.**
1975: Rapport géologique-154. Région de Grondines; Service de l'exploration géologique, Ministère des richesses naturelles, direction générale des Mines, 175 p.

**Cloutier, M., Parent, M., and Bolduc, A.**
1997: Géologie des formations superficielles, région de Saint-Marc-des-carrieres, Québec; Commission géologique du Canada, Dossier public 3544, échelle 1/100 000.

**Coleman, M.L., Shepherd, T.J., Durham, J.J., Rousse, J.E., and Moore, G.R.**
1982: Reduction of water with zinc for hydrogen isotope analysis; Analytical Chemistry, v. 54, no. 6, p. 993–995.

**Coplen, T.B.**
1993: Uses of Environmental Isotopes; *in* Regional Ground-Water Quality, (ed.) W.M. Alley; Van Nostrand Reinhold, New York, New York, p. 227–254.

**Craig, H.**
1961: Isotopic variations in meteoric waters; Science, v. 133, p. 1702–1703.

**Dansgaard, W.**
1964: Stable isotopes in precipitation; Tellus, v. 16, no. 4, p. 436–468.

**Drever, J.I.**
1997: The Geochemistry of Natural Waters: Surface and Groundwater Environments; Prentice Hall, New Jersey, 436 p. (third edition).

**Dudziak A.**
1994: Diurnal variation of $^{13}C/^{12}C$ ratio in soil $CO_2$ under wheat and grass; *in* Extended abstracts, Isotope Workshop II, (ed.) M.O. Jedrysek. May 1994, International Isotope Society, University of Wroclaw, Ksiaz Castle, Poland, p. 17–19.

**Ebhardt, G. and Fritsch, P.**
1992: Influence of fine-grained cover beds on the chemistry of shallow ground water; *in* Progress in Hydrogeochemistry, G. Matthess, F. Frimmel, P. Hirsch, H.D. Schulz, and E. Usdowski; Springer, New York, p. 226–237.

**Epstein, S. and Mayeda, T.**
1953: Variation of $^{18}O$ content of waters from natural sources; Geochimica et Cosmochimica Acta, v. 4, p. 213–224.

**Fagnan, N.**
1998: Cartographie hydrogéologique régionale et vulnérabilité des aquifères de la MRC de Portneuf; Mémoire de Maîtrise, Université du Québec, INRS Géoressources, 263 p.

**Fagnan N., Bourque, É., Michaud, Y., Lefebvre, R., Boisvert, É., Parent, M. et Martel, R.**
in press: Hydrogéologie des complexes deltaïques sur la marge nord de la Mer de Champlain; Hydrogéologie, BRGM, Numéro spécial sur l'hydrogéologie du Québec.

**Fagnan, N., Michaud, Y., Lefebvre, R., Boisvert, É., Parent, M., Martel, R., Paradis, D. et Larose-Charette, D.**
1998: Cartographie hydrogéologique régionale du Piémont Laurentien dans la MRC de Portneuf : hydrostratigraphie et piézométrie des aquifères granulaires de surface; Commission géologique du Canada, Dossier public 3664-b, 1 feuille.

**Fontes, J.Ch.**
1980: Environmental isotopes in groundwater hydrology; *in* Handbook of Environmental Isotope Geochemistry, (ed.) P. Fritz and J.Ch. Fontes, Elsevier, Amsterdam, Netherlands, p. 75–140.
1994: Isotope palaeohydrology and the prediction of long-term repository behaviour; Terra Nova, v. 6, p. 20–36.

**Fritz, P., Drimmie, R.J., Frape, S.K., and O'Shea, K.**
1987: The isotopic composition of precipitation and groundwater in Canada; *in* Proceedings, International Symposium on the Use of Isotope Techniques in Water Resources Development; International Atomic Energy Agency, IAEA-SM-299/17, p. 539–550.

**Fry, B. and Sherr, E.B.**
1988: $\delta^{13}C$ measurements as indicators of carbon flow in marine and freshwater ecosystems; *in* Stable Isotopes in Ecological Research, (ed.) P.W. Rundel, J.R. Ehleringer and K.A. Nagy; Ecological Studies 68, Springer Verlag, New York, New York, p. 196–229.

**Gat, J.R.**
1996: Oxygen and hydrogen isotopes in the hydrologic cycle; Annual Review of Earth and Planetary Science, v. 24, p. 225–262.

**Gat, J.R. and Carmi, I.**
1970: Evolution of the isotopic composition of atmospheric waters in the Mediterranean Sea area; Journal of Geophysical Research, v. 75, p. 3039–3048.

**Gat, J.R. and Dansgaard, W.**
1972: Stable isotope survey of fresh water occurrences in Israel and the Northern Jordan Rift Valley; Journal of Hydrology, v. 16, p. 177–212.

**Gerber, R.E. and Howard, K.W.F.**
1996: Evidence for recent groundwater flow through Late Wisconsinan till near Toronto; Canadian Geotechnical Journal, v. 33, p. 538–555.

**Gerritse, R.G. and Van Driel, W.**
1984: The relationship between adsorption of trace metals, organic matter, and pH in temperate soils; Journal of Environmental Quality, v.13, no. 2, p. 197–204.

**Globensky, Y.**
1987: Géologie des Basses-Terres du Saint-Laurent; Ministère de l'énergie et des ressources du Québec, MM 85-02, 63 p.

**Heller, R.**
1981: Abrégé de physiologie végétale; Masson, Paris, France, 244 p.

**Kendall, C., Sklash, M.G., and Bullen, T.D.**
1995: Isotope tracers of water and solute sources in catchments; *in* Solute Modelling in Catchment Systems, John Wiley and Sons, Chichester, United Kingdom, p. 261–303.

**Klopmann, W., Dever, L., and Edmunds, W-M.**
1994: Isotopic and geochemical investigations of Chalk; Groundwater of the Champagne Region, France. Zeitschrift der Deutschen Geologischen Gesellschaft, no. 145,Verlag Ferdinand Enke, Stuttgart, Federal Republic of Germany, p. 143–152.

**Lavoie, D.**
1993: Lithostratigraphy and paleoenvironmental evolution of the Upper Ordovician Trenton Group, southern Quebec; *in* Current Research, Part D; Geological Survey of Canada, Paper 93-1D, p. 161–172.

**Lohmann, K.C.**
1988: Geochemical patterns of meteoric diagenetic systems and their application to studies of Paleokarst; *in* Paleokarst, (ed.) N.P. James and P.W. Choquette, Springer-Verlag, New York, New York, p. 58–80.

**Lohmann, K.C. and Walker, J.C.G.**
1989: The $d^{18}O$ record of Phanerozoic abiotic marine calcite cements; Geophysical Research Letters, v. 16, no. 4, p. 319–322.

**Michaud, Y., Lefebvre, R., Martel, R., Parent, M., Bolduc, A., Boisvert, E., Bourque, E., Fagnan, N., and Paradis, D.**
1997: Le projet piémont laurentien. Application de la cartographie hydrogéologique régionale à la gestion de la ressource en eaux souterraines; Vecteur Environnement, vol. 30, n° 4, p. 22–23.

**Mook, W.G.**
1980: Carbon-14 in hydrogeological studies; *in* Handbook of Environmental Isotope Geochemistry, (ed.) P. Fritz and J.Ch. Fontes; Elsevier, Amsterdam, Netherlands, p. 49–74.

**Moore, R.D.**
1989: Tracing runoff sources with deuterium and oxygen-18 during spring melt in a headwater catchment, southern Laurentians, Québec; Journal of Hydrology, v. 112, p. 135–148.

**O'Leary, M.H.**
1988: Carbon isotope in photosynthesis; Bioscience, v. 38, p. 328–336.

**Paradis, D., Lefebvre, R., and Michaud, Y.**
1997: Analyse hydrologique pour l'évaluation de la recharge en eau souterraine dans le bassin versant de la rivière Portneuf sur le Piémont Laurentien (Québec); dans Recherches en cours 1997-E; Commission géologique du Canada, p. 83–88.

**Parent, M., Michaud, Y., Boisvert, É., Bolduc, A.M., Fagnan, N., Fortier, R., Cloutier, M. et Doiron, A.**
1998: Cartographie hydrogéologique régionale du Piémont Laurentien dans la MRC de Portneuf : géologie et stratigraphie des formations superficielles; Commission géologique du Canada, Dossier public 3664-a, 1 feuille.

**Pawellek, F. and Veizer, J.**
1994: Carbon cycle in the upper Danube and its tributaries: $d^{13}C_{DIC}$ constraints; Israel Journal of Earth Sciences, v. 43, p. 187–194.

**Probst, J.L., Mortatti, J., and Tardy, Y.**
1994: Carbon river fluxes and weathering $CO_2$ consumption in the Congo and Amazon river basins; Applied Geochemistry, v. 9, p. 1–13.

**Vitali, F., Savard, M.M., and Bourque, É.**
1997: Premiers résultats de la caractérisation isotopique des aquifères de la région de Portneuf, Québec; dans Recherches en cours 1997-E; Commission géologique du Canada. p. 89–95.

**Wigley, T.M., Plummer, L.N., and Pearson, F.J.**
1978: Mass transfer and carbon isotope evolution in natural water systems; Geochimica et Cosmochimica Acta, v. 42, p. 1117–1139.

**Wilson, C.W.**
1971: Le climat du Québec; Service météorologique du Canada, Études climatologique, vol. 11, Part I.

Geological Survey of Canada Project 960001 HD

# New observations on relict volcanic features in medium-grade gneiss of the Montauban group, Grenville Province, Quebec

L. Nadeau, P. Brouillette, and C. Hébert[1]
GSC Quebec, Sainte-Foy

*Nadeau, L., Brouillette, P., and Hébert, C., 1999: New observations on relict volcanic features in medium-grade gneiss of the Montauban group, Grenville Province, Quebec;* in *Current Research 1999-E; Geological Survey of Canada, p. 149–160.*

**Abstract:** The Montauban region, south-central Grenville Province, is known for its small, stratiform, polymetallic Au-Ag-Zn-Pb ore deposits. The amphibolite-facies orebodies and hydrothermally altered wall rocks occur within the ca. 1.45 Ga Montauban group, a sequence dominated by quartzofeldspathic gneiss with minor quartzite and amphibolite, locally pillowed metabasalt, and sporadic outcrops of marble and calc-silicate rocks.

Occurrences of lapilli tuff are reported, namely from the structural footwall-stratigraphic hanging wall of the orebodies. This is the first unequivocal example of felsic volcanic rocks in the Montauban group. Proximal lapilli tuff and vesicular basaltic pillow lava occur with thinly bedded intermediate to felsic rocks interpreted as distal pyroclastic subaqueous fallout deposits, and laterally intercalated epiclastic sediments.

Such volcanic rocks are consistent with deposition of the Montauban group in a shallow submarine environment at the late stage of an andesitic to felsic volcanic cycle, a common occurrence in mature island-arc or backarc settings where Au-rich volcanogenic sulphide deposits are formed.

**Résumé :** La région de Montauban, dans le centre sud de la Province de Grenville, est connue pour ses petits gisements stratiformes polymétalliques de Au-Ag-Zn-Pb. La zone minéralisée et son enveloppe d'altération hydrothermale, métamorphisées au faciès des amphibolites, appartiennent au groupe de Montauban. Ce groupe, qui remonte à 1,45 Ga environ, se compose principalement de gneiss quartzofeldspathiques, mais renferme aussi des quantités mineures de quartzite et d'amphibolite, dont des métabasaltes en coussins par endroits, ainsi que des affleurements épars de marbre et de roches calco-silicatées.

Des tufs à lapilli ont été identifiés à plusieurs endroits, dont l'un d'intérêt particulier se situe dans le mur structural de la zone minéralisée, mais dans le toit stratigraphique de celle-ci. Ces affleurements fournissent les premiers exemples non ambigus de roches volcaniques felsiques au sein du groupe de Montauban. Les tufs à lapilli et les laves basaltiques en coussins vésiculaires, qui correspondent à des dépôts de faciès proximal, sont associés à des roches intermédiaires à felsiques finement litées, qui seraient des cendres volcaniques de faciès distal. Ces roches sont imbriquées latéralement avec des roches sédimentaires épiclastiques.

Cette association lithologique indique que le groupe de Montauban s'est accumulé en milieu sous-marin peu profond, au stade tardif d'un cycle volcanique andésitique à felsique. Ces conditions sont typiques des environnements matures d'arc insulaire et de bassin d'arrière-arc où se forment des dépôts de sulfures massifs volcanogènes riches en or.

[1] Géologie Québec, 5700 4e avenue ouest, Charlesbourg, Québec G1H 6R1

## INTRODUCTION

The origin of large tracts of medium- to high-grade quartzofeldspathic gneiss in the Grenville Province remains obscure, thus hindering lithostratigraphic and tectonic reconstruction. Quartzofeldspathic gneiss in the Montauban region is no exception (Fig. 1, 2, 3). This gneiss and associated subordinate amphibolite, locally containing preserved relict pillow structure, are included in the Montauban group, named and defined by Rondot (1978). In the absence of geochemical fingerprinting, the recognition of relict primary features provides essential clues for the proper interpretation of these rocks. Until recently, the metabasaltic pillow lava at Mont Tétreault constituted the only known locality of volcanic rock in the region. Recently, however, a number of additional occurrences of relict volcanic features, including felsic lapilli tuff, have been found, hence shedding new light on the origin of some of the quartzofeldspathic gneissic rocks of the Montauban group. In addition, U-Pb dating of igneous zircon from a lapilli tuff indicates an age of extrusion ca. 1.45 Ga for the volcanic rocks of the Montauban group (Nadeau and van Breemen, 1994).

In this paper, we provide detailed field descriptions, a photographic record, and the location of these occurrences (Table 1); we discuss the nature and origin of the associated quartzofeldspathic gneiss; and we explore the relevance of these observations to the volcanic stratigraphy and paleotectonic setting. Studies in progress are focusing on detailed petrography and geochemistry.

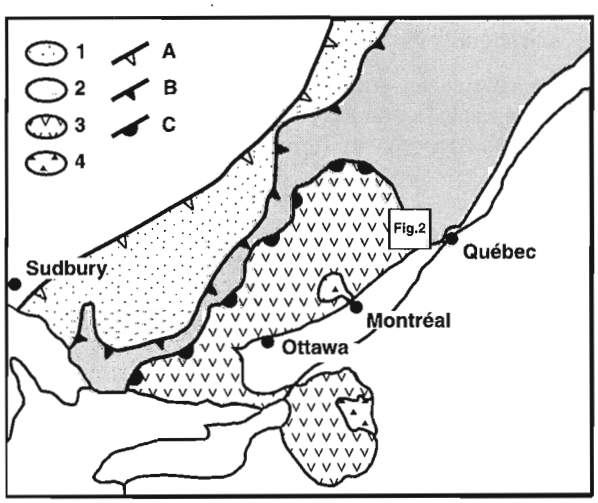


***Figure 1.*** *Location sketch map and tectonic subdivisions of the Grenville Province (modified from Rivers et al., 1989). Legend: 1, parautochthonous belt; 2, allochthonous polycyclic belt; 3, allochthonous monocyclic belt; 4, anorthosite-mangerite-charnockite-granite suite; A, Grenville Front; B, allochthon boundary thrust; C, monocyclic belt boundary thrust.*

### *Historical development*

The occurrence of gold- and silver-bearing polymetallic lead-zinc sulphide mineralization in calc-silicate rocks and associated quartzofeldspathic gneiss at Montauban has been known since 1910. Intermittent mining took place from 1914 to 1989. Through 1965, estimated total production was 2.7 million metric tonnes of massive sulphide ore grading 6.8% Zn, 2.3% Pb, 1.3 g/t Au, and 131 g/t Ag (Lavergne, 1985). In addition, 2571 kg of gold and 8068 kg of silver were

**Table 1.** Type and localities of relict volcanic features.

| Locality | Easting (UTM zone 18, NAD 27) | Northing | Geographic name |
|---|---|---|---|
| Metabasaltic pillow lava | | | |
| 1.1 | 701000 | 5190175 | Mont Tétreault |
| 2 | 699100 | 5194550 | Lac aux Sables |
| 3 | 708875 | 5202675 | Rousseau |
| Sheared metabasaltic pillow lava | | | |
| 4 | 704100 | 5193150 | Notre-Dame-de-Montauban |
| 5 | 702300 | 5192250 | Cyprès |
| 6 | 712600 | 5206750 | Rivière-à-Pierre |
| 7 | 693900 | 5227200 | Dussault |
| Fragmental mafic rock | | | |
| 8 | 707900 | 5195650 | Lac des Pins |
| Felsic lapilli tuff | | | |
| 1.3 | 701525 | 5189500 | Montauban-les-Mines |
| 9 | 710375 | 5209400 | Lac Gagnon |
| 10 | 689300 | 5207600 | Lac Roy |
| Hydrothermally altered lapilli tuff | | | |
| 1.4 | 701875 | 5189300 | Montauban-les-Mines |
| Thinly bedded intermediate and felsic tuff | | | |
| 1.2 | 701500 | 5189700 | Montauban-les-Mines |

***Figure 2.*** *Geological sketch map of the Montauban region, and occurrences of relict volcanic features. Legend: 1, granite-monzonite of the Rivière-à-Pierre suite; 2, metamonzonite-metagabbro of Lejeune complex; 3, Lapeyrère gabbronorite; 4, granulitic gneiss of Mékinac-Taureau domain; 5, metadiorite-metagabbro and tectonic mélange of Jésuite complex; 6, Saint-Ubalde leucogranitic orthogneiss; 7, Lac à l'Ours granodioritic orthogneiss; 8–11, La Bostonnais complex including: 8, granodioritic-monzodioritic migmatitic orthogneiss, 9, metagabbro-diorite, 10, metagranodiorite-tonalite, 11, granodioritic-tonalitic migmatitic orthogneiss; 12–15, Montauban group including: 12, metabasalt, 13, quartzite, 14, hornblende-biotite paragneiss, 15, sillimanite±muscovite±garnet-biotite paragneiss; 16, sheared lithological contact; 17, oblique-extensional ductile shear zone; 18, tectonic boundary of Mékinac–Taureau domain; 19, tectonic boundary beneath Portneuf–Mauricie domain; 20, boundary of Parc des Laurentides domain; 21, post-Grenvillian normal fault. Circled numbers are localities discussed in the text.*

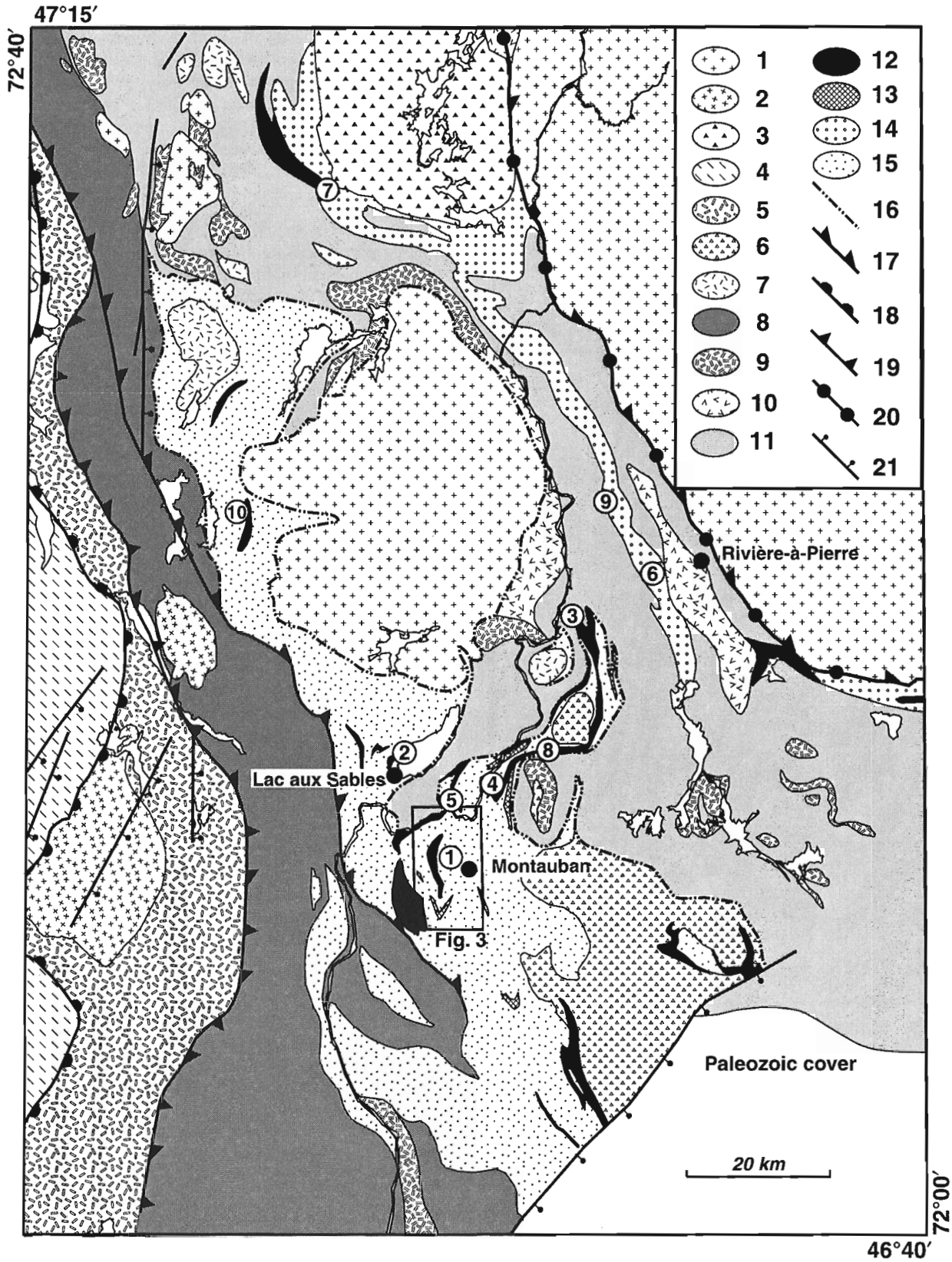
47°15′
72°40′
72°00′
46°40′
1
2
3
4
5
6
7
8
9
10
11
12
13
14
15
16
17
18
19
20
21
Rivière-à-Pierre
Lac aux Sables
Montauban
Fig. 3
Paleozoic cover
20 km

extracted between 1983 and 1989 from 0.9 million tonnes of disseminated sulphide ore grading 3.6 g/t Au and 17.7 g/t Ag (Hébert and Gobeil, 1991).

Although modest, the mineral deposits at Montauban are of special interest because they occur in hydrothermal alteration zones which share many similarities with recently documented high-sulfidation volcanogenic massive sulphide deposits (Sillitoe et al., 1996; Hannington et al., 1998), and

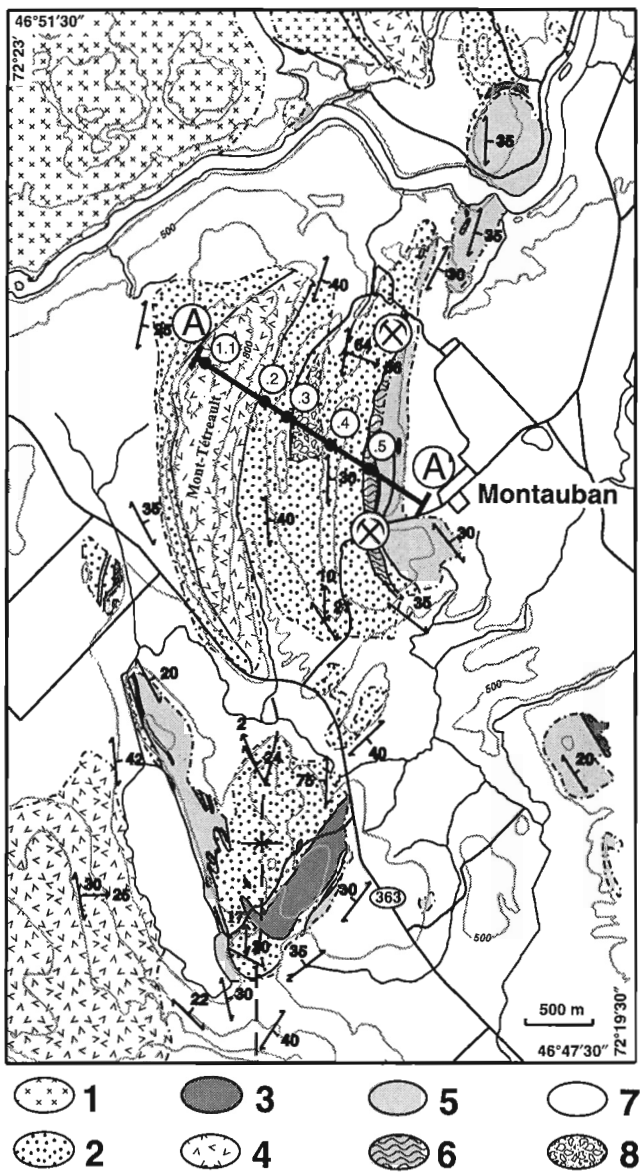


***Figure 3.*** *Geological sketch map of the Montauban area (modified from Smith (1956)) with localities of relict volcanic features. Legend: 1, La Bostonnais complex granodiorite; 2–6) Montauban group including: 2, layered sillimanite±garnet±muscovite-biotite gneiss, 3, quartzite, 4, metabasaltic pillow lava and amphibolite, 5, grey composite gneiss, 6, mine sequence; 7, overburden; and 8, mine tailings. Section A-A' refers to Figure 9. Circled numbers on figure refer to locality 1 (e.g. .2, .3, etc. refer to specific sites).*

along with Calumet and Balmat-Edwards, they are the most significant base-metal deposits in the Grenville Province. The mineralogy of the Montauban orebodies and the conformable association of these orebodies with calc-silicate rocks and metamorphosed hydrothermally altered wall rocks underpin the interpretation that they are either sedimentary-hosted exhalative deposits (SEDEX; Prabhu, 1981; Morin, 1987) or volcanogenic massive sulphide deposits (VMS; Sangster, 1972; Stamatelopoulou-Seymour and MacLean, 1977; MacLean et al., 1982; Bernier et al., 1987; Bernier and MacLean, 1993).

The latter interpretation requires that the quartzofeldspathic gneiss hosting the ore deposits is chiefly volcanic in origin, hence calling for a reappraisal of its previous interpretation as detrital metasediments. This interpretation was proposed on account of their prominent layering, the presence of thin and discontinuous quartzite layers, and the sporadic occurrence of calc-silicate rocks (e.g. Bancroft, 1915; Osborne, 1939; Smith, 1956; Pyke, 1967; Prabhu and Webber, 1984; Morin, 1987). Osborne (1939) was first to suggest that some amphibolite could be volcanic in origin. The discovery by Pyke (1966, 1967) of metabasaltic pillow lava at Mont Tétreault, approximately 1 km west and structurally in the footwall of the ore zone (Fig. 2, 3), constitutes the first direct evidence for the occurrence of volcanic rocks in the sequence.

Following this discovery, several workers applied geochemical discriminants, using major element data, to try to unravel the origin of the associated layered quartzofeldspathic gneiss. Recognizing igneous differentiation trends and close compositional similarities between some of the gneiss and intermediate and acidic volcanic rocks of the Noranda district of Quebec and Kuroko district of Japan, Stamatelopoulou-Seymour (1975) and Stamatelopoulou-Seymour and MacLean (1977) suggested that the protoliths were probably intermediate and acidic tuffs and derived epiclastic sediments. Conversely, Prabhu and Webber (1984), using the lithogeochemical data set of Prabhu (1981), concluded that most of the quartzofeldspathic gneiss was derived from greywacke or sandstone, emphasizing the local association with quartzite, calc-silicate gneiss, and mica schist to support their conclusions. They recognized, however, that about 20% of their samples could have had an igneous origin.

Subsequent workers have interpreted the quartzofeldspathic gneiss as chiefly sedimentary (Morin, 1987; Jourdain et al., 1987), or eluded the question by referring to them as "derived from volcaniclastic rocks" (Bernier and MacLean, 1993), a general term applying to "...all clastic volcanic materials formed by any process of fragmentation, dispersed by any kind of transportation agent, deposited in any environment or mixed in any significant proportion with nonvolcanic fragments..." (Fisher and Schmincke, 1984, p. 89).

## *Local geological setting*

The geology of the Montauban area and its regional tectonic framework have been studied anew by Morin (1987) and Hocq and Dufour (1999). The Montauban group (Rondot, 1978) is made up of a medium-grade sequence of well

layered, intermediate to felsic gneiss with intercalated subordinate amphibolite, locally pillowed metabasalt, and minor quartzite, which set the region apart from adjacent high-grade Grenvillian terranes (Fig. 2). The following remarks are limited to those aspects of the local geology that are directly relevant to the present study.

The rocks of the Montauban area have been regionally metamorphosed to almandine-amphibolite facies, with estimated peak metamorphic conditions in the range 4.5–6.5 kbar and 550–620°C (Bernier and MacLean, 1993). Pronounced mineral foliation is generally parallel to compositional layering. The planar fabric undulates smoothly along strike and dips gently to moderately eastward (Fig. 3). Mineral lineation is variably developed, generally subtle in quartzofeldspathic gneiss but may be pronounced in amphibolite. Locally occurring stretched pillows and lapilli fragments with aspect ratios on the order of 1:3:<10 suggests significant ductile deformation.

The large-scale deformation pattern of the Montauban region is not fully understood. Fold interference and possibly ductile faulting preclude tracing of structural markers in discontinuous outcrops. Minor folds are sporadically exposed between the abandoned mine workings and Mont Tétreault. They are consistently Z-type with easterly shallowly to moderately dipping axial planes, and subhorizontal to shallow-plunging axes parallel to the local mineral and stretching lineations. This is consistent with the sequence being part of the inverted limb of a larger north-plunging and west-verging synform (Fig. 3; *see also* Morin (1987) and Jourdain et al. (1987)).

### *The mine sequence*

The petrogenesis of the mine sequence has been described in detail by Bernier and MacLean (1993). This informal unit includes the various rock types genetically associated with the orebodies and forming their wall rocks (Fig. 3). The mine sequence is structurally conformable with regional structural fabric, at most a few tens of metres thick, and extends more than 2.5 km along strike, with the ore occurring as discontinuous tabular bodies several hundreds of metres long. The following two types of orebody are present: Pb-Zn massive sulphides in calc-silicate rocks, and Au-Ag-rich disseminated sulphides in garnet-gahnite-biotite quartzitic gneiss. The latter are mantled by distinctive cordierite-anthophyllite and cordierite-biotite gneiss and schist. The orebodies and immediate wall rocks are incompletely enveloped in quartzitic biotite-muscovite gneiss with distinctive lenticular sillimanite mats up to 1 cm thick. This rock unit, locally called 'nodular-sillimanite gneiss', is considered to reach a maximum thickness close to 10 m adjacent the cordierite-anthophyllite quartzitic gneiss.

## PRESERVED VOLCANIC FEATURES

### *Metabasaltic pillow lava*

Pyke (1966) was the first to recognize pillow in mafic rocks at Mont Tétreault (locality 1.1; Fig. 4). The rocks retain neither primary texture nor mineralogy in thin section. They have a

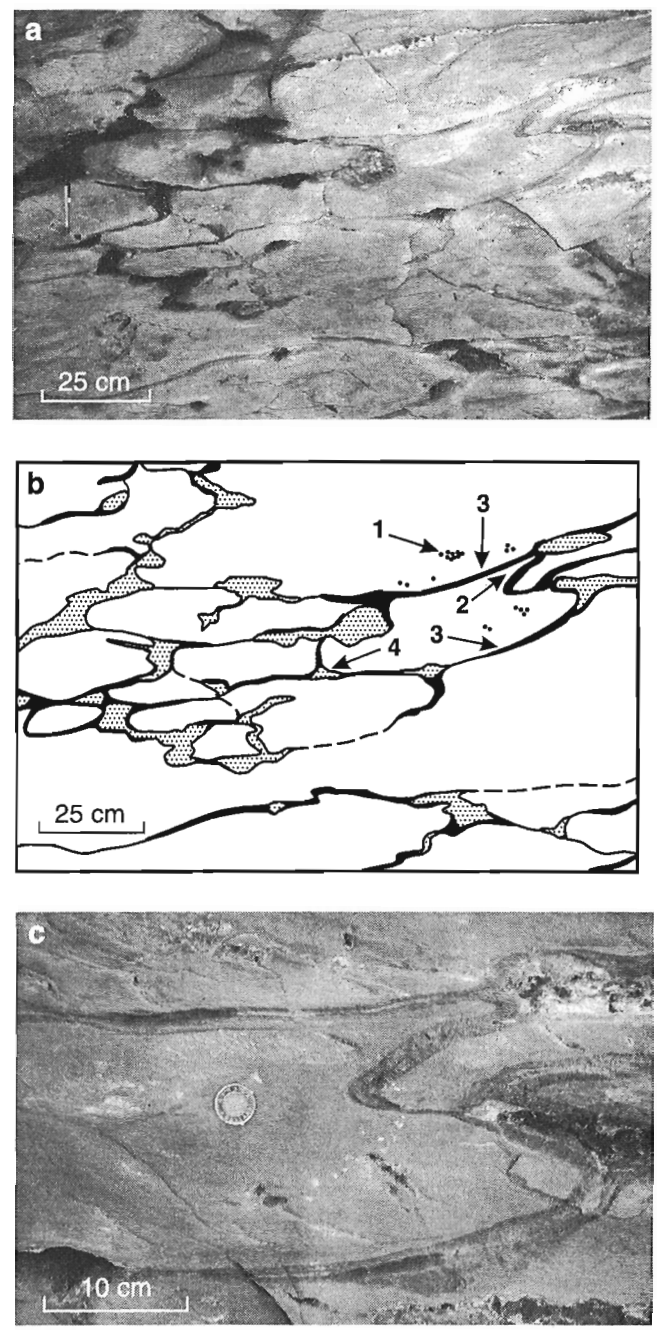


***Figure 4.*** *Pillow structure in metabasalt at Mont Tétreault (locality 1.1):* ***a)*** *decimetric size, bulbous, slightly flattened pillows are viewed in section at high angle to the stretching direction. The weathered recessed pillow interspaces are filled with calc-silicate minerals.* ***b)*** *line drawing of* ***a)*** *highlighting the pillow morphology: note that the distribution of the vesicles 1), the pillow peduncle 2), the curvature of the selvage 3), and the triangular shape of the interspace 4) indicate a top-side-down facing direction;* ***c)*** *close-up showing the thin pillow selvage, coarsening of relict grain size in the pillow core, and a few weathered, recessed calcite-filled vesicles.*

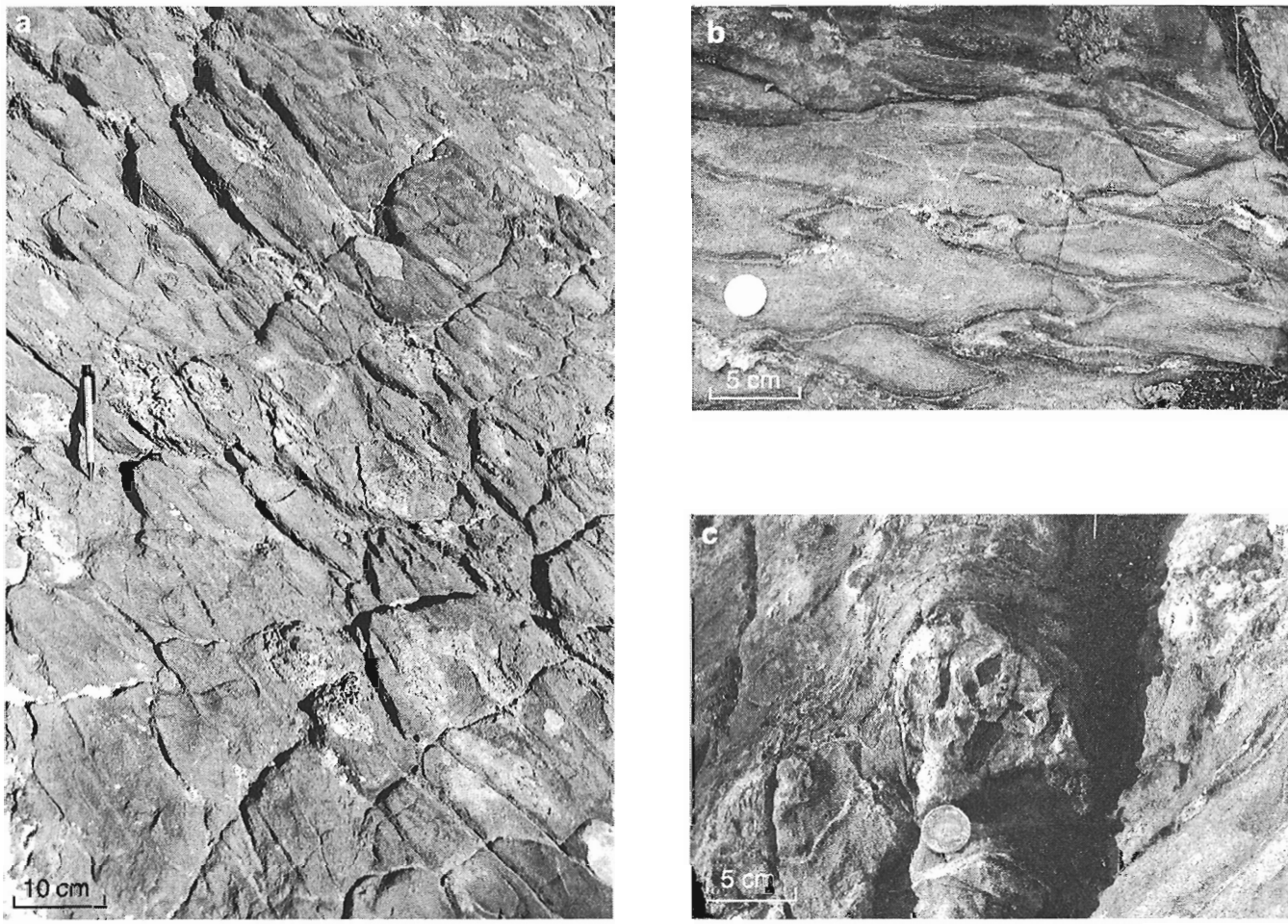


***Figure 5.*** *Pillowed metabasalt at Rousseau (locality 3):* ***a), b)*** *deformed pillows in sections respectively oblique and at high angle to the stretching direction; note the decimetric size of the pillows and the thickness of the selvages;* ***c)*** *close-up showing hyaloclastic interpillow matrix.*

fine-grained, granoblastic nematoblastic texture, and are essentially composed of hornblende-augite-plagioclase, in places with accessory epidote and tiny garnet crystals which occur sporadically along pillow salvages suggesting subtle compositional variations.

At the type locality, pillows are recognized by their flattened bulbous shapes, with well defined, 1–2 cm thick fine-grained salvages (Fig. 4). They are a few decimetres in diameter, and display ellipsoidal shape in oblique section looking down the stretching direction (Fig. 4a). Contacts between pillows are smoothly undulating, sharp and thin with weathered, recessed, irregular interspaces filled with calcite and calc-silicate minerals (Fig. 4b). Salvages exhibit granoblastic texture with a grain size markedly finer than that of the pillow cores. Locally, calcite-filled vesicles up to 5 mm in diameter are preserved, testifying to shallow subaqueous extrusion. The facing direction, deduced from overall morphology, indicates that the section at Mont Tétreault is overturned (Fig. 4b). Well preserved pillows with a hyaloclastic interpillow matrix are exposed at locality 3 (Fig. 5), and segments of pillow salvage have been recognized in displaced blocks at locality 2. In addition, heterogeneous amphibolite with calc-silicate pods resembling pillow interspaces occurs at locality 4, 5, 6, and 7.

### *Fragmental and altered mafic rocks*

The mafic rocks at Lac des Pins exhibit a number of features that set them apart from the pillowed basalt described above. The rocks grade within 20 m across strike in discontinuous outcrops from lower-strained foliated amphibolite containing abundant flattened felsic fragments up to 5 cm thick by 40 cm long, to a compositionally equivalent, thinly layered, mylonitic straight gneiss (compare Fig. 6a and 6d). The fragments in the lower-strain rocks are presumed primary because they are randomly distributed, and show no structures such as rootless isoclinal fold closures that might suggest boudinage, or isoclinal folding. The less strained rocks resemble an agglomerate, with cognate, fine-grained, flattened, felsic blocks (Fig. 6a). The fragments are matrix supported and compose up to 25% of the rock. The unit is exposed over 10 m of structural thickness and contains two layers of homogeneous amphibolite, perhaps derived from massive basaltic flows.

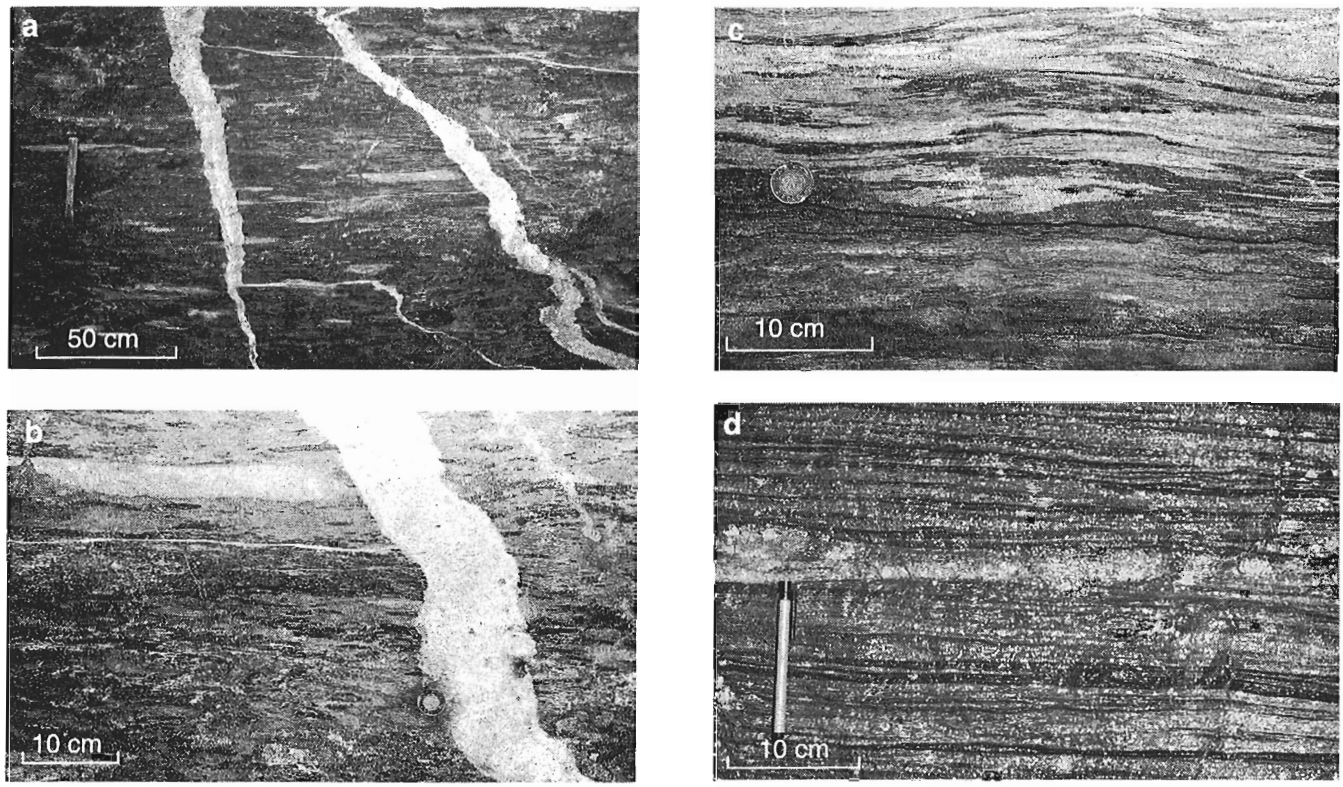


***Figure 6.*** *Hydrothermally altered metabasalt with felsic fragments at Lac des Pins (locality 8):* ***a)*** *flattened, matrix-supported, felsic fragments in amphibolite;* ***b), c)*** *close-up highlighting the composite nature of the matrix, and the delicately sutured contact between dark hornblende-rich, and lighter clinopyroxene-rich parts of the matrix; and* ***d)*** *derived straight gneiss.*

The matrix in the lower strain rocks is heterogeneous (Fig. 6b, c). Locally it contains hornblende-free and markedly more felsic, light greenish, irregular, flame-like patches of clinopyroxene and plagioclase interspersed and contrasting with dark green to black hornblende-plagioclase matrix. The composite nature of the matrix is tentatively attributed to the effects of hydrothermal alteration accentuated by the development of distinct high-grade metamorphic assemblages. These parageneses and textural relationships are best seen on newly uncovered, glacially polished surfaces. Elsewhere, the outcrop surface is variably weathered, with high-standing, black, hornblende-plagioclase amphibolite and, irregular, deeply weathered, rusty-brown, pyritic zones. Ubiquitous disseminated pyrite may also be related to hydrothermal alteration.

### *Felsic lapilli tuff*

Metamorphosed lapilli tuff consisting of approximately 40% white ellipsoidal, monomictic, very fine-grained, felsic fragments in a grey foliated matrix is well exposed at locality 1.3 (Fig. 3, 7a, 7b). The fragments and the matrix are finely recrystallized and have a sugary texture. The fragments are matrix supported, generally less than 1 cm thick, and range in length from 1 cm to approximately 15 cm. Most are 3–5 cm long. The present shape of the fragments is likely to reflect both the initial flattened form of the lapilli, and subsequent regional deformation. The matrix is slightly coarser grained and more mafic than the clasts with approximately 5% biotite. Mesoscopic bedding is not apparent in this unit which is discontinuously exposed across strike over a distance of 10 m. Beside being the first unambiguous felsic volcanic rock to be recognized in the area, the lapilli tuff at locality 1.3 is of special interest because it contains zircons with a distinctive internal igneous morphology that have yielded a U-Pb age ca. 1.45 Ga (Nadeau and van Breemen, 1994). This age is taken to mark the age of volcanism and deposition of the Montauban group. Similar lapilli tuff occurs as metre-thick units at locality 9 and 10 (Fig. 2), and form distinctive decimetre-thick beds within the 'thinly bedded intermediate and felsic tuff' described below (Fig. 7c).

Most of the rocks exposed between the lapilli tuff at locality 1.3 and the mine sequence, including occurrences of nodular-sillimanite gneiss, retain the thick and poorly marked bedding characteristic of the lapilli tuff. The rocks differ, however, in mineralogy and composition. They grade from granitic to rusty, sulphide-bearing, quartz-muscovite±sillimanite enriched. The siliceous rocks are here attributed to

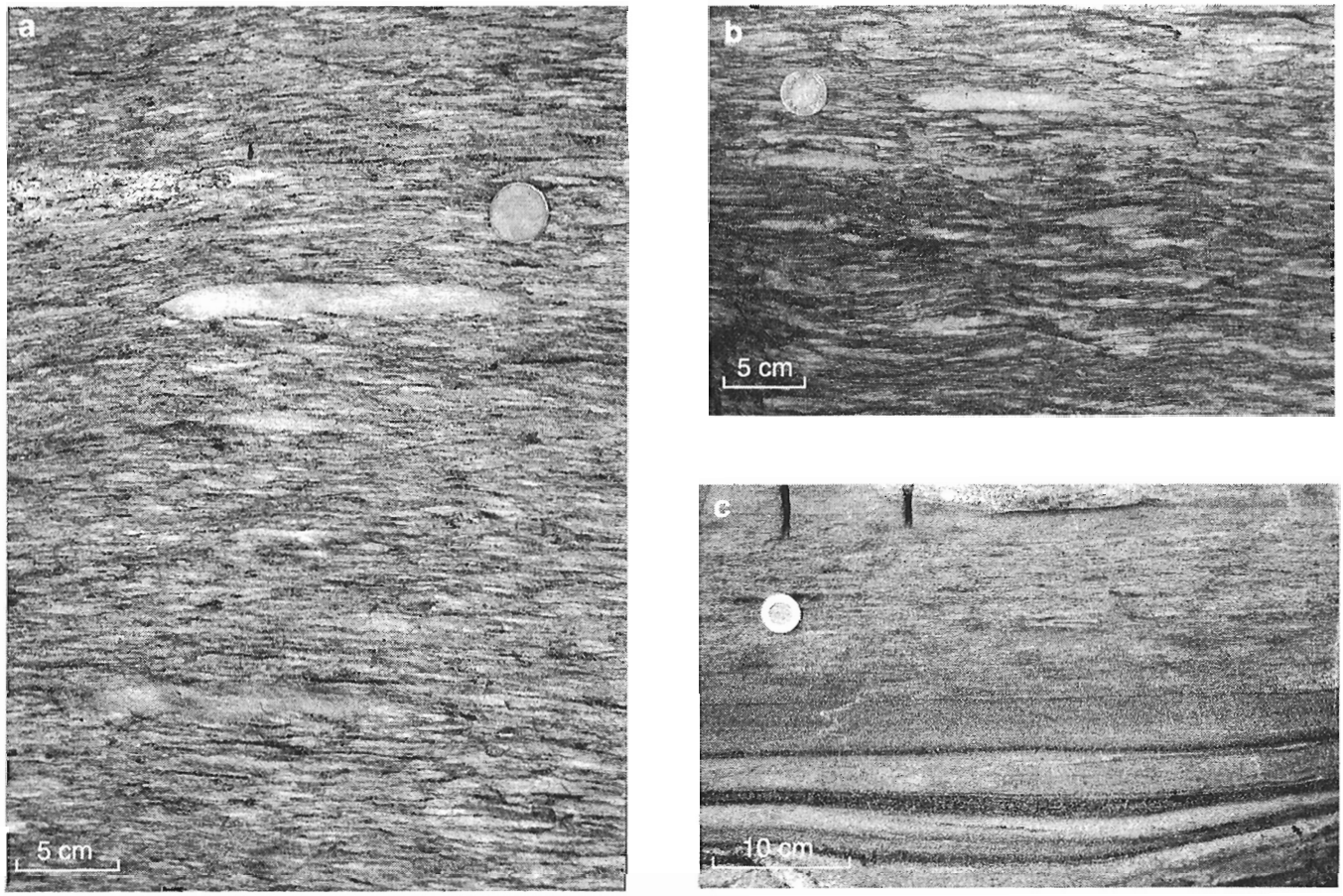


***Figure 7.*** *Felsic lapilli tuff of the Montauban section (locality 1.3):* ***a), b)*** *flattened and recrystallized, matrix-supported felsic lapilli;* ***c)*** *decimetre-thick bed of flattened granoblastic lapilli tuff in contact with thinly bedded intermediate and felsic tuff; the variation in texture suggests an overturned bedding polarity.*

acid leaching after advanced argillic hydrothermal alteration (Sillitoe et al., 1996; Hannington et al., 1998). In addition, nodular-sillimanite gneiss, distinguished by its porphyroblastic muscovite-sillimanite mats, appears to occur preferentially in rocks retaining palimpsests of lapilli fragments.

### *Thinly bedded intermediate and felsic tuff*

Rocks between the Mont Tétreault metabasalt (locality 1.1) and the lapilli tuff (locality 1.3) are thinly bedded quartzofeldspathic gneiss (Fig. 8). It is stressed that this gneiss shows neither mesoscopic ductile strain gradients, isoclinal folds, nor evidence of structural repetition. Minor decimetre-scale folds with a constant Z-type asymmetry occur sporadically throughout the section; crosscutting granitic sheets show little evidence of folding. Given the middle amphibolite-facies metamorphism and the absence of mylonitic structures, the very fine- to fine-grained granoblastic textures of these rocks are here interpreted to reflect a fine-graded protolith.

The salient characteristics of these bedded rocks are listed below.

1. Relict bedding is primarily compositional and, to a lesser extent textural; this is most obvious on weathered surfaces (Fig. 8).
2. Laminae and thin beds (1–10 cm) dominate over thicker beds (Fig. 8a). Beds thicker than 30 cm are rare.
3. Beds are generally sharply defined, and plane parallel.
4. Thin beds and laminae are laterally persistent in thickness, texture, and composition for several metres throughout the outcrops. Thicker beds are tabular and appear to be continuous along strike.
5. Compositional variations from layer to layer are chiefly in the proportion of mafic minerals (Fig. 8c). The colour index is less than 5% in the more felsic layers, ranging to approximately 20% in darker beds, and locally reaching approximately 40% in the most mafic laminae.
6. Compositional zoning is usually more pronounced in thinner than thicker beds (Fig. 8c), the latter being more homogeneous and massive (Fig. 8b).

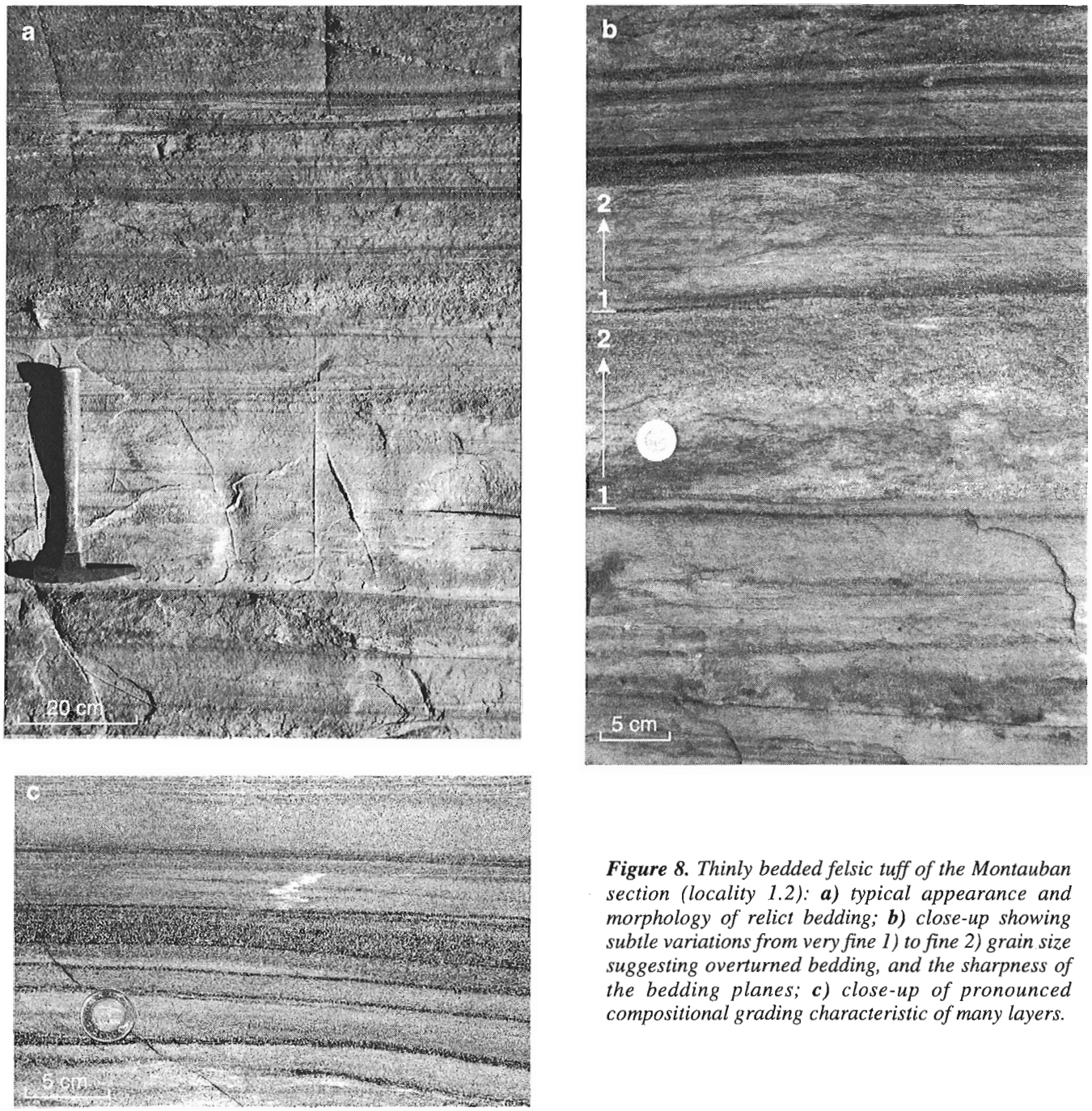


***Figure 8.*** *Thinly bedded felsic tuff of the Montauban section (locality 1.2):* ***a)*** *typical appearance and morphology of relict bedding;* ***b)*** *close-up showing subtle variations from very fine 1) to fine 2) grain size suggesting overturned bedding, and the sharpness of the bedding planes;* ***c)*** *close-up of pronounced compositional grading characteristic of many layers.*

7. The rocks generally exhibit a fine-grained, equigranular, granoblastic texture; medium- and coarse-grained varieties are absent. The mafic-rich laminae and the darker parts of the compositional zoned beds tend, however, to be slightly coarser grained than their felsic counterparts.
8. With the exception of rare beds that contain matrix-supported lenticular, recrystallized felsic fragments interpreted as lapilli tuff (Fig. 7c), the beds show no relict primary coarse clastic textures.
9. Changes in granoblastic grain size commonly occur between beds which otherwise appear mineralogically and compositional alike. These changes are considered to reflect variation in primary grain size. Similarly, subtle variation in grain size in some beds may reflect relict graded bedding.
10. Lastly, the absence of erosional and volcanic flow structures is striking.

## DISCUSSION

### *Origin of the thinly bedded felsic tuffs*

Given 1) the scarcity of porphyroblastic growth; 2) the lack of metamorphic remobilization; 3) the absence of evidence for isoclinal folding, transposition, and structural repetition; 4) the present very fine, granoblastic grain size; and 5) the pervasive nature of primary compositional layering, the rocks are interpreted to retain relict bedding, genuine depositional structures, and initial stratigraphic relationships.

The following observations and inferences together favour the interpretation that the thinly bedded tuffs are indeed metavolcanic rocks, mostly distal pyroclastic subaqueous fallout deposits with limited epiclastic reworking, although none of these criteria taken by itself is diagnostic of such an origin. Our supporting arguments are the following:

1. The thinly bedded tuffs lies stratigraphically between pillowed basalt and a thick unit of lapilli tuff.
2. The sequence includes a number of beds of coarse clastic rocks interpreted as lapilli tuff.
3. Given the quartzofeldspathic composition of the rocks and the thickness and thinly bedded nature of the section, the absence of metapelitic schist, quartzite, marble, and of polymictic conglomerate argues against a terrigenous sedimentary origin. The overall compositional monotony of the sequence is thus consistent with a volcanic origin.
4. The lack of erosional–depositional structures that are characteristic of terrigenous sediments and of volcanic flow deposits, rules out substantial reworking, transport, and deposition by water and density currents. The likelihood of some reworking, however, cannot be excluded and the sequence may contain subordinate epiclastic sediments.
5. The lateral persistence of the beds and lamellae and the well defined and plane-parallel nature of bedding are characteristic of fallout deposits (Fisher and Schmincke, 1984).
6. The preservation, in spite of amphibolite-facies metamorphism, of a very fine and uniform grain size in granoblastic and apparently nonmylonitic rocks requires an even finer initial grain size, and a very high degree of uniformity in texture and in the distribution of the rock constituents. Such features are common in fallout ash deposits (Fisher and Schmincke, 1984).
7. The felsic-to-mafic zoning conspicuous in many beds of the sequence is characteristic of most pyroclastic flow and fallout deposits (Smith, 1979; Hildreth, 1981; Fisher and Schmincke, 1984). In keeping with our finding that zoning tends to be more pronounced in the thinner beds, small-volume pyroclastic eruptions tend to show stronger compositional contrasts than larger volume eruptions (Fisher and Schmincke, 1984).
8. In the absence of lava and pyroclastic flows, the morphology and thickness of the beds suggest intermediate to distal depositional facies, which typically consist of fallout ash deposited farther from the source than lava and pyroclastic flows can travel, and of interbedded, reworked pyroclastic and epiclastic sediments (Fisher and Schmincke, 1984).

### *Stratigraphic polarity*

Our structural observations are consistent with the conclusions of previous workers (Smith, 1956; Pyke, 1966; Morin, 1987; Jourdain et al., 1987) that the rock succession between the mine sequence and the metabasalt at Mont Tétreault is the inverted eastern limb of a shallow, north-plunging synform overturned to the west (Fig. 3). The absence of evidence of structural repetition intimates that the rocks belong to a continuous stratigraphic succession. Recognizing the local and regional complexity of the fold pattern, the kilometre-scale fold mentioned above was variously interpreted as a first-phase fold (Smith, 1956; Pyke, 1966; Rondot, 1978), as a second-phase Ramsay type 3 interference fold (Morin, 1987), or as a second phase structure of unspecified geometry (Jourdain et al., 1987; Bernier and MacLean, 1993). Accordingly, some workers did not specify the stratigraphic polarity of the section (Prabhu and Webber, 1984; Bernier and MacLean, 1993), whereas others inferred that the Mont Tétreault metabasalt was deposited either stratigraphically below (Rondot, 1978; MacLean et al., 1982; Morin, 1987) or above (Stamatelopoulou-Seymour and MacLean, 1977; Jourdain, 1987) the mine sequence. With the exception of Pyke (1966), none of the workers cited has described or located the mesoscopic facing indicators on which they based their interpretation.

Along with those of Pyke (1966), our observations of pillows at Mont Tétreault suggest that the succession is stratigraphically overturned (Fig. 4a, b). This is consistent with the polarity deduced from the compositional zoning and relict graded bedding identified in a number of tuff beds (Fig. 8b, c). If this is correct, the metabasalt was deposited stratigraphically above the mine sequence.

### *Volcanic stratigraphy*

Having deduced the nature of the rock and the stratigraphic polarity of the succession, it is now possible to make a tentative interpretation in terms of the eruption history and of volcanic facies, emphasizing the position of the rock unit relative to the eruptive centre. Five informal units are recognized between Montauban village and Mont Tétreault (Fig. 3, 9). In stratigraphic order, these are:

1. The grey composite gneiss (Smith, 1956) consisting of vaguely layered migmatitic biotite-hornblende quartzofeldspathic gneiss. Although generally considered to be conformably overlain by the mine sequence, the contact is locally marked by a ductile fault such as exposed in the abandoned open-pit mine (locality 1.5; Fig. 3).

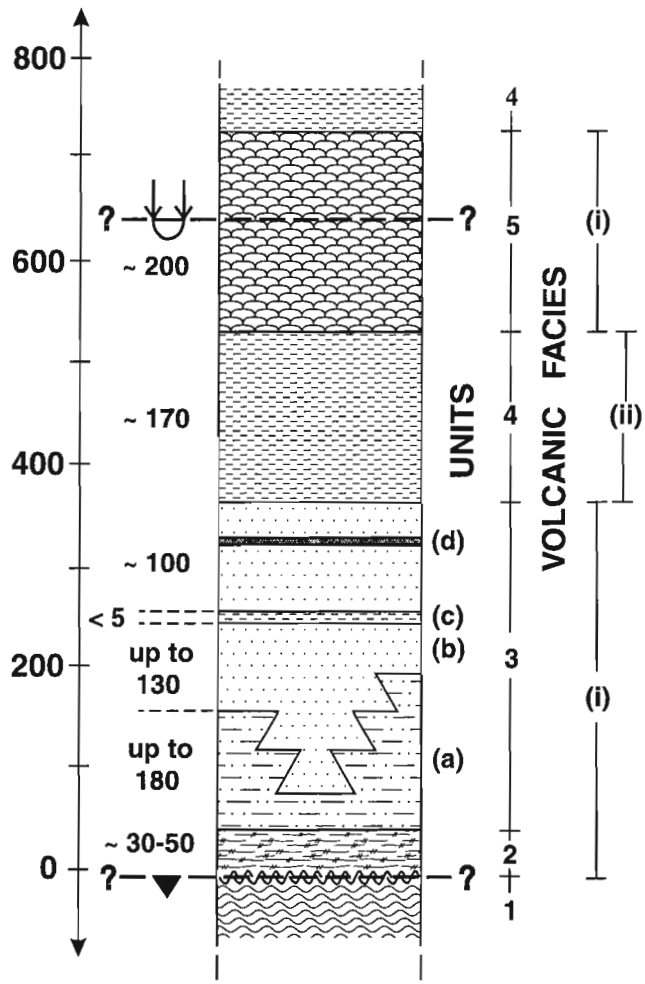


***Figure 9.*** *Volcanic stratigraphy in the structural footwall of the Montauban ore deposits; see Figure 3 for location. Rock units: 1, grey composite gneiss; 2, mine sequence; 3, lapilli tuff including thickly bedded hydrothermally altered (a) and unaltered (b), lapilli tuff, subordinate thinly bedded felsic tuff (c), and possibly rare massive metre-thick pyroclastic flow, (d); 4, thinly bedded felsic tuff; and 5, metabasaltic pillow lava. Volcanic facies: (i) proximal, and (ii) distal. Structural thicknesses in metres. Note that the contact between units 1 and 2 is locally faulted and that the pillow lava may occupy the core of a tight fold.*

2. The mine sequence, comprising the polymetallic and Au-rich volcanogenic massive sulphide-type orebodies and their associated, metamorphosed, hydrothermally altered wall rocks (locality 1.5; Fig. 3). Volcanogenic massive sulphide-type orebodies invariably occur in proximal facies where hydrothermal alteration systems are extensively developed.

3. The lapilli tuff unit is dominated by unaltered rhyolitic lapilli tuff (locality 1.3), and derived hydrothermally altered pyrite-bearing muscovite±sillimanite quartzitic gneiss (locality 1.4), with minor thinly bedded pyroclastic tuff, and possibly a few massive rhyolitic flows. The abundance of metamorphosed hydrothermally altered rocks and the thickness of the lapilli tuff testify to a proximal facies.

4. The thinly bedded felsic tuff unit, composed of intermediate to felsic, centimetre-thick bedded fallout tuffs, in places with pronounced compositional zoning, and rare intercalated decimetre-thick lapilli tuff beds. Such volcanic rocks are distinctive of distal facies.

5. The metabasalt unit is composed of less than metre-scale, vesicular, thin-rimmed basaltic pillow lava with calcitic interpillow matrix, and possibly thin massive flows, all of which are characteristic of a proximal shallow submarine environment.

These volcanic rocks are likely to be laterally intercalated with epiclastic sediments, as the distance to the volcanic centre increases. Indeed, compositional akin gneiss, which could be in part reworked volcanic rocks, are widespread in the region (Fig. 2) suggesting that the Montauban group is composed essentially of metamorphosed volcanic and derived epiclastic sedimentary rocks. Whereas the proximal units (2, 3, 5) reflect a small number of eruptions, the thinly bedded felsic tuff unit records a large number of events. Hence, the rock sequence testifies to a multiple and evolving eruption history with significant changes with time in the source of magma, from rhyolitic to basaltic, and in either or both the location of the active volcanic centre and the intensity and type of volcanism.

## *Paleotectonic setting and exploration model*

The Montauban group has been attributed to either island- or backarc (e.g. Bernier and MacLean, 1993), or continental rift (e.g. Morin, 1987) paleotectonic settings. By extension, the associated mineral deposits were interpreted as VMS (e.g. Bernier and MacLean, 1993) or SEDEX (e.g. Morin, 1987) types. These conflicting interpretations arose from the opposing views that the wall rocks are dominantly of volcanic or sedimentary origin, respectively.

Admittedly, the volcanic sequence discussed above likely represents only a small portion of the parent volcanic edifice. Our observations support the view of Bernier and MacLean (1993) and demonstrate that the best preserved part of the Montauban group is derived chiefly from metamorphosed intermediate to felsic volcanic rocks with minor vesicular metabasalt. Accordingly, we suggest that these rocks were deposited in a relatively shallow marine environment in the late stage of an andesitic to felsic volcanic cycle. This setting is common in mature island-arcs or backarcs where VMS deposits are commonly formed.

In addition, the occurrence of Au- and Ag-rich ore in association with hydrothermally altered, shallow marine felsic volcanic rocks suggests that the Montauban Au-rich deposits may belong to the recently recognized high-sulphidation VMS type (Sillitoe et al., 1996; Hannington et al., 1998). Exploration for this type of deposit in the region should therefore concentrate on the recognition of hydrothermally altered rocks, whether or not they are associated with mafic rocks or a significant Pb-Zn ore zone.

## ACKNOWLEDGMENTS

The present report has benefited from insightful discussions in the field with numerous colleagues of Géologie Québec, Friends of the Grenville, and GSC. In particular we gratefully acknowledge careful and constructive reviews by L. Corriveau, T. Clark, A. Davidson, and T. Feininger. This was a joint project between Géologie Québec and the Geological Survey of Canada. Géologie Québec contribution no. 1999-5110-01.

## REFERENCES

**Bancroft, J.A.**
1915: Geology of a part of Montauban and Chavigny townships and of De Grondines seignory; Department of Colonization, Mines and Fisheries, Quebec, Mines Branch Annual Report, p. 103–143.

**Bernier, L.R. and MacLean, W.H.**
1993: Lithogeochemistry of a metamorphosed VMS alteration zone at Montauban, Grenville Province, Quebec; Exploration and Mining Geology, v. 2, p. 367–386.

**Bernier, L.R., Pouliot, G., and MacLean, W.H.**
1987: Geology and metamorphism of the Montauban north gold zone, a metamorphosed polymetallic exhalative deposit, Grenville Province, Quebec; Economic Geology, v. 82, p. 2076–2090.

**Fisher, R.V. and Schmincke, H.U.**
1984: Pyroclastic Rocks; Springer-Verlag, Berlin, 472 p.

**Hannington, M.D., Poulsen, K.H., Thompson, J.F.H., and Sillitoe, R.H.**
1998: Volcanogenic gold in the massive sulfide environment; *in* (ed.) C.T. Barrie and M.D. Hannington; Reviews in Economic Geology, v. 8, p. 319–350.

**Hébert, C. et Gobeil, A.**
1991: Province de Grenville, zone de favorabilité pour l'exploration minérale, principaux indices et producteurs (anciens et actuels); Ministère de l'Énergie et des Ressources, Québec; PRO 91-08, 4 p.

**Hildreth, W.**
1981: Gradients in silicic magma chambers: implications for lithospheric magmatism; Journal of Geophysical Research, v. 86, p. 10153–10192.

**Hocq, M. et Dufour, S.**
1999: Compilation et interprétation de la région de Montauban; Ministère des Ressources naturellles, Québec, carte no: SI-31I16-C3G-99D, echelle 1/50 000.

**Jourdain, V., Roy, D.W., and Simard, J.M.**
1987: Stratigraphy and structural analysis of the North Gold Zone at Montauban-les-Mines, Quebec; Canadian Institute of Mining Bulletin, v. 80, p. 61–67.

**Lavergne, G.**
1985: Gîtes minéraux à tonnage évalué et production minérale du Québec; Ministères des Ressources naturelles, Québec, DV 85-08, 44 p.

**MacLean, W.H., Stamatelopoulou-Seymour, K., and Prabhu, M.K.**
1982: Sr, Y, Zr, Nb, Ti and REE in Grenville amphibolites at Montauban-les-Mines, Quebec; Canadian Journal of Earth Sciences, v. 19, p. 633–644.

**Morin, G.**
1987: Gîtologie de la région de Montauban; Ministère de l'Énergie et des Ressources, Québec, MM 86-02, 59 p.

**Nadeau, L. and van Breemen, O.**
1994: Do the 1.45-1.39 Ga Montauban group and the La Bostonnais Complex constitute a Grenvillian accreted terrane?; Geological Association of Canada, Program with Abstract, v. 19, p. A81.

**Osborne, F.F.**
1939: The Montauban mineralized zone, Quebec; Economic Geology, v. 34, p. 712–726.

**Prabhu, M.K.**
1981: Geology, geochemistry and genesis of the Montauban lead-zinc deposits; Ph.D. thesis, McGill University, Montreal, Quebec, 271 p.

**Prabhu, M.K. and Webber, G.R.**
1984: Origin of quartzofeldspathic gneisses at Montauban-les-Mines, Quebec; Canadian Journal of Earth Sciences, v. 21, p. 336–345.

**Pyke, D.R.**
1966: Geology of the Montauban-Colbert area, Champlain and Portneuf townships; Quebec Department of Mines, Geological Report, RP-545, 18 p.
1967: Geology of the Montauban area; Ph.D. thesis, McGill University, Montreal, Quebec, 181 p.

**Rivers, T., Martignole, J., Gower, C.F., and Davidson, A.**
1989: New tectonic divisions of the Grenville Province, southeast Canadian Shield; Tectonics, v. 8, p. 63–84.

**Rondot, J.**
1978: Région de Saint-Maurice, Québec; Ministère des Richesses naturelles, Québec, DPV-594, 85 p.

**Sangster, D.F.**
1972: Precambrian volcanogenic massive sulfide deposits in Canada: a review; Geological Survey of Canada, Paper 72-22, 44 p.

**Sillitoe, R.H., Hannington, M.D., and Thompson, J.F.H.**
1996: High sulfidation deposits in the volcanogenic massive sulfide environment; Economic Geology, v. 91, p. 204–212.

**Smith, J.R.**
1956: Rapport géologique 65: la région de Montauban-les-Mines, comté de Portneuf; Ministère des Mines, Québec, RG-65, 43 p.

**Smith, R.L.**
1979: Ash-flow magmatism; Geological Society of America, Special Paper 180, p. 5–27.

**Stamatelopoulou-Seymour, K.**
1975: Metamorphosed volcanogenic Pb-Zn deposits at Montauban, Quebec; M.Sc. thesis, McGill University, Montreal, Quebec, 230 p.

**Stamatelopoulou-Seymour, K. and MacLean, W.H.**
1977: The geochemistry of possible metavolcanic rocks and their relationship to mineralization at Montauban-les-Mines, Quebec; Canadian Journal of Earth Sciences, v. 14, p. 2440–2452.

Geological Survey of Canada Project 920002

# Mineralogical investigation of a clay deposit for cosmetic and therapeutic purposes, Baie-St-Ludger, Quebec

Catharine A. Burton[1], Jeanne B. Percival, and Denise Saulnier[2]
Mineral Resources Division, Ottawa

*Burton, C.A., Percival, J.B., and Saulnier, D., 1999: Mineralogical investigation of a clay deposit for cosmetic and therapeutic purposes, Baie-St-Ludger, Quebec;* in *Current Research 1999-E; Geological Survey of Canada, p. 161–168.*

**Abstract:** Since ancient times, clay materials have been used as cosmetic and therapeutic materials due to their inherent physico-chemical properties. This study reports detailed mineralogical analyses of a clay deposit in Baie-St-Ludger, eastern Quebec, as part of its assessment as a potential cosmetic or therapeutic clay material for external use. The samples were compared to a small suite of commercially available clay products of similar application. These silty-clay to silt marine sediments are dominated by illite (biotitic) and plagioclase feldspar with subordinate amounts of K-feldspar, quartz, and amphibole (hornblende). Chlorite occurs only in minor to trace amounts. The commercial samples generally contain more kaolinite and less non-clay silicates than the field samples. This difference should not be a deterrent for developing this deposit for commercial purposes, as at least one of the commercial products examined is mineralogically similar.

**Résumé :** Depuis la préhistoire, on a utilisé des minéraux argileux comme produits cosmétiques ou thérapeutiques à cause de leurs propriétés physico-chimiques inhérentes. Cette étude fait état d'analyses minéralogiques détaillées d'un gisement d'argile dans la baie Saint-Ludger (Est du Québec) réalisées dans la cadre de son évaluation comme matière argileuse potentiellement cosmétique/thérapeutique d'usage externe. On a comparé les échantillons à une petite série de produits argileux disponibles dans le commerce et utilisés à des fins semblables. Ces sédiments marins silto-argileux à silteux sont composés surtout d'illite (biotitique) et de plagioclase avec des quantités moins élevées de feldspath potassique, de quartz et d'amphibole (hornblende). La chlorite n'est présente qu'en quantités mineures ou à l'état de traces. Les échantillons commerciaux contenaient généralement plus de kaolinite et moins de silicates non argileux que les échantillons de terrain. Cette différence ne devrait pas constituer un obstacle à la mise en valeur du gisement à des fins commerciales puisqu'au moins un des produits commerciaux examinés présentait une minéralogie similaire.

[1] 17 Elmsley Crescent, Nepean, Ontario K2H 6T9
[2] Argile eau mer, 5594 rue Waverly, Montréal, Québec H2T 2Y1

## INTRODUCTION

Clay minerals, sensitive indicators of low-temperature geological environments, are the most abundant minerals on or near the Earth's surface. They occur in weathering, sedimentary, diagenetic, and hydrothermal environments through transformation of non-clay minerals, precipitation from solution, and crystallization of amorphous colloidal material. Clay minerals are widely used in our day-to-day lives. They are important in agriculture for nutrient cycling, in engineering for foundation and slope stability, and in the environment as sorbents for organic and inorganic contaminants. Clay minerals are used extensively in the ceramic industry, not only for china, stoneware, brick, tiles and sewer pipes, but also in the electronics field in dielectric, piezoelectric, semiconductors, and insulator ceramics. They are used in the metallurgical, pulp and paper, wine, cosmetic, and pharmaceutical industries.

Since ancient times, clays have been used as cosmetic and therapeutic materials. Health spas in Europe and North America use clay materials in mud baths and facial mud packs as part of their routine cleansing procedures. During the past few decades, there has been a resurgence in the use of clay materials in cosmetic and therapeutic products as evidenced by the increased number that are commercially available. There is also a voluminous amount of information about the benefits of clays in cosmetics on the Internet. At one site, Salon Web (www.salonweb.com), a glossary of cosmetic terms can be viewed. Kaolin is defined as a 'white clay used to absorb impurities from the skin', whereas silica is used as an 'absorbent, anti-caking and abrasive' ingredient. Clay minerals have inherent physico-chemical properties such as ion exchange, adsorption, and absorption that make them ideal in therapeutic applications. According to popular articles on naturopathy, in addition to the properties listed above, they are considered to have additional beneficial characteristics such as being antiseptic and antitoxic, promoting healing and blood clotting, relaxing and revitalizing skin, etc. (Dextreit, 1976; Passebecq, 1978; Bourgeois, 1981; Masson, 1983).

This study reports the detailed mineralogical analyses of a clay deposit in Baie-St-Ludger, eastern Quebec, as part of its assessment as a potential (external use only) cosmetic and therapeutic clay material. The samples were compared to a small suite of commercially available clay products of similar application. The commercial products analyzed, however, are not representative of all products currently on the market.

## GEOLOGICAL SETTING

Baie-St-Ludger is located on the north shore of the St. Lawrence River, on the Manicouagan Peninsula, 20 km west of Baie-Comeau (Fig. 1). The main settlements of the area include Chute-aux-Outardes to the northwest, and Baie-Comeau to the northeast.

The southern part of the region, including the Manicouagan Peninsula, consists of a coastal plain composed of extensive silt-clay deposits overlain by sands. The plain is terraced and rises to approximately 90 m above sea level at the Laurentian Highlands boundary (Sauvé, 1962). The area is similar to the region to the northeast where Dredge (1983) described beach ridges, river and wave-cut scarps, dunes, landslide scars, and bogs characterizing the low, local relief.

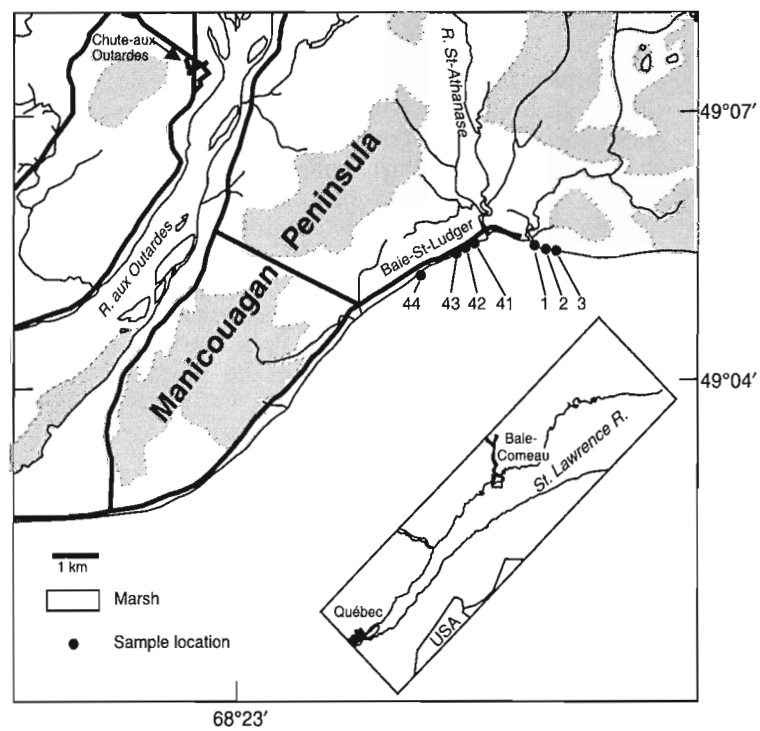


***Figure 1.***

*Detailed map showing location of study area and samples. The Manicouagan Peninsula comprises Pleistocene sand and clay plain.*

During retreat of the last ice sheet, marine waters inundated the isostatically depressed St. Lawrence and Ottawa valleys. The Goldthwait Sea occupied the St. Lawrence Valley east of Quebec City (Elson, 1969), whereas the Champlain Sea occupied the remaining St. Lawrence and lower Ottawa valleys. The Goldthwait Sea reached the limit of 170 m in the Baie-Comeau area (Bernatchez, 1997). Large quantities of fine-grained debris were deposited from meltwaters into the Goldthwait and Champlain seas, exceeding 100 m in thickness in some localities (Ochietti, 1989). On the Manicouagan Peninsula, the clay deposits reach a thickness of up to 80 m (Simard, 1972). Dredge (1976) reported that three major types of deposits in the Goldthwait Sea represent a continuous offlap sequence of sedimentation. These deposits coarsen upwards and include marine offshore silts and clays, nearshore marine deltaic sands, both capped by littoral sands deposited during marine regression. The marine clays of the Goldthwait Sea are similar to the Champlain Sea sediments (e.g. Leda Clay) with respect to their geotechnical behaviour. In the study area, the last major landslide in the sensitive clays took place in the Baie-St-Ludger area in 1964 (Simard, 1972; J. Aylsworth, pers. comm., 1999). However, a more recent landslide occurred during the exceptional flooding during the summer of 1996, approximately at the same location as the one in 1964 (P. Bernatchez, pers. comm., 1999).

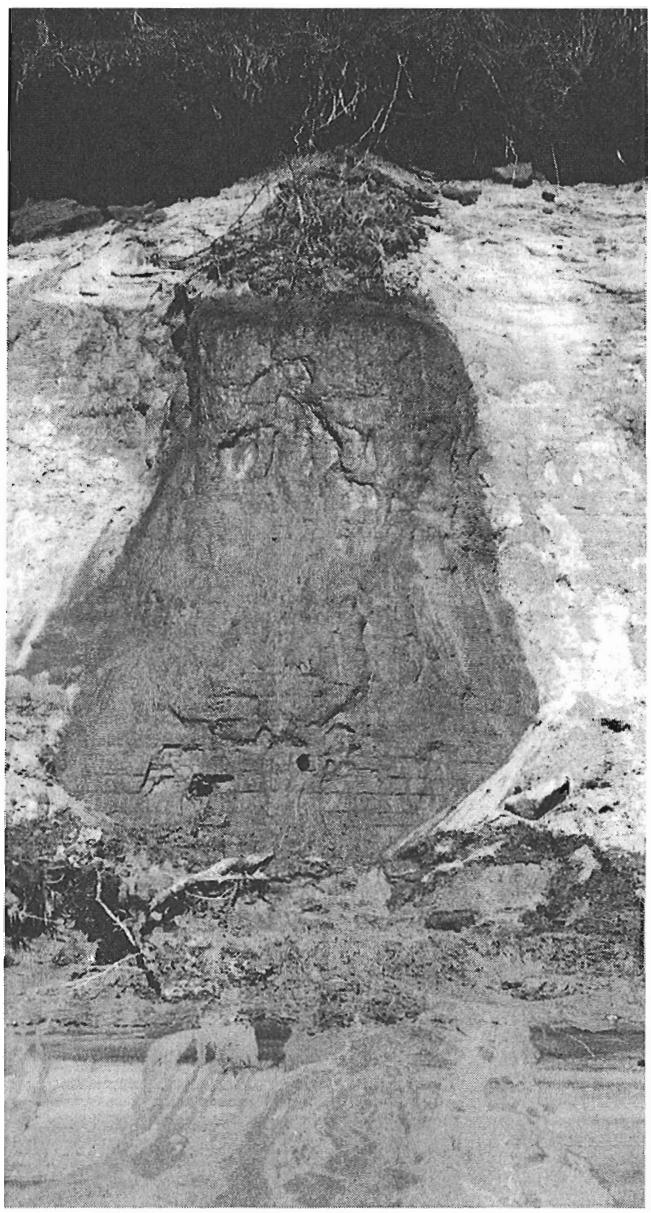

***Figure 2.*** *Example of the bedded silty-clay deposit along the shore of the St. Lawrence River, Baie-St-Ludger, Quebec (height approx. 8 m). GSC photo 1999-008A*

The materials under study are typical glaciomarine (deltaic) or marine silts and clays. They consist of thick units of silty clay alternating with thin bands of clay or silt (dark layers) (Fig. 2, 3). Marine shells (white) can be seen in the lower right-hand part of Fig. 3. The lack of pebbles in this section further suggests that the materials are marine in origin rather then glacio-fluvial. In general, these silty-clay units are overlain by 'bedded sands' (littoral?) as shown at the top of Figure 4. Note the slumping of material in the central part of this photograph.

## MATERIALS AND METHODS

Samples for detailed analyses were collected from seven sites along the Baie-St-Ludger beach (Fig. 1). An auger was used to obtain material about 1 m from the vertically exposed surface. Samples were then placed in glass jars for transportation (Fig. 3). Nine samples were submitted for grain size and mineralogical characterization from the seven sites. In addition, nine clay-based samples were selected, randomly, from the cosmetic market for comparison purposes. These commercial samples, however, are not representative of all products on the market and were labelled so as to protect the anonymity of each company.

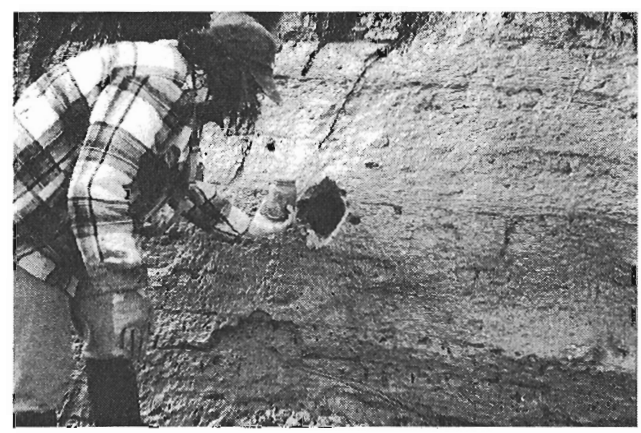

***Figure 3.*** *Close-up of bedded silty-clay deposit showing silty-clay layers separated by thin (dark) bands of clay-rich material. D.S. collecting sample for testing. Note the white, shelly material in lower right corner of the photo. GSC photo 1999-008D*

For grain-size analyses, a subsample of the material was disaggregated using a milk shaker. Particle-size distribution was then determined using a Galai (formerly Brinkmann) Particle Size Analyzer (Model 2010). Details on theory and application of laser systems are given in Lindsay et al. (1998). Results were reduced to percentages of sand-, silt-, and clay-size material for reporting purposes.

The mineralogy of the clay-size samples was determined by X-ray powder diffraction analysis (XRD). The clay-size fraction was separated using centrifugation followed by freeze-drying. A 40 mg suspension (in water) of each sample was pipetted onto glass slides and air-dried overnight to produce an oriented mount. X-ray patterns of the air-dried samples were digitally recorded using a Philips PW1710 automated powder diffractometer equipped with a graphite monochromator, with Co Kα radiation set at 40 kV and 30 mA. The samples were also X-rayed following saturation with ethylene glycol and heat treatment (550°C). Data was processed using a PC-based program, JADE® (Materials Data, Inc.) which enables manipulation of the X-ray pattern for optimization (e.g. correction for background, instrument error) in identification of mineral species and calculation of abundances. Semiquantitative analyses are possible through comparison with a set of reference standards using a predetermined reference intensity ratio (RIR). The RIRs available from the International Centre for Diffraction Data (ICDD) database are based on a weighted factor of a mineral relative to corundum. The weighted factors or RIRs used at the GSC laboratory have been, in many cases, recalculated using quartz as the internal standard.

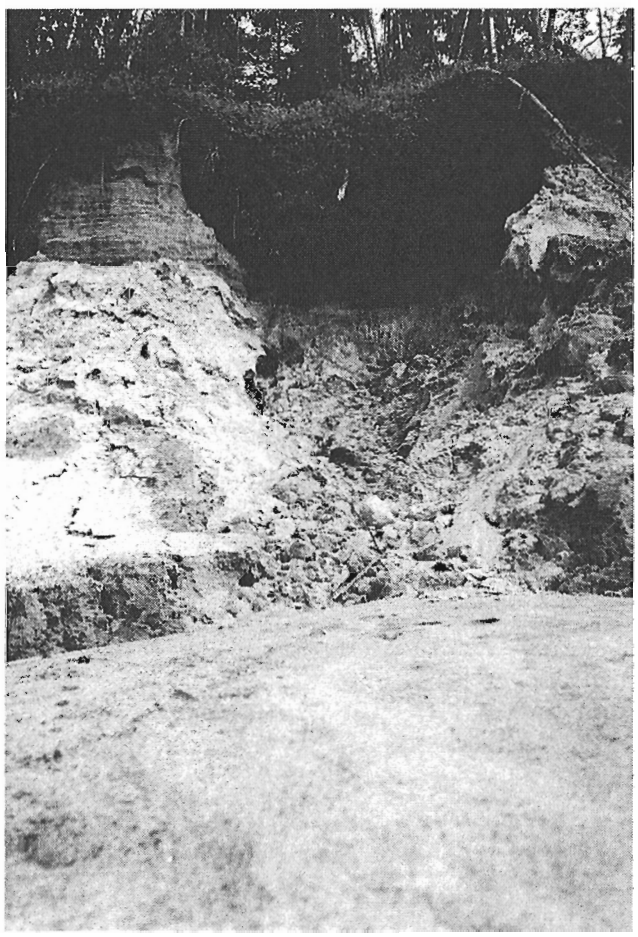

***Figure 4.*** *Bedded silty clay unit overlain by bedded (littoral?) sands. Note the slump in the central part of the photo (height approx. 6 m). GSC photo 1999-008B*

Grain mounts were prepared for scanning electron microscopy (SEM) by either pipetting a very dilute (<10–20 ppm) suspension onto a carbon-coated planchette or dusting double-sided, carbon-coated tape with loose powders. All mounts were then carbon-coated for examination. A Leica Cambridge Stereoscan S360 SEM was used. The SEM was equipped with an Oxford/Link eXL-II energy-dispersion X-ray analyzer, Oxford/Link Pentafet Be window/light-element detector, and an Oxford/Link Tetra backscattered-electron detector. The SEM is operated at an accelerating voltage of 20kV. SEM images are captured at 768 by 576 by 256 grey scale and digitally stored for further processing.

Two bulk samples (41A and 43) were subjected to a complete series of chemical analyses at Analex and Technitrol-Écho laboratories in Montreal. Laboratoire Analex measured total bacteria, yeast, mold, and per cent organic matter, whereas Laboratoire Technitrol-Écho tested for industrial contaminants such as hydrocarbons (e.g. oils and greases), organic contaminants (e.g. phenols), pesticides, Hg, and As. Major elements and cations in pore waters were analyzed by XRF and ICP-ES, respectively, at Centre de Recherches minérales, Québec.

## RESULTS AND DISCUSSION

### *Texture*

The field samples have, in general, the appearance of a soft, light grey to grey (hue 5Y) clay. However, the samples tend to be silt rich, which is typical of marine sediments on the North Shore (Table 1). On a standard ternary plot of clay-silt-sand, sample 1 would be classified as a sandy silt and sample 3 as a silty sand, whereas the remaining field samples are silts. The mean content of clay-size material is 8.4%. These results are similar to those reported by Bernatchez and Baker (1995) for samples taken between Baie-St-Ludger and Point-Lebel. Their samples contain, on average, 19.0% sand, 72.9% silt, and 8.1% clay. These samples appear to be more silt rich than equivalent samples to the northeast. Dredge (1983) described both a bedded and massive clayey silt unit in the Sept-Îles area, with mean clay contents ranging from 37% to 31%, respectively.

**Table 1.** Particle-size analysis of field samples and commercially-available cosmetic samples.

| Sample type/no. | %Pebbles | %Sand | %Silt | %Clay |
|---|---|---|---|---|
| ***Field*** | | | | |
| 1 | 0.00 | 44.12 | 53.85 | 2.03 |
| 2 | 0.00 | 18.18 | 77.95 | 3.86 |
| 3 | 0.00 | 54.09 | 43.58 | 2.33 |
| 41A | 0.00 | 0.17 | 85.26 | 14.58 |
| 41B | 0.00 | 0.76 | 88.91 | 10.33 |
| 42A | 0.00 | 5.77 | 83.95 | 10.29 |
| 42B | 0.00 | 4.09 | 86.12 | 9.78 |
| 43 | 0.00 | 2.24 | 83.76 | 13.98 |
| 44 | 0.00 | 4.63 | 86.64 | 8.74 |
| ***Commercial*** | | | | |
| ABP | 0.00 | 0.00 | 90.23 | 9.78 |
| ABWC | 0.00 | 0.00 | 68.68 | 31.32 |
| ANI | 0.00 | 2.82 | 82.80 | 14.36 |
| AVC | 1.03 | 1.10 | 85.15 | 13.75 |
| AVGC | 0.00 | 2.32 | 86.35 | 11.30 |
| CPN | 0.00 | 0.00 | 68.74 | 31.26 |
| CVH | 0.00 | 0.00 | 86.55 | 13.44 |
| KIC | 0.00 | 8.34 | 83.23 | 8.42 |
| M100 | 0.00 | 6.80 | 90.20 | 2.99 |

The commercial samples were powdered, and ranged in colour from white to pale green to dark brown. Some of the products are described as simply 'green clay powder'. No information is given as to content, although a few products did show partial chemical analyses. These materials are comparable with respect to particle-size distribution and can be classified as silts or clayey-silts (i.e. commercial samples ABWC and CPN). Only one sample, AVC, contained pebbles. The mean clay content of the commercial samples is higher than the field samples, at 15.2%.

## *Composition*

Semiquantitative mineralogical results are given in Table 2. All field samples are dominated by illite (biotitic) and plagioclase feldspar with subordinate amounts of K-feldspar, quartz, and amphibole (hornblende). Chlorite occurs only in minor to trace amounts. One sample contains a trace amount of smectite. In general, samples contained an unknown quantity of X-ray amorphous material, probably organic, resulting in slightly broadened X-ray peaks. Under the SEM, clay-size particles (<2 μm) tended to be subangular to subrounded. Furthermore, all samples contained trace amounts of pyroxene, anhydrite, titanite, rutile, and Fe-oxides; ilmenite was observed only in sample 44 and apatite in 41A. The mineralogy

**Table 2.** Semiquantitative clay mineralogical results using X-ray powder diffraction analyses and JADE® software.

| Sample type/no. | Qtz | Kfs | Pl | Amp | Chl | Ill | Kao | Sm | ML | Cal |
|---|---|---|---|---|---|---|---|---|---|---|
| ***Field*** | | | | | | | | | | |
| 1 | 11 | 19 | 32 | 11 | 3 | 24 | | | | |
| 2 | 9 | 17 | 31 | 15 | 4 | 24 | | tr | | |
| 3 | 14 | 17 | 38 | 12 | 3 | 16 | | | | |
| 41A | 12 | 10 | 32 | 16 | 2 | 28 | | | | |
| 41B | 10 | 15 | 32 | 18 | 3 | 22 | | | | |
| 42A | 15 | 16 | 36 | 14 | 3 | 16 | | | | |
| 42B | 14 | 14 | 36 | 14 | 3 | 19 | | | | |
| 43 | 10 | 13 | 29 | 10 | 4 | 34 | | | | |
| 44 | 12 | 14 | 31 | 15 | 3 | 25 | | | | |
| ***Commercial*** | | | | | | | | | | |
| ABP | | | | | | | | 100 | | |
| ABWC | | | | | | 1 | 99 | | | |
| ANI | 3 | 5 | | | tr | 11 | 81 | tr | tr | |
| AVC | 2 | | | | | 68 | 26 | tr | tr | 4 |
| AVGC | 1 | | | | 11 | 74 | 9 | tr | m-tr | 4 |
| CPN | | | | | | | 100 | | | |
| CVH-1 | | | | | | 13 | 87 | | | |
| CVH-2 | | | | | | 15 | 85 | tr | | |
| KIC | 6 | | 27 | 14 | 27 | 27 | | | | |
| M100 | | | | | | | | A | | |

Qtz = quartz; Kfs = K-feldspar; Pl = plagioclase feldspar; Amp = amphibolite; Chl = chlorite; Ill = illite; Kao = kaolinite; Sm = smectite (expandable clay mineral, not quantified); ML = mixed-layer clay mineral; Cal = calcite; A = abundant; m = minor; tr = trace.
ML component may be an illite-smectite or chlorite-smectite mixed-layer mineral; these cannot be quantified at this time.

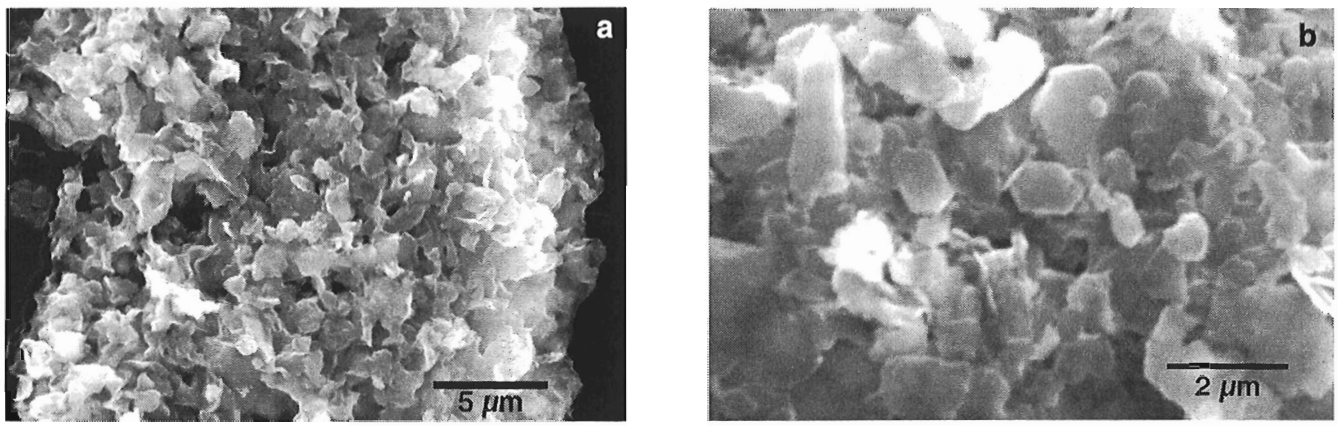


***Figure 5.*** *SEM photomicrographs (secondary electron images) of monominerallic commercial clay products:* ***a****) sample ABP composed of Na-smectite showing typical crenulated texture (magnification 4400x); and* ***b****) sample CPN, composed of kaolinite showing well-developed hexagonal plates (magnification 11 600x).*

reflects the mineralogy of Precambrian rocks (as rock flour) that occur in the area. The mineralogical composition compares favourably to that of the Sept-Îles area where offshore sediments are dominated by non-clay minerals quartz and feldspar, especially plagioclase, with minor amounts of amphibole, illite, and chlorite (Dredge, 1983). The semiquantitative results presented here are comparable to marine-clay data from the Goldthwait Sea summarized in Torrance (1988). For example, samples from Outardes-2 contained, on average for 14 samples, 17% quartz, 42% plagioclase, 18% K-feldspar, 17% amphibole, 6% illite, 1% chlorite, and 3% dolomite (Foscal-Mella, 1976).

The commercial samples were more variable in their mineralogical composition. A few of the samples were monominerallic. Sample ABP contained 100% Na-smectite (Fig. 5a), whereas CPN and ABWC are essentially composed of kaolinite, with about 1% illite in ABWC. An example of the kaolinite hexagonal plates from sample CPN is shown in Figure 5b. It is interesting to note that CPN is produced for internal use. Sample M100 is shown to have an abundance of smectite only, as this sample is highly amorphous and contains an unquantifiable amount (by XRD) of organic matter. The smectite is Ca rich. Samples ANI, CVH-1, and CVH-2 are kaolinite rich (81–87%) with a minor amount of illite and lesser amounts of quartz, K-feldspar (ANI), smectite, and mixed-layer clays. Sample AVC contains only minor kaolinite (26%) and is dominated by illite (65%) with trace amounts of quartz, calcite, smectite, and mixed-layer clays. SEM analyses showed that the quartz grains were highly spherical. In addition, a grain of zircon and Al-phosphate (probably variscite) were also present. Sample KIC appears more similar to the field samples. It contains subequal amounts of plagioclase, illite, and chlorite with minor amounts of amphibole and quartz. This particular product is sold as a facial mask, and it is possible that the presence of non-phyllosilicates is beneficial for the skin (exfoliant). Another commercial product analyzed some years ago in the mineralogy laboratory (qualitative, unpub. data) was very similar to the field and KIC samples. It contained quartz, both feldspars, amphibole, illite (probably biotite), and some chlorite. This product was advertised as a glacial marine mud from British Columbia. An additional two samples analyzed as part of this study contained 100% organic matter (as algae) and were not suitable for comparison.

The field samples contain up to 28% organic matter, mostly as plant material. This amount of organic matter is considered normal in cosmetic products. As mentioned above, some commercial products only contain organic material (e.g. algae).

**Table 3.** Major-element analysis (XRF) of bulk samples 41A and 43 and cation content of their pore waters (ICP-ES).

| Oxide | No. 41A | No. 43 | Cation | No. 41A | No. 43 |
|---|---|---|---|---|---|
| $SiO_2$ ( wt %) | 59.8 | 60.0 | Al (mg/L) | 60.2 | 37.3 |
| $TiO_2$ | 0.66 | 0.66 | Ba | 0.49 | 0.28 |
| $Al_2O_3$ | 16.2 | 16.2 | Ca | 9.9 | 5.8 |
| $Cr_2O_3$ | 0.02 | 0.02 | Cd | <0.002 | <0.002 |
| $Fe_2O_3$t | 6.25 | 6.00 | Cr | 0.15 | 0.09 |
| MnO | 0.09 | 0.10 | Cu | 0.49 | 0.32 |
| MgO | 3.34 | 3.30 | Fe | 56.7 | 36.6 |
| CaO | 3.92 | 4.17 | K | 24.6 | 16.8 |
| $Na_2O$ | 3.80 | 3.83 | Mg | 27.7 | 17.3 |
| $K_2O$ | 2.81 | 2.76 | Mn | 0.74 | 0.45 |
| C org | 0.03 | 0.04 | Na | 34.5 | 57.0 |
| $CO_2$T | 0.22 | 0.33 | Ni | 0.11 | 0.07 |
| $P_2O_5$ | 0.21 | 0.22 | P | 1.7 | 1.0 |
| S | 0.05 | 0.04 | Pb | 0.12 | 0.06 |
| Cl | <0.10 | <0.10 | Zn | 0.16 | 0.10 |
| LOI | 1.78 | 1.91 | | | |
| **Total** | 99.28 | 99.68 | | | |

Major-element chemistry for two field samples is given in Table 3. Their composition is midway between that of a quartz diorite and a diorite, suggesting that the marine sediments may have derived from diorite occurring locally north of the Manicouagan Peninsula. Sauvé (1962) indicated that the rocks in the Manicouagan area include diorites, granites and high-grade gneisses and paragneisses. The cation composition of the pore waters is also shown in Table 3. The Na content is comparable to some samples of Champlain Sea clays (Ottawa Valley), but is generally one to two orders of magnitude lower (*see* Torrance, 1988). This probably resulted from postdepositional leaching of salt by fresh water. Elements of concern would include As, Cd, Ni, and Pb. There was insufficient sample to analyze for As. Both Ni and Pb can cause contact (skin) dermatitis (Cecutti and Nieboer, 1981; Jaworski, 1978) whereas Cd is not normally absorbed through the skin. In contrast to Ni and Pb, Cu and Zn are beneficial to the skin (as well as internally). For example, Zn was applied topically in the form of calamine during the early Egyptian period. Zinc-containing compounds are widely used today in powders and ointments to treat skin lesions (Pories et al., 1971). Levels measured in the pore waters for Cr, Ni, and Pb are within the acceptable limits for external use (Hildgen, pers. comm., 1999); Cd was undetectable. Industrial and agricultural contaminants were undetectable or within the acceptable range (in trace amounts) for the intended purposes. Greases were found in trace amounts but may be related to the auger used to collect the samples (Hildgen, unpub. rept., 1998).

In general, the commercial samples are comparable in their grain size characteristics to the field samples. However, the commercial samples tend to contain more kaolinite and less non-clay silicates than the field samples. This difference should not be a deterrent for developing this deposit for commercial purposes as at least one of the products examined is mineralogically similar. The levels of metals in the porewaters associated with these materials are within acceptable levels for external use.

## NEXT STEPS

The silty clay materials from the Baie-St-Ludger deposit are currently being assessed for their trace-element content (i.e. as essential nutrients) and their capacity to retain vitamins. If these results are promising and meet the standard requirements they will be presented to Health Canada to obtain any necessary permits for production. Following this, a complete environmental assessment of the deposit and its environ will be required before extraction of the materials can commence.

## ACKNOWLEDGMENTS

Special thanks to E. Hillary for digitizing and computer drafting of map, P. Hunt for SEM analyses, R. Kelly for reproductions of field photographs, and R. Lacroix for final preparation of the SEM photomicrographs. Reviews by L. Dredge and P. Bernatchez (Université Laval) are gratefully appreciated.

## REFERENCES

**Bernatchez, P.**
1997: Géomorphologie et environnements quaternaires du bassin de la rivière aux Anglais, région de Baie-Comeau: étude de la formation de dépôts coquilliers; M.Sc. thesis, Department of Geography and Remote Sensing, University of Sherbrooke, Sherbrooke, Quebec, 233 p.

**Bernatchez, P. and Baker, N.**
1995: Analyse du littoral de la péninsule de Manicouagan; B.Sc. thesis, Department of Geography and Remote Sensing, University of Sherbrooke, Sherbrooke, Quebec, 123 p.

**Bourgeois, P.**
1981: Soignez-vous avec l'argile; Éditions Vecchi, Paris, 124 p.

**Cecutti, A. and Nieboer, E.**
1981: Effects of nickel on animals and humans; *in* Effects of Nickel in the Canadian Environment, National Research Council of Canada, Report 18568, p. 217–260.

**Dextreit, R.**
1976: L'argile qui guérit: mémento de médecine naturelle, Nouvelle Édition Complétée; Éditions Vivre en Harmonie, Paris, 152 p.

**Dredge, L. A.**
1976: The Goldthwait Sea and its sediments: Godbout-Sept-Îles region, Quebec North Shore; *in* Report of Activities, Part C; Geological Survey of Canada, Paper 76-1C, p. 176–180.
1983: Surficial geology of the Sept-Îles area, Quebec North Shore; Geological Survey of Canada, Memoir 408, 40 p.

**Elson, J. A.**
1969: Late Quaternary marine submergence of Quebec; La Revue de géographie de Montréal, v. 23, p. 247–258.

**Foscal-Mella, G.**
1976: Analyse minéralogique des argiles glaciaires; M.Sc. thesis, École Polytechnique, Montréal, Quebec, 148 p.

**Jaworski, J.F.**
1978: Effects of lead in the environment — 1978: quantitative aspects; National Research Council of Canada, Report 16736, 779 p.

**Lindsay, P.J., Percival, J.B., Tsai, A.C., and Wygergangs, M.H.M.**
1998: Investigation of automated particle size analysis techniques; *in* Current Research 1998-E; Geological Survey of Canada, p. 173–182.

**Masson, R.**
1983: La santé par l'argile; M.A. Éditions, Paris, 125 p.

**Ochietti, S.**
1989: Quaternary geology of St. Lawrence Valley and adjacent Appalachian subregion; *in* Chapter 4 of Quaternary Geology of Canada and Greenland, (ed.) R. J. Fulton; Geological Survey of Canada, Geology of Canada, no. 1, p. 350–363 (*also* Geological Society of America, The Geology of North America, v. K-1, p. 350–363).

**Passebecq, A.**
1978: L'Argile pour votre santé: applications thérapeutiques et esthétiques; Éditions Dangles, Paris, 129 p.

**Pories, W.J., Strain, W.H., and Rob, C.G.**
1971: Zinc deficiency in delayed healing and chronic disease; *in* Environmental Geochemistry in Health and Disease, (ed.) H.L. Cannon and H.C. Hopps; Geological Society of America, Memoir 123, p. 73–95.

**Sauvé, P.**
1962: Preliminary report on lower Manicouagan River area Saguenay County; Department of Natural Resources, Geological Surveys Branch, Québec, P.R. no. 481, 6 p .

**Simard, G.**
1972: Levé hydrogéologique Pointe-Lebel et Pointe-aux-Outardes, comté de Saguenay; Ministère des Richesses naturelles, Service de l'Hydrogéologie, Québec, rapport H.G.P.-6, 27 p.

**Torrance, J.K.**
1988: Mineralogy, pore-water chemistry, and geotechnical behaviour of Champlain Sea and related sediments; *in* The Late Quaternary Development of the Champlain Sea Basin, (ed.) N.R. Gadd; Geological Association of Canada, Special Paper 35, p. 259–275.

Geological Survey of Canada Project 680023-ZC

# Nouveau site de la transgression de Mitis à Champlain, vallée du Saint-Laurent, Québec

A.M. Bolduc
CGC-Québec, Sainte-Foy

*Bolduc, A.M., 1999 : Nouveau site de la transgression de Mitis à Champlain, vallée du Saint-Laurent, Québec;* dans *Recherches en cours 1999-E; Commission géologique du Canada, p. 169–174.*

**Résumé :** Les fluctuations du niveau marin dans l'Est du Canada sont relativement bien documentées à l'est de Québec, sur les deux rives de l'estuaire du Saint-Laurent. La présente étude contribue à la reconstitution du prolongement vers l'ouest d'au moins une de ces fluctuations. À Champlain, en Mauricie, la basse terrasse située à une altitude de 6 à 9 m a.n.m. peut être attribuée à la transgression de Mitis. En effet, une datation au $^{14}C$ sur des troncs (*Prunus* sp.) enfouis sous environ 2 m de silts sableux donne un âge de 2 190 ± 60 ans BP (GSC-6304). Bien que la dynamique de la rivière Champlain ait pu contribuer à l'enfouissement du matériel organique, l'âge obtenu indique que ces événements se seraient produits dans un contexte de haut niveau marin associé à la transgression de Mitis. Ces données laissent penser que la basse terrasse entourant le lac Saint-Pierre a été construite à cette époque.

**Abstract:** Sea level fluctuations in eastern Canada are relatively well documented east of Québec City on both shores of the St. Lawrence Estuary. This study contributes to the recognition of one of those fluctuations west of Québec City. At Champlain, in the Mauricie area, the low terrace located at an altitude of 6 to 9 m a.s.l. can be attributed to the Mitis transgression. Indeed, wood logs (*Prunus* sp.) found below 2 m of silty sands have been radiocarbon dated at 2190 ± 60 BP (GSC-6304). The dynamics of the Champlain River may have played a role in the burial of the organic matter, but the age obtained on the logs indicates that these events took place during a high marine stand associated with the Mitis transgression. These data suggest that the low terrace around Lake Saint-Pierre may have been built during that time.

## INTRODUCTION

Lors des travaux de cartographie des formations en surface dans la région de la Mauricie, au Québec méridional (Bolduc, 1999), une petite coupe, située dans un méandre de la rivière Champlain et contenant des troncs d'arbres à sa base, a particulièrement retenu notre attention. Puisque l'enfouissement des matériaux organiques ne semble pas être attribuable à un glissement de terrain (absence de cicatrice de glissement dans la région immédiate), il doit donc (1) être associé à la dynamique fluviale de la rivière Champlain, (2) être le témoin d'une fluctuation du niveau marin relatif qui aurait eu lieu depuis le retrait de la Mer de Champlain, (3) ou encore être le résultat de l'interaction de ces deux phénomènes.

Deux fluctuations du niveau marin relatif sont documentées le long du Saint-Laurent. Il s'agit de la transgression laurentienne (5.6–4 ka, Dionne, 1997) et de la transgression de Mitis (2.5–1.5 ka, Dionne, 1992). La transgression laurentienne (Dionne, 1997) est reconnue sur la rive sud du Saint-Laurent, entre autres à Berthier-sur-Mer, à Montmagny et à Cap-Saint-Ignace. Quant à la transgression de Mitis, elle a été reconnue non seulement sur la rive sud du Saint-Laurent, entre Berthier-sur-Mer et Matane, mais aussi sur la rive nord du fleuve, à Deschambault, à Québec, à Petite-Rivière et à Pointe-aux-Allouettes (Dionne, 1992; fig. 1).

Le site de Champlain aurait également pu être le vestige d'une fluctuation du niveau marin inconnue à ce jour. L'âge de 2 190 ±60 ans BP (GSC-6304), obtenu sur un morceau de bois enfoui, suggère toutefois que le site fait partie de la terrasse Mitis ou, à tout le moins, qu'il est le résultat d'un événement s'étant produit dans le contexte de la transgression de Mitis.

## EMPLACEMENT

Le site se situe en bordure de la rivière Champlain (fig. 2; 72° 19′ 31" de latitude O., 46° 27′ 43" de longitude N.) à environ 20 km au nord-est de Trois-Rivières. On s'y rend en empruntant l'autoroute 40, sortie Champlain, puis la route 359 vers le sud jusqu'à Champlain, puis la route 138 vers l'est jusqu'à la route Sainte-Marie nord et enfin le rang de Picardie sur 500 m vers l'est. À cet endroit, la route passe très près d'un méandre de la rivière Champlain où des troncs enfouis sous environ 2 m de silt sableux sont visibles dans une coupe.

## LA BASSE TERRASSE

Les premières descriptions détaillées d'une basse terrasse située en bordure du Saint-Laurent nous viennent de Goldthwait (1911). L'auteur décrit alors ce qu'il appelle le «rivage Micmac», qui se prolonge sur plus de 350 km sur la rive sud du Saint-Laurent, entre Lévis à l'ouest et Matane à l'est. On le retrouve également sur la rive nord, entre Québec et Saint-Joachim, soit sur une distance d'environ 50 km. Il s'agit d'une surface à peine plus élevée que le niveau des hautes mers (20 pieds, soit 6 m), délimitée du côté du fleuve par la

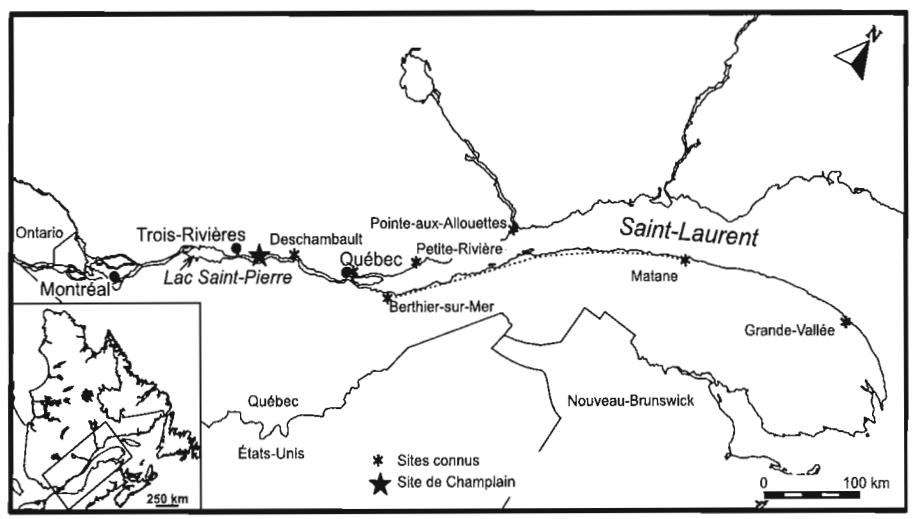


***Figure 1.*** *Sites de la transgression de Mitis le long du Saint-Laurent. Sur la côte sud, entre Berthier-sur-Mer et Matane, plusieurs sites ont été reconnus (Dionne, 1992). Le site de Grande Vallée est un équivalent de la terrasse Mitis (Dionne, 1992). D'autres sites pourraient également exister jusqu'au lac Saint-Pierre, aux endroits où existe une basse terrasse entre 6 et 10 m a.n.m.*

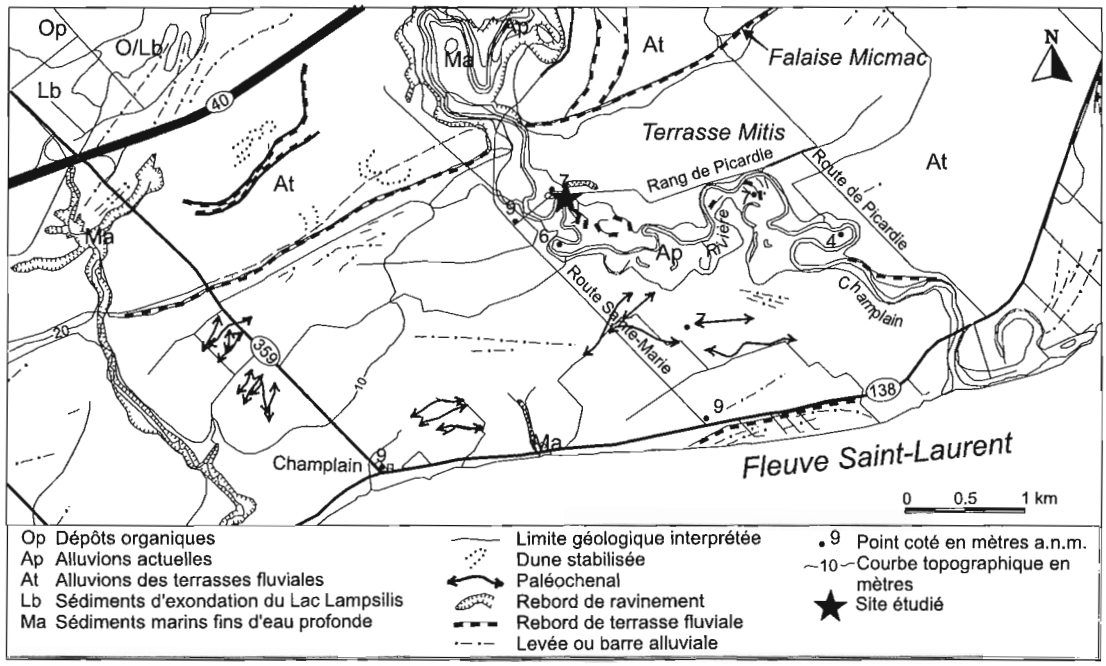


***Figure 2.*** *Carte des formations en surface de la région de Champlain. Le site étudié, identifié par le symbole ★, se trouve sur la rive est de la rivière Champlain. La largeur de la basse terrasse varie de moins de 500 m à plus de 3 km. La falaise Micmac est bien évidente dans le paysage, surtout à l'est de la rivière Champlain. Modifié de Bolduc (1999).*

microfalaise moderne qui borde le Saint-Laurent et à l'arrière par une falaise morte d'environ 20 m de hauteur et pouvant atteindre jusqu'à 40 m (Goldthwait, 1911).

Goldthwait (1911) souligne l'étonnante maturité de ce rivage par rapport au rivage moderne et au rivage qui représente la limite maximale de l'invasion marine postérieure au retrait glaciaire. Il favorise l'hypothèse selon laquelle la basse terrasse sur toute sa longueur et la falaise morte sise à l'arrière de la terrasse auraient été formées au cours d'un même événement, soit une lente submergence des rives du Saint-Laurent après le retrait de la mer. La rive sud du Saint-Laurent aurait ensuite émergée jusqu'au niveau actuel.

Il a fallu attendre les travaux de Dionne (1963) pour relancer l'intérêt dans cet élément géomorphologique présent le long du fleuve et de l'estuaire du Saint-Laurent. Il appert alors que le rivage Micmac défini par Goldthwait (1911) est en fait une série beaucoup plus complexe d'éléments géomorphologiques situés entre 0 et 30 m a.n.m., mais dont la genèse diffère d'un tronçon à un autre. En plus du tronçon reconnu par Goldthwait (1911) sur la rive nord, la basse terrasse est aussi présente au moins entre Deschambault et Charlevoix (Dionne, 1992).

Afin d'éviter toute confusion, Dionne (1963) propose de nommer «terrasse Mitis» les sections du rivage Micmac qui peuvent être directement attribuées à une transgression holocène et qui se situent aux environs de 6 m a.n.m. À l'exception de deux sites (Pointe-aux-Allouettes [Dionne, 1992, 1996a] et une partie de Petite-Rivière [Dionne, 1996b]), toutes les datations effectuées sur des débris organiques provenant de la terrasse Mitis indiquent que cette terrasse a été construite vers 2 000 ans BP (Dionne, 1992). Les sédiments de la terrasse Mitis sont principalement sablo-graveleux et recouvrent un substrat rocheux ou silto-sableux reposant sur un substrat argileux (Dionne, 1992).

## DESCRIPTION DU SITE DE CHAMPLAIN

Le site est situé à un peu plus de 2 km au nord du Saint-Laurent (fig. 2). La falaise morte de 20 m qui délimite la basse terrasse (falaise Micmac, *sensu* Goldthwait, 1911) se trouve à environ 500 m au nord du site étudié. Elle est taillée entièrement dans des matériaux meubles, soit une séquence de sable (entre 5 et 10 m d'épaisseur) sus-jacent à de l'argile (environ 40 m d'épaisseur, Banque de données des puisatiers, ministère de l'Environnement du Québec). Le socle rocheux

a été atteint lors d'un seul forage, soit à plus de 50 m sous la surface de la haute terrasse qui, elle, est à environ 28 m a.n.m. Entre la falaise Micmac et le fleuve, la surface de la basse terrasse est légèrement bosselée et faiblement inclinée vers le Saint-Laurent. Elle est délimitée au sud par la microfalaise moderne qui borde le Saint-Laurent. Les points cotés dans le secteur varient de 4 à 9 m (fig. 2). De petites levées alluviales et de nombreux chenaux et méandres abandonnés caractérisent la surface de la terrasse (Bolduc, 1999). La basse terrasse sous la cote de 10 m est présente de façon presque continue depuis le lac Saint-Pierre (Bolduc, 1999) jusqu'à Grondines (Cloutier et al., 1997).

Entre la falaise Micmac et le fleuve Saint-Laurent, la rivière Champlain serpente dans un couloir d'environ 500 m de largeur et entaille les dépôts de la terrasse jusqu'à une profondeur d'environ 3 m. De nombreux méandres abandonnés et de petits niveaux de terrasse associés à la dynamique holocène de la rivière caractérisent ce tronçon.

La coupe étudiée se situe sur la rive est de la rivière Champlain. Même si la base de la coupe est mal exposée, on peut y distinguer des silts argileux massifs (fig. 3, unité «A») dont l'épaisseur varie de 0 à 50 cm. Ces silts argileux sont surmontés sur une épaisseur d'environ 50 cm d'un enchevêtrement de troncs dans une matrice lâche de silts sableux (fig. 3, unité «B»). Aucun des débris n'est en position de vie. L'altitude du lit organique est de 5 m, compte tenu du point coté le plus près (7 m, fig. 2) et de l'épaisseur du silt recouvrant les troncs. Le niveau organique ligneux est enfoui sous une unité silto-sableuse massive d'environ 2 m d'épaisseur (fig. 3, unité «C»).

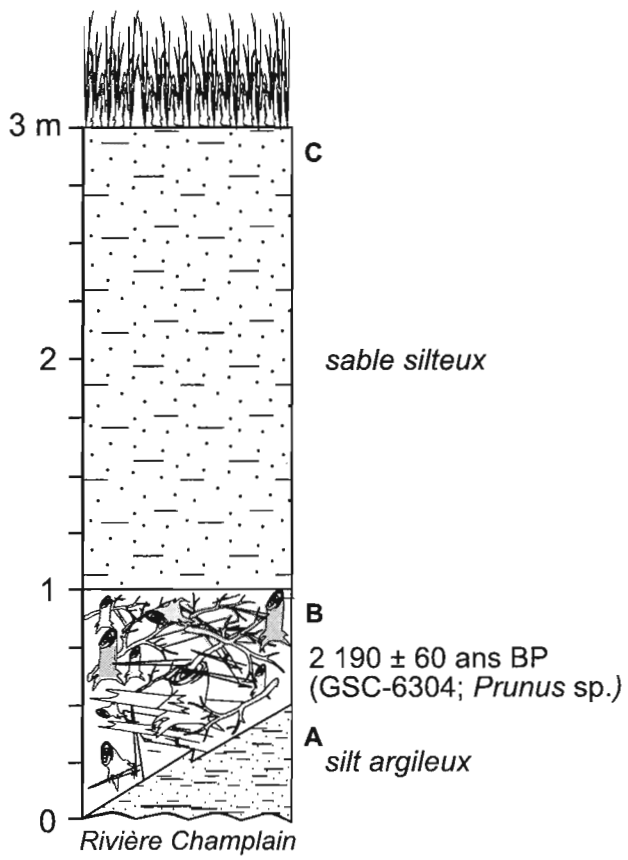


***Figure 3.*** *Coupe stratigraphique de la terrasse Mitis à Champlain. Les silts argileux à la base* ***(A)*** *sont recouverts par un lit de troncs entremêlés* ***(B)*** *que recouvrent des sables silteux massifs* ***(C)****.*

## DATATION

L'échantillon de bois destiné à la datation a été prélevé sur un tronc de *Prunus* d'environ 20 cm de diamètre. Ce genre, auquel appartiennent les cerisiers (quatre espèces au Québec), est largement réparti la région et est typique des milieux perturbés, tels que les bordures de rivières à méandres (C. Bégin, comm. pers., 1999). Le bois a été daté à 2 190 ± 60 ans BP (GSC-6304, $\delta^{13}C$ = -25.6 %; âge normalisé pour $\delta^{13}C$ = -25 % : 2 180 ± 60 BP).

Cet âge représente l'âge de l'accumulation de la terrasse Mitis (Dionne, 1992). En effet, l'âge des débris organiques contenus dans la terrasse s'échelonne de 2 800 ± 200 ans BP (UQ-1389, Dionne, 1996b) à 1 800 ± 70 (Beta-18330, Dionne, 1996b), la médiane étant à 2 030 ± 50 ans BP (Dionne, 1992).

## DISCUSSION

L'enfouissement des troncs en bordure d'une rivière à méandres telle que la rivière Champlain peut être un résultat de la dynamique fluviale. En effet, l'action de la rivière sur la berge en érosion mène à son effondrement, ce qui entraîne la végétation de surface vers le bas du talus. Cette végétation peut être transportée sur une distance plus ou moins grande avant de se stabiliser et d'être enfouie dans un tronçon de rivière en sédimentation. Il n'est donc pas étonnant de retrouver de telles accumulations végétales par endroits le long du corridor alluvial de la rivière. La présence de lits organiques du même âge à l'extérieur de ce corridor alluvial permettrait d'écarter cette hypothèse de la mise en place des troncs au site de Champlain. Toutefois, la correspondance entre l'âge du site et l'âge connu de la terrasse Mitis laisse penser que l'enfouissement des troncs serait associé directement à la transgression ou indirectement à l'influence d'une remontée du niveau marin sur la dynamique fluviale de la rivière Champlain.

Il est plus que probable que toute la séquence de dépôts exposée dans la coupe est associée à la transgression de Mitis. Les silts argileux à la base de la coupe pourraient aussi correspondre à la surface d'érosion originale, puisque dans certains des puits avoisinants, de l'argile, présumément d'origine marine, se retrouve jusqu'à une altitude de 19 m a.n.m. (Banque de données des puisatiers, ministère de l'Environnement du Québec). Toutefois, selon l'hypothèse la plus vraisemblable, la séquence de sables, de silts et d'argiles

mise en place dans la Mer de Champlain et lors de son retrait aurait été érodée au moment de la transgression de Mitis dont le niveau maximal aurait atteint de 8 à 10 m (Dionne, 1996b). Ces sédiments auraient ensuite été redéposés dans la zone littorale à sublittorale. Le même scénario aurait pu se produire au moment de la transgression laurentienne qui, pour sa part, aurait atteint une altitude de 12 m (Dionne, 1997). Lors de la transgression de Mitis, les sédiments champlainiens et laurentiens auraient peut-être été érodés. Une analyse paléoécologique ou la mise à jour d'un lit organique associé à la transgression laurentienne permettrait d'éclaircir ce point.

Si les troncs ont été enfouis lors de la construction de la terrasse, ils pourraient provenir d'une surface plus élevée et avoir été érodés par l'action des vagues lors de la transgression de Mitis. En effet, puisque aucun des troncs n'est en position de vie, il ne peut s'agir que de débris charriés et enfouis lors de la transgression et non pas d'une flore enfouie *in situ* comme c'est le cas à Petite Rivière, par exemple (Dionne, 1996b). Ce niveau organique n'est sans doute pas continu sous la terrasse Mitis, mais il pourrait se retrouver sporadiquement à plusieurs endroits. Il faudrait effectuer des sondages peu profonds (<3 m) et examiner des coupes naturelles et anthropiques afin de mettre à jour certains sites additionnels et ainsi de déterminer avec certitude si la basse terrasse de la région de Champlain remonte bien à la transgression de Mitis, tel que suggéré ici.

La transgression de Mitis aurait duré environ 1000 ans, soit de 2800 à 1800 ans BP dans la région de Petite Rivière (Dionne, 1996b) ou de 2500 à 1500 ans BP dans la région de Montmagny (Dionne, 1998). En acceptant que les troncs enfouis du site de Champlain représentent le début de la transgression de Mitis à cet endroit, il aura fallu entre 300 et 600 ans pour que l'influence de cette fluctuation du niveau marin se fasse sentir dans cette région. Il se peut aussi que les troncs aient été érodés par la rivière Champlain vers 2190 ± 60 ans BP (GSC-6304) et que la terrasse Mitis n'ait été construite qu'ultérieurement, mais avant la fin de la transgression, soit avant 1800 à 1500 ans BP (Dionne, 1996b, 1998).

Bien que la séquence supérieure de sables silteux puisse être le résultat d'une sédimentation alluviale par la rivière Champlain, elle pourrait également correspondre à un dépôt intertidal contemporain de la transgression de Mitis. Dans ce cas et étant donné l'épaisseur de cette unité, l'âge des troncs enfouis et l'âge estimé de la fin de la transgression, le taux moyen de sédimentation aurait été de l'ordre de 3 à 5 mm/année. Il est toutefois probable que l'événement qui a entraîné les troncs jusqu'au site a également provoqué l'accumulation d'une forte proportion des sédiments sus-jacents. Dans ce cas, une partie importante des 2 m de silts sableux aurait été déposée lors d'un seul événement lié à l'interaction entre la dynamique fluviale et la transgression marine et le reste des silts sableux se serait accumulé sur une longue période de temps. Une analyse paléoécologique détaillée permettrait de vérifier cette hypothèse. Lors de l'émersion du site, de petites levées alluviales ont été construites et de petits chenaux ont été érodés à la surface de la terrasse.

## CONCLUSION

La basse terrasse est un élément géomorphologique omniprésent le long des deux rives du Saint-Laurent. Elle est bien documentée et bien datée à plusieurs endroits où elle peut être associée à une fluctuation mineure du niveau marin, soit la transgression de Mitis. Cependant, jusqu'à présent, aucune donnée n'avait été recueillie en amont de Deschambault (Dionne, 1992). Étant donné la faible dénivellation du fleuve, on doit s'attendre à ce que des vestiges de la terrasse soient présents jusqu'à Sorel et de part et d'autre du lac Saint-Pierre. La falaise morte de 20 m qui est bien évidente le long de la rive nord du lac Saint-Pierre et du fleuve serait le rivage Micmac *sensu* Goldthwait (1911). Bien qu'il existe une autre explication de la présence de troncs enfouis en bordure d'une rivière à méandres telle que la rivière Champlain, nous proposons que le site de Champlain représente un témoin du prolongement vers l'ouest de la transgression de Mitis.

## REMERCIEMENTS

La présente étude a été financée par la CGC Québec dans le cadre de son activité «Hydrogéologie régionale» du projet «Les séquences quaternaires du piémont laurentien». Je tiens à remercier l'effectif du laboratoire de géochronologie de la Division de la science des terrains, en particulier R. McNeely pour la datation du bois, et C. Keith de la firme Wood Technology Consultants (contractuel pour la Division de la science des terrains) pour l'identification de l'échantillon soumis. Je remercie sincèrement L. Dubé pour l'exécution des figures et C. Bégin, lecteur critique, pour ses commentaires et discussions qui ont grandement amélioré ce manuscrit.

## RÉFÉRENCES

**Bolduc, A.M.**
1999: Géologie des formations superficielles, région de Trois-Rivières, Québec; Commission géologique du Canada, Dossier public 2994 (échelle de 1/50 000).

**Cloutier, M., Parent, M. et Bolduc, A.M.**
1997: Géologie des formations superficielles, région de Saint-Marc-des-Carrières, Québec; Commission géologique du Canada, Dossier public 3544 (échelle de 1/100 000).

**Dionne, J.-C.**
1963: Le problème de la terrasse et de la falaise Mic Mac; Revue canadienne de géographie, vol. 17, p. 9–25.
1992: État des connaissances sur la terrasse Mitis : ligne de rivage Micmac de Goldthwait; Bulletin de l'Association québécoise pour l'étude du Quaternaire, vol. 18, p. 32–33.

**Dionne, J.-C.** (suite)
1996a: La terrasse Mitis à la Pointe-aux-Allouettes, côte nord du moyen estuaire du Saint-Laurent, Québec; Géographie physique et Quaternaire, vol. 50, p. 57–72.
1996b: La basse terrasse à Petite-Rivière (Charlevoix, Québec) : un exemple d'activité néotectonique à l'Holocène; Géographie physique et Quaternaire, vol. 50, p. 311–330.
1997: Nouvelles données sur la transgression laurentienne, côte sud du moyen estuaire du Saint-Laurent, Québec; Géographie physique et Quaternaire, vol. 51, p. 201–210.
1998: Relative sea-level variations during the Holocene, Middle Saint Lawrence Estuary; Association géologique du Canada–Association minéralogique du Canada, Réunion annuelle conjointe, Québec 1998; Guide d'excursion B1, 49 p.

**Goldthwait, J.W.**
1911: The twenty-foot terrace and sea cliff of the Lower St. Lawrence; American Journal of Science, v. 32, p. 291–317.

Projet 960001 HD de la Commission géologique du Canada

# Textural characteristics of low to high resistivity, low anisotropy volcanic tuffs, Bathurst mining camp, New Brunswick

S. Connell, T.J. Katsube, and P.A. Hunt
Mineral Resources Division, Ottawa

*Connell, S., Katsube, T.J., and Hunt, P.A., 1999: Textural characteristics of low to high resistivity, low anisotropy volcanic tuffs, Bathurst mining camp, New Brunswick;* in *Current Research 1999-E; Geological Survey of Canada, p. 175–181.*

**Abstract:** Detailed textural analysis by scanning electron microscopy (SEM) has been carried out on four rock samples from the Bathurst mining camp, New Brunswick. The purpose was to characterize the degree to which deformation and veining can affect the electrical characteristics of tuffaceous rocks. Resistivities parallel and perpendicular to foliation are in the ranges of 100–1000 Ω·m and 1700–2200 Ω·m, respectively.

Results indicate that resistivity values are affected by varying degrees of silicification and quartz veining accompanied by iron-oxide stringers. They also indicate that clay-sized phyllosilicates have the potential to increase the electrical conductivity along the long axis of the grain and increase the resistivity perpendicular to the foliation when aligned parallel to foliation. Further analysis is required to determine the difference in effect, if any, of the resistivity of Mg-rich chlorite as compared to that of Fe-rich chlorite.

**Résumé :** On a réalisé une analyse détaillée par microscopie électronique à balayage de la texture de quatre échantillons de roche du camp minier de Bathurst (Nouveau-Brunswick) afin de déterminer dans quelle mesure la déformation et la présence de filons peuvent influer sur les caractéristiques des roches tufacées. Les résistivités dans les directions parallèle et perpendiculaire à la foliation sont de l'ordre de 100 à 1000 Ω·m et de 1700 à 2200 Ω·m, respectivement.

Les résultats indiquent que les valeurs de résistivité sont affectées par le degré de silicification et la présence de filons de quartz accompagnés de filonnets d'oxyde de fer. Ils indiquent aussi que les phyllosilicates de la grosseur de l'argile ont le potentiel d'accroître la conductivité électrique le long de l'axe longitudinal du grain et d'accroître la résistivité dans la direction perpendiculaire à la foliation, quand ils sont alignés parallèlement à la foliation. D'autres analyses sont requises pour déterminer l'effet sur la résistivité, le cas échéant, des chlorites magnésiennes par rapport aux chlorites riches en fer.

## INTRODUCTION

Detailed textural analysis by scanning electron microscopy (SEM) has been carried out on four rock samples from the Bathurst mining camp, New Brunswick (Table 1). The purpose was to characterize the degree to which deformation and veining can affect the electrical characteristics of tuffaceous rocks. Electrical anisotropies are low for these samples, averaging 2:1. This was expected, given the weak to moderate foliation present, although, it is also low for samples with veins. These sample specimens were chosen based mainly on electrical resistivity values determined in previous studies (Katsube et al., 1998b, c; Connell et al., 1998; Table 2). Resistivities parallel and perpendicular to foliation are in the ranges of 100–1000 Ω·m and 1700–2200 Ω·m, respectively, values well within the range of those previously reported (Keller, 1966) for rhyolitic tuffs (10–1400 Ω·m). A previous study (Connell et al., 1999b) suggested that the low electrical anisotropy of rocks similar to these samples were likely attributed to the weak to moderate foliation along with the mineralogy. This paper documents the relationships observed between the rock texture and electrical resistivity ($\rho_r$) and anisotropy ($\lambda$) values.

## METHODS OF INVESTIGATION

The four sample specimens selected for this study display low to high electrical resistivity values and were collected from various regions in the Bathurst mining camp, New Brunswick. One sample is from the Restigouche deposit (Katsube et al., 1998b). The other three samples are from the Stratmat deposit (Connell et al., 1998). Information on drill hole identification, sample depth, formation, and lithology for all foliated tuffs examined are listed in Table 1. The sample specimens used in this study (MXD-1, MXF-1, MXF-9, and MXF-21) were selected from a larger set of 21 volcanic tuffs specimens (Katsube et al., 1997, 1998a, b, c; Connell et al., 1998), on the basis of their electrical characteristics. For the most part, each sample specimen selected for this study, displays lower resistivity values which are well within the accepted range for rhyolitic tuffs (10–1400 Ω·m; Keller, 1966). Sample specimen MXF-9, which is considerably more resistive than the others, was selected as it represented the high resistivity end of the crystal tuffs measured. Sample specimen MXF-21 was selected to represent the conductive end. Detailed information on a few of the more resistive samples from this suite of volcanic tuffs can be found elsewhere (Connell et al., 1999a).

**Table 1.** Sample identification.

| Sample number | Deposit | Drill hole | Depth (m) | Lithology |
|---|---|---|---|---|
| MXD-1 | Restigouche | R-95-2 | 23.9 | Lapilli tuff |
| MXF-1 | Stratmat | ST218 | 37.8 | Lapilli tuff |
| MXF-9 | Stratmat | ST219 | 72.3 | Crystal tuff |
| MXF-21 | Stratmat | ST221 | 86.5 | Crystal tuff |

Specimens for the electrical measurements were previously taken (e.g. Katsube et al., 1998b; Connell et al., 1998) from these samples and were cut into rectangular shapes with the edges either parallel or perpendicular to foliation. First, a detailed visual examination was performed and the key features were recorded or described, as shown in the block diagrams of Figures 1, 2, 3, and 4. Following the analysis of the electrical resistivity values, achieved through geo-impedance spectroscopy, specimen surfaces which best represented the areas of interest were polished and prepared for scanning electron microscope (SEM) analysis. Results of the electrical measurements of these sample specimens were previously reported (Katsube et al., 1998b; Connell et al., 1998). The SEM analysis allowed a close examination of the sample mineralogy, texture, and fabric, including the connectivity of the sulphide and other mineral grains.

An image analysis procedure using a scanning electron microscope (SEM) was used to study, in detail, the textural characteristics of a specimen surface (e.g. grain shape, orientation, mineralogy, connectivity). A Leica/Cambridge S-360 scanning electron microscope (SEM) with an Oxford/Link eXL-II energy dispersive X-ray analyzer was used in this

**Table 2.** Results of electrical resistivity measurements.

| Specimen | Lithology | $\delta_B$ (g/mL) | Mean $\rho_r$, ($10^3$ m) | | | Anisotropy $\lambda$ |
|---|---|---|---|---|---|---|
| | | | $\alpha$ | $\beta$ | $\gamma$ | |
| MXD-1A | Lapilli tuff | 2.86 | 0.49 | 0.8 | – | 1.6:1 |
| MXD-1B | Lapilli tuff | 2.86 | 0.74 | – | – | – |
| MXD-1C | Lapilli tuff | 2.8 | 1.57 | – | – | – |
| MXF-1A | Lapilli tuff | 3.1 | 1.32 | – | – | – |
| MXF-1B | Lapilli tuff | 3.15 | 2.16 | 0.98 | – | 2:1 |
| MXF-9 | Crystal tuff | 3.11 | 15.95 | 6 | 3.13 | 5:1 |
| MXF-21 | Crystal tuff | 3.24 | 1.72 | 1.17 | 0.41 | 3:1, 4:1 |

$\rho_r$ = Bulk electrical resistivity
$\delta_B$ = Bulk density (g/mL)
$\alpha$ = Direction measured perpendicular to foliation (if any)
$\beta$ = Direction measured parallel to foliation (if any)
$\gamma$ = Direction measured parallel to lineation (if any)
– = No data

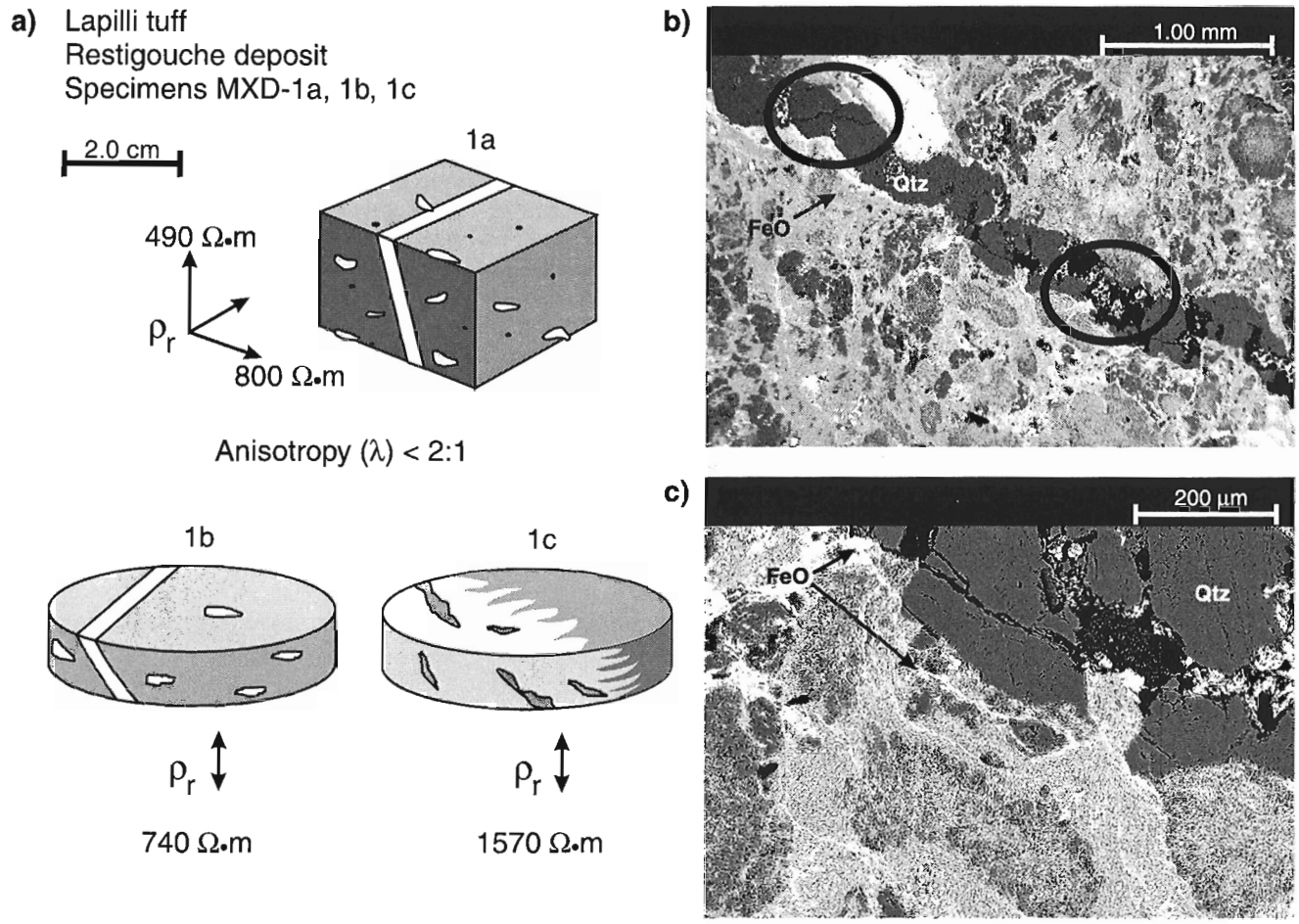


***Figure 1.*** *a) Schematic representation for specimens MXD-1a, MXD-1b, and MXD-1c and b) and c) SEM images for specimen MXD-1a, with electrical resistivities ($\rho_r$) and electrical anisotropy ($\lambda$) value. The SEM images (backscattered image, BSI) highlight the quartz (Qtz) vein with the iron oxide (FeO) stringers.*

study. Operating conditions for the SEM were generally 20 kV accelerating voltage at a 25 mm working distance. Backscattered electron images (BSI) were produced as a result. A detailed description of the SEM methods and procedures can be found elsewhere (Reed, 1997).

## ANALYTICAL RESULTS

Schematic representations of sample specimens MXD-1a, b, and c are displayed in Figure 1a. Either adjacent or below each block diagram are displayed the directions of electrical resistivities. Specimen MXD-1a has a resistivity value ($\rho_r$) of 490 Ω·m parallel to a quartz vein and 800 Ω·m perpendicular to the vein. Specimens MXD-1b and MXD-1c have resistivities of 740 Ω·m and 1570 Ω·m, respectively. Specimen MXD-1c is believed to have a higher $\rho_r$ value (1570 Ω·m) as a result of increased silicification. The sample is a lapilli tuff with quartz, K-feldspar, apatite, monazite, rutile, zircon, and iron oxide identified under the scanning electron microscope (SEM). The SEM images for the left-side of specimen MXD-1a are displayed in Figure 1b and 1c. From the $\rho_r$ values (740 Ω·m) of specimen MXD-1b, it seems reasonable to conclude that the $\rho_r$ value for sample MXD-1, barren of the quartz vein, is 740 Ω·m, since the measurement is performed in a direction such that the traversing electrical current would not be interrupted by the quartz vein that would normally be considered an electrical insulator. The fact that the $\rho_r$ value (800 Ω·m) for specimen MXD-1a in the direction perpendicular to its quartz vein is similar to that of MXD-1b, but that the $\rho_r$ value (490 Ω·m) parallel to the quartz vein is smaller than that of the other direction, implies that the quartz vein of this specimen is not acting as an electrical insulator, as might be the case for specimen MXD-1b, but is a poor conductor. The SEM images display visible iron-oxide stringers which could be acting as poor conductors parallel to the vein, and explains the lower $\rho_r$ (490 Ω·m) in this direction. In addition, the SEM images show considerable numbers of fractures in the vein, suggesting that the normally expected insulating nature of the quartz vein to a traversing electrical current is unlikely to exist, in this case. Two sections are highlighted in Figure 1b. The upper highlighted area shows an open microfracture (black crack) clearly traversing the quartz vein. The lower highlighted area shows two black sections indicating open

pores traversing the vein. These open microfractures and pores would be saturated with pore water under in situ conditions and would allow electrical currents to traverse the vein. This could explain the reason for the $\rho_r$ value of sample specimen MXD-1a in the direction perpendicular to the vein being 800 Ω·m, rather than being more than 1000 Ω·m, which would be normal for such a case (*see* Fig. 2a).

Schematic representations of sample specimens MXF-1a and MXF-1b are displayed in Figure 2a. The directions of the electrical resistivities are displayed adjacent to each block diagram. Specimen MXF-1a has a siliceous vein which cross-cuts the foliation. The resistivity measured perpendicular to the vein is 1320 Ω·m. Specimen MXF-1b has a resistivity of 2160 Ω·m perpendicular to foliation and 980 Ω·m parallel to foliation. These data suggest that the resistivities of this sample parallel and perpendicular to the foliation are about 1000 Ω·m and 2000 Ω·m, respectively, and that the quartz vein (≤ mm in thickness) has raised the parallel resistivity to about 1300 Ω·m. The low λ for this sample (2:1) reflects the weak to moderate foliation of the tuff. Plagioclase, Mg-rich chlorite, and biotite in the groundmass with some rutile and pyrite have been identified by the SEM. The plagioclase is the darker grey on the SEM image and the biotite and chlorite are indicated by lighter grey (Fig. 2b, c). The vein consists of quartz, K-feldspar, calcite, pyrite, chalcopyrite, and galena (Fig. 2b). Both images are of the surface perpendicular (left-hand surface of sample specimen MXF-1a) to the foliation for specimen MXF-1a and the upper image (Fig. 2b) is a closeup of the vein. The quartz vein increases the resistivity by only about 300 Ω·m, but does not act as a good insulator, probably a result of the porous nature (a result of crystal growth) and varied mineralogy (e.g. calcite) in the vein. The relatively large micropores are highlighted in Figure 2b.

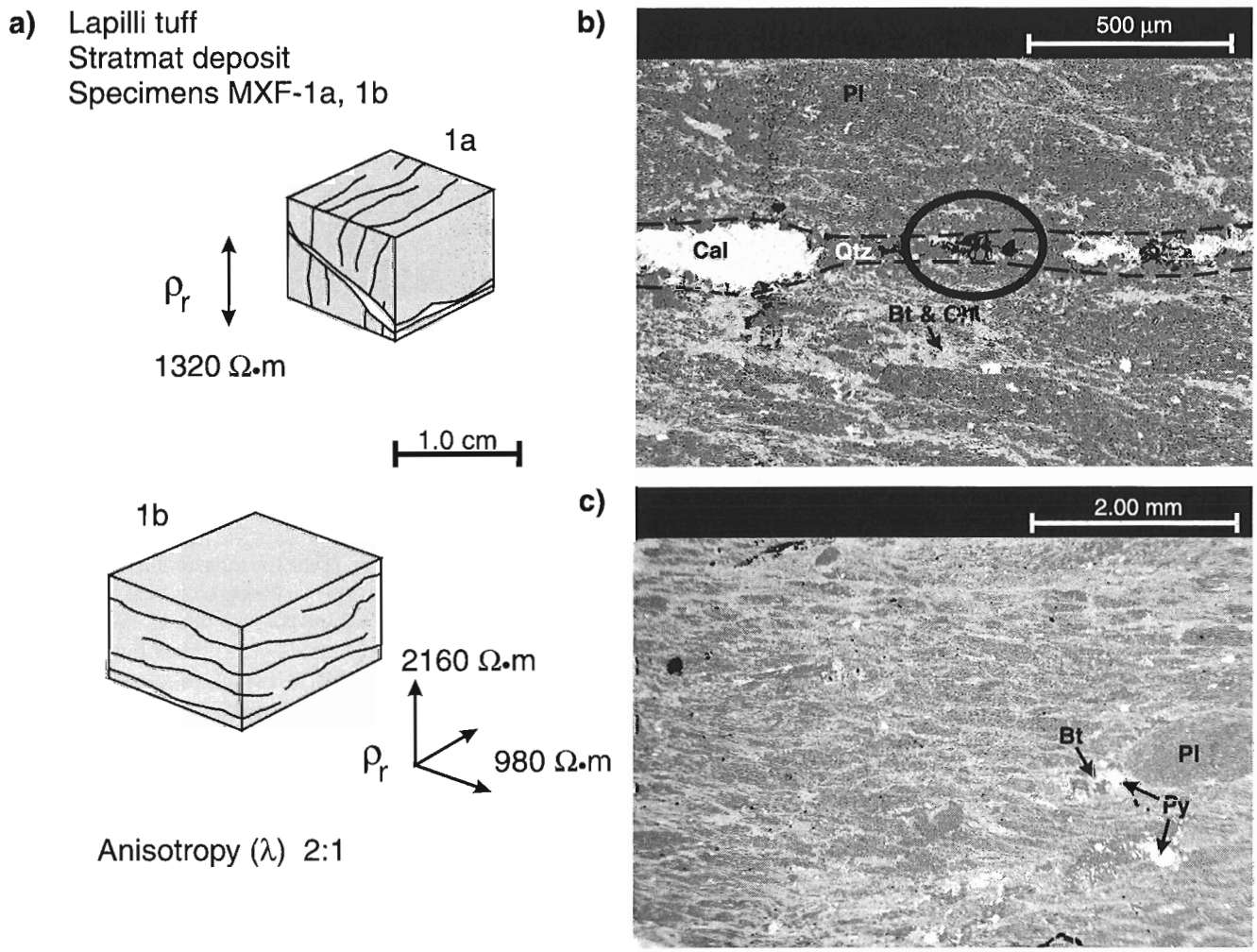


***Figure 2. a)*** *Schematic representation for specimens MXF-1a and MXF-1b and* ***b)*** *and* ***c)*** *SEM images for specimen MXF-1a, with $\rho_r$ and λ values (lower left-hand section of Fig. 1a). The SEM images (BSI) highlight the quartz (Qtz)-calcite (Cal) vein (dashed line) and displays the distribution of plagioclase (Pl), biotite (Bt), and chlorite (Chl) within the groundmass of* ***b)****. Disseminated pyrite (Py) grains are also indicated in* ***c)****.*

The schematic representation of sample specimen MXF-9 is displayed in Figure 3a. The directions of electrical resistivities are shown below the block diagram with 3050–5600 Ω·m and 15 680 Ω·m in the directions parallel and perpendicular to foliation ($S_1$), respectively. The anisotropy for this sample is less than 5:1. The mineralogy of this tuff includes plagioclase, quartz, chlorite, sphalerite, pyrite, rutile, biotite, apatite, and zircon, which were identified under SEM (Fig. 3b, c). A preferential alignment of chlorite grains (parallel to the foliation) is seen in Figure 3c, and an enlargement is seen in Figure 3b. These thin chlorite layers are interspersed in a groundmass dominated by plagioclase and quartz. The lower $\rho_r$ values (3000–6000 Ω·m) are associated with the direction of the thin chlorite layers, and the high $\rho_r$ values (16 000 Ω·m) are in the direction perpendicular to the foliation.

The schematic representation of sample specimen MXF-21 is displayed in Figure 4a. The $\rho_r$ values for the three directions (α, β, and γ) are displayed adjacent to the block diagram. This sample shows a lineation in the γ-direction and a foliation that coincides with the β-γ plane. The mineralogy is similar to that of sample specimen MXF-9, but the electrical resistivities are considerably lower. The $\rho_r$ value parallel to the lineation and foliation (γ-direction) is 410 Ω·m. The value parallel to foliation and perpendicular to lineation (β-direction) is 1170 Ω·m and the value perpendicular to foliation and lineation (α-direction) is 1720 Ω·m. The resulting electrical anisotropies are about 3:1 to 4:1. These low anisotropy values are expected, due to the discontinuity of the linear feature defined by quartz (Fig. 4a, b). The SEM images (Fig. 4b, c, d) indicate that the groundmass is predominantly silica (dark grey) and biotite with clay-sized minerals (light grey).

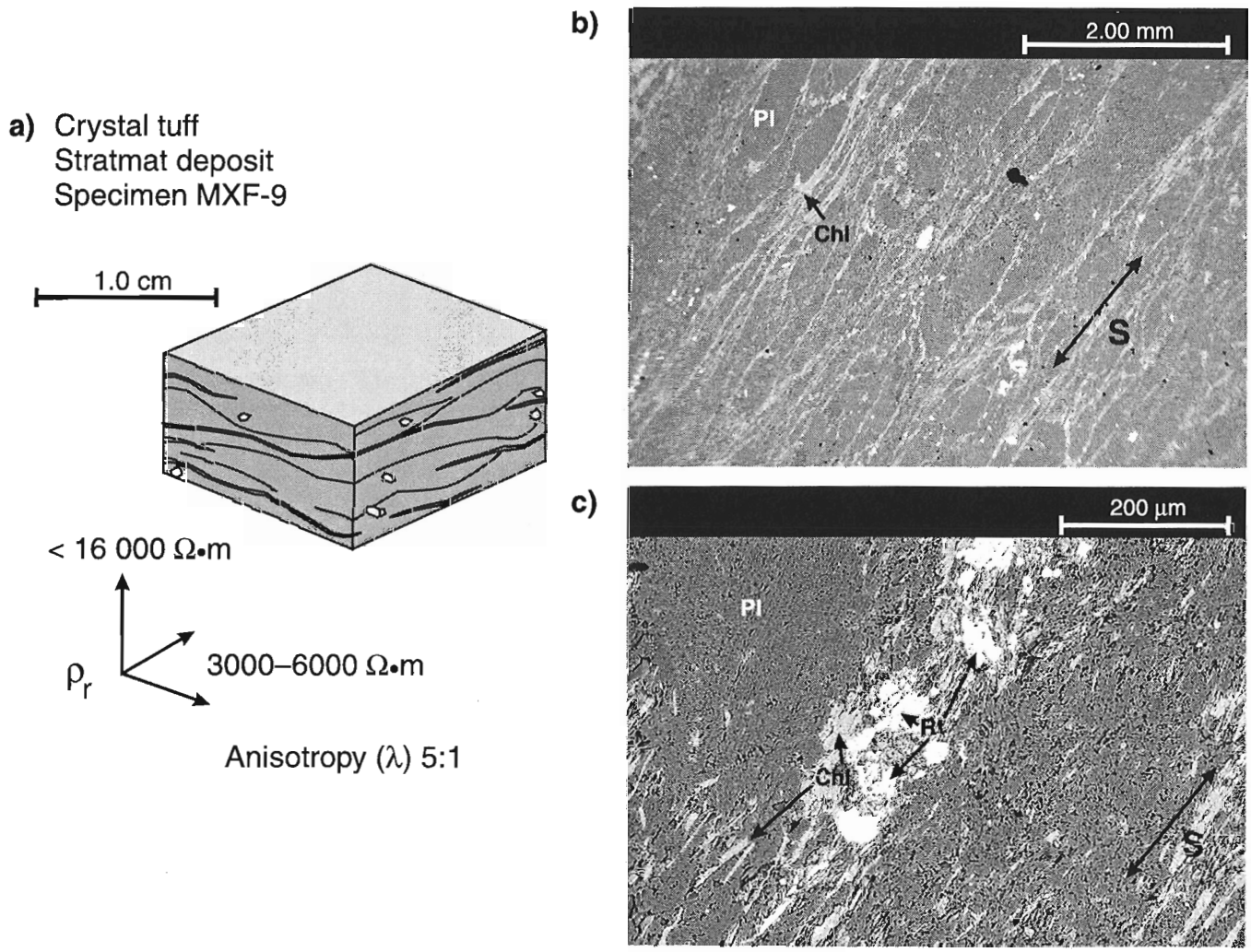


***Figure 3.*** *a) Schematic representation and* ***b)*** *and* ***c)*** *SEM images for specimen MXF-9, with $\rho_r$ for the two directions and their λ value (lower left-hand section of Fig. 3a). The SEM images (BSI) show the orientation and distribution of plagioclase (Pl), chlorite (Chl), and rutile (Rt) within the specimen. The foliation direction is indicated by $S_1$.*

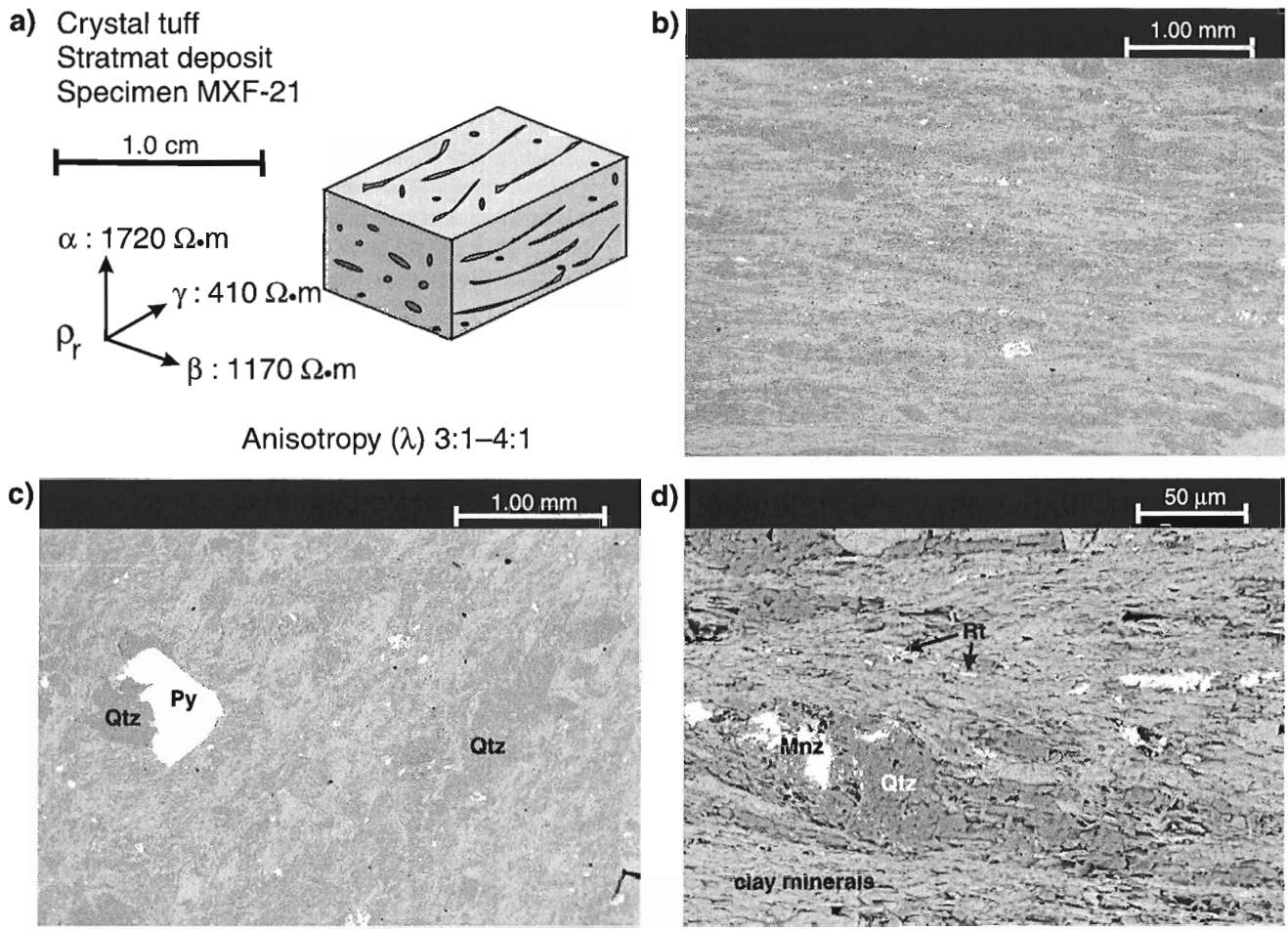


***Figure 4.*** *a) Schematic representation and* ***b), c),*** *and* ***d)*** *SEM images for specimen MXF-21, with* $\rho_r$ *for the three directions and* $\lambda$ *value. Minerals identified in the SEM images (BSI) include quartz (Qtz), pyrite (Py), rutile (Rt), monazite (Mnz), and clay size minerals.*

Figure 4b represents the right-hand surface of the block diagram (Fig. 4a), parallel to the lineation and perpendicular to foliation. Figure 4c represents the left-hand surface of the block diagram, perpendicular to the lineation. Figure 4d is a closeup of Figure 4b. Trace to minor amounts of apatite, pyrite, sphalerite, monazite, rutile, zircon, and galena grains disseminated throughout the groundmass were also identified by the SEM. The lower $\rho_r$ values are associated with the lineation which is visually defined by quartz. The SEM images indicate that the foliation is characterized by preferential alignment of the grains, such as platy minerals, aligned parallel to foliation and/or lineation (Fig. 4d).

## DISCUSSION AND CONCLUSIONS

The electrical anisotropy ($\lambda$) values for these four volcanic tuff samples are in the range of 2:1 to 5:1 and the electrical resistivity ($\rho_r$) values in the direction parallel and perpendicular to their foliation are in the ranges of 410–3130 Ω·m and 490–15 950 Ω·m (Fig. 1, 2, 3, 4) respectively.

Sample MXD-1 is a good example of how local textural variations can affect the electrical response of a rock. From a 9 cm section of core, resistivity values ranged from 490–1570 Ω·m (Fig. 1). These fluctuations resulted from varying degrees of silicification and quartz veining accompanied by iron-oxide stringers.

SEM analysis identified a higher Mg content in the chlorite found in sample specimens MXF-1, MXF-9, and MXF-21. This Mg-rich chlorite, in contrast to Fe-rich chlorite, is commonly associated with Kuroko-type deposits (McCutcheon, 1992). Further analysis is required to determine the effect, if any, of Mg-rich chlorite as opposed to Fe-rich chlorite affecting the resistivity. The possibility of elemental variations affecting electrical properties was raised in a previous publication (Connell et al., 1999b) where Fe-rich and K-depleted halos in a felsic volcanic rock appeared to be one of the few features contributing to the anisotropy of the sample specimen.

Sample MXF-9 and MXF-21 show variations within a rock type and represent the high and low resistivity end of all the crystal tuffs from the Bathurst mining camp. The $\rho_r$ values in the three directions, $\alpha$, $\beta$, and $\gamma$ for the two specimens MXF-9 and MXF-21, have a difference of 9:1, 5:1, and 7.6:1 in ratios, respectively. The differences in $\rho_r$ values are likely a result of mineralogy and grain shape and/or orientation. The mineralogy is essentially the same between the two sample specimens except for the abundance of plagioclase in sample specimen MXF-9. Sample MXF-21 clearly has a higher clay mineral content. The resulting effect being more pronounced when the minerals are aligned parallel to each other. While not as strong conductors as sulphides, clay minerals have the potential to increase the electrical conductivity along the long axis of the grains but allow the resistivity to increase in the direction perpendicular to the foliation.

It is likely that the slightly lower values (410 $\Omega$·m) in the $\gamma$-direction for sample specimen MXF-21, are related to the preferential alignment of the grains. The higher $\rho_r$ values in the $\alpha$-direction are likely due to the alignment of the quartz in the $\beta$-$\gamma$ direction. The result is quartz grains that interrupt the electrical current flow in the $\alpha$-direction, but do not act as insulators because of the lack of continuous quartz grain contact. This is probably the reason the $\rho_r$ values in the $\alpha$-direction are in the 1700 $\Omega$·m range rather than the more than 16 000 $\Omega$m range which was the case for $\rho_r$ values for sample specimen MXF-9, in the direction perpendicular to foliation (Fig. 3). The reason for the intermediate value of 1170 $\Omega$m in the $\beta$-direction is not clear at present.

These four samples are characterized by low $\lambda$ values (2:1 to 5:1), and a lack of very low $\rho_r$ values (<10 $\Omega$·m) in the conductive direction due to the absence of sulphides or clay and sulphide layers (Connell et al., 1999b), and a lack of very high $\rho_r$ (>10 000 $\Omega$·m) in the resistive direction (except for sample MXF-9) due to the absence of well defined siliceous layers acting as good electrical insulators. In the case of sample MXF-9, the high $\rho_r$ value (16 000 $\Omega$·m) in the direction perpendicular to the foliation is associated with the higher plagioclase and quartz content in the groundmass. Except for sample MXD-1, the conductive direction of these samples appears to be associated with chloritic layers or other mineral grains aligned parallel to that direction. In the case of sample MXD-1 (Fig. 1), the quartz vein, which has unusual characteristics, appears to define the $\lambda$ value. Contrary to the usual cases where quartz veins act as electrical insulators (e.g. Katsube et al., 1997), the quartz veins in this case are either ineffective due to frequent fractures, or act as a poor electrical conductor due to iron-oxide stringers. Consequently, the connecting porosity and resistivity-formation factor may control the electrical resistivities of these samples.

## ACKNOWLEDGMENTS

This work has been supported by funds from P. Keatings' (Continental Geoscience Division) project. The authors are grateful to P. Keating for critically reviewing this paper. This manuscript was greatly improved as a result of discussions and comments by K. Shaw (Lacuna Digital Imaging Inc.).

## REFERENCES

**Connell, S., Katsube, T.J., Best, M.E., Goodfellow, W.D., and Mwenifumbo, J.**
1998: Electrical characteristics of mineralized and nonmineralized rocks at the Stratmat deposit, Bathurst mining camp, New Brunswick; *in* Current Research 1998-E; Geological Survey of Canada, p. 149–162.

**Connell, S., Katsube, T.J., and Hunt, P.A.**
1999a: Textural characteristics of moderate to strongly foliated volcanic tuffs that display high resistivity and anisotropy values, Bathurst mining camp, New Brunswick; *in* Current Research 1999-E; Geological Survey of Canada.

**Connell, S., Katsube, T.J., Hunt, P.A., and Walker, D.**
1999b: Textural characteristics of rocks that display significant electrical anisotropy; *in* Current Research 1999-D; Geological Survey of Canada, p. 9–15.

**Katsube, T.J., Connell, S., Goodfellow, W.D., and Scromeda, N.**
1998a: Electrical characteristics of non-mineralized rocks from the Bathurst mining camp, New Brunswick; *in* Current Research 1998-E; Geological Survey of Canada, p. 125–137.

**Katsube, T.J., Connell, S., Goodfellow, W.D., Scromeda, N., and Best, M.E.**
1998b: Electrical characteristics of mineralized and non-mineralized rocks at the Caribou deposit, Bathurst mining camp, New Brunswick; *in* Current Research 1998-D; Geological Survey of Canada, p. 25–35.
1998c: Electrical characteristics of mineralized and non-mineralized rocks at the Restigouche deposit, Bathurst mining camp, New Brunswick; *in* Current Research 1998-E; Geological Survey of Canada, p. 139–148.

**Katsube, T.J., Scromeda, N., Best, M.E., and Goodfellow, W.D.**
1997: Electrical characteristics of mineralized and non-mineralized rocks at the Brunswick No.12 deposit, Bathurst mining camp, New Brunswick; *in* Current Research 1997-E; Geological Survey of Canada, p. 97–107.

**Keller, G.V.**
1966: Electrical properties of rocks and minerals; *in* Handbook of Physical Constants, (ed.) S.P. Clark, Jr.; Geological Society of America, Memoir 97, p. 553–577.

**McCutcheon, S.R.**
1992: Base-metal deposits of the Bathurst-Newcastle district: Characteristcs and depositional models: Exploration Mining Geology, v. 1, no. 2, p. 105–119.

**Reed, S.J.B.**
1997: Electron Microprobe Analysis; Cambridge University Press, Cambridge, U.K., 346 p. (second edition).

Geological Survey of Canada Project 870057

# Textural characteristics of moderate to strongly foliated volcanic tuffs that display high resistivity and anisotropy values, Bathurst mining camp, New Brunswick

S. Connell, T.J. Katsube, and P.A. Hunt
Mineral Resources Division, Ottawa

*Connell, S., Katsube, T.J., and Hunt, P.A., 1999: Textural characteristics of moderate to strongly foliated volcanic tuffs that display high resistivity and anisotropy values, Bathurst mining camp, New Brunswick;* in *Current Research 1999-E; Geological Survey of Canada, p. 183–188.*

**Abstract:** Detailed texture analysis by scanning electron microscopy (SEM) has been carried out on three volcanic tuff specimens (Bathurst mining camp, New Brunswick). The purpose was to determine the cause of the high electrical anisotropy ($\lambda$ = 24:1 to 67:1) and the high electrical resistivity ($\rho$), and to characterize the degree to which deformation and/or foliation can affect the electrical signature of tuffaceous rocks. Resistivities perpendicular and parallel to foliation are 7000–15 000 Ω·m and 150–600 Ω·m, respectively.

Results indicate that the high $\rho$ values (7000–15 000 Ω·m) in the direction perpendicular to the foliation are due to the tight siliceous and/or feldspathic layers acting as electrical insulators to the traversing electrical current. They also indicate that the increased chlorite content resulting from the recrystallization of various minerals during metamorphism and parallel alignment of grains may be the source of the lower $\rho$ values (150–600 Ω·m) in the direction parallel to the foliation.

**Résumé :** On a réalisé une analyse détaillée par microscopie électronique à balayage de la texture de trois échantillons de tuf volcanique du camp minier de Bathurst (Nouveau-Brunswick) afin de déterminer la cause de l'anisotropie électrique élevée ($\lambda$ = 24/1 à 67/1) et de la résistivité électrique ($\rho$) élevée et aussi de déterminer dans quelle mesure la déformation ou la foliation peuvent influer sur la signature électrique des roches tufacées. Les résistivités dans les directions perpendiculaire et parallèle à la foliation sont de 7000 à 15 000 Ω·m et de 150 à 600 Ω·m, respectivement.

Les résultats indiquent que les valeurs élevées de $\rho$ (7000–15 000 Ω·m) dans la direction perpendiculaire à la foliation sont dues aux couches siliceuses ou feldspathiques compactes qui agissent comme des isolateurs électriques envers le courant électrique qui les traverse. Ils indiquent aussi que la teneur plus élevée en chlorite, qui est attribuable à la recristallisation de divers minéraux pendant le métamorphisme, et l'alignement parallèle des grains peuvent être à l'origine des faibles valeurs de $\rho$ (150–600 Ω·m) dans la direction parallèle à la foliation.

## INTRODUCTION

Detailed texture analysis by scanning electron microscopy (SEM) has been carried out on three specimens representing two tuffaceous samples from the Bathurst mining camp, New Brunswick (Table 1). The purpose was to determine the cause of the relatively high electrical anisotropy ($\lambda$ = 24:1 to 67:1), the high electrical resistivity ($\rho_r$) (values up to 10 times higher than those commonly seen in tuffs), and also to characterize the degree to which deformation and/or foliation can affect the electrical signature of this rock type. These three specimens represent typical examples of tuffs that have strong foliation and high anisotropy characteristics. They were chosen from previous studies based mainly on their high anisotropy values (Katsube et al., 1998b). Resistivities perpendicular and parallel to foliation are 6930 to 14 820 $\Omega$·m and 150–600 $\Omega$·m (Table 2), respectively. Previously reported values (Keller, 1966) for rhyolitic tuffs are 10–1400 $\Omega$·m. A previous study (Connell et al., 1999b) suggested that the anisotropic properties resulted from grain connectivity or layering of electrically conductive minerals and the preferred orientation of grains parallel to foliation. This paper documents the relationships observed between the rock texture and electrical resistivity ($\rho$) and anisotropy ($\lambda$) values.

## METHODS OF INVESTIGATION

The three specimens selected for this study were collected from the Caribou deposit in the Bathurst mining camp, New Brunswick. Information on drillhole identification numbers, sample depth, formation, and lithology for these foliated tuffs are listed in Table 1. The specimens used in this study (MXC-2a, MXC-2b, and MXC-8) were selected from a suite of 21 specimens representing 16 tuffaceous samples, which was compiled from previously studied samples from various deposits in the Bathurst mining camp (Katsube et al., 1997, 1998a, b, c; Connell et al., 1998). This suite of samples consists of felsic, crystal and lapilli tuff specimens with resistivity values of 5730–24 690 $\Omega$·m in the directions perpendicular to foliation and 200–6000 $\Omega$·m in the directions parallel to foliation. The samples are weak to strongly foliated and have anisotropy values of 2:1 to 67:1. The selected specimens, studied in this paper, were chosen on the basis of their characteristic strong foliation and high anisotropy. Analytical results of the rest of the samples can be found elsewhere (e.g. Connell et al., 1999a).

**Table 1.** Sample identification.

| Sample number | Deposit | Drill hole | Depth (m) | Lithology |
|---|---|---|---|---|
| MXC-2a | Caribou | 62-48 | 20.19 | Volcanic tuff |
| MXC-2b | Caribou | 62-48 | 20.19 | Volcanic tuff |
| MXC-8 | Caribou | 62-48 | 61.87 | Volcanic tuff |

These specimens were previously cut into rectangular shapes with the edges either parallel or perpendicular to foliation for the electrical measurements (e.g. Katsube et al., 1998b). In this study, a detailed visual examination was performed on these specimens and key textural features recorded, as shown in the block diagrams of Figures 1, 2, and 3. Following analysis of the electrical resistivity data, previously achieved through geo-impedance spectroscopy, specimen surfaces which best represented the areas of interest were polished and prepared for scanning electron microscope (SEM) analysis. The SEM analysis allowed a close examination of the sample mineralogy, texture, and fabric, including the connectivity of the sulphide and other mineral grains. A Leica/Cambridge S-360 scanning electron microscope (SEM) with an Oxford/Link eXL-II energy dispersive X-ray analyzer was used. Operating conditions for the SEM were generally 20 kV accelerating voltage at a 25 mm working distance. Backscattered electron images (BSI) were produced. Detailed description of the SEM methods and procedures can be found elsewhere (Reed, 1997).

## ANALYTICAL RESULTS

A schematic representation of specimen MXC-2a is displayed in Figure 1a. The directions of the electrical resistivities are shown to the left of the block diagram with 150 $\Omega$·m in the directions parallel to foliation and 6930 $\Omega$·m in the direction perpendicular to foliation. This implies an electrical anisotropy ($\lambda$) of 46:1 (Table 2). This is a volcanic tuff containing quartz, chlorite, K-feldspar, biotite, apatite, plagioclase, pyrite, and sphalerite identified under the SEM. The foliation is defined by fairly continuous layers of quartz and K-feldspar which are visible in hand specimen. The dark green, discontinuous layers visible in hand specimen, are likely chloritic. The chlorite is visible on the SEM images as

**Table 2.** Results of electrical resisitivity measurements.

| Sample | Lithology | $\delta_B$ (g/mL) | Mean $\rho_r$ ($10^3$ $\Omega$·m) | | Anisotropy $\lambda$ |
|---|---|---|---|---|---|
| | | | $\alpha$ | $\beta$ | |
| MXC-2A | Volcanic tuff | 2.74 | 6.93 | 0.15 | 46:1 |
| MXC-2B | Volcanic tuff | 2.73 | 14.82 | 0.22 | 67:1 |
| MXC-8 | Volcanic tuff | 2.74 | 14.59 | 0.61 | 24:1 |

$\rho_r$ = Bulk electrical resistivity
$\delta_B$ = Bulk density (g/mL)
$\alpha$ = Direction measured perpendicular to foliation, if any
$\beta$ = Direction measured parallel to foliation, if any

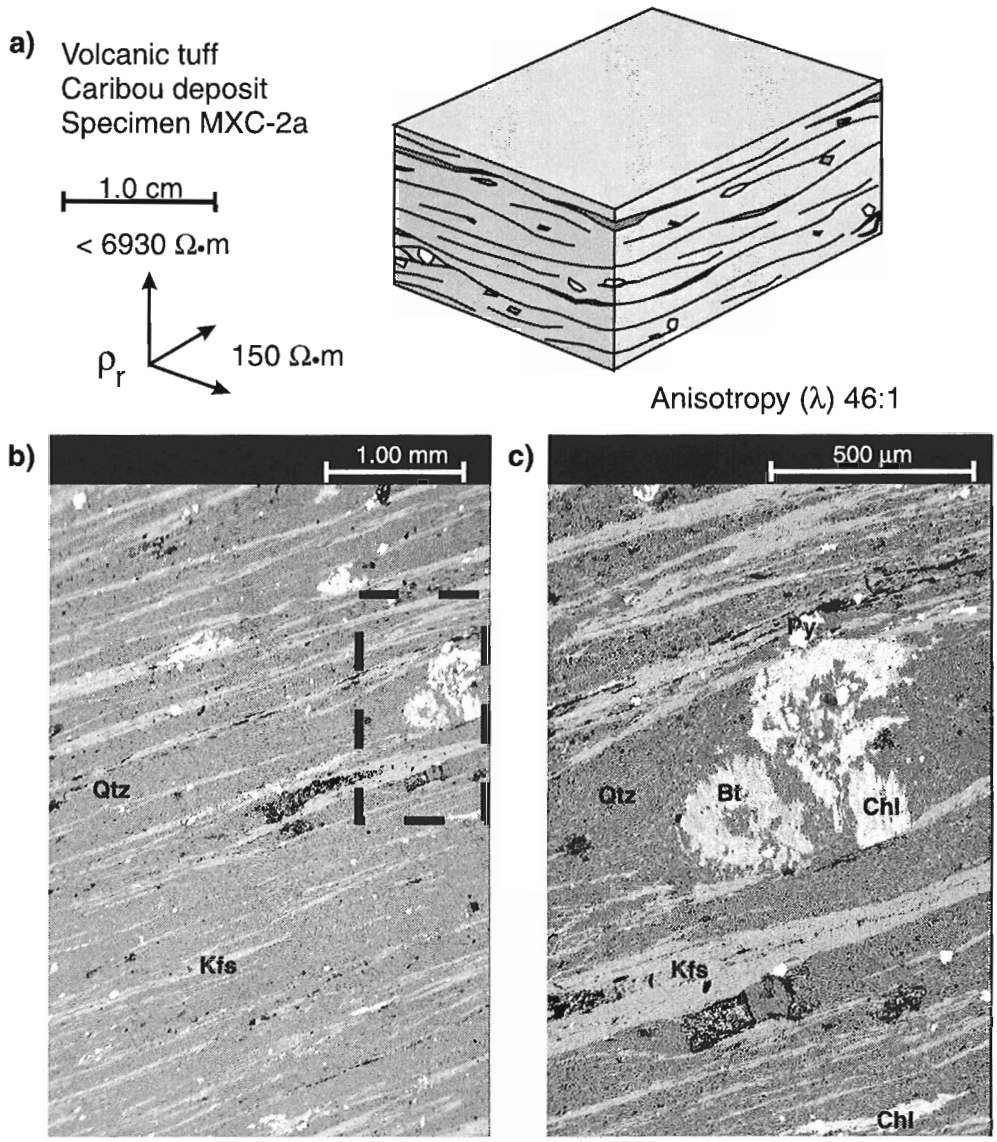


***Figure 1. a)*** *Schematic representation and* ***b), c)*** *SEM images for specimen MXC-2a, with electrical resistivities (ρ) for the two directions and their electrical anisotropy (λ) value. The SEM images (backscattered image, BSI) show quartz (Qtz) and K-feldspar (Kfs) layering with patches of chlorite (Chl), disseminated pyrite (Py) and a biotite (Bt) porphyroblast altering to chlorite.*

light grey, almost white. The disseminated blebs of pyrite are visible in the SEM images as bright white grains. Figure 1b represents an overall view, showing the continuous quartz layer and discontinuous K-feldspar layers. These layers are medium and light grey, respectively. Figure 1c shows a biotite and chlorite porphyroblast with chlorite possibly pseudomorphous after biotite. The higher resistivity in the perpendicular direction is likely attributed to the planar feature defined by the quartz layers. An even higher resistivity is achieved when the planar features become more continuous (the K-feldspar layers do not pinch out as much) and the grains are tighter, as seen in MXC-2b (Fig. 2). The source of low resistivity in the direction parallel to foliation is likely attributed to grain orientation.

A schematic representation of specimen MXC-2b is displayed in Figure 2a. This specimen was cut from the same section of core as the previously described specimen (MXC-2a). The directions of electrical resistivities are shown below the block diagram with 220 Ω·m in the directions parallel to foliation and 14 820 Ω·m in the directions perpendicular to foliation, implying a λ value of 67:1. The SEM analysis identified quartz and K-feldspar layers with patches of chlorite. Biotite, pyrite, rutile, and apatite were also identified. Foliation is defined by fairly continuous, alternating layers of quartz (dark grey on SEM image) and K-feldspar (medium grey on SEM image *see* Fig. 2b, 2c). Although specimens MXC-2a and MXC-2b are almost identical, there is a

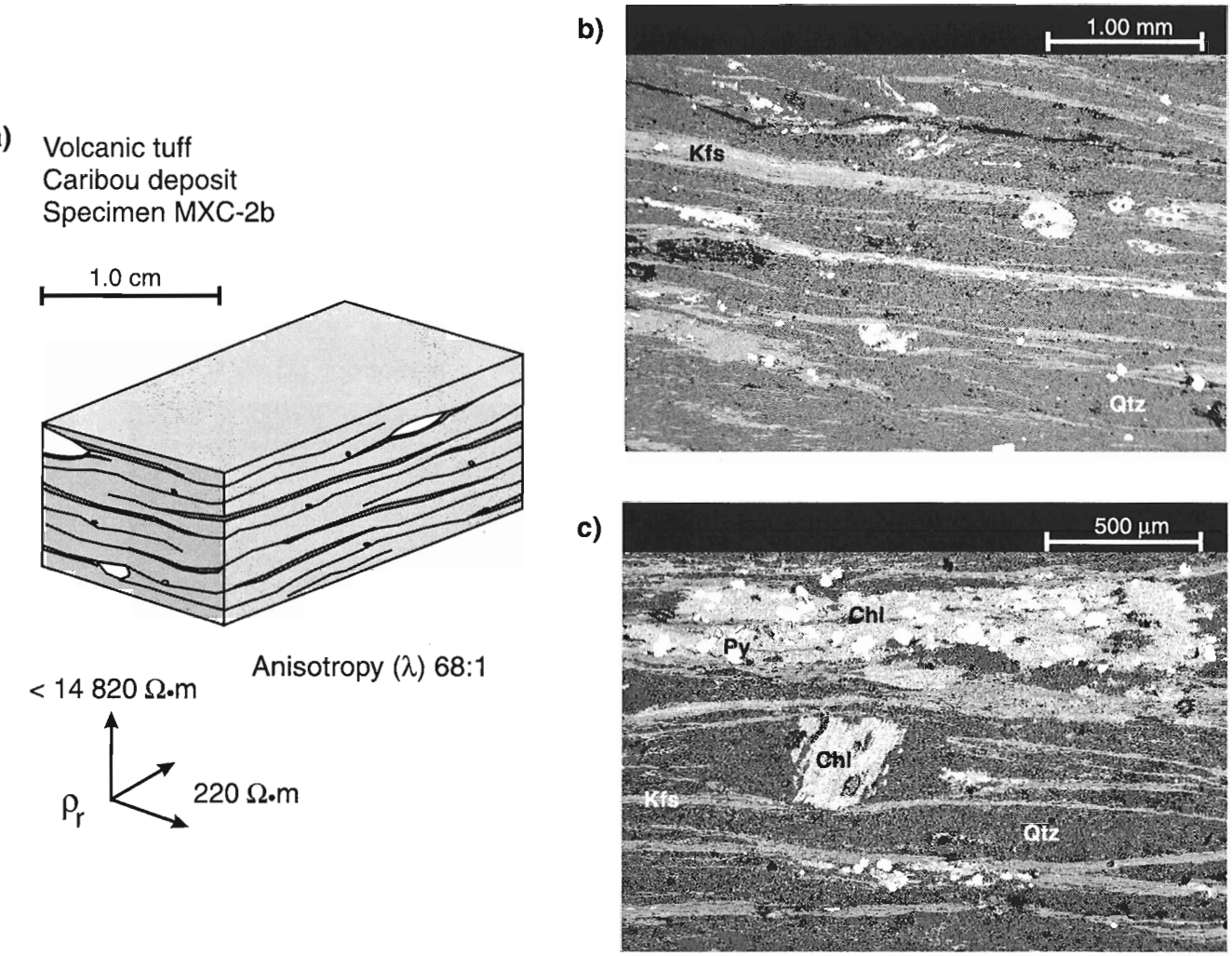


***Figure 2.*** *a) Schematic representation and* ***b), c)*** *SEM images for specimen MXC-2b, with* ρ *for the two directions and their* λ *value (lower left-hand section). The SEM images (BSI) show quartz (Qtz) and K-feldspar (Kfs) layering with patches of chlorite (Chl) and disseminated pyrite (Py).*

considerable difference in the resistivity values obtained for the direction perpendicular to foliation. Resistivity values in this direction are twice as high for specimen MXC-2b as for specimen MXC-2a. The main difference between the two specimens is visible in hand sample. This specimen (MXC-2b) has more continuous chloritic and siliceous and/or feldspathic layers. The increased resistivity in the direction perpendicular to foliation is likely attributed to the tighter (densely packed mineral grains), and more continuous quartz layers. Fine-grained pyrite blebs are disseminated throughout the sample but are concentrated in chloritic patches as shown in Figure 2c. As the sulphide grains are not connected it is unlikely that they have much of an effect on the electrical resistivities.

A schematic representation of specimen MXC-8a is displayed in Figure 3a. The directions of electrical resistivities are shown below the block diagram with 610 Ω·m in the direction parallel to foliation and 14 590 Ω·m in the direction perpendicular to foliation. The anisotropy for this sample is 24:1. The specimen is from the same drillhole as those previously described, but from a greater depth (Table 1). The mineralogy is very similar, with plagioclase, K-feldspar, quartz, chlorite, apatite, monazite, rutile, and zircon identified under SEM. The foliation is defined by continuous layers of quartz and plagioclase feldspar with alternating, discontinuous layers of K-feldspar and chlorite (Fig. 3b). The K-feldspar grains appear to have been sheared as shown in Figure 3c. The grain shape and orientation of the K-feldspar is such that it might be less resistive to the flow of electrical current parallel to foliation, although the resistivity in this direction is higher compared to the previous cases. Thick quartz and plagioclase layers (1–3 mm) have been observed, but their effect on the resistivity is not clear. The chlorite is patchy and there does not appear to be any parallel alignment of the grains; therefore, it is unlikely that it has any effect on the resistivity parallel to foliation.

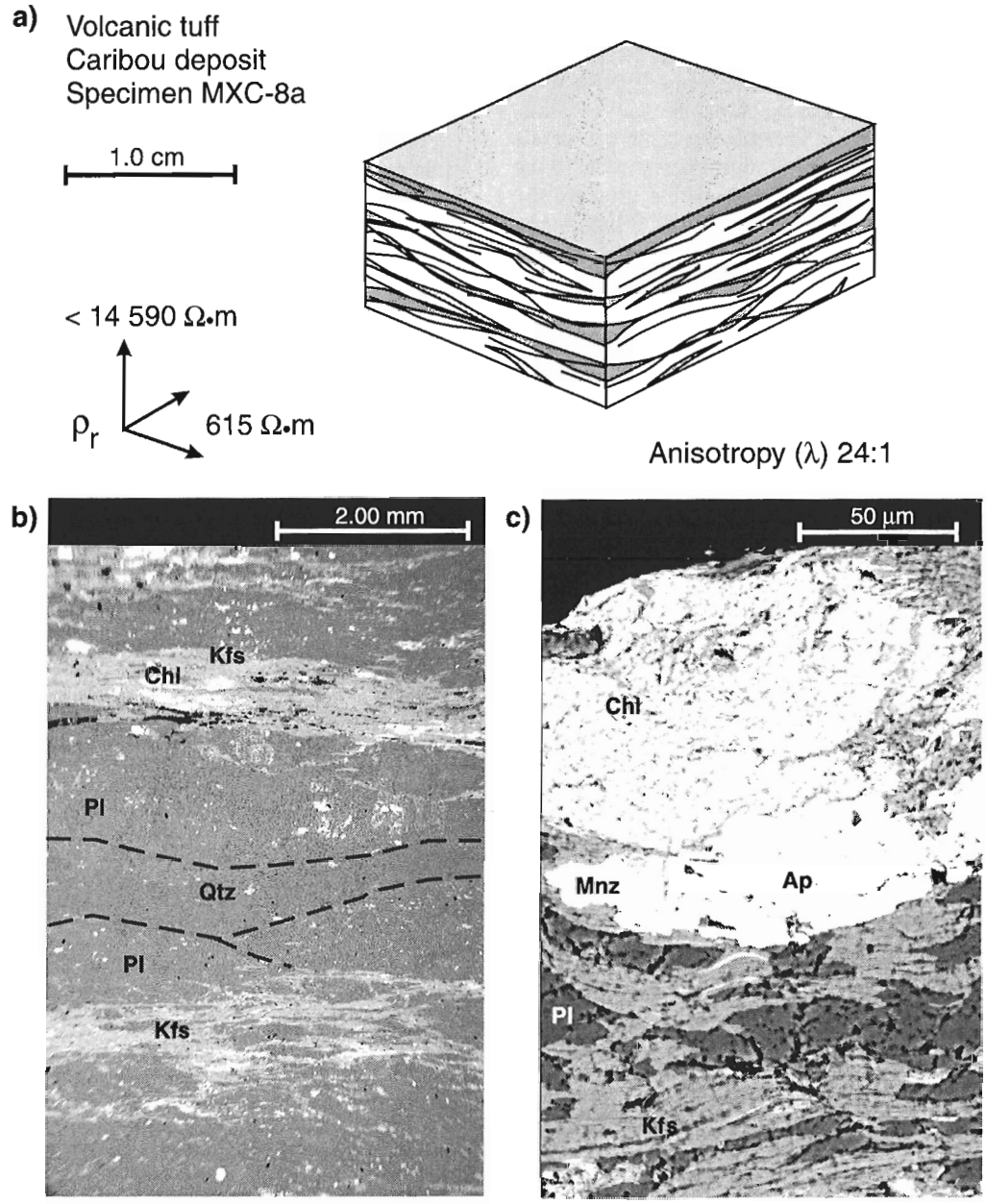


***Figure 3.*** *a) Visual description and* ***b)****,* ***c)*** *SEM images for specimen MXC-8a, with ρ for the two directions and their λ value. The SEM images (BSI) show quartz (Qtz), plagioclase feldspar (Pl) and K-feldspar (Kfs) layering with patches of chlorite (Chl). Monazite (Mnz) and apatite (Ap) are also identified.*

## DISCUSSION AND CONCLUSIONS

The electrical anisotropy (λ) values for these three volcanic tuff samples are in the range of 24:1 to 68:1, and the electrical resistivity values in the direction parallel and perpendicular to their foliation are in the ranges of 150–600 Ω·m and 7000–15 000 Ω·m (Fig. 1, 2, 3), respectively. The high electrical resistivities (7000–15 000 Ω·m) in the direction perpendicular to the foliation are likely a result of the siliceous and/or feldspathic layers (parallel to foliation) acting as insulators to the traversing electrical current.

There are no obvious sources (e.g. sulphides) of the lower electrical resistivities (150–600 Ω·m) in the directions parallel to the foliation except for the parallel alignment of grains.

The K-feldspar layers are associated with chlorite in these specimens. Greenschist-facies conditions are present with an increase in grade marked by the introduction of biotite at the expense of chlorite in silicic and epiclastic rocks (van Staal, 1992). This implies that there is a possibility of platy minerals (e.g. biotite) aligned parallel to foliation associated with the K-feldspar layers. This type of texture would increase the pore-space connectivity in the direction of the foliation and become the cause of the lower resistivity in that direction. Formation-factor measurements would indicate whether or not the electrical anisotropy is a result of mineralogy (i.e. connectivity of platy minerals) or connectivity of pore space (Katsube and Salisbury, 1994) both of which are related to the degree of foliation.

Specimen MXC-2a (Fig. 1) shows resistivity values of 7000 Ω·m in the perpendicular direction which are lower than those (15 000 Ω·m) of the other two samples (MXC-2b, MXC-8a). The scanning electron microscope (SEM) images show continuous siliceous and/or feldspathic layers for all specimens and do not show any distinct differences between the two sets of samples. However, there are indications that the siliceous and/or feldspathic layers of sample MXC-2a may be less continuous in the direction of the foliation, compared to those in the other two specimens. This is seen in Figure 1b, where pinching off of the feldspathic layers are suggested. This may result in very tortuous K-feldspar layers in the perpendicular direction, and be the source of the high resistivity, but lower for that direction compared to the other two specimens. The reason for MXC-8 (600 Ω·m) having the higher parallel resistivity compared to MXC-2a (150 Ω·m) and MXC-2b (220 Ω·m) is not explained. However, resistivities of 150–220 Ω·m and 600 Ω·m can be considered as being in the same category, compared to the perpendicular resistivities of 7000 to 15 000 Ω·m.

Consequently, these results indicate that the high resistivity values (7000–15 000 Ω·m) in the direction perpendicular to the foliation are due to the tightly packed (low pore space) siliceous and/or feldspathic layers acting as electrical insulators to the traversing electrical current in that direction. They also indicate that the increased chlorite content associated with the K-feldspar layers, resulting from the recrystallization of various minerals (biotite) during metamorphism, may be the source of the lower electrical resistivities (150–600 Ω·m) in the direction parallel to the foliation. Increased chlorite content implies an increase in platy mineral grains aligned parallel to foliation and implies increased pore-space connection in that direction. Further analysis (i.e. formation-factor measurements) is required to identify the source of the high and low resistivities.

## ACKNOWLEDGMENTS

This work has been supported by funds from P. Keatings' (GSC-CGD) project. The authors are grateful to J.B. Percival (Continental Geoscience Division) for critically reviewing this paper. The authors also greatly appreciate useful comments and suggestions from K. Shaw (Lacuna Digital Imaging Inc.).

## REFERENCES

**Connell, S., Katsube, T.J., Best, M.E., Goodfellow, W.D., and Mwenifumbo, J.**
1998: Electrical characteristics of mineralized and non-mineralized rocks at the Stratmat deposit, Bathurst mining camp, New Brunswick; *in* Current Research 1998-E; Geological Survey of Canada, p. 149–162.

**Connell, S., Katsube, T.J., and Hunt, P.A.**
1999a: Textural characteristics of low to high resistivity, low anisotropy volcanic tuffs, Bathurst mining camp, New Brunswick; *in* Current Research 1999-E; Geological Survey of Canada.

**Connell, S., Katsube, T.J., Hunt, P.A., and Walker, D.**
1999b: Textural characteristics of rocks that display significant electrical anisotropy; *in* Current Research 1999-D; Geological Survey of Canada, p. 9–15.

**Katsube, T.J. and Salisbury, M.**
1994: Implications of laboratory electrical measurements on interpretation of EM-surveys and origin of the Sudbury Structure; Geophysical Research Letters (GRL), v. 21, p. 947–950.

**Katsube, T.J., Scromeda, N., Best, M.E., and Goodfellow, W.D.**
1997: Electrical characteristics of mineralized and non-mineralized rocks at the Brunswick No.12 deposit, Bathurst mining camp, New Brunswick; *in* Current Research 1997-E; Geological Survey of Canada, p. 97–107.

**Katsube, T.J., Connell, S., Goodfellow, W.D., and Scromeda, N.**
1998a: Electrical characteristics of non-mineralized rocks from the Bathurst mining camp, New Brunswick; *in* Current Research 1998-E; Geological Survey of Canada, p. 125–137.

**Katsube, T.J., Connell, S., Goodfellow, W.D., Scromeda, N., and Best, M.E.**
1998b: Electrical characteristics of mineralized and nonmineralized rocks at the Caribou deposit, Bathurst mining camp, New Brunswick; *in* Current Research 1998-D; Geological Survey of Canada, p. 25–35.
1998c: Electrical characteristics of mineralized and non-mineralized rocks at the Restigouche deposit, Bathurst mining camp, New Brunswick; *in* Current Research 1998-E; Geological Survey of Canada, p. 139–148.

**Keller, G.V.**
1966: Electrical properties of rocks and minerals; in Handbook of Physical Constants, (ed.) S.P. Clark, Jr.; Geological Society of America, Memoir 97, p. 553–577.

**Reed, S.J.B.**
1997: Electron Microprobe Analysis; Cambridge University Press, Cambridge, U.K., 346 p. (second edition).

**Van Staal, C.R.**
1992: The Ordovician Tetaouche Group, Bathurst camp, northern New Brunswick, Canada: history, tectonic setting, and distribution of massive sulphide deposits; Exploration Mining Geology, v. 1, p. 3–103.

Geological Survey of Canada Project 870057

# Textural characteristics of low to high resistivity sedimentary rocks, Bathurst mining camp, New Brunswick

S. Connell, T.J. Katsube, and P.A. Hunt
Mineral Resources Division, Ottawa

*Connell, S., Katsube, T.J., and Hunt, P.A., 1999: Textural characteristics of low to high resistivity sedimentary rocks, Bathurst mining camp, New Brunswick;* in *Current Research 1999-E; Geological Survey of Canada, p. 189–194.*

**Abstract:** Detailed textural analysis by scanning electron microscopy has been carried out on three sedimentary rock samples from the Bathurst mining camp (New Brunswick) to investigate the reason for unusual features they display. They are characterized by a lack of increased resistivity by quartz-filled fractures intersecting bedding, resistivity-increasing effects parallel to bedding and resistivity-reducing effects perpendicular to the bedding by shear fractures absent of any electrically insulating or conductive minerals.

Results indicate that, for the former case, the lack of quartz continuity in the fractures allows the electrical current to flow across the fracture without an increase in electrical resistivity. For the latter case, the continuity of electrically conductive zones parallel to bedding, mainly due to pyrite lined with iron oxide, are cut by shear fractures intersecting the bedding, resulting in increased resistivity. In addition, conductive segments concentrated in the shear zone result in reduced resistivity perpendicular to bedding.

**Résumé :** On a réalisé une analyse détaillée par microscopie électronique à balayage de la texture de trois échantillons de roche sédimentaire du camp minier de Bathurst (Nouveau-Brunswick) pour expliquer les caractéristiques inhabituelles qu'ils présentaient. Ces roches sont caractérisées par une absence d'augmentation en résistivité malgré la présence de fractures remplies de quartz qui recoupent le litage et par une augmentation de la résistivité dans la direction parallèle au litage et une diminution de la résistivité dans la direction perpendiculaire au litage causées par la présence de fractures de cisaillement dépourvues de minéraux conducteurs ou isolants.

Les résultats indiquent que, dans le premier cas, le manque de continuité du quartz dans les fractures permet au courant électrique de les traverser sans augmentation de la résistivité. Dans le deuxième cas, la continuité des zones conductrices parallèles au litage, surtout attribuable à la présence de pyrite recouverte d'oxyde de fer, est interrompue par les fractures de cisaillement qui recoupent le litage, ce qui augmente la résistivité. De plus, les segments conducteurs concentrés dans la zone de cisaillement entraînent à une diminution de la résistivité dans la direction perpendiculaire au litage.

## INTRODUCTION

Detailed texture analysis by scanning electron microscopy (SEM) has been carried out on three sedimentary rock samples from the Bathurst mining camp (New Brunswick; Table 1) which display unusual electrical characteristics. Their anisotropy values are in the range of 2:1 to more than 30:1, and their resistivity values are in the ranges of 37–14 000 Ωm and 12–12 000 Ωm for the directions perpendicular and parallel to foliation (Table 2), respectively (Katsube et al., 1998). These resistivity ranges are considerably broader than previously reported (Keller, 1966) values for shale samples (163–192 Ωm). Usually, resistivities are lower in the direction parallel to bedding, shearing, and fracture cleavages, and are higher in the direction perpendicular to bedding and quartz veins (Katsube et al., 1997, 1998; Connell et al., 1999b). However, this is not necessarily the case for these three samples. Connell et al. (1999b), suggested that the anisotropic properties in sedimentary rocks are a result of bedding and the connectivity and/or alignment of clay-sized mineral grains. The purpose of this paper is to document the textural characteristics of these samples, and their relationships to the electrical characteristics.

## METHODS OF INVESTIGATION

The three samples selected for this study display a relatively wide range of resistivity values (12–22 000 Ωm), and were collected from several regions in the Bathurst mining camp (New Brunswick) by Wayne Goodfellow (Katsube et al., 1998). One sample is from the Caribou deposit area (sample MXG-3), another from the Brunswick No.12 area (sample MXG-8), and the third was sampled from the Heath Steele area (sample MXG-16). Information on drillhole identification, sample depth, formation, and lithology for all samples examined are listed in Table 1.

**Table 1.** Sample identification.

| Sample number | Deposit | Drillhole | Depth (ft.) | Lithology |
|---|---|---|---|---|
| MXG-3 | Caribou | H-55 | 412 | Carbonaceous argillite |
| MXG-8 | Brunswick No.12 | HA248 | 175 | Maroon sediment |
| MXG-16 | Heath Steele | 289A-B4 | 1424 | Black shale |

The samples were cut into rectangular shapes with the edges either parallel or perpendicular to foliation. First, a detailed visual examination was performed and the key features recorded, as shown in the block diagrams of Figures 1, 2, and 3. Following analysis of the electrical resistivity data, previously obtained by geo-impedance spectroscopy (Katsube et al., 1998), surfaces which best represented the areas of interest were polished and prepared for scanning electron microscope (SEM) analysis. The SEM analysis allowed a close examination of the sample mineralogy, texture, and fabric, including the connectivity of the sulphide and other mineral grains. The image analysis procedure followed in this study, examines in detail, the textural characteristics of a specimen surface (e.g. grain shape, orientation, mineralogy, connectivity). A Leica/Cambridge S-360 scanning electron microscope (SEM), Oxford/Link eXL-II energy dispersive X-ray analyzer, was used for this study. Operating conditions for the SEM were generally 20 kV accelerating voltage at a 25 mm working distance. Backscattered electron images (BSI) were produced as a result. Detailed descriptions of the SEM methods and procedures can be found elsewhere (Reed, 1997).

## ANALYTICAL RESULTS

A schematic representation of specimen MXG-3, a carbonaceous argillite, is displayed in Figure 1a. To the left of the block diagram the directions of the electrical resistivities ($\rho_r$) are displayed, with 3000 Ωm in the direction perpendicular to bedding and 90–150 Ωm parallel to bedding. The electrical anisotropy ($\lambda$) for this sample is more than 30:1 (Table 2). Scanning electron microscope (SEM) images of the left-hand surface and top surface of the specimen are displayed in Figures 1c and 1b, respectively. Figure 1d is an enlargement of the surface perpendicular to bedding. The SEM analysis identified quartz, clay minerals (K, Al, Si, as major elements with minor Mg), and a few pyrite grains. Fracture cleavages ($S_1$) filled with quartz are evident in hand sample and are visible in Figure 1b and 1c. However, these quartz-filled fractures do not appear to have an increasing effect on the resistivities parallel to bedding. Quartz-filled fractures or veins usually increase resistivity values by at least 1000 Ωm, even if they are in the order of 1–2 mm in thickness (e.g. Katsube et al., 1997, 1998). The lack of continuity of the quartz content in the microfractures,

**Table 2.** Results of electrical resistivity measurements.

| Sample | Lithology | $\delta_B$ (g/mL) | Mean $\rho_r$, ($10^3$ Ω·m) | | | Anisotropy $\lambda$ |
|---|---|---|---|---|---|---|
| | | | $\alpha$ | $\beta$ | $\gamma$ | |
| MXG-3 | Carbonaceous argillite | 3.05 | 3.37 | 0.15 | 0.09 | 37:1 |
| MXG-8A | Maroon sediment | 3.03 | 13.73 | 11.76 | 6.66 | 2:1 |
| MXG-8B | Maroon sediment | 3.12 | 21.54 | 7.66 | | 2.5:1 |
| MXG-16 | Black shale | 2.94 | 0.037 | 0.012 | 0.32 | 27:1 |

$\rho_r$ = Bulk electrical resistivity
$\delta_B$ = Bulk density (g/mL)
$\alpha$ = Direction measured perpendicular to foliation, if any
$\beta$ = Direction measured parallel to foliation, if any
$\gamma$ = Direction measured parallel to lineation (or other feature), if any

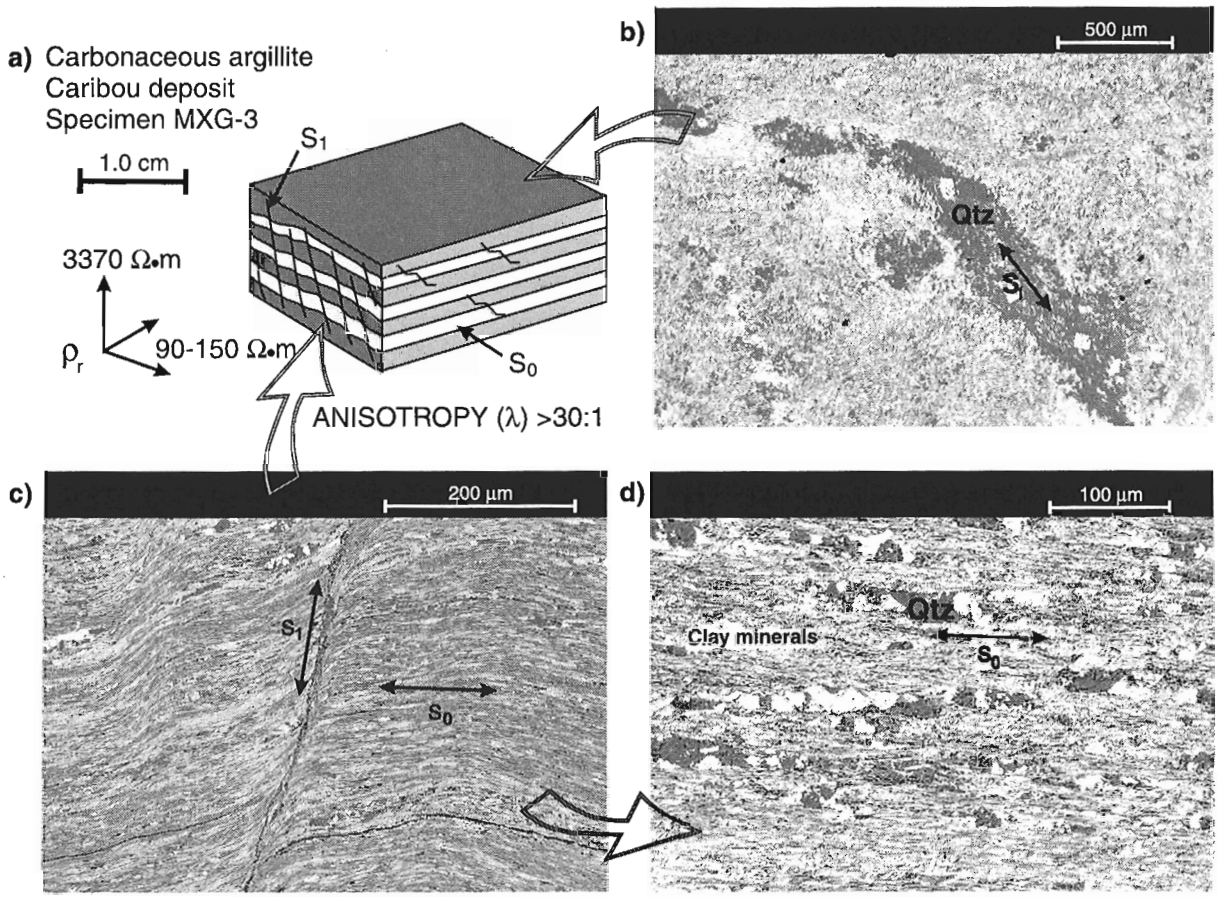


***Figure 1.*** *a) Schematic representation, and* ***b), c),*** *and* ***d)*** *SEM images for sample MXG-3 with electrical resistivities ($\rho_r$) and electrical anisotropy ($\lambda$) values adjacent and below the block diagram, respectively. The SEM images (BSI) show bedding ($S_0$) and the fracture and/or shear planes ($S_1$) which are most often filled with quartz (Qtz).*

seen in Figure 1b, likely fails to cause any serious interruption of the electrical current traversing the fracture, and is suggested to be the reason for not increasing the resistivities in the directions parallel to the bedding ($S_0$). In hand sample, bedding ($S_0$) is defined by dark and light grey layers, likely attributed to the silica content. Under the SEM, bedding ($S_0$) is defined by variations in grain size without much change in mineralogy (Fig. 1c, 1d). For the most part, the grains are preferentially aligned parallel to bedding. The bedding appears to be crenulated throughout, maintaining a fairly continuous flow path for the electrical current.

A schematic representation of specimens MXG-8a and MXG-8b is displayed in Figure 2a. Adjacent to each of the block diagrams are the directions of electrical resistivities with 13 730 Ωm and 6660–11 760 Ωm perpendicular and parallel to bedding, respectively, for specimen MXG-8a and 21 540 Ωm and 7660 Ωm perpendicular and parallel to bedding, respectively, for specimen MXG-8b. The sample is a strongly silicified maroon sediment. The bedding and/or primary foliation is defined by faint variations in colour only, as seen in hand sample. The $\lambda$ values are low for this sample (2:1 to 2.5:1) as expected, due to the high silica content and absence of any distinct directional variations in grain shape, grain size, or mineralogy. The SEM images of the right-hand surface of specimen MXG-8b are displayed in Figures 1c and 1b. A dominantly quartz matrix is identified by the SEM, shown as dark grey on the images (Fig. 1b, 1c). The bright subhedral to euhedral grains disseminated throughout the matrix are iron oxide (likely magnetite). The less intense, slightly smaller nodules are likely a garnet, possibly calderite. The medium grey patches are almost all Mn with small Ca and Mg peaks identified under SEM. The vein is carbonate, Mn-Al-Si-Fe, and Ba-sulphide. The carbonate and Ba-sulphide show up as bright white in the vein on the lower right-hand SEM image (Fig. 2c). The existence of the vein has not made any obvious impact on the resistivity value in the direction parallel to the bedding, probably due to the already high intrinsic values in that direction. That is, the effect of the vein is negligible in this high-resistivity background.

The schematic representation of specimen MXG-16, a black shale, is displayed in Figure 3a. Visual examination of the rectangular specimen revealed well defined bedding ($S_0$) and shear zones ($S_1$), as shown in the upper-left section of the figure. The directions of electrical resistivities are shown below the block diagram, with 37 Ωm in the direction

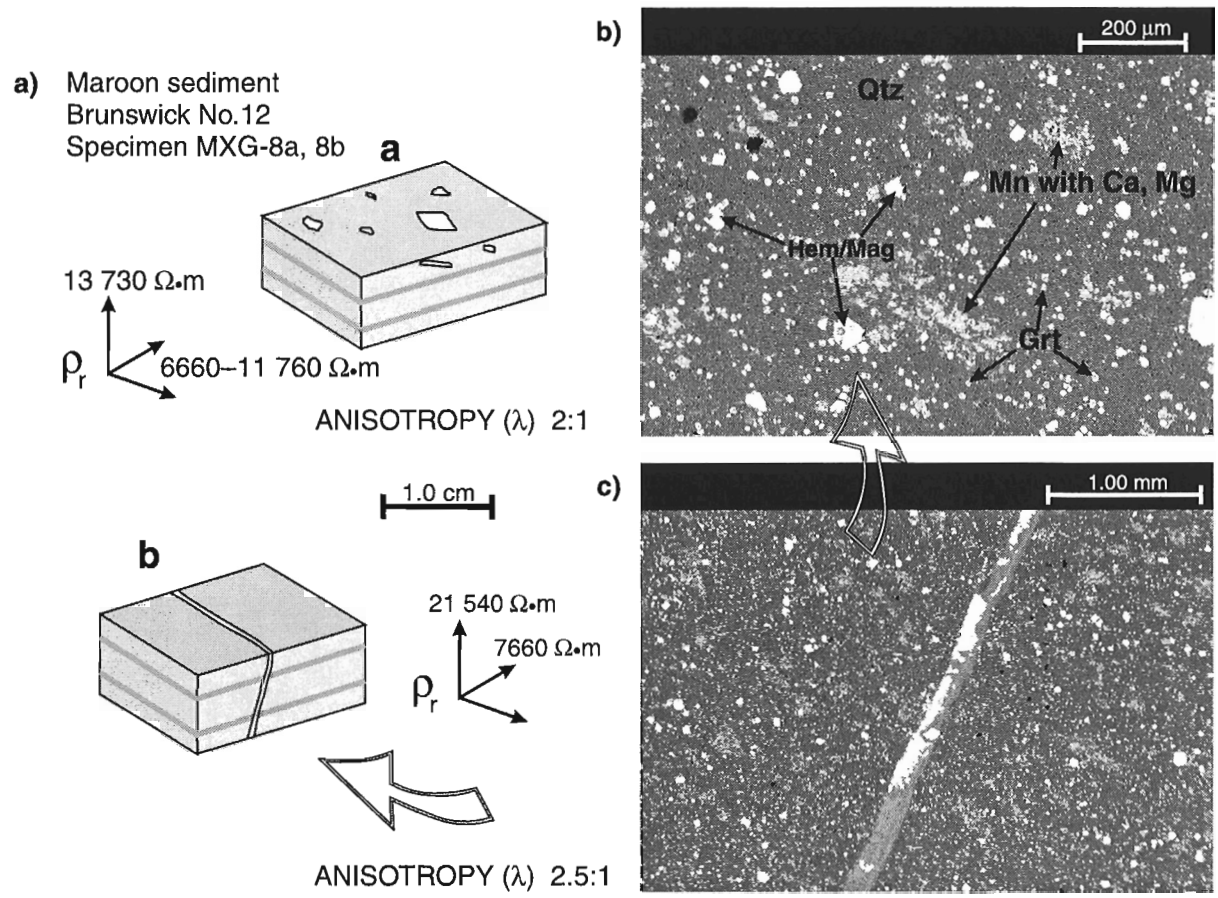


***Figure 2.*** *a) Schematic representation for samples MXG-8a and MXG-8b, and* ***b)*** *and* ***c)*** *SEM images for sample MXG-8b, with* $\rho_r$ *and* $\lambda$ *value adjacent to each block diagram. The SEM images (BSI) show the distribution of hematite-magnetite (Hem/Mag), garnet (Grt), and Mn, Ca, and Mg patches in the matrix material (Qtz).*

perpendicular to bedding and parallel to the fractures (α-direction), 12 Ωm in the direction parallel to bedding and the fractures (β-direction), and 320 Ωm parallel to bedding and perpendicular to the fractures (γ-direction). The SEM images of several sections of the right-hand side of the specimen are displayed in Figures 1b, 1c, and 1d. Results of the SEM analysis indicate that this black shale (carbonaceous sediment) consists of clay-sized aluminosilicate minerals preferentially oriented parallel to bedding ($S_0$), suggesting good pore-space connectivity in that direction. In addition, pyrite stringers with iron-oxide linings oriented parallel to bedding have been observed. These stringers suggest that there exist zones of high pyrite concentration lined with iron oxide along a number of these bedding planes. The sample contains various heavy minerals in minor amounts, such as rutile, zircon, and monazite. Minor amounts of graphite have also been detected (Fig. 3b). The possible good pore-space connectivity, due to the preferentially oriented minerals, with the zones of pyrite lined with iron oxide are most likely the source of the low electrical resistivity (12 Ωm) in the β-direction parallel to bedding. Figures 3a, 3b, and 3c suggest that shearing ($S_1$) in the α-direction has stretched and partially cut the pyrite–iron-oxide-rich zones, as shown in Figure 4. In addition, Figure 3b suggests that as a result of the shearing, the good pore-space connectivity along the bedding has been reduced. That is, the good electrical conductivity in the β-direction (12 Ωm) has been interrupted by the shearing and has raised the electrical resistivity along the bedding in the γ-direction which is perpendicular to the shearing ($S_1$) to 320 Ωm. The electrical resistivity perpendicular to the bedding (α-direction) is 37 Ωm, which is considerably smaller than those for the same direction in similar rock types (e.g. >1500 Ωm for sample MXG-20, Connell et al., 1999b). This is likely due to the pyrite–iron-oxide segments from numerous pyrite–iron-oxide-rich horizons along the bedding, forming partial short circuits in the a-direction within the sheared zone, as suggested by Figure 3b, and described in Figure 4.

***Figure 4.*** *Diagram showing the stretching and breaking of the zones of high pyrite–iron-oxide content and good pore-space connectivity by the shearing that occurred in the direction perpendicular to the bedding; Py = pyrite.*

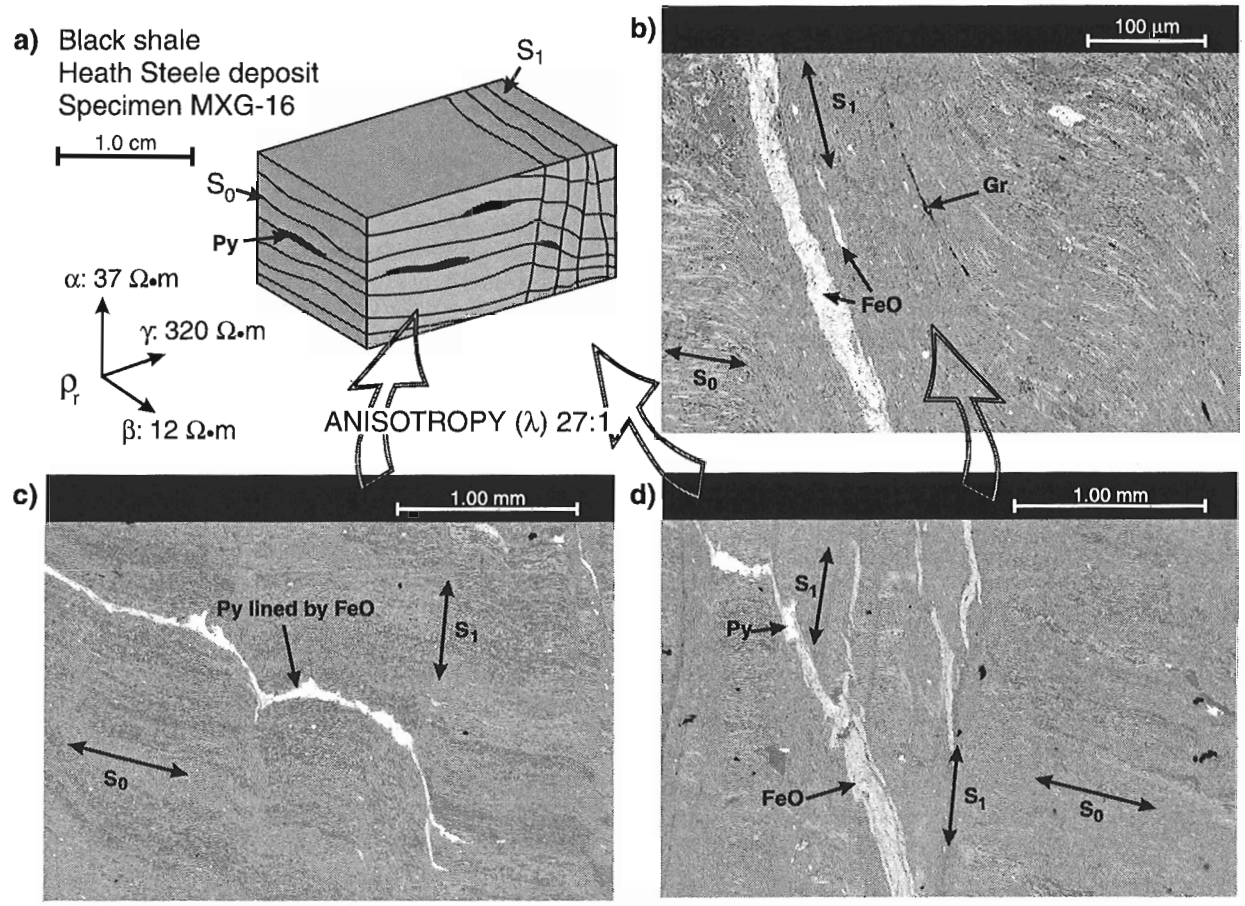


***Figure 3.*** *a) Schematic representation, and* ***b)****,* ***c)****, and* ***d)*** *SEM images for sample MXG-16, with* $\rho_r$ *for the directions and their* $\lambda$ *value adjacent and below the block diagram respectively. The SEM images (BSI) show views perpendicular to bedding (*$S_0$*). Areas with pyrite (Py), iron oxide (FeO), and graphite (Gr) are highlighted, and in particular, their association with the fracture and/or shear plane (*$S_1$*).*

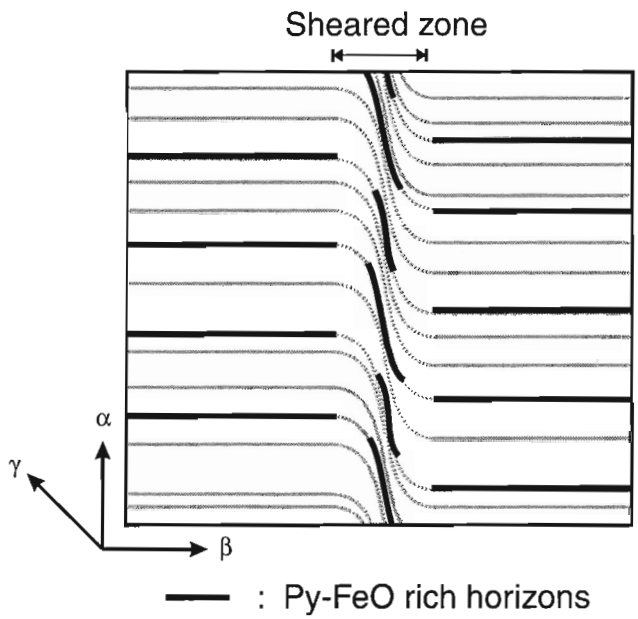


## DISCUSSION AND CONCLUSIONS

Sample MXG-3, a carbonaceous argillite, is characterized by electrical resistivities ($\rho_r$) of 3000 Ωm in the direction perpendicular to bedding and 90–150 Ωm parallel to bedding with an electrical anisotropy ($\lambda$) of more than 30:1 (Table 2). These $\rho_r$ values for the direction parallel to bedding are normal for rock textures with grains preferentially aligned parallel to bedding, which result in a fairly continuous flow path for the electrical current. These characteristics are similar to those previously observed for a fine-grained sedimentary rock (Connell et al., 1999b) from this region (Bathurst mining camp), and the $\rho_r$ values parallel to bedding (90–150 Ωm) are similar to those (163–192 Ωm) reported for shale samples (Keller, 1966). The unusual characteristics of this sample are the $\rho_r$ values apparently not being affected by the quartz-filled fractures that intersect the bedding. As indicated in previous studies (e.g. Katsube et al., 1997, 1998; Connell et al.,1999a), quartz fillings or veins usually act as important electrical insulators and are a cause of increased $\rho_r$ values.

Analysis by scanning electron microscope (SEM) of this sample indicates a lack of continuity of the quartz content in these microfractures. This likely explains the reason for the absence of any serious $\rho_r$ increasing effect from quartz-filled fractures.

Sample MXG-8 is a silicified maroon sediment with $\rho_r$ values of approximately 14 000–22 000 Ωm and 6600–12 000 Ωm in the perpendicular and parallel directions, respectively, and a $\lambda$ value of 2:1 to 2.5:1. There is a thin carbonate vein that intersects the bedding. These high $\rho_r$ values in the direction perpendicular to the bedding are usual for silicified sediments (Katsube et al., 1997, 1998; Connell et al., 1999a), but the high $\rho_r$ values in the direction parallel to the bedding and the lack of any impact of the vein are unusual. Results of the SEM analysis indicate that the bedding is defined by faint variations in colour only. In addition, the high $\rho_r$ values parallel to the bedding and low $\lambda$ values are due to the high silica content and absence of any distinct directional variations in grain shape, grain size, or mineralogy. It is interpreted that the existence of the carbonate vein has not made any obvious impact on the resistivity value in the direction parallel to the bedding, due to the already high intrinsic values in that direction.

Sample MXG-16 is a black shale with distinct bedding features and shear fractures intersecting the bedding. The $\rho_r$ values are 12 Ωm in the direction parallel to both bedding and shearing, 320 Ωm parallel to bedding and perpendicular to the fractures, and 37 Ωm perpendicular to bedding and parallel to the shear zones. Very low $\rho_r$ values (e.g. 12 Ωm) in the direction parallel to the bedding is often seen (e.g. Katsube et al., 1997; Connell et al., 1999b). The unusual characteristics of this sample are the low $\rho_r$ values (37 Ωm) in the direction perpendicular to the bedding, and the increased $\rho_r$ value (from 12 Ωm to 320 Ωm) in the direction parallel to the bedding and perpendicular to a fracture system not containing insulating material (e.g. quartz). The SEM analyses indicate that the very low $\rho_r$ value (12 Ωm) in the direction parallel to the bedding is a result of possible good pore-space connectivity, due to the preferentially oriented minerals, with the zones of pyrite lined with iron oxide. They also suggest that the increased $\rho_r$ values parallel to the bedding and perpendicular to the shearing is a result of the shearing having stretched and partially cut the pyrite–iron-oxide-rich zones. In addition, the same analyses also suggest that the relatively low $\rho_r$ values (37 Ωm) perpendicular to the bedding (usually >7000 Ωm) is a result of pyrite–iron-oxide segments, from numerous pyrite–iron-oxide-rich horizons along the bedding. These pyrite–iron-oxide segments form partial short circuits within the sheared zone, as suggested in Figure 4.

Consequently, all three samples examined in this study display visually clear to relatively clear bedding features, but show unusual electrical characteristics, as previously indicated. Their anisotropy values are in the range of 2:1 to more than 30:1, and resistivity values are in the ranges of 37–14 000 Ωm and 12–12 000 Ωm for the directions perpendicular and parallel to foliation, respectively, as already reported. The unusual features can be characterized by the lack of any resistivity-increasing effect by quartz- or carbonate- filled fractures that intersect the bedding, or by a resistivity-increasing effect parallel to the bedding and a resistivity-reducing effect perpendicular to the bedding by shearing absent of any electrically insulating or conductive material. Detailed textural analysis by scanning electron microscopy (SEM) suggests that for the former case, the lack of continuity of the electrically insulating material that fills the fractures has allowed the electrical current to flow across the fractures without much impeding effect, resulting in no obvious increase in the electrical resistivity (90–150 Ωm). For the latter case, zones of very low resistivity parallel to bedding due to good pore-space connectivity combined with the zones of pyrite lined with iron-oxide has been cut by shear fractures that intersect the bedding, resulting in increased resistivities (12–320 Ωm). In addition, platy segments of the pyrite–iron-oxide-rich zones that have been stretched and broken off from the bedding plane by shearing, are concentrated in the sheared zone and form partial electrical short-circuits in the direction parallel to shearing. The authors suggest that this results in the unusually low resistivity values (37 Ωm) obtained in the direction perpendicular to the bedding.

## ACKNOWLEDGMENTS

This work has been supported by funds from P. Keatings' (Continenal Geoscience Division) project. The authors are grateful to P. Keating for critically reviewing this paper. The authors also appreciate the useful comments and suggestions from K. Shaw (Lacuna Digital Imaging Inc.).

## REFERENCES

**Connell, S., Katsube, T.J., and Hunt, P.A.**
1999a: Textural characteristics of moderate to strongly foliated volcanic tuffs that display high resistivity and anisotropy values, Bathurst mining camp, New Brunswick; in Current Research 1999-E; Geological Survey of Canada.

**Connell, S., Katsube, T.J., Hunt, P.A., and Walker, D.**
1999b: Textural characteristics of rocks that display significant electrical anisotropy; *in* Current Research 1999-D; Geological Survey of Canada, p. 9–15.

**Katsube, T.J., Connell, S., Goodfellow, W.D., and Scromeda, N.**
1998: Electrical characteristics of nonmineralized rocks from the Bathurst mining camp, New Brunswick; *in* Current Research 1998-E, Geological Survey of Canada, p. 125–137.

**Katsube, T.J., Scromeda, N., Best, M.E., and Goodfellow, W.D.**
1997: Electrical characteristics of mineralized and nonmineralized rocks at the Brunswick No. 12 deposit, Bathurst mining camp, New Brunswick; *in* Current Research 1997-E; Geological Survey of Canada, p. 97–107.

**Keller, G.V.**
1966: Electrical properties of rocks and minerals; *in* Handbook of Physical Constants, (ed.) S.P. Clark, Jr., Geological Society of America, Memoir 97, p. 553–577.

**Reed, S.J.B.**
1997: Electron Microprobe Analysis; Cambridge University Press, Cambridge, U.K., 346 p. (second edition).

Geological Survey of Canada Project 870057

# Preliminary GIS analysis of biogeochemical relationships, particularly Hg, in Kejimkujik National Park, Nova Scotia[1]

A. Rencz, K. Telmer[2], A. Sangster, P. Smith[3], and D. Kliza
Mineral Resources Division, Ottawa

*Rencz, A., Telmer, K., Sangster, A., Smith, P., and Kliza, D., 1999: Preliminary GIS analysis of biogeochemical relationships, particularly Hg, in Kejimkujik National Park, Nova Scotia;* in *Current Research 1999-E; Geological Survey of Canada, p. 195–202.*

**Abstract:** Kejimkujik National Park, Nova Scotia has among the highest levels of Hg in loons in North America. This study was designed to investigate sources and processes that may lead to these anomalous levels.

Several media types were sampled, including dominant trees, lake waters, lake sediments, and rocks and analyzed for trace elements including Hg. Published values for Hg in yellow perch are included. The range of Hg values in the various media in this project are slightly higher than values in the literature. Current results illustrate that the variables which are the most related to levels of Hg in yellow perch are lake water dissolved organic carbon and Hg (total values), per cent of coniferous forest in a drainage basin, per cent of water in the lake basin, lake water pH, and Zn concentration in rocks. There is no obvious correlation with Hg in samples of vegetation or surface rocks.

**Résumé :** Les huards du parc Kejimkujik (Nouvelle-Écosse) présentent des taux de mercure parmi les plus élevés en Amérique du Nord. Cette étude a été conçue dans le but d'examiner les sources et les processus qui ont pu mener à ces taux anomalement élevés.

Plusieurs types de milieux ont été échantillonnés, dont des arbres dominants, des eaux lacustres, des sédiments lacustres et des roches, et analysés en vue de déterminer leur teneur en éléments traces, y compris le mercure. Des valeurs déjà publiées pour le mercure dans la perchaude sont incluses. La fourchette des taux de mercure dans les différents milieux analysés lors de ce projet est légèrement plus élevée que celle signalée dans la documentaion. Les résultats actuels montrent que les paramètres qui sont le plus étroitement reliés aux taux de mercure dans la perchaude sont le carbone organique dissous et la concentration de mercure (valeurs totales) des eaux lacustres, le pourcentage de forêt de conifères dans le bassin versant, le pourcentage d'eau dans le bassin lacustre, le pH des eaux lacustres et la teneur en Zn des roches. Il n'y a aucune corrélation évidente avec le mercure dans les échantillons de végétation ou de roches.

[1] Contribution to the Geological Survey of Canada's Metals In The Environment (MITE) Initiative

[2] University of Victoria, P.O. Box 3055 Station CSC, Victoria, British Columbia V8W 3P6
[3] Nova Scotia Department of Natural Resources, P.O. Box 698, Halifax, Nova Scotia B3J 2T9

## INTRODUCTION

Metals enter the biogeochemical cycle from natural and anthropogenic sources. Many factors combine to establish total levels of a metal in the environment. As a first approximation, it is important to understand factors contributing to total metal levels. Ultimately, the factors which affect bioavailability, the movement of metals through the food chain, are the most critical to ecological health and hence most critical to determine and quantify. As metals move through compartments of ecosystems, from their various sources to the atmosphere and hydrosphere, through the biosphere and ultimately to a sink, the processes controlling their distribution fall under the expertise of many scientific disciplines. To fully appreciate the relative importance of each process in the ecological cycle of metals, multidisciplinary approaches capable of linking responses from one reservoir to another must be undertaken.

Kejimkujik National Park, Nova Scotia, noted for having the highest Hg concentrations in loon blood in North America (Burgess et al., 1998b), has been the location of numerous toxicology studies and which have produced a wealth of baseline data. The present state of knowledge at Kejimkujik National Park is that loons, being at the top of the food chain and therefore at the top of the Hg biomagnification pyramid, tend to bioaccumulate Hg and that they have been adversely affected by Hg accumulations (Burgess et al., 1998c; Nocera and Taylor 1998); however, the underlying reason for the high Hg levels in loons and the source of the Hg remains unknown. There are existing databases on lake-water chemistry, watershed morphology, hydrology, land use and vegetation cover, and Hg levels in biota, including perch, loons, and vegetation. There are data on atmospheric input, including Hg and $SO_4$ and geochemical data for the rocks (surface and drill core) of the area.

The overall objective of this project is to determine the relative importance of atmospheric deposition, geological sources, and geochemical and biological processes on Hg concentrations in aquatic and terrestrial systems. The basic question is why are Hg levels so high in certain parts of the ecosystem at Kejimkujik National Park, Nova Scotia. Fieldwork is based in Kejimkujik National Park, Nova Scotia; however, we consider that results will be applicable to other areas in Canada and abroad, particularly areas dominated by wetland conditions. Rasmussen et al. (1998) reported on a similar study in Ontario. This report will provide some of the basic data already available, including new limnological data acquired by GSC and a preliminary look at relationships between the variables.

## STUDY AREA

Kejimkujik National Park is located on the southern upland of Nova Scotia (Fig. 1). This area is basically a flat plain lacking the major escarpments, mountains, and valleys found in other parts of the province. Most of the visible landforms in the park are a direct result of the last glaciation which started approximately 100 000–80 000 years ago. These include drumlins, shallow lakes connected by wandering rivers and streams, and granite boulders. The glacial action was greatly influenced by the underlying bedrock. Most of the glacial landforms are in areas with slate bedrock, as it was soft and easily eroded. The drumlins in the park all trend southeastwards, indicating the direction of the strongest ice advance from the northwest to the southeast.

The forest cover of the park is representative of the Atlantic Uplands forest region, including mixed coniferous and deciduous vegetation. There is a mixture of tree species but the dominant trees include white pine (*Pinus strobus*),

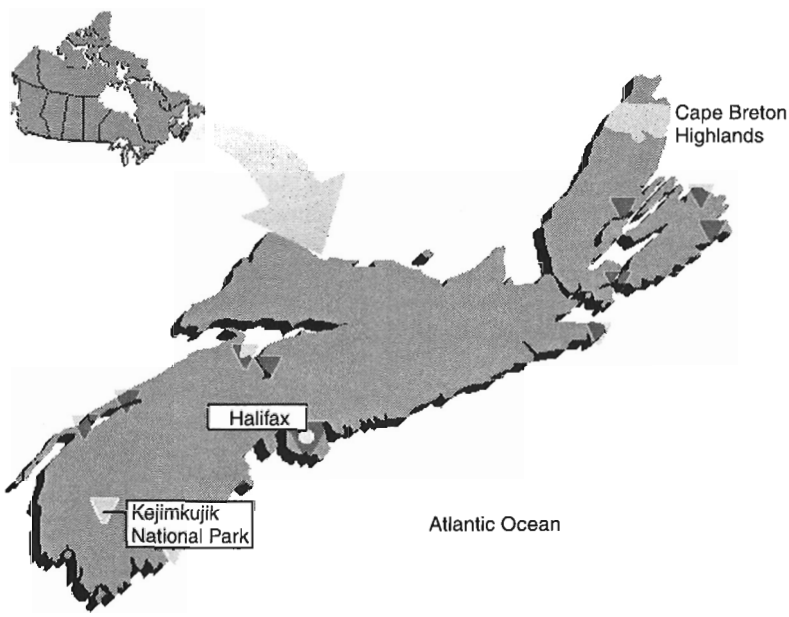


***Figure 1.***

*Location of Kejimkujik National Park, Nova Scotia.*

eastern hemlock (*Tsuga canadensis*), white birch (*Betula papyrifera*), and red maple (*Acer rubrum*). While much of the forest in the area has been disturbed by past logging, there is no longer logging within the park. The average age of forests in Kejimkujik National Park is less than 100 a as a result of the history of fire and logging. However, there are a few groves of towering eastern hemlock that have survived for over 300 a.

## METHODS

### *Data collection*

There are a variety of data and sources for the data that will be used in this study. A list of data currently available and used in this report is provided in Table 1. A brief description of each layer follows.

#### Lake-water chemistry

Fifty lakes, mostly within the boundaries of Kejimkujik National Park, were sampled by helicopter over a three-day period in October of 1997. Samples were filtered, acidified, and returned to the lab for analysis. Analysis for major and trace elements including Hg were done by acid digestion and subsequent ICP mass spectroscopy. Total organic carbon (TOC) was measured and dissolved organic carbon (DOC) was calculated. In addition, field measurements were made of the following parameters: dissolved oxygen, alkalinity, temperature, pH, and conductivity.

#### Lake-sediment chemistry

Eight sediment cores were taken from lakes in August of 1998. Cores were taken from the deepest part of the lake. In the field, each core was separated into 2 cm intervals to a depth of 20 cm and then in 5 cm intervals to the bottom of the core (average core lengths were about 40 cm). Samples were returned to the lab, freeze-dried, and centrifuged. Analysis for major and trace elements including Hg were done by acid digestion and subsequent ICP mass spectroscopy.

#### Biogeochemistry

Samples of tissue from the dominant tree species were collected at 53 sites in and around Kejimkujik National Park in August of 1998. Dominant trees included red maple (*Acer rubrum*), white pine (*Pinus strobus*), eastern hemlock (*Tsuga canadensis*), and white birch (*Betula papyrifera*). Not all species were present at each of the sites. Samples were placed in paper bags, air dried, and returned to the lab. Samples were sorted into leaf and twig tissue, ground to ensure homogeneity, and sent for chemical analyses. Trace elements including Hg were analyzed by acid digestion followed by ICP mass spectroscopy. Mercury samples were also analyzed by the Milestone Advance Mercury Analyzer using a drying time of 50 s and a decomposition time of 160 s but the results are not yet processed.

**Table 1.** Data layers and sample size for Kejimkujik National Park study.

| Data description | Data type | Sample size |
|---|---|---|
| Lake water chemistry | point | 50 |
| Lake sediment chemistry | point | 8 |
| Biogeochemistry | point | 53 |
| Rock chemistry | point | 117 |
| Fish chemistry* | point | 24 |
| Geology — lithology | raster | |
| Land cover classification | raster | |
| Drainage basins | raster | |

* N. Burgess (pers. comm., 1998)

#### Rock chemistry and lithology

A geological map of the study area is currently being compiled by the Nova Scotia Department of Natural Resources from existing data and field observations. The bedrock of Kejimkujik National Park is typical of rocks of the Meguma Terrane found throughout about 50% of the landmass of Nova Scotia from the town of Canso to Yarmouth. The area contains three general rock sequences each of which could be a source of Hg, 1) the Cambro-Ordovician Meguma Group, 2) the Siluro-Devonian Whiterock Group, and 3) the Devono-Carboniferous South Mountain batholith and related intrusive rocks.

The Meguma Group consists of a lower greywacke unit and an overlying black, organic, carbon-rich sulphidic slate. It underlies the south and eastern portions of Kejimkujik National Park as well as most of the Atlantic shore of Nova Scotia. Various facies are known to be strongly anomalous in As and Zn, and unpublished data (A. Sangster, 1999) suggests that locally Hg contents may vary directly with both of these elements.

From a geological perspective, Hg tends to be concentrated in sedimentary rocks that are deposited in reducing environments associated with abundant organic material such as black sulphidic shales and coal basins. The environment in and adjacent to Kejimkujik National Park is potentially favourable to the presence of Hg in such rocks and its liberation to the environment. Geological fieldwork concentrated on compiling existing geological information into a common base and collecting unweathered rock samples. One hundred and eighteen rock samples were collected from a variety of geological formations in the area. Rocks were returned to the lab, ground, and sent out for chemical analysis. Analysis of trace elements was done by acid digestion followed by ICP mass spectroscopy. Mercury samples were analyzed by cold vapour atomic absorption spectrometry using the Milestone AMA-254 as described by Hall and Pelchat (1997).

#### Fish chemistry

Fish chemistry data were provided by N. Burgess from Environment Canada. The data set consisted of Hg content (total) in yellow perch (*Perca flavescens*) from 24 lakes in Kejimkujik National Park (Burgess et al., 1998a). Values used were mean total Hg concentrations in whole yellow

perch of 50 g body weight. The entire fish was homogenized as it was considered that loons eat the entire fish. The lake-water sampling locations (50 lakes) included these lakes.

### Land-cover classification

The type of land cover is both affected by its chemical substrate and contributes to its composition. Seven different land-cover classes were identified and these were classified using LANDSAT Thematic Mapper data (LANDSAT TM). The seven classes included two classes of water, and one each of coniferous forest, deciduous forest, mixed forest, bogs/wetland, and cultural areas.

LANDSAT TM data are a measure of reflected and emitted light from the visible through the thermal infrared segment of the electromagnetic spectrum. The six bands in the visible and reflected part of the spectrum are measured with 30 m spatial resolution whereas the thermal band (lower energy) is measured with 120 m pixels.

## *Data preparation*

The objective of the study was to determine those factors, which may influence the level of Hg in the fish. The initial step was to construct a database that would permit analysis of relationships between variables. This would permit a series of questions to be investigated. For example to determine whether or not significant relationships exist between Hg and dissolved organic carbon concentrations in water and the concentration of Hg in fish as others have found. This was done by compiling all the information into a geospatially registered database. In this case, the main variable to be investigated was the level of Hg in yellow perch; however, there are many other relationships that need to clarified.

The construction of the database was complicated as the sample points were not always at the same location. For example fish samples will not be from the exact co-ordinates as a vegetation sample or even a lake-water sample. To overcome this limitation, the data were expressed on a catchment basin basis, with the assumption that the basin is a basis for standardizing the comparisons and the basin generally outlines an area of influence (Fig. 2). The catchment area for lakes were manually drawn on 1:50 000 topographic maps and digitized.

There are several data types in the list of variables (Table 1) and each type must be treated differently to compile the final database. A Universal Transverse Mercator projection (UTM) with NAD 83 was used as the projection system for this study.

## *Raster data*

The land cover and geological maps represent raster data. For each of these data layers the areal extent of a theme within each of the catchment areas was calculated. These areas (as percentages of each basin and as square kilometres) were then appended to the point-data file for each drainage basin.

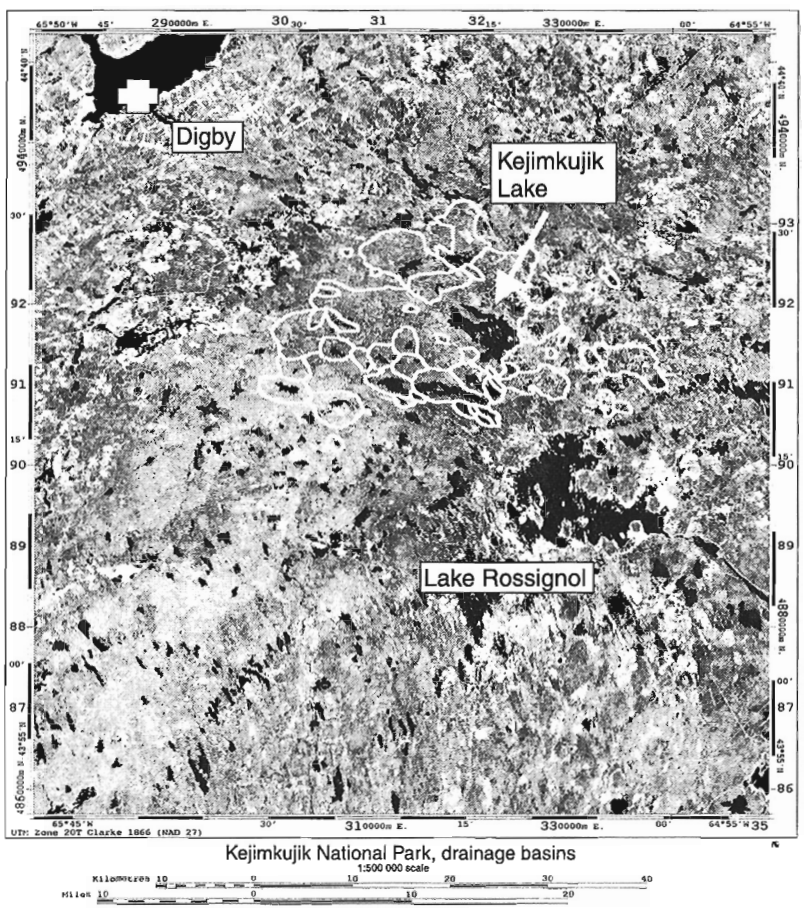


*Figure 2.*

*Outline of the drainage basins within Kejimkujik National Park, Nova Scotia.*

### *Point data*

#### Geochemical data

The lake-water geochemical data were simply appended to the fish data for the corresponding lake. The geochemical data for vegetation and rocks were first interpolated using an inverse distance weighted formula (idw) and then the average concentration for each element was calculated for each catchment basin. These values were then appended to the point data for the corresponding lake basin.

#### Lake morphology

There are several parameters that will be tested, but for the purposes of this report only the maximum lake depth and area of the catchment basin were taken. Other parameters associated with lake morphology will be included in the final study (e.g. average lake depth and lake depth fluctuations).

The intent is to develop a data file based on the lake basins. For each basin there would be a series of attributes that would permit a testing of relationships. For this report the file consists of 50 lake basins and currently available data. Eventually this data will be combined with data from other sources and data that will be collected as part of the ongoing study in Kejimkujik National Park.

## RESULTS

### *Statistics for each of the data layers*

The data presentation will provide a preliminary look at relationships between the variables. This will be in the form of x-y scatter plots that will compare two variables at a time. Future work will include multivariate analysis.

#### Raw data and variance in results

Preliminary chemical results are available for three tree species, rock samples, and lake waters. The data on yellow perch was provided by N. Burgess (pers. comm., 1998). Data compilation is not yet complete for all layers in Table 1. Table 2 illustrates the range of values for selected elements in the different media. The Hg concentrations in the trees are comparable to values in the literature (Rasmussen, 1994). Mercury concentrations in the leaf tissue showed a five-fold range in values, which is attributed to site differences as samples were from the same species, same tissue, same height, and samples were gathered over a narrow time window (5 d). Similarly the Hg (total) levels in lake waters were comparable to values in the literature (Beauchamp et al., 1997) and for other values at Kejimkujik National Park (Clair et al., 1998). There is also a five-fold range in the Hg values for lake waters which is attributed to site differences as samples were taken using the same protocol at each site and sampling was limited to a two-day period. The values in the rocks appear relatively low but are comparable to levels in the literature (Rose et al., 1979). There is a wide range in the values and this is directly related to the mineralogy of the rock sampled.

**Table 2.** Range of Hg concentrations in various media for Kejimkujik National Park, Nova Scotia and values reported in the literature.

| Media | Hg (total) *Kejimkujik* | N *samples* | Hg (total) *Reported values** |
|---|---|---|---|
| White pine, leaf | 21–46 ppb | 31 sites | |
| Red maple, leaf | 17–85 ppb | 33 sites | 16–41 ppb[1] |
| Perch[4] | | 24 lakes | 0.159–0.722 µg/g[4] |
| Rock | 0.04–12.5 ppb | 117 samples | granite 0.04[2] ppb<br>shale 0.02–0.4[2] ppb |
| Water | 2[2]–10 ppt | 50 lakes | 1–10 ppt[3] |

* selected values from the literature
[1] Rasmussen (1994)
[2] Rose et al. (1979)
[3] Beauchamp et al. (1997)
[4] N. Burgess (pers. comm., 1998)

The pH values in the lake waters varied from 4.1 to 6.2 and dissolved organic carbon varied from 2.2 to 13.1 ppm.

#### Relationships between dissolved organic carbon and other variables

It has been shown that dissolved organic carbon is strongly correlated to the level of Hg in waters (e.g. *see* Lodenius, 1994; Clair et al., 1998) and in particular to the process of methylation which is important in controlling the level of bioavailable Hg. This section will look at variables that are related to the level of Hg and thereby have a significant impact on the total level of Hg in the system as well as the level of bioavailable Hg. Figure 3 illustrates the relationship between several factors in the environment and dissolved organic carbon. In each of the four figures there are weak but visual relationships between dissolved organic carbon and each of the variables. There is a positive correlation between the percentage of bogs within a catchment basin and the level of dissolved organic carbon in lake waters. There is a negative association between lake-water pH and dissolved organic carbon that is apparent at low pH values. Similarily a negative correlation between the per cent cover of water within a drainage basin and dissolved organic carbon is only apparent at high dissolved organic carbon levels and low percentage water cover. Figure 3c illustrates a weak negative correlation between reflectance values in channel 1 of Landsat Thematic Mapper and dissolved organic carbon. As more data is entered into the database these relationships can be quantitatively studied and interactions between multiple variables can be investigated through multivariate statistics.

#### Relationships between Hg in waters (total) and other variables

Figure 4 illustrates the relationship between four variables and the level of Hg (total) in the water. As noted above, only a few variables are included in this report. In this case the relationships are visually stronger than in Figure 3. There is a positive correlation between Hg levels and the level of Zn in the rocks and in the level of dissolved organic carbon. There is a negative correlation between the concentration of Hg in lake

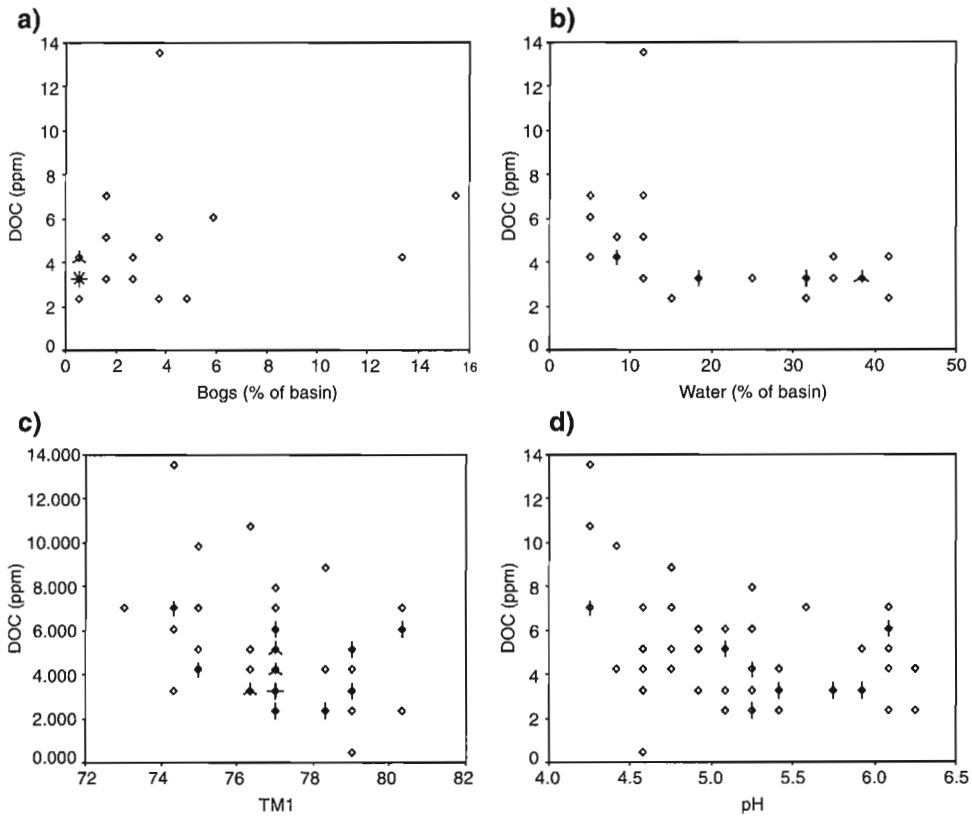


*Figure 3.*

*Scattergrams showing relationship between four variables and level of dissolved organic carbon in lake waters at Kejimkujik National Park, Nova Scotia. Circles represent one sample, and number of 'petals' represent number of samples with the same value.*

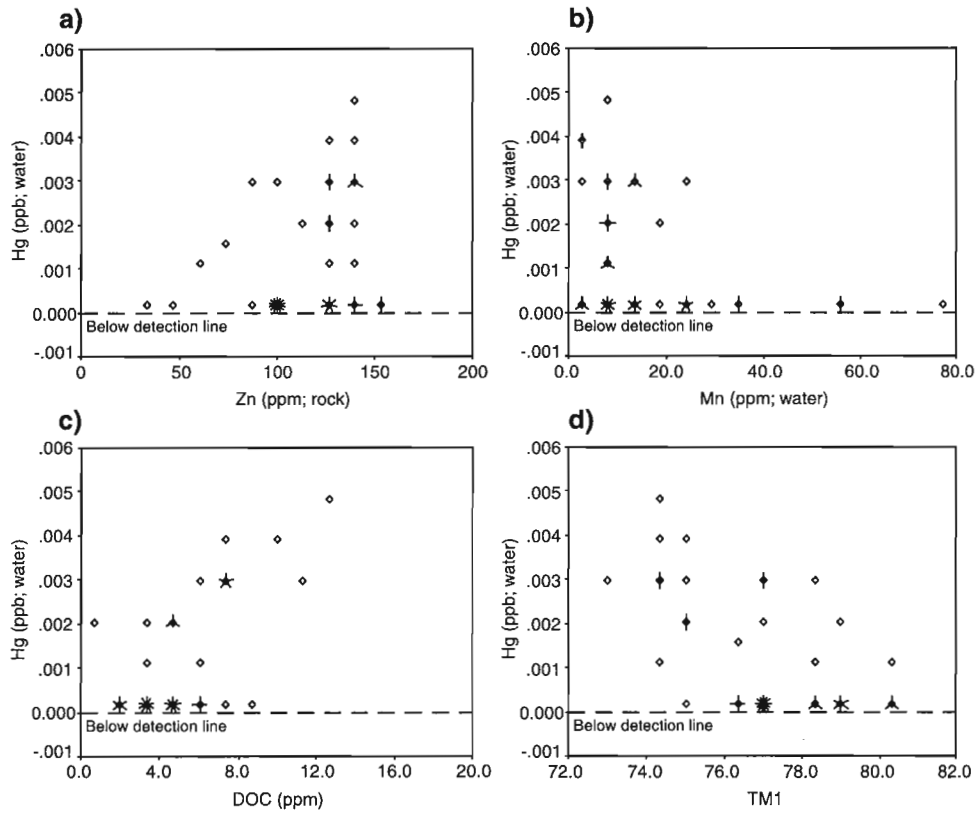


*Figure 4.*

*Scattergrams showing relationship between four variables and level of Hg in lake waters at Kejimkujik National Park, Nova Scotia. Circles represent one sample, and number of 'petals' represent number of samples with the same value.*

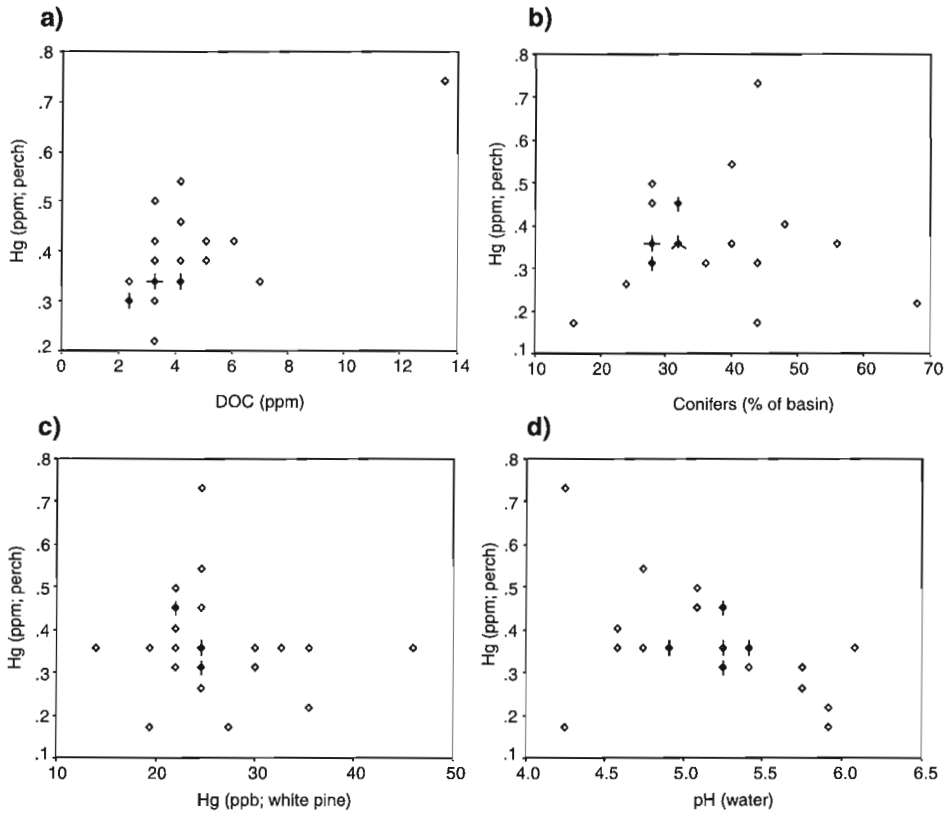


*Figure 5.*

*Scattergrams showing relationship between four variables and level of Hg in perch at Kejimkujik National Park, Nova Scotia. Circles represent one sample, and number of 'petals' represent number of samples with the same value.*

waters and the level of Mn in lake waters. The relationship between reflectance levels in band 1 of LANDSAT Thematic Mapper data with Hg in waters shows a weak negative correlation but there is considerable variability in the pattern (Fig. 4).

### Relationships between Hg in fish and other variables

Figure 5 illustrates the relationship between four variables and the level of Hg in yellow perch. There are positive relationships between dissolved organic carbon, per cent coniferous forest in a catchment basin, and Hg concentration (total) in water with the level of Hg in perch. The concentration of Zn in the underlying rocks appears to be related to the Hg levels in yellow perch. There is no obvious pattern in the relationship between levels of Hg in white pine and Hg levels in perch (compared on a catchment basin basis).

## DISCUSSION

The preliminary results from Kejimkujik National Park, Nova Scotia illustrate that the values of total Hg in the vegetation, rocks, and lake waters are not considerably higher than elsewhere. However the level of Hg in the fish and the loons are among the highest in North America. In fact, the high levels of Hg are suggested as a potential cause of lower rates of loon reproductive success in the park (Burgess et al., 1998c). The reasons for these high levels in the biota are the focus of this and other studies in the park.

The preliminary data sets illustrate certain relationships that merit further investigation. As with other studies, the level of dissolved organic carbon in lake waters appears very important in controlling the total Hg in water and in the food chain (Lodenius, 1994; Clair et al., 1998). The factors contributing to the high dissolved organic carbon include the percentage of bogs and coniferous forest in the catchment basin. The size of the catchment basin and the water/land ratio are important controls on the Hg levels. It is potentially very significant that the level of Zn in the underlying rocks is related to the Hg levels in fish. This could indicate a relationship with Hg-bearing minerals, a link with sulphide minerals and its relationship with lake pH, or a combination of these attributes. In Nova Scotia, much of the area around Kejimkujik National Park is underlain by black sulphidic shale and greywacke known as the Meguma Group of rocks. Although little is known of their Hg geochemistry, the rocks are rich in arsenic and locally zinc and gold — all elements that tend to occur with Hg in natural environments. Unpublished results (A. Sangster, pers comm., 1999) for a drill hole (26 samples) near Clarksville, Nova Scotia illustrate a clear association of Hg with the levels of zinc and arsenic.

There does not appear to be a strong correlation between any one variable and the level of Hg in yellow perch. This would suggest that all the variables interact to some degree and undoubtedly that other variables not yet studied will play a major role. The next stages of the research will include other variables and if planned work proceeds then a range of variables including atmospheric input, groundwater input, and diagenetic processes will be included.

## ACKNOWLEDGMENTS

The project has been funded through the MITE Project at the Geological Survey of Canada and support from the Nova Scotia Department of Natural Resources. Pat Rasmussen and Graeme Bonham-Carter, both with the Geological Survey of Canada, and Mr. Neil Burgess with Environment Canada have reviewed parts of the paper, however the authors are responsible for the content.

## REFERENCES

**Beauchamp, S., Burgess, N., Dentremont, A., Tordon, R., Brun, G., Leger, D., Schroeder, W., and Abraham, J.**
1997: Mercury in air, water and biota in Kejimkujik National Park, Nova Scotia, Canada; *in* Proceedings of the Third International Conference of Science and the Management of Protected Area, May 12–16, 1997, Calgary, Alberta, 13 p.

**Burgess, N.M., d'Entremont, A.A., Drysdale, C., Vaidya, O., and Brun, G.L.**
1998a: Mercury in yellow perch in Kejimkujik National Park; *in* Mercury in Atlantic Canada: a Progress Report, (ed.) N. Burgess, S. Beauchamp, G. Brun, T. Clair, C. Roberts, L. Rutherford, R. Tordon, and O. Vaidya; Environment Canada - Atlantic Region, Sackville, New Brunswick, p. 72–76.

**Burgess, N.M., Evers, D.C., and Kaplan, J.D.**
1998b: Mercury levels in common loons breeding in the Maritimes and their prey; *in* Mercury in Atlantic Canada: a Progress Report, (ed.) N. Burgess, S. Beauchamp, G. Brun, T. Clair, C. Roberts, L. Rutherford, R. Tordon, and O. Vaidya; Environment Canada - Atlantic Region, Sackville, New Brunswick, p. 96–100.

**Burgess, N.M., Evers, D.C., Kaplan, J.D., Duggan, M., and Kerekes, J.J.**
1998c: Mercury and reproductive success of common loons breeding in the Maritimes; *in* Mercury in Atlantic Canada: a Progress Report, (ed.) N. Burgess, S. Beauchamp, G. Brun, T. Clair, C. Roberts, L. Rutherford, R. Tordon, and O. Vaidya; Environment Canada - Atlantic Region, Sackville, New Brunswick, p. 104–109.

**Clair, T.A., Burgess, N.M., Brun, G.L., and Léger, D.**
1998: The relationship between organic carbon, pH, total mercury and location in Atlantic Canada lakes; *in* Mercury in Atlantic Canada: a Progress Report, (ed.) N. Burgess, S. Beauchamp, G. Brun, T. Clair, C. Roberts, L. Rutherford, R. Tordon, and O. Vaidya; Environment Canada - Atlantic Region, Sackville, New Brunswick, p. 54–62.

**Hall, G.E.M. and Pelchat, P.**
1997: Evaluation of a direct solid sampling atomic adsorption spectrometer for the trace determination of mercury in geological samples; Analyst, v. 122, p. 921–924.

**Lodenius, M.**
1994: Mercury in terrestrial ecosystems: a review; *in* Mercury Pollution: Integration and Synthesis, (ed.) C.W. Watras and J.W. Huckabee; Lewis Publishers, London, U.K., p. 343–354.

**Nocera, J. and Taylor, P.**
1998: *In situ* behavioral response of common loons associated with elevated mercury (Hg) exposure; Conservation Ecology (online) v. 2, issue 2, article 10. (Site visited April 27, 1999. Available on the Internet at http://www.consecol.org/vol2/iss2/art10.)

**Rasmussen, P.**
1994: Mercury in vegetation of the Precambrian Shield; *in* Mercury Pollution: Integration and Synthesis, (ed.) C.W. Watras and J.W. Huckabee; Lewis Publishers, London, U.K., p. 417–425.

**Rasmussen, P., Villard, D., Gardener, H., Fortescue, J., Schiff, S., and Shilts, W.**
1998: Mercury in lake sediments of the Precambrian Shield, near Huntsville, Ontario, Canada; Environmental Geology, v. 33, no.2-3, p. 96–108.

**Rose, A.W., Hawkes, H.E., and Webb, J.S.**
1979: Geochemistry in Mineral Exploration; Academic Press, U.K., 657 p.

Geological Survey of Canada Project 890043 AR

# History of major debris flows on the Scotian Rise, offshore Nova Scotia

David J.W. Piper, Kenneth I. Skene[1], and Nancy Morash
Geological Survey of Canada (Atlantic)

*Piper, D.J.W., Skene, K.I., and Morash, N., 1999: History of major debris flows on the Scotian Rise, offshore Nova Scotia;* in *Current Research 1999-E; Geological Survey of Canada, p. 203–212.*

**Abstract:** Regional single-channel seismic reflection profiles of the Pliocene–Quaternary section on the Scotian Rise have been correlated with biostratigraphic control on Laurentian Fan and the central Scotian Slope. The distribution and age of debris-flow deposits on the rise is correlated with sediment failures on the slope. Debris-flow deposits are as old as the mid-Pliocene, suggesting that glaciation is not a determining cause of sediment failure. On the Scotian Slope, the widespread occurrence of shallow gas and the age and character of several failures suggest that sublimation of gas hydrate, resulting in excess pore pressures, is the principal trigger for sediment failure.

**Résumé :** Des profils régionaux de sismique-réflexion monocanal de la section pléistocène–quaternaire du glacis Néo-Écossais ont été corrélés avec des contrôles biostratigraphiques sur le cône Laurentien et le centre du talus Néo-Écossais. La répartition et l'âge des coulées de débris sur le glacis sont corrélés avec des glissements de sédiments sur le talus. Les coulées de débris datent au moins du Pléistocène moyen, ce qui permet de penser que la glaciation n'est pas une cause déterminante des glissements de sédiments. Sur le talus Néo-Écossais, la présence étendue de gaz près de la surface ainsi que l'âge et les caractéristiques de plusieurs glissements laissent supposer que la sublimation d'hydrates de gaz, qui mène à une surpression interstitielle, est le principal facteur de déclenchement des glissements de sédiments.

[1] Mobil Oil Canada, 330-5th Avenue SW, P.O. Box 800, Calgary, Alberta T2P 2J7

## INTRODUCTION

Major sediment failure is a potential hazard to petroleum development on the continental slope and rise. Several well known glaciated continental margins show widespread failures involving the upper hundred or so metres of sediment (New England: O'Leary and Dobson, 1992; Norway: Bugge et al., 1987, 1988). Similar failures are known from the Scotian margin (Fig. 1). Detailed studies of sediment failure near the Albatross B-13 and Shubenacadie H-100 wells (e.g. Mosher et al., 1994; Mulder and Moran, 1995; Mulder et al., 1997, 1999) have not solved the problem of the origin and triggering mechanism for the failures on the Scotian Slope. These sediment failures originate in water depths of 500–1000 m b.s.l. and in the last 30 ka appear restricted to the time interval from 15 ka to 10 ka, a time when glacial ice was retreating from the Scotian Shelf. Thus triggering mechanisms involving the loading effects of ice appear unlikely, except perhaps seismicity induced by ice loading (Stein et al., 1979). Mosher et al. (1994) used infinite slope analysis to show that slopes near the Shubenacadie H-100 well are stable and that failure would require excess pore pressures and/or earthquake accelerations.

Sparse, high-resolution seismic-reflection profiles from the Scotian Rise show that debris-flow or flow-slide deposits are widespread (Piper, 1991; Hughes Clarke et al., 1992). On the western Scotian margin, which is not highly dissected by canyons, some debris-flow deposits on the continental rise can be clearly linked to failures on the continental slope (e.g. Mulder et al., 1997). On the other hand, the eastern Scotian Slope is deeply dissected by canyons and it is much more difficult to recognize failure scars there.

In this study, we use the spatial and stratigraphic distribution of debris-flow deposits on the Scotian Rise to determine the age and distribution of failures on the Scotian Slope. We use this information to draw conclusions about triggering mechanisms. Our principal database on the continental rise is single-channel seismic-reflection profiles collected on cruises 93026, 96029, and 98039 (Fig. 1) using a 40 cubic inch sleeve gun. In addition, we have examined industry multichannel seismic line GSI-108 and data presented by Swift (1987).

## STRATIGRAPHY

Stratigraphic correlation on the Scotian Rise is difficult because of the lack of wells and the problem of seismic continuity through the slope salt-diapir province. We have identified late Pliocene strata on the rise from two tie points, one on Laurentian Fan and the other on the central Scotian Slope (Fig. 2, Table 1).

### *Laurentian Fan*

On Laurentian Fan, samples of outcropping mudstone sampled from DSV Alvin and dated as Late Pliocene can be correlated with regional seismic stratigraphy (Hughes Clarke, 1988, p. 132–133). The outcrop is some 100 m deeper than regional stratigraphic marker A defined by Piper and Normark (1982) and further correlated on Laurentian Fan by Skene (1998) (Fig. 3).

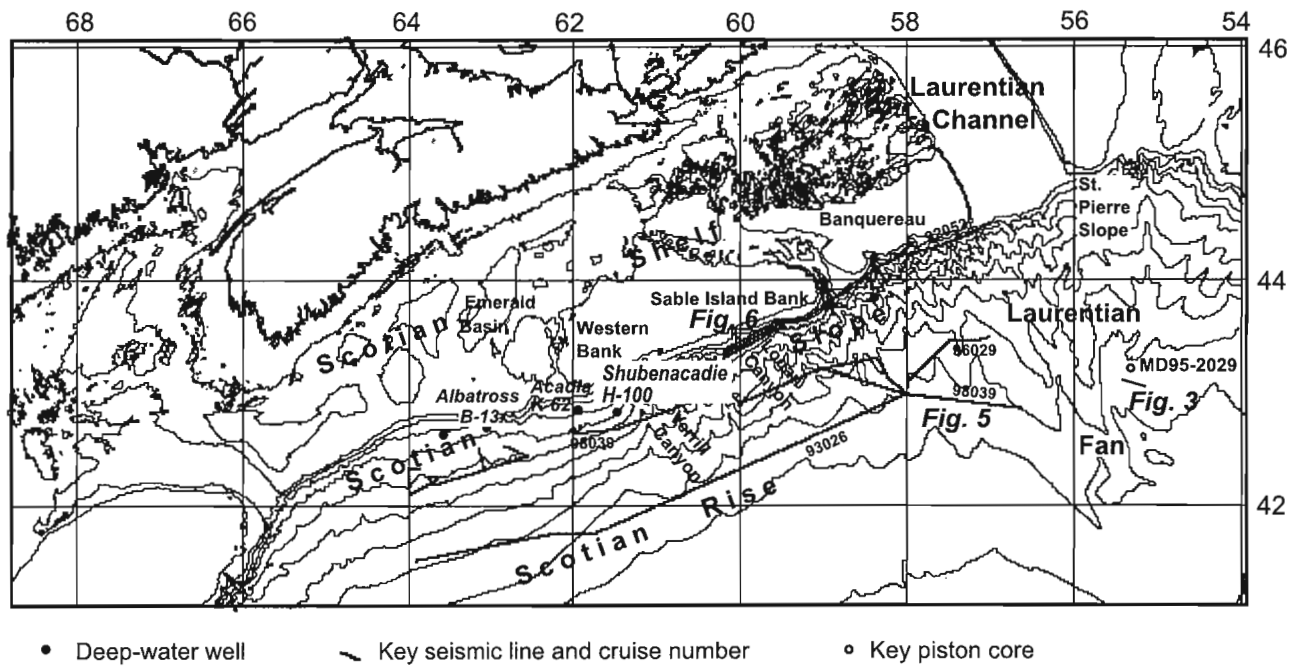


***Figure 1.*** *General map of Scotian margin showing deep-water wells, piston core, and seismic lines used for stratigraphic correlation and to map debris-flow deposits.*

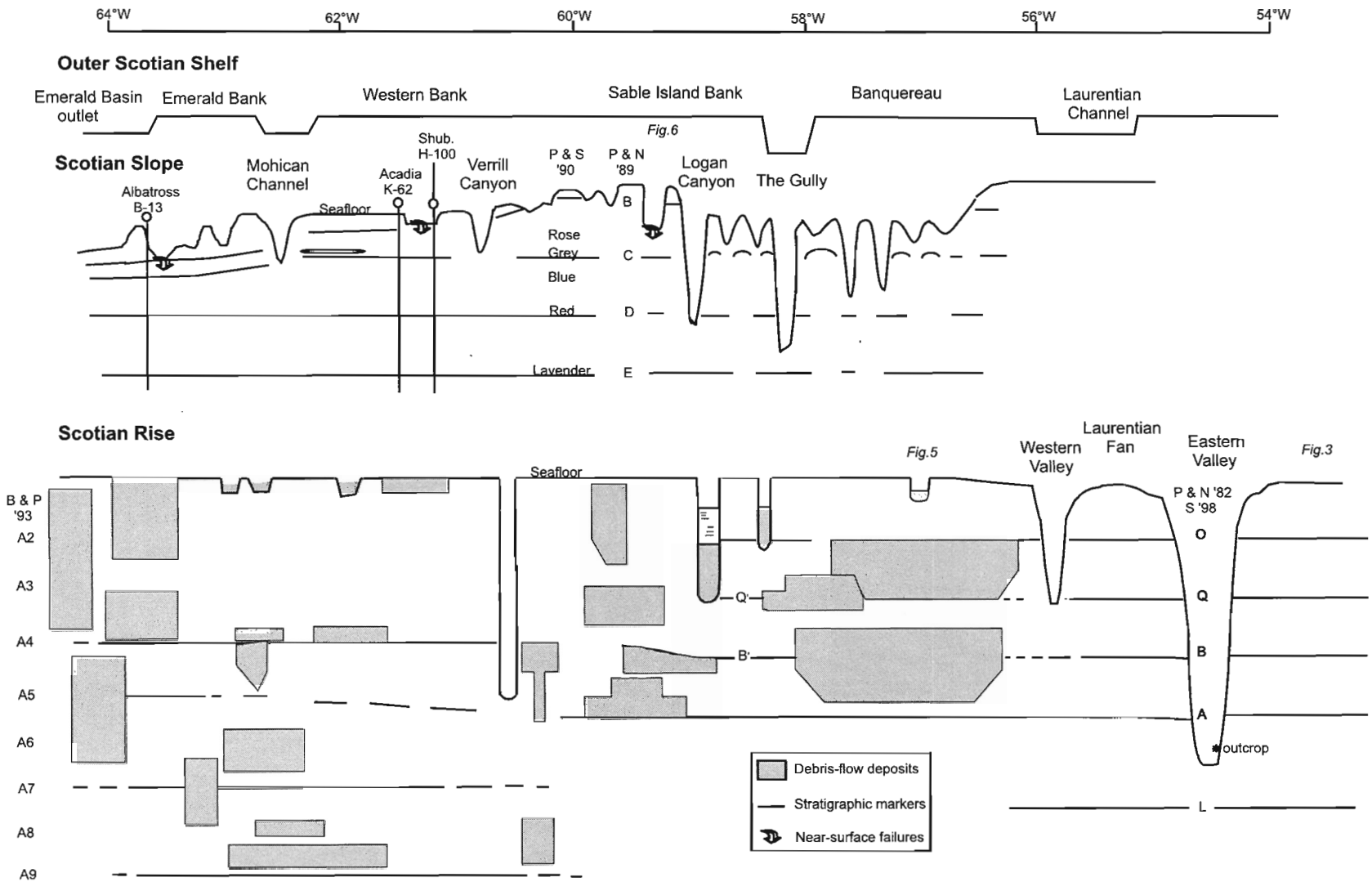


***Figure 2.*** *Schematic east-west sections showing the distribution of key stratigraphic reflectors and debris-flow deposits on the Scotian Slope and Scotian Rise. Shub.=Shubenacadie; P & S '90=Piper and Sparkes (1990); P & N "89=Piper and Normark (1989); B & P '93=Berry and Piper (1993); P & N '82=Piper and Normark (1982); S '98=Skene (1998). See also Table 1.*

**Table 1.** Stratigraphic nomenclature on the Scotian Slope, Scotian, and Laurentian Fan.

| Age | Scotian Slope | | | Scotian Rise | Laurentian Fan | |
|---|---|---|---|---|---|---|
| | Piper and Normark (1989) | Piper et al. (1987) | Piper and Sparkes (1990) | Berry and Piper (1993) | Piper and Normark (1982) | Skene (1998) |
| | A | | | | | |
| Isotopic stage 6 | B | | Carmine | | | O |
| | | | | | Q | Q |
| | | Gold | | A4 | | |
| | | | Rose | | | B |
| Base Quaternary | C | | Grey | A5 | A | A |
| | | Blue | Blue | A9 | | |
| | D | Red | Red | | | |
| Middle Pliocene | E | Light green | Lavender Orange Pink | | L | |
| Base Pliocene | | | Canary | | | |

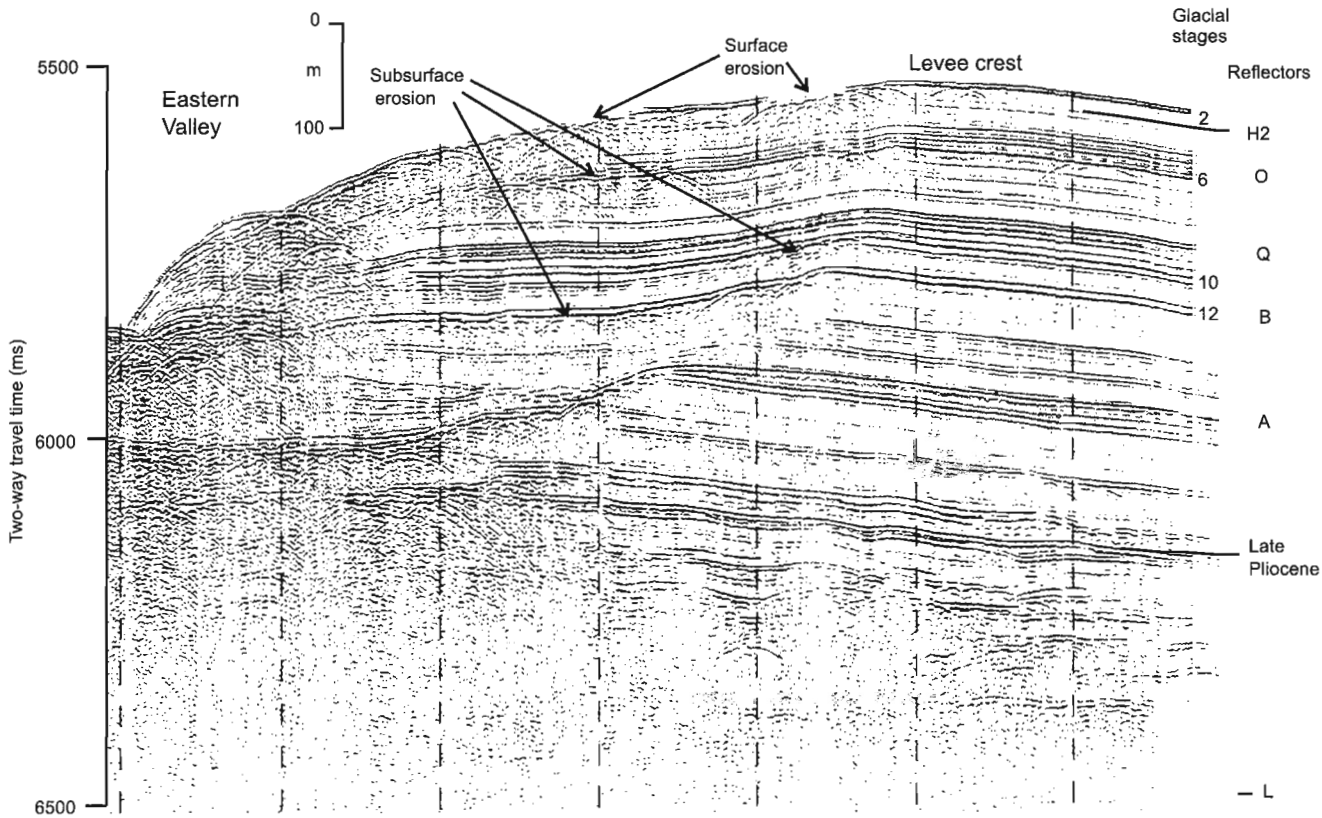


***Figure 3.*** *Seismic-reflection profile from the eastern levee of Eastern Valley of Laurentian Fan, showing key stratigraphic reflectors and correlation with core MD95-2029 (Cruise HU84-040).*

Berry and Piper (1993) attempted to date the shallowest part of the Laurentian Fan seismic stratigraphy by extrapolation of sedimentation rates and correlation of reflector character with the central Scotian Rise. More recent sampling suggests that their interpretation was wrong. Core MD95-2029 sampled Heinrich event 2 (21 ka) (H2, Fig. 4) at a core depth of 27–28 m (Piper and Skene, 1998). Cores collected on this cruise experienced some stretching, perhaps as much as 6 m (F. Rack, pers. comm., 1998; R.N. Hiscott, pers. comm., 1998). Correlation of core MD95-2029 with standard piston cores 73031-007 and 96029-069 and 96029-070 (Fig. 4) suggests that the uppermost part of the core was stretched about 5 m, but that deeper intervals (marked by bioturbated horizons within a uniform red mud sequence) were not stretched. Therefore, the true subbottom depth is probably of H2 is thus about 22 m. Using this subbottom depth, H2 can be correlated with a high amplitude reflection at 30 ms (22 m) subbottom corresponding to significant variability in bulk density between 25 m and 28 m in core MD95-2029 (Fig. 4). The prominent near-surface reflector in the 3.5 kHz profiles corresponds to an interval of variable bulk density at 6–8 m in stretched core MD95-2029, corresponding to 2–3 m b.s.f.(below sea floor) in nearby cores.

We have attempted to extrapolate sedimentation rates on a seismic reflection profile from cruise HU84-040 (Fig. 3). Reflector L has been argued by Piper and Normark (1989) to date from the base of the late Pliocene, when turbidites first reached the Sohm Abyssal Plain. If there were a constant sedimentation rate above reflector L, reflector A would approximately correspond to the base of the Quaternary. On the Laurentian Fan, there was a major re-arrangement of valley patterns at reflector A, correlative with the initiation of widespread canyon cutting on the Scotian Slope, and probably triggered by the fall in sea level at the base of the Quaternary (Piper and Normark, 1989). Another change in style on Laurentian Fan occurs at reflector B, most clearly visible on the eastern levee of Eastern Valley (Fig. 6.13 of Skene, 1998) and the western levee of Western Valley (Fig. 6.15 of Skene, 1998). Substantial cut and fill above reflector B (Fig. 3; *see also* Piper and Normark, 1982, their Fig. 9) may be related to catastrophic ice-margin flood discharge, probably at the end of major glacial stages (J. Shaw, pers. comm., 1997). Four horizons of rather similar surface erosion are visible in Figure 3, near the present surface, at reflector O, just below reflector Q, and at reflector B. The style of this erosion is quite different from that seen at reflector A. The near-surface erosion corresponds to erosion by subglacial flood discharge during ice-retreat about 15 ka. The erosion surface at reflector O is three times deeper than the reflector at Heinrich event 2 (21 ka) — linear extrapolation of sedimentation rate would suggest an age of about 60 ka. On the distal Sohm Abyssal Plain, which appears to receive most of its sediment from the Laurentian Fan, H2 occurs at 5 m b.s.f. and the end of the penultimate glacial (stage 6) at 12 m b.s.f. (Hundert, 1999). If changes in sedimentation rates on Laurentian Fan through time are comparable, then the top of stage 6 would be at about 50 m b.s.f. in Figure 3, a little shallower than reflector O at 65 m b.s.f.. These two approaches bracket reflector O as representing the end of glacial isotopic stage 6 at about 130 ka. An analogous extrapolation suggests that reflector B might represent the top of glacial stage 12 and reflector Q the top of glacial stage 8. Piper et al. (1994) identified marine isotope stage 12 (0.45 Ma) as the time that glacial ice first excavated the modern deep Laurentian Channel on the continental shelf.

### *Central Scotian Slope and Scotian Rise*

On the central Scotian Slope and Scotian Rise, between the Acadia K-62 and Albatross B-13 wells, we have used two techniques to modify the stratigraphic correlation proposed by Berry and Piper (1993). Although direct correlation between the continental slope and rise is difficult because of widespread salt diapirism, one low-resolution industry seismic line (A160 shot for Shell Canada Resources in 1982: Berry and Piper, 1993) allows correlation of the "Blue" reflector of Piper et al. (1987) on the Scotian Slope to the rise, where it corresponds to A9 of Berry and Piper (1993) (Table 1). "Blue" was dated as late Pliocene using biostratigraphy from the Acadia K-62 and the Shubenacadie H-100 wells (Gradstein *in* Piper et al., 1987).

In general, the area on the Scotian Slope between Mohican Channel and the Acadia K-62 well lacks failure surfaces and debris-flow deposits, in contrast to the areas both east and west (Fig. 2). The exception is a prominent debris-flow deposit at about the "Rose" stratigraphic horizon of Piper and Sparkes (1990), correlated with just above the base of the Quaternary in the Acadia K-62 well (Piper et al., 1987). The Mohican Channel to Acadia K-62 sector of the Scotian Rise also has a well stratified sediment section, in contrast to debris-flow deposits to the east and west. Within this section, there is one prominent debris-flow deposit (Fig. 2), just above reflector A5. We therefore correlate this unique debris-flow deposit with the unique debris-flow deposit at "Rose" on the corresponding continental slope.

Cenozoic sediment thickness on the continental rise, interpreted mainly from low-resolution industry seismic line GSI-108 and regional studies, such as Uchupi and Austin (1979) and Swift (1987), thins substantially from the major depocentre of the Laurentian Fan westward onto the Scotian Rise. We cannot correlate precisely along high-resolution strike lines on the Scotian Rise, because of intermittent pinchouts, but our general correlation (Fig. 2) is consistent with this westward thinning.

## DEBRIS-FLOW DEPOSITS ON THE SCOTIAN RISE

Debris-flow and slide deposits are widespread on the Scotian Rise (Hughes Clarke et al., 1992; Mulder et al., 1997). In high-resolution seismic reflection profiles, such deposits are recognized by their acoustic transparency, erosional base, irregular surface, and commonly convex-up morphology

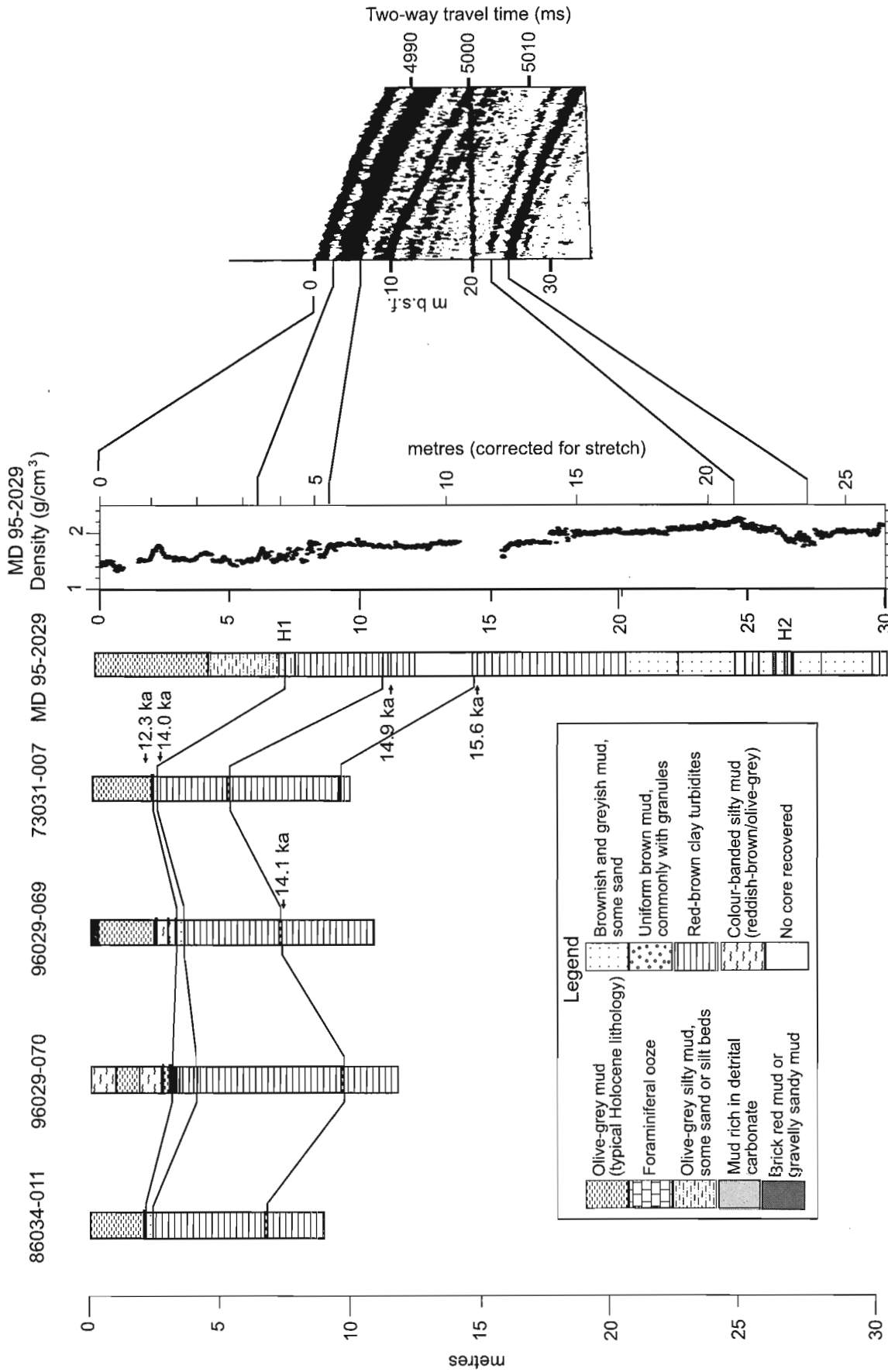


***Figure 4.*** *Core MD95-2029 and nearby cores showing lithological correlation and correlation of the bulk-density profile in MD95-2029 with the 3.5 kHz profile (cf. Fig. 9 of Berry and Piper (1993)).*

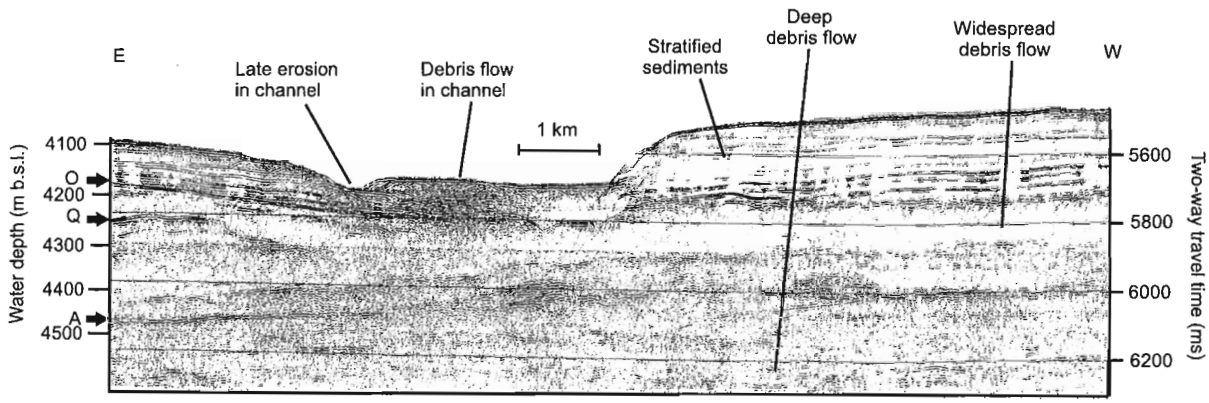


***Figure 5.*** *Seismic-reflection profile showing stacked debris-flow deposits and key stratigraphic reflectors on the eastern Scotian Rise (Cruise HU98-039). Symbols O, Q, and A are reflectors identified in Table 1 and Figure 2.*

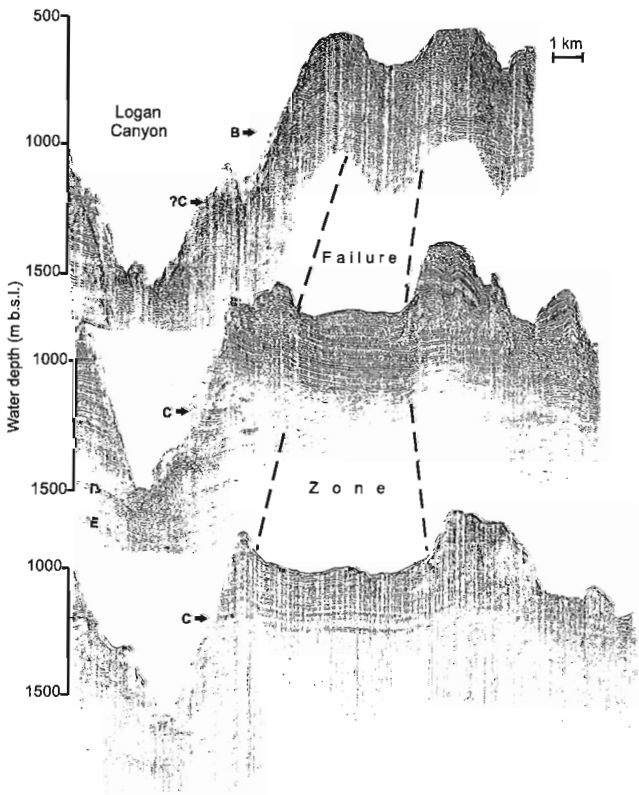


***Figure 6.*** *Seismic-reflection profile showing large scar left by sediment failure(s) on the Scotian Slope immediately west of Logan Canyon (Cruise PZ92-052). Symbols B and C are reflectors identified in Table 1 and Figure 2.*

(Shor and Piper, 1989). At their margins, debris-flow deposits interfinger with well stratified sediments. Debris-flow deposits have two styles of occurrence — as channel fills and as laterally extensive sheets (Fig. 5). Along the continental rise, zones with common stacked debris-flow deposits alternate with zones in which predominantly stratified sediments have accumulated, as shown schematically in Figure 2.

On the Scotian Rise south of Banquereau, debris-flow deposits are widespread in the interval from Laurentian Fan reflectors A to O (interpreted base Quaternary to isotopic stage 6) (Fig. 5). Above reflector O, thick stratified sediments accumulated and debris-flow deposits are generally restricted to a few channels. Although some debris-flow deposits are recognized below reflector A (Fig. 5), seismic penetration is insufficient to map their distribution systematically (Fig. 2).

On the Scotian Rise south of Sable Island Bank, the stratigraphic distribution of debris-flow deposits is similar. An exception is in the area south of Logan Canyon, where a series of near-surface debris flows on the rise can be traced upslope into a major slump scar more than 300 m deep (Fig. 6).

Immediately west of Verrill Canyon, near-surface failures on the continental slope described by Piper et al. (1985) and Mosher et al. (1994) appear to correspond to near-surface debris flows on the Scotian Rise (Fig. 2). The widespread debris flows on the continental slope near the Albatross B-13 well (Mulder et al., 1997) are represented by near-surface channel-filling debris flows on the rise (Berry, 1992). However, debris flows are visible deeper in the section and appear to date back to at least the middle Pliocene (applying our revised stratigraphy to Berry and Piper (1993)). Farther west, a thick sequence of debris flows from the seabed down to below reflector A7 of Berry and Piper (1993) (possibly late Pliocene) are downslope from the deep-water outlet of Emerald Basin, an area of substantial sediment instability (Hill, 1983, 1984; Piper and Sparkes, 1987).

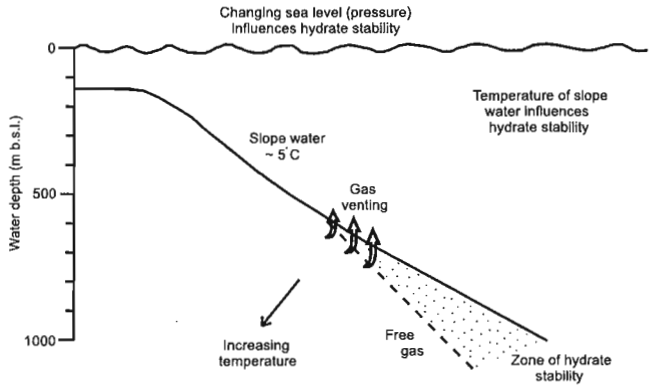


***Figure 7.*** *Cartoon illustrating the role of gas hydrate on slope stability.*

## DISCUSSION

Debris-flow deposits have accumulated on the Scotian Rise at least since the middle Pliocene. This substantially predates the first crossing of the Scotian Shelf by continental ice sheets, probably in the middle Pleistocene (Piper et al., 1994), suggesting that ice loading effects are not responsible for triggering widespread sediment failures.

On the Laurentian Fan, there was a major rearrangement of valley patterns at refector A, which most probably corresponds to the fall in sea level at the base of the Quaternary (Piper and Normark, 1989). Following that event, channels developed on the western Laurentian Fan, perhaps resulting in a decrease in sedimentation rates in the east. Another change in style on Laurentian Fan occurs at reflector B and substantial cut and fill above reflector B may be related to catastrophic ice-margin flood discharge, probably at the end of major glacial stages (J. Shaw, pers. comm., 1997). Our seismo-stratigraphic correlations show that on the east Scotian Rise, widespread debris flows ceased to be deposited at about reflector Q, shortly after the onset of shelf-crossing glaciations at reflector B. At least on the central Scotian Slope, canyon cutting did not begin until the Pleistocene (Piper et al., 1987) and a similar timing is likely on the east Scotian Slope (Clifford, 1986; Piper and Normark, 1989, their Fig. 11). Therefore, the distribution of debris-flow deposits is unlikely to be related to canyon excavation. The widespread occurrence of single debris-flow deposits is also difficult to reconcile with failure triggered by canyon wall oversteepening.

The head scarps of most well studied sediment failures on the Scotian margin and St. Pierre slope are in the same water depth (500–700 m) as the most abundant pockmarks (Baltzer et al., 1994; Mosher et al., 1994; Piper et al., 1999), which suggest a causal link between excess pore pressures due to shallow gas and the occurrence of failures. The presence of areas of undisturbed seabed down to 700 m water depth indicates that bearing capacity failure from an ice load on the shelf (Mulder and Moran, 1995) is unlikely to be a cause of the observed failures, as more common failures in shallower water would be expected. Failures in this water depth are also difficult to account for by excess pore pressure due to ice-loading (Mulder and Moran, 1995; Mulder et al., 1999), which is unlikely to be significant in water depths of more than 250 m.

On many other continental margins, gas hydrate has been implicated in large sediment failures (Paull et al., 1991; Piper et al., 1997). Methane hydrate would be stable in near-surface sediment on the Scotian margin in water depths of more than about 600 m b.s.l. (cf. Cranston et al., 1994) (Fig. 7). If they formed a less permeable cap to seafloor sediments, free gas in sediments beneath the zone of hydrate stability could lead to excess pore pressures and hence sediment instability. The link between shelf-crossing glaciation and the end of debris-flow initiation may be in the widespread tunnel valleys on the eastern Scotian Shelf (Loncarevic et al., 1992) that appear to continue in the deep canyons of the eastern Scotian Slope. Cutting of deep slope canyons on the eastern Scotian Slope seaward of the shelf tunnel valleys could have allowed excess pore pressures to dissipate laterally along permeable horizons. The remarkable preservation of a narrow ridge between Logan Canyon and the major failure to the west (Fig. 6) is consistent with this interpretation.

Pockmarks and gassy cores indicate that free gas is widespread on the Scotian margin. High-resolution sidescan data show that pockmarks are common on the continental slope and more abundant in water depths of 500–700 m than at 1000–2000 m (Baltzer et al., 1994). There is no evidence that this distribution results from either differences in bottom sediment type or the distribution of deep sources or pathways for gas. We suggest, rather, that this distribution is the result of up-dip migration of gas along the base of the hydrate layer, which then preferentially escapes to the surface where the hydrate cap thins or becomes discontinuous (Fig. 7). Excess pore pressure may also develop as a result of high sedimentation rates seaward of major glacial outlets, notably south of Emerald Basin (Piper and Sparkes, 1987). The actual trigger for failure may be seismicity, iceberg scour (during the Pleistocene, in water depths of less than 700 m), or perhaps storm-wave loading.

Although circumstantial evidence for gas hydrate is widespread, we know of no direct evidence for the presence of gas hydrate on the Scotian margin. No bottom-simulating reflections or bottom-simulating wipeouts have been reported. Gas hydrate has not been recovered in cores and no detailed geochemical measurements have been made on gas samples. Thus further work will be necessary to demonstrate the possible role of gas hydrate in slope instability.

Failures near the Albatross and Shubenacadie wells took place in the interval 15–12 ka (Piper and Skene, 1998), and younger failures are not known. We speculate that during this time, deep slope waters were warmed as a result of

withdrawal of glacial ice from the continental margin, thus resulting in sublimation of gas hydrate. The occurrence of high-latitude glaciation around the Norwegian–Greenland and Labrador seas since the middle Pliocene suggests that a cold Labrador Current has existed since that time. Cold slope waters derived from this current would have promoted the formation of gas hydrate on the Scotian margin and fluctuations in the current provide a mechanism for sublimation at intervals through the late Pliocene and Quaternary.

## CONCLUSIONS

1. A general Pliocene–Quaternary stratigraphic framework has been developed for the Scotian Rise.
2. Debris-flow deposits are widespread on the Scotian Rise since at least the middle Pliocene; they are less frequent on the eastern Scotian Rise since the middle Pleistocene.
3. Shallow gas is widespread on the Scotian Slope. The co-occurrence of pockmarks and sediment failures suggest that excess pore pressures due to shallow gas are important in causing failure on the continental slope. The preservation of unfailed sediment adjacent to deep canyons where excess pore pressures could dissipate supports this conclusion.
4. The ages of failures suggest that sublimation of gas hydrate as a result of warming of slope waters is the principal cause of sediment failure.

## REFERENCES


**Baltzer, A., Cochonat, P., and Piper, D.J.W.**
1994: In situ geotechnical characterisation of sediments on the Scotian Slope, eastern Canadian continental margin; Marine Geology, v. 120, p. 291–308.

**Berry, J.A.**
1992: A detailed study of a debris flow system on the Scotian Rise; M.Sc. thesis, Dalhousie University, Halifax, Nova Scotia, 202 p.

**Berry, J.A. and Piper, D.J.W.**
1993: Seismic stratigraphy of the central Scotian Rise: a record of continental margin glaciation; Geo-Marine Letters, v. 13, p. 197–206.

**Bugge, T., Befrig, S., Belderson, R.H., Eidrin, T., Jansen, E., Kenyon, N.H., Holtedahl, H., and Sejrup, H.P.**
1987: A giant three-stage submarine slide off Norway; Geo-Marine Letters, v. 7, p. 191–198.

**Bugge, T., Belderson, R.H. and Kenyon, N.H.**
1988: The Storegga Slide; Philosophical Transactions of the Royal Society A, v. 325, p. 357–388.

**Clifford, V.**
1986: The late Cenozoic seismo-stratigraphy of the East Scotian Slope; B.Sc. honours thesis, Saint Mary's University, Halifax, Nova Scotia, 64 p.

**Cranston, R.E., Ginsburg, G.D., Soloviev, V.A., and Lorenson, T.D.**
1994: Gas venting and hydrate deposits in the Okhotsk Sea; Bulletin of the Geological Society of Denmark, v. 41, p. 80–85.

**Hill, P.R.**
1983: Detailed morphology of a small area on the Nova Scotian continental slope; Marine Geology, v. 53, p. 55–76.
1984: Sedimentary facies of the Nova Scotian upper and middle continental slope, offshore Eastern Canada; Sedimentology, v. 31, p. 293–309.

**Hughes Clarke, J.E.**
1988: The geological record of the 1929 "Grand Banks" earthquake and its relevance to deep-sea clastic sedimentation; Ph.D. thesis, Dalhousie University, Halifax, Nova Scotia, 171 p.

**Hughes Clarke, J.E., O'Leary, D., and Piper, D.J.W.**
1992: The relative importance of mass wasting and deep boundary current activity on the continental rise off western Nova Scotia; *in* Geologic Evolution of Atlantic Continental Rises, (ed.) C.W. Poag and P.C. de Graciansky; van Nostrand Reinhold, New York, p. 266–281.

**Hundert, T.**
1999: An investigation into Quaternary sediments on the continental margin of southeastern Canada; B.Sc. thesis, Saint Mary's University, Halifax, Nova Scotia, 47 p.

**Loncarevic, B.D., Piper, D.J.W., and Fader, G.B.**
1992: Applications of high-quality bathymetry to geological interpretation of the Scotian Shelf; Geoscience Canada, v. 19, p. 5–12.

**Mosher, D.C., Moran, K., and Hiscott, R.N.**
1994: Late Quaternary sediment, sediment mass-flow processes and slope stability on the Scotian Slope; Sedimentology, v. 41, p. 1039–1061.

**Mulder, T. and Moran, K.**
1995: Relationship among submarine instabilities, sea-level variations and the presence of an ice sheet on the continental shelf: an example from the Verrill Canyon area, Scotian Shelf; Paleoceanography, v. 10, p. 137–154.

**Mulder, T., Berry, J.A., and Piper, D.J.W.**
1997: Links between geomorphology and geotechnical characteristics of large debris flow deposits in the Albatross area on the Scotian slope (E. Canada); Marine Georesources and Geotechnology, v. 15, p. 253–281.

**Mulder, T., Moran, K., and Piper, D.J.W.**
in press: Mechanisms for late Quaternary submarine landslides off Nova Scotia, Canada; Marine Geology.

**O'Leary, D.W. and Dobson, M.R.**
1992: Southeastern New England Continental Rise: origin and history of slide complexes; *in* Geologic Evolution of Atlantic Continental Rises, (ed.) C.W. Poag and P.C. de Graciansky; van Nostrand Reinhold, New York, p. 214–265

**Paull, C.K., Ussler, W., III, and Dillon, W.P.**
1991: Is the extent of glaciation limited by marine gas-hydrates; Geophysical Research Letters, v. 18, p. 432–434.

**Piper, D.J.W.**
1991: Surficial Geology and Physical Properties 6. Deep water surficial geology; *in* East Coast Basin Atlas Series: Scotian Shelf; Atlantic Geoscience Centre, Geological Survey of Canada, p. 121.

**Piper, D.J.W. and Normark, W.R.**
1982: Acoustic interpretation of Quaternary sedimentation and erosion on the channelled upper Laurentian Fan, Atlantic margin of Canada; Canadian Journal of Earth Sciences, v. 19, p. 1974–1984.
1989: Late Cenozoic sea-level changes and the onset of glaciation: impact on continental slope progradation off eastern Canada; Marine and Petroleum Geology, v. 6, p. 336–348.

**Piper, D.J.W. and Skene, K.I.**
1998: Latest Pleistocene ice-rafting events on the Scotian margin (eastern Canada) and their relationship to Heinrich events; Paleoceanography, v. 13, p. 205–214.

**Piper, D.J.W. and Sparkes, R.**
1987: Proglacial sediment instability features on the Scotian Slope at 63°W; Marine Geology, v. 76, p. 1–11.
1990: Pliocene - Quaternary geology, central Scotian Slope; Geological Survey of Canada, Open File 2233, scale 1:250 000.

**Piper, D.J.W., Cochonat, P., and Morrison, M.L.**
1999: Sidescan sonar evidence for progressive evolution of submarine failure into a turbidity current: the 1929 Grand Banks event; Sedimentology, v. 46, p. 79–98.

**Piper, D.J.W., Farre, J.A., and Shor, A.N.**
1985: Late Quaternary slumps and debris flows on the Scotian Slope; Geological Society of America Bulletin, v. 96, p. 1508–1517.

**Piper, D.J.W., Mudie, P.J., Aksu, A.E., and Skene, K.I.**
1994: A 1 Ma record of sediment flux south of the Grand Banks used to infer the development of glaciation in southeastern Canada; Quaternary Science Reviews, v. 13, p. 23–37.

**Piper, D.J.W., Normark, W.R., and Sparkes, R.**
1987: Late Cenozoic acoustic stratigraphy of the central Scotian Slope, eastern Canada; Canadian Bulletin of Petroleum Geology, v. 35, p. 1–11.

**Piper, D.J.W., Pirmez, C., Manley, P.L., Long, D., Flood, R.D., Normark, W.R., and Showers, W.**
1997: Mass transport deposits of Amazon Fan; Scientific Results, Ocean Drilling Program, v. 155, p. 109–146.

**Shor, A.N. and Piper, D.J.W.**
1989: A large Pleistocene blocky debris flow on the central Scotian Slope; Geo-Marine Letters, v. 9, p. 153–160.

**Skene, K.I.**
1998: Architecture of submarine channel levees; Ph.D. thesis, Dalhousie University, Halifax, Nova Scotia, 365 p.

**Stein, S., Sleep, N.H., Geller, R.J., Wang, S., and Kroeger, G.C.**
1979: Earthquakes along the passive margin of eastern Canada; Geophysical Research Letters, v. 6, p. 537–540.

**Swift, S.A.**
1987: Late Cretaceous - Cenozoic development of Outer Continental Margin, Southwest Nova Scotia; American Association of Petroleum Geologists Bulletin, v. 71, p. 678–701.

**Uchupi, E. and Austin, J.**
1979: The stratigraphy and structure of the Laurentian cone region; Canadian Journal of Earth Sciences, v. 16, p. 1726–1752.

---

Geological Survey of Canada Project 980013

# AUTHOR INDEX

## NOTE TO CONTRIBUTORS

Submissions to the Discussion section of Current Research are welcome from both the staff of the Geological Survey of Canada and from the public. Discussions are limited to six double-spaced typewritten pages (about 1500 words) and are subject to review by the Managing Editor. Discussions are restricted to the scientific content of Geological Survey reports. General discussions concerning sector or government policy will not be accepted. All manuscripts must be computer word-processed on an IBM compatible system and must be submitted with a diskette using WordPerfect. Illustrations will be accepted only if, in the opinion of the editor, they are considered essential. In any case no redrafting will be undertaken and reproducible copy must accompany the original submissions. Discussion is limited to recent reports (not more than two years old) and may be in either English or French. Every effort is made to include both Discussion and Reply in the same issue. Current Research is published in January and July. Submissions should be sent to the Managing Editor, Geological Survey of Canada, 601 Booth Street, Ottawa K1A 0E8.

## AVIS AUX AUTEURS D'ARTICLES

Nous encourageons tant le personnel de la Commission géologique que le grand public à nous faire parvenir des articles destinés à la section discussion de la publication Recherches en cours. Le texte doit comprendre au plus six pages dactylographiées à double interligne (environ 1500 mots), texte qui peut faire l'objet d'un réexamen par la rédactrice en chef administrative. Les discussions doivent se limiter au contenu scientifique des rapports de la Commission géologique. Les discussions générales sur le Secteur ou les politiques gouvernementales ne seront pas acceptées. Le texte doit être soumis à un traitement de texte informatisé par un système IBM compatible et enregistré sur disquette WordPerfect. Les illustrations ne seront acceptées que dans la mesure où, selon l'opinion du rédacteur, elles seront considérées comme essentielles. Aucune retouche ne sera faite aux illustrations et dans tous les cas, une copie qui puisse être reproduite doit accompagner le texte original. Les discussions en français ou en anglais doivent se limiter aux rapports récents (au plus de deux ans). On s'efforcera de faire coïncider les articles destinés aux rubriques discussions et réponses dans le même numéro. La publication Recherches en cours paraît en janvier et en juillet. Les articles doivent être envoyés à la rédactrice en chef administrative, Commission géologique du Canada, 601, rue Booth, Ottawa K1A 0E8.

Geological Survey of Canada Current Research is released twice a year, in January and July. The four parts published in January 1999 (Current Research 1999-A to D) are listed below and can be purchased separately.

Recherches en cours, une publication de la Commission géologique du Canada, est publiée deux fois par année, en janvier et en juillet. Les quatre parties publiées en janvier 1999 (Recherches en cours 1999-A à D) sont énumérées ci-dessous et sont vendues séparément.

| | |
|---|---|
| Part A: | Cordillera and Pacific Margin |
| Partie A : | Cordillère et marge du Pacifique |
| Part B: | Interior Plains and Arctic Canada |
| Partie B : | Plaines intérieures et région arctique du Canada |
| Part C: | Canadian Shield |
| Partie C : | Bouclier canadien |
| Part D: | Eastern Canada and national and general programs |
| Partie D : | Est du Canada et programmes nationaux et généraux |
| Part E: | this volume |
| Partie E : | ce volume |